

2nd synthetic biology forum: System and synthetic biology for biofuels and bioproducts

Edited by

Jean Marie François, Min Jiang, Mingjie Jin
and Shihui Yang

Published in

Frontiers in Bioengineering and Biotechnology



FRONTIERS EBOOK COPYRIGHT STATEMENT

The copyright in the text of individual articles in this ebook is the property of their respective authors or their respective institutions or funders. The copyright in graphics and images within each article may be subject to copyright of other parties. In both cases this is subject to a license granted to Frontiers.

The compilation of articles constituting this ebook is the property of Frontiers.

Each article within this ebook, and the ebook itself, are published under the most recent version of the Creative Commons CC-BY licence. The version current at the date of publication of this ebook is CC-BY 4.0. If the CC-BY licence is updated, the licence granted by Frontiers is automatically updated to the new version.

When exercising any right under the CC-BY licence, Frontiers must be attributed as the original publisher of the article or ebook, as applicable.

Authors have the responsibility of ensuring that any graphics or other materials which are the property of others may be included in the CC-BY licence, but this should be checked before relying on the CC-BY licence to reproduce those materials. Any copyright notices relating to those materials must be complied with.

Copyright and source acknowledgement notices may not be removed and must be displayed in any copy, derivative work or partial copy which includes the elements in question.

All copyright, and all rights therein, are protected by national and international copyright laws. The above represents a summary only. For further information please read Frontiers' Conditions for Website Use and Copyright Statement, and the applicable CC-BY licence.

ISSN 1664-8714
ISBN 978-2-83251-028-5
DOI 10.3389/978-2-83251-028-5

About Frontiers

Frontiers is more than just an open access publisher of scholarly articles: it is a pioneering approach to the world of academia, radically improving the way scholarly research is managed. The grand vision of Frontiers is a world where all people have an equal opportunity to seek, share and generate knowledge. Frontiers provides immediate and permanent online open access to all its publications, but this alone is not enough to realize our grand goals.

Frontiers journal series

The Frontiers journal series is a multi-tier and interdisciplinary set of open-access, online journals, promising a paradigm shift from the current review, selection and dissemination processes in academic publishing. All Frontiers journals are driven by researchers for researchers; therefore, they constitute a service to the scholarly community. At the same time, the *Frontiers journal series* operates on a revolutionary invention, the tiered publishing system, initially addressing specific communities of scholars, and gradually climbing up to broader public understanding, thus serving the interests of the lay society, too.

Dedication to quality

Each Frontiers article is a landmark of the highest quality, thanks to genuinely collaborative interactions between authors and review editors, who include some of the world's best academicians. Research must be certified by peers before entering a stream of knowledge that may eventually reach the public - and shape society; therefore, Frontiers only applies the most rigorous and unbiased reviews. Frontiers revolutionizes research publishing by freely delivering the most outstanding research, evaluated with no bias from both the academic and social point of view. By applying the most advanced information technologies, Frontiers is catapulting scholarly publishing into a new generation.

What are Frontiers Research Topics?

Frontiers Research Topics are very popular trademarks of the *Frontiers journals series*: they are collections of at least ten articles, all centered on a particular subject. With their unique mix of varied contributions from Original Research to Review Articles, Frontiers Research Topics unify the most influential researchers, the latest key findings and historical advances in a hot research area.

Find out more on how to host your own Frontiers Research Topic or contribute to one as an author by contacting the Frontiers editorial office: frontiersin.org/about/contact

2nd synthetic biology forum: System and synthetic biology for biofuels and bioproducts

Topic editors

Jean Marie François — Institut Biotechnologique de Toulouse (INSA), France

Min Jiang — Nanjing Tech University, China

Mingjie Jin — Nanjing University of Science and Technology, China

Shihui Yang — Hubei University, China

Citation

François, J. M., Jiang, M., Jin, M., Yang, S., eds. (2022). *2nd synthetic biology forum: System and synthetic biology for biofuels and bioproducts*.

Lausanne: Frontiers Media SA. doi: 10.3389/978-2-83251-028-5

Table of contents

- 06 **Prompting Fab Yeast Surface Display Efficiency by ER Retention and Molecular Chaperon Co-expression**
Meng Mei, Junhong Li, Shengchen Wang, Ki Baek Lee, Brent L. Iverson, Guimin Zhang, Xin Ge and Li Yi
- 17 **Recent Advances of CRISPR/Cas9-Based Genetic Engineering and Transcriptional Regulation in Industrial Biology**
Shangjie Zhang, Feng Guo, Wei Yan, Zhongxue Dai, Weiliang Dong, Jie Zhou, Wenming Zhang, Fengxue Xin and Min Jiang
- 28 **Progress and Prospects of Bioelectrochemical Systems: Electron Transfer and Its Applications in the Microbial Metabolism**
Tianwen Zheng, Jin Li, Yaliang Ji, Wenming Zhang, Yan Fang, Fengxue Xin, Weiliang Dong, Ping Wei, Jiangfeng Ma and Min Jiang
- 38 **Omics Analysis Reveals the Mechanism of Enhanced Recombinant Protein Production Under Simulated Microgravity**
Jie Huangfu, Hye Su Kim, Ke Xu, Xiaoyu Ning, Lei Qin, Jun Li and Chun Li
- 49 **Pleiotropic Functions and Biological Potentials of Silver Nanoparticles Synthesized by an Endophytic Fungus**
Radhika Chandankere, Jayabaskaran Chelliah, Kamalraj Subban, Vanitha C. Shanadrahalli, Amreesh Parvez, Hossain M. Zayed, Yogesh C. Sharma and Xianghui Qi
- 63 **Endogenous Type I CRISPR-Cas: From Foreign DNA Defense to Prokaryotic Engineering**
Yanli Zheng, Jie Li, Baiyang Wang, Jiamei Han, Yile Hao, Shengchen Wang, Xiangdong Ma, Shihui Yang, Lixin Ma, Li Yi and Wenfang Peng
- 80 **Multiple Small RNAs Interact to Co-regulate Ethanol Tolerance in *Zymomonas mobilis***
Runhua Han, Katie Haning, Juan C. Gonzalez-Rivera, Yongfu Yang, Runxia Li, Seung Hee Cho, Ju Huang, Bobi A. Simonsen, Shihui Yang and Lydia M. Contreras
- 99 **The Synergistic Action of Electro-Fenton and White-Rot Fungi in the Degradation of Lignin**
Lipeng Hou, Dandan Ji, Weifang Dong, Lin Yuan, Fengshan Zhang, Yan Li and Lihua Zang
- 110 **Molecular Mechanism Associated With the Impact of Methane/Oxygen Gas Supply Ratios on Cell Growth of *Methylobacterium buryatense* 5GB1 Through RNA-Seq**
Lizhen Hu, Yongfu Yang, Xin Yan, Tianqing Zhang, Jing Xiang, Zixi Gao, Yunhao Chen, Shihui Yang and Qiang Fei

- 120 **Enhanced Bacitracin Production by Systematically Engineering S-Adenosylmethionine Supply Modules in *Bacillus licheniformis***
Dongbo Cai, Bowen Zhang, Jiang Zhu, Haixia Xu, Pei Liu, Zhi Wang, Junhui Li, Zhifan Yang, Xin Ma and Shouwen Chen
- 132 **Production of Terpenoids by Synthetic Biology Approaches**
Caizhe Zhang and Kui Hong
- 141 **Exploring a Highly D-Galactose Specific L-Arabinose Isomerase From *Bifidobacterium adolescentis* for D-Tagatose Production**
Guoyan Zhang, Yingfeng An, Amreesh Parvez, Hossain M. Zayed, Junhua Yun and Xianghui Qi
- 151 **High-Efficiency Secretion and Directed Evolution of Chitinase BcChiA1 in *Bacillus subtilis* for the Conversion of Chitinaceous Wastes Into Chitooligosaccharides**
Sijia Wang, Gang Fu, Jinlong Li, Xunfan Wei, Huan Fang, Dawei Huang, Jianping Lin and Dawei Zhang
- 162 **Recent Development of Extremophilic Bacteria and Their Application in Biorefinery**
Daochen Zhu, Wasiu Adewale Adebisi, Fiaz Ahmad, Sivasamy Sethupathy, Blessing Danso and Jianzhong Sun
- 180 **Intracellular Redox Perturbation in *Saccharomyces cerevisiae* Improved Furfural Tolerance and Enhanced Cellulosic Bioethanol Production**
Chen-Guang Liu, Kai Li, Ke-Yi Li, Chularat Sakdaronnarong, Muhammad Aamer Mehmood, Xin-Qing Zhao and Feng-Wu Bai
- 190 **Engineering the Effector Domain of the Artificial Transcription Factor to Improve Cellulase Production by *Trichoderma reesei***
Qing-Shan Meng, Fei Zhang, Wei Wang, Chen-Guang Liu, Xin-Qing Zhao and Feng-Wu Bai
- 199 **Acidic Versus Alkaline Bacterial Degradation of Lignin Through Engineered Strain *E. coli* BL21(Lacc): Exploring the Differences in Chemical Structure, Morphology, and Degradation Products**
Gabriel Murillo Morales, Sameh S. Ali, Haibing Si, Weimin Zhang, Rongxian Zhang, Keyvan Hosseini, Jianzhong Sun and Daochen Zhu
- 215 **Global Reprogramming of Gene Transcription in *Trichoderma reesei* by Overexpressing an Artificial Transcription Factor for Improved Cellulase Production and Identification of Ypr1 as an Associated Regulator**
Fei Zhang, Jia-Xiang Li, Verawat Champreda, Chen-Guang Liu, Feng-Wu Bai and Xin-Qing Zhao

- 231 **The Magnesium Concentration in Yeast Extracts Is a Major Determinant Affecting Ethanol Fermentation Performance of *Zymomonas mobilis***
Runxia Li, Mingjie Jin, Jun Du, Mian Li, Shouwen Chen and Shihui Yang
- 244 **A Novel Butanol Tolerance-Promoting Function of the Transcription Factor Rob in *Escherichia coli***
Zhiquan Wang, Tingli Xue, Dongsheng Hu and Yuanyuan Ma



Prompting Fab Yeast Surface Display Efficiency by ER Retention and Molecular Chaperon Co-expression

Meng Mei¹, Junhong Li¹, Shengchen Wang¹, Ki Baek Lee², Brent L. Iverson³, Guimin Zhang¹, Xin Ge^{2*} and Li Yi^{1*}

¹ State Key Laboratory of Biocatalysis and Enzyme Engineering, Hubei Collaborative Innovation Center for Green Transformation of Bio-Resources, Hubei Key Laboratory of Industrial Biotechnology, School of Life Sciences, Hubei University, Wuhan, China, ² Department of Chemical and Environmental Engineering, University of California, Riverside, Riverside, CA, United States, ³ Department of Chemistry, University of Texas, Austin, TX, United States

OPEN ACCESS

Edited by:

Min Jiang,
Nanjing Tech University, China

Reviewed by:

Lei Wang,
Institute of Biophysics (CAS), China
Dae-Hyuk Kweon,
Sungkyunkwan University,
South Korea

*Correspondence:

Xin Ge
xge@engr.ucr.edu
Li Yi
liyi@hbu.edu.cn

Specialty section:

This article was submitted to
Synthetic Biology,
a section of the journal
Frontiers in Bioengineering and
Biotechnology

Received: 20 August 2019

Accepted: 12 November 2019

Published: 26 November 2019

Citation:

Mei M, Li J, Wang S, Lee KB, Iverson BL, Zhang G, Ge X and Yi L (2019) Prompting Fab Yeast Surface Display Efficiency by ER Retention and Molecular Chaperon Co-expression. *Front. Bioeng. Biotechnol.* 7:362. doi: 10.3389/fbioe.2019.00362

For antibody discovery and engineering, yeast surface display (YSD) of antigen-binding fragments (Fabs) and coupled fluorescence activated cell sorting (FACS) provide intact paratopic conformations and quantitative analysis at the monoclonal level, and thus holding great promises for numerous applications. Using anti-TNF α mAbs Infliximab, Adalimumab, and its variants as model Fabs, this study systematically characterized complementary approaches for the optimization of Fab YSD. Results suggested that by using divergent promoter *GAL1-GAL10* and endoplasmic reticulum (ER) signal peptides for co-expression of light chain and heavy chain-Aga2 fusion, assembled Fabs were functionally displayed on yeast cell surface with sigmoidal binding responses toward TNF α . Co-expression of a Hsp70 family molecular chaperone Kar2p and/or protein-disulfide isomerase (Pdi1p) significantly improved efficiency of functional display (defined as the ratio of cells displaying functional Fab over cells displaying assembled Fab). Moreover, fusing ER retention sequences (ERSs) with light chain also enhanced Fab display quality at the expense of display quantity, and the degree of improvements was correlated with the strength of ERSs and was more significant for Infliximab than Adalimumab. The feasibility of affinity maturation was further demonstrated by isolating a high affinity Fab clone from 1:10³ or 1:10⁵ spiked libraries.

Keywords: yeast surface display, Fab, divergent promotor, ER retention sequence, molecular chaperone

INTRODUCTION

Monoclonal antibodies (mAbs) represent the fastest growing class of therapeutics in the last decades. By the end of 2018, at least 116 mAb-based biopharmaceutical products are active on the market (Walsh, 2018; DeFrancesco, 2019). Notably, mAbs occupies seven spots out of the top ten best-selling drugs in 2018 (Urquhart, 2019). As 54 new mAbs in late-stage clinical trials are under regulatory review, it is expected that mAb-based products will continue to dominate the biopharmaceutical approvals in the near future. From the biotechnology viewpoint, an essential development step is the affinity maturation of lead mAbs to achieve high potencies desirable for therapeutic practices. Following the generation of combinatorial libraries, a high-throughput selection/screening method needs to be exploited to isolate mAb variants with improved affinities. Compared to selection approaches, which rely on overall binding strength such as phage panning,

fluorescence activated cell sorting (FACS) is advantageous by providing quantitative analysis of each library member. During subsequent rounds of sorting, the concentration of a fluorophore-labeled antigen can be fine-tuned in a real-time manner, leading to efficiently distinguish high affinity clones from others. In addition, the multiparameter nature of FACS allows to normalize the difference on antibody expression levels among cells and/or various antibody clones. Accordingly, a dual color sorting with one channel for antibody expression and the other for antigen binding has been proven highly effective for enriching affinity improved clones (Feldhaus et al., 2003; van den Beucken et al., 2003).

For FACS, recombinant antibodies or their fragments must be present on cell surface. Compared to mammalian cells, yeast has been widely used for antibody surface display due to its low cost, ease to handle, and facile construction of antibody libraries (Boder and Wittrup, 1997; Pepper et al., 2008). Derived from human immunoglobulin G (IgG), the design of single-chain variable fragment (scFv) links a heavy chain variable domain (V_H) with its associated light chain variable domain (V_L) via a flexible linker. As the smallest human antibody fragment with binding function, scFv can be efficiently displayed on yeast cell surface such as by fusion with α -agglutinin aga2 (Boder and Wittrup, 1997). Consequently, yeast surface display (YSD) of scFv achieved great successes for antibody discovery and engineering using either immunized or naïve/synthetic libraries (Feldhaus et al., 2003; Miller et al., 2008). However, the conformation of V_H and V_L domains in scFv format may not be the same as in its natural IgG, in which the heavy and light chains also interact through their constant heavy 1 (C_H1) and constant light (C_L) domains. Although such conformational variations are usually subtle, its impact on binding affinity can be substantial and problematic for affinity maturation studies (Casadevall and Janda, 2012). In fact, it is not uncommon that significant potency loss happens when an affinity matured scFv clone is converted back to its associated IgG (Steinwand et al., 2014; Yang et al., 2018). As the antigen-binding fragment (Fab) contains half heavy chain (V_H - C_H1) and entire light chain (V_L - C_L), this format can reserve V_H and V_L domains in their intact conformations. Therefore, it is argued that the best combination for affinity maturation is to display Fabs on yeast surface and to screen by FACS.

Since the initial studies of YSD in 1990s (Boder and Wittrup, 1997), recent researches have demonstrated the feasibility of displaying Fabs (Rosowski et al., 2018; Wang et al., 2018), and full-length IgGs (Rhiel et al., 2014) on yeast cell surface. These developments apply different technologies including bi-directional promoter design for co-expression (Rosowski et al., 2018), type II restriction enzymes for library construction (Roth et al., 2019), immobilized ZZ domain for surface display (Rhiel et al., 2014), and leucine-zipper interactions for Fab assembly (Wang et al., 2018). It has been proven that Fab was more reliable than scFv for YSD (Sivelle et al., 2018), and Fab YSD was suitable for antibody affinity maturation (Yang et al., 2018). Despite these tremendous advances, systematic study for Fab YSD optimization is still lacking.

One characteristic of protein production in yeast cells is that various molecular chaperons exist in the endoplasmic reticulum (ER) to facilitate the protein folding and post-translational modifications. Kar2p, also known as BiP, is a major member of the Hsp70 chaperone family, which binds to unfolded polypeptide chains and mediates protein folding within the ER (Rose et al., 1989; Valkonen et al., 2003; Hernandez-Elvira and Torres-Quiroz, 2018). Only correctly folded proteins can be released from Kar2p, while abnormally folded or improperly assembled proteins are retained by Kar2p for later degradation. In addition, ER-associated protein disulfide isomerase (Pdi1p) catalyzed the disulfide bonds formation in eukaryotic cells (Farquhar et al., 1991; Niu et al., 2016; Beal et al., 2019). These molecular chaperons are crucial for the Fab assembly, whose efficiency depends on the correct folding of V_H - C_H1 and V_L - C_L domains as well as the formation of intra- and inter-molecular disulfide bonds. Moreover, ER retention, mediated by characteristic ER retention sequence (ERS), is a mechanism that ensures only properly folded/assembled proteins are exported from the ER to the Golgi (Munro and Pelham, 1987). This phenomenon provides a means of quality control during protein synthesis, maturation and assembly, because misfolded or incorrectly assembled proteins are retained in the ER and targeted for degradation (Ellgaard et al., 1999). Our previous work on characterization of HDEL-type ERS suggested that the ERS sequence HDEL exhibited a protein ER retention ability 2-fold stronger than that of KDEL but was 50% of FEHDEL, the strongest endogenous ERS in *Saccharomyces cerevisiae* (Munro and Pelham, 1987; Mei et al., 2017). Further systematic study of all endogenous ERS indicated that an engineered sequence WEHDEL could confer 2-fold stronger retention ability than FEHDEL. Building on above knowledge, using anti-tumor necrosis factor α (TNF α) mAbs Infliximab (Keane et al., 2001), Adalimumab (D2E7), and its variants (Rajpal et al., 2005) as model Fabs, this study characterized the impacts of molecular chaperons Kar2p and Pdi1p and four ERSs, i.e., WEHDEL, FEHDEL, HDEL, and KDEL, on Fab YSD efficiency. In addition, the feasibility of Fab maturation through high-throughput screening was demonstrated by FACS sorting of large spiked libraries.

MATERIALS AND METHODS

Construction of Fab and scFv Yeast Surface Display Vectors

Genes encoding V_H - C_H1 and V_L - C_L fragments (Salfeld et al., 2003; Rajpal et al., 2005) were chemically synthesized, amplified by PCR and cloned to *PstI/EcoRI* sites and *BamHI/XhoI* sites, respectively, on pESD (Yi et al., 2015) to generate pESD-Fab. pESD-HC (heavy chain only) and pESD-LC (light chain only) were also generated as controls. Fragments encoding Adalimumab variant scFvs, V_L -(G4S)₃- V_H , were assembled by overlapping PCR and cloned to *PstI/EcoRI* sites on pESD to generate pESD-scFv. Kar2p and Pdi1p wild-type (wt) genes were amplified by PCR using the genome of *S. cerevisiae* EBY100 as the templates and fused with protomer *GALI* region by overlapping PCR. Using Kar2p and Pdi1p wt genes as the templates, their

mutants were generated through site mutagenesis. Obtained *GAL1*-Kar2p/Pdi1p cassettes were cloned to *KpnI*/*BglII* sites on pESD-Fab to give pESD-Fab-Kar2p/Pdi1p. Additional *GAL1*-Kar2p cassette was cloned to *SacI* site on pESD-Fab-Pdi1p to give pESD-Fab-Pdi1p-Kar2p. ERSs were introduced at C-termini of light chains by extension PCR and cloned to pESD-Fab to give pESD-Fab-ERS. All cloning works were performed in *Escherichia coli* XL-Gold and confirmed by DNA sequencing.

Expression and Purification of TNF α -His₆

Gene of human TNF α (NCBI ID: 7124) was chemically synthesized, cloned to pET-28a, and transformed to *E. coli* BL21 (DE3) cells for culture in LB medium at 37°C. When OD₆₀₀ reached 0.6–0.8, cells were induced with 0.5 mM IPTG at 18°C for 20 h. After induction, cells were collected and resuspended in lysis buffer containing 50 mM Tris (pH 8.0), 150 mM NaCl, 0.5 mg/mL lysozyme, 1 mM PMSF, and 10 mM imidazole for 1 h on ice, followed by sonication. Cell debris was then removed by centrifugation at 10,000 \times g at 4°C for 20 min, and the supernatant containing TNF α -His₆ was subjected to Ni-NTA affinity purification at 4°C (Qiagen, Valencia, CA, USA). Purity of produced TNF α -His₆ was tested by SDS-PAGE, and its concentration was measured by UV absorbance.

Flow Cytometry Analysis of Displayed Fabs and scFvs on Yeast Cell Surface

Generated yeast surface display plasmids were transformed to *S. cerevisiae* EBY100 competent cells (Cooper and Hausman, 2000). Transformed cells were cultivated in SD-CAA medium (20 g/L D-glucose, 6.7 g/L yeast nitrogen base, 5 g/L casamino acids, 5.4 g/L Na₂HPO₄, 8.6 g/L NaH₂PO₄·H₂O, pH 7.4) at 30°C with shaking at 230 rpm. When OD₆₀₀ reached 0.5–1.0, cells were collected by centrifugation at 3,000 \times g for 2 min and inoculated to SG-CAA medium (20 g/L galactose, 6.7 g/L yeast nitrogen base, 5 g/L casamino acids, 5.4 g/L Na₂HPO₄, 8.6 g/L NaH₂PO₄·H₂O, pH 7.4). After induction at 18°C for 48 h, cells were harvested by centrifugation, washed three times with PBS (pH 7.4), supplemented with 0.5% BSA and 1 mM EDTA, and re-suspended as 0.1 OD₆₀₀ cells per 20 μ L PBS (pH 7.4), 0.5% BSA. For Fab and scFv display analysis, cells were incubated with 0.1 μ M anti-HA-FITC and/or 0.1 μ M anti-FLAG-iFluor647 (GenScript, Nanjing, China) for 15 min in dark. Flow cytometry analysis was performed by using Beckman Coulter CytoFLEX (Brea, CA) equipped with 488 and 633 nm lasers and 525/40 and 660/20 nm band-pass filters. To test binding function of cell surface displayed antibody fragments, cells were incubated with 1 pM –20 nM purified TNF α -His₆ at 25°C for 30 min and subsequently labeled with 0.1 μ M anti-His₆-iFluor647 (GenScript, Nanjing, China). Percentages of TNF α ⁺ cells were quantified by FACS. The cells carrying Fab heavy chain (V_H-C_{H1}) without light chain and light chain (V_L-C_L) without heavy chain were used as controls.

FACS Enrichment for High Affinity Fab Clone From Spiked Libraries

Cells bearing Fab cb2-6 and Fab D2E7 display vectors were mixed at 1:10³ or 1:10⁵ ratios. After cultivation and induction,

mixed cells were labeled with TNF α -His₆ of predetermined concentrations, and subsequently labeled with 0.1 μ M anti-His₆-iFluor647 and 0.1 μ M anti-HA-FITC. Sorting was performed in the single cell mode by using Beckman Coulter MoFlo XDP flow cytometer (Brea, CA, USA) equipped with 488 and 633 nm lasers and 525/40 and 660/20 nm band-pass filters. In each round, 10⁷–10⁹ cells were sorted, and 0.6–1.0% cells with the highest FITC/iFluor647 double signals were collected. Collected cells were cultivated in SD-CAA and induced in SG-CAA for the next round of sorting. Aliquots of collected cells were also recovered on SD-CAA plates for monoclonal analysis. Yeast plasmids were extracted by using Zymolyase (Amsbio, Abingdon, UK) and transformed into *E. coli* XL-Gold for amplification and sequence analysis.

Yeast Total RNA Extract and qRT-PCR

After galactose induction, total RNA was extracted from yeast cell samples by using RNAiso kit (TaKaRa Bio, Kusatsu, Japan). Reverse transcription was performed by using PrimeScript II first-strand cDNA synthesis kit (TaKaRa Bio) with Random 6 mers. The cDNA levels of *Kar2p* and *Pdi1p* were then analyzed with CFX real-time PCR (Bio-Rad, Hercules, CA, USA). Relative expression levels against endogenous *Taf10* were determined with efficiency correction and associated technical errors were calculated. The final results were normalized by the relative mRNA levels of *Kar2p* and *Pdi1p* in EBY100 cells.

RESULTS

Design for Fab Yeast Surface Display

For successful display of a Fab, its heavy chain (V_H-C_{H1}) and light chain (V_L-C_L) need to be co-expressed. In our design, a divergent *GAL1*-*GAL10* promoter derived from previous studies (West et al., 1987; Boder et al., 2005; Jiang and Boder, 2010) is exploited by cloning Fab heavy chain and light chain at downstream of *GAL10* and *GAL1*, respectively (Figure 1A). Therefore, in the presence of galactose, expression of both chains will be induced simultaneously. Yeast endoplasmic reticulum (ER) signal sequences are included at N-termini of both chains for their translocation and secretory expression. Once translated, Fab assembly between heavy and light chains, especially via the intermolecular disulfide connecting C-termini of C_{H1} and C_L, is critical for its binding function (Padlan et al., 1986). Since protein disulfide-bond formation in eukaryotic cells mainly occurs in ER (Frand et al., 2000), targeting ER via signal sequences also enhances Fab assembly. For surface display, V_H-C_{H1} is fused to the N-terminus of Aga2p, which leads transportation to cell surface through the α -agglutinin system by a disulfide linkage to the cell wall-anchored Aga1p (Boder and Wittrup, 1997). In addition, a FLAG tag and a HA tag are introduced to the heavy and light chain expression cassettes, respectively, for facile detections (Figure 1A).

Display of Assembled Fabs on Yeast Cell Surface

Fab display plasmids of anti-TNF α mAb D2E7 and its variants were constructed and transformed into *S. cerevisiae* EBY100

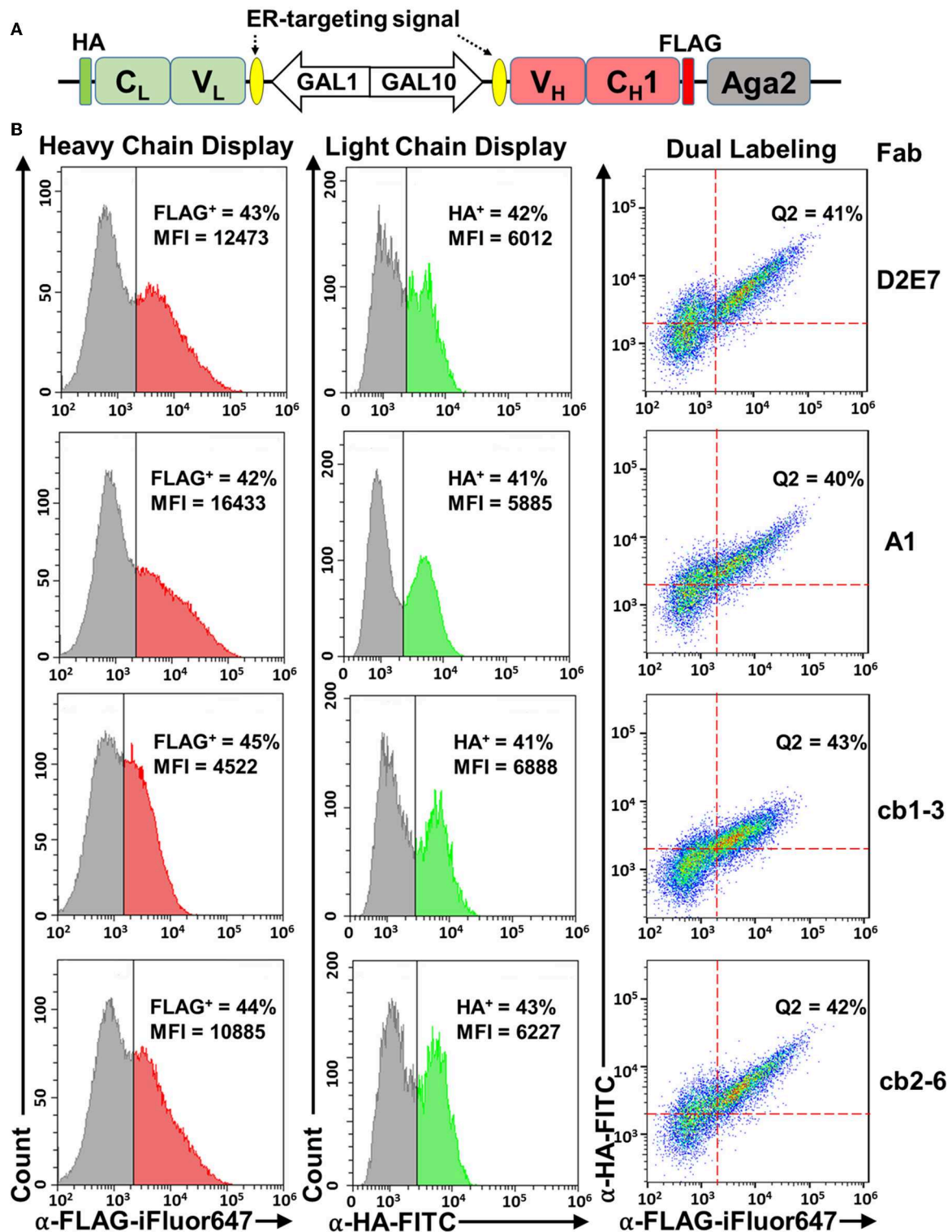


FIGURE 1 | Fab yeast surface display using a divergent promoter, ER-targeting signals, and Aga2 fusion. **(A)** pESD-Fab. Expression cassettes for light (V_L - C_L) and heavy (V_H - C_H1) chains were located downstream of *GAL1*-*GAL10* promoter and endoplasmic reticulum (ER)-targeting signals. Light chain was fused with a HA tag, and heavy chain was fused with a FLAG tag to the N-terminus of Aga2. **(B)** Validation of heavy chain display (left panels), light chain display (middle panels), and Fab assembly (right panels) on yeast cell surface by flow cytometry. Expression was induced by 20 g/L galactose and cells were incubated with 0.1 μ M anti-FLAG-iFluor647 and/or 0.1 μ M anti-HA-FITC antibodies. Fab display of Adalimumab (D2E7) and three variants were tested. Percentages of cells displaying assembled Fabs were shown as Q2 (FLAG⁺/HA⁺ double positive). MFI, mean fluorescence intensity.

cells. After cultivation and induction with 20 g/L galactose, cells were analyzed by flow cytometry. To detect surface displayed D2E7 heavy chain, which was fused with a FLAG tag to the N-terminus of Aga2, cells were incubated with 0.1 μ M iFluor 647 conjugated anti-FLAG antibodies. FACS results showed the successful anchoring of D2E7 heavy chain on yeast cell surface, with 43% cells were FLAG⁺ (**Figure 1B**, left panel). In contrast, <0.6% cells bearing D2E7 light chain without its heavy chain gene were FLAG⁺ (**Figure S1A**). Similarly, the display of HA-tagged D2E7 light chain was detected with 0.1 μ M FITC conjugated anti-HA antibodies, and the results indicated that 42% cells were HA⁺ (**Figure 1B**, middle panel), while <0.4% cells bearing D2E7 heavy chain without its light chain gene were HA⁺ (**Figure S1B**). In addition, <0.6% cells bearing D2E7 light chain without its heavy chain gene were HA⁺ (**Figure S1C**). As D2E7 light chain expression cassette (V_L-C_L-HA) did not possess the fusion partner Aga2 for anchoring, display of D2E7 light chain on cell surface was presumably caused by its Fab assembly between secreted light chain and anchored heavy chain. To confirm the presence of both chains on individual cells, induced cells were further dual labeled with 0.1 μ M anti-FLAG-iFluor647 and 0.1 μ M anti-HA-FITC. FACS results revealed that 41 \pm 3% cells were FLAG⁺/HA⁺ double positive (**Figure 1B**, right panel), suggesting the display of intermolecularly assembled D2E7 Fab. Display profiles of D2E7 variants A1, cb1-3, and cb2-6 were also characterized in the same approaches. Results suggested the similar display levels for their heavy chains (42–45% FLAG⁺, **Figure 1B**, left panel), their light chains (41–43% HA⁺, **Figure 1B**, middle panel), and assembled Fabs (40–42% FLAG⁺/HA⁺ double positive, **Figure 1B**, right panel). Notably, the mean fluorescence intensity (MFI) of FLAG⁺ cells for cb1-3 was considerably less than other tested Fab clones, suggesting that cb1-3 presumably exhibited a lower expression level or less display efficiency of its heavy chain.

Yeast Surface Displayed Fabs Were Functional

To test binding functions of displayed D2E7 Fab and its variants, human TNF α as a His₆ tagged protein was recombinantly produced in *E. coli* with a typical yield of 24 mg purified TNF α -His₆ per liter of culture (**Figure 2A**). Cells bearing D2E7 Fab construct were incubated with 1 pM–20 nM TNF α -His₆ followed by labeling with 0.1 μ M iFluor 647 conjugated anti-His₆ antibodies. In parallel, cells displaying D2E7 heavy chain without its light chain was prepared as the control. FACS results indicated that, when 20 nM TNF α -His₆ was used, only 0.5% of cells displaying D2E7 V_H-C_H1 were TNF α ⁺ (**Figure 2B**), suggesting that TNF α cannot be recognized by either unassembled D2E7 heavy chain or yeast host cell EBY100. In contrast, when D2E7 Fab was displayed, after incubation with even 1 pM TNF α -His₆, 5.3% cells were TNF α ⁺ (**Figure 2C**). The percentages of TNF α ⁺ cells increased with higher TNF α -His₆ concentrations: 9.6% at 10 pM, 15% at 100 pM, 42% at 500 pM, and 46% at 1 μ M. The proportion of TNF α ⁺ cells became plateaued 55% when 5–20 nM TNF α -His₆ was applied, suggesting that under used culture and induction conditions, 55% cells displayed functional D2E7

Fab. Plotting MFIs of TNF α ⁺ cells over TNF α concentrations demonstrated a sigmoidal correlation (**Figure 2D**). Dose-response relationships on TNF α ⁺ cell percentages and associated MFIs were also measured for D2E7 variants A1, cb1-3, and cb2-6. Results showed that \sim 60% cells displayed functional Fabs (**Figure S2A**) with expected sigmoidal curves between MFIs and TNF α concentrations (**Figures S2B–D**). All these results suggested that yeast surface displayed Fabs exhibited their specific binding functions. Notably, when 1–100 pM TNF α was used for cell labeling, MFIs of TNF α ⁺ cells were higher for variants cb1-3 and cb2-6 than D2E7 (**Figure 2C**, **Figure S2A**), likely due to their improved affinities (Rajpal et al., 2005).

Functional Display Efficiency Was Improved by Co-expression of Molecular Chaperones

As molecular chaperones in the ER assist folding of newly synthesized proteins and prevent them from misfolding and/or formation of aggregates (Hartl and Hayer-Hartl, 2002), we next investigated the effects of a Hsp70 family member Kar2p (Rose et al., 1989) on Fab surface display. To achieve co-expression of Kar2p, its gene was cloned downstream of an additional *GAL1* promoter allowing its simultaneous induction with galactose (**Figure 3A**). When EBY100 cells producing D2E7 Fab and Kar2p were labeled with anti-FLAG-iFluor647 or anti-HA-FITC for detecting displayed heavy chain or light chain, results revealed that co-expression of Kar2p in fact reduced the percentages of cells displaying D2E7 heavy chain from 43 \pm 2% to 25 \pm 3% and cells displaying assembled D2E7 Fab from 40 \pm 2% to 24 \pm 2% (**Figures 3B,C**, **Table S1**). MFIs of FLAG⁺ cells and HA⁺ cells also decreased when Kar2p was co-expressed, suggesting that less amounts of heavy chain and assembled Fab were displayed. To test the binding function of displayed D2E7 Fab, induced cells were sequentially labeled with 0.1 nM TNF α -His₆ and 0.1 μ M anti-His₆-iFluor647. We used the ratio of TNF α ⁺ percentage (cells displaying functional Fab) over HA⁺ percentage (cells display assembled Fab) to assess the efficiency of functional display. As results shown in **Figure 3D**, co-expression of Kar2p increased the efficiency of functional display of D2E7 Fab from 36 \pm 2% to 53 \pm 1%.

To further evaluate the contribution of Kar2p on Fab folding, we constructed inactive Kar2p mutants as controls. As a Hsp70 chaperon, Kar2p's nucleotide binding domain carries ATPase activity to promote the interaction between its substrate binding domain and unfolded protein substrates. Therefore, by alanine substitutions of its ADP/ATP recognizing residues E313/K316/S320 (Yan et al., 2011), or incorporating the mutants of temperature-sensitive alleles C63Y/F196L/G417S (Kimata et al., 2003), inactive Kar2p_{E313A/K316A/S320A} and Kar2p_{C63Y/F196L/G417S} were generated. Same strategy was used that co-expression of these Kar2p variants was under the control of additional *GAL1* promoter (**Figure S3A**). Co-expression of Kar2p variants with D2E7 Fab resulted in drops of cell percentages displaying D2E7 heavy chain (to 20 \pm 2% and 23 \pm 2% respectively) and assembled D2E7 Fab

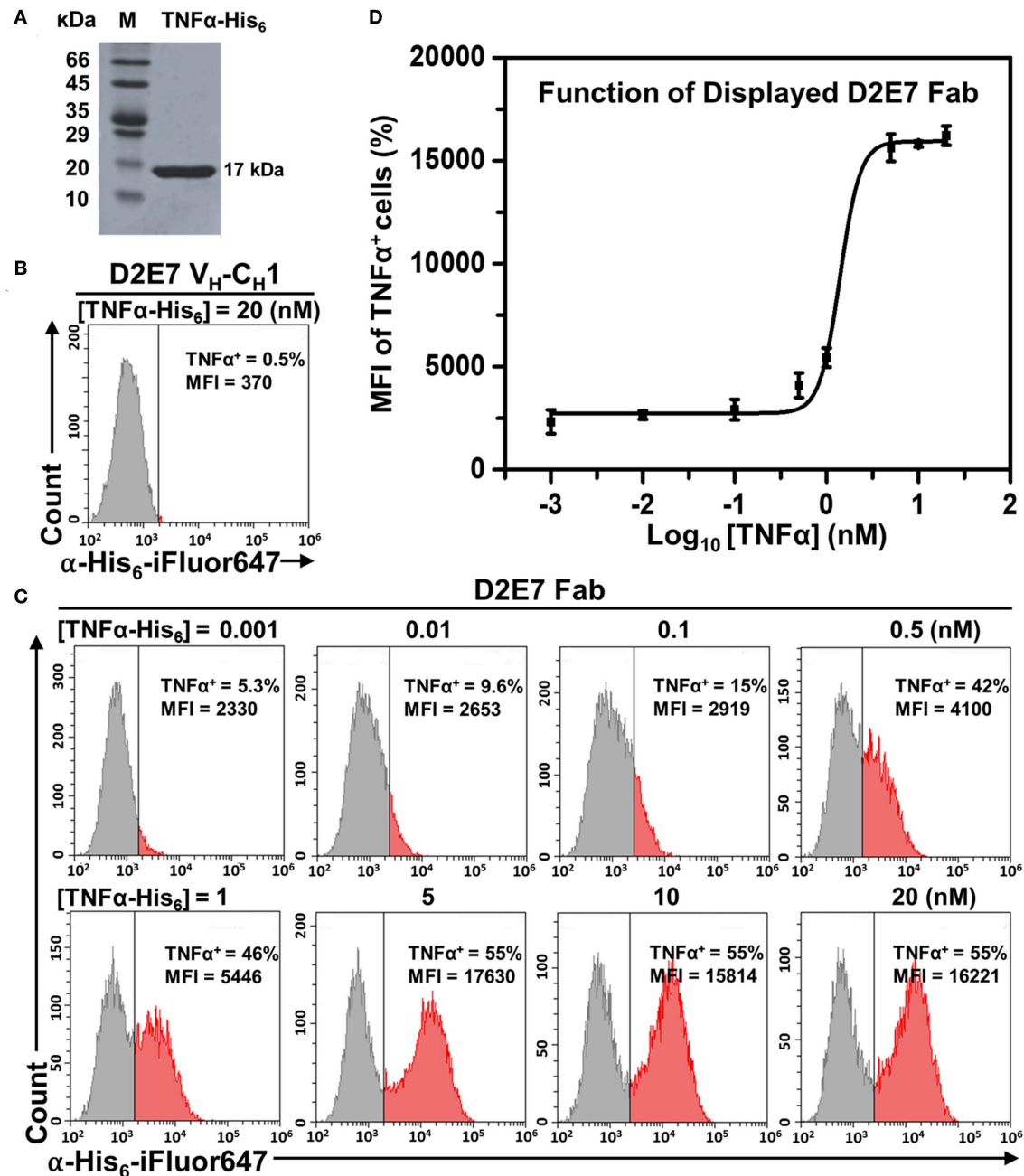
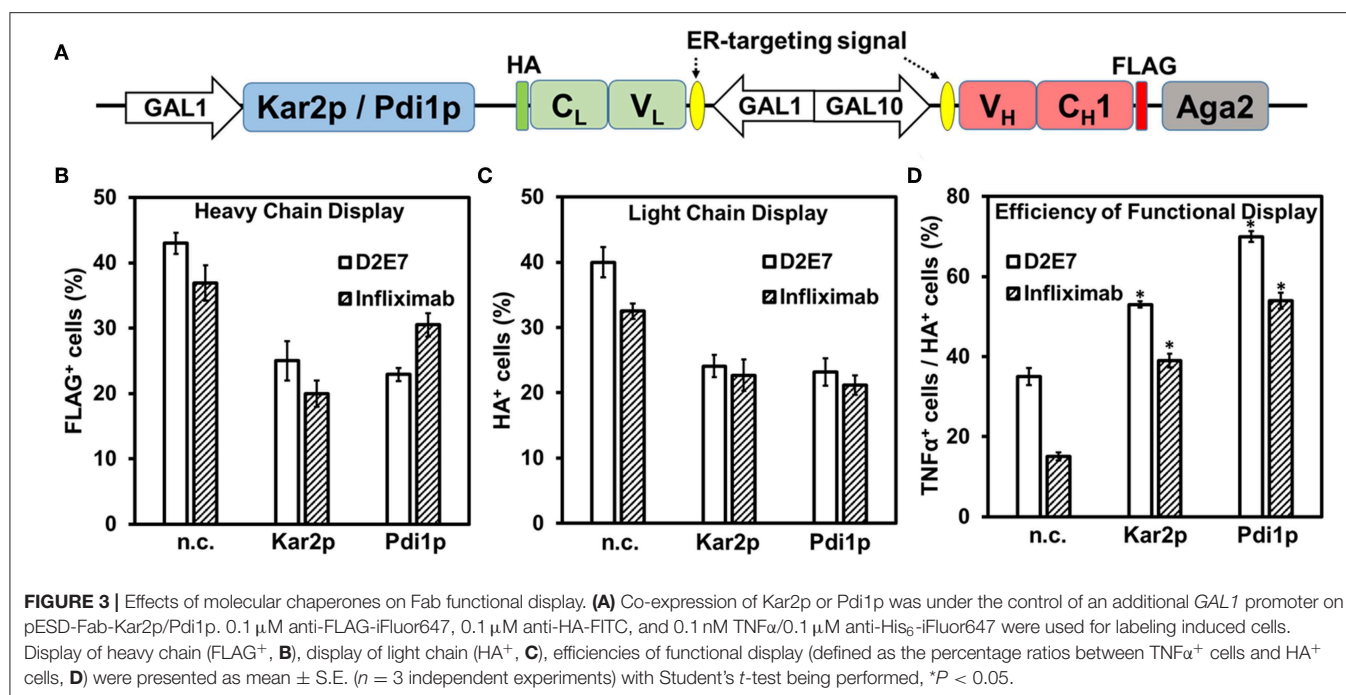


FIGURE 2 | Function characterizations of displayed Fab D2E7. **(A)** Recombinant production of human $\text{TNF}\alpha$ as a His_6 tagged protein. **(B)** Flow cytometry analysis of cells carrying the gene of Adalimumab (D2E7) heavy chain ($\text{V}_H\text{-C}_H1$) without its light chain. Expression was induced by 20 g/L galactose and cells were labeled with 20 nM $\text{TNF}\alpha\text{-His}_6$ and 0.1 μM anti- $\text{His}_6\text{-iFluor647}$. **(C)** Flow cytometry analysis of cells carrying D2E7 Fab display construct. Induced cells were labeled with 1 pM – 20 nM $\text{TNF}\alpha\text{-His}_6$ and 0.1 μM anti- $\text{His}_6\text{-iFluor647}$ for $\text{TNF}\alpha^+$ cell quantification. **(D)** Sigmoidal curves depicting fluorescence intensities of $\text{TNF}\alpha^+$ cells as a function of $\text{TNF}\alpha$ concentrations. Data are presented as mean \pm S.E. ($n = 3$ independent experiments). MFI, mean fluorescence intensity.

(to $19 \pm 2\%$ and $21 \pm 3\%$) (Figures S3B–D, Table S1). As expected, these biochemically inactive Kar2p variants failed to improve display efficiencies of functional D2E7 Fab, as $\text{TNF}\alpha^+/\text{HA}^+$ ratios of $32 \pm 4\%$ and $38 \pm 2\%$ were statistically indifferent from the D2E7 Fab producing cells without chaperon co-expression.

Often as the rate-limiting step of protein folding in ER, disulfide bond formation is critical for V_H and V_L domain folding and their assembly to form a functional Fab. Therefore, we further tested the effects of ER-associated protein-disulfide isomerase (Pdi1p) on Fab surface display. Similar to Kar2p, Pdi1p gene was cloned downstream of a *GAL1* promoter for



its co-expression. Induced cells were labeled with anti-FLAG-iFluor647 for detecting heavy chain display, anti-HA-FITC for detecting Fab assembly, and TNF α -His₆ and anti-His₆-iFluor647 for detecting Fab function. Results indicated that when Pdi1p was co-expressed, the cell percentage displaying D2E7 heavy chain decreased from $43 \pm 2\%$ to $23 \pm 1\%$, and the cell percentage displaying D2E7 Fab decreased from $40 \pm 2\%$ to $23 \pm 2\%$. However, the functional display efficiency (defined as the ratio of TNF α ⁺ cells over HA⁺ cells) enhanced from $36 \pm 2\%$ to $70 \pm 1\%$ (Figure 3). We also constructed Pdi1p_{C4S} mutant by changing the four catalytic cysteines of its thioredoxin-like domains to serines (Tian et al., 2006; Wang et al., 2013), and Pdi1p_{C6S} mutant which carried two additional Cys->Ser substitutions important for Pdi1p re-oxidation mediated by sulfhydryl oxidase ER oxidoreductin 1 (Ero1p) (Frand and Kaiser, 2000; Niu et al., 2016). Co-expression of inactive Pdi1p_{C4S}/Pdi1p_{C6S} with D2E7 Fab decreased cell percentage displaying its heavy chain and assembled Fab without improvements on functional display efficiencies (Figure S3, Table S1).

Infliximab is another therapeutic mAb targeting TNF α (Keane et al., 2001), however its display as a scFv on yeast cell surface has been proved difficult (Sivelle et al., 2018). To investigate whether co-expression of Kar2p or Pdi1p can improve the display quality of this challenging antibody clone, we constructed Infliximab Fab yeast display and its co-expression vectors for Kar2p or Pdi1p (Figure 3A). Similar to testing displayed D2E7 Fab, induced cells were labeled and measured for Infliximab heavy chain display (FLAG⁺ cells), Fab assembly (HA⁺ cells), and its function (TNF α ⁺ cells). Results showed that when Kar2p or Pdi1p was co-expressed, while the percentages of cells displaying Infliximab heavy chain decreased from $37 \pm 3\%$ to $20 \pm 2\%$ or $30 \pm 2\%$, and the percentages of cells displaying Infliximab Fab decreased

from $33 \pm 1\%$ to $23 \pm 2\%$ or $21 \pm 2\%$, its efficiency of functional display (TNF α ⁺/HA⁺) increased from $15 \pm 1\%$ to $39 \pm 2\%$ or $53 \pm 2\%$, representing an 2.6- or 3.6-fold improvement, respectively (Figures 3B–D, Table S1). Applying inactive Kar2p or Pdi1p variants toward Infliximab Fab failed to improve its functional display efficiencies (Figure S3, Table S1). Collectively, results with two tested anti-TNF α clones suggested that molecular chaperone Kar2p or Pdi1p significantly improved the quality of displayed Fabs.

We also tested the effects of dual chaperones Kar2p and Pdi1p co-expression on Fab YSD. Simultaneous co-expression of Kar2p and Pdi1p was under the control of additional *GAL1* promoters on pESD-Fab-Pdi1p-Kar2p. Results indicated that the efficiencies of functional display (TNF α ⁺/HA⁺) were improved from 36 and 15% to 65 and 56% for D2E7 and Infliximab Fab, respectively, while their light chain display amounts (as HA⁺) decreased from 40 and 33% to 20 and 16% (Figure S4). These results suggested that, similar to the effects of Kar2p/Pdi1p alone, simultaneous co-expression of these two chaperones improved the quality of displayed Fabs at the expense of display quantity.

Functional Display Efficiency Was Improved by Fusion With ER Retention Sequences

We hypothesized that the ER retention sequence (ERS), a specific short sequence that mediates protein retention in the ER (Munro and Pelham, 1987; Mei et al., 2017), can extend the residence time of Fab fragments in yeast ER and thus facilitate their proper folding and assembly. Infliximab was our primary target because of its relatively low yeast surface display efficiency (Table S1). To determine the effect of ERS on Fab assembly, five ERSs of

different strength were fused to the C-terminus of Infliximab light chain (V_L - C_L) (**Figure 4A**). Induced cells were labeled with anti-FLAG-iFluor647 for detecting heavy chain display, anti-HA-FITC for detecting Fab assembly, and TNF α -His₆ and anti-His₆-iFluor647 for detecting Fab function. Similar to effects of tested molecular chaperons (**Figure 3**), fusion with ERSs decreased the surface display amounts of Infliximab heavy chain (FLAG⁺ cells) and assembled Fab (HA⁺ cells) (**Figures 4B,C**). However, the percentages and MFIs of TNF α ⁺ cells increased as ERS strength increased (**Figure 4D**, **Table S2**). When 1 nM TNF α was used for labeling, TNF α ⁺ % increased with the efficiency of functional Infliximab Fab display (TNF α ⁺ cells / HA⁺ cells) improved from $29 \pm 2\%$ without ERS, to $42 \pm 2\%$ with weak ERS KDEL, and to $55 \pm 4\%$ and $64 \pm 2\%$ with strong ERSs FEHDEL and WEHDEL, which represented a 2.0- and 2.3-fold of improvement (**Figure 4D**). When labeled with 0.1 nM TNF α , strong ERSs FEHDEL and WEHDEL comparably enhanced functional display efficiency from $16 \pm 1\%$ to $33 \pm 4\%$ and $39 \pm 2\%$, with increased percentages and MFIs of TNF α ⁺ cells. Similar to Infliximab Fab, strong ERSs FEHDEL and WEHDEL increased percentages and MFIs of TNF α ⁺ cells and prompted the functional display efficiency of D2E7 Fab for 1.5- and 1.9-fold (**Figure S5**, **Table S3**), while weak ERSs, HDEL, and KDEL, did not significantly affect display amounts or functional display efficiencies. Overall, these results suggested that ERSs with high retention strength improved the quality of yeast surface displayed Fab, presumably due to extended residence time in the ER that facilitated the formation of functional Fabs.

Enrichment of a High Affinity Fab Clone From Spiked Libraries

To validate the feasibility of yeast surface Fab display for affinity maturation, we mimicked the enrichment procedure with spiked libraries. Compared to D2E7 scFv of 0.96 nM binding potency, its variant cb2-6 scFv exhibited a reported affinity of 1.1 pM (Rajpal et al., 2005). When 10 pM TNF α was used for labeling yeast cells displaying D2E7 or cb2-6 Fab fragments, 9.6 or 20% cells were TNF α ⁺, respectively (**Figure 2C**), suggesting the possibility to efficiently isolate cb2-6 from D2E7. Cells bearing cb2-6 Fab gene were mixed with cells bearing D2E7 Fab gene at a ratio 1:10³, and mixed cells were cultured for Fab expression. When labeled with anti-FLAG-iFluor647 and anti-HA-FITC, 43% of mixed cells were double positive indicating the successful display of assembled Fabs (**Figure 5A**, left panel). In the first round of FACS sorting (R1), 10⁸ mixed cells were labeled with 0.1 μ M anti-HA-FITC for detecting Fab assembly, and 1 nM TNF α -His₆ plus 0.1 μ M anti-His₆-iFluor647 for detecting TNF α binding. Top 1.0% double positive clones, equivalent to 10⁶ cells, were collected. Similar FACS sorting was performed for six more rounds with gradually reduced TNF α concentrations—100 pM for R2, R3, and R4; 10 pM for R5 and R6; and finally 1 pM for R7. For each round, 10⁷ cells were sorted, and 5×10^4 – 7×10^4 cells with the highest signals on both Fab display and TNF α binding were collected, equivalent to a selection gate of 0.60–0.72% (**Figure 5A** right panels). After certain rounds of FACS, 10 clones were randomly picked for plasmid extraction

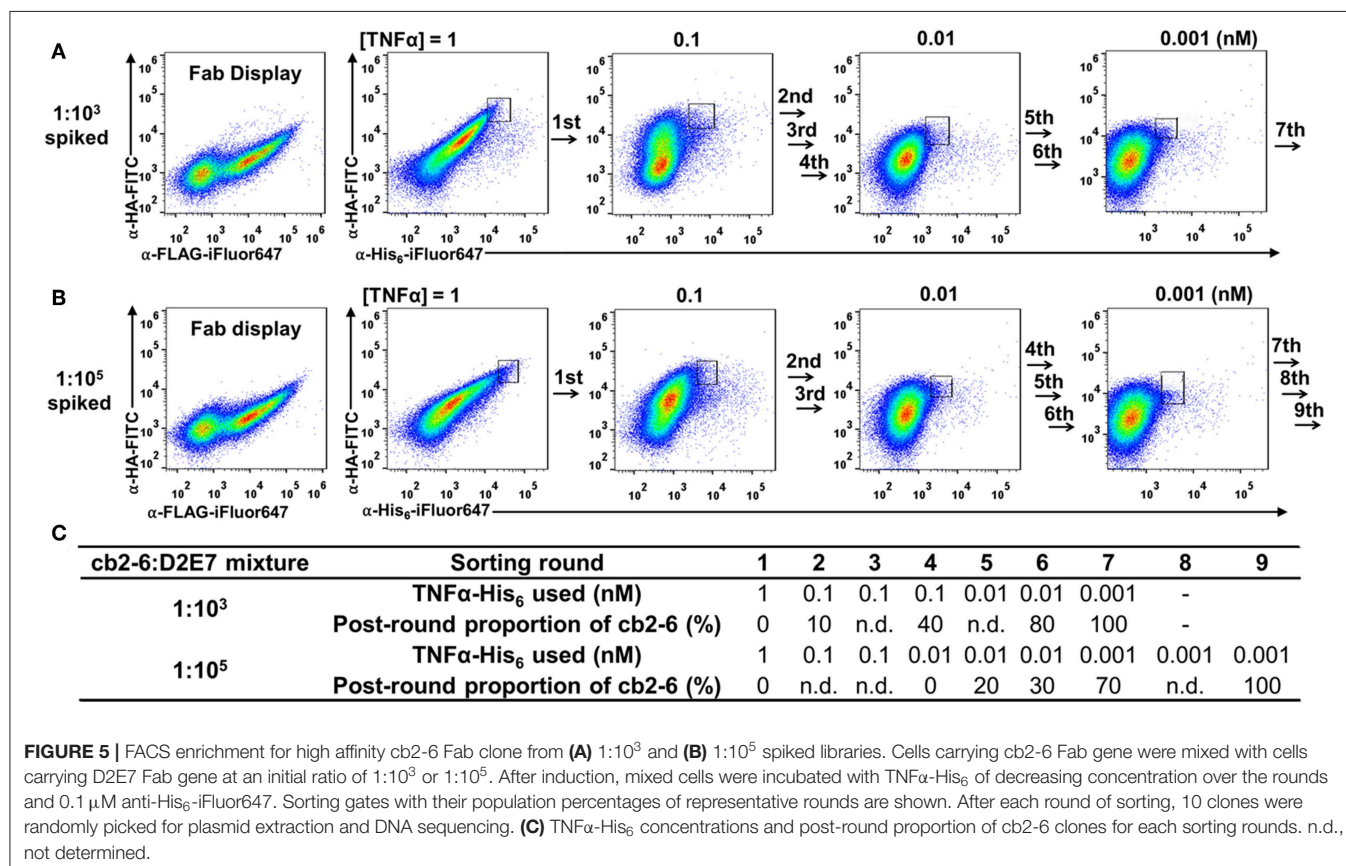
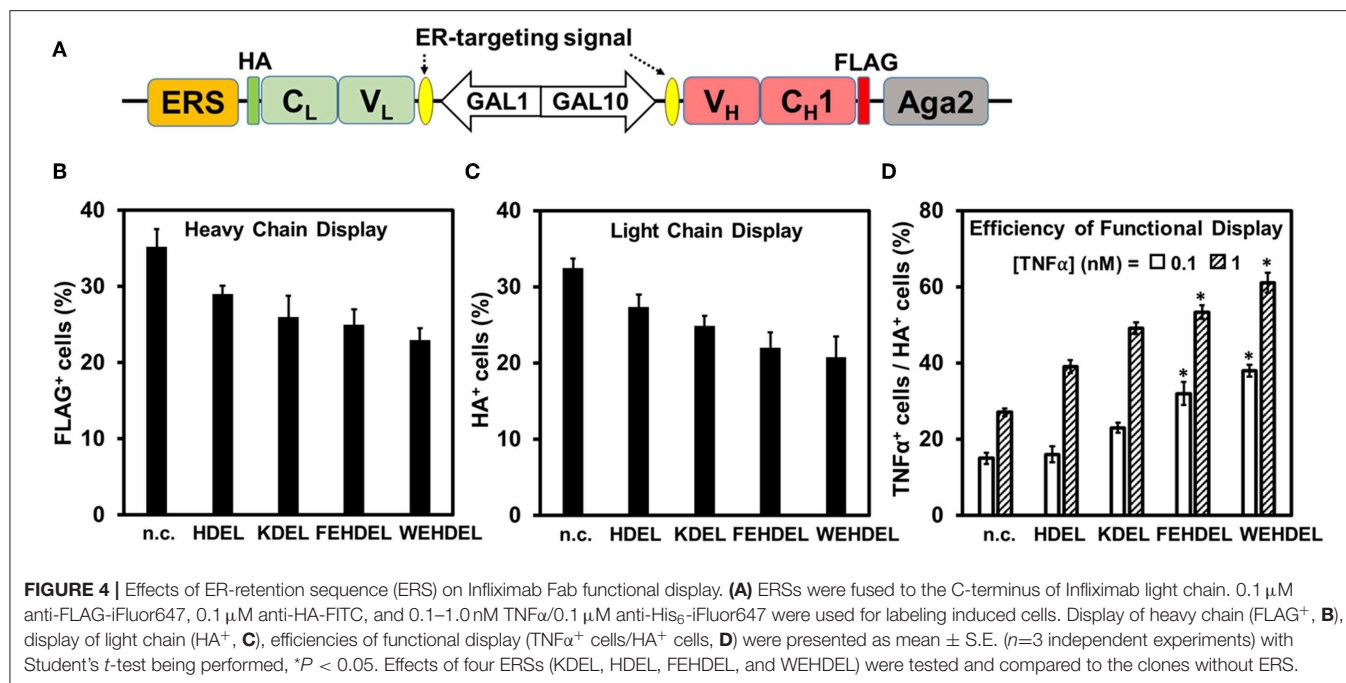
and DNA sequencing. Results indicated that the proportions of cb2-6 clones were enriched to 10% post-R2 and 40% post-R4, and reached to 80% post-R6 and 100% post-R7 (**Figure 5C**).

Successful isolation of cb2-6 from a 1:10³ mixture encouraged us to further test a more diluted library. The cb2-6 Fab cells was mixed with the D2E7 Fab cells at a ratio of 1:10⁵, a library size needed for affinity maturation practices (Boder and Wittrup, 1997). After induction for Fab expression and display, 43% of cells were FLAG⁺ and HA⁺ double positive (**Figure 5B**, left panel). Starting with this 1:10⁵ spiked library, total nine rounds of FACS were performed with decreasing TNF α concentrations from 1 nM to 1 pM (**Figures 5B,C**). 10⁹ mixed cells in R1 and 10⁷–10⁸ cells in later rounds were subjected for sorting with selection gates of 0.60–0.90% for the cells with the highest double signals on Fab display and TNF α binding. DNA sequencing results of randomly picked post-sorting clones indicated that cb2-6 increased its proportions to 20 and 40% post-R5 and post-R6, and achieved dominance of 70% post-R7 and finally 100% post-R9.

DISCUSSION

Currently, scFv is the antibody format commonly used for yeast surface display (YSD) (Feldhaus and Siegel, 2004). Absent in natural IgGs, the introduction of an artificial flexible peptide linker, such as (G₄S)₃, between V_H and V_L domains can result in paratopic conformations different from those of intact IgGs (Gu et al., 2010). Although usually subtle and satisfactory for antigen binding specificity, such conformational variations can be troublesome for quantitative tasks such as affinity maturation (Yang et al., 2018). Preserving the entire antigen binding region, it has been suggested that Fab format retains the natural conformations and thus were widely used for determining the structures of antigen-antibody complex (Rothlisberger et al., 2005). Additionally, Fabs were more suitable for YSD of various antibody clones than scFvs (Sivelle et al., 2018). In this study, scFvs of D2E7 and its mutants A1, cb1-3, and cb-6 were also constructed for YSD (**Figure S6A**). Fluorescent staining for surface display and followed FACS analysis showed that scFv display levels varied from 31 to 46% (**Figure S6B**). In contrast, the same Ab clones in their Fab format showed a similar Fab display level with a narrow disparity of 41–43% (**Figure 1B** middle panels). Furthermore, for Infliximab, only its Fab but not scFv can be well-displayed on yeast cell surface (Sivelle et al., 2018). Collectively, our results, consistent with others (Rosowski et al., 2018; Wang et al., 2018; Yang et al., 2018), suggested that Fab is a reliable and practicable format for YSD.

As the largest organelle of most eukaryotic cells, the endoplasmic reticulum (ER) is the site where secretory polypeptides fold into their correct three-dimensional conformations, assemble into multi-subunit proteins, and achieve covalent modifications such as disulfide bond formation and initial glycosylation (Cooper and Hausman, 2000). By fusing ER targeting signals upstream of both heavy and light chains, Fabs successfully assembled and secreted for functional surface display (**Figure 1**). Interestingly, only around 40–45% of



induced cells presented assembled Fabs on cell surface, which could be attributed to either inefficient induction/expressions or improper domain folding/assembly. As folding and processing

of polypeptide chains in the ER is facilitated by the molecular chaperones (Nishikawa et al., 2005; Buck et al., 2007), mounting evidence suggests that the secretion of scFvs increased with

co-expression of a wide range of molecular chaperones (Shusta et al., 1998; Wentz and Shusta, 2007). In this study, a major member of the Hsp70 chaperone family Kar2p or the ER-associated Pdi1p was co-expressed to assist Fab production and surface display. Consistent with Kar2p functions, our results suggested that when assisted with Kar2p, the absolute amounts of Fab display (percentage and MFIs of HA⁺ cells) decreased, while functional display efficiency (defined as the ratio of cells displaying functional Fab over cells displaying assembled Fab) significantly improved for both D2E7 and Infliximab Fabs (Figure 3). Similarly, co-expression of Pdi1p also improved efficiency of functional display for Fabs in our study (Figure 3). Notably, the improvements were more significant for Infliximab (2.6- and 3.6-fold with Kar2p and Pdi1p) than D2E7 (1.5- and 2.0-fold, respectively). When inactive Kar2p or Pdi1p variants were co-expressed for comparison, Fab display amounts were decreased without improvements on functional display efficiencies (Figure S3, Table S1).

It was speculated that the co-expression of molecular chaperons might increase the burden of transcriptional and translational machinery in yeast cells. Indeed, qRT-PCR data suggested that the mRNA levels of co-expressed Kar2p or its variants were increased 9- to 16-fold compared to the level of physiological Kar2p in the D2E7 and Infliximab Fab producing cells (Figure S7A). Similarly, the mRNA levels of co-expressed Pdi1p and its variants were increased 9- to 17-fold over the background Pdi1p (Figure S7B). In our studies, we also attempted to increase the Fab folding and assembly efficiencies through retaining the light chain (V_L-C_L) longer in the yeast ER by anchoring the ERS at its C-terminus (Figure 4). Theoretically, the stronger ERS will increase the retention time and concentration of V_L-C_L domain in the yeast ER, thus enhancing the Fab folding and assembly efficiencies. Consistently, our results suggested that fusion with ERSs improved the quality of displayed Fabs (Figure 4, Figure S4). However, it was also noticed that retaining the V_L-C_L domain in the yeast ER decreased the display amounts of both heavy and light chains along with the strength of ERS.

In summary, this study characterized four complementary approaches for optimization of Fab yeast surface

display—divergent promoter, ER signal peptide, molecular chaperones, and ER retention sequences. All these findings highlighted the importance to consider tradeoffs between quality and quantity of Fab yeast surface display for individual antibody clones. Encouraged by the success of Fab YSD and the feasibility of affinity maturation through FACS, current efforts have been focusing on surveying novel approaches, e.g., secretory organelle manipulation, to further improving antibody YSD. As Fab YSD and coupled FACS provide intact paratopic conformations and quantitative analysis at the monoclonal level, we expect this technology holds great potential for numerous applications in monoclonal antibody discovery and engineering.

DATA AVAILABILITY STATEMENT

All datasets generated for this study are included in the article/Supplementary Material.

AUTHOR CONTRIBUTIONS

MM, JL, SW, and KL performed experiments. MM, XG, and LY designed the experiments and wrote the manuscript. BI and GZ were involved in analysis and interpretation of experimental data. LY conceived the idea and supervised the whole research. All authors read and approved the final manuscript.

FUNDING

This study was supported by the National Key Research and Development Program of China 2018YFA090091 to LY and GZ, National Natural Science Foundation of China 31870057 to LY, and National Science Foundation 1453645 and National Institute of General Medical Sciences R01GM115672 to XG.

SUPPLEMENTARY MATERIAL

The Supplementary Material for this article can be found online at: <https://www.frontiersin.org/articles/10.3389/fbioe.2019.00362/full#supplementary-material>

REFERENCES

- Beal, D. M., Bastow, E. L., Staniforth, G. L., von der Haar, T., Freedman, R. B., and Tuite, M. F. (2019). Quantitative analyses of the yeast oxidative protein folding pathway *in vitro* and *in vivo*. *Antioxid. Redox Signal.* 31, 261–274. doi: 10.1089/ars.2018.7615
- Boder, E. T., Bill, J. R., Nields, A. W., Marrack, P. C., and Kappler, J. W. (2005). Yeast surface display of a noncovalent MHC class II heterodimer complexed with antigenic peptide. *Biotechnol. Bioeng.* 92, 485–491. doi: 10.1002/bit.20616
- Boder, E. T., and Wittrup, K. D. (1997). Yeast surface display for screening combinatorial polypeptide libraries. *Nat. Biotechnol.* 15, 553–557. doi: 10.1038/nbt0697-553
- Buck, T. M., Wright, C. M., and Brodsky, J. L. (2007). The activities and function of molecular chaperones in the endoplasmic reticulum. *Semin. Cell Dev. Biol.* 18, 751–761. doi: 10.1016/j.semcdb.2007.09.001
- Casadevall, A., and Janda, A. (2012). Immunoglobulin isotype influences affinity and specificity. *Proc. Natl. Acad. Sci. U.S.A.* 109, 12272–12273. doi: 10.1073/pnas.1209750109
- Cooper, G. M., and Hausman, R. E. (2000). *The Cell: A Molecular Approach*. Sunderland, MA: Sinauer Associates.
- DeFrancesco, L. (2019). Drug pipeline: 4Q18. *Nat. Biotechnol.* 37, 206–208. doi: 10.1038/s41587-019-0052-z
- Ellgaard, L., Molinari, M., and Helenius, A. (1999). Setting the standards: quality control in the secretory pathway. *Science* 286, 1882–1888. doi: 10.1126/science.286.5446.1882
- Farquhar, R., Honey, N., Murrant, S. J., Bossier, P., Schultz, L., Montgomery, D., et al. (1991). Protein disulfide isomerase is essential for viability in *Saccharomyces cerevisiae*. *Gene* 108, 81–89. doi: 10.1016/0378-1119(91)90490-3
- Feldhaus, M. J., and Siegel, R. W. (2004). Yeast display of antibody fragments: a discovery and characterization platform. *J. Immunol. Methods* 290, 69–80. doi: 10.1016/j.jim.2004.04.009
- Feldhaus, M. J., Siegel, R. W., Opresko, L. K., Coleman, J. R., Feldhaus, J. M., Yeung, Y. A., et al. (2003). Flow-cytometric isolation of human antibodies from a nonimmune *Saccharomyces cerevisiae* surface display library. *Nat. Biotechnol.* 21, 163–170. doi: 10.1038/nbt785

- Frand, A. R., Cuozzo, J. W., and Kaiser, C. A. (2000). Pathways for protein disulphide bond formation. *Trends Cell Biol.* 10, 203–210. doi: 10.1016/S0962-8924(00)01745-1
- Frand, A. R., and Kaiser, C. A. (2000). Two pairs of conserved cysteines are required for the oxidative activity of Ero1p in protein disulfide bond formation in the endoplasmic reticulum. *Mol. Biol. Cell* 11, 2833–2843. doi: 10.1091/mbc.11.9.2833
- Gu, X., Jia, X., Feng, J., Shen, B., Huang, Y., Geng, S., et al. (2010). Molecular modeling and affinity determination of scFv antibody: proper linker peptide enhances its activity. *Ann. Biomed. Eng.* 38, 537–549. doi: 10.1007/s10439-009-9810-2
- Hartl, F. U., and Hayer-Hartl, M. (2002). Molecular chaperones in the cytosol: from nascent chain to folded protein. *Science* 295, 1852–1858. doi: 10.1126/science.1068408
- Hernandez-Elvira, M., and Torres-Quiroz, F. (2018). The unfolded protein response pathway in the yeast *Kluyveromyces lactis*: a comparative view among yeast species. *Cells* 7:106. doi: 10.3390/cells7080106
- Jiang, W., and Boder, E. T. (2010). High-throughput engineering and analysis of peptide binding to class II MHC. *Proc. Natl. Acad. Sci. U.S.A.* 107, 13258–13263. doi: 10.1073/pnas.1006344107
- Keane, J., Gershon, S., Wise, R. P., Mirabile-Levens, E., Kasznica, J., Schwieterman, W. D., et al. (2001). Tuberculosis associated with infliximab, a tumor necrosis factor alpha-neutralizing agent. *N. Engl. J. Med.* 345, 1098–1104. doi: 10.1056/NEJMoa011110
- Kimata, Y., Kimata, Y. I., Shimizu, Y., Abe, H., Farcasanu, I. C., Takeuchi, M., et al. (2003). Genetic evidence for a role of BiP/Kar2 that regulates Ire1 in response to accumulation of unfolded proteins. *Mol. Biol. Cell* 14, 2559–2569. doi: 10.1091/mbc.e02-11-0708
- Mei, M., Zhai, C., Li, X., Zhou, Y., Peng, W., Ma, L., et al. (2017). Characterization of aromatic residue-controlled protein retention in the endoplasmic reticulum of *Saccharomyces cerevisiae*. 292, 20707–20719. doi: 10.1074/jbc.M117.812107
- Miller, K. D., Pefaur, N. B., and Baird, C. L. (2008). Construction and screening of antigen targeted immune yeast surface display antibody libraries. *Curr. Protoc. Cytom.* Chapter 4, Unit 4.7. doi: 10.1002/0471142956.cy0407s45
- Munro, S., and Pelham, H. R. (1987). A C-terminal signal prevents secretion of luminal ER proteins. *Cell* 48, 899–907. doi: 10.1016/0092-8674(87)90086-9
- Nishikawa, S., Brodsky, J. L., and Nakatsukasa, K. (2005). Roles of molecular chaperones in endoplasmic reticulum (ER) quality control and ER-associated degradation (ERAD). *J. Biochem.* 137, 551–555. doi: 10.1093/jb/mvi068
- Niu, Y., Zhang, L., Yu, J., Wang, C. C., and Wang, L. (2016). Novel roles of the non-catalytic elements of yeast protein-disulfide isomerase in its interplay with endoplasmic reticulum oxidoreductin 1. *J. Biol. Chem.* 291, 8283–8294. doi: 10.1074/jbc.M115.694257
- Padlan, E. A., Cohen, G. H., and Davies, D. R. (1986). Antibody Fab assembly: the interface residues between CH1 and CL. *Mol. Immunol.* 23, 951–960. doi: 10.1016/0161-5890(86)90125-2
- Pepper, L. R., Cho, Y. K., Boder, E. T., and Shusta, E. V. (2008). A decade of yeast surface display technology: where are we now? *Comb. Chem. High Throughput Screen* 11, 127–134. doi: 10.2174/138620708783744516
- Rajpal, A., Beyaz, N., Haber, L., Cappuccilli, G., Yee, H., Bhatt, R. R., et al. (2005). A general method for greatly improving the affinity of antibodies by using combinatorial libraries. *Proc. Natl. Acad. Sci. U.S.A.* 102, 8466–8471. doi: 10.1073/pnas.0503543102
- Rhiel, L., Krah, S., Gunther, R., Becker, S., Kolmar, H., and Hock, B. (2014). REAL-select: full-length antibody display and library screening by surface capture on yeast cells. *PLoS ONE* 9:e114887. doi: 10.1371/journal.pone.0114887
- Rose, M. D., Misra, L. M., and Vogel, J. P. (1989). KAR2, a karyogamy gene, is the yeast homolog of the mammalian BiP/GRP78 gene. *Cell* 57, 1211–1221. doi: 10.1016/0092-8674(89)90058-5
- Rosowski, S., Becker, S., Toleikis, L., Valldorf, B., Grzeschik, J., Demir, D., et al. (2018). A novel one-step approach for the construction of yeast surface display Fab antibody libraries. *Microb. Cell Fact.* 17:3. doi: 10.1186/s12934-017-0853-z
- Roth, L., Grzeschik, J., Hinz, S. C., Becker, S., Toleikis, L., Busch, M., et al. (2019). Facile generation of antibody heavy and light chain diversities for yeast surface display by golden gate cloning. *Biol. Chem.* 400, 383–393. doi: 10.1515/hsz-2018-0347
- Rothlisberger, D., Honegger, A., and Pluckthun, A. (2005). Domain interactions in the Fab fragment: a comparative evaluation of the single-chain Fv and Fab format engineered with variable domains of different stability. *J. Mol. Biol.* 347, 773–789. doi: 10.1016/j.jmb.2005.01.053
- Salfeld, J. G., Allen, D. J., Hoogenboom, H. R., Kaymakalan, Z., Labkovsky, B., et al. (2003). D2E7. U.S. Patent US6509015B1. Ludwigshafen: BASF Aktiengesellschaft.
- Shusta, E. V., Raines, R. T., Pluckthun, A., and Wittrup, K. D. (1998). Increasing the secretory capacity of *Saccharomyces cerevisiae* for production of single-chain antibody fragments. *Nat. Biotechnol.* 16, 773–777. doi: 10.1038/nbt0898-773
- Sivelle, C., Sierocki, R., Ferreira-Pinto, K., Simon, S., Maillere, B., and Nozach, H. (2018). Fab is the most efficient format to express functional antibodies by yeast surface display. *MAbs* 10, 720–729. doi: 10.1080/19420862.2018.1468952
- Steinwand, M., Droste, P., Frenzel, A., Hust, M., Dubel, S., and Schirrmann, T. (2014). The influence of antibody fragment format on phage display based affinity maturation of IgG. *MAbs* 6, 204–218. doi: 10.4161/mabs.27227
- Tian, G., Xiang, S., Noiva, R., Lennarz, W. J., and Schindelin, H. (2006). The crystal structure of yeast protein disulfide isomerase suggests cooperativity between its active sites. *Cell* 124, 61–73. doi: 10.1016/j.cell.2005.10.044
- Urquhart, L. (2019). Top drugs and companies by sales in 2018. *Nat. Rev. Drug Discov.* 18:245. doi: 10.1038/d41573-019-00049-0
- Valkonen, M., Penttilä, M., and Sawloheimo, M. (2003). Effects of inactivation and constitutive expression of the unfolded- protein response pathway on protein production in the yeast *Saccharomyces cerevisiae*. *Appl. Environ. Microbiol.* 69, 2065–2072. doi: 10.1128/AEM.69.4.2065-2072.2003
- van den Beucken, T., Pieters, H., Steukers, M., van der Vaart, M., Ladner, R. C., Hoogenboom, H. R., et al. (2003). Affinity maturation of Fab antibody fragments by fluorescent-activated cell sorting of yeast-displayed libraries. *FEBS Lett.* 546, 288–294. doi: 10.1016/S0014-5793(03)00602-1
- Walsh, G. (2018). Biopharmaceutical benchmarks 2018. *Nat. Biotechnol.* 36, 1136–1145. doi: 10.1038/nbt.4305
- Wang, B., DeKosky, B. J., Timm, M. R., Lee, J., Normandin, E., Misasi, J., et al. (2018). Functional interrogation and mining of natively paired human VH:VL antibody repertoires. *Nat. Biotechnol.* 36, 152–155. doi: 10.1038/nbt.4052
- Wang, C., Li, W., Ren, J., Fang, J., Ke, H., Gong, W., et al. (2013). Structural insights into the redox-regulated dynamic conformations of human protein disulfide isomerase. *Antioxid. Redox Signal* 19, 36–45. doi: 10.1089/ars.2012.4630
- Wentz, A. E., and Shusta, E. V. (2007). A novel high-throughput screen reveals yeast genes that increase secretion of heterologous proteins. *Appl. Environ. Microbiol.* 73, 1189–1198. doi: 10.1128/AEM.02427-06
- West, R. W. Jr., Chen, S. M., Putz, H., Butler, G., and Banerjee, M. (1987). GAL1-GAL10 divergent promoter region of *Saccharomyces cerevisiae* contains negative control elements in addition to functionally separate and possibly overlapping upstream activating sequences. *Genes Dev.* 1, 1118–1131. doi: 10.1101/gad.1.10.1118
- Yan, M., Li, J., and Sha, B. (2011). Structural analysis of the Sil1-Bip complex reveals the mechanism for Sil1 to function as a nucleotide-exchange factor. *Biochem. J.* 438, 447–455. doi: 10.1042/BJ20110500
- Yang, Z., Du, M., Wang, W., Xin, X., Ma, P., Zhang, H., et al. (2018). Affinity maturation of an TpoR targeting antibody in full-length IgG form for enhanced agonist activity. *Protein Eng. Des. Sel.* 31, 233–241. doi: 10.1093/protein/gzy002
- Yi, L., Taft, J. M., Li, Q., Gebhard, M. C., Georgiou, G., and Iverson, B. L. (2015). Yeast endoplasmic reticulum sequestration screening for the engineering of proteases from libraries expressed in yeast. *Methods Mol. Biol.* 1319, 81–93. doi: 10.1007/978-1-4939-2748-7_5

Conflict of Interest: Two patent applications related to this study have been filed.

The authors declare that the research was conducted in the absence of any commercial or financial relationships that could be construed as a potential conflict of interest.

Copyright © 2019 Mei, Li, Wang, Lee, Iverson, Zhang, Ge and Yi. This is an open-access article distributed under the terms of the Creative Commons Attribution License (CC BY). The use, distribution or reproduction in other forums is permitted, provided the original author(s) and the copyright owner(s) are credited and that the original publication in this journal is cited, in accordance with accepted academic practice. No use, distribution or reproduction is permitted which does not comply with these terms.



Recent Advances of CRISPR/Cas9-Based Genetic Engineering and Transcriptional Regulation in Industrial Biology

Shangjie Zhang¹, Feng Guo¹, Wei Yan¹, Zhongxue Dai¹, Weiliang Dong^{1,2}, Jie Zhou^{1,2}, Wenming Zhang^{1,2*}, Fengxue Xin^{1,2*} and Min Jiang^{1,2*}

¹ State Key Laboratory of Materials-Oriented Chemical Engineering, College of Biotechnology and Pharmaceutical Engineering, Nanjing Tech University, Nanjing, China, ² Jiangsu National Synergetic Innovation Center for Advanced Materials (SICAM), Nanjing Tech University, Nanjing, China

OPEN ACCESS

Edited by:

Pablo Ivan Nikel,
Novo Nordisk Foundation Center for
Biosustainability (DTU
Biosustain), Denmark

Reviewed by:

Hodaka Fujii,
Hirosaki University, Japan
Chonghua Ren,
South China Normal University, China
Kun Xu,
Northwest A&F University, China

*Correspondence:

Wenming Zhang
zhangwm@njtech.edu.cn
Fengxue Xin
xinfengxue@njtech.edu.cn
Min Jiang
jiangmin@njtech.edu.cn

Specialty section:

This article was submitted to
Synthetic Biology,
a section of the journal
Frontiers in Bioengineering and
Biotechnology

Received: 02 September 2019

Accepted: 19 December 2019

Published: 28 January 2020

Citation:

Zhang S, Guo F, Yan W, Dai Z,
Dong W, Zhou J, Zhang W, Xin F and
Jiang M (2020) Recent Advances of
CRISPR/Cas9-Based Genetic
Engineering and Transcriptional
Regulation in Industrial Biology.
Front. Bioeng. Biotechnol. 7:459.
doi: 10.3389/fbioe.2019.00459

Industrial biology plays a crucial role in the fields of medicine, health, food, energy, and so on. However, the lack of efficient genetic engineering tools has restricted the rapid development of industrial biology. Recently, the emergence of clustered regularly interspaced short palindromic repeats/CRISPR-associated protein 9 (CRISPR/Cas9) system brought a breakthrough in genome editing technologies due to its high orthogonality, versatility, and efficiency. In this review, we summarized the barriers of CRISPR/Cas9 and corresponding solutions for efficient genetic engineering in industrial microorganisms. In addition, the advances of industrial biology employing the CRISPR/Cas9 system were compared in terms of its application in bacteria, yeast, and filamentous fungi. Furthermore, the cooperation between CRISPR/Cas9 and synthetic biology was discussed to help build complex and programmable gene circuits, which can be used in industrial biotechnology.

Keywords: industrial biology, CRISPR/Cas9, synthetic biology, gene circuits, genetic engineering

INTRODUCTION

Industrial biotechnology has advanced significantly in recent years due to the improvement of genomic engineering tools. Genetic engineering is a complex technology that manipulates genes at molecular level. The recombinant exogenous genes can be replicated, transcribed, translated, and expressed in receptor cells to produce various valuable chemicals. During the long-time evolution of microorganisms, a unique adaptive immune system, named as clustered regularly interspaced short palindromic repeat sequences and CRISPR-associated protein 9 (CRISPR/Cas9), was employed by bacteria and archaea to defend against foreign-invading DNA (Figure 1; Horvath and Barrangou, 2010). This system is consisted of a Cas9 nuclease, a target-recognizing CRISPR RNA (crRNA), and auxiliary non-coding trans-activating crRNAs (tracrRNAs) (Jiang and Doudna, 2017). The precursor crRNA (pre-crRNA) is able to combine with several tracrRNAs, and can be recognized and processed by RNase III into mature crRNA::tracrRNAs (dual RNA hybrid). A single-guide RNA (sgRNA) can be constructed by fusing a crRNA containing the targeting guide sequence to a tracrRNA and then combines to Cas9 protein, generate DNA double-strand breaks (DSBs), and then alter the target gene by cellular DNA repair mechanisms (Cong et al., 2013). The DSBs can be repaired through two different ways: non-homologous end-joining (NHEJ) and homologous

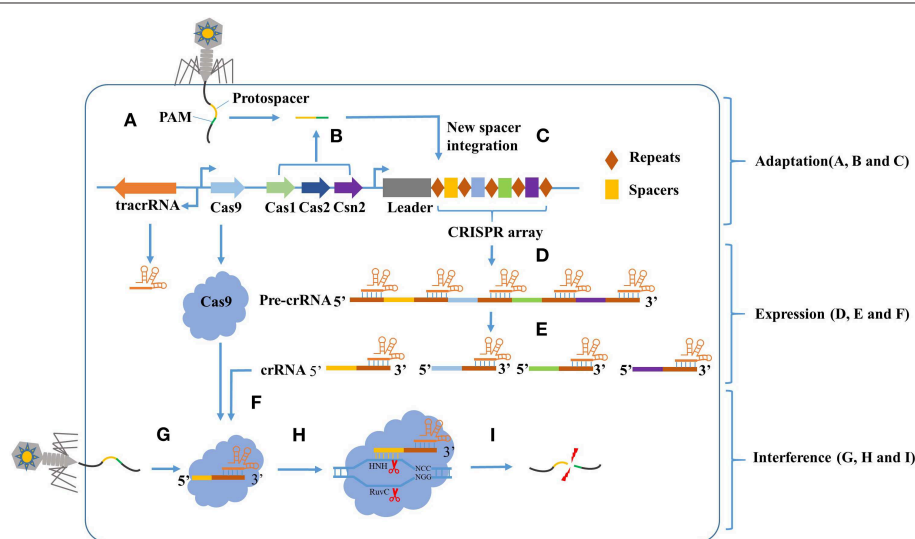


FIGURE 1 | The CRISPR-Cas9 mediated adaptive immunity is divided into three phases: Adaptation, Expression, and Interference. In the adaptation phase, **(A)** the host is invaded by phage DNA during infection. **(B)** Subsequently, the invading DNA is processed by various Cas genes into small DNA fragments (protospacer). The selection of protospacer depends in part on the specific recognition of protospacer adjacent motif (PAM) present within the viral genome. **(C)** The small DNA fragments is then incorporated into the CRISPR locus of the bacterial genome as a new spacer, flanked by a repeat sequence. In the expression phase, **(D)** the CRISPR locus is transcribed into a long precursor CRISPR RNA (pre-crRNA). **(E)** Then, the tracrRNA combine to pre-crRNA to a dual RNA hybrid, this dual RNA hybrid will be recognized and cut by RNase III with the existence of Cas9 protein, resulting in mature crRNA. **(F)** The mature crRNA will combine to Cas9 protein and guide the DNA cleavage. In the Interference phase, when phage DNA invades again, the Cas9:crRNA complex identifies a sequence that is complementary to the spacer and adjacent to the PAM. **(I)** Finally, the invading DNA is cleaved by Cas9 protein to prevent infection.

repair (HR) (Capecchi, 1989). NHEJ can introduce insertion and deletion at the target site. HR uses a foreign DNA donor template to recombine with the target site for introducing a specific point mutation or insertion of the desired sequence.

Previous methods of manufacturing targeted DSBs relied on protein–DNA recognition systems, such as zinc-finger nucleases (ZFNs) and transcription activator-like effector nucleases (TALENs). However, these systems were limited due to their complex and expensive operation. On the contrary, the CRISPR/Cas9 system has been widely employed in various fields owing to its high efficiency, low cost, and convenience (Gaj et al., 2013; Hsu et al., 2014). Hence, in this review, the potential of CRISPR/Cas9 in industrial biotechnology was demonstrated by introducing its applications in bacteria, yeasts, and filamentous fungi. The future prospect of cooperation between CRISPR/Cas9 and synthetic biology to build complex and programmable gene circuits was also summarized.

VERSATILE DESIGNS OF CRISPR/CAS9 FOR HIGHLY EFFICIENT GENE EDITING

Although the CRISPR/Cas9 system has been successfully used in bacteria, yeasts, and fungi, its gene editing efficiency is still unsatisfactory. How to improve the gene editing efficiency has been the focus in this field. Several strategies employed to improve genome editing efficiency with CRISPR/Cas9 were accordingly summarized.

Improvement of Homologous Recombination Efficiency

The mechanism of gene editing is repairing the DSBs generated by CRISPR/Cas9 through NHEJ or HR. Once DSBs occurs, most industrial microorganisms prefer the NHEJ pathway over HR even with exogenous donors, which retards the precise genome editing. In order to increase the frequency of HR, two main strategies were employed: (1) coupling the CRISPR/Cas9 system to lambda Red oligonucleotide recombineering and (2) deleting *KU70* or *KU80* heterodimer involved in NHEJ repair. For instance, Jiang et al. established a two-plasmid-based CRISPR/Cas9 system in *Escherichia coli*, in which *Streptococcus pyogenes* Cas9 and crRNA array were expressed in the low-copy plasmid (pCas) and high-copy plasmid (pCRISPR) series (Jiang et al., 2013; Mali et al., 2013). Although this novel genetic engineering tool had a better performance than did the traditional one, it still needed further modifications to obtain higher efficiency. Based on this system, a triple-plasmid strategy was designed with the third plasmid carrying the λ -Red genes expressed from ParaB. In contrast, this three-plasmid system increased the percentage of mutant cells from 19 to 65%. In another study, a CRISPR/Cas9 system, which had 94% efficiency toward single-gene non-sense mutations, was accordingly established in *Komagataella pastoris*. However, the integration efficiency was really low (2%), when a donor template with 1-kbp homologous arms was provided (Weninger et al., 2016). To improve the integration efficiency with markerless donor cassettes, the *KU70* gene was accordingly knocked out and

improved the knock-in efficiency up to nearly 100% (Weninger et al., 2018).

Adoption of Optimal Promoter for Expression of Cas9 and gRNA

In most studies, Cas9 protein and gRNA were separated into independent vectors. The Cas9 protein was commonly expressed in a low-copy plasmid with constitutive promoters, because high-level expression of Cas9 will lead to negative influence on microbial growth. In contrast, the expression of gRNA should choose high-copy plasmids with a strong promoter. The RNA polymerase III (pol III) promoters had been successfully employed in many cases; however, it was difficult to find suitable RNA pol III promoters. Thus, the sgRNA was flanked with two ribozyme sequences, 5' end hammerhead (HH) and 3' end hepatitis delta virus (HDV) to express under a strong RNA polymerase II promoter (Figure 2; Nødvig et al., 2015). In addition, synthesized hybrid promoters provide another feasible substitute for gRNA expression (Cai et al., 2019). For instance, the gene editing efficiency by harnessing the common RNA pol III promoter SNR52 to express sgRNA in oleaginous yeast *Yarrowia lipolytica* only reached 26%. In order to optimize the expression of sgRNA, Schwartz et al. constructed an RNA polymerase II (Pol II) TEF promoter for sgRNA with HH and HDV ribozymes in 5' end and 3' end, and fused the Pol III promoters RPR1, SCR1, and SNR52 with a glycine tRNA (tRNA^{Gly}) (Schwartz et al., 2015). Finally, the highest disruption efficiency of 92% reached with synthetic SCR1'-tRNA^{Gly} promoter. In addition, the disruption efficiency using the SNR52'-tRNA^{Gly} promoter was improved by 28% than the initial SNR52 promoter.

Other Methods

Optimization of Cas9 Protein Codons

The importance of codon optimization of Cas9 is different in different strains. For example, the natural *S. pyogenes* Cas9 has

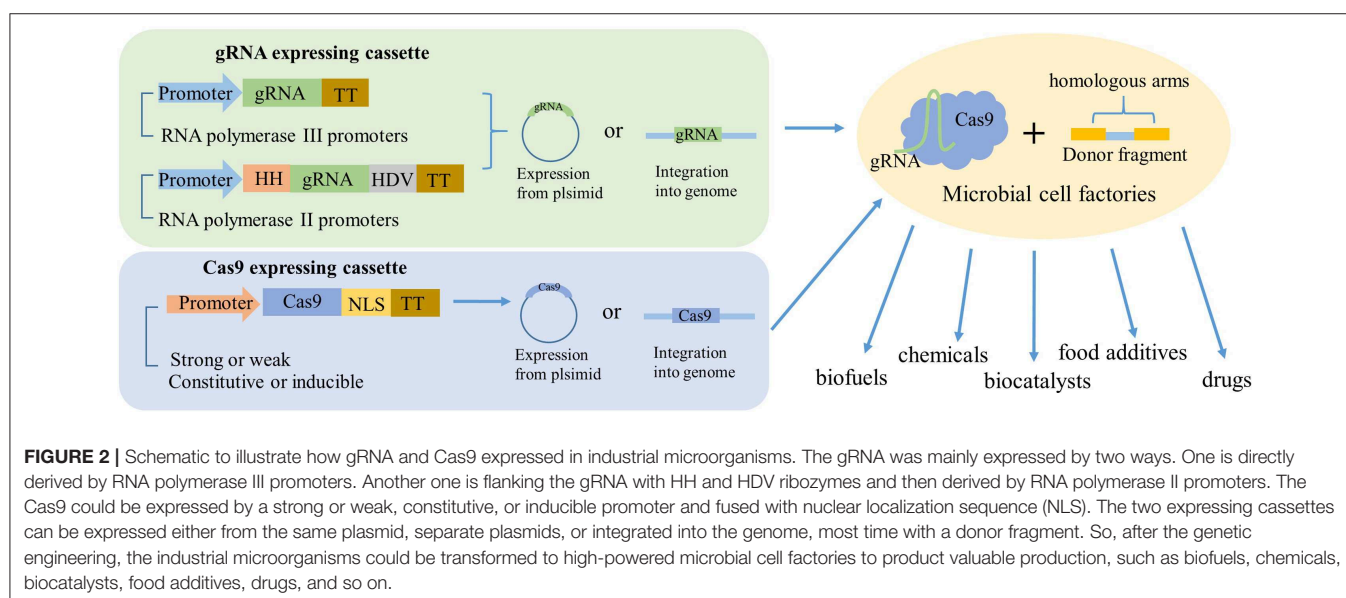
shown high targeting efficiency in *Saccharomyces cerevisiae* (Bao et al., 2015). However, the targeting efficiency was unsatisfactory when using native *S. pyogenes* Cas9 in *K. pastoris*. By employing the human codon optimized Cas9 (HsCas9), the targeting efficiency improved from 32 to 73%, indicating that optimization of Cas9 protein codons plays a crucial role in improving the targeting efficiency. Hence, when the performance of the CRISPR/Cas9 system was unsatisfactory, optimization of Cas9 codons may be a good solution.

Adoption of Suitable sgRNA Binding Sites

For industrial microorganisms, the sgRNA binding site is crucial in terms of the targeting efficiency. In order to improve the efficiency, different sgRNAs targeting sites should be tested. For instance, Peng et al. found that the targeting efficiency was distributed between 13 and 100% when using six different sgRNAs targeting six different sites of *mepA* gene, and the sgRNAs with the GC content under 60% had better performance. This result showed that different sgRNAs had great influence on editing efficiency and adoption of suitable sgRNA is important for a high success rate. A series of website tools had been set for sgRNA design and summarized in previous literature (Chuai et al., 2017).

Prolongation of Incubation

The targeted chromosomal region could escape sgRNA/Cas9 endonuclease activity in some cases. The effective solution is to prolong the incubation under the appropriate selection pressure to generate iterative DSBs until mutagenic repair occurs. To confirm the effect of prolonged incubation on the mutation efficiency, So et al. introduced two plasmids that contained same sgRNA sequence and different length of homologous arms (30 and 500 bp) to the targeted gene into *Bacillus subtilis*, respectively (So et al., 2017). The mutation efficiencies were improved from 85% to almost 100% after incubation for 9 h. Results



demonstrated that the mutation efficiency can be maximized by prolonging incubation.

CRISPR/CAS9-MEDIATED GENETIC ENGINEERING IN INDUSTRIAL BIOLOGY

Industrial microorganisms can produce various value-added chemicals from low-cost feedstock including renewable biomass and organic wastes (Yao et al., 2018). To enhance the performances of industrial microorganisms, genetic modifications were usually implemented to construct desired microbial cell factories. Although various methods are available for genetic modifications, it is time-consuming and labor-intensive. Fortunately, as a surprising “gift,” the CRISPR/Cas9 system greatly improved the efficiency of genetic engineering. Here, we reviewed the applications of the CRISPR/Cas9 system in bacteria, yeasts, and filamentous fungi with special emphasis on *E. coli* and *S. cerevisiae*, which were the most commonly used cell factory.

The Application of CRISPR/Cas9 in Bacteria

Escherichia coli is often used to produce a variety of valuable chemicals, drugs, and biofuels in industrial biotechnology. A traditional method of gene knockout in *E. coli* was to adopt the Red homologous recombination system to mediate the homologous recombination of DNA. However, it is inefficient and especially not suitable for recombination of multiple sites (Murphy and Campellone, 2003). To improve the genetic engineering efficiency, Jiang et al. construct a triple-plasmid system as mentioned above. This novel genetic engineering tool significantly improved the efficiency of genetic modification and thus accelerated the development of industrial biology. In previous studies, Cas9 and gRNA were expressed in two plasmids, respectively, as the simultaneous expression would burden the organism metabolism and cause cell death. Hence, Cas9 or gRNA should be repressed before a genome editing event. Cas9 and gRNA can be assembled into one plasmid containing a pBAD promoter, which is repressed by glucose and induced by arabinose and a temperature-sensitive replicon repA101ts, so that transformed *E. coli* could grow on glucose-amended plates and be edited under the induction with 2 g/L of arabinose. This fast and easy procedure for genome editing could perform continuously, as multiple loci only required one plasmid construction and one step of transformation. To further improve the simultaneous editing efficiency of multiple loci, a CRISPR/Cas9-assisted multiplex genome editing technique was developed. The CRISPR/Cas9-assisted multiplex genome editing technique contained three plasmids: pRedCas9 containing both λ -Red recombineering and Cas9 system under the control of pBAD promoter, pMgRNAs containing gRNAs, and pDonorDNAs carrying multiple donor DNA cassettes (Feng et al., 2018). In another versatile study, Li et al. firstly coexpressed a plasmid containing a gRNA targeting the *bla* gene and Cas9 with the λ -Red recombineering system into

E. coli (Li et al., 2015). Then, the genetic editing started with cotransformation of donor DNA and gRNA plasmid into preceding cells. Comparing to the previously established system, this optimized system has a higher gene editing efficiency and less operating time, almost 100% for codon replacements and knockout genes within 2 days. It was noteworthy that using a double-strand DNA as a donor template has a better performance than a single-strand DNA in gene deletions. Subsequently, this optimized system was employed to strengthen the MEP pathway by substituting the promoters and ribosome binding sites, inserting a heterologous β -carotene biosynthetic pathway and optimizing the central carbon metabolism (Li et al., 2015). Finally, the best producer yielded 2.0 g/L β -carotene in fed-batch fermentation. This extensive work can hardly be completed without employing CRISPR-based tools, revealing their great potential for efficient and diverse manipulation of genomic DNA. The Cas9-recombineering method was further exploited with the development of the CRISPR-enabled trackable genome engineering (CREATE) tool (Garst et al., 2017). Application of this tool in *E. coli* allowed for simultaneous transformation of multiple libraries of plasmid-borne recombined templates (Garst et al., 2017). The CREATE strategy was employed to construct genome libraries of isopropanol pathway by introducing multiple ribosome binding site variations in *E. coli*, leading to the construction and testing of $\sim 1,000$ strains in a few days. The best performer reached a titer of 7.1 g/L isopropanol within 24 h (Liang et al., 2017).

Besides the versatile applications in *E. coli*, the CRISPR-based tools also had satisfactory performances in other bacteria (Table 1). For instance, genetic engineering technologies for solventogenic *Clostridium* were still immature due to low transformation efficiency, inadequate endogenous homologous recombination, and poorly understood physiology and metabolism (Papoutsakis, 2008; Pyne et al., 2014; Bruder et al., 2016). Recently, CRISPR/Cas9 for *Clostridium saccharoperbutylacetonicum* N1-4, a hyper-butanol-producing strain, was developed. The genome engineering efficiency was improved from 20 to 75% by selecting optimized promoter P_{J23119} from *E. coli* for gRNA expression. After deleting two essential genes of phosphotransacetylase (PTA) and butyrate kinase (BUK) for acetate and butyrate production, the butanol production reached 19.0 g/L, which is one of the highest levels ever reported from batch fermentations (Wang et al., 2017). This Cas9-based editing tool could be easily adapted for use in closely related microorganisms, paving the way for elucidating the mechanism of solvent production and constructing robust strains with desirable butanol-producing features. In addition, the Cas9-based editing tools have also been successfully employed for the production of bulk chemicals, such as succinate in *Synechococcus elongatus* (Li et al., 2016), isopropanol-butanol-ethanol in *Clostridium acetobutylicum* (Wasels et al., 2017), and γ -amino-butyric acid (GABA) in *Corynebacterium glutamicum* (Cho et al., 2017). The wide application of the CRISPR/Cas9 system in a variety of bacteria genera demonstrates that it plays a critical role in the prosperous development of bioindustrial.

TABLE 1 | Applications of the CRISPR/Cas9 system in bacteria.

Species	Cassettes for CRISPR/Cas9		Editing efficiency	Advances in genetic modification using CRISPR/Cas9	Strategies for improving efficiency	References
	Cas9 protein	gRNA				
<i>Bacillus subtilis</i>	<i>lacA5'</i> -Cas9- <i>tracrRNA-lacA3'</i>	<i>thrC5'</i> - <i>P_{xydA}</i> - <i>SphI</i> +1- <i>gRNA-thrC3'</i>	100 and 85% for single, double gene mutations, and 69% for chromosomal insertion of a 2.9 kb hyaluronic acid (HA) biosynthetic operon	Multiplex knockout	Choose optimal homology lengths (1,000 bp) for editing template, optimize PAM site	Westbrook et al., 2016
	<i>Pgrac</i> - <i>SpCas9</i>	Para-sgRNA-donor DNA	Point mutation (68%), single-gene deletion in <i>spo0A</i> (100%), and gene insertion (97%)	Traceless, high efficient	Incubation for longer periods to generate iterative DSB	So et al., 2017
<i>Clostridium autoethanogenum</i>	Cas9 was introduced into plasmid pLZtet3no and pIPL12	sgRNA was introduced into plasmid pMTL83157	Over 50% for gene deletion	Construct a small library of tetracycline-inducible promoters for efficient gene deletion	Construct variants of inducible promoter to control the expression of Cas9. Cas9 protein was codon adapted to <i>C. autoethanogenum</i>	Nagaraju et al., 2016
<i>Clostridium cellulolyticum</i>	Optimized <i>SpCas9</i> was introduced into plasmid pLyc017	gRNA was introduced into plasmid pCR8/GW/TOPO TA	High editing efficiency (>95%)	High editing efficiency even using short homologous arms (0.2 kb), deliver foreign genes into the genome in a single step without a marker	Generate single-nick triggered homologous recombination and choose optimal homology lengths for editing template	Xu T. et al., 2015
<i>Corynebacterium glutamicum</i>	<i>P_{tac}</i> -SD- <i>SpCas9</i> was introduced into plasmid pXMJ19	<i>P_{trc}</i> -sgRNA was introduced into plasmid pEC-XK99E	Deletion efficiencies were almost 100% for <i>porB</i> , <i>mepA</i> , <i>clpX</i> , and Ncgl0911 genes	High editing efficiency even using short homologous arms (0.3 kb)	Choose strong promoters for the expression of Cas9 and sgRNA	Liu J. et al., 2017
<i>Clostridium ljungdahlii</i>	<i>P_{thrI}</i> - <i>SpCas9</i>	<i>P_{araE}</i> -sgRNA	Deletion efficiencies were 100%, >75%, 100%, and >50% for <i>pta</i> , <i>adhE1</i> , <i>ctf</i> , and <i>pyrE</i>	More rapid, no added antibiotic resistance gene, scarless, and minimal polar effects	Choose strong promoters for the expression of Cas9 and sgRNA	Park et al., 2019
<i>Clostridium pasteurianum</i>	<i>P_{thrI}</i> - <i>SpCas9</i>	<i>P_{sRNA}</i> -gRNA	Deletion efficiencies were 100% for <i>cpaAIR</i>	High efficient	Inducible expression of cas9 was recommended to mitigate toxicity for high editing efficiency	Pyne et al., 2016
<i>Lactobacillus reuteri</i>	<i>tracrRNA</i> , <i>cas9</i> , and CRISPR arrays derived from pCAS9 were introduced into plasmid pNZ9530		100% for genes mutations	High efficient	Employ oligonucleotide-mediated recombineering (RecT)	Jee-Hwan and Jan-Peter, 2014
<i>Streptomyces albus</i>	<i>P_{rpsLP}</i> -Cas9-T _{fd}	<i>P_{gapdhP}</i> -gRNA-T _{fd}	Multiplex gene deletions with editing efficiency ranging from 70 to 100%	Reduce the time and labor needed to perform precise genome manipulation	Choose strong promoters for the expression of Cas9 and gRNA; Cas9 gene was optimized to favor the <i>Streptomyces</i> codon bias	Wang et al., 2016
<i>Streptomyces coelicolor</i>						Wang et al., 2016
<i>Streptomyces lividans</i>						Wang et al., 2016
<i>Streptomyces viridochromogenes</i>						Wang et al., 2016

The Application of the CRISPR/Cas9 System in Yeasts

Yeasts play critical roles in industrial biology, as a wide range of products can be produced by yeasts, including biopharmaceuticals, biocatalysts, food additives, fine chemicals, and renewable biofuels (Raschmanova et al., 2018). Due to their robust physiology, yeasts could be cultivated in harsh growth conditions, such as low pH and elevated temperatures. Furthermore, yeasts can be introduced in complex eukaryotic post-translational modification systems, which are absent in bacterial hosts and often vital for biopharmaceuticals production (Thomas et al., 2013). Until now, a series of genetic engineering tools based on CRISPR/Cas9 had been exploited in yeast to improve the efficiency of genetic modification (Mitsui et al., 2019).

For decades, *S. cerevisiae* has been a well-known model organism in research and application areas (Jakočiunas et al., 2016). To verify the efficiency of the CRISPR/Cas9 system in *S. cerevisiae*, the endogenous genomic negative selectable marker *CAN1* (encoding arginine permease) can be chosen as a target gene (Dicarlo et al., 2013). To further improve the gene knockout efficiency, 90-bp double-strand oligonucleotides (dsOligo) including homologous arms to the target site and an internal stop codon as the HR template were designed. The recombined frequency of mutations selected from the medium containing canavanine (a toxic arginine analog that can kill cells containing functional *CAN1* gene) was almost 100%, providing foundations for simple and powerful genome engineering tools in yeasts. This system can be used to knock out *LEU2*, *TRP1*, *URA3*, and *HIS3* in polyploid industrial yeast *S. cerevisiae* ATCC 4124 with efficiency of up to 60%, and a quadruple-deficient strain ($\Delta ura3$, $\Delta trp1$, $\Delta leu2$, $\Delta his3$) was successfully constructed (Zhang et al., 2014). In order to further improve the genetic editing efficiency of the CRISPR/Cas9 system, the USER cloning technology was accordingly employed to assemble multiple sgRNAs in one plasmid for efficient gene disruption and promoter engineering of one to five target loci in one step (Jakočiunas et al., 2015a). This one-step marker-free genome editing approach achieved high efficiencies of 50–100% from single to quintuple edits. However, the low efficiency of cotransformation of gRNA plasmids and corresponding HR donors hindered large-scale genome engineering applications (Lian et al., 2018). To solve this problem, a homology-integrated CRISPR (HI-CRISPR) system by fusing a 100-bp HR template to the 5' end of the crRNA sequences was constructed, leading to 87% efficiency of multiplex knockout of *CAN1*, *ADE2*, and *LYP1* (Bao et al., 2015). This HI-CRISPR system further improved the efficiency of multiplex genome editing and genome-scale engineering.

In addition to gene knockout, the CRISPR/Cas9 system can also mediate gene insertion using the homologous arm of donor DNA to the target gene. To better control cellular levels of correctly folding sgRNA, HDV ribozyme was fused to the 5' end of sgRNA to protect the 5' end of the sgRNA from 5' exonucleases. This HDV-gRNA expression strategy

significantly increased the efficiency of multiplex genome editing in diploid yeast strains, in which the heterologous cellodextrin transporter (*cdt-1*) and endogenous β -glucosidase (*ghl-1*) were inserted. As a result, the efficiency of utilizing cellobiose was increased by 10 times through site-directed mutagenesis of *cdt-1* and *ghl-1* genes via the multiplexed CRISPR/Cas9 system (Ryan et al., 2014). Meanwhile, Ronda et al. cotransformed one episomal vector expressing three gRNAs with three donor DNAs containing β -carotene synthesis genes of *BTS1*, *crtYB*, and *crtI* into *S. cerevisiae*, enabling it to synthesize β -carotene (Ronda et al., 2015). Similarly, three exogenous genes (*XYL1*, *XYL2*, and *XYL3*) encoding for xylose reductase, xylitol dehydrogenase, and xylulokinase from *Scheffersomyces stipites* were integrated into the loci of *PHO13* and *ALD6* in *S. cerevisiae* by employing the CRISPR/Cas9 system (Tsai et al., 2015). The refactored strains achieved the ability of utilizing xylose and could be readily used for large-scale fermentations, as no antibiotic-resistant markers were adopted. In addition, a more versatile genome engineering tool, Cas9-facilitated multiloci integration of *in vivo* assembled DNA parts (CasEMBLR), was constructed by combining DNA assembly, HR of DSBs using donor DNAs, and multiplex gRNA expression cassettes (Jakočiunas et al., 2015b). As a proof of concept, this CasEMBLR was employed to assemble and integrate the gene expression cassettes (upstream homology arm, promoter, structural gene, terminator, and downstream homology arm) of *CrtYB*, *CrtI*, and *CrtE* into the loci of *ADE2*, *HIS3*, and *URA3*, with a marker-free engineering efficiency of 31%.

CRISPR/Cas9 was also implemented in many other industrial yeasts (Table 2). For example, to construct more suitable promoters for sgRNA in *Schizosaccharomyces pombe*, Jacobs et al. constructed an expression cassette by adding the leader RNA from *rrk1* gene between the promoter and sgRNA sequence, and fused the HH ribozymes with 3' end of the mature sgRNA to achieve correct 3' sgRNA processing. This system achieved a high efficiency of 98% when a donor template was cotransformed. To further simplify the operation of the CRISPR/Cas9 system in *S. pombe*, Zhang et al. developed a cloning-free procedure including a gapped Cas9-encoding plasmid and a PCR-amplified sgRNA insert. *Ura4* and *rrk1* promoter-leader was just between the gap of Cas9-encoding plasmid. The PCR-amplified sgRNA insert was consisted of sgRNA target sequence and scaffold, and flanked with the homologous arms of *ura4* and promoter-leader. Accordingly, a circular plasmid including Cas9 and sgRNA could generate two gap-repairing fragments. This cloning-free procedure could change the sgRNA target sequence only using an 83-bp sgRNA primer instead of cloning the whole sgRNA plasmid.

The Applications of the CRISPR/Cas9 System in Filamentous Fungi

Due to the considerable economic value of their metabolites, filamentous fungi have been applied to produce antibiotics, organic acids, pigments, polyunsaturated fatty acids, and so on (Dufossé et al., 2014; Ji et al., 2014; Xu X. et al.,

TABLE 2 | Applications of CRISPR/Cas9 system in yeast.

Species	Cassettes for CRISPR/Cas9		Editing efficiency	Advances in genetic modification using CRISPR/Cas9	Strategies for improving efficiency	References
	Cas9 protein	gRNA				
<i>Kluyveromyces lactis</i>	P _{FBA1} -ScCas9-CYC1TT	P _{SNR52} -gRNA-SUP4TT	Multiple-gene cassette insertion into multiple-gene loci: 2.1%	Multiplex knock-in	Delete <i>KU80</i> gene to increase the frequency of HR	Horwitz et al., 2015
<i>Komagataella pastoris</i>	P _{HTA1} -HsCas9-DAS1TT	P _{HTB1} -HH ribozyme-gRNA-HDV ribozyme-AOX1TT	87–94% for single-gene disruption and 69% for double-gene disruptions	Multiplex knockout	Choose optimal promoters for the expression of Cas9 and gRNA	Walter et al., 2016
<i>Kluyveromyces marxianus</i>	P _{Tef1p} -Cas9-CYC1TT	P _{RPR1} -tRNA ^{Gly} -sgRNA	66% for single-gene disruption	High editing efficiency	Choose optimal promoters for the expression of sgRNA	Löbs et al., 2017
<i>Ogataea polymorpha</i>	P _{TDH3} -Cas9	P _{tRNA} -sgRNA	45% for single-gene disruption	High editing efficiency	Modify system using a tRNA-sgRNA fusion gene to increase the mutation efficiency	Numamoto et al., 2017; Wang et al., 2018
<i>Schizosaccharomyces pombe</i>	P _{ADH1} -HsCas9-CYC1TT	P _{RRK1} -rrk1 leader-gRNA-HH ribozyme	Single-gene disruption (allele swap): 85%–90%	Highly efficient knockout	Add the leader RNA from <i>rrk1</i> gene between the promoter and the gRNA sequence	Jacobs et al., 2014
<i>Yarrowia lipolytica</i>	P _{UAS1B8-TEF(136)} -YCAs9	P _{SCR1} -tRNA ^{Gly} -gRNA-poly T	Single-gene disruptions (NHEJ/HR): 90–100%/64–88%	Highly efficient knock out	Choose optimal promoters for the expression of sgRNA; delete <i>KU70</i> gene to increase the frequency of HR	Schwartz et al., 2015
	P _{TEF1} -HsCas9-CYC1TT	P _{TEF1} -HH ribozyme-gRNA-HDV ribozyme-MIG1TT	Single-gene disruption (NHEJ/HR): 62%–98%/72%; multiple-gene disruptions (NHEJ): 19–37%	Highly efficient, scarless, single or multigene editing	Choose strong promoters for the expression of Cas9; delete <i>KU70</i> gene to increase the frequency of HR; Cas9 protein was codon adapted to <i>Y. lipolytica</i>	Gao et al., 2016

2015). However, challenges of delivery through fungal cell wall and lack of available promoters and plasmids hindered the development of genetic engineering tools in filamentous fungi. In addition, the low editing efficiency and consequent large amount of labor time impeded the further application of filamentous fungi in the industry. The emerged CRISPR/Cas9 has brought a breakthrough for genetic manipulation in filamentous fungi.

Conventional genetic engineering strategies to improve the efficiency of HR were to delete *KU70* or *KU80* heterodimer (Weld et al., 2006). However, if *KU70* or *KU80* is interrupted, the filamentous fungi will become more sensitive to growth environments with specific requirements for some chemicals, such as phleomycin, bleomycin, and methyl/ethyl methanesulfonate (Liu et al., 2015). To overcome this obstacle, the CRISPR/Cas9 system in the filamentous fungus of *Trichoderma reesei* using specific optimized codon and *in vitro* RNA transcription was established (Hao and Su, 2019).

The highest frequency of single HR in *T. reesei* using a pair of ≥ 600 -bp homology arms was almost 100%. Subsequently, a microhomology-mediated end-joining system based on CRISPR/Cas9 in *Aspergillus fumigatus* was also established by flanking the sgRNA with HH and HDV. This system achieved accurate target gene editing with a high efficiency of 95–100% via very short (~ 35 -bp) homology arms, indicating that it can function as a powerful and versatile genome editing tool in *A. fumigatus* (Zhang et al., 2016). In addition to the successful application in different species of *Aspergillus*, this evolved system has also been employed in several different filamentous fungal species, broadening the application of the CRISPR/Cas9 system (Hao and Xia, 2015; Weber et al., 2016; Weyda et al., 2017).

Taken together, the CRISPR/Cas9-mediated gene editing technology not only efficiently edited individual target gene but also showed satisfactory performances in multigene editing, which greatly promoted the development of genetic manipulations in filamentous fungi.

COMBINATION OF CAS9-MEDIATED TRANSCRIPTIONAL REGULATION WITH SYNTHETIC BIOLOGY

In addition to the overexpression or deletion of genes, which occur in desired metabolite pathways, regulation of gene expression at the transcription levels is also very important to obtain high yields of metabolites (Mougiakos et al., 2018). Conventional methods to regulate gene expression were to use different promoters with desired strength or RNA interference (Crook et al., 2014). However, with the increased numbers of target genes, the task of testing promoters with suitable strength was time-consuming and labor-intensive. In addition, in order to achieve transcriptional control in terms of level and timing, a complex and sophisticated genetic circuit including activating and repressive transcription factors is indispensable. According to the unique features of the CRISPR/Cas9 system, Jinek et al. constructed a catalytically deactivated Cas9 (dCas9) by introducing inactivating mutations into two nuclease domains of the Cas9 endonuclease, one in the HNH nuclease domain (H840A) and the other in the RuvC-like (D10A) domain (Jinek et al., 2012). This dCas9 protein lost the activity of DNA cleavage but retained the ability to specifically bind to target DNA sequences complementary to the sgRNA. Soon after, this CRISPR/dCas9 system was employed to synthesize a transcriptional repressor. Qi et al. showed that RNA guiding of dCas9 to target genes or promoters would block RNA polymerase binding and genetic transcription, leading to the repression of gene expression (Qi et al., 2013). This CRISPR interference (CRISPRi) system subsequently was used to create efficient, programmable, and genome-wide scale transcriptional regulators (Gilbert et al., 2013, 2014; Silvana et al., 2015). Similarly, CRISPR activation (CRISPRa) was constructed through the fusion of dCas9 to transcriptional activators or activation domains, allowing for transcriptional upregulation of select genes (David et al., 2013). To investigate whether the system could activate the transcription of reporter gene, dCas9 with an omega (ω) protein was fused, which could improve RNA polymerase activity and activate the transcription in *E. coli*. As a result, the transcription level of the reporter gene was increased by 2.8 times (David et al., 2013). In order to broaden the application of CRISPRa, several transcription activator domains have been excavated, such as VP64 and p65AD (Farzadfard et al., 2013; Silvana et al., 2015). Therefore, CRISPRi/a was allowed for facile transcriptional modification of gene networks and satisfied as an important tool to control enzyme expression levels in endogenous or synthetic pathways (Donohoue et al., 2017).

The core concept of synthetic biology is to transform existing natural systems and construct gene circuits by building and integrating standardized components and modules (Dai et al., 2018). However, an ultimate challenge in the construction of gene circuits was lack of effective, programmable, secure, and sequence-specific gene editing tools. The CRISPRi/a system was poised to solve this problem owing to its programmable targeting, efficacy as activator or repressor, high specificity, and

rapid and tight binding kinetics (Sternberg et al., 2014; Xu and Qi, 2019). The CRISPR/Cas9 transcriptional regulator (CRISPR-TF) has been developed to become an important component of scalable device libraries, which were essential in creating complex genetic circuits. Nissim et al. constructed a multi-RNA-mediated gene network regulatory toolkit including RNA-triple-helix structures, introns, microRNAs, ribozymes, Cas9-based CRISPR-TFs, and Cas6/Csy4-based RNA processing to perform tunable synthetic circuits (Nissim et al., 2014). Nielsen et al. also constructed multiple transcriptional logic gates by employing CRISPR/dCas9 and linked them to perform logical computations in living cells (Nielsen and Voigt, 2014). In specific applications, researchers constructed a set of NOT gates by designing five synthetic $\sigma 70$ promoters in *E. coli*. These promoters were inhibited by the corresponding sgRNAs, and interrelationships between various components did not exhibit crosstalk. Furthermore, they used these NOT gates to build larger lines, including the Boolean-complete NOR gate and three gates, which were consisted of four-layered sgRNAs. The previously designed gene synthetic lines were ligated into the native regulatory network using an export sgRNA capable of targeting the transcriptional regulator (MalT) in *E. coli*. By using these methods, the output of synthetic lines can be converted into switches of various cell phenotypes, such as sugar utilization, chemotaxis, and phage resistance.

Comparing with traditional methods of regulating expression, these complex gene circuits based on CRISPRi/a could carry out more precise regulation in terms of levels and timing. In addition, a cascade of responses in these circuits could be triggered by only one signal, which is more advanced than complex promoter engineering. Implementation of CRISPRi/a to design precise gene circuits in biosynthesis pathways will facilitate an unprecedented level of control of metabolic flux and promote the rapid development of the bioindustry.

CONCLUSION AND FUTURE DIRECTIONS

In the past, non-model microbes have been greatly limited in product diversity and yield due to the lack of efficient genetic engineering tools. These problems could be solved under the wide application of the CRISPR/Cas9 system, which will bring a bright future in the industrial biotechnology. Comparing to the conventional marker-based genome editing tools, the CRISPR/Cas9 system enabled fast strain engineering of prototrophic wild and industrial strains, allowing for multiple genome editing simultaneously with marker cassette integration (Stovicek et al., 2017). The high-throughput screening of industrial strains was another bottleneck in industrial biology (Donohoue et al., 2017). Recently, droplet-based microfluidics technology attracted great attention in terms of strain isolation and characterization due to its high-throughput screening efficiency. The combination of the CRISPR/Cas9 system and droplet-based microfluidics technologies maybe bring new breakthroughs in industrial biology in the future.

Although CRISPR/Cas9-mediated genome editing techniques were increasingly used in biotechnology, some disadvantages still existed (Zhang et al., 2019). First, the off-target effect is still a main issue needed to be solved. The designed sgRNAs may form mismatches with non-target DNA sequences, resulting in unexpected gene mutations. These unexpected gene mutations may cause genomic instability and disrupt the function of other normal genes. Although a variety of methods have optimized off-target effects, further improvement is still needed. Hence, conformational changes associated with sgRNA and DNA recognition need to be further explored to obtain higher genome editing accuracy (Mir et al., 2017). In addition, time-dependent control of Cas9 protein activity and the ratio of Cas9 to sgRNA also require further investigation. High expression of Cas9 protein, whether in gene knockout or gene insertion, will affect the growth and recovery rate of host bacteria after transformation, and cause fatal damage to cells in most cases. The existing methods to increase the HR frequency are not suitable to many non-conventional industrial microorganisms. Hence, exploitation of novel approaches to improve homologous recombination efficiency in these strains is critical for precise and efficient CRISPR/Cas9-mediated genetic engineering. Besides, the intellectual property and scientific ethics issues also hindered the wide application of CRISPR/Cas9. The patent dispute has come to an end in the United States, but the war is continuing in Europe and other countries, delaying its adaptation for industrial biotechnology and pharmaceutical applications. Just like the first test-tube baby that appeared in

1978, employing CRISPR/Cas9 for gene therapy also caused some controversies. Therefore, if the laws in the application of the CRISPR/Cas system were completed, it would promote rapid development in the fields of medicine, genomics, agriculture, and so on.

AUTHOR CONTRIBUTIONS

SZ conceived, designed, and drafted the paper. SZ and FG wrote the part of the application of CRISPR-Cas9 in bacteria. WY and ZD wrote the part of the application of CRISPR-Cas9 system in Yeast. JZ and WD wrote the part of the applications of CRISPR-Cas9 system in filamentous fungi. MJ, WZ, and FX wrote the part of Cas9-mediated transcriptional regulation and critically revised the manuscript. All authors read and approved the final manuscript.

FUNDING

This work was supported by National Key R&D Program of China (2018YFA0902200), National Natural Science Foundation of China (Nos. 21978130, 31961133017, 21706125, 21978129), Jiangsu Province Natural Science Foundation for Youths (BK20170993, BK20170997), the Jiangsu Synergetic Innovation Center for Advanced Bio-Manufacture, Jiangsu Key Lab of Biomass-based Green Fuels and Chemicals Foundation (JSBEM201908), and Project of State Key Laboratory of Materials-Oriented Chemical Engineering (ZK201601).

REFERENCES

- Bao, Z., Xiao, H., Liang, J., Zhang, L., Xiong, X., Sun, N., et al. (2015). Homology-integrated CRISPR-Cas (HI-CRISPR) system for one-step multigene disruption in *Saccharomyces cerevisiae*. *ACS Synth. Biol.* 4, 585–594. doi: 10.1021/sb500255k
- Bruder, M. R., Pyne, M. E., Moo-Young, M., Chung, D. A., and Chou, C. P. (2016). Extending CRISPR-Cas9 technology from genome editing to transcriptional engineering in *Clostridium*. *Appl. Environ. Microbiol.* 82, 6109–6119. doi: 10.1128/AEM.02128-16
- Cai, P., Gao, J. Q., and Zhou, Y. J. (2019). CRISPR-mediated genome editing in non-conventional yeasts for biotechnological applications. *Microb. Cell Fact.* 18:63. doi: 10.1186/s12934-019-1112-2
- Capecchi, M. R. (1989). Altering the genome by homologous recombination. *Science* 244, 1288–1292. doi: 10.1126/science.2660260
- Cho, J. S., Choi, K. R., Prabowo, C. P. S., Shin, J. H., Yang, D., Jang, J., et al. (2017). CRISPR/Cas9-coupled recombineering for metabolic engineering of *Corynebacterium glutamicum*. *Metab. Eng.* 42, 157–167. doi: 10.1016/j.ymben.2017.06.010
- Chu, G. H., Wang, Q. L., and Liu, Q. (2017). *In silico* meets *in vivo*: towards computational CRISPR-based sgRNA design. *Trends Biotechnol.* 35, 12–21. doi: 10.1016/j.tibtech.2016.06.008
- Cong, L., Ran, F. A., Cox, D., Lin, S., Barretto, R., Habib, N., et al. (2013). Multiplex genome engineering using CRISPR/Cas systems. *Science* 339, 819–823. doi: 10.1126/science.1231143
- Crook, N. C., Schmitz, A. C., and Alper, H. S. (2014). Optimization of a yeast RNA interference system for controlling gene expression and enabling rapid metabolic engineering. *ACS Synth. Biol.* 3, 307–313. doi: 10.1021/sb4001432
- Dai, Z., Zhang, S., Yang, Q., Zhang, W., Qian, X., Dong, W., et al. (2018). Genetic tool development and systemic regulation in biosynthetic technology. *Biotechnol. Biofuels* 11:152. doi: 10.1186/s13068-018-1153-5
- David, B., Wenyan, J., Poulami, S., Ann, H., Feng, Z., and Marraffini, L. A. (2013). Programmable repression and activation of bacterial gene expression using an engineered CRISPR-Cas system. *Nucleic Acids Res.* 41, 7429–7437. doi: 10.1093/nar/gkt520
- Dicarlo, J. E., Norville, J. E., Prashant, M., Xavier, R., John, A., and Church, G. M. (2013). Genome engineering in *Saccharomyces cerevisiae* using CRISPR-Cas systems. *Nucleic Acids Res.* 41, 4336–4343. doi: 10.1093/nar/gkt135
- Donohoue, P. D., Barrangou, R., and May, A. P. (2017). Advances in industrial biotechnology using CRISPR-Cas systems. *Trends Biotechnol.* 36, 134–146. doi: 10.1016/j.tibtech.2017.07.007
- Dufossé, L., Fouillaud, M., Caro, Y., Mapari, S. A., and Sutthiwong, N. (2014). Filamentous fungi are large-scale producers of pigments and colorants for the food industry. *Curr. Opin. Biotech.* 26, 56–61. doi: 10.1016/j.copbio.2013.09.007
- Farzadfar, F., Perli, S. D., and Lu, T. K. (2013). Tunable and multifunctional eukaryotic transcription factors based on CRISPR/Cas. *ACS Synth. Biol.* 2, 604–613. doi: 10.1021/sb400081r
- Feng, X., Zhao, D. D., Zhang, X. L., Ding, X., and Bi, C. H. (2018). CRISPR/Cas9 assisted multiplex genome editing technique in *Escherichia coli*. *Biotechnol. J.* 13:e1700604. doi: 10.1002/biot.201700604
- Gaj, T., Gersbach, C. A., and Iii, C. F. B. (2013). ZFN, TALEN, and CRISPR/Cas-based methods for genome engineering. *Trends Biotechnol.* 31, 397–405. doi: 10.1016/j.tibtech.2013.04.004
- Gao, S., Tong, Y., Wen, Z., Zhu, L., Ge, M., Chen, D., et al. (2016). Multiplex gene editing of the *Yarrowia lipolytica* genome using the CRISPR-Cas9 system. *J. Ind. Microbiol. Biotechnol.* 43, 1085–1093. doi: 10.1007/s10295-016-1789-8
- Garst, A. D., Bassalo, M. C., Pines, G., Lynch, S. A., Halwegedwards, A. L., Liu, R., et al. (2017). Genome-wide mapping of mutations at single-nucleotide resolution for protein, metabolic and genome engineering. *Nat. Biotechnol.* 35, 48–55. doi: 10.1038/nbt.3718

- Gilbert, L., Horlbeck, M., Adamson, B., Villalta, J., Chen, Y., Whitehead, E., et al. (2014). Genome-scale CRISPR-mediated control of gene repression and activation. *Cell* 159, 647–661. doi: 10.1016/j.cell.2014.09.029
- Gilbert, L. A., Larson, M. H., Leonardo, M., Zairan, L., Brar, G. A., Torres, S. E., et al. (2013). CRISPR-mediated modular RNA-guided regulation of transcription in eukaryotes. *Cell* 154, 442–451. doi: 10.1016/j.cell.2013.06.044
- Hao, F., and Xia, L. (2015). Cellulase production by recombinant *Trichoderma reesei* and its application in enzymatic hydrolysis of agricultural residues. *Fuel* 143, 211–216. doi: 10.1016/j.fuel.2014.11.056
- Hao, Z., and Su, X. (2019). Fast gene disruption in *Trichoderma reesei* using *in vitro* assembled Cas9/gRNA complex. *BMC Biotechnol.* 19:2. doi: 10.1186/s12896-018-0498-y
- Horvath, P., and Barrangou, R. (2010). CRISPR/Cas, the immune system of bacteria and archaea. *Science* 327, 167–170. doi: 10.1126/science.1179555
- Horwitz, A., Walter, J., Schubert, M., Kung, S., Hawkins, K., Platt, D., et al. (2015). Efficient multiplexed integration of synergistic alleles and metabolic pathways in yeasts via CRISPR-Cas. *Cell Syst.* 1, 88–96. doi: 10.1016/j.cels.2015.02.001
- Hsu, P., Lander, E., and Zhang, F. (2014). Development and applications of CRISPR-Cas9 for genome engineering. *Cell* 157, 1262–1278. doi: 10.1016/j.cell.2014.05.010
- Jacobs, J. Z., Ciccaglione, K. M., Tournier, V., and Zaratiegui, M. (2014). Implementation of the CRISPR-Cas9 system in fission yeast. *Nat. Commun.* 5:5344. doi: 10.1038/ncomms6344
- Jakočiunas, T., Bonde, I., Herrgård, M., Harrison, S. J., Kristensen, M., Pedersen, L. E., et al. (2015a). Multiplex metabolic pathway engineering using CRISPR/Cas9 in *Saccharomyces cerevisiae*. *Metab. Eng.* 28, 213–222. doi: 10.1016/j.ymben.2015.01.008
- Jakočiunas, T., Jensen, M. K., and Keasling, J. D. (2016). CRISPR/Cas9 advances engineering of microbial cell factories. *Metab. Eng.* 34, 44–59. doi: 10.1016/j.ymben.2015.12.003
- Jakočiunas, T., Rajkumar, A. S., Zhang, J., Arsovska, D., Rodriguez, A., Jendresen, C. B., et al. (2015b). CasEMBLR: Cas9-facilitated multiloci genomic integration of *in vivo* assembled DNA parts in *Saccharomyces cerevisiae*. *ACS Synth. Biol.* 4, 1226–1234. doi: 10.1021/acssynbio.5b00007
- Jee-Hwan, O., and Jan-Peter, V. P. (2014). CRISPR-Cas9-assisted recombineering in *Lactobacillus reuteri*. *Nucleic Acids Res.* 42:e131. doi: 10.1093/nar/gku623
- Ji, X. J., Ren, L. J., Nie, Z. K., Huang, H., and Ouyang, P. K. (2014). Fungal arachidonic acid-rich oil: research, development and industrialization. *Crit. Rev. Biotechnol.* 34, 197–214. doi: 10.3109/07388551.2013.778229
- Jiang, F., and Doudna, J. A. (2017). CRISPR–Cas9 structures and mechanisms. *Annu. Rev. Biophys.* 46, 505–529. doi: 10.1146/annurev-biophys-062215-010822
- Jiang, W., Bikard, D., Cox, D., Zhang, F., and Marraffini, L. A. (2013). RNA-guided editing of bacterial genomes using CRISPR-Cas systems. *Nat. Biotechnol.* 31, 233–239. doi: 10.1038/nbt.2508
- Jinek, M., Chylinski, K., Fonfara, I., Hauer, M., Doudna, J. A., and Charpentier, E. (2012). A programmable dual-RNA-guided DNA endonuclease in adaptive bacterial immunity. *Science* 337, 816–821. doi: 10.1126/science.1225829
- Li, H., Shen, C. R., Huang, C. H., Sung, L. Y., Wu, M. Y., and Hu, Y. C. (2016). CRISPR-Cas9 for the genome engineering of *Cyanobacteria* and succinate production. *Metab. Eng.* 38, 293–302. doi: 10.1016/j.ymben.2016.09.006
- Li, Y., Lin, Z., Huang, C., Zhang, Y., Wang, Z., Tang, Y. J., et al. (2015). Metabolic engineering of *Escherichia coli* using CRISPR–Cas9 mediated genome editing. *Metab. Eng.* 31, 13–21. doi: 10.1016/j.ymben.2015.06.006
- Lian, J., Hamedirad, M., and Zhao, H. (2018). Advancing metabolic engineering of *Saccharomyces cerevisiae* using the CRISPR/Cas system. *Biotechnol. J.* 13:e1700601. doi: 10.1002/biot.201700601
- Liang, L., Liu, R., Garst, A. D., Lee, T., Nogué, V. S. I., Beckham, G. T., et al. (2017). CRISPR enabled trackable genome engineering for isopropanol production in *Escherichia coli*. *Metab. Eng.* 41, 1–10. doi: 10.1016/j.ymben.2017.02.009
- Liu, J., Wang, Y., Lu, Y., Zheng, P., Sun, J., and Ma, Y. (2017). Development of a CRISPR/Cas9 genome editing toolbox for *Corynebacterium glutamicum*. *Microb. Cell Fact.* 16:205. doi: 10.1186/s12934-017-0815-5
- Liu, R., Chen, L., Jiang, Y., Zhou, Z., and Zou, G. (2015). Efficient genome editing in filamentous fungus *Trichoderma reesei* using the CRISPR/Cas9 system. *Cell Discov.* 1:15007. doi: 10.1038/celldisc.2015.7
- Löbs, A. K., Engel, R., Schwartz, C., Flores, A., and Wheeldon, I. (2017). CRISPR–Cas9-enabled genetic disruptions for understanding ethanol and ethyl acetate biosynthesis in *Kluyveromyces marxianus*. *Biotechnol. Biofuels* 10:164. doi: 10.1186/s13068-017-0854-5
- Mali, P., Yang, L., Esvelt, K. M., Aach, J., Guell, M., DiCarlo, J. E., et al. (2013). RNA-guided human genome engineering via Cas9. *Science* 339, 823–826. doi: 10.1126/science.1232033
- Mir, A., Edraki, A., Lee, J., and Sontheimer, E. J. (2017). Type II-C CRISPR-Cas9 biology, mechanism, and application. *ACS Chem. Biol.* 13, 357–365. doi: 10.1021/acscchembio.7b00855
- Mitsui, R., Yamada, R., and Ogino, H. (2019). CRISPR system in the yeast *Saccharomyces cerevisiae* and its application in the bioproduction of useful chemicals. *World J. Microb. Biotechnol.* 35:111. doi: 10.1007/s11274-019-2688-8
- Mougiakos, I., Bosma, E. F., Ganguly, J., Van, D. O. J., and Van, K. R. (2018). Hijacking CRISPR-Cas for high-throughput bacterial metabolic engineering: advances and prospects. *Curr. Opin. Biotech.* 50, 146–157. doi: 10.1016/j.copbio.2018.01.002
- Murphy, K. C., and Campellone, K. G. (2003). Lambda Red-mediated recombinogenic engineering of enterohemorrhagic and enteropathogenic *E. coli*. *BMC Mol. Biol.* 4:11. doi: 10.1186/1471-2199-4-11
- Nagaraju, S., Davies, N. K., Walker, D. J. F., Köpke, M., and Simpson, S. D. (2016). Genome editing of *Clostridium autoethanogenum* using CRISPR/Cas9. *Biotechnol. Biofuels* 9:219. doi: 10.1186/s13068-016-0638-3
- Nielsen, A. A., and Voigt, C. A. (2014). Multi-input CRISPR/Cas genetic circuits that interface host regulatory networks. *Mol. Syst. Biol.* 10, 763–763. doi: 10.15252/msb.20145735
- Nissim, L., Perli, S., Fridkin, A., Perez-Pinera, P., and Lu, T. (2014). Multiplexed and programmable regulation of gene networks with an integrated RNA and CRISPR/Cas toolkit in human cells. *Mol. Cell* 54, 698–710. doi: 10.1016/j.molcel.2014.04.022
- Nødvig, C. S., Nielsen, J. B., Kogle, M. E., and Mortensen, U. H. (2015). A CRISPR-Cas9 system for genetic engineering of filamentous fungi. *PLoS ONE* 10:e0133085. doi: 10.1371/journal.pone.0133085
- Numamoto, M., Maekawa, H., and Kaneko, Y. (2017). Efficient genome editing by CRISPR/Cas9 with a tRNA-sgRNA fusion in the methylotrophic yeast *Ogataea polymorpha*. *J. Biosci. Bioeng.* 124, 487–492. doi: 10.1016/j.jbiosc.2017.06.001
- Papoutsakis, E. T. (2008). Engineering solventogenic clostridia. *Curr. Opin. Biotechnol.* 19, 420–429. doi: 10.1016/j.copbio.2008.08.003
- Park, J., Yu, B. J., Choi, J. I., and Woo, H. M. (2019). Heterologous production of squalene from glucose in engineered *Corynebacterium glutamicum* using multiplex CRISPR interference and high-throughput fermentation. *J. Agric. Food Chem.* 67, 308–319. doi: 10.1021/acs.jafc.8b05818
- Pyne, M. E., Bruder, M., Moo-Young, M., Chung, D. A., and Chou, C. P. (2014). Technical guide for genetic advancement of underdeveloped and intractable *Clostridium*. *Biotechnol. Adv.* 32, 623–641. doi: 10.1016/j.biotechadv.2014.04.003
- Pyne, M. E., Bruder, M. R., Mooyoung, M., Chung, D. A., and Chou, C. P., (2016). Harnessing heterologous and endogenous CRISPR-Cas machineries for efficient markerless genome editing in *Clostridium*. *Sci. Rep.* 6:25666. doi: 10.1038/srep25666
- Qi, L. S., Larson, M. H., Gilbert, L. A., Doudna, J. A., Weissman, J. S., Arkin, A. P., et al. (2013). Repurposing CRISPR as an RNA-guided platform for sequence-specific control of gene expression. *Cell* 152, 1173–1183. doi: 10.1016/j.cell.2013.02.022
- Raschmanova, H., Weninger, A., Glieder, A., Kovar, K., and Vogl, T. (2018). Implementing CRISPR-Cas technologies in conventional and non-conventional yeasts: current state and future prospects. *Biotechnol. Adv.* 36, 641–665. doi: 10.1016/j.biotechadv.2018.01.006
- Ronda, C., Maury, J., Jakočiūnas, T., Jacobsen, S. A. B., Germann, S. M., Harrison, S. J. et al. (2015). CrEdit: CRISPR mediated multi-loci gene integration in *Saccharomyces cerevisiae*. *Microb. Cell Fact.* 14:97. doi: 10.1186/s12934-015-0288-3
- Ryan, O. W., Skerker, J. M., Maurer, M. J., Li, X., Tsai, J. C., Poddar, S., et al. (2014). Selection of chromosomal DNA libraries using a multiplex CRISPR system. *Elife Sci.* 3:e03703. doi: 10.7554/eLife.03703

- Schwartz, C. M., Hussain, M. S., Blenner, M., and Wheeldon, I. (2015). Synthetic RNA polymerase III promoters facilitate high-efficiency CRISPR-Cas9-mediated genome editing in *Yarrowia lipolytica*. *ACS Synth. Biol.* 5, 356–9. doi: 10.1021/acssynbio.5b00162
- Silvana, K., Brigham, M. D., Trevino, A. E., Julia, J., Abudayyeh, O. O., Clea, B., et al. (2015). Genome-scale transcriptional activation by an engineered CRISPR-Cas9 complex. *Nature* 517, 583–588. doi: 10.1038/nature14136
- So, Y., Park, S. Y., Park, E. H., Park, S. H., Kim, E. J., Pan, J. G., et al. (2017). A highly efficient CRISPR-Cas9-mediated large genomic deletion in *Bacillus subtilis*. *Front. Microbiol.* 8:1167. doi: 10.3389/fmicb.2017.01167
- Sternberg, S. H., Sy, R., Martin, J., Greene, E. C., and Doudna, J. A. (2014). DNA interrogation by the CRISPR RNA-guided endonuclease Cas9. *Nature* 507, 62–67. doi: 10.1038/nature13011
- Stovicek, V., Holkenbrink, C., and Borodina, I. (2017). CRISPR/Cas system for yeast genome engineering: advances and applications. *FEMS Yeast Res.* 17:fox030. doi: 10.1093/femsyr/fox030
- Thomas, V., Hartner, F. S., and Anton, G. (2013). New opportunities by synthetic biology for biopharmaceutical production in *Pichia pastoris*. *Curr. Opin. Biotech.* 24, 1094–1101. doi: 10.1016/j.copbio.2013.02.024
- Tsai, C. S., Kong, I. I., Lesmana, A., Million, G., Zhang, G. C., Kim, S. R., et al. (2015). Rapid and marker-free Cas9/CRISPR refactoring yields equivalent xylose-utilization performance in yeast. *Biotechnol. Bioeng.* 112, 2406–2411. doi: 10.1002/bit.25632
- Walter, J. M., Chandran, S. S., and Horwitz, A. A. (2016). CRISPR-Cas-Assisted Multiplexing (CAM): simple same-day multi-locus engineering in yeast. *J. Cell. Physiol.* 231, 2563–2569. doi: 10.1002/jcp.25375
- Wang, L., Deng, A., Zhang, Y., Liu, S., Liang, Y., Bai, H., et al. (2018). Efficient CRISPR-Cas9 mediated multiplex genome editing in yeasts. *Biotechnol. Biofuels* 11:277. doi: 10.1186/s13068-018-1271-0
- Wang, S., Dong, S., Wang, P., Tao, Y., and Wang, Y. (2017). Genome Editing in *Clostridium saccharoperbutylacetonicum* N1-4 with the CRISPR-Cas9 system. *Appl. Environ. Microbiol.* 83:e00233-17. doi: 10.1128/AEM.00233-17
- Wang, Y., Cobb, R. E., and Zhao, H. (2016). High-efficiency genome editing of *Streptomyces* species by an engineered CRISPR/Cas system. *Method Enzymol.* 575, 271–284. doi: 10.1016/bs.mie.2016.03.014
- Wasels, F., Jean-Marie, J., Collas, F., López-Contreras, A. M., and Ferreira, N. L. (2017). A two-plasmid inducible CRISPR/Cas9 genome editing tool for *Clostridium acetobutylicum*. *J. Microbiol. Methods* 140, 5–11. doi: 10.1016/j.mimet.2017.06.010
- Weber, J., Valiente, V., Nødvig, C. S., Mattern, D. J., Slotkowski, R. A., Mortensen, U. H., et al. (2016). Functional reconstitution of a fungal natural product gene cluster by advanced genome editing. *ACS Synth. Biol.* 6, 62–68. doi: 10.1021/acssynbio.6b00203
- Weld, R. J., Plummer, K. M., Carpenter, M. A., and Ridgway, H. J. (2006). Approaches to functional genomics in filamentous fungi. *Cell Res.* 16, 31–44. doi: 10.1038/sj.cr.7310006
- Weninger, A., Fischer, J., Raschmanová, H., Kniely, C., Vogl, T., and Glieder, A. (2018). Expanding the CRISPR/Cas9 toolkit for *Pichia pastoris* with efficient donor integration and alternative resistance markers. *J. Cell. Biochem.* 119, 3183–3198. doi: 10.1002/jcb.26474
- Weninger, A., Hatzl, A. M., Schmid, C., Vogl, T., and Glieder, A. (2016). Combinatorial optimization of CRISPR/Cas9 expression enables precision genome engineering in the methylotrophic yeast *Pichia pastoris*. *J. Biotechnol.* 235, 139–149. doi: 10.1016/j.jbiotec.2016.03.027
- Westbrook, A. W., Moo-Young, M., and Chou, C. P. (2016). Development of a CRISPR-Cas9 tool kit for comprehensive engineering of *Bacillus subtilis*. *Appl. Environ. Microbiol.* 82, 4876–4895. doi: 10.1128/AEM.01159-16
- Weyda, I., Yang, L., Vang, J., Ahring, B. K., Lübeck, M., and Lübeck, P. S. (2017). A comparison of Agrobacterium-mediated transformation and protoplast-mediated transformation with CRISPR-Cas9 and bipartite gene targeting substrates, as effective gene targeting tools for *Aspergillus carbonarius*. *J. Microbiol. Methods* 135, 26–34. doi: 10.1016/j.mimet.2017.01.015
- Xu, T., Li, Y., Shi, Z., Hemme, C. L., Li, Y., Zhu, Y., et al. (2015). Efficient genome editing in *Clostridium cellulolyticum* via CRISPR-Cas9 nickase. *Appl. Environ. Microb.* 81, 4423–4431. doi: 10.1128/AEM.00873-15
- Xu, X., and Qi, L. S. (2019). A CRISPR-dCas toolbox for genetic engineering and synthetic biology. *J. Mol. Biol.* 431, 34–47. doi: 10.1016/j.jmb.2018.06.037
- Xu, X., Zhang, X., Wu, Z., and Wang, Z. (2015). Accumulation of yellow *Monascus* pigments by extractive fermentation in nonionic surfactant micelle aqueous solution. *Appl. Microbiol. Biotechnol.* 99, 1173–1180. doi: 10.1007/s00253-014-6227-0
- Yao, R., Liu, D., Jia, X., Zheng, Y., Liu, W., and Xiao, Y. (2018). CRISPR-Cas9/Cas12a biotechnology and application in bacteria. *Synth. Syst. Biotechnol.* 3, 135–149. doi: 10.1016/j.synbio.2018.09.004
- Zhang, C., Meng, X., Wei, X., and Lu, L. (2016). Highly efficient CRISPR mutagenesis by microhomology-mediated end joining in *Aspergillus fumigatus*. *Fungal Genet. Biol.* 86, 47–57. doi: 10.1016/j.fgb.2015.12.007
- Zhang, G. C., Kong, I. I., Kim, H., Liu, J. J., Cate, J. H., and Jin, Y. S. (2014). Construction of a quadruple auxotrophic mutant of an industrial polyploid *Saccharomyces cerevisiae* strain by using RNA-guided Cas9 nuclease. *Appl. Environ. Microbiol.* 80, 7694–7701. doi: 10.1128/AEM.02310-14
- Zhang, Y.-T., Jiang, J.-Y., Shi, T.-Q., Sun, X.-M., Zhao, Q.-Y., Huang, H., et al. (2019). Application of the CRISPR/Cas system for genome editing in microalgae. *Appl. Microbiol. Biotechnol.* 103, 3239–3248. doi: 10.1007/s00253-019-09726-x

Conflict of Interest: The authors declare that the research was conducted in the absence of any commercial or financial relationships that could be construed as a potential conflict of interest.

Copyright © 2020 Zhang, Guo, Yan, Dai, Dong, Zhou, Zhang, Xin and Jiang. This is an open-access article distributed under the terms of the Creative Commons Attribution License (CC BY). The use, distribution or reproduction in other forums is permitted, provided the original author(s) and the copyright owner(s) are credited and that the original publication in this journal is cited, in accordance with accepted academic practice. No use, distribution or reproduction is permitted which does not comply with these terms.



Progress and Prospects of Bioelectrochemical Systems: Electron Transfer and Its Applications in the Microbial Metabolism

Tianwen Zheng, Jin Li, Yaliang Ji, Wenming Zhang, Yan Fang, Fengxue Xin, Weiliang Dong, Ping Wei, Jiangfeng Ma* and Min Jiang

State Key Laboratory of Materials-Oriented Chemical Engineering, College of Biotechnology and Pharmaceutical Engineering, Nanjing Tech University, Nanjing, China

OPEN ACCESS

Edited by:

Yuan Lu,
Tsinghua University, China

Reviewed by:

Yang-Chun Yong,
Jiangsu University, China
Enrico Marsili,
Nazarbayev University, Kazakhstan

*Correspondence:

Jiangfeng Ma
majiangfeng@njtech.edu.cn

Specialty section:

This article was submitted to
Synthetic Biology,
a section of the journal
Frontiers in Bioengineering and
Biotechnology

Received: 04 September 2019

Accepted: 08 January 2020

Published: 31 January 2020

Citation:

Zheng T, Li J, Ji Y, Zhang W,
Fang Y, Xin F, Dong W, Wei P, Ma J
and Jiang M (2020) Progress
and Prospects of Bioelectrochemical
Systems: Electron Transfer and Its
Applications in the Microbial
Metabolism.
Front. Bioeng. Biotechnol. 8:10.
doi: 10.3389/fbioe.2020.00010

Bioelectrochemical systems are revolutionary new bioengineering technologies which integrate microorganisms or enzymes with the electrochemical method to improve the reducing or oxidizing metabolism. Generally, the bioelectrochemical systems show the processes referring to electrical power generation or achieving the reducing reaction with a certain potential poised by means of electron transfer between the electron acceptor and electron donor. Researchers have focused on the selection and optimization of the electrode materials, design of electrochemical device, and screening of electrochemically active or inactive model microorganisms. Notably, all these means and studies are related to electron transfer: efflux and consumption. Thus, here we introduce the basic concepts of bioelectrochemical systems, and elaborate on the extracellular and intracellular electron transfer, and the hypothetical electron transfer mechanism. Also, intracellular energy generation and coenzyme metabolism along with electron transfer are analyzed. Finally, the applications of bioelectrochemical systems and the prospect of microbial electrochemical technologies are discussed.

Keywords: bioelectrochemical system, electron transfer, microbial fuel cells, microbial electrolysis cells, energy generation, coenzyme metabolism

INTRODUCTION

Bioelectrochemical systems, revolutionary new bioengineering technologies, integrate microorganisms or other bio-based catalysts with an electrochemical method to improve the reducing or oxidizing metabolism. Generally, bioelectrochemical systems show the process of electrical power generation or achieve the reduction reaction with a certain potential poised by means of electron transfer between the electron acceptor and electron donor (Fernandez et al., 2015).

Previously, bioelectrochemical systems have been widely applied in the form of microbial fuel cells (MFCs), since Michael Potter (1911) first studied the generation of an electrical current by several microorganisms, which convert chemical energy into electrical energy by degradation of various substrates, especially organic compounds from waste water (Gul and Ahmad, 2019). As a reversal process compared to MFCs, microbial electrolytic cells (MECs) were used to convert electrical energy to chemical energy with the help of microorganisms or enzymes to

produce useful products such as formate, methanol, ethanol, or hydrocarbons. These molecules were then converted or used directly as a sustainable alternative to fossil fuels (Yuan et al., 2019). With the growing desire for environment-friendly and energy-saving processes (Zhang and Angelidaki, 2015), bioelectrochemical systems attracted much attention for their green and sustainable characteristics (Ghosh and Ghangrekar, 2015).

To expand the application of bioelectrochemical systems, researchers have focused on the selection and optimization of the electrode materials, design of the electrochemical devices, and screening of electrochemically active or inactive model microorganisms. Recently, bioelectrochemical systems have been widely applied in nitrate removal, solid waste processing, desalination and materials science (Zhen et al., 2016). Notably, all of these uses and studies are related to electron transfer and energy transformation, i.e., the interchange of chemical energy and electrical energy.

Here, we first introduce the basic concepts of bioelectrochemical systems, and elaborate on the mechanisms of extracellular and intracellular electron transfer. We also analyze the hypothetical electron transfer mechanism, intracellular energy generation and coenzyme metabolism. Finally, the applications of bioelectrochemical systems and prospective microbial electrochemical technologies are discussed.

CLASSIFICATION OF BIOELECTROCHEMICAL SYSTEMS

An electrochemical system is a series of electrochemical models, or devices, in which electronic behaviors occur with different types of catalysts. In terms of bioelectrochemical systems, it mainly describes a series of technologies that are used for biotechnology applications including electricity generation (Butler et al., 2010) and the production of valuable products (Villano et al., 2011). Generally, they can be divided into two categories depending on the catalyst adopted. The first one are those that use microorganisms as catalysts, and the second are those that use enzymes as the catalyst.

Microbial Electrochemical Systems

According to the direction of electron transfer and the type of reaction, microbial electrochemical systems can be divided into MFCs and microbial electrolysis or electrosynthesis cells (MECs). MFCs, are electrochemical systems with microorganisms acting as biocatalysts in the anode chamber, have been widely used for electricity generation with various substrates (Table 1). In MFCs, electrons released through intracellular metabolism (substrate oxidation) transfer to the anode, and are finally captured by the cathode electrode *via* an external circuit to be used for the reduction of oxygen, or another electron acceptor, with the generation of current (Logan et al., 2006). Recently, many MFCs have been reported that act as an innovative wastewater treatment technique for pollution removal and energy generation, due to their high degradation rate (He et al., 2015; Yazdi et al., 2015; Zhao et al., 2015a).

Bioelectrochemical systems have been successfully applied in MFCs using diverse microorganisms such as *Shewanella putrefaciens* (Yang et al., 2017), *Shewanella oneidensis* MR-1 (Bretschger et al., 2007) and *Escherichia coli* DH5 α (Li et al., 2018), which can produce a maximum power density range from 3800 to 4400 mW/m². However, these fuel cells have a low cost-effectiveness due to high material costs and mediocre power generation, which are still the major limitations to extending the range of applications (Zhou et al., 2013). Also, some electrodes are manufactured with gold, platinum and other expensive materials which raises the cost (Sadeghifar and Rashid-Nadimi, 2017).

Microbial fuel cells systems adopt bacteria as catalysts, and the biofilm is formed on the surface of the anode, which can improve the electron transfer. Thus, the practical application of MFCs may be further confined by microorganisms - since the efficiency and stability of microbial reactions mainly relies on the external environment which is far different from their indigenous environments (Pareek et al., 2019), due to issues such as low temperatures, high salinity and high toxicity (Zhang et al., 2017). Another limitation is the internal resistance of the fuel cell caused mainly by the proton exchange membrane, which results in low current density and power density (Shreeram et al., 2018). Table 1 lists the recent research on MFCs.

Microbial electrolytic cells also use microorganisms as catalysts, and the cells are inoculated into the cathode chamber which acts as an electron acceptor and gains electrons, thus accelerating the intracellular reduction metabolism (Villano et al., 2011; Ding et al., 2012; Jafary et al., 2015). Essentially, MECs are a reverse process compared to MFCs. In MFCs, the oxidation reaction occurs in the anode chamber, after which the released electrons are transferred to the cathode chamber in a process that involves substrate reduction. For MECs, the potential poised on the cathode chamber is the most important factor and is determined by the bacteria and electron shuttles added, as they can have different potential differences (Table 2). However, the potential poised on the cathode is not equal to the theoretical potential difference of electron shuttles as the electron or energy losses in bioelectrochemical system (Zhen et al., 2016). There are also many issues restraining the scale up of MECs, especially as most of the microbial electrosynthesis systems suffer from low energy efficiencies and low production rates (Su and Ajo-Franklin, 2019). Another limitation on MECs is chemical incompatibility between the abiotic and biotic catalysis, for example, fouling of the electrode by microbes, or toxicity to the microbes caused by electrode leaching (Gildemyn et al., 2017). A vital index in the application of MECs is the long-term stability, which suffers from low turnover frequencies and oxygen sensitivity of certain enzymes relevant to CO₂ reduction (Yuan et al., 2019).

By using cyclic voltammogram detection, it was found that the potential poised cathode can drive the electron shuttle reduction at high rates and then the intracellular reducing metabolism can be accomplished by current stimulation. During the whole process, the cathode provides electrons to pump intracellular reducing power and energy generation (She et al., 2006). However, it remains to be investigated whether the

TABLE 1 | Brief summary of microbial fuel cells.

Strains	Anode electrode	Cathode electrode	Substrate	Electrode surface (cm ²)	Electron shuttles	Power output	References
Anaerobic sludge	Graphite felt	Graphite felt	Glucose	10	NA ^a	28.6 mW/m ²	Song et al., 2016
Anaerobic sludge	Activated carbon cloth	Carbon cloth	Waste water	66.5	NA	142 mW/m ²	Yazdi et al., 2015
Activated sludge	Modified carbon cloth	Modified carbon cloth	Sodium acetate	2.5	NA	2355 mW/m ²	Yuan et al., 2016
Activated sludge	Carbon brush	Bilirubin oxidase	Acetate	9	NA	6530 mW/m ²	Santoro et al., 2016
Consortium	Ammonia-treated carbon cloth	Carbon fiber	Cellulose	1.13	NA	5.4 mW/m ²	Farzaneh et al., 2009
<i>Geobacter</i> biofilm	Modified graphite rod	Modified graphite rod	Acetate	5.81	NA	100 mW/m ²	Commault et al., 2015
<i>Geobacter sulfurreducens</i>	PTEE carbon cloth	PTEE carbon cloth	Acetate	7	NA	9.8 mW/m ²	Qu et al., 2012
<i>Escherichia coli</i>							
<i>Shewanella oneidensis</i>	CP/G/Au	CP/G/Au	Lactate	6	-	508 mW/m ²	Zhao C. et al., 2015
<i>Spartina anglica</i>	Plant root	Plant root	Waste water	27	NA	679 mW/m ²	Wetser et al., 2015
Recombinant consortium	Carbon cloth	Carbon cloth	Glucose Xylose	6.25	Flavins	104.7 mW/m ²	Li et al., 2019
<i>Shewanella oneidensis</i>	Carbon cloth	Carbon cloth	Lactate	1	Flavins	2630 mW/m ²	Lin et al., 2018

^aNo electron shuttles added in electrochemical system.

TABLE 2 | The standard potential of electrons shuttles.

Electron shuttles	Standard potential (E ⁰ /V)	Electron mediators	Standard potential (E ⁰ /V)
Methyl viologen	−0.446	NAD ⁺ /NADH	−0.315
H ₂	−0.414	Methane/HCO ₃ [−]	−0.24
Neutral red	−0.325	FAD/FADH ₂	−0.219
Riboflavin	−0.208	MK/MKH ₂	−0.074
Anthraquinone-2,6-disulfonate (AQDS)	−0.184	Fumarate/Succinate	+0.031

electrons released from the cathode can be efficiently transferred between the cathode and bacteria (Schroder, 2007). In a word, in these two microbial electrochemical systems, the possibility of electron transfer and the rate of electron transfer between cells and electrodes are the key factors used to determine the efficiency of the entire system (Li et al., 2015; Santoro et al., 2015).

Enzymatic Electrochemical Systems

Another type of bioelectrochemical system is that using enzymes as catalysts. The electrodes with enzymes serve as external electron donors or electron acceptors (Amano et al., 2016; Lee et al., 2016). Since the enzymatic reaction is the sole reaction occurring in this electrochemical system, and the electron transfer kinetic potential is predetermined, and the oxidoreductase can be regenerated by capturing or releasing electrons at the surface of electrode, the enzymatic electrochemical system is widely used in the study of electron transfer mechanisms *in vitro* (Kracher et al., 2016).

Since previous studies have applied electrochemical methods to study the biological electron and ion transfer and proved its high sensitivity and reliability, it would be an efficient and convenient strategy to analyze the mechanism of enzyme

reaction. When NADH:quinone complex I was fixed on the surface of a gold modified electrode, the process of electron and proton transfer recurred effectively *in vivo* with the electrode as the sole electron acceptor (Oscar et al., 2014). Moreover, in order to increase the load of the enzyme for a higher catalytic rate, high surface area materials were introduced into this system with a high density current output (Bari et al., 2016).

Although all these electrochemical systems have been studied for decades, upgraded electrochemical devices and novel biocompatible electrode materials are absolutely imperative. Moreover, the mechanisms of energy output and electron transfer are still in their infancy.

ELECTRON TRANSFER IN THE BIOELECTROCHEMICAL SYSTEM

Extracellular Electron Transfer

Electron Transfer in Enzyme Electrochemical Systems

In enzyme electrochemical systems, the oxidoreductases are selected, purified and fixed on the surface of modified electrodes, which act as electron donors or electron acceptors and participate in enzymatic reactions along with the interaction of an electrode (Compagnone and Guilbault, 1997; Bari et al., 2016). So, the key problem to be solved is the bidirectional electron transfer from the electrode to the active site of the enzymes. However, the transition and transfer of electrons between the electron carriers have certain restrictions, as the relative distance between the two given electron carriers within the enzyme increases, the electron transfer rate will decline rapidly and affect the efficiency of the enzymatic reaction. When the distance is longer than 10 angstroms, electron transfer will only be achieved through the presence of electron mediators (Mayo et al., 1986). Therefore, the electrodes are modified to facilitate the immobilization of the enzyme and thus effectively accelerate

electron transfer between oxidases and the electrodes (Freguia et al., 2012; Oscar et al., 2014). Furthermore, conductive nanoparticles can also be used to assist the long distance transfer of electrons. In this way, a long distance electron transfer from FAD/FADH₂ (glucose oxidase) to an electrode was achieved (Degani and Heller, 1987).

Although efficient electron transfer can be achieved by various means, the applications of enzyme electrochemical are restricted to a small field by taking into consideration the decreasing activity of enzymes during recycling. Among them, enzyme electrochemical sensor systems is a relatively mature field and widely used for substance detection, such as heavy metals (Ruecha et al., 2015), glucose (Gutierrez et al., 2016) and other organic substances (Wang et al., 2016). Additionally, enzyme electrochemical systems have also been successfully applied to studying the mechanism of electron transfer during enzyme reactions. By cyclic voltammetry detection, Kracher et al. (2016) verified the mechanism of electron transfer in lytic polysaccharide monooxygenases (LPMOs) during the oxidative degradation of cellulose with multi-enzyme modified electrodes.

Extracellular Electron Transfer in Microbial Electrochemical Systems

Unlike enzyme electrochemical systems, microorganisms act as catalysts in MFCs and MECs. In MFCs, reducing equivalents stored in the organic substrate are released in the form of electrons, which are captured by the anode and then transferred to the cathode through the external circuit with the generation of electricity (Santoro et al., 2016). In MECs, a given voltage is poised at the cathode. The electrons involved in intracellular reduction and energy metabolism are released from the cathode electrode and captured by strains (Carmona-Martínez et al., 2015; Yin et al., 2016). Since the cell membrane is insulated, a necessary prerequisite for the electrochemical reactions to occur is that the electrons can smoothly transfer across the membrane (Kracher et al., 2016). Due to reactions occurring on the electrodes of different substances exhibiting different electrochemical behaviors and the different mechanisms of electron transfer between microorganisms and electrodes, three major mechanisms exist in electron transfer between the electrodes and the microorganisms (Figure 1). They are relying on nanowires (conductive pili), relying on outer membrane proteins and/or mediated by endogenous or exogenous electron shuttles (Choi and Sang, 2016).

For the electrochemical active strains, different groups of strains evolved different conductive mechanisms. *Shewanella* has a complete set of extracellular electron transport chains. The electron transport channels which were formed by outer membrane cytochromes (Mtr and CymA system) mediate the direct electron transfer between cells and electrodes (Ross et al., 2012; Carmona-Martínez et al., 2013). Meanwhile, the synthesis and release of riboflavin assists electron transmembrane transfer, but this process requires a specific transport system (Brutinel and Gralnick, 2012). Another model electrochemical active strain, *Geobacter*, can synthesize conductive pili (nanowires) through cell growth and is directed involved in the extracellular electron transfer between cell and electrodes (Schroder, 2007;

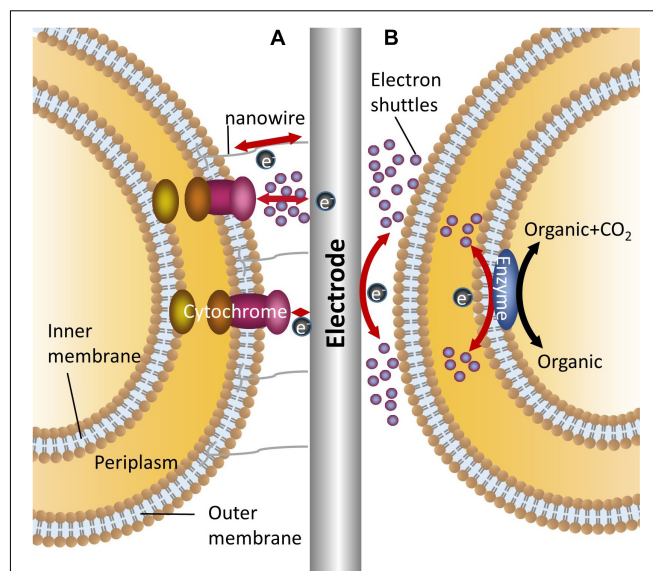


FIGURE 1 | Mechanisms for bidirectional electron transfer between bacteria and electrodes. **(A)** Represents two mechanisms of direct electron transfer, one is mediated by nanowire, the other is mediated by outer membrane cytochromes with or without electron shuttles; **(B)** Shows the indirect electron transfer mediated by electron shuttles.

Lovley, 2008). Also, outer membrane cytochromes are necessary for electron capturing (Butler et al., 2010).

Nanowires, outer membrane cytochromes and other appendages are key components for effective electron capture in electrochemical active strains. In order to improve the extracellular electron transfer efficiency, the development of biofilms can benefit the whole process (Verea et al., 2014; Laura et al., 2015). The presence of biofilm ensures direct long distance electron transfer, high catalytic rates and high power outputs. In recent years, newly developed and modified porous conductive materials have been used for facilitating biofilm formation on electrode surfaces (Karthikeyan et al., 2015; Yuan et al., 2016). Although the electrodes that have porous or three-dimensional surfaces in MFCs will improve the performance of the whole system with enhanced efficiency of electricity output, it also depends on the conductive characteristic of the selected electrode material (Ledezma et al., 2015). When using stainless steel and carbon felt as electrodes for current generation, Dumas et al. (2008) found that carbon felt has high porosity characteristics for microbial attachment, but weaker conductivity compared to stainless steel electrodes which caused lower level current generation. However, in terms of other electrochemical active or inactive strains, the electrons cannot transfer directly between the cells and electrodes, and biofilm on electrode surfaces limited the electron and mass transfer (Rabaey et al., 2007; Freguia et al., 2008).

The electrochemically inactive bacteria do not have a fully functional extracellular electron transfer system and almost all the strains of this type are not able to secrete electron carriers (Masuda et al., 2010). However, electrochemically inactive bacteria can react with electrodes through the addition of an

electron shuttle. In the majority of model strains, such as *Escherichia coli*, *Actinobacillus succinogenes* (Park et al., 1999) and *Clostridium* (He et al., 2016), bidirectional electron transfer can be achieved in the presence of electron shuttles. With neutral red, *A. succinogenes* can gain electrons from a cathode and use these for intracellular metabolism (Park et al., 1999). Although bacteria can be divided into electrochemically active and inactive types, the boundary is not so clear. For example, one study has demonstrated that the screened *E. coli* gained the ability of direct electron transfer from intracellular to extracellular and achieved electricity generation without electron shuttles (Park et al., 1999). However, that does not mean all the electrochemically inactive bacteria can gain the same ability of direct electron transfer.

Interspecies Electron Transfer

After the microorganisms were incubated into electrochemical systems, a start-up period was needed to activate the process of electricity generation. During this period, electrochemically active strains, in which electrons could be transferred directly were absorbed onto the surface of the electrode to form biofilm. And thus, a shorter start-up period of MFC could be obtained as the distance of electron transfer decreased (Zhao et al., 2015b).

A co-culture of *Geobacter* and *Methanosaeta* or *Methanosarcina* species has been confirmed to promote the electro-synthesis of methane as strains shared electrons via direct interspecies electron transfer (Zheng et al., 2015). In this way, interspecies electron transfer can promote and strengthen the symbiotic electrochemical behavior with microbial co-culture fermentation, which was beneficial to achieve synergy between different microbial species and the production of bio-gas or other high value biofuels from cheap raw materials (Zheng et al., 2015).

The more general concept is that conductive materials can promote interspecies electron transfer and strengthen co-culture fermentation. In order to introduce more species to symbiotic co-culture systems and expand the application of interspecies electron transfer, electron shuttles can also be used for indirect electron transfer among strains. It is demonstrated that electron transfer mediated by active carbon particles within cells does not need to rely on cellular conductive structures (such as conductive pili or nanowires) or the assistance of cytochromes (Liu et al., 2012; Amelia-Elena et al., 2014). Moreover, the interspecific electron transfer can be achieved in the presence of activated carbon particles, and the catalytic properties of the mixed bacteria can be strengthened even when co-cultured with electrochemically inactive bacteria (Qu et al., 2012).

It is worthy of notice that co-cultures of bacteria with different electron shuttles may have different functions. In the presence of AQDS, co-cultures of *Geobacter metallireducens* and *Geobacter sulfurreducens* can achieve higher rates of ethanol consumption and better cell growth as more energy is generated (Smith et al., 2015). When the co-cultured bacteria were *Geobacter metallireducens* and *Monascus barkeri*, no obvious effects on the synthesis of methane from ethanol was obtained because of the higher potential of AQDS (Table 2; Liu et al., 2012). This can be explained due to the differing levels of intracellular energy that can be gained along with electron transfer from electron donor

to electron acceptor *via* various electron shuttles and electron transfer chains.

Intracellular Electron Transfer Chain

The only goal of nanowires, electron shuttles and modified electrodes is to strengthen the interaction between cells and electrodes, and to increase the rate of extracellular electron transfer. The intracellular electron transfer chain (ETC, also called the respiratory chain) consists of a series of electron or proton carriers, including cytochromes, coenzyme Q and lots of oxidoreductases. Within the ETC, electrons are transferred from high potential electron donor to a low potential electron acceptor along with ATP synthesis (Hara and Kondo, 2015).

For electrochemically active bacteria, cytochromes that are anchored at the membrane can facilitate electron transfer and intracellular metabolism (Richter et al., 2009). As electrochemically active bacteria, *Shewanella* and *Geobacter* have an excellent ability for intracellular electron transfer, and thus are widely used in MFCs (Lovley, 2012). Previous studies have demonstrated that some strains can change electron transfer routes depending on the potential difference of available electron donors or acceptors (Kracke et al., 2015), and *Shewanella* can achieve bidirectional electron transfer with only one intracellular electron transfer system in MFCs and MECs (Figure 2; Shi et al., 2010; Ross et al., 2012). The only difference was the electron mediator that was used. The MFC adopted ubiquinone, while the MEC adopted menaquinone, as it has a lower potential difference to ubiquinone. Compared with *Shewanella*, three electron leaking mechanisms exist in *Geobacter*: electron transfer OmcZ between cells, OmcE/OmcS used for Fe (III) reduction, and nanowire used for interactions with electrodes (Richter et al., 2009; Shi et al., 2010; Ross et al., 2012; Sturm et al., 2015).

Electrochemically inactive bacteria can interact with electrodes in the presence of electron shuttles (Table 2). Bio-based electron shuttles, such as riboflavin, coenzyme Q or its analogs, can integrate into inherent electron transfer chains directly *via* membrane transporters or diffusion, and participate in intracellular reducing and energy metabolism (Schroder, 2007). Compared with bio-based electron shuttles, chemical based electron shuttles have a faster diffusion rate, and their high polarization characteristics ensure effective bidirectional transportation across membranes (Federico et al., 2007; Pandit and Mahadevan, 2011). However, the relationship between chemical-based electron shuttles and intracellular ETC is not clear. Some studies showed that neutral red can integrate into membranes and execute the function of native electron transfer mediators (Park et al., 1999). Recently, Harrington et al. (2015) verified that neutral red can interact with menaquinone and then transfer the electrons into intracellular ETC. Another type of electron shuttles are reduced chemical substances, such as hydrogen and formate (Zhao et al., 2006).

Until now, it has been confirmed that electron shuttles can capture or release electrons between electrodes and intracellular ETC even though the mechanism is not clear. Compared with electrochemically active strains, the electron transfer efficiency of intracellular ETC in electrochemically inactive strains is not effective. Thus, metabolic engineering strategies have been

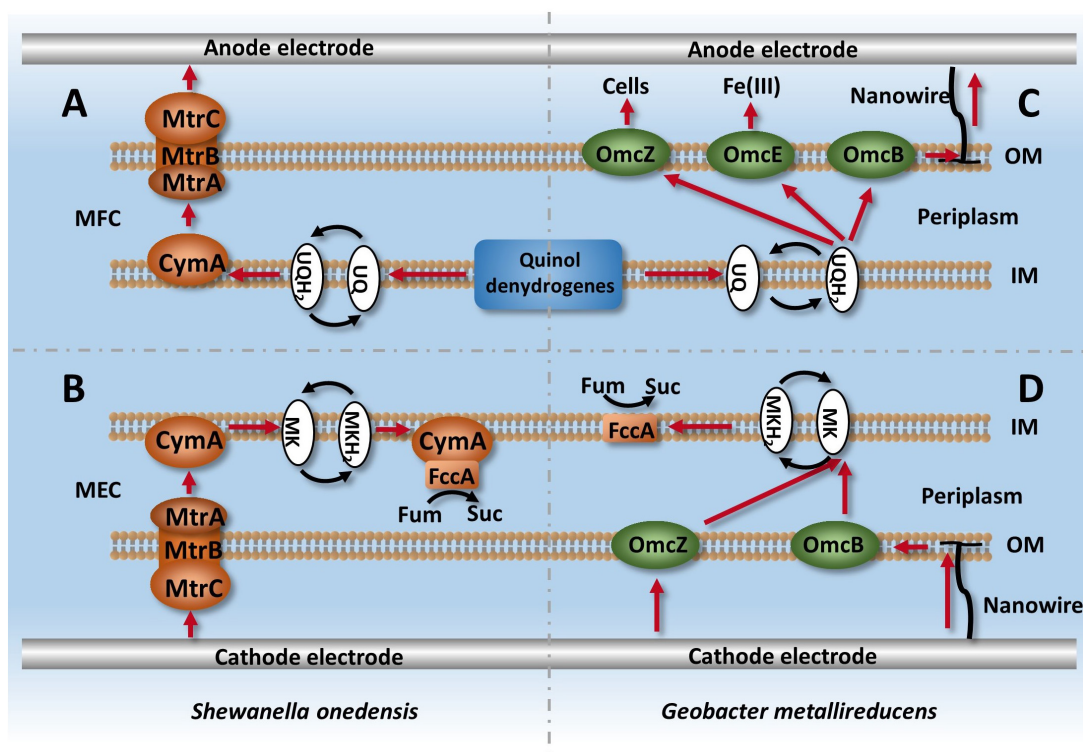


FIGURE 2 | Intracellular electron transfer chains in *Shewanella* and *Geobacter*. **(A)** Describes the process of electron leaking from intracellular metabolism via Mtr and CymA systems in *Shewanella*, **(B)** Describes the process of electron capturing by strains from cathodes and used for fumarate reduction. **(C,D)** describe the ETCs of *Geobacter* in MFC and MEC systems, respectively.

applied to reconstruct the intracellular ETC to promote electron transfer in electrochemically inactive bacteria. Sturm-Richter et al. (Sturm et al., 2015) found that heterologous expression of intracellular ETC from *Shewanella* (CymA and Mtr system) in *E. coli* can reprogram the intracellular metabolism and accelerate the intracellular electron transfer rate by 183% (Sturm et al., 2015). In addition, higher electricity power output was achieved with the assistance of methylene blue. Similar results showed that the rate of extracellular electron transfer can also be increased by heterologous introduction of a synthetic flavin pathway in *Shewanella* (Yang et al., 2015).

THE EFFECTS AND APPLICATIONS OF BIOELECTROCHEMICAL SYSTEMS IN MICROBIAL METABOLISM

Electrons are not simply transferred along with the potential gradient between the electrode and cell, or by intracellular electron transfer chains in bioelectrochemical systems, and the reason for the presence of electron carriers is not just to transfer electrons by a simple pattern from an electrode to intracellular ETC. The capturing of electrons is often accompanied by the cotransport of protons (Pandit and Mahadevan, 2011), which can be released and involved in intracellular reduction and energy metabolism. In addition, the

reducing power (NADH or FADH₂) and ATP play a vital role in intracellular redox metabolism, metabolite synthesis and transportation, stress responses and transcriptional regulation (Balzer et al., 2013; Man et al., 2016). The perturbation of intracellular ATP and NADH levels has effects on the whole cellular metabolism and redirects the metabolic flux (Holm et al., 2010).

Energy Metabolism

In bioelectrochemical systems, bacteria can gain energy in two ways. First, the native respiration chain is the main route of energy generation. For electrochemically active strains, insoluble metals act as electron acceptors and participate in extracellular ETC in nature. When *Geobacter* and *Shewanella* were inoculated in MFC system, they could gain energy continuously by degrading organic acids for cell growth and metabolism. And the redox balance was maintained by releasing electrons to the anode, which replaces insoluble metals as the final electron acceptor (Lin et al., 2018; Li et al., 2019; Wang et al., 2019).

The second way is also derived from electron transfer. As electrons transferred from cathodes into an intracellular environment, along with the cotransport of protons, the hypothetical mechanism of ATP generation is that the released proton will promote the formation of proton motive force (PMF) and drive ATP synthesis (Rose and Regan, 2015).

Compared with aerobic respiration, the energy generated by oxidative phosphorylation is not enough for cell growth at high rates under anaerobic conditions. The main reason is that due to the low supply level of intracellular ATP, as the intermediate metabolites acted as electron acceptors they were not matched by oxygen levels (Unden and Bongaerts, 1997). Generally, as synthesis of the cell appendages is an energy consuming process, an electron shuttle can be used for supplying more energy through highly effective electron transfer under the same conditions (Liu et al., 2012). In some cases, bacteria can gain enough energy to maintain cell growth and metabolism in MEC systems, even though they do not have a complete native electron transfer chain (Smith et al., 2015).

Co-enzyme Metabolism

The concentration of co-enzymes, NADH or NADPH, represents the level of intracellular reducing power and are involved in many oxidation-reduction reactions. As redox reactions occur inevitably along with electron generation and consumption, the release or capture of electrons in bioelectrochemical systems will disturb the intracellular steady state environment and cause a shift of metabolic flux (Chen et al., 2012).

In electrochemical systems, oxidation and reduction reactions are performed in the anode and cathode chamber, respectively. In MECs, *Geobacter* can catalyze fumarate reduction with the cathode electrode as the sole electron donor, and this reduction was catalyzed by fumarate dehydrogenase (NADH-dependent) (Mahadevan et al., 2006). For electrochemically inactive bacteria, previous studies have also found that the electrons can be transferred from the cathode to ferric iron *via* NADH generation when using ferric citrate as the electron acceptor by *E. coli*, and the whole process can be achieved without any membrane electron transport carriers (Emde et al., 1989). Meanwhile, an analysis of the theory revealed that the intracellular reducing power (NADH) could be enhanced through biological electrolytic synthesis, and the increased concentration of NADH could affect the intracellular reducing and energy reaction (Pandit and Mahadevan, 2011).

Reversely, the efflux of electrons from the anode chamber may create a relative oxidizing intracellular environment. In an MFC system with *Lactococcus lactis*, homolactic fermentation switched to mixed acid fermentation to keep the balance of intracellular reducing power along with the electricity power output (Freguia et al., 2009).

The Applications of Bioelectrochemical Systems

Based on the effects of bioelectrochemical systems in microbial metabolism, diverse microbial electrochemical technologies were mainly applied to the production of valuable compounds and the generation of power (Fan et al., 2018).

Microbial electrosynthesis is a novel hybrid of biobased and electrochemical approaches to utilize microbial cells to convert dissolved CO₂ into value-added organic compounds, such as CH₄ production with *Methanococcus maripaludis*

through a self-secreted compounds to promote CO₂ reduction (Deutzmann et al., 2015), and acetate production with *Sporomusa ovata* using a novel cathode to facilitate direct delivery of CO₂ to microbes (Bian et al., 2018).

Electro-fermentation (EF) also uses electrochemistry to affect microbial metabolism. The electron transfer in either anodic EF or cathodic EF can regulate the ORP and the NAD⁺/NADH ratio and then affect the intracellular metabolism (Moscoviz et al., 2016). Recently, an anodic electro-fermentation was carried out using *Corynebacterium glutamicum* to produce L-lysine, and the results showed that adoption of anodic electro-fermentation can balance the redox and energy states of *C. glutamicum* and thus improve the anaerobic production of L-lysine (Vassilev et al., 2018). Cathodic electro-fermentation was also performed for simultaneous biogas upgrading and biochemical production, and the highest biogas content [96% (v/v)] and acetate production (358 mg/L) were achieved (Omar et al., 2018).

Photosynthetic MFCs that combined photosynthesis and generation of electric energy, have also gained much attention recently due to their more sustainable energy production than that of non-photosynthetic MFCs (Pillot et al., 2019). The microbes in photosynthetic MFCs usually contain certain specialized light harvesting complexes that function as the units of photosynthesis. These light harvesting units can sustainably convert solar energy into chemical energy, which are then utilized by traditional exoelectrogens to produce electric energy (Rashid et al., 2019). The integration of photosynthesis with MFC technology has opened several neoteric possibilities for sustainable bioenergy generation.

FUTURE PROSPECTS AND CONCLUSION

All types of microbial electrochemical technologies are based on the energy interchange: chemical energy into electrical energy (MFCs), electric energy into chemical energy (MECs) and solar energy into electrical energy (Photosynthetic MFCs). For all types of bioelectrochemical systems, energy conversion efficiency is the key factor that determines bioelectrochemical system performance, especially the energy conversion step in which electrical energy is involved. Electron transfer plays an important role in this step, which it is implied is a future direction for METs research. The electron's behavior, intracellular reducing power and energy metabolism in bioelectrochemical systems is of increasing concern in the context of precise regulation of fermentation and degradation. Understanding the mechanism of electron transfer *via* extracellular and intracellular electron transfer chains would extend the future application of bioelectrochemical systems.

AUTHOR CONTRIBUTIONS

TZ, JL, and YJ wrote the manuscript. WZ, YF, FX, WD, PW, and MJ provided literature and data. JM contributed to the writing of the manuscript and the overall manuscript design.

FUNDING

This work was supported by the National Key Research and Development Program of China (2018YFA0901500), the

National Natural Science Foundation of China (21727818 and 21706124), the Key Science and Technology Project of Jiangsu Province (BE2016389), and the Jiangsu Synergetic Innovation Center for Advanced Bio-Manufacture of China.

REFERENCES

- Amano, Y., Koto, A., Matsuzaki, S., Sakamoto, H., Satomura, T., and Suye, S. I. (2016). Construction of a biointerface on a carbon nanotube surface for efficient electron transfer. *Mater. Lett.* 174, 184–187. doi: 10.1016/j.matlet.2016.03.113
- Amelia-Elena, R., Pravin Malla, S., Fanghua, L., Beatrice, M., Shanshan, C., Nevin, K. P., et al. (2014). Direct interspecies electron transfer between *Geobacter metallireducens* and *Methanoscarcina barkeri*. *Appl. Environ. Microbiol.* 80:4599. doi: 10.3389/fmicb.2016.00236
- Balzer, G. J., Thakker, C., Bennett, G. N., and San, K. Y. (2013). Metabolic engineering of *Escherichia coli* to minimize byproduct formate and improving succinate productivity through increasing NADH availability by heterologous expression of NAD⁺-dependent formate dehydrogenase. *Metab. Eng.* 20, 1–8. doi: 10.1016/j.ymben.2013.07.005
- Bari, C. D., Goñi-Urtiaga, A., Pita, M., Shleev, S., Toscano, M. D., Sainz, R., et al. (2016). Fabrication of high surface area graphene electrodes with high performance towards enzymatic oxygen reduction. *Electrochim. Acta* 191, 500–509. doi: 10.1016/j.electacta.2016.01.101
- Bian, B., Manal, A., Krishna, K., Defei, L., Suman, B., Zhiping, L., et al. (2018). Porous nickel hollow fiber cathodes coated with CNTs for efficient microbial electrosynthesis of acetate from CO₂ using *Sporomusa ovata*. *J. Mater. Chem. A* 6.35, 17201–17211. doi: 10.1039/c8ta05322g
- Bretschger, O., Obraztsova, A., Sturm, C. A., Chang, I. S., Gorby, Y. A., Reed, S. B., et al. (2007). Current production and metal oxide reduction by *Shewanella oneidensis* MR-1 wild type and mutants. *Appl. Environ. Microbiol.* 73, 7003–7012. doi: 10.1128/aem.01087-07
- Brutinel, E. D., and Gralnick, J. A. (2012). Shuttling happens: soluble flavin mediators of extracellular electron transfer in *Shewanella*. *Appl. Microbiol. Biotechnol.* 93, 41–48. doi: 10.1007/s00253-011-3653-0
- Butler, J. E., Young, N. D., and Lovley, D. R. (2010). Evolution of electron transfer out of the cell: comparative genomics of six *Geobacter* genomes. *BMC Genom.* 11:40. doi: 10.1186/1471-2164-11-40
- Carmona-Martínez, A. A., Harnisch, F., Kuhlicke, U., Neu, T. R., and Schröder, U. (2013). Electron transfer and biofilm formation of *Shewanella putrefaciens* as function of anode potential. *Bioelectrochemistry* 93, 23–29. doi: 10.1016/j.bioelechem.2012.05.002
- Carmona-Martínez, A. A., Trably, E., Milferstedt, K., Lacroix, R., Etcheverry, L., and Bernet, N. (2015). Long-term continuous production of H₂ in a microbial electrolysis cell (MEC) treating saline wastewater. *Water Res.* 81, 149–156. doi: 10.1016/j.watres.2015.05.041
- Chen, F., Feng, X. H., Liang, J. F., and Xu, H. (2012). An oxidoreduction potential shift control strategy for high purity propionic acid production by *Propionibacterium freudenreichii* CCTCC M207015 with glycerol as sole carbon source. *Bioprocess Biosyst. Eng.* 36, 1165–1176. doi: 10.1007/s00449-012-0843-9
- Choi, O., and Sang, B. I. (2016). Extracellular electron transfer from cathode to microbes: application for biofuel production. *Biotechnol. Biofuels* 9, 1–14. doi: 10.1186/s13068-016-0426-0
- Commault, A. S., Gavin, L., and Weld, R. J. (2015). Maintenance of *Geobacter*-dominated biofilms in microbial fuel cells treating synthetic wastewater. *Bioelectrochemistry* 106, 150–158. doi: 10.1016/j.bioelechem.2015.04.011
- Compagnone, D., and Guilbault, G. G. (1997). Glucose oxidase/hexokinase electrode for the determination of ATP. *Anal. Chim. Acta* 340, 109–113. doi: 10.1016/s0003-2670(96)00451-5
- Degani, Y., and Heller, A. (1987). Direct electrical communication between chemically modified enzymes and metal electrodes. I. Electron transfer from glucose oxidase to metal electrodes via electron relays, bound covalently to the enzyme. *J. Am. Chem. Soc.* 110, 708–715.
- Deutzmann, J. S., Sahin, M., and Spormann, A. M. (2015). Extracellular enzymes facilitate electron uptake in biocorrosion and bioelectrosynthesis. *mBio* 6:e00496-15. doi: 10.1128/mBio.00496-15
- Ding, A., Yu, Y., Sun, G., and Wu, D. (2012). Impact of applied voltage on methane generation and microbial activities in an anaerobic microbial electrolysis cell (MEC). *Chem. Eng. J.* 283, 260–265. doi: 10.1016/j.cej.2015.07.054
- Dumas, C., Basseguy, R., and Bergel, A. (2008). Microbial electrocatalysis with *Geobacter sulfurreducens* biofilm on stainless steel cathodes. *Electrochim. Acta* 53, 2494–2500. doi: 10.1016/j.electacta.2007.10.018
- Emde, R., Swain, A., and Schink, B. (1989). Anaerobic oxidation of glycerol by *Escherichia coli* in an amperometric poised-potential culture system. *Appl. Microbiol. Biotechnol.* 32, 170–175. doi: 10.1007/bf00165883
- Fan, L., Guo, K. J., Duan, H. W., Shao, L. M., and He, P. J. (2018). Exploit carbon materials to accelerate initiation and enhance process stability of CO anaerobic open-culture Fermentation. *ACS Sustain. Chem. Eng.* 6, 2787–2796. doi: 10.1021/acssuschemeng.7b04589
- Farzaneh, R., Defeng, X., Rachel, W., Regan, J. M., Richard, T. L., and Logan, B. E. (2009). Simultaneous cellulose degradation and electricity production by *Enterobacter cloacae* in a microbial fuel cell. *Appl. Environ. Microbiol.* 75, 3673–3678. doi: 10.1128/AEM.02600-08
- Federico, A., Alessandro, C., Mauro, M., Stefania, P., Priscilla, R., and Simona, R. (2007). Electron transfer from a solid-state electrode assisted by methyl viologen sustains efficient microbial reductive dechlorination of TCE. *Environ. Sci. Technol.* 41, 2554–2559. doi: 10.1021/es0624321
- Fernandez, M. D. L., Sanromán, M. D. L., Marks, S., Makinia, J., Campo, A. G. D., Rodrigo, M., et al. (2015). A grey box model of glucose fermentation and syntrophic oxidation in microbial fuel cells. *Bioresour. Technol.* 200:396. doi: 10.1016/j.biortech.2015.10.010
- Freguia, S., Masuda, M., Tsujimura, S., and Kano, K. (2009). *Lactococcus lactis* catalyzes electricity generation at microbial fuel cell anodes via excretion of a soluble quinone. *Bioelectrochemistry* 76, 14–18. doi: 10.1016/j.bioelechem.2009.04.001
- Freguia, S., Rabaey, K., Yuan, Z., and Keller, J. (2008). Sequential anode–cathode configuration improves cathodic oxygen reduction and effluent quality of microbial fuel cells. *Water Res.* 42, 1387–1396. doi: 10.1016/j.watres.2007.10.007
- Freguia, S., Virdis, B., Harnisch, F., and Keller, J. (2012). Bioelectrochemical systems: microbial versus enzymatic catalysis. *Electrochim. Acta* 82, 165–174. doi: 10.1002/cssc.201100835
- Ghosh, R. S., and Ghangrekar, M. M. (2015). Enhancing organic matter removal, biopolymer recovery and electricity generation from distillery wastewater by combining fungal fermentation and microbial fuel cell. *Bioresour. Technol.* 176, 8–14. doi: 10.1016/j.biortech.2014.10.158
- Gildemyn, S., Verbeeck, K., Jansen, R., and Rabaey, K. (2017). The type of ion selective membrane determines stability and production levels of microbial electrosynthesis. *Bioresour. Technol.* 224, 358–364. doi: 10.1016/j.biortech.2016.11.088
- Gul, M. M., and Ahmad, K. S. (2019). Bioelectrochemical systems: sustainable bio-energy powerhouses. *Biosens. Bioelectron.* 142:111576. doi: 10.1016/j.bios.2019.111576
- Gutierrez, F. A., Rubianes, M. D., and Rivas, G. A. (2016). Electrochemical sensor for amino acids and glucose based on glassy carbon electrodes modified with multi-walled carbon nanotubes and copper microparticles dispersed in polyethylenimine. *J. Electroanal. Chem.* 765, 16–21. doi: 10.1016/j.jelechem.2015.10.029
- Hara, K. Y., and Kondo, A. (2015). ATP regulation in bioproduction. *Microb. Cell Factor.* 14:198. doi: 10.1186/s12934-015-0390-6
- Harrington, T. D., Tran, V. N., Mohamed, A., Renslow, R., Biria, S., Orfe, L., et al. (2015). The mechanism of neutral red-mediated microbial electrosynthesis in *Escherichia coli*: menaquinone reduction. *Bioresour. Technol.* 192, 689–695. doi: 10.1016/j.biortech.2015.06.037
- He, A. Y., Yin, C. Y., Xu, H., Kong, X. P., Xue, J. W., Zhu, J., et al. (2016). Enhanced butanol production in a microbial electrolysis cell by *Clostridium beijerinckii* IB4. *Bioprocess Biosyst. Eng.* 39, 245–254. doi: 10.1007/s00449-015-1508-2

- He, C. S., Mu, Z. X., Yang, H. Y., Wang, Y. Z., Mu, Y., and Yu, H. Q. (2015). Electron acceptors for energy generation in microbial fuel cells fed with wastewaters: a mini-review. *Chemosphere* 140, 12–17. doi: 10.1016/j.chemosphere.2015.03.059
- Holm, A. K., Blank, L. M., Marco, O., Andreas, S., Christian, S., Jensen, P. R., et al. (2010). Metabolic and transcriptional response to cofactor perturbations in *Escherichia coli*. *J. Biol. Chem.* 285, 17498–17506. doi: 10.1074/jbc.M109.095570
- Jafary, T., Wan, R. W. D., Ghasemi, M., Kim, B. H., Jahim, J. M., Ismail, M., et al. (2015). Biocathode in microbial electrolysis cell; present status and future prospects. *Renew. Sustain. Energy Rev.* 47, 23–33.
- Karthikeyan, R., Wang, B., Xuan, J., Wong, J. W. C., Lee, P. K. H., and Leung, M. K. H. (2015). Interfacial electron transfer and bioelectrocatalysis of carbonized plant material as effective anode of microbial fuel cell. *Electrochim. Acta* 157, 314–323. doi: 10.1016/j.electacta.2015.01.029
- Kracher, D., Scheiblbrandner, S., Felice, A. K. G., Breslmayr, E., Preims, M., Ludwicka, K., et al. (2016). Extracellular electron transfer systems fuel cellulose oxidative degradation. *Science* 352:aaf3165. doi: 10.1126/science.aaf3165
- Kracke, F., Vassilev, I., and Krömer, J. O. (2015). Microbial electron transport and energy conservation – the foundation for optimizing bioelectrochemical systems. *Front. Microbiol.* 6:575. doi: 10.3389/fmicb.2015.00575
- Laura, R., Yolanda, R., Baeza, J. A., Albert, G., and Pilar, C. (2015). Microbial community analysis in a long-term membrane-less microbial electrolysis cell with hydrogen and methane production. *Bioelectrochemistry* 106, 359–368. doi: 10.1016/j.bioelechem.2015.06.003
- Ledezma, P., Donose, B. C., Freguia, S., and Keller, J. (2015). Oxidised stainless steel: a very effective electrode material for microbial fuel cell bioanodes but at high risk of corrosion. *Electrochim. Acta* 158, 356–360. doi: 10.1016/j.electacta.2015.01.175
- Lee, C. Y., Reuillard, B., Sokol, K. P., Laftoglou, T., Lockwood, C. W., Rowe, S. F., et al. (2016). A decahaem cytochrome as an electron conduit in protein-enzyme redox processes. *Chem. Commun.* 52, 7390–7393. doi: 10.1039/c6cc02721k
- Li, F., An, X., Wu, D., Xu, J., Chen, Y., Li, W., et al. (2019). Engineering microbial consortia for high-performance cellulosic hydrolyzates-fed microbial fuel cells. *Front. Microbiol.* 10:6937. doi: 10.3389/fmicb.2019.00409
- Li, H., Liao, B., Xiong, J., Zhou, X., Zhi, H., Liu, X., et al. (2018). Power output of microbial fuel cell emphasizing interaction of anodic binder with bacteria. *J. Power Sources* 379, 115–122. doi: 10.1016/j.jpowsour.2018.01.040
- Li, J. J., Gao, M. M., Zhang, G., Wang, X. H., Wang, S. G., Song, C., et al. (2015). Perchlorate reduction in microbial electrolysis cell with polyaniline modified cathode. *Bioresour. Technol.* 177, 74–79. doi: 10.1016/j.biortech.2014.11.065
- Lin, T., Ding, W., Sun, L., Wang, L., Liu, C.-G., and Song, H. (2018). Engineered *Shewanella oneidensis*-reduced graphene oxide biohybrid with enhanced biosynthesis and transport of flavins enabled a highest bioelectricity output in microbial fuel cells. *Nano Energy* 50, 639–648. doi: 10.1016/j.nanoen.2018.05.072
- Liu, F., Rotaru, A. E., Shrestha, P. M., Malvankar, N. S., and Lovley, D. R. (2012). Promoting direct interspecies electron transfer with activated carbon. *Energy Environ. Sci.* 5, 8982–8989. doi: 10.1016/j.biortech.2018.03.050
- Logan, B. E., Bert, H., René, R., Uwe, S. D., Jürg, K., Stefano, F., et al. (2006). Microbial fuel cells: methodology and technology. *Environ. Sci. Technol.* 40, 5181–5192.
- Lovley, D. R. (2008). The microbe electric: conversion of organic matter to electricity. *Curr. Opin. Biotechnol.* 19, 564–571. doi: 10.1016/j.copbio.2008.10.005
- Lovley, D. R. (2012). Electromicrobiology. *Ann. Rev. Microbiol.* 66:391. doi: 10.1146/annurev-micro-092611-150104
- Mahadevan, R., Bond, D., Butler, J. N., Coppi, M., Palsson, B., Schilling, C., et al. (2006). Characterization of metabolism in the Fe(III)-reducing organism *Geobacter sulfurreducens* by constraint-based modeling. *Appl. Environ. Microbiol.* 72, 1558–1568. doi: 10.1128/aem.72.2.1558-1568.2006
- Man, Z., Rao, Z., Xu, M., Guo, J., Yang, T., Zhang, X., et al. (2016). Improvement of the intracellular environment for enhancing L-arginine production of *Corynebacterium glutamicum* by inactivation of H₂O₂-forming flavin reductases and optimization of ATP supply. *Metab. Eng.* 38, 310–321. doi: 10.1016/j.ymben.2016.07.009
- Masuda, M., Freguia, S., Wang, Y. F., Tsujimura, S., and Kano, K. (2010). Flavins contained in yeast extract are exploited for anodic electron transfer by *Lactococcus lactis*. *Bioelectrochemistry* 78, 173–175. doi: 10.1016/j.bioelechem.2009.08.004
- Mayo, S. L., Ellis, W. R., Crutchley, R. J., and Gray, H. B. (1986). Long-range electron transfer in heme proteins. *Science* 233, 948–952. doi: 10.1126/science.3016897
- Moscovitz, R., Toledo-Alarcón, J., Trably, E., and Bernet, N. (2016). Electro-fermentation: how to drive fermentation using electrochemical systems. *Trends Biotechnol.* 34, 856–865. doi: 10.1016/j.tibtech.2016.04.009
- Omar, B., Abou-Shanab, R., El-Gammal, M., Fotidis, I. A., Kougias, P. G., Zhang, Y., et al. (2018). Simultaneous biogas upgrading and biochemicals production using anaerobic bacterial mixed cultures. *Water Res.* 142, 86–95. doi: 10.1016/j.watres.2018.05.049
- Oscar, G. S., David, O., Marcos, P., Batista, A. P., Alvaro, A., Pereira, M. M., et al. (2014). Reconstitution of respiratory complex I on a biomimetic membrane supported on gold electrodes. *Langmuir* 30, 9007–9015. doi: 10.1021/la501825r
- Pandit, A. V., and Mahadevan, R. (2011). In silico characterization of microbial electrosynthesis for metabolic engineering of biochemicals. *Microb. Cell Factor.* 10, 1–14. doi: 10.1186/1475-2859-10-76
- Pareek, A., Shanthi Sharan, J., and Venkata Mohan, S. (2019). Exploring chemically reduced graphene oxide electrode for power generation in microbial fuel cell. *Mater. Sci. Energy Technol.* 2, 600–606. doi: 10.1016/j.mset.2019.06.006
- Park, D. L. M., Guettler, M. V., Jain, M. K., and Zeikus, J. G. (1999). Microbial utilization of electrically reduced neutral red as the sole electron donor for growth and metabolite production. *Appl. Environ. Microbiol.* 65, 2912–2917. doi: 10.1128/aem.65.7.2912-2917.1999
- Pillot, G., Davidson, S., Auria, R., Combet-Blanc, Y., Godfroy, A., and Liebgott, P.-P. (2019). Production of current by syntrophy between exoelectrogenic and fermentative hyperthermophilic microorganisms in heterotrophic biofilm from a deep-sea hydrothermal chimney. *Microb. Ecol.* 79, 38–49. doi: 10.1007/s00248-019-01381-z
- Potter, M. C. (1911). Electrical effects accompanying the decomposition of organic compounds. *Proc. R. Soc. B Biol. Sci.* 84, 260–276. doi: 10.1098/rspb.1911.0073
- Qu, Y., Feng, Y., Wang, X., and Logan, B. E. (2012). Use of a coculture to enable current production by *Geobacter sulfurreducens*. *Appl. Environ. Microbiol.* 78, 3484–3487. doi: 10.1128/AEM.00073-12
- Rabaey, K., Rodriguez, J., Blackall, L. L., Keller, J., Gross, P., Batstone, D., et al. (2007). Microbial ecology meets electrochemistry: electricity-driven and driving communities. *ISME J.* 1, 9–18. doi: 10.1038/ismej.2007.4
- Rashid, N., Lee, B., and Chang, Y.-K. (2019). “Recent trends in microalgae research for sustainable energy production and biorefinery applications,” in *Microalgae Biotechnology for Development of Biofuel and Wastewater Treatment*, eds M. Alam, and Z. Wang (Singapore: Springer), 3–20. doi: 10.1007/978-981-13-2264-8_1
- Richter, H., Nevin, K. P., Jia, H., Lowy, D. A., Lovley, D. R., and Tender, L. M. (2009). Cyclic voltammetry of biofilms of wild type and mutant *Geobacter sulfurreducens* on fuel cell anodes indicates possible roles of OmcB, OmcZ, type IV pili, and protons in extracellular electron transfer. *Energy Environ. Sci.* 2:506. doi: 10.1039/b816647a
- Rose, N. D., and Regan, J. M. (2015). Changes in phosphorylation of adenosine phosphate and redox state of nicotinamide-adenine dinucleotide (phosphate) in *Geobacter sulfurreducens* in response to electron acceptor and anode potential variation. *Bioelectrochemistry* 106, 213–220. doi: 10.1016/j.bioelechem.2015.03.003
- Ross, D. E., Flynn, J. M., Baron, D. B., Gralnick, J. A., and Bond, D. R. (2012). Towards electrosynthesis in *Shewanella*: energetics of reversing the mtr pathway for reductive metabolism. *PLoS One* 6:e16649. doi: 10.1371/journal.pone.0016649
- Ruecha, N., Rodthongkum, N., Cate, D. M., Volckens, J., Chailapakul, O., and Henry, C. S. (2015). Sensitive electrochemical sensor using a graphene-polyaniline nanocomposite for simultaneous detection of Zn(II) Cd(II), and Pb(II). *Anal. Chim. Acta* 874, 40–48. doi: 10.1016/j.aca.2015.02.064
- Sadeghifar, M., and Rashid-Nadimi, S. (2017). Nanoporous gold electrode prepared from gold compact disk as the anode for the microbial fuel cell. *J. Iran. Chem. Soc.* 15, 607–612. doi: 10.1007/s13738-017-1260-4
- Santoro, C., Serov, A., Villarrubia, C. W. N., Stariha, S., Babanova, S., Artyushkova, K., et al. (2015). High catalytic activity and pollutants resistivity using Fe-AAPyr cathode catalyst for microbial fuel cell application. *Sci. Rep.* 5:16596. doi: 10.1038/srep16596
- Santoro, C., Soavi, F., Serov, A., Arbizzani, C., and Atanassov, P. (2016). Self-powered supercapacitive microbial fuel cell: the ultimate way of boosting and

- harvesting power. *Biosens. Bioelectron.* 78, 229–235. doi: 10.1016/j.bios.2015.11.026
- Schroder, U. (2007). Anodic electron transfer mechanisms in microbial fuel cells and their energy efficiency. *Phys. Chem. Chem. Phys.* 9, 2619–2629. doi: 10.1039/b703627m
- She, P., Song, B., Xing, X. H., Loosdrecht, M. V., and Liu, Z. (2006). Electrolytic stimulation of bacteria *Enterobacter dissolvens* by a direct current. *Biochem. Eng. J.* 28, 23–29. doi: 10.1016/j.bej.2005.08.033
- Shi, L., Squier, T., Zachara, J., and Fredrickson, J. (2010). Respiration of metal (hydr)oxides by *Shewanella* and *Geobacter*: a key role for multihaem c-type cytochromes. *Mol. Microbiol.* 65, 12–20. doi: 10.1111/j.1365-2958.2007.05783.x
- Shreeram, D. D., Panmanee, W., Mcdaniel, C. T., Daniel, S., Schaefer, D. W., and Hassett, D. J. (2018). Effect of impaired twitching motility and biofilm dispersion on performance of *Pseudomonas aeruginosa*-powered microbial fuel cells. *J. Indust. Microbiol. Biotechnol.* 45, 103–109. doi: 10.1007/s10295-017-1995-z
- Smith, J. A., Nevin, K. P., and Lovley, D. R. (2015). Syntrophic growth via quinone-mediated interspecies electron transfer. *Front. Microbiol.* 6:121. doi: 10.3389/fmicb.2015.00121
- Song, T. S., Jin, Y., Bao, J., Kang, D., and Xie, J. (2016). Graphene/biofilm composites for enhancement of hexavalent chromium reduction and electricity production in a biocathode microbial fuel cell. *J. Hazard. Mater.* 317, 73–80. doi: 10.1016/j.jhazmat.2016.05.055
- Sturm, G., Richter, K., Doetsch, A., Heide, H., Louro, R. O., and Gescher, J. (2015). A dynamic periplasmic electron transfer network enables respiratory flexibility beyond a thermodynamic regulatory regime. *ISME J.* 9, 1802–1811. doi: 10.1038/ismej.2014.264
- Su, L., and Ajo-Franklin, C. M. (2019). Reaching full potential: bioelectrochemical systems for storing renewable energy in chemical bonds. *Curr. Opin. Biotechnol.* 57, 66–72. doi: 10.1016/j.copbio.2019.01.018
- Uden, G., and Bongaerts, J. (1997). Alternative respiratory pathways of *Escherichia coli*: energetics and transcriptional regulation in response to electron acceptors. *Biochim. Biophys. Acta Bioenerget.* 1320, 217–234. doi: 10.1016/s0005-2728(97)00034-0
- Vassilev, I., Gießelmann, G., Schwechheimer, S. K., Wittmann, C., Virdis, B., and Krömer, J. O. (2018). Anodic electro-fermentation: anaerobic production of L-Lysine by recombinant *Corynebacterium glutamicum*. *Biotechnol. Bioeng.* 115, 1499–1508. doi: 10.1002/bit.26562
- Verea, L., Oumarou, S., Campos, J., Gineza, F., Verde, A., and Sebastian, P. J. (2014). Performance of a microbial electrolysis cell (MEC) for hydrogen production with a new process for the biofilm formation. *Int. J. Hydrogen Energy* 39, 8938–8946. doi: 10.1016/j.ijhydene.2014.03.203
- Villano, M., Monaco, G., Aulenta, F., and Mauro, M. (2011). Electrochemically assisted methane production in a biofilm reactor. *J. Power Sources* 196, 9467–9472. doi: 10.1016/j.jpowsour.2011.07.016
- Wang, G., Guo, Y., Cai, J., Wen, H., Mao, Z., Zhang, H., et al. (2019). Electricity production and the analysis of the anode microbial community in a constructed wetland-microbial fuel cell. *RSC Adv.* 9, 21460–21472.
- Wang, Y., Lun, J., Leng, Q., Wu, Y., He, X., and Wang, K. (2016). Electrochemical sensor for glutathione detection based on mercury ion triggered hybridization chain reaction signal amplification. *Biosens. Bioelectron.* 77, 914–920. doi: 10.1016/j.bios.2015.10.071
- Wetser, K., Sudirjo, E., Buisman, C. J. N., and Strik, D. P. B. T. B. (2015). Electricity generation by a plant microbial fuel cell with an integrated oxygen reducing biocathode. *Appl. Energy* 137, 151–157. doi: 10.1016/j.apenergy.2014.10.006
- Yang, L., Deng, W., Zhang, Y., Tan, Y., Ma, M., and Xie, Q. (2017). Boosting current generation in microbial fuel cells by an order of magnitude by coating an ionic liquid polymer on carbon anodes. *Biosens. Bioelectron.* 91, 644–649. doi: 10.1016/j.bios.2017.01.028
- Yang, Y., Ding, Y., Hu, Y., Cao, B., Rice, S. A., Kjelleberg, S., et al. (2015). Enhancing bidirectional electron transfer of *Shewanella oneidensis* by a synthetic flavin pathway. *ACS Synth. Biol.* 4:815. doi: 10.1021/sb500331x
- Yazdi, H., Alzate-Gaviria, L., and Ren, Z. J. (2015). Pluggable microbial fuel cell stacks for septic wastewater treatment and electricity production. *Bioresour. Technol.* 180, 258–263. doi: 10.1016/j.biortech.2014.12.100
- Yin, Q., Zhu, X., Zhan, G., Bo, T., Yang, Y., Tao, Y., et al. (2016). Enhanced methane production in an anaerobic digestion and microbial electrolysis cell coupled system with co-cultivation of *Geobacter* and *Methanosarcina*. *J. Environ. Sci. China* 42, 210–214. doi: 10.1016/j.jes.2015.07.006
- Yuan, M., Kummer, M. J., and Minteer, S. D. (2019). Strategies for bioelectrochemical CO₂ reduction. *Chemistry* 25, 14258–14266. doi: 10.1002/chem.201902880
- Yuan, Y., Shin, H., Kang, C., and Kim, S. (2016). Wiring microbial biofilms to the electrode by osmium redox polymer for the performance enhancement of microbial fuel cells. *Bioelectrochemistry* 108, 8–12. doi: 10.1016/j.bioelechem.2015.11.001
- Zhang, D., Li, Z., Zhang, C., Zhou, X., Xiao, Z., Awata, T., et al. (2017). Phenol-degrading anode biofilm with high coulombic efficiency in graphite electrodes microbial fuel cell. *J. Biosci. Bioeng.* 123, 364–369. doi: 10.1016/j.jbiosc.2016.10.010
- Zhang, Y., and Angelidaki, I. (2015). Bioelectrochemical recovery of waste-derived volatile fatty acids and production of hydrogen and alkali. *Water Res.* 81, 188–195. doi: 10.1016/j.watres.2015.05.058
- Zhao, C., Gai, P. P., Song, R., Zhang, J. R., and Zhu, J. J. (2015). Graphene/Au composites as an anode modifier for improving electricity generation in *Shewanella*-inoculated microbial fuel cells. *Anal. Methods* 7, 4640–4644. doi: 10.1039/c5ay00976f
- Zhao, F., Falk, H., Uwe, S. D., Fritz, S., Peter, B., and Iris, H. (2006). Challenges and constraints of using oxygen cathodes in microbial fuel cells. *Environ. Sci. Technol.* 40, 5193–5199. doi: 10.1021/es060332p
- Zhao, Z., Zhang, Y., Quan, X., and Zhao, H. (2015a). Evaluation on direct interspecies electron transfer in anaerobic sludge digestion of microbial electrolysis cell. *Bioresour. Technol.* 200:235. doi: 10.1016/j.biortech.2015.10.021
- Zhao, Z., Zhang, Y., Wang, L., and Quan, X. (2015b). Potential for direct interspecies electron transfer in an electric-anaerobic system to increase methane production from sludge digestion. *Sci. Rep.* 5:11094. doi: 10.1038/srep11094
- Zhen, G., Lu, X., Kobayashi, T., Kumar, G., and Xu, K. (2016). Promoted electromethanogenesis in a two-chamber microbial electrolysis cells (MECs) containing a hybrid biocathode covered with graphite felt (GF). *Chem. Eng. J.* 284, 1146–1155. doi: 10.1016/j.cej.2015.09.071
- Zheng, S., Zhang, H., Li, Y., Zhang, H., Wang, O., Zhang, J., et al. (2015). Co-occurrence of *Methanosarcina mazei* and *Geobacteraceae* in an iron (III)-reducing enrichment culture. *Front. Microbiol.* 6:941. doi: 10.3389/fmicb.2015.00941
- Zhou, M., Wang, H., Hassett, D. J., and Gu, T. (2013). Recent advances in microbial fuel cells (MFCs) and microbial electrolysis cells (MECs) for wastewater treatment, bioenergy and bioproducts. *J. Chem. Technol. Biotechnol.* 88, 508–518. doi: 10.1002/jctb.4004

Conflict of Interest: The authors declare that the research was conducted in the absence of any commercial or financial relationships that could be construed as a potential conflict of interest.

Copyright © 2020 Zheng, Li, Ji, Zhang, Fang, Xin, Dong, Wei, Ma and Jiang. This is an open-access article distributed under the terms of the Creative Commons Attribution License (CC BY). The use, distribution or reproduction in other forums is permitted, provided the original author(s) and the copyright owner(s) are credited and that the original publication in this journal is cited, in accordance with accepted academic practice. No use, distribution or reproduction is permitted which does not comply with these terms.



Omics Analysis Reveals the Mechanism of Enhanced Recombinant Protein Production Under Simulated Microgravity

Jie Huangfu^{1,2†}, Hye Su Kim^{1†}, Ke Xu^{1,3}, Xiaoyu Ning¹, Lei Qin^{1*}, Jun Li^{1*} and Chun Li¹

¹ Department of Biochemical Engineering/Institute for Synthetic Biosystems, School of Chemistry and Chemical Engineering, Beijing Institute of Technology, Beijing, China, ² China National Research Institute of Food & Fermentation Industries, Beijing, China, ³ Key Lab for Industrial Biocatalysis, Ministry of Education, Department of Chemical Engineering, Tsinghua University, Beijing, China

OPEN ACCESS

Edited by:

Mingjie Jin,
Nanjing University of Science and
Technology, China

Reviewed by:

Xinqing Zhao,
Shanghai Jiao Tong University, China
Feng Qi,
Fujian Normal University, China

*Correspondence:

Lei Qin
qinlei@bit.edu.cn
Jun Li
junlibiotech@bit.edu.cn

[†]These authors have contributed
equally to this work

Specialty section:

This article was submitted to
Synthetic Biology,
a section of the journal
Frontiers in Bioengineering and
Biotechnology

Received: 05 November 2019

Accepted: 14 January 2020

Published: 20 February 2020

Citation:

Huangfu J, Kim HS, Xu K, Ning X,
Qin L, Li J and Li C (2020) Omics
Analysis Reveals the Mechanism of
Enhanced Recombinant Protein
Production Under
Simulated Microgravity.
Front. Bioeng. Biotechnol. 8:30.
doi: 10.3389/fbioe.2020.00030

Simulated microgravity (SMG) is regarded as a suitable environment to produce recombinant proteins. This study showed that β -glucuronidase expressing *Escherichia coli* had higher productivity of recombinant protein and higher plasmid copy number under SMG compared with the normal gravity condition. The cellular changes were analyzed at both transcriptomic and proteomic levels. The upregulation of a group of ribosome/RNA polymerase genes and a cluster of genes involving energy metabolism at transcriptomic level stood out for improved production of recombinant protein under SMG. The protein folding modulators such as chaperones were upregulated at proteomic level, which could be a result of the increased activity of protein synthesis and can help recombinant protein production. Protein export was also strengthened, which was revealed at both transcriptomic and proteomic levels. The results demonstrated that SMG is a favorable environment for recombinant protein production arousing the upregulation of protein synthesis, protein folding, and protein export.

Keywords: simulated microgravity, omics, recombinant protein, ribosome protein assembly, protein folding

INTRODUCTION

Microgravity is a special environmental condition for microorganisms. The significant characteristics of this extreme and unique environment are the low sedimentation, low shear stress, and low turbulence (Nickerson et al., 2004). The reduced gravity might elicit a number of distinct physiological variations to microorganisms, such as microbial growth (Rosenzweig et al., 2010), resistance to multiple stresses and antibiotics (Gao et al., 2001; Wilson et al., 2002), and substrate utilizations (Brown et al., 2002). Since the microgravity experiment in space takes enormous resources and time, the techniques of clino-rotation have been devised to simulate microgravity on the ground. Under the simulated microgravity (SMG), microorganism has a shorter lag phase, a higher growth rate, and a higher cell density compared to the normal gravity (NG) (Baker et al., 2004).

Escherichia coli is widely used for expressing recombinant proteins; however, there are still bottlenecks for obtaining large amounts of soluble and functional proteins (San-Miguel et al., 2013). Variation in environmental condition was reported to influence the recombinant protein production (Hoffmann and Rinas, 2004; Jamal et al., 2009). Some studies have demonstrated that

SMG had impact on the heterologous protein production. It was reported that SMG enhanced the production of recombinant proteins of LacZ and glycodelin in the human cells compared with a stirred bioreactor under NG (Navran, 2007). A previous study found that SMG enhanced the expression of the recombinant β -glucuronidase in *E. coli* (Xiang et al., 2010). However, the research about the mechanism of SMG on the expression of recombinant proteins by bacteria is still lacking.

The potent expression of desired recombinant proteins involves efficient protein translation and functional protein folding. The ribosomes, consisting of a huge complex RNA and proteins, are protein factories for protein synthesis and assembly. The ribosome is comprised of two subunits: large subunit [5 small ribosomal RNA (rRNA), 23 small rRNA, and 33 r-proteins] and small subunit (16 small ribosomal RNA and 21 r-proteins) in *E. coli* (Kaltschmidt and Wittmann, 1970). Ribosomal proteins have significant function on maintaining the rRNA structure and messenger RNA (mRNA) helicase activity in ribosome biogenesis (Ogle et al., 2001; Takyar et al., 2005). For protein folding, the nascent polypeptide chains have received assistance from many molecular chaperones (Frydman and Hartl, 1996). In *E. coli*, different proteins interact with different chaperones according to polypeptide chain length. Small proteins (<30 kDa), taking 70% of total, interact with Trigger factor *tig*, a ribosome-associated chaperone (Hartl and Hayer-Hartl, 2009). Longer proteins, belonging to 20% of total, interact with *dnaK* and *dnaJ* (Hsp70 system) (Clerico et al., 2015). About 10% of polypeptide chains are transported to *groEL* and *groES* chaperonin system (Hayer-Hartl et al., 2016). Understanding how SMG affects protein translation and protein folding could be profitable to discover new potentials for increased recombinant proteins.

In this study, we examined the effects of SMG on expressing *Aspergillus oryzae* β -glucuronidase (pGUS) by the recombinant *E. coli*. The potent changes of ribosome protein assembly and protein folding were revealed by the multilevel omics analysis. This result could be helpful to comprehensively understand the physiological adaptation of recombinant *E. coli* under SMG and provide new insight into developing unconventional bioprocess to enhance recombinant protein production.

MATERIALS AND METHODS

Strain and SMG Cultivation

The recombinant *E. coli* BL21 (DE3)/pET28a-pGUS previously constructed (Shi et al., 2011) was authorized and used in this study. Conditions referred as SMG and NG were designed by rotating the high-aspect rotating-wall vessel (HARV; diameter, 8 cm; depth, 1 cm) horizontally and vertically on the rotating cell culture systems (RCCS-4D, 50 ml; Synthecon Inc., Houston, TX), respectively.

An overnight bacterial culture was inoculated into 30 ml Luria-Bertani (LB) medium (10 g/L tryptone, 5 g/L yeast extract, and 10 g/L NaCl) in a shaker flask at 37°C for 10 h. The cell suspension was diluted (1:10) in two HARV vessels filled with fresh LB medium containing 50 μ g/ml kanamycin. Both of the two HARVs were first incubated at 37°C for 4 h. After

that, the cells were induced by adding 0.8 mM isopropyl β -D-1-thiogalactopyranoside (IPTG). The SMG culture process was carried out under different rotary speeds (10, 15, 20, and 30 rpm), induction temperatures (17, 27, and 37°C), and induction time (4, 6, and 8 h) to find the optimal condition for the efficient recombinant protein production. The NG culture process was carried out at the same condition. Cell growth curve was tested periodically by measuring the OD₆₀₀ using an ultraviolet spectrophotometer (Hitachi, Japan) through triplicate independent experiments. All experiments were carried out in triplicate.

Protein Expression Analysis and Enzyme Assay

The strain after cultivation was collected by centrifugation at 8,000 rpm for 15 min. The pellets were suspended in 200 mM phosphate buffer (pH 6.0) and ultrasonicated on the ice. After centrifugation, the supernatant (soluble protein) and pellet (inclusion body) were separated. A semiquantitative determination of the soluble protein and inclusion body was detected by sodium dodecyl sulfate polyacrylamide gel electrophoresis. Bovine serum albumin was used as an internal standard to determine the total protein concentration by the Coomassie brilliant blue R250 staining method. The pGUS activity was assayed by high-performance liquid chromatography (Shimadzu, Japan) from cell crude extract after sonication using glycyrrhizin as the substrate. One unit of activity was defined as the amount of enzyme that released 1 μ mol of biosynthesized β -D-mono-glucuronide-glycyrrhizin in the reaction mixture per minute (Feng et al., 2006). All the experiments from a biological sample were carried out in triplicate.

Plasmid Stability and Copy Number Analysis

The strains were cultured overnight in liquid LB medium without kanamycin under SMG and NG, respectively. Then, the cells were collected and diluted (1:100) into fresh liquid LB medium at every 8 h to continue SMG and NG culturing. Fifty microliters of diluted sample (10^4 cells/ml) was plated on LB plate (without kanamycin) and incubated at 37°C overnight. After that, the colonies were stamped on selective plates (with kanamycin). The relative ratio of colonies on the plates with kanamycin represents the plasmid stability. Three induction temperatures (17, 27, and 37°C) were chosen to investigate the SMG effect on the plasmid copy number. After adding 0.8 mM IPTG for 4 h, the cells were collected, and the plasmids were extracted. The DNA quantity was assessed using the NanoDrop 2000c spectrophotometer (Thermo Scientific, Waltham, MA). The plasmid number was calculated as the plasmid DNA concentration per OD₆₀₀.

RNA-seq

Cells under SMG and NG were incubated at 15 rpm and 27°C for 4 h, and subjected to IPTG induction at 17°C for 4 h. After that, total RNA was isolated using the RNA isolation system (Roche). Genomic DNA was removed using DNaseI. RNA quality was assessed using the NanoDrop 2000c spectrophotometer. Sequencing was carried out by Solexa Genome Analyzer

commercially. To obtain information regarding the expression level among the genes, the number of relative reads per coding region using a window of 250 bp was calculated. Gene expression was calculated using the transcripts per million (TPM) method. The raw reads of 35 bp were truncated as 28-mers and remapped with the Efficient Local Alignment of Nucleotide Data allowing for 1 and 2 nt mismatches. The output file containing only the sequences that mapped once in the genome was further analyzed to ascertain genome coverage and to assign the number of reads per locus (open reading frame or intergenic region). To identify the differential expression genes (DEGs), the libraries were initially compared by pairs; for this, the number of reads for each coding region was determined. The number of total reads was normalized between these libraries, and the ratio of reads between SMG and NG was calculated. The genes showing a ratio larger than 2.0 and lower than 0.5 were considered potential candidates. Finally, the number of reads for the four libraries was normalized, and the Student's *t*-test was applied for each gene. Those genes that showed a *P*-value lower or equal to 0.05 (corrected for multiple testing) were considered as statistically significant. The genome sequence and annotation files of *E. coli* K12 MG1655 were obtained from NCBI, and the experimentally verified operons in the bacterium were downloaded from RegulonDB (<http://regulondb.ccg.unam.mx/>). Categories of differentially expressed genes were identified according to Gene Ontology and Kyoto Encyclopedia of Genes and Genomes using Cytoscape software. On average, 6,415,574 and 6,603,164 reads were obtained from

both *E. coli*-pGUS-SMG and *E. coli*-pGUS-NG, respectively. The mapping statistics of the samples were summarized in **Table S1**. The levels of DEGs were calculated on TPM. All of the genes with a TPM ≥ 0.1 were used as DEGs in the following analysis.

Proteomic Analysis

Cells were incubated and induced at the same conditions with previous description for RNA-seq. The cells were then centrifuged and washed with ice-cold phosphate-buffered saline (pH 7.2) for three times. Then, the cells were suspended in an ice-cold lysis buffer containing 8 M urea in 50 mM Tris-HCl (pH = 7.4), 65 mM dithiothreitol, 1 mM ethylenediaminetetraacetic acid, 1% (v/v) Triton, 1 mM phenylmethylsulfonyl fluoride (added freshly), 2% (v/v) protease inhibitor cocktail (added freshly), and phosphatase inhibitor cocktail (1 tablet/10 ml of lysis buffer, added freshly), and ultrasonicated in an ice bath. The supernatant was reserved for the determination of protein content using the bicinchoninic acid method. Proteomic analysis was performed through precipitation by chloroform/methanol treatment, then redissolution in 0.2 ml buffer containing 8 M urea, 50 mM Tris-HCl, pH 8.2. Two milligrams of the above redissolved proteins was reduced by 20 mM dithiothreitol at 37°C for 2 h and oxidized by 40 mM indole-3-acetic acid at 25°C for 45 min in the dark. The protein mixture was further diluted to 2 ml with 50 mM Tris-HCl buffer (pH = 8.3). After adding 40 μ g of sequencing trypsin, the protein mixture was digested at 37°C overnight.

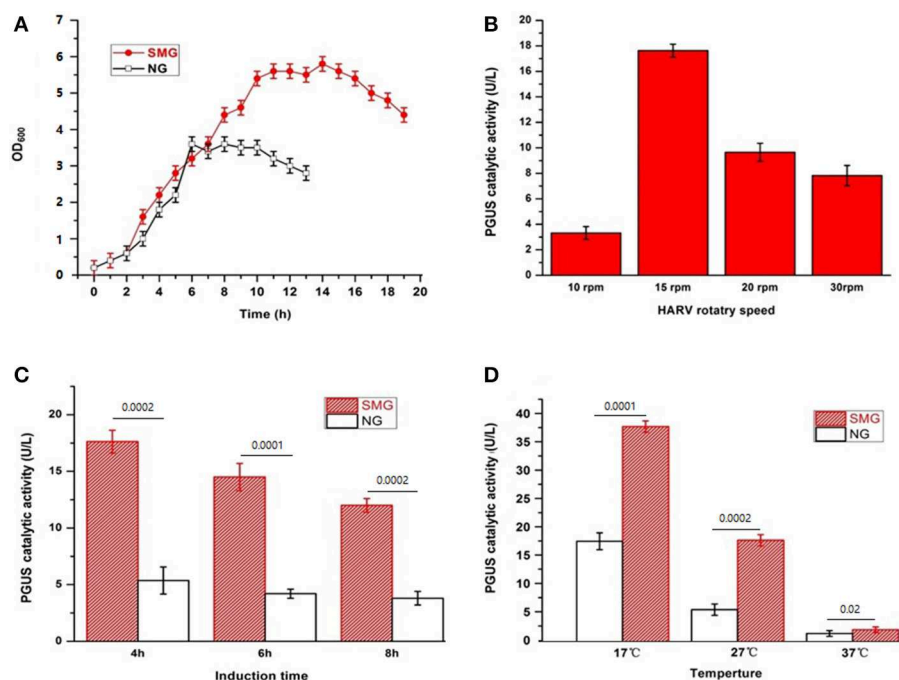


FIGURE 1 | The characteristics of the recombinant *E. coli*-pGUS under SMG and NG. **(A)** Growth curve of the strain at 37°C under SMG and NG at 15 rpm. Optimal HARV rotary speed **(B)**, induction time **(C)**, and induction temperature **(D)** for the recombinant pGUS expressed under SMG were determined. The default condition for the optimization of induction was 15 rpm, 4 h, and 27°C. Significance was assessed using two-sided, paired Student's *t*-test, and *P*-values are indicated as numbers in the graphs, *n* = 3.

The obtained digests were reserved at -80°C . The tryptic digests were desalted with C18 solid-phase cartridges and lyophilized. Protein analysis technology was used by LTQ-OrbitrapVelos mass spectrometer (Thermo, San Jose, CA) with one-dimensional reversed-phase liquid chromatography separating system in the positive ion mode. MS/MS experiments of the five most abundant precursor ions were acquired, and the fragmentation data were exported using the Data Analysis Software (version 3.4, Bruker Daltonic). The protein identification was validated by the *E. coli* open reading frame protein database using the MASCOT Daemon (version 2.1.3) search engine. The results were filtered using the SFOER software with optimized criteria, and the corresponding false discovery rate was below 1%. Proteins with a $\log_2(\text{fold change}) > 1$ and $\log_2(\text{fold change}) < -1$ ($P < 0.05$ for the *t*-test of each of the two samples) were assigned as differential expressed proteins (DEPs).

RESULTS

Characteristics of the Recombinant *E. coli*-pGUS Under SMG

Our previous studies have shown the significant improvement of recombinant protein secretion and glycosylation in pGUS expressing *Pichia pastoris* (Huangfu et al., 2016). Now, we want to discover the impact of SMG using *E. coli*-based expression system as the easiest and cheapest host. The growth curves of the strain *E. coli*-pGUS under SMG at 27°C exhibited the enhanced growth rate and the delayed entering into stationary phase (Figure 1A). The strain under SMG at 37°C also showed higher growth rate compared with that under NG (data not shown). The maximum catalytic activity of recombinant pGUS appeared under SMG with 15 rpm, 4 h IPTG induction, and 17°C induction temperature (Figures 1B,C). At different induction temperatures (17, 27, and 37°C), the enzyme activities increased by 2.16-, 2.46-, and 1.55-fold compared with NG, respectively (Figure 1D).

The pGUS expression efficiencies of the total protein increased under SMG at all inducing temperatures, which increased by 15.3, 48.2, and 52.4% at 17, 27, and 37°C , respectively (Figure 2). SMG also had clear effects on the plasmid stability and the plasmid copy number (Figure 3). The plasmid stability under SMG was slightly lower than that under NG (Figure 3A), but the plasmid copy number under SMG was significantly higher than that under NG (Figure 3B). These results indicated that the cells growth, enzyme activities, and protein expression efficiencies were all facilitated under SMG. Moreover, the higher plasmid copy number under SMG might result in higher protein productivity.

Transcriptome Revealed the Mechanism of Enhanced Protein Expression Under SMG

This study compared transcriptomic performance under SMG and NG by RNA-seq (Figure 4A). Among the DEGs between SMG and NG, 316 genes were upregulated and 276 genes were downregulated. The most differential pathways were clustered into the categories of translation

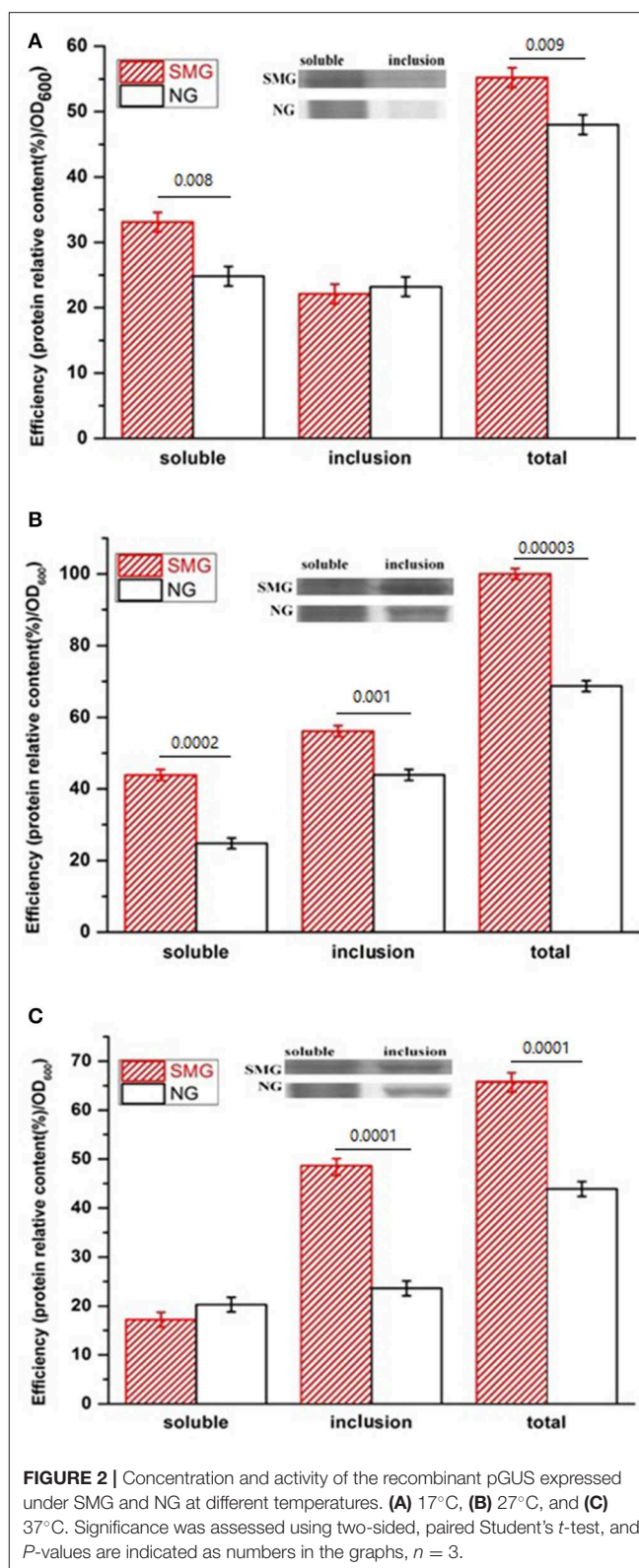


FIGURE 2 | Concentration and activity of the recombinant pGUS expressed under SMG and NG at different temperatures. **(A)** 17°C , **(B)** 27°C , and **(C)** 37°C . Significance was assessed using two-sided, paired Student's *t*-test, and *P*-values are indicated as numbers in the graphs, $n = 3$.

hub (ribosomal, RNA polymerase, and aminoacyl-tRNA biosynthesis), metabolism hub [glycolysis/gluconeogenesis, tricarboxylic acid cycle (TCA) cycle, purine metabolism,

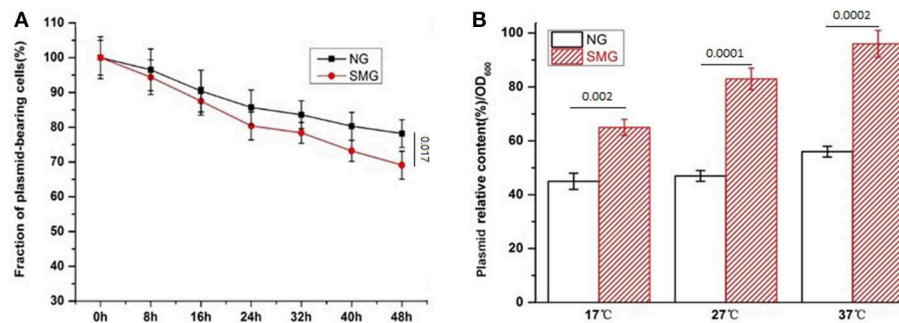


FIGURE 3 | The stability (A) and copy number (B) of the plasmids in the recombinant *E. coli*-pGUS under SMG. For (B), significance was assessed using two-sided, paired Student's *t*-test, and *P*-values are indicated as numbers in the graphs, *n* = 3.

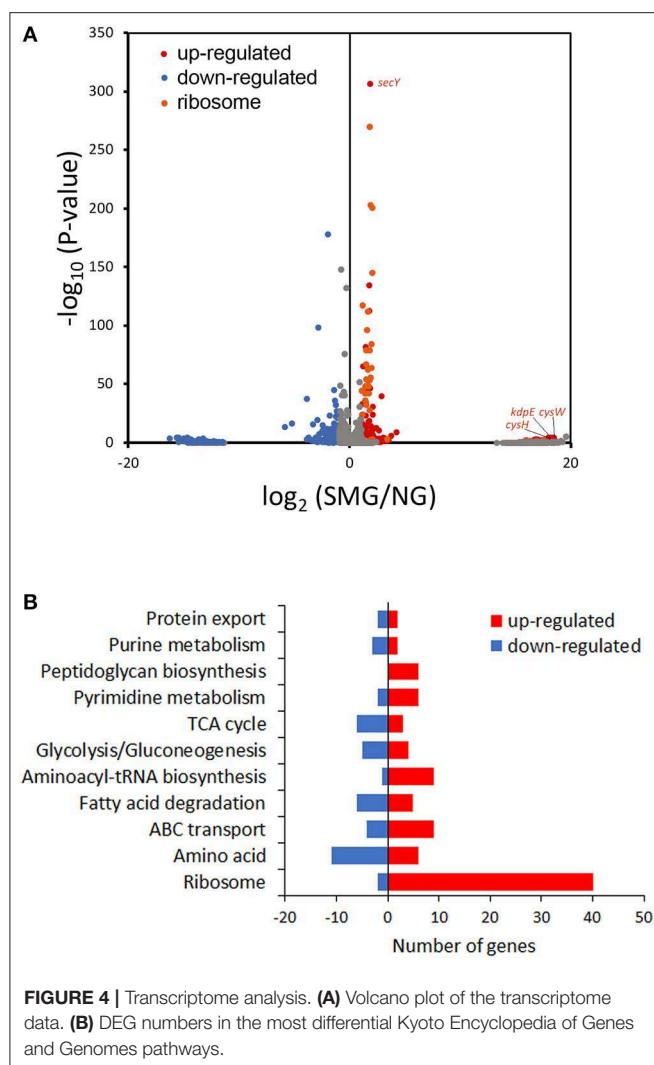


FIGURE 4 | Transcriptome analysis. (A) Volcano plot of the transcriptome data. (B) DEG numbers in the most differential Kyoto Encyclopedia of Genes and Genomes pathways.

pyrimidine metabolism, fatty acid degradation, amino acid, and peptidoglycan biosynthesis], and transport hub (ATP-binding cassette transporters and protein export) (Figure 4B and Table S5).

As a result, the ribosome is the major group of significantly upregulated genes compared with other classified clusters (Figure 4). Most of the genes belonging to the ribosome cluster were upregulated (Table 1), in which 39 genes were significantly upregulated, accounting for 12.4% of all the DEGs. The ribosomal assembly related genes encoding 30S and 50S ribosomal subunit proteins (e.g., *rplO*, *rpsK*, *rplV*, *rplP*, *rpsD*, *rplR*, *rpsC*, *rpsE*, and *rplB*) were all upregulated in the recombinant pGUS-expressing *E. coli* (Table 1) and in *Pseudomonas aeruginosa* (Crabbé et al., 2011). The aminoacyl-transfer RNA (tRNA) biosynthesis were also reinforced under SMG (Table 2), in which the DEGs accounts for 2.9% of the total DEGs. The transcriptional levels of the DNA-directed RNA polymerase genes (including *rpoA*, *rpoB*, *rpoC*, and *rpoZ*) were also observed to be upregulated (Table 3). These upregulated ribosome-related genes and RNA polymerase genes may increase the rate of protein synthesis and contribute to the enhancement of the protein production under SMG environment.

The overall transcriptional level of glycolysis was upregulated (Table 4 and Figure S1), which could contribute to the enhanced uptake of carbon sources and the conversion of precursors to biomass. The aerotaxis receptor *aer* was upregulated by 2.99-fold (\log_2). The upregulation of gene *aer* indicated that SMG could guide cells toward oxygen and energy-generating niches. Most of oxidative phosphorylation genes (encoding NADH dehydrogenase, succinate dehydrogenase, cytochrome c oxidase, cytochrome bd complex, and ATPase) were upregulated (Table 5). These upregulated energy-generating genes may directly lead to high metabolic efficiency and high cell viability.

Interestingly, the genes about cysteine synthesis, *cysW* and *cysH*, were both substantially upregulated [increased by 17.93- and 17.58-fold (\log_2), respectively] (Figure 4A). Thus, cysteine, acting as a building unit for protein translation and involves in redox homeostasis, may contribute to higher recombinant protein production responding to SMG, while the mechanism is still unknown and needs to be further studied in future.

Protein folding is an outstanding feature issuing in efficient metabolism conversion under SMG. *kdpE* is a transcription factor for potassium homeostasis. In this study, *kdpE* was significantly upregulated by 17.85-fold (\log_2) under SMG (Figure 4A). Chaperone *groEL* is just one of the K^+ -activated

TABLE 1 | Transcription changes of ribosomal genes.

Gene	Function descriptions	log ₂ (SMG/NG)	-lg(P-value)
<i>rpmE</i>	50S ribosomal subunit protein L31	17.46	0.40
<i>ykgM</i>	putative ribosomal protein	17.46	0.40
<i>rplO</i>	50S ribosomal subunit protein L15	2.09	145.07
<i>rpsK</i>	30S ribosomal subunit protein S11	2.01	83.80
<i>rplV</i>	50S ribosomal subunit protein L22	2.00	64.04
<i>rplP</i>	50S ribosomal subunit protein L16	1.94	55.21
<i>rpsD</i>	30S ribosomal subunit protein S4	1.87	202.58
<i>rplR</i>	50S ribosomal subunit protein L18	1.84	79.02
<i>rpmC</i>	50S ribosomal subunit protein L29	1.83	28.01
<i>rpsS</i>	30S ribosomal subunit protein S19	1.82	53.62
<i>rplQ</i>	50S ribosomal subunit protein L17	1.78	47.84
<i>rplW</i>	50S ribosomal subunit protein L23	1.72	42.12
<i>rpsC</i>	30S ribosomal subunit protein S3	1.69	113.34
<i>rpsE</i>	30S ribosomal subunit protein S5	1.69	112.30
<i>rplD</i>	50S ribosomal subunit protein L4	1.66	62.19
<i>rpmA</i>	50S ribosomal subunit protein L27	1.64	18.69
<i>rplT</i>	50S ribosomal subunit protein L20	1.61	47.36
<i>rplB</i>	50S ribosomal subunit protein L2	1.60	96.49
<i>rpsQ</i>	30S ribosomal subunit protein S17	1.52	32.19
<i>rplF</i>	50S ribosomal subunit protein L6	1.51	78.93
<i>rplC</i>	50S ribosomal subunit protein L3	1.50	54.34
<i>rplE</i>	50S ribosomal subunit protein L5	1.49	67.09
<i>rpsN</i>	30S ribosomal subunit protein S14	1.42	47.74
<i>rpmJ</i>	50S ribosomal subunit protein L36	1.42	34.72
<i>ykgO</i>	putative ribosomal protein	1.42	34.72
<i>rpsH</i>	30S ribosomal subunit protein S8	1.41	43.43
<i>rpmD</i>	50S ribosomal subunit protein L30	1.40	14.19
<i>rpsM</i>	30S ribosomal subunit protein S13	1.40	36.00
<i>rpmI</i>	50S ribosomal subunit protein L35	1.30	35.67
<i>rpsA</i>	30S ribosomal subunit protein S1	1.18	116.84
<i>rplU</i>	50S ribosomal subunit protein L10	1.17	23.71
<i>rpsJ</i>	30S ribosomal subunit protein S10	1.07	19.14
<i>rplL</i>	50S ribosomal subunit protein L12	0.99	11.74
<i>rplX</i>	50S ribosomal subunit protein L24	0.94	12.37
<i>rplS</i>	50S ribosomal subunit protein L19	0.91	7.33
<i>rpmF</i>	50S ribosomal subunit protein L32	0.72	2.64
<i>rpmG</i>	50S ribosomal subunit protein L33	0.71	2.23
<i>rplN</i>	50S ribosomal subunit protein L14	0.69	11.25
<i>rplA</i>	50S ribosomal subunit protein L1	0.61	8.11
<i>rpsR</i>	30S ribosomal subunit protein S18	0.60	1.26
<i>rpmB</i>	50S ribosomal subunit protein L28	0.58	1.78
<i>rpsP</i>	30S ribosomal subunit protein S16	0.54	2.36
<i>rplI</i>	50S ribosomal subunit protein L9	0.52	1.25
<i>rpsO</i>	30S ribosomal subunit protein S15	0.48	4.68
<i>rplM</i>	50S ribosomal subunit protein L13	0.46	2.95
<i>rpsB</i>	30S ribosomal subunit protein S2	0.45	3.89
<i>rplU</i>	50S ribosomal subunit protein L21	0.36	1.27
<i>rplK</i>	50S ribosomal subunit protein L11	0.33	1.87
<i>rpsT</i>	30S ribosomal subunit protein S20	0.28	0.27
<i>rpsG</i>	30S ribosomal subunit protein S7	0.25	0.77
<i>rpsI</i>	30S ribosomal subunit protein S9	0.23	0.60
<i>rpsL</i>	30S ribosomal subunit protein S12	0.19	0.41
<i>rplY</i>	50S ribosomal subunit protein L25	0.16	0.18
<i>rpsU</i>	30S ribosomal subunit protein S21	-0.18	0.99
<i>rpsF</i>	30S ribosomal subunit protein S6	-0.53	8.39

TABLE 2 | Transcription changes of aminoacyl-tRNA biogenesis genes.

Gene	Function descriptions	log ₂ (SMG/NG)	-lg(P-value)
<i>cysS</i>	Phenylalanine-tRNA ligase subunit alpha	1.13	3.73
<i>ileS</i>	Isoleucine-tRNA ligase	1.12	44.21
<i>glyS</i>	Glycine-tRNA ligase subunit beta	0.92	7.04
<i>aspS</i>	Aspartate-tRNA ligase	0.92	6.23
<i>valS</i>	Valine-tRNA ligase	0.80	11.71
<i>proS</i>	Proline-tRNA ligase	0.76	3.58
<i>metG</i>	Methionine-tRNA ligase	0.75	3.92
<i>alaS</i>	Alanine-tRNA ligase/DNA-binding transcriptional repressor	0.65	12.77
<i>selA</i>	Selenocysteine synthase	0.64	0.34
<i>asnS</i>	Asparagine-tRNA ligase	0.56	2.41
<i>pheT</i>	Phenylalanine-tRNA ligase subunit beta	0.46	3.20
<i>lysS</i>	Lysine-tRNA ligase, constitutive	0.44	1.25
<i>lysU</i>	Lysine-tRNA ligase/Ap4A synthetase/Ap3A synthetase	0.44	1.25
<i>leuS</i>	Leucine-tRNA ligase	0.38	2.53
<i>argS</i>	Arginine-tRNA ligase	0.29	0.44
<i>glyQ</i>	Glycine-tRNA ligase subunit alpha	0.29	0.41
<i>glxS</i>	Glutamate-tRNA ligase	0.21	0.39
<i>thrS</i>	Threonine-tRNA ligase	0.21	1.08
<i>tyrS</i>	Tyrosine-tRNA ligase	0.05	0.05
<i>hisS</i>	Histidine-tRNA ligase	0.01	0.20
<i>serS</i>	Serine-tRNA ligase	0.00	0.25
<i>cysS</i>	Cysteine-tRNA ligase	0.00	0.14
<i>trpS</i>	Tryptophan-tRNA ligase	-0.20	0.81
<i>glnS</i>	Glutamine-tRNA ligase	-0.57	6.68
<i>fnt</i>	10-formyltetrahydrofolate:l-methionyl-tRNA(fMet) N-formyltransferase	-0.71	5.78

type I enzymes. Therefore, it was suggested that SMG could provide a better environment for improving the activities of chaperones to reduce protein aggregation upon environmental stress. However, the transcriptional level of some chaperone genes did not show significant upregulation under SMG, such as *dnaJ*, *groEL*, *cpxP*, and *ppiD* (Tables S2–S4), which was also observed in previous studies (Tucker et al., 2007; Wilson et al., 2007). Meanwhile, *secY* encoding a transmembrane transporter was significantly upregulated (Figure 4A), suggesting that the activity of protein export was strengthened due to the high protein production.

PROTEOMIC ANALYSIS REVEALED THE MECHANISM OF ENHANCED PROTEIN EXPRESSION UNDER SMG

Under SMG condition, there might be differential expression clusters of proteins to cope with the enhanced recombinant protein production which can prevent protein misfolding and protein aggregation. In proteomics investigation, the number

TABLE 3 | Transcription changes of RNA polymerase genes.

Gene	Function descriptions	log ₂ (SMG/NG)	-lg(P-value)
<i>rpoA</i>	RNA polymerase subunit alpha	1.82	270.07
<i>rpoB</i>	RNA polymerase subunit beta	2.03	200.53
<i>rpoC</i>	RNA polymerase subunit beta'	1.72	134.96
<i>rpoZ</i>	RNA polymerase subunit omega	0.59	0.69

TABLE 4 | Transcription changes of glycolysis genes.

Gene	Function descriptions	log ₂ (SMG/NG)	-lg(P-value)
<i>chbF</i>	Monoacetylchitobiose-6-phosphate hydrolase	17.24	2.14
<i>glpX</i>	Fructose-1,6-bisphosphatase 2	16.02	0.57
<i>yggF</i>	Fructose 1,6-bisphosphatase	16.02	0.57
<i>fbaA</i>	Fructose-bisphosphatase aldolase class II	15.23	0.22
<i>ascB</i>	6-phospho-beta-glucosidase	15.08	0.40
<i>bglA</i>	6-phospho-beta-glucosidase A	15.08	0.40
<i>bglB</i>	6-phospho-beta-glucosidase B	15.08	0.40
<i>eutG</i>	Putative alcohol dehydrogenase in ethanolamine utilization	14.72	0.22
<i>glk</i>	Glucokinase	2.22	1.56
<i>ascF</i>	Beta-glucoside specific PTS enzyme IIBC component	1.05	0.32
<i>frmA</i>	S-(hydroxymethyl)glutathione dehydrogenase	1.02	1.42
<i>aceF</i>	Pyruvate dehydrogenase, E2 subunit	0.92	20.53
<i>aldB</i>	Aldehyde dehydrogenase B	0.91	3.69
<i>yeaD</i>	Putative aldose 1-epimerase	0.85	1.58
<i>pfkA</i>	6-phosphofructokinase I	0.82	1.40
<i>pgi</i>	Glucose-6-phosphate isomerase	0.64	0.11
<i>yiaY</i>	L-threonine dehydrogenase	0.64	0.11
<i>ptsG</i>	Glucose-specific PTS enzyme IIBC component	0.61	0.64
<i>pykF</i>	Pyruvate kinase I	0.54	1.59
<i>pykA</i>	Pyruvate kinase II	0.54	1.59
<i>aceE</i>	Pyruvate dehydrogenase E1 component	0.51	9.80
<i>ydbK</i>	Putative pyruvate-flavodoxin oxidoreductase	0.49	1.13
<i>acs</i>	Acetyl-CoA synthetase (AMP-forming)	0.36	5.54
<i>eno</i>	Enolase	0.36	1.31
<i>gpmA</i>	2,3-bisphosphoglycerate-dependent phosphoglycerate mutase	0.34	0.31
<i>agp</i>	Glucose-1-phosphatase	0.19	0.63
<i>lpd</i>	Lipoamide dehydrogenase	0.11	0.30
<i>adhP</i>	Ethanol dehydrogenase/alcohol dehydrogenase	0.09	0.01
<i>pck</i>	Phosphoenolpyruvate carboxykinase (ATP)	0.04	0.21
<i>pgm</i>	Phosphoglucumutase	-0.09	0.73
<i>pgk</i>	Phosphoglycerate kinase	-0.13	1.11
<i>gapA</i>	Glyceraldehyde-3-phosphate dehydrogenase A	-0.19	5.79
<i>crr</i>	Enzyme IIA(Glc)	-0.20	1.28
<i>fbp</i>	Fructose-1,6-bisphosphatase 1	-0.32	2.98
<i>adhE</i>	Aldehyde-alcohol dehydrogenase	-0.32	4.64
<i>tpiA</i>	Triose-phosphate isomerase	-0.36	1.95
<i>galM</i>	Galactose-1-epimerase	-0.53	0.30

TABLE 5 | Transcription changes of oxidative phosphorylation genes.

Gene	Function descriptions	log ₂ (SMG/NG)	-lg(P-value)
<i>nuoJ</i>	NADH:quinone oxidoreductase subunit J	1.20	2.54
<i>frdC</i>	Fumarate reductase membrane protein FrdC	1.19	0.92
<i>cydB</i>	Cytochrome bd-I ubiquinol oxidase subunit II	1.13	0.82
<i>appB</i>	Cytochrome bd-II ubiquinol oxidase subunit II	1.13	0.82
<i>nuoI</i>	NADH:quinone oxidoreductase subunit I	1.03	2.87
<i>nuoM</i>	NADH:quinone oxidoreductase subunit M	1.01	3.00
<i>nuoL</i>	NADH:quinone oxidoreductase subunit L	0.84	3.06
<i>nuoK</i>	NADH:quinone oxidoreductase subunit K	0.79	0.27
<i>nuoN</i>	NADH:quinone oxidoreductase subunit N	0.71	1.81
<i>atpA</i>	ATP synthase F1 complex subunit alpha	0.66	7.57
<i>atpH</i>	ATP synthase F1 complex subunit delta	0.64	1.98
<i>nuoF</i>	NADH:quinone oxidoreductase subunit F	0.60	2.95
<i>atpC</i>	ATP synthase F1 complex subunit epsilon	0.57	1.67
<i>atpB</i>	ATP synthase Fo complex subunit a	0.54	2.19
<i>nuoC</i>	NADH:quinone oxidoreductase subunit CD	0.52	3.85
<i>frdB</i>	Fumarate reductase iron-sulfur protein	0.49	0.78
<i>atpG</i>	ATP synthase F1 complex subunit gamma	0.48	1.83
<i>ndh</i>	NADH:quinone oxidoreductase II	0.47	0.85
<i>atpE</i>	ATP synthase Fo complex subunit c	0.38	0.36
<i>atpF</i>	ATP synthase Fo complex subunit b	0.36	1.37
<i>nuoG</i>	NADH:quinone oxidoreductase subunit G	0.36	2.30
<i>atpD</i>	ATP synthase F1 complex subunit beta	0.32	1.25
<i>sdhA</i>	Succinate:quinone oxidoreductase, FAD binding protein	0.31	5.46
<i>sdhB</i>	Succinate:quinone oxidoreductase, iron-sulfur cluster binding protein	0.30	2.10
<i>nuoE</i>	NADH:quinone oxidoreductase subunit E	0.20	0.33
<i>cyoB</i>	Cytochrome bo3 ubiquinol oxidase subunit 1	0.19	1.46
<i>frdA</i>	Fumarate reductase flavoprotein subunit	0.17	0.29
<i>sdhD</i>	Succinate:quinone oxidoreductase, membrane protein	0.04	0.08
<i>ppa</i>	Inorganic pyrophosphatase	0.01	0.16
<i>nuoH</i>	NADH:quinone oxidoreductase subunit H	-0.12	0.44
<i>cyoD</i>	Cytochrome bo3 ubiquinol oxidase subunit 4	-0.15	0.78
<i>cyoA</i>	Cytochrome bo3 ubiquinol oxidase subunit 2	-0.18	4.03
<i>cydA</i>	Cytochrome bd-I ubiquinol oxidase subunit I	-0.21	0.26
<i>appC</i>	Cytochrome bd-II ubiquinol oxidase subunit I	-0.21	0.26
<i>cyoC</i>	Cytochrome bo3 ubiquinol oxidase subunit 3	-0.22	2.10
<i>nuoB</i>	NADH:quinone oxidoreductase subunit B	-0.23	0.97
<i>sdhC</i>	Succinate:quinone oxidoreductase, membrane protein	-0.39	1.48
<i>nuoA</i>	NADH:quinone oxidoreductase subunit A	-0.54	1.94
<i>ppk</i>	Polyphosphate kinase	-0.81	6.17
<i>frdD</i>	Fumarate reductase membrane protein	-1.48	1.94

of the DEPs are identified as 69 (without IPTG induction) and 199 (with IPTG induction) under SMG, respectively, compared with NG. Without IPTG induction, 32 proteins were significantly upregulated and only 1 protein (*rpsS*) was drastically downregulated (Table S6). With the induction, 181 proteins were upregulated and 6 proteins were downregulated (Table S8). The large amount of upregulated proteins reflected that SMG not only improved the production of heterogenous proteins but also increased the expression of most of endogenous proteins. The DEPs were classified into three hubs: metabolism hub (TCA cycle, glycolysis/gluconeogenesis, fatty acid biosynthesis, amino acid metabolism, pyrimidine/purine metabolism), translation hub (RNA polymerase, ribosome), and folding/transport hub (chaperone, protein export) (Tables S7, S9). Similar to the result of transcriptome, the differential pathways from proteome still focused on carbon metabolism, translation, and protein transport. Chaperone was discovered differentially expressed at protein level, which was not found in the transcriptional level.

Protein–protein interactions were analyzed for deeper understanding (Figure 5). Without IPTG induction, chaperone proteins *groEL* (Hsp60), *dnaK* (Hsp70), and *clpB* (Hsp100) are mostly upregulated under SMG comparing to NG (\log_2 change fold was 2.03, 1.79, and 0.8, respectively) (Figure 5A). These proteins functioning as folding modulators are associated with inclusion body prevention. With the induction, we found that chaperones such as *dnaK*, *groEL*, *ibpA*, *clpB*, and *hspG* were all upregulated under SMG (\log_2 change fold was 3.02, 1.93, 1.88, 2.49, and 2.92, respectively) (Figure 5B). These upregulated DEPs suggested that SMG environment could enhance the translation and expression of chaperones to provide the suitable environment for correct protein folding.

It was found that proteins involving in Sec-dependent pathway also had differential expression levels under SMG. The upregulation of *secA*, *secB*, *ffh*, and *ftsY* showed that protein export is also an important step for high-efficient recombinant protein production (Figure 5).

In addition, a panel of enzymes involved in carbon metabolism was upregulated. For example, the expression of *glbA* (citrate synthase, a gatekeeper gene to TCA cycle) was upregulated by 2.81-fold (\log_2), which could improve energy metabolism and cell growth.

DISCUSSION

One of the obstacles for obtaining large amounts of recombinant proteins in *E. coli* is the inclusion bodies (De Marco, 2009). It is known that altering the growth conditions can affect soluble protein expression level by varying the folding environments of the recombinant protein, such as initial culture density, temperature, and duration of the expression stage (San-Miguel et al., 2013). Besides, the growth and induction of cells under heat-shock, osmotic stress, and osmole supplementation conditions have been shown to enhance solubility of some recombinant proteins (Harrison

and Bagajewicz, 2015). However, there is still a limitation for further improvement of the protein production. In this study, SMG can be regarded as a special environment due to the variation of gravity, mass transfer, and nutrient supply for cell to respond and thus have physiochemical changes. Several studies have found that SMG enhanced the production of recombinant proteins (Navran, 2007; Xiang et al., 2010; Huangfu et al., 2016). According to the omics analysis in this study, the crucial upregulated clusters under SMG are the groups of ribosomes/RNA polymerase genes, which directly contributed to the high-efficient protein synthetic ratio. Transcriptomic data of our study were compared with the previous studies about *P. aeruginosa* (Crabbé et al., 2011), *E. coli* K12 (Vukanti et al., 2008), and *Salmonella typhimurium* (Wilson et al., 2007). Most of the upregulated genes in the ribosome and RNA polymerase were in line with these previous studies. We have overexpressed certain ribosome genes which were significantly upregulated in this omics study (data not shown). Unfortunately, this approach resulted in unremarkable improvement of protein production because the overexpression of a few genes cannot increase the overall ribosome/RNA polymerase level, which was regulated by dozens of genes. To monitor ribosome dynamics or to map ribosome profiling might be helpful to improve protein production in the future. Chaperones demonstrated more of upregulation at proteomic level than that of the transcriptomic level under SMG. The overexpression of chaperones may be a result of the increased ribosome activity (ability to produce proteins). Thus, the highly expressed chaperones could reduce protein aggregation resulting in further improved recombinant protein quality. Previous studies suggested that folding modulators including *dnaK*, *clpB*, and *groL* were overexpressed as the culture temperature increases (Hoffmann and Rinas, 2010). Since the overexpression of heterologous protein was regarded as an intracellular stress which may aggravate protein misfolding, the upregulated chaperones can be helpful to prevent the formation of inclusion bodies (Baneyx and Mujacic, 2004). Sec system is the main pathway for protein secretion, in which *secY* and *secA* exert important roles (Allen et al., 2016). Our result showed that *secY* and *secA* were significantly upregulated at both transcriptomic and proteomic levels, respectively, which implicated the activity of protein export was substantially increased under SMG.

As known, because mRNAs would go through complicated translational regulations, there are always inconsistent genes/proteins between the transcriptomics and proteomics data, which can reflect cells undergoing different states. We analyzed both the consistent and inconsistent genes/proteins between the transcriptomics and the proteomics. Between the DEGs and DEPs, 108 genes/proteins were at the intersection in both the transcriptomics and proteomics profiling (Figure 6A). Ribosome and carbon metabolism were the two biggest clusters of the intersection, both of which accounted for 35% of the overlapped genes/proteins, followed by aminoacyl-tRNA biosynthesis (9%), glycine/serine/threonine metabolism (7%), RNA degradation (5%), oxidative phosphorylation (5%), and

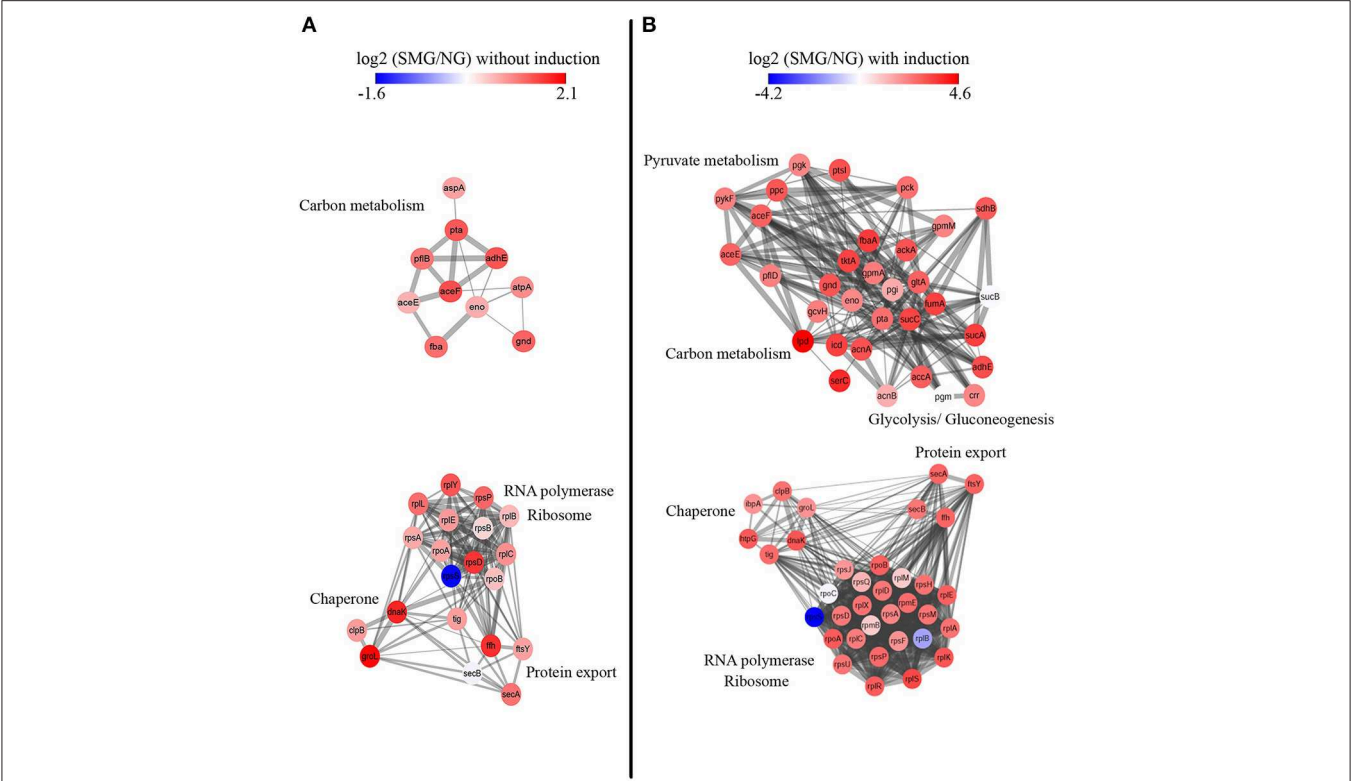


FIGURE 5 | Protein–protein interaction network analysis. STRING clusters represent proteins involved in carbon metabolism and RNA polymerase, ribosome, chaperone, and protein export. Proteins are colored either in red (representing upregulation) or in blue (representing downregulation) according to their differential expression levels. Left panel **(A)** is the proteins without IPTG induction, and right panel **(B)** is the proteins with IPTG induction.

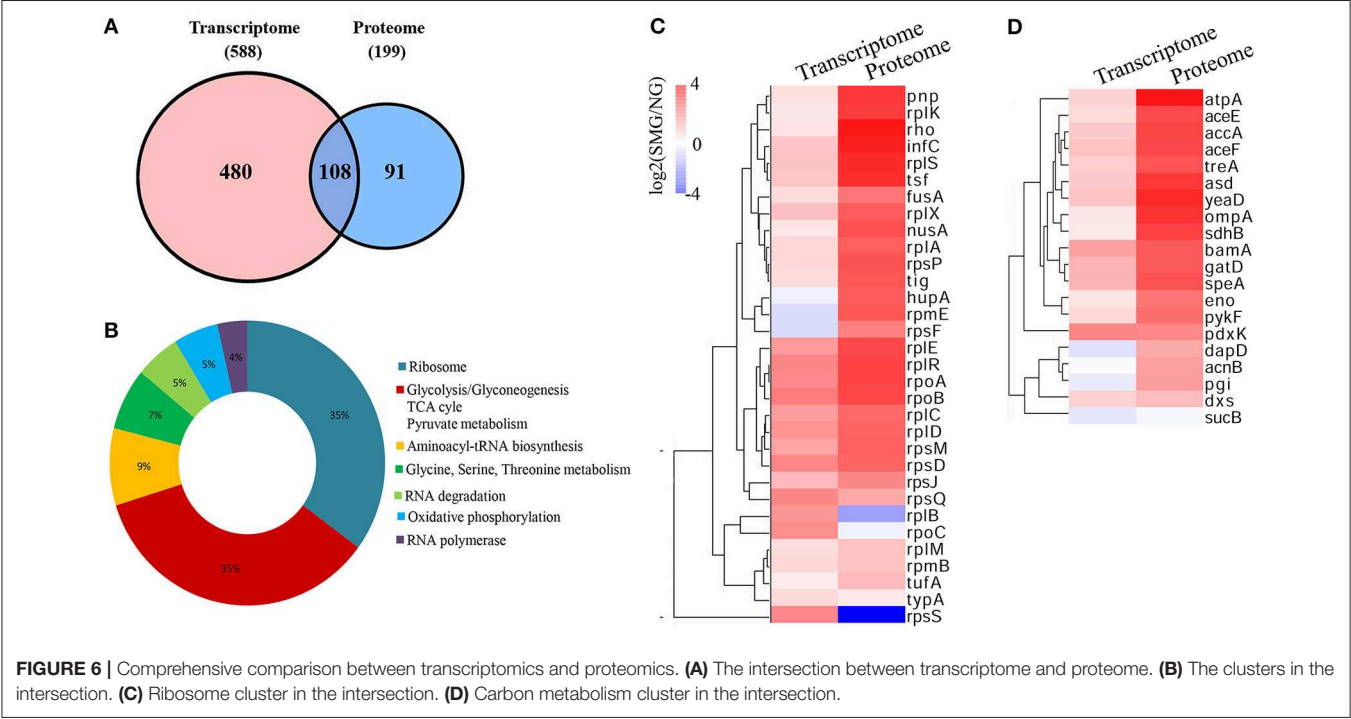


FIGURE 6 | Comprehensive comparison between transcriptomics and proteomics. **(A)** The intersection between transcriptome and proteome. **(B)** The clusters in the intersection. **(C)** Ribosome cluster in the intersection. **(D)** Carbon metabolism cluster in the intersection.

RNA polymerase (4%) (**Figure 6B**). Most of the ribosome and glycolytic enzymes are found more upregulated in the protein level than that in the transcription level under SMG, such as *rplA*, *eno*, *pykF*, etc. (**Figures 6C,D**). For example, *tig* (encoding the Trigger factor) is upregulated by 0.5-fold (\log_2) in transcriptomic level and 2.59-fold (\log_2) in proteomic level. Meanwhile, a few genes were not consistent between the transcriptomics and the proteomics. For example, *rplB* and *rpsS* were upregulated at transcriptional level, while their encoded proteins were downregulated under SMG (**Figure 6C**). This suggested that the SMG environment could influence the translation process of some specific mRNA in an unknown manner, which is an important subject and needs to be studied in depth in the future.

DATA AVAILABILITY STATEMENT

All datasets generated for this study are included in the article/**Supplemental Material**.

REFERENCES

- Allen, W. J., Corey, R. A., Oatley, P., Sessions, R. B., Baldwin, S. A., Radford, S. E., et al. (2016). Two-way communication between SecY and SecA suggests a Brownian ratchet mechanism for protein translocation. *Elife* 16:e15598. doi: 10.7554/eLife.15598.031
- Baker, P. W., Meyer, M. L., and Leff, L. G. (2004). *Escherichia coli* growth under modeled reduced gravity. *Microgravity Sci. Technol.* 15, 39–44. doi: 10.1007/BF02870967
- Baneyx, F., and Mujacic, M. (2004). Recombinant protein folding and misfolding in *Escherichia coli*. *Nat. Biotechnol.* 22, 1399–1408. doi: 10.1038/nbt1029
- Brown, R. B., Klaus, D., and Todd, P. (2002). Effects of space flight, clinorotation, and centrifugation on the substrate utilization efficiency of *E. coli*. *Microgravity Sci. Technol.* 13:24. doi: 10.1007/BF02881678
- Clerico, E. M., Tilitsky, J. M., Meng, W., and Gierach, L. M. (2015). How hsp70 molecular machines interact with their substrates to mediate diverse physiological functions. *J. Mol. Biol.* 427, 1575–1588. doi: 10.1016/j.jmb.2015.02.004
- Crabbé, A., Schurr, M. J., Monsieurs, P., Morici, L., Schurr, J., Wilson, J. W., et al. (2011). Transcriptional and proteomic responses of *Pseudomonas aeruginosa* PAO1 to spaceflight conditions involve Hfq regulation and reveal a role for oxygen. *Appl. Environ. Microbiol.* 77, 1221–1230. doi: 10.1128/AEM.01582-10
- De Marco, A. (2009). Strategies for successful recombinant expression of disulfide bond-dependent proteins in *Escherichia coli*. *Microbial Cell Factories* 8:26. doi: 10.1186/1475-2859-8-26
- Feng, S., Li, C., Xu, X., and Wang, X. (2006). Screening strains for directed biosynthesis of β -d-mono-glucuronide-glycyrrhizin and kinetics of enzyme production. *J. Mol. Catal. B Enzymat.* 43, 63–67. doi: 10.1016/j.molcatb.2006.06.016
- Frydman, J., and Hartl, F. U. (1996). Principles of chaperone-assisted protein folding: differences between *in vitro* and *in vivo* mechanisms. *Science* 272, 1497–1502. doi: 10.1126/science.272.5267.1497
- Gao, Q., Fang, A., Pierson, D., Mishra, S., and Demain, A. (2001). Shear stress enhances microcin B17 production in a rotating wall bioreactor, but ethanol stress does not. *Appl. Microbiol. Biotechnol.* 56, 384–387. doi: 10.1007/s002530100610
- Harrison, R. G., and Bagajewicz, M. J. (2015). Predicting the solubility of recombinant proteins in *Escherichia coli*. *Methods Mol. Biol.* 1258, 403–408. doi: 10.1007/978-1-4939-2205-5_23
- Hartl, F. U., and Hayer-Hartl, M. (2009). Converging concepts of protein folding *in vitro* and *in vivo*. *Nat. Struct. Mol. Biol.* 16, 574–581. doi: 10.1038/nsmb.1591
- Hayer-Hartl, M., Bracher, A., and Hartl, F. U. (2016). The GroEL–GroES chaperonin machine: a nano-cage for protein folding. *Trends Biochem. Sci.* 41, 62–76. doi: 10.1016/j.tibs.2015.07.009
- Hoffmann, F., and Rinas, U. (2004). Roles of heat-shock chaperones in the production of recombinant proteins in *Escherichia coli*. *Adv. Biochem. Eng. Biotechnol.* 89, 143–161. doi: 10.1007/b93996
- Hoffmann, F., and Rinas, U. (2010). Kinetics of heat-shock response and inclusion body formation during temperature-induced production of basic fibroblast growth factor in high-cell-density cultures of recombinant *Escherichia coli*. *Biotechnol. Prog.* 16, 1000–1007. doi: 10.1021/bp0000959
- Huangfu, J., Xu, Y., Li, C., and Li, J. (2016). Overexpressing target helper genes enhances secretion and glycosylation of recombinant proteins in *Pichia pastoris* under simulated microgravity. *J. Ind. Microbiol. Biotechnol.* 43, 1429–1439. doi: 10.1007/s10295-016-1817-8
- Jamal, A., Ko, K., Kim, H.-S., Choo, Y.-K., Joung, H., and Ko, K. (2009). Role of genetic factors and environmental conditions in recombinant protein production for molecular farming. *Biotechnol. Adv.* 27, 914–923. doi: 10.1016/j.biotechadv.2009.07.004
- Kaltschmidt, E., and Wittmann, H. G. N. (1970). Ribosomal proteins, XII. Number of proteins in small and large ribosomal subunits of *Escherichia coli* as determined by two-dimensional gel electrophoresis. *Proc. Natl. Acad. Sci. U.S.A.* 67, 1276–1282. doi: 10.1073/pnas.67.3.1276
- Navran, S. (2007). Rotary bioreactor for recombinant protein production. *Cell Technol. Cell Prod.* 567–569. doi: 10.1007/978-1-4020-5476-1_98
- Nickerson, C. A., Ott, C. M., Wilson, J. W., Ramamurthy, R., and Pierson, D. L. (2004). Microbial responses to microgravity and other low-shear environments. *Microbiol. Mol. Biol. Rev.* 68, 345–361. doi: 10.1128/MMBR.68.2.345-361.2004
- Ogle, J. M., Brodersen, D. E., Clemons, W. M., Tarry, M. J., Carter, A. P., and Ramakrishnan, V. (2001). Recognition of cognate transfer RNA by the 30S ribosomal subunit. *Science* 292, 897–902. doi: 10.1126/science.1060612
- Rosenzweig, J. A., Abogunde, O., Thomas, K., Lawal, A., Nguyen, Y.-U., Sodipe, A., et al. (2010). Spaceflight and modeled microgravity effects on microbial growth and virulence. *Appl. Microbiol. Biotechnol.* 85, 885–891. doi: 10.1007/s00253-009-2237-8
- San-Miguel, T., Pérez-Bermúdez, P., and Gavidia, I. (2013). Production of soluble eukaryotic recombinant proteins in *E. coli* is favoured in early log-phase cultures induced at low temperature. *Springerplus* 2:89. doi: 10.1186/2193-1801-2-89
- Shi, Y., Yang, X., Garg, N., and van der Donk, W. A. (2011). Production of lantipeptides in *Escherichia coli*. *J. Am. Chem. Soc.* 133, 2338–2341. doi: 10.1021/ja109044r

AUTHOR CONTRIBUTIONS

JH, HK, KX, and XN carried out the experiments and drafted the manuscript. JH, JL, and CL participated in experimental design and supported the experiments. LQ, JL, and CL conceived and coordinated the study and drafted the manuscript. All authors read and approved the final manuscript.

FUNDING

We gratefully acknowledge the financial support from the National Natural Science Foundation of China (21425624, 21576027, 21808013, and 21736002) and the Beijing Municipal Science and Technology Commission (Z181100005118009).

SUPPLEMENTARY MATERIAL

The Supplementary Material for this article can be found online at: <https://www.frontiersin.org/articles/10.3389/fbioe.2020.00030/full#supplementary-material>

- Takyar, S., Hickerson, R. P., and Noller, H. F. (2005). mRNA helicase activity of the ribosome. *Cell* 120, 49–58. doi: 10.1016/j.cell.2004.11.042
- Tucker, D. L., Ott, C. M., Huff, S., Fofanov, Y., Pierson, D. L., Willson, R. C., et al. (2007). Characterization of *Escherichia coli* MG1655 grown in a low-shear modeled microgravity environment. *BMC Microbiol.* 7:15. doi: 10.1186/1471-2180-7-15
- Vukanti, R., Mintz, E., and Leff, L. (2008). Changes in gene expression of *E. coli* under conditions of modeled reduced gravity. *Microgravity Sci. Technol.* 20:41. doi: 10.1007/s12217-008-9012-9
- Wilson, J., Ott, C., Zu Bentrup, K. H., Ramamurthy, R., Quick, L., Porwollik, S., et al. (2007). Space flight alters bacterial gene expression and virulence and reveals a role for global regulator Hfq. *Proc. Natl. Acad. Sci. U.S.A.* 104, 16299–16304. doi: 10.1073/pnas.0707155104
- Wilson, J. W., Ott, C. M., Ramamurthy, R., Porwollik, S., McClelland, M., Pierson, D. L., et al. (2002). Low-shear modeled microgravity alters the *Salmonella enterica* serovar Typhimurium stress response in an RpoS-independent manner. *Appl. Environ. Microbiol.* 68, 5408–5416. doi: 10.1128/AEM.68.11.5408-5416.2002
- Xiang, L., Qi, F., Dai, D., Li, C., and Jiang, Y. (2010). Simulated microgravity affects growth of *Escherichia coli* and recombinant β -D-glucuronidase production. *Appl. Biochem. Biotechnol.* 162, 654–661. doi: 10.1007/s12010-009-8836-0

Conflict of Interest: The authors declare that the research was conducted in the absence of any commercial or financial relationships that could be construed as a potential conflict of interest.

Copyright © 2020 Huangfu, Kim, Xu, Ning, Qin, Li and Li. This is an open-access article distributed under the terms of the Creative Commons Attribution License (CC BY). The use, distribution or reproduction in other forums is permitted, provided the original author(s) and the copyright owner(s) are credited and that the original publication in this journal is cited, in accordance with accepted academic practice. No use, distribution or reproduction is permitted which does not comply with these terms.



Pleiotropic Functions and Biological Potentials of Silver Nanoparticles Synthesized by an Endophytic Fungus

Radhika Chandankere^{1,2}, Jayabaskaran Chelliah², Kamalraj Subban², Vanitha C. Shanadrahalli², Amreesh Parvez¹, Hossain M. Zayed¹, Yogesh C. Sharma³ and Xianghui Qi^{1*}

¹ School of Food and Biological Engineering, Jiangsu University, Zhenjiang, China, ² Department of Biochemistry, Indian Institute of Science, Bengaluru, India, ³ Department of Chemistry, Indian Institute of Technology, Banaras Hindu University, Varanasi, India

OPEN ACCESS

Edited by:

Shihui Yang,
Hubei University, China

Reviewed by:

Hui Li,
Jiangnan University, China
YanJun Jiang,
Hebei University of Technology, China
Jiandong Cui,
Tianjin University of Science &
Technology, China

*Correspondence:

Xianghui Qi
qxh@ujs.edu.cn

Specialty section:

This article was submitted to
Synthetic Biology,
a section of the journal
Frontiers in Bioengineering and
Biotechnology

Received: 07 December 2019

Accepted: 03 February 2020

Published: 21 February 2020

Citation:

Chandankere R, Chelliah J, Subban K, Shanadrahalli VC, Parvez A, Zayed HM, Sharma YC and Qi X (2020) Pleiotropic Functions and Biological Potentials of Silver Nanoparticles Synthesized by an Endophytic Fungus. *Front. Bioeng. Biotechnol.* 8:95. doi: 10.3389/fbioe.2020.00095

In recent years, the biological synthesis of silver nanoparticles (AgNPs) from microorganisms has become an emerging trend for developing biocompatible nanomaterials that finds applications in nano and biomedical sectors. In the present study, we demonstrated a facile, green and eco-friendly method for AgNPs synthesis using the endophytic fungi (*Colletotrichum incarnatum* DM16.3) isolated from medicinal plant *Datura metel* and its *in vitro* antithrombin and cytotoxic activity. At first, biosynthesis of colloidal AgNPs was predicted by visual observation of color change and UV-visible spectra demonstrated specific surface plasmon resonance peak at 420 nm which confirmed the presence of nanoparticles. Microscopic analyses revealed the structure of highly aggregated, spherical and crystalline AgNPs in the diameter range of 5–25 nm. Transform infrared spectroscopy (FT-IR) spectral analysis confirmed the presence of probable biomolecules required for the reduction of silver ions. *In vitro* evaluation of thrombin activity demonstrates that AgNPs could exert strong inhibition against both thrombin activity (87%) and thrombin generation (84%), respectively. Further, *in silico* based mechanistic analysis yielded a better insight in understanding the probable amino acids responsible for AgNPs binding with thrombin protein. Similarly, *in vitro* cytotoxicity of synthesized AgNPs on human epithelial cells using MTT assay did not produce any substantial effects after 24 h exposure which indicates excellent biocompatibility nature, whereas notable toxicity was observed on human cancerous (HeLa) cells at 50 $\mu\text{g/mL}$ (IC_{50} value). In addition, assessment of AgNPs at 10 $\mu\text{g/mL}$ concentration via crystal violet method on biofilm forming Gram-positive (*Vibrio cholerae*) and Gram-negative bacteria (*Bacillus cereus*) revealed inhibition up to 85 and 46%, respectively. Overall, this study showed the possibility of microbially synthesized AgNPs as a potent inhibitor for managing acute thrombosis and highlighted their role for other biomedical applications.

Keywords: silver nanoparticles, antithrombin potential, endophytic fungus, biogenic synthesis, *Colletotrichum incarnatum*

INTRODUCTION

Fungal nanotechnology is an upcoming field of nanotechnology and it has consequently gained tremendous impetus in fabricating nanoparticles with a wide range of applications toward human welfare (Vivian et al., 2018). Metallic nanoparticles (NPs) are being employed in the field of agri-food, diagnostics, therapeutics, and medical device development, with fungal NPs recently used in application ranging from drug development to the pharmaceutical and food industries (Baker et al., 2015). Fungi are the preferred microorganisms as they are fast-growing, easy to handle and produce large quantities of proteins needed for the synthesis of NPs. Previously, different types of metal NPs have been biosynthesized namely, titanium, copper, zinc, gold, and silver (Mukherjee et al., 2001; Kirthi et al., 2011; Balakumaran et al., 2015; Jafarirad et al., 2016; Prabhu et al., 2017; Mohamed et al., 2019). Among these NPs, silver nanoparticles (AgNPs) are found to be superior, as they have a larger surface area that results in greater surface energy, catalytic activity, and biochemical reactivity (Syed and Ahmad, 2012; Neethu et al., 2018; Ying et al., 2018; Zhou et al., 2018). Some of the most commonly used fungal genera for the biosynthesis of AgNPs are *Fusarium*, *Trichoderma*, *Cladosporium*, *Aspergillus*, *Penicillium*, and *Phanerochaete* (Bhainsa and D'Souza, 2006; Vahabi et al., 2011; Syed and Ahmad, 2012; Neethu et al., 2018).

Recently, fungal-mediated AgNPs bound with herbal drugs have been found more beneficial and competent over conventional forms of drugs. Amongst fungi, not much work has been done on the fabrication of endophytic fungi from medicinal plants for the synthesis of AgNPs and reports are still limited (Singh et al., 2013). According to the literature, endophytic fungi are a promising source for drug discovery by providing a unique way of fabricating a range of AgNPs, which showed a broad pharmacologic potential (Loo et al., 2018; Naidu et al., 2019). Medicinal plant-derived endophytic fungi have received broad attention due to the unusual living environment, that is exposed to the high temperature and salinity (Vahabi et al., 2011). In this context, we have used *Datura metel* belonging to the Solanaceae family which is a widely distributed herb native to China and India and is described as the divine drug in the traditional medicines used for the treatment of a number of ailments. According to the literature, various endophytic microorganisms were isolated from *D. metel* that have various biological activities, such as anticancer, antioxidant, antimicrobial, anti-inflammatory, and antifungal (Narendra and Uday, 2014; Baker et al., 2015; Dakal et al., 2016; Loo et al., 2018; Majeed et al., 2018; Zhou et al., 2018).

Thrombosis is the formation/presence of a thrombus (blood clot), which hinders the flow of blood in blood vessels, resulting in abnormal coagulation. In other words, this coagulation caused by the bacterial infection is frequently related to the prothrombotic case as it came across the hemostatic abnormalities and further activates the coagulation factors ending up in the formation of unusual clots in the arteries and veins (Kuriakose et al., 2013). In brief, the key reason for the thrombosis in infection is due to the inhibition of fibrinolysis and the generation of tissue factor-mediated thrombin (Xiaowen et al., 2019). Henceforth,

antithrombotic drugs (ATPs) are essential to combat these disorders by hindering the thrombosis using thrombin inhibitors drugs. Previously, researchers have reported thrombin inhibitory activity of leaf and flower extracts of *Catharanthus roseus* (Kuriakose et al., 2013). According to the literature, any bioactive compound used for human welfare has to be assessed for its ecotoxicity (Chandankere et al., 2014). Also, it is reported that the plants need to be included to develop a comprehensive toxicity profile for NPs due to its low execution costs (Yin et al., 2012; Zhou et al., 2018). Therefore, based on the potential of AgNPs, the current study also aims to develop an innovative bioactive agent in eco-friendly fungal-based nanomaterials.

As the gamut of the research on various bioactive compounds from endophytic fungi harbored in medicinal plants (Singh et al., 2013; Rasool and Hemalatha, 2017), herein we have selected *D. metel* for isolation of a novel fungal isolate. In the present study, *C. incarnatum* DM16.3 was isolated from the healthy leaves of *D. metel* and exploited for the biosynthesis of AgNPs. The novel finding of the present study is the demonstration of thrombin inhibitory activity of the AgNPs synthesized by *C. incarnatum* with an insight into its molecular simulation dynamics studies. The morphology and structure of the biosynthesized AgNPs were characterized using UV-visible absorption spectroscopy, scanning electron microscopy (SEM), and transform infrared spectroscopy (FT-IR). Subsequently, experiments were conducted for *in vitro* antibiofilm studies against the human pathogens and cytotoxic assay toward normal and cancerous cells. In addition, phytotoxicity of AgNPs was evaluated against the seeds of two model bio-indicator plants, namely *Cucumis sativus* and *Vigna radiata* to reveal the ecotoxicity of AgNPs.

MATERIALS AND METHODS

Chemicals and Biological Strains

Silver nitrate (AgNO₃) was purchased from HiMedia Laboratories Pvt. Ltd., Mumbai, India. All other fine chemicals were obtained from Sigma-Aldrich (HiMedia). The pathogenic indicator strains used in this study were Gram-negative bacteria (*Vibrio cholerae*) and Gram-positive bacteria (*Bacillus cereus*) that were procured from the Microbial Type Culture Collection, Chandigarh, India. Both strains were cultured in Luria Broth (HiMedia) at 37°C under aerobic conditions. All the cultures were stored at −80°C in broth supplemented with 20% glycerol.

Plant Material and Isolation of Endophytic Fungus

Healthy leaves of *D. metel* were collected from the nursery of the Indian Institute of Science campus, Bengaluru, India. The leaves were washed thoroughly with running tap water to remove epiphytic fungi. The leaf samples were then rinsed with sterile distilled water and treated with 20% commercial bleach supplemented with 0.1% Tween-20 for 5 min, followed by rinsing with sterile distilled water. The samples were soaked for 20 min in 100 mL solution consisted of (in 100 mL) fungicide; Bavistin (30 mg), Tetracycline (0.6 mg), and Rifampicin (0.6 mg)

supplemented with 0.1% Tween-20. After treatment, samples were rinsed with sterile distilled water. The surface-sterilized samples were cut into small segments (1–2 mm) aseptically. All the sterile segments were evenly placed on Petri dishes containing potato dextrose agar (PDA) medium supplemented with 100 mg/L ampicillin and incubated at $25 \pm 2^\circ\text{C}$ for 7 days. The Petri dishes were observed at regular intervals for the fungal growth and mycelia emerged from the surface of the leaf segments were transferred on to the fresh PDA plates, and incubated for 48 h.

Morphological and Identification of Endophytic Fungal Isolated

Photomicrographs of conidiogenous cells and conidia of the isolated fungal strain were taken by the phase-contrast microscope fitted with a camera by using a Zeiss light microscope (Olympus BX43). The mycelial samples, conidiogenous cells, and young and mature conidia were suspended in sterile distilled water and observed under $400\times$.

The fungal genomic DNA was isolated by sodium dodecyl sulfate (SDS) method as described previously (Das et al., 2018). Briefly, the strain was inoculated in the shake flask containing

250 mL PDA medium and incubated at $25 \pm 2^\circ\text{C}$ for 5 days. The mycelium was harvested by filtration through cheese cloth and blot dried. Two grams of mycelium were weighed and ground in liquid nitrogen using sterile mortar and pestle. The powdered samples were thoroughly mixed with 4 mL of extraction buffer [1 M Tris-HCl (pH 8.0), 0.5 M EDTA (pH 8.0), 10% SDS, and 5 M NaCl], 3 μL RNase A, and 10 μL β -mercaptoethanol, and incubated at 60°C for 1 h. subsequently, an equal volume of Tris-HCl (pH 8.0): water-saturated (2:2) phenol was added, mixed well and centrifuged at $6000 \times g$ for 5 min. The supernatant was removed and pellets were suspended in the equal volume of chloroform: isoamyl alcohol mixture (24:1) and centrifuged at $6000 \times g$ for 5 min. Later, the upper aqueous layer was mixed thoroughly with 0.1 vol of 3 M ammonium acetate and 2 vol of 100% ice-cold ethanol. The solution was incubated at -20°C overnight and centrifuged at $12,000 \times g$ for 15 min and the supernatant was discarded. Then the pellet was washed with 70% ice-cold ethanol by centrifugation at $7500 \times g$ for 5 min, air-dried and re-suspended in 100 μL of TE buffer/Sterile distilled water. DNA purity was ascertained from the A_{260}/A_{280} absorbance ratios. A master mix was prepared using the $10 \times$ Taq buffer, 10 mM dNTPs, Taq polymerase and pipetted into each PCR tubes along with 2 μL of primer (1 μL of forward and 1 μL of reverse primer) and 1 μL of purified DNA extract was added and the total concentration of each tube was made up to 25 μL using sterilized water.

To amplify the internal transcribed spacer (ITS) regions of the fungal endophyte, ITS 1 and 2 primers were used. ITS 1 (5'-TCCGTAGGTGAACCTGCGG-3') and ITS 2 (5'-GCTGCGTTCTTCATCGATGC-3') primers amplified the predicted ~ 300 -bp fragment. DNA was amplified in 25 μL of the reaction mixture in PCR tubes and the PCR tubes were given a small spin and were placed in a PCR thermocycler (MinicyclerTM, Germany) and programmed as follows: the thermal cycle consisted of initial denaturation at 94°C for 6 min, denaturation at 94°C for 50 s, annealing at 54°C for 50 s, extension at 72°C for 50 s, followed by 35 cycles and a final extension at 72°C for 10 min. The amplified DNA fragments were analyzed by agarose gel electrophoresis. Purification of the PCR product was done by GeneJETTM Gel Extraction kit, Fermentas and then send for sequencing at MWG Biotech Ltd., Bangalore, India.

Biosynthesis of Silver Nanoparticles

For the biosynthesis of AgNPs, *C. incarnatum* DM16.3 was grown in 250 mL Erlenmeyer flasks containing 100 mL of PDA broth medium (pH 7.0, adjusted by 10% Na_2CO_3). The culture was incubated on a rotary ($120 \times g$) shaker at $25 \pm 2^\circ\text{C}$ for 96 h. After incubation, the mycelia were harvested by filtering through Whatman filter paper No. 1 and washed thrice with sterile distilled water to remove any medium component. 10 g of harvested wet mycelial mass was then re-suspended in 100 mL of 1 mM aqueous solution of AgNO_3 in 250 mL Erlenmeyer flasks followed by incubation at the same condition mentioned above. The mycelium biomass was harvested after complete incubation by filtering through Whatman filter paper No. 1. This was followed by repeated washing with distilled

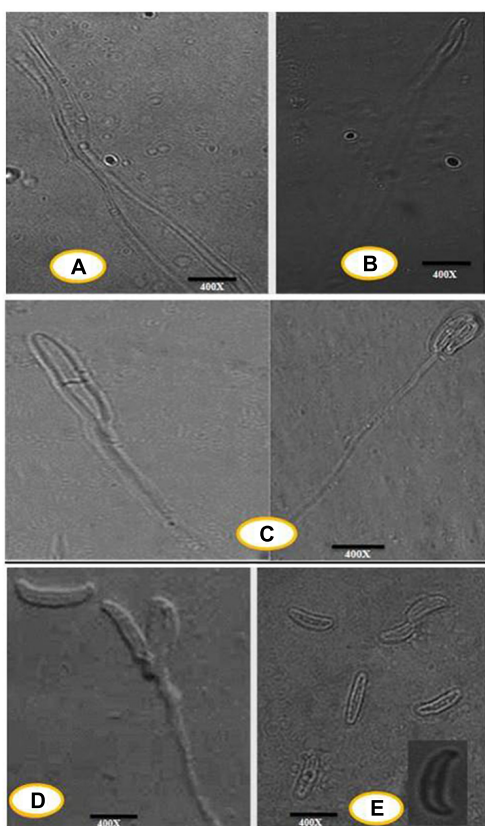


FIGURE 1 | (A) Progressive proliferation of conidiogenous cells developments X400. (B) Progressive proliferation accumulation of wall layers may eventually plug the opening X400. (C–D) Polyphialides (more than one conidiogenous locus) X400. (E) Young conidia, mature conidia (insert) X400.

water to remove any medium component from the biomass. Then, 10 g of harvested mycelium was re-suspended in 100 mL of 1 mM aqueous solution of AgNO_3 solution (prepared in deionized water) and incubated at same condition mentioned above. Concurrently, a positive control of incubating the fungus mycelium with deionized water was also maintained. After the incubation, the cell filtrate (CF) was obtained by passing it through Whatman filter paper No. 1. Later, the CF containing AgNPs was repeated centrifugation at $8000 \times g$ for 10 min and the pellets of AgNPs were re-dispersed into pure acetone. After air-drying of the purified AgNPs, they were stored at 4°C for further analysis.

Characterization of Silver Nanoparticles

Preliminary confirmation of AgNPs formed in the mycelium free fungal filtrate was done through visual observation of color change. The time-dependent formation of AgNPs was observed using a UV-visible spectrophotometer. Biosynthesized AgNPs were confirmed by sampling the reaction solution at regular intervals and the absorption spectra were scanned at a resolution of 1 nm between the wavelength of 300 and 700 nm in a spectrophotometer (SPECORD S-600, Analytik Jena, Germany).

For electron microscopy analysis, the fine powder of AgNPs was dispersed in ethanol on a carbon-coated copper grid. The grid was removed after 10 min and air-dried. The images

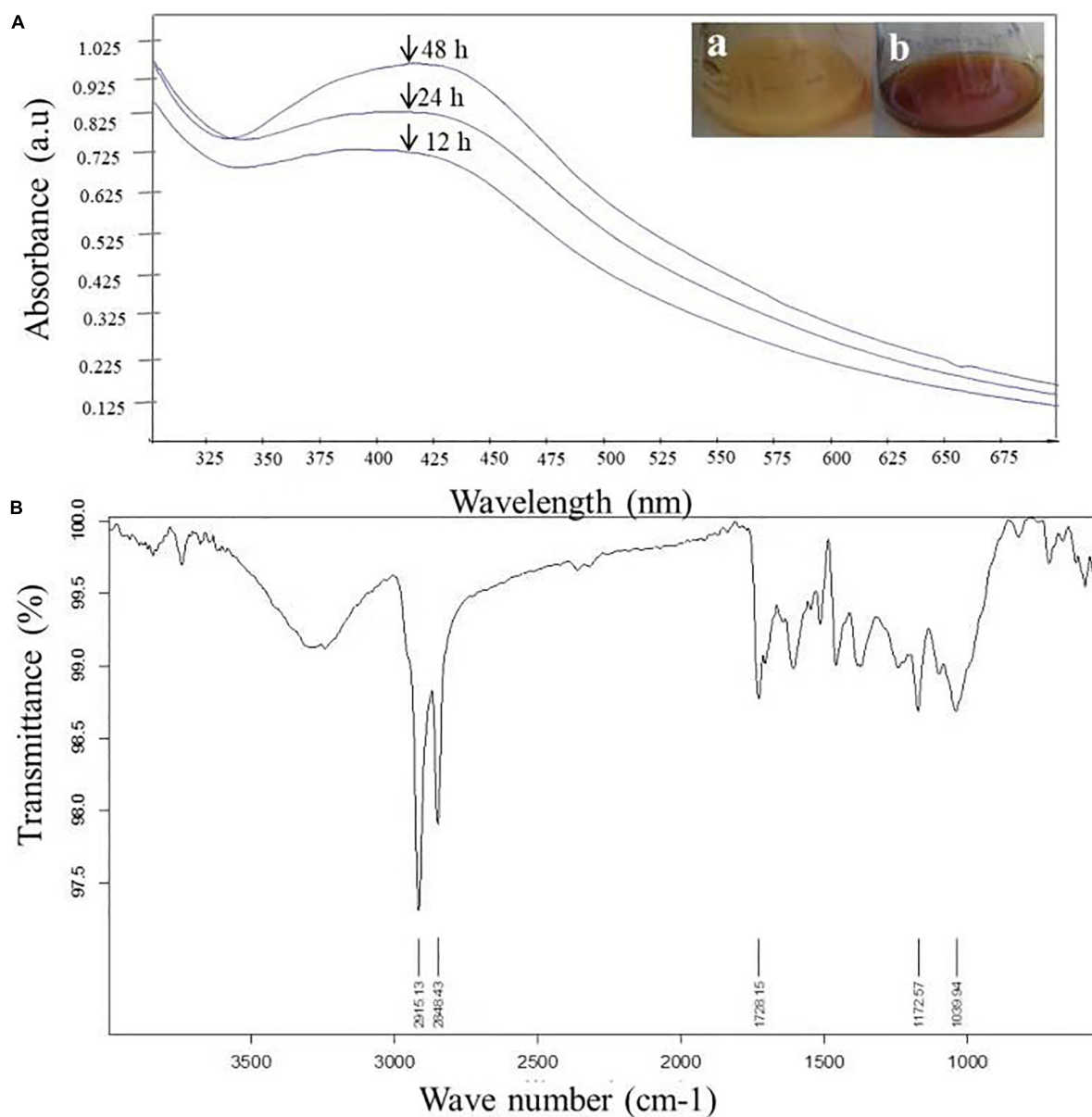


FIGURE 2 | (A) UV-Vis spectra of AgNPs from *C. incarnatum* DM16.3 at different times. **(B)** FTIR spectrum of biosynthesized AgNPs (Inset (a) Erlenmeyer flask with *C. incarnatum* DM16.3 before exposure and (b) after exposure to AgNO_3 ions). **(B)** FTIR spectrum of biosynthesized AgNPs.

of AgNPs were taken using transmission electron microscopy (TEM) assisted with energy-dispersive X-ray spectroscopy (EDX) (FEI Tecnai F30 S-TWIN). Further, the selected area electron diffraction (SAED) pattern was analyzed. For FT-IR analysis, the biosynthesized AgNPs synthesized were air-dried at room temperature. All the measurements were carried out in the range of 500–4000 cm^{-1} at a resolution of 4 cm^{-1} . The spectrum was recorded using a Cary 630 FT-IR instrument (Agilent, India). Different modes of vibrations were recognized and assigned to verify different functional groups present in the AgNPs extracted by *Colletotrichum* sp. DM16.3. All the data were corrected with the background spectrum.

For X-ray diffraction (XRD) analysis of AgNPs, a thin film of sample solution was spread evenly on an XRD grid and dried by using a vacuum dryer. XRD patterns were obtained on Shimadzu PS 7000 instrument operated at 40 kV and 30 mA with Cu K α 1 radiation (λ 1.54443). The diffracted intensities were recorded from 2 to 80° 2 θ angles. The thin film on silicon cover glass (1 mm \times 1 mm \times 1 mm) containing the dried AgNPs sample was analyzed using Atomic Force Microscope, followed by visualization under AFM (N6520B series 6000, Agilent, United States). The thermal behavior of biosynthesized AgNPs was carried out using Netzsch STA 409 thermal analysis system (Selb, Germany). About \sim 8 mg of dried

AgNPs sample was loaded on the platinum pan and heated under nitrogen atmosphere at 10°C min $^{-1}$ in the range of 20–1000°C. The analyses were performed under a gradual increase in temperature by plotting the weight percentage and heat flow against temperature.

Thrombin Inhibition Assay and *in silico* Studies

The antithrombin assay uses a synthetic substrate of thrombin, a tripeptide linked to an inactive fluorophore (AMC), called thrombin substrate III and was conducted as described in the literature (Chan and Don, 2013). Briefly, the aqueous crude AgNPs sample (5, 10, 25, 50, 100, 200 $\mu\text{g/mL}$) was incubated with Tris buffer, pH 7.5 in a black 96-well plate. Then thrombin substrate III was added (0.2 mM) followed by the addition of thrombin (1 U/mL). Ninety-six-well plate was read at 450 nm of emission and 390 nm of excitation in a fluorimeter (SpectraMax M5e, Molecular Devices, Inc., United States) (Neethu et al., 2018). The thrombin inhibition was calculated as the decrease in fluorescence by AgNPs compared to the control fluorescence.

For *in silico* studies, the X-ray crystallographic structure of thrombin protein (PDB: 1PPB) (Bode et al., 1989) was used for docking with Ag and fungal AgNP. The AgNP structure was

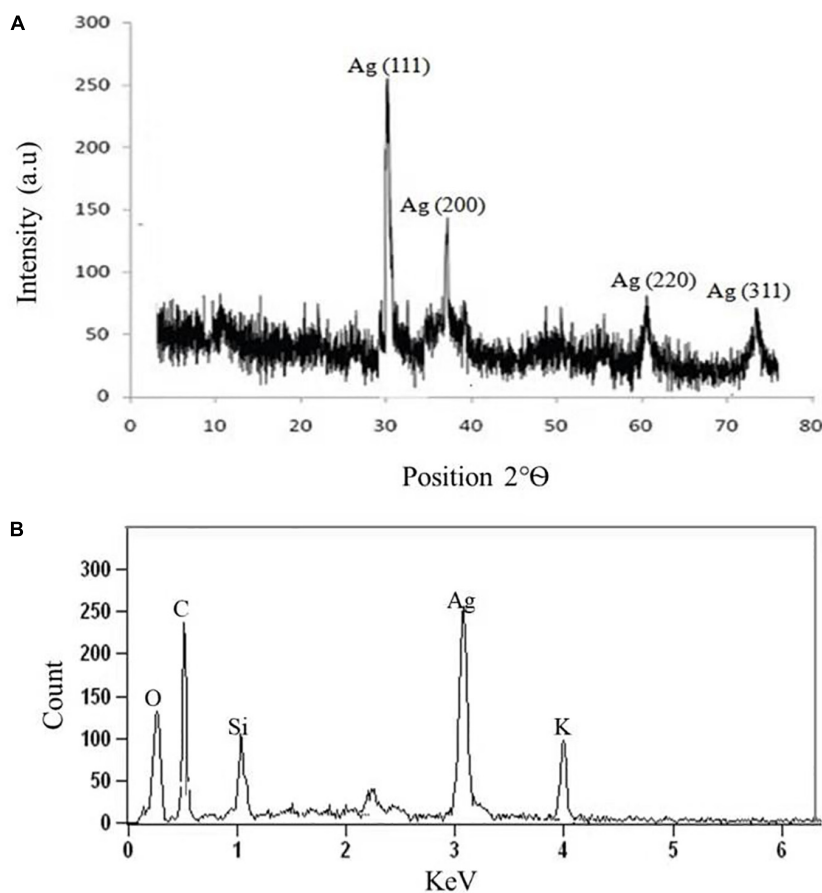


FIGURE 3 | (A) X-ray diffraction. **(B)** Energy dispersive X-ray spectra of biosynthesized AgNPs from *C. incarnatum* DM16.3.

provided by Dr. M. Bagheri of Tehran University of Medical Sciences (Kyrychenko et al., 2015). The AgNP structure for docking was prepared in the discovery studio visualizer to remove polyvinylpyrrolidone. Docking of the Ag and AgNP was done using PATCHDOCK server (Schneidman-Duhovny et al., 2005). All the molecular dynamics simulation for the interaction of Ag and AgNP with thrombin were performed using MDWeb server (Adam et al., 2012). The GROMACS full step was used for solvation and energy minimization followed by MD trajectory generation through GROMACS-NTP at 300K for 0.5 ns.

Thrombin Generation Assay

In this assay, the capacity of AgNPs that inhibits the thrombin generated from plasma was assessed. The 5-weeks-old specific-pathogen free rat was acclimatized for 1 week before conducting experiments. The animal handling was carried out in accordance with the guidelines of the Committee for the Purpose of Control and Supervision of Experiments on Animals (CPCSEA). All the procedures considered were in accordance with the Animal Care

and Use Committee of the National Institute of Food and Drug Safety Evaluation (NIFDS). The protocol was approved by the Institutional Animal Ethics Committees of Indian Institute of Science, Bangalore, India. Briefly, rat blood was collected via the abdominal aorta using a vacutainer tube containing sodium citrate and centrifuged at $5000 \times g$ for 10 min to collect plasma. The same assay conditions of the thrombin inhibition mentioned above (see section “Characterization of Silver Nanoparticles”) were followed, except that 200 μ L of rat plasma was used instead of Tris buffer and 7 μ L (0.045 U/mL) of thrombin was added. The thrombin added in this assay acted as an agonist to promote the generation of thrombin from rat plasma.

Biofilm Inhibition Assays

The effect of AgNPs was determined on the biofilm formation by both Gram-positive (*B. cereus*) and Gram-negative (*V. cholerae*) bacterial pathogens. Biofilm formation was carried out using a crystal violet assay in a 96-well polystyrene microliter plate using the modified method described earlier (Ezealisiji et al., 2017).

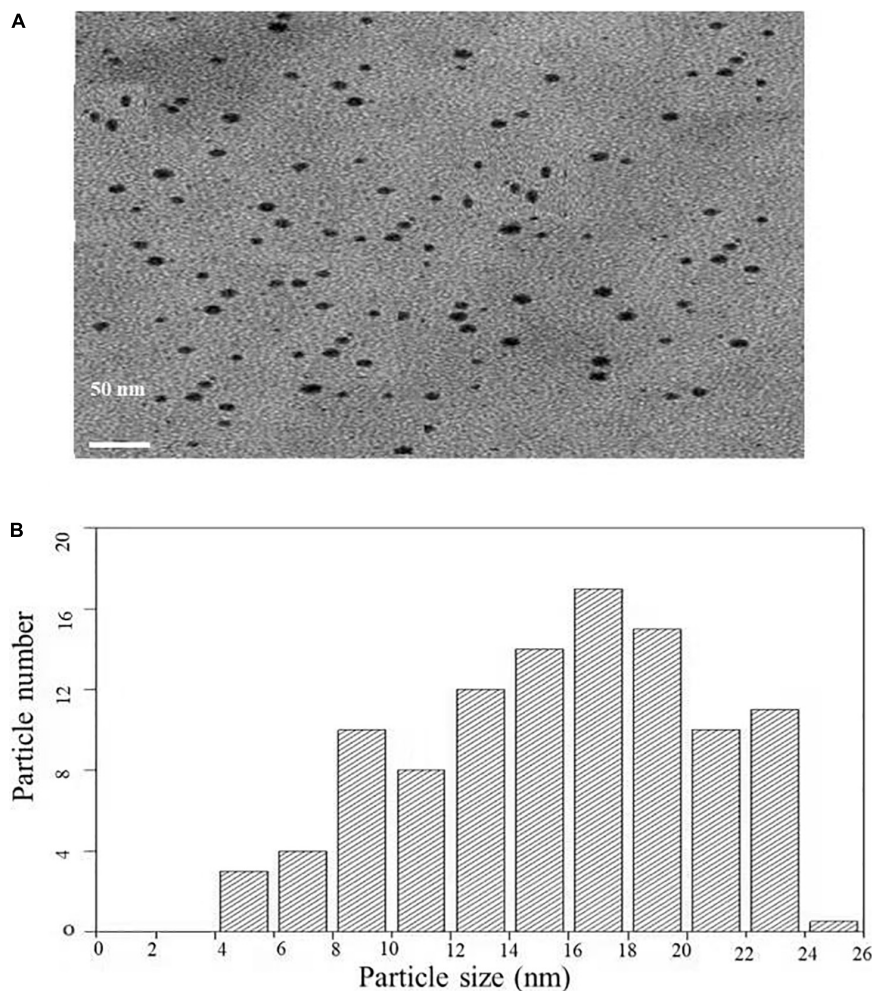


FIGURE 4 | (A) Transmission electron microscopic image of AgNPs biosynthesized from *C. incarnatum* DM16.3. **(B)** Histogram analysis of the particle size distribution.

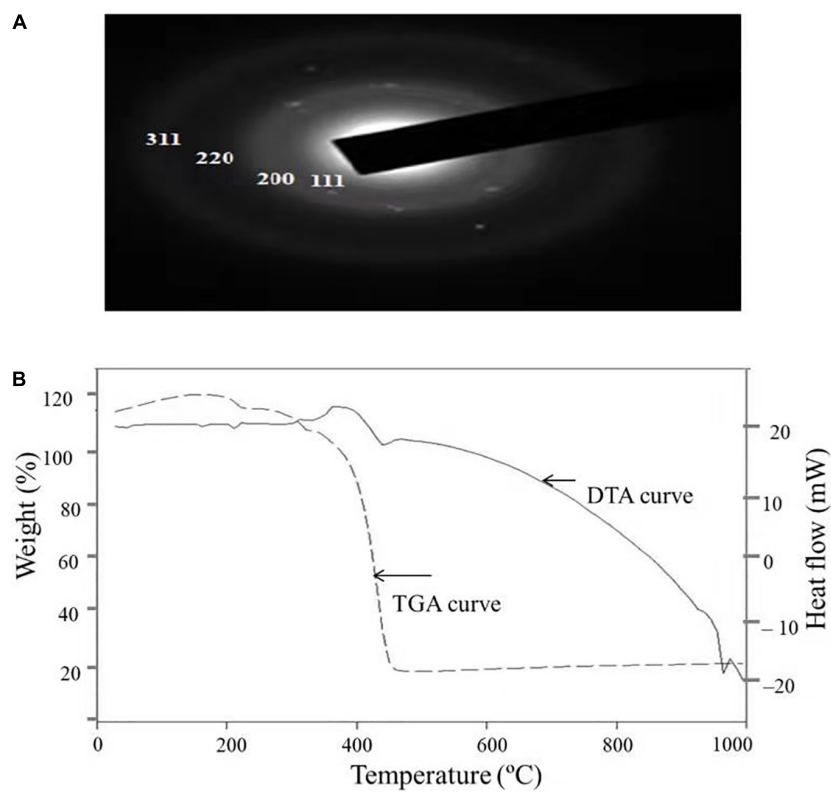


FIGURE 5 | (A) SAED patterns of the AgNPs. **(B)** TGA-DTA thermogram of biosynthesized AgNPs from *C. incarnatum* DM16.3.

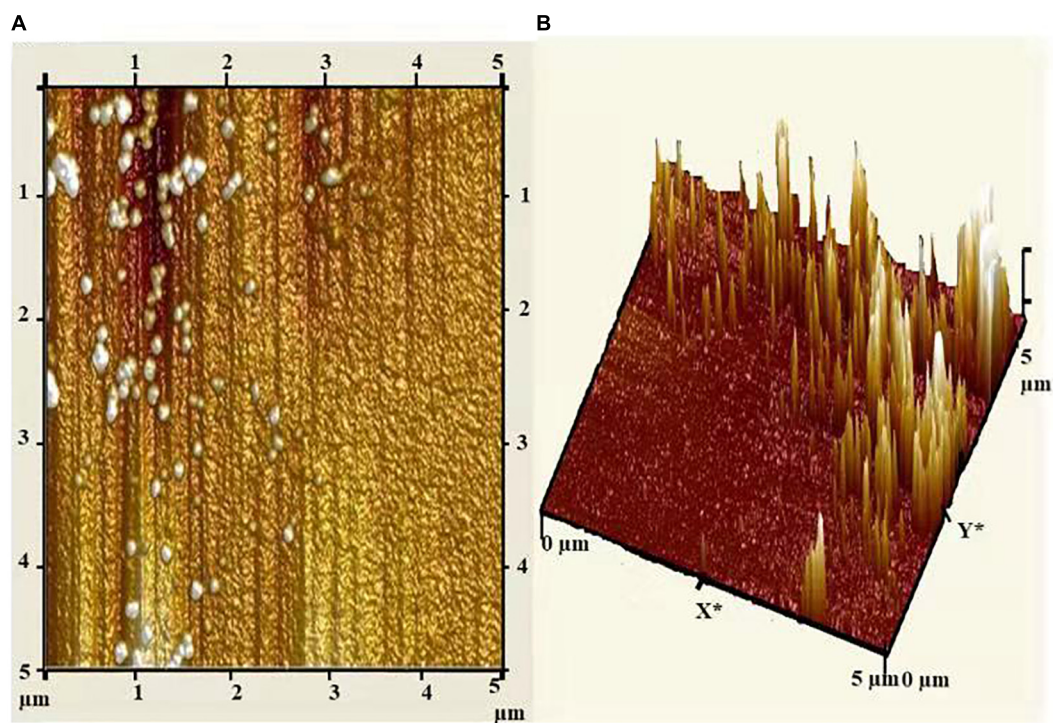


FIGURE 6 | (A) Atomic force micrograph, and **(B)** topographical image of biosynthesized AgNPs from *C. incarnatum* DM16.3.

Briefly, individual wells of the sterile microliter plate were filled with 160 μL of LB broth and inoculated with 20 μL of individual overnight grown bacterial suspension (0.6 OD at 600 nm). To the mixture, 20 μL of AgNPs solution at different concentration (0.25, 0.5, 1, 2, 5, and 10%) was added. The microliter plate was incubated for 24 h at 37°C. After incubation, the medium was discarded and gently washed with phosphate buffer saline (pH 7.2). A volume of 200 μL of a crystal violet dye (0.1%, w/v) was inoculated to each well and left for 15 min at the ambient temperature of 25°C. Then, the excess stain was rinsed off by thorough washing with sterilized Millipore water and plates were kept for drying. After drying, 200 μL of 95% (v/v) ethanol was added to the wells. The absorbance at 620 nm was measured on an ELISA reader, and values obtained were considered as an index of bacteria adhering to the surface of well wall for developing biofilms. All the experiments were performed in triplicates. The percentage of biofilm inhibition was calculated using the equation:

$$\text{Biofilm inhibition (\%)} = 100 - [\text{OD}_{620} \text{ of cells treated with AgNPs} \times 100] / \text{OD}_{620} \text{ of non - AgNPs control}]$$

Cytotoxicity Assay

The cytotoxicity of fungal AgNPs was evaluated by the cell viability assay [MTT [3-(4,5-dimethylthiazol-2-yl)-2,5-diphenyltetrazolium bromide] carried on HeLa (human cervical carcinoma) cell line as described earlier (Das et al., 2018). Briefly, cells were grown in Dulbecco's Modified Eagle's medium (DMEM) supplemented with 10% FBS (fetal bovine serum) in a CO₂ incubator at 37°C for 24 h under 5% CO₂. Penicillin and streptomycin each of 100 $\mu\text{g}/\text{mL}$ concentration, respectively were added to the medium to prevent microbial growth. After the incubation period, the cells grown in 96-well flat-bottom plates were treated with different concentrations of AgNPs ranging between 5 and 100 $\mu\text{g}/\text{mL}$. Then, 10 μL of 5 mg/mL MTT solution in PBS was added to each well and incubated for 2 h at 37°C. The plate was then read at 570 nm in an ELISA reader. The results were expressed as the percentage of cell viability against the control without treatment of AgNP. The percentage of 50% of cell viability (IC₅₀) was calculated using the equation:

$$\text{Cell viability (\%)} = \left(\frac{\text{OD}_{570} \text{ of AgNPs treated cells}}{\text{OD}_{570} \text{ untreated cells}} \right) \times 100$$

Phytotoxicity Assessment

The toxicity assessment of AgNPs was conducted by phytotoxicity assay based on the seed germination and root elongation of selected crop seeds using the method discussed by Chandankere et al. (2014), with slight modifications. *Cucumis sativus* (cucumber) and *V. radiata* (Mung bean) crop seeds were selected as bio-indicators. In brief, ten seeds were dipped in 5% Sodium hypochlorite solution for 30 min to ensure seed surface sterility and then soaked with AgNPs solution

overnight. The seeds soaked in normal tap water were treated as control. Five milliliter of AgNPs solution was dispensed into a sterilized Petri-plate with Whatman filter paper No. 1 and the treated seeds were kept on the filter paper. Finally, Petri-plates were covered and incubated at room temperature for 5 days. Thereafter, the germination percentage and root elongation were estimated. Distilled water and AgNO₃ were used as positive and

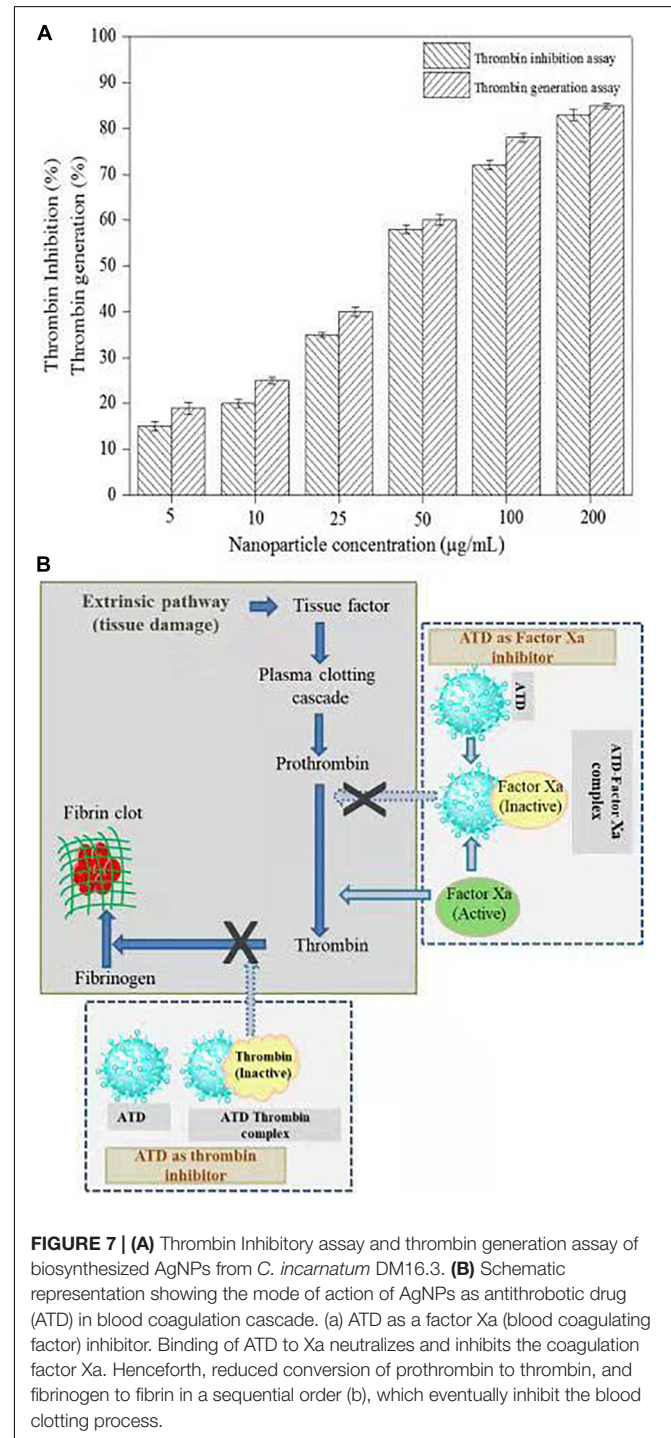


FIGURE 7 | (A) Thrombin Inhibitory assay and thrombin generation assay of biosynthesized AgNPs from *C. incarnatum* DM16.3. **(B)** Schematic representation showing the mode of action of AgNPs as antithrombotic drug (ATD) in blood coagulation cascade. (a) ATD as a factor Xa (blood coagulating factor) inhibitor. Binding of ATD to Xa neutralizes and inhibits the coagulation factor Xa. Henceforth, reduced conversion of prothrombin to thrombin, and fibrinogen to fibrin in a sequential order (b), which eventually inhibit the blood clotting process.

negative control, respectively. Finally, the germination index was calculated as:

$$GI (\%) = [(Sg_{NP}/Sg_c) \times (Re_{NP}/Re_c)] \times 100,$$

where GI is the germination index; Sg_{NP} and Sg_c are the seed germinated in AgNPs treated and control, respectively; Re_{NP} and Re_c are the root elongation in AgNPs treated and control, respectively.

RESULTS AND DISCUSSION

Isolation and Identification of Endophytic Fungus

An efficient AgNPs producing endophytic fungal isolate, designated as DM16.3, was successfully isolated from the leaf segment of *D. metel*. Morphological identification of DM16.3 was done by colony characteristic examination. DM16.3 is opaque and smooth with black to green color, raised filamentous fungus as observed on the PDA plate (**Figure 1A**). **Figures 1A–E** represents the reproductive structures of isolated fungal strain DM16.3. The size of fusoid young conidia was in the range of $3\text{--}9 \times 1.1\text{--}2.0 \mu\text{m}$, produced in chains or single long lateral phialides. Macroconidia were fusoid and sickle-shaped with one or two septa, and $22\text{--}35 \times 2.1\text{--}3.3 \mu\text{m}$ in size. **Supplementary Figure S1** represents the agarose gel electrophoresis image showing partial rDNA ITS sequence (~ 250 bp) from DM16.3 by genomic PCR. The result of BLASTn showed that the isolate DM16.3 was highly homologous to species from class Sordariomycetes and phylum Sordariomycete. The ITS region of rDNA sequences of DM16.3 showed 99% similarity to *Colletotrichum incarnatum* and sequence analyzed with NCBI GenBank accession number KT358850. In the present paper, the fungal strain DM16.3 is designated as *C. incarnatum* DM16.3.

Characterization of Silver Nanoparticles

UV-Visible Spectral Analysis

The very first visual observation of biogenic synthesized NP is color change. On the exposure to 1 mM of silver ion solution, the initial yellow colored CF of *C. incarnatum* DM16.3 turned into dark brown color solution, while the control flask remained unchanged after the 48 h incubation period. The color change of cell filtrate was probably due to the surface plasmon vibrations of the synthesized NPs. **Figure 2A** represents the UV-visible spectra recorded from the *C. incarnatum* DM16.3 reaction flask at different time intervals. The characteristic surface plasmon absorption peaks were recorded at 420 nm, which further confirmed the formation of AgNPs. These observations are in agreement with what was reported in an earlier study (Chan and Don, 2013).

Fourier Transform Infrared Analysis

Figure 2B depicts the FTIR spectrum of the freeze-dried powder of AgNPs. It was carried out to discover the potential contact among silver and biomaterial, which could be responsible for the synthesis of AgNPs. The results demonstrated five distinct

peaks at 1172, 1728, 2848, 2915, and 3285 cm^{-1} . The peaks at 1728 and 3285 cm^{-1} corresponds to the binding vibration of amide I and II groups of proteins, respectively, with N-H stretching. The peaks at 2915 and 1172 could represent the methylene group and carboxylic group (C-O stretching) of the proteins, respectively (Balaji et al., 2009). These results support the presence of protein on the surface of the NPs synthesized by *C. incarnatum* DM16.3. Our finding was in concurrence with Nithya and Ragunathan (2012), who reported that proteins present in the fungal filtrate can act as the capping agent for bio-reduction and stabilization of AgNPs.

X-Ray Diffraction Analysis

The crystalline nature of AgNPs synthesized by *C. incarnatum* DM16.3 was studied with XRD analysis. Intense XRD peaks at 2θ values of 32.01, 38.29, 63.21, and 75.48° assigned to the planes of (111), (200), (220), and (311), respectively, were obtained ranging from 10 to 80° (**Figure 3A**). The values concur well with those reported for silver (face centric cubic) by the Joint Committee on Powder Diffraction Standards file no. 04-0783, indicating the crystalline nature of Ag. Many researchers have also reported the crystalline nature of AgNPs using various fungal endophytes (Balaji et al., 2009; Baker et al., 2015).

A representative EDX pattern (**Figure 3B**) confirms the presence of Ag in support of XRD results. These results clearly showed the crystalline nature of AgNPs formed by endophytic fungus *C. incarnatum* DM16.3 (Bhainsa and D'Souza, 2006). A strong optical absorption band in the silver region at approximately 3 eV revealed the presence of elemental silver along with the C and O signatures that might be from the stabilizing proteins presented as capping agents on the surface of AgNPs. Liang et al. (2017) reported the silver peak at 3 eV, which is typical for the absorption of AgNPs due to surface plasmon resonance confirming the presence of nanocrystalline elemental silver.

Transmission Electron Microscopy Analysis

Transmission electron microscopy analysis was carried out to determine the size and morphology of biosynthesized AgNPs. **Figure 4A** represents the TEM micrograph of well dispersed and spherical shaped AgNPs. The morphology of AgNPs is predominantly spherical in size ranging from 5 to 25 nm as observed in particle size histogram (**Figure 4B**). However, Balaji et al. (2009) reported the synthesis of AgNPs by *Fusarium oxysporum* which was found to be hexagonal and irregular in shape.

Figure 5A depicts the SAED pattern obtained from AgNPs. The SAED image exhibited four bright diffraction rings arising due to reflection from (111), (200), (220), and (311) planes of face centric cubic (fcc) silver which was supported by XRD results. These results confirm the nanocrystalline nature of the AgNPs synthesized by *C. incarnatum* DM16.3.

Thermal Properties and Atomic Force Microscopy Analysis

Thermal properties of any NP are considered as the important attributes for various industrial applications. Therefore, the thermal behavior of biosynthesized AgNPs was studied

thermogravimetric (TG) and differential thermal (DT) analysis and is depicted in **Figure 5B**. Apart from the gradual change in weight, the TG curve exhibited a drastic weight loss between 340 and 420°C. It was observed that the AgNPs was thermally stable up to 420°C after the weight loss of 13.75%, beyond which no

further weight loss occurred. The same was established by the exothermic peak observed at 420 in the DT curve which mainly attributed to the crystallinity of AgNPs. The results showed that complete thermal decomposition and crystallization of the sample occurred simultaneously (Xiaowen et al., 2019).

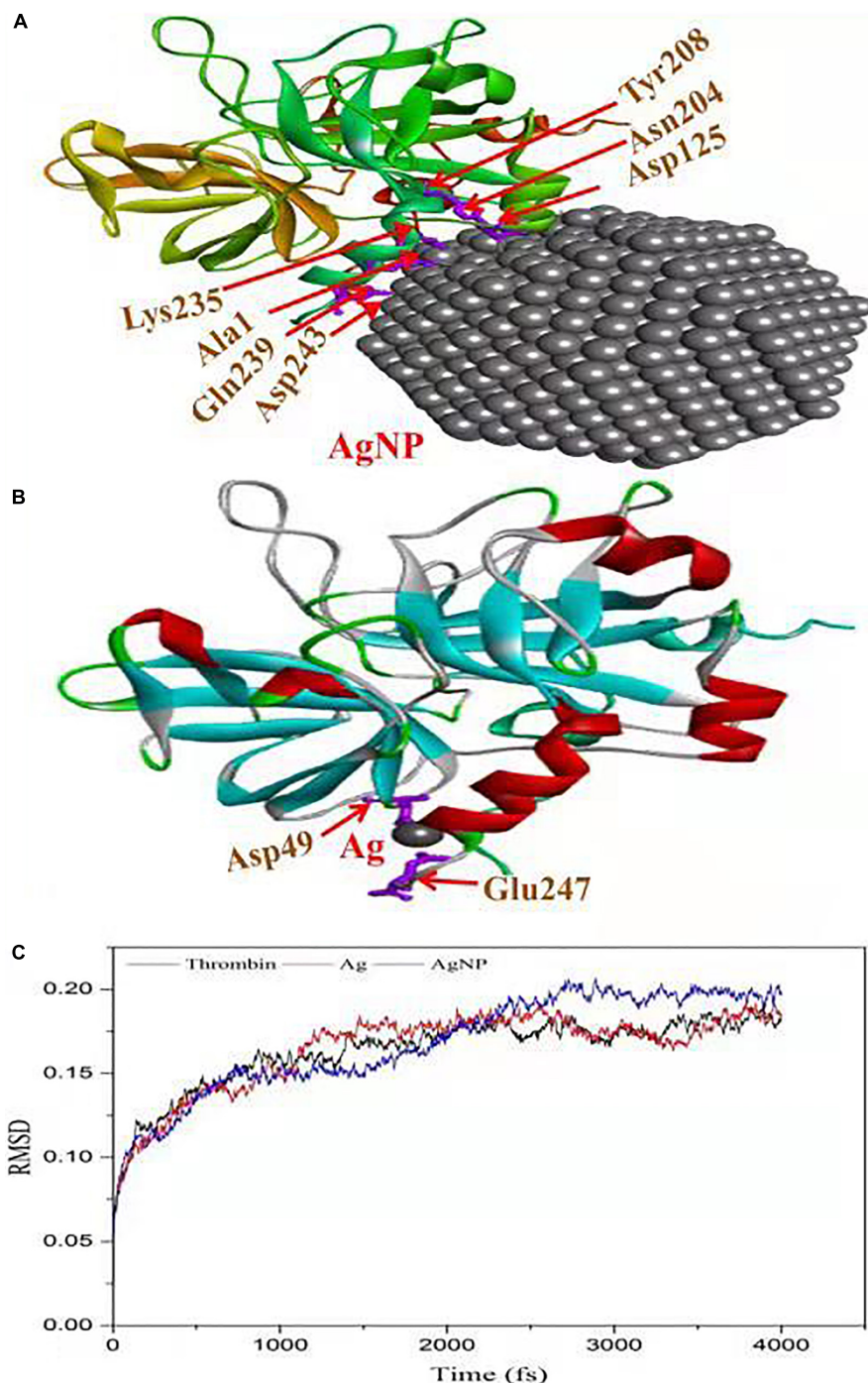


FIGURE 8 | Molecular docking of thrombin protein with AgNP and single Ag atom; **(A)** Orientation of AgNP and thrombin juxtaposed towards the various amino acid residues namely Asp243, Gln239, Ala1, Lys235, Asp125, ASN204 and Tyr208. **(B)** The docking model shows an interaction of Ag to thrombin through Asp49 and Glu2476. **(C)** RMSD analysis of molecular dynamics (MD) simulations for thrombin, Ag and AgNP.

Atomic force microscopy (AFM) analysis of biosynthesized AgNPs showed insight into the size, shape, and distribution of NPs. **Figure 6A** illustrated that the AgNPs were dispersed uniformly with an average particle size of 5–25 nm, which was in concurrence with TEM and XRD results. Furthermore, the topography of the picture demonstrated the three-dimensional structure of the NPs which is depicted in **Figure 6B**.

Biological Effect of Biosynthesized AgNPs

Thrombin Inhibition and Generation Assay

Thrombin is a serine protease that regulated hemostasis responsible in the formation of obstructive blood clots, also

known as thrombosis, that is a life-threatening condition related to many diseases such as stroke and cancer-associated thrombosis (Kuriakose et al., 2013). Henceforth, in the field of biomedical, there is an immense interest to develop an antithrombotic agent. In this context, AgNPs extracted from *C. incarnatum* DM16.3 was tested for thrombin inhibition capability. The AgNPs were incubated with the thrombin substrate at 5–200 µg/mL concentrations for 5 min, followed by the addition of thrombin (1 U/mL). With the treatment of AgNPs solution, there was 16, 21, 37, 56, 74, and 84% inhibition of thrombin activity at 5, 10, 25, 50, 100, and 200 µg/mL, respectively (**Figure 7A**). This result suggests that the synthesized AgNPs can exert thrombin inhibitory effect in a concentration-dependent manner. This, to the best of our knowledge, is the first report on the thrombin inhibitory effect of AgNPs synthesized from an endophytic fungus, *C. incarnatum* DM16.3. Earlier, Kuriakose et al. (2013) have reported similar thrombin inhibitory activity for leaf and flower extract of *C. roseus*. Nevertheless, its effect on endogenous thrombin generation potential has not been studied. Further in our studies, AgNPs inhibition of thrombin generation was carried out using rat plasma, which interestingly showed that AgNPs (200 µg/mL) could result in about 80% inhibition of thrombin generation activity. This result was concurrent with thrombin inhibition assay, where AgNPs exhibited 84% inhibition of thrombin activity. The authors have proposed the mode of action of AgNPs as an ATP and **Figure 7B** explicit the schematic representation showing the mode of action of AgNPs as ATD in the blood coagulation cascade.

The *in vitro* analysis of AgNPs revealed that it inhibited thrombin. In the next step, to assess and predict the biological interaction of AgNP with thrombin, molecular docking studies were carried out. The closest interacting amino acid residues which contribute to the binding of thrombin protein with AgNP and Ag are presented in **Figures 8A,B**, respectively. The docking study revealed that AgNP had interacted well with thrombin that might cause changes in the structure of the thrombin. In order to investigate the effect of Ag and AgNP on thrombin stability, molecular dynamics simulation was performed. Root mean square deviation (RMSD) was monitored to analyze structural stability over time. The average RMSD of thrombin, thrombin-Ag, and thrombin-AgNP complex were 0.1632, 0.1641, and 0.1679, respectively. In contrast to RMSD, thrombin and thrombin-Ag complex attained equilibrium state at 3000 fs, whereas thrombin-AgNP complex needed 0.15 ns to attain equilibrium (**Figure 8C**). Our MD simulation analysis revealed that AgNP binding had caused thrombin unstable, which was in concurrence with the *in vitro* thrombin inhibition analysis.

Cytotoxicity Assay

To evaluate the cytotoxicity of AgNPs, the normal cells (MCF-12A, human breast epithelial cell line) and cancerous cells (HeLa, human cervical carcinoma cell line) were treated with varying concentrations of AgNPs (5, 10, 25, 50, and 100 µg/mL) for 24 h. The biosynthesized AgNPs were found to have negligible toxicity and the viability of MCF-12A cells was slightly affected up to 100 µg/mL (**Figure 9**). The cell viability of MCF-12A was reduced to 6.73% at 100 µg/mL of AgNPs. Due to the negligible toxicity of

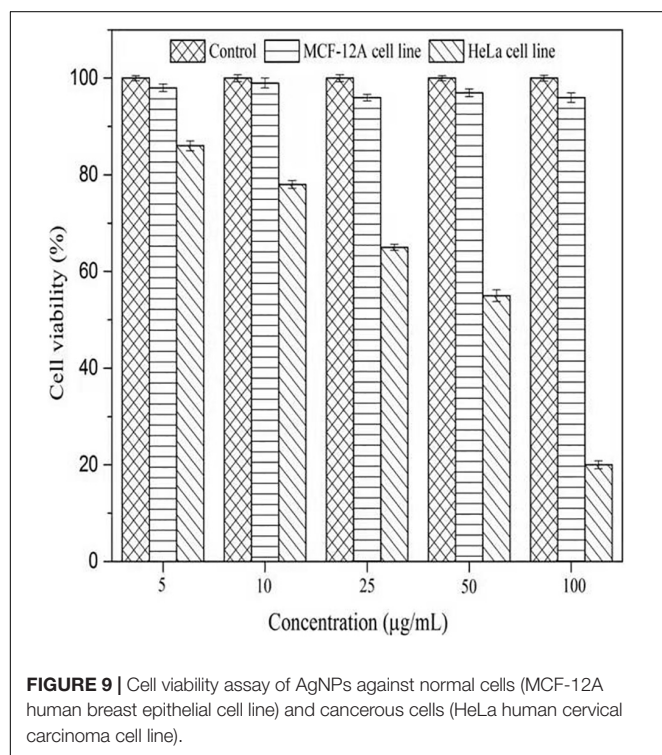


TABLE 1 | Inhibition of bacterial biofilm by different concentration of AgNPs synthesized by *C. incarnatum* DM16.3.

Microorganism	Concentration of AgNPs (µg/mL)	Biofilm inhibition (%)
<i>Vibrio cholerae</i>	0.25	29.5 ± 0.5
	0.5	37.2 ± 0.8
	1	45.1 ± 0.2
	2	58.6 ± 0.9
	5	69.0 ± 0.5
	10	85.1 ± 0.2
<i>Bacillus cereus</i>	0.25	15.1 ± 0.2
	0.5	23.9 ± 0.6
	1	29.3 ± 0.1
	2	34.7 ± 0.9
	5	40.1 ± 0.7
	10	45.6 ± 0.2

AgNPs against normal cell lines, *C. incarnatum* DM16.3 derived AgNP can be effectively used as an anticancer agent. In contrast, the viability was reduced in a dose-dependent manner in HeLa cell lines and the cytotoxicity of the AgNPs was observed with the inhibitory concentration (IC₅₀) value of AgNPs was 50 µg/mL. The cytotoxic effects of AgNPs might be due to the interference with the proper functioning of cellular proteins that thereafter provoked apoptosis by the mitochondrial pathway in HeLa cells (Liang et al., 2017). A significant reduction in the HeLa cell lines viability was observed at a higher concentration of AgNPs. The cell viability was reduced to 80.29% at 100 µg/mL. The cell viability was reduced by 6.73% in the case of MCF-12A and 80.29% for HeLa cell line at 100 µg/mL concentration. Xiaowen et al. (2019) showed IC₅₀ value to be 500 µg/mL of AgNPs against human breast carcinoma cell line (MDA-MB-231). But the effective doses used in these studies were considerably higher than those observed in the present study (IC₅₀, 50 µg/mL).

Antibiofilm Potential

The bacteria have the ability to form an organic polymer matrix referred as “biofilms” on the surface, which is involved in

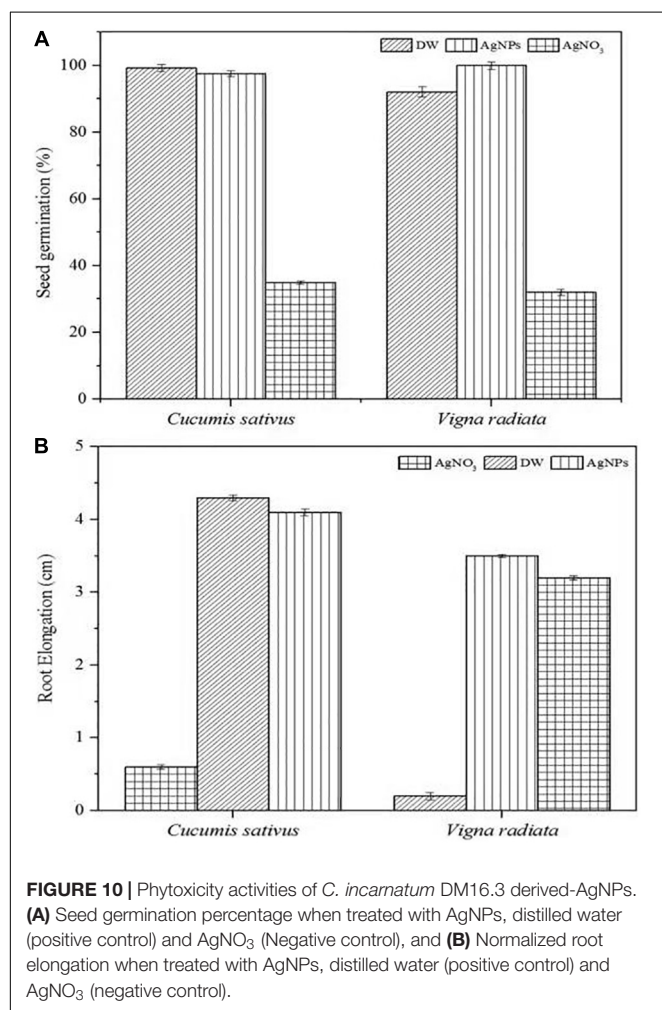
key problems associated with the medicine and food industry. According to Singh et al. (2013), AgNPs have a significant effect on microbial adhesion and biofilm disruption, which has become an effective method to diminish biofilm formation and combat colonization by pathogenic microorganisms. In the present study, extracted AgNPs were tested for biofilm inhibition potential against *B. cereus* (Gram-positive) and *V. cholerae* (Gram-negative) having known for their ability to form a biofilm. **Table 1** explicit the inhibition of bacterial biofilm by different concentrations of AgNPs synthesized by *C. incarnatum* DM16.3. Test organisms were grown in 96 µL plate wells with different concentrations (0.25–10 µg/mL) of AgNPs to form biofilm for 24 h. In both cases, the amount of biofilm formation was decreased by an increase in AgNPs concentration. The results illustrate that the activity of AgNPs is highest at the concentration of 10 µg/mL, with the inhibition rate of 85.1% (IC₅₀, 2 µg/mL) and ~46.5% against *Vibrio* sp. and *Bacillus* sp., respectively. From the results, it was observed that the AgNPs were better antibiofilm agents against the Gram-negative bacteria. This difference in the inhibitory activity of AgNPs might be due to the presence of an external layer with negative charges in Gram-negative bacteria that is attracted by the weak positive charge of the AgNPs (Dakal et al., 2016). In contrast, the Gram-positive bacteria presents a thick layer that reduces the binding of AgNPs (Magdi and Bhushan, 2005). Our results were in concurrence with the literature which reports significant inhibitory activities against Gram-negative bacteria (Xiaowen et al., 2019).

Phytotoxic Activity

The phytotoxic analyses of AgNPs were tested on the seeds of *C. sativus* and *V. radiata*. The phytotoxicity assay performed was based on seed germination and root elongation. The results revealed that the AgNPs obtained from *C. incarnatum* DM16.3 did not show any inhibitory effect on seed germination and root elongation against both the tested seeds when compared with the control that exhibited inhibitory characteristics. However, the highest seed germination (%) and root elongation were observed in *C. sativus* with 99.4% and 4.0 cm, whereas the lowest seed germination (%) and root elongation was obtained against AgNO₃ with 28.5% and 0.4 cm, respectively (**Figures 10A,B**). Interestingly, leaves and secondary root growth was noticed in both the tested seeds. Our observation was in agreement with Yin et al. (2012) who reported a non-appearance of phytotoxicity of the AgNPs against *Lolium multiflorum*. A growth index of 80% has been used as a bio-indicator to confirm the absence of phytotoxicity of the AgNPs (Jiang et al., 2018).

CONCLUSION

This study has shown that the endophytic fungus *C. incarnatum* DM16.3 isolated from the leaves of *D. metel* is a promising strain for the biosynthesis of AgNPs. Extensive characterization of the synthesized AgNPs revealed that these NPs were



spherical in shape with a size ranged from 5 to 25 nm. The composition and crystalline nature of AgNPs was confirmed by FTIR, XRD, EDS, and SAED analyses. This is the first report on the role of AgNPs been extracted by endophytic fungus *C. incarnatum* as a thrombin inhibiting agent. The *in silico* docking revealed that the AgNPs had interacted well with thrombin that might cause changes in the structure of the thrombin, further inhibited thrombin. The biosynthesized AgNPs were further tested for the antibiofilm activities and exhibited significant biofilm inhibition activities against Gram-negative bacterium. AgNPs also reported noteworthy cytotoxic by inhibiting the HeLa cell lines and non-toxic effect against normal cell lines. Furthermore, AgNPs have not exhibited any phytotoxic activities on seeds of crops claiming its safety to the environment. Thus, we conclude that the biosynthesized AgNPs may be used as a promising and eco-friendly drug agent in biomedical applications. Nevertheless, further research works, particularly *in vivo* studies should be carried out before AgNPs could be considered for biological application.

DATA AVAILABILITY STATEMENT

All datasets generated for this study are included in the article/**Supplementary Material**.

ETHICS STATEMENT

The animal handling was carried out in accordance with the guidelines of the Committee for the Purpose of Control and Supervision of Experiments on Animals (CPCSEA). All the procedures considered were in accordance with the Animal Care

and Use Committee of the National Institute of Food and Drug Safety Evaluation (NIFDS).

AUTHOR CONTRIBUTIONS

RC and JC designed the experiment and analyzed the data. RC and HZ wrote the manuscript. RC, VS, and AP conducted the experiment. YS contributed to the resources access. HZ and XQ contributed to the data interpretation and commented on the manuscript. XQ conceived and supervised the overall project. All authors listed have contributed to manuscript revision, read, and approved the submitted version.

FUNDING

The National Key R&D Program of China (Grant No. 2017YFC1600806), National Natural Science Foundation of China (Grant Nos. 31972042, 31950410550, and 31571806), China Postdoctoral Science Foundation (Grant Nos. 2019T120402 and 2017M621657), and high-level talents project of Six Talent Peaks in Jiangsu Province of China (Grant No. SWYY-018) supported this work. The authors are grateful to the University Grants Commission, New Delhi for providing financial assistance under the Dr. D. S. Kothari Post-doctoral Fellowship Scheme (No. F.4-2/2006 (BSR)/BL/14-15/0383).

SUPPLEMENTARY MATERIAL

The Supplementary Material for this article can be found online at: <https://www.frontiersin.org/articles/10.3389/fbioe.2020.00095/full#supplementary-material>

REFERENCES

- Adam, H., Pau, A., Carles, F., Cicin-Sain, D., Orozco, M., and Lius, J. (2012). MDWeb and MDMoby: an integrated web-based platform for molecular dynamics simulation. *Bioinformatics* 28, 1278–1279. doi: 10.1093/bioinformatics/bts139
- Baker, S., Kumar, K. M., Santosh, P., Rakshith, D., and Satish, S. (2015). Extracellular synthesis of silver nanoparticles by novel *Pseudomonas veronii* AS41G inhabiting *Annona squamosa* L. and their bactericidal activity. *Spectrochim. Acta A* 136, 1434–1440. doi: 10.1016/j.matlet.2011.05.077
- Balaji, D. S., Basavaraja, S., Deshpande, R., Mahesh, D. B., Prabhakar, B. K., and Venkataraman, A. (2009). Extracellular biosynthesis of functionalized silver nanoparticles by strains of *Cladosporium cladosporioides* fungus. *Coll. Surf. B* 68, 88–92. doi: 10.1016/j.colsurfb.2008.09.022
- Balakumaran, D., Ramachandran, R., and Kalaichelvan, P. T. (2015). Mycosynthesis of silver and gold nanoparticles: optimization, characterization and antimicrobial activity against human pathogens. *Microbiol. Res.* 178, 9–17. doi: 10.1016/j.micres.2015.09.009
- Bhainsa, K. C., and D'Souza, S. F. (2006). Extracellular biosynthesis of silver nanoparticles using the fungus *Aspergillus fumigatus*. *Coll. Surf. B* 472, 160–164. doi: 10.1016/j.colsurfb.2005.11.026
- Bode, W., Baumann, U., Huber, R., Stone, S. R., and Hofsteenge, J. (1989). The refined 1.9 Å crystal structure of human alpha-thrombin: interaction with D-Phe-Pro-Arg chloromethylketone and significance of the Tyr-Pro-Pro-Trp insertion segment. *EMBO J.* 8, 3467–3475. doi: 10.1002/j.1460-2075.1989.tb08511.x
- Chan, Y. S., and Don, M. M. (2013). Biosynthesis and structural characterization of Ag nanoparticles from white rot fungi. *Mat. Sci. Eng. C* 33, 282–288. doi: 10.1016/j.msec.2012.08.041
- Chandankere, R., Yao, J., Chai, M., Masakorala, K., Jain, A. K., and Choi, M. M. F. (2014). Properties and characterization of biosurfactant in crude oil biodegradation by bacterium *Bacillus methylotrophicus* USTBa. *Fuel* 122, 134–148. doi: 10.1016/j.fuel.2014.01.023
- Dakal, T. C., Kumar, A., Majumdar, R. S., and Yadav, V. (2016). Mechanistic basis of antimicrobial actions of silver nanoparticles. *Front. Microbiol.* 16:1831. doi: 10.3389/fmicb.2016.01831
- Das, M. P., Livingstone, J. R., Veluswamy, P., and Das, J. (2018). Exploration of *Wedelia chinensis* leaf-assisted silver nanoparticles for antioxidant, antibacterial and *in vitro* cytotoxic applications. *J. Food Drug Anal.* 26, 917–925. doi: 10.1016/j.jfda.2017.07.014
- Ezealisiji, M. K., Noundou, S. X., and Ukwueze, E. S. (2017). Green synthesis and characterization of monodispersed silver nanoparticles using root bark aqueous extract of *Annona muricata* Linn and their antimicrobial activity. *Appl. Nanosci.* 7, 905–911. doi: 10.1007/s13204-017-0632-5
- Jafarirad, S., Mehrabi, M., Divband, B., and Kosari-Nasab, M. (2016). Biofabrication of zinc oxide nanoparticles using fruit extract of *Rosa canina* and their toxic potential against bacteria: a mechanistic

- approach. *Mater. Sci. Eng. C* 59, 296–302. doi: 10.1016/j.msec.2015.09.089
- Jiang, K., Wu, B., Zhou, J., and Yanna, L. (2018). Silver nanoparticles with different particle sizes enhance the allelopathic effects of Canada goldenrod on the seed germination and seedling development of lettuce. *Ecotoxicology* 27, 1116–1125. doi: 10.1007/s10646-018-1966-9
- Kirthi, V. A., Rahuman, A. A., Rajakumar, G., Marimuthu, S., Santhoshkumar, T., Jayaseelan, C., et al. (2011). Biosynthesis of titanium dioxide nanoparticles using bacterium *Bacillus subtilis*. *Mater. Lett.* 65, 2745–2747. doi: 10.1016/j.matlet.2011.05.077
- Kuriakose, G. C., Krishna, T. H. A., Gudde, R. S., Jayabaskaran, C., and Surin, W. R. (2013). Thrombin-inhibitory activity of aqueous leaf and flower extract of *Catharanthus roseus*. *Int. J. Gen. Med. Pharm.* 2, 11–18.
- Kyrychenko, A., Korsun, O. M., Gubin, I. I., Kovalenko, S. M., and Kalugin, O. N. (2015). Atomistic simulations of coating of silver nanoparticles with poly(vinylpyrrolidone) oligomers: effect of oligomer chain length. *J. Phys. Chem.* 119, 7888–7899. doi: 10.1021/jp510369a
- Liang, M., Wei, S., Jian-Xin, L., Xiao-Xi, Z., Zhi, H., Wen, L., et al. (2017). Optimization for extracellular biosynthesis of silver nanoparticles by *Penicillium aculeatum* Su1 and their antimicrobial activity and cytotoxic effect compared with silver ions. *Mater. Sci. Eng. C* 77, 963–971. doi: 10.1016/j.msec.2017.03.294
- Loo, Y. Y., Rukayadil, Y., Nor-Khaizura, M. A. R., Kuan, C. H., Chieng, B. W., Nishibuchi, M., et al. (2018). In vitro antimicrobial activity of green synthesized silver nanoparticles against selected gram-negative foodborne pathogens. *Front. Microbiol.* 9:1555. doi: 10.3389/fmicb.2018.01555
- Magdi, H. M., and Bhushan, B. (2005). Extracellular biosynthesis and characterization of gold nanoparticles using the fungus *Penicillium chrysogenum*. *Microsyst. Technol.* 21, 2279–2285. doi: 10.1007/s00542-015-2666-5
- Majeed, S., Danish, M., Husna, A., Zahrudin, B., and Das, G. K. (2018). Biosynthesis and characterization of silver nanoparticles from fungal species and its antibacterial and anticancer effect. *Karbala Int. J. Mod. Sci.* 4, 86–92. doi: 10.1007/s10529-019-02699-x
- Mohamed, A. A., Fouda, A., Abdel-Rahman, M. A., El-Din, S. H., Gamal, M. S., Salem, S. S., et al. (2019). Fungal strain impacts the shape, bioactivity and multifunctional properties of green synthesized zinc oxide nanoparticles. *Biocatal. Agric. Biotechnol.* 19:101103. doi: 10.1016/j.bcab.2019.101103
- Mukherjee, P., Ahmad, A., Mandal, D., Senapati, S., Sainkar, S. R., Khan, M. I., et al. (2001). Bioreduction of AuCl₄⁻ ions by the fungus, *Verticillium* sp. and surface trapping of the gold nanoparticles formed. *Angew. Chem. Int. Ed. Eng.* 40, 3585–3588.
- Naidu, K. S., Murugan, N., Adam, J. K., and Serhsen, T. (2019). Biogenic synthesis of silver nanoparticles from avicennia marina seed extract and its antibacterial potential. *Bionanoscience* 9, 266–273. doi: 10.1007/s12668-019-00612-4
- Narendra, K., and Uday, M. (2014). Biosynthesis of metal nanoparticles: a review. *J. Nanotechnol.* 4, 62–70. doi: 10.1155/2014/510246
- Neethu, S. S., Midhun, S. J., Sunil, M. A., Soumya, S., and Jyothis, M. (2018). Efficient visible light induced synthesis of silver nanoparticles by *Penicillium polonicum* ARA 10 isolated from *Chetomorpha antennina* and its antibacterial efficacy against *Salmonella enterica* Serovar typhimurium. *J. Photochem. Photobiol. B* 180, 175–185. doi: 10.1016/j.jphotobiol.2018.02.005
- Nithya, R., and Ragunathan, R. (2012). Synthesis of silver nanoparticles using a probiotic microbe and its antibacterial effect against multidrug resistant bacteria. *Afr. J. Biotechnol.* 11, 1013–1021.
- Prabhu, T. Y., Rao, V. K., Sai, V. S., and Pavani, T. (2017). A facile biosynthesis of copper nanoparticles: a micro-structural and antibacterial activity investigation. *J. Saudi Chem. Soc.* 21, 180–185. doi: 10.1016/j.jscs.2015.04.002
- Rasool, U., and Hemalatha, S. (2017). Marine endophytic actinomycetes assisted synthesis of copper nanoparticles (CuNPs): Characterization and antibacterial efficacy against human pathogens. *Mater. Lett.* 194, 176–180. doi: 10.1016/j.matlet.2017.02.055
- Schneidman-Duhovny, D., Inbar, Y., Nussinov, R., and Wolfson, H. J. (2005). PatchDock and SymmDock: servers for rigid and symmetric docking. *Nuclear Acids* 33, 363–367. doi: 10.1093/nar/gki481
- Singh, D., Rathod, V., Ningangouda, S., Herimath, J., and Kulkarni, P. (2013). Biosynthesis of silver nanoparticle by endophytic fungi *Penicillium* sp. isolated from *Curcuma longa* (turmeric) and its antibacterial activity against pathogenic gram negative bacteria. *J. Pharm. Res.* 7, 448–453. doi: 10.1016/j.jopr.2013.06.003
- Syed, A., and Ahmad, A. (2012). Extracellular biosynthesis of platinum nanoparticles using the fungus *Fusarium oxysporum*. *Coll. Sur. B* 97, 27–31. doi: 10.1016/j.colsurfb.2012.03.026
- Vahabi, K., Mansoori, G. A., and Karimi, S. (2011). Biosynthesis of silver nanoparticles by fungus *Trichoderma reesei* (a route for large-scale production of AgNPs). *Insci. J.* 1, 65–79. doi: 10.5640/insc.010165
- Vivian, C., Lisa, O. G., and Tong, K. S. (2018). Synthesis of silver nanoparticles mediated by endophytic fungi associated with orchids and its antibacterial activity. *Mater. Today Proc.* 5, 22093–22100. doi: 10.1016/j.matpr.2018.07.074
- Xiaowen, H., Saravankumar, K., Jin, T., and Myeong-Hyeon, W. (2019). Mycosynthesis, characterization, anticancer and antibacterial activity of silver nanoparticles from endophytic fungus *Talaromyces purpureogenus*. *Int. J. Nanomed.* 14, 3427–3438. doi: 10.2147/IJN.S200817
- Yin, L., Colman, B. P., McGill, B. M., Wright, J. P., and Bernhardt, E. S. (2012). Effects of Silver nanoparticle exposure on germination and early growth of eleven wetland plants. *PLoS One* 7:47674. doi: 10.1371/journal.pone.0047674
- Ying, X. U., Shengzhe, L. U., WenXiao, F., Mei, C., Taofeng, H. E., Xinhui, L., et al. (2018). Preparation, characterization, pharmacokinetics and hemolytic test of bufalin-loaded polybutylcyanoacrylate nanoparticles. *Lat. Am. J. Pharm.* 37, 2434–2440.
- Zhou, Y., Huang, J., Shi, W., Wu, Y., Liu, Q., Zhu, J., et al. (2018). Ecofriendly and environment-friendly synthesis of size-controlled silver nanoparticles/graphene composites for antimicrobial and SERS actions. *Appl. Surf. Sci.* 457, 1000–1008. doi: 10.1016/j.apsusc.2018.07.040

Conflict of Interest: The authors declare that the research was conducted in the absence of any commercial or financial relationships that could be construed as a potential conflict of interest.

Copyright © 2020 Chandankere, Chelliah, Subban, Shanadrahalli, Parvez, Zabeed, Sharma and Qi. This is an open-access article distributed under the terms of the Creative Commons Attribution License (CC BY). The use, distribution or reproduction in other forums is permitted, provided the original author(s) and the copyright owner(s) are credited and that the original publication in this journal is cited, in accordance with accepted academic practice. No use, distribution or reproduction is permitted which does not comply with these terms.



Endogenous Type I CRISPR-Cas: From Foreign DNA Defense to Prokaryotic Engineering

Yanli Zheng, Jie Li, Baiyang Wang, Jiamei Han, Yile Hao, Shengchen Wang, Xiangdong Ma, Shihui Yang, Lixin Ma, Li Yi* and Wenfang Peng*

State Key Laboratory of Biocatalysis and Enzyme Engineering, Hubei Collaborative Innovation Center for Green Transformation of Bio-resources, Hubei Key Laboratory of Industrial Biotechnology, School of Life Sciences, Hubei University, Wuhan, China

OPEN ACCESS

Edited by:

C. Perry Chou,
University of Waterloo, Canada

Reviewed by:

Scott Bailey,
Johns Hopkins University,
United States
Matthew Wook Chang,
National University of Singapore,
Singapore

*Correspondence:

Li Yi
liy@hubu.edu.cn
Wenfang Peng
wenfang@hubu.edu.cn

Specialty section:

This article was submitted to
Synthetic Biology,
a section of the journal
Frontiers in Bioengineering and
Biotechnology

Received: 30 October 2019

Accepted: 24 January 2020

Published: 04 March 2020

Citation:

Zheng Y, Li J, Wang B, Han J,
Hao Y, Wang S, Ma X, Yang S, Ma L,
Yi L and Peng W (2020) Endogenous
Type I CRISPR-Cas: From Foreign
DNA Defense to Prokaryotic
Engineering.
Front. Bioeng. Biotechnol. 8:62.
doi: 10.3389/fbioe.2020.00062

Establishment of production platforms through prokaryotic engineering in microbial organisms would be one of the most efficient means for chemicals, protein, and biofuels production. Despite the fact that CRISPR (clustered regularly interspaced short palindromic repeats)-based technologies have readily emerged as powerful and versatile tools for genetic manipulations, their applications are generally limited in prokaryotes, possibly owing to the large size and severe cytotoxicity of the heterogeneous Cas (CRISPR-associated) effector. Nevertheless, the rich natural occurrence of CRISPR-Cas systems in many bacteria and most archaea holds great potential for endogenous CRISPR-based prokaryotic engineering. The endogenous CRISPR-Cas systems, with type I systems that constitute the most abundant and diverse group, would be repurposed as genetic manipulation tools once they are identified and characterized as functional in their native hosts. This article reviews the major progress made in understanding the mechanisms of invading DNA immunity by type I CRISPR-Cas and summarizes the practical applications of endogenous type I CRISPR-based toolkits for prokaryotic engineering.

Keywords: endogenous type I CRISPR-Cas systems, mechanisms of action, DNA targeting, genome editing, selective killing, antimicrobials, gene expression modulation

INTRODUCTION

Throughout the past billion years, bacteria and archaea have evolved a range of defense mechanisms to defend themselves against their viral predators (Doron et al., 2018), including restriction-modification systems, abortive infections and phage adsorption blocks, and the recently discovered CRISPR-Cas (clustered regularly interspaced short palindromic repeats-CRISPR-associated) systems (Jansen et al., 2002). Unique among these mechanisms, CRISPR immunity functions by storing records of previous invasions to provide immunological memory for a rapid and robust response upon subsequent viral infections.

CRISPR-Cas systems consist of two genetic components, the CRISPR array and *cas* genes encoding Cas proteins. The CRISPR array, featuring the CRISPR-Cas systems, is composed of conserved direct repeats, which are separated by unique sequences derived from the invasive mobile genetic elements (termed as *spacers*) (Bolotin et al., 2005; Mojica et al., 2005; Pourcel et al., 2005). Generally, the CRISPR immunity is driven by the Cas proteins in three distinct molecular stages.

The first stage is termed *spacer acquisition*, in which a short DNA stretch is captured from an invading genetic element and incorporated into a CRISPR array as the first spacer immediately after a leader sequence. Then, in the process of *crRNA (CRISPR RNA) biogenesis*, the entire CRISPR array is transcribed into a precursor CRISPR RNA (pre-crRNA) molecule driven by promoter elements embedded in the leader sequence. Following the transcription, cleavage within the repeats of the pre-crRNA by ribonucleases gives mature crRNAs, with each carrying a unique foreign sequence. In the final stage of *target interference*, each crRNA forms a ribonucleoprotein effector complex with Cas proteins and guides the effector machinery to the matching region of the invader through base pairing for destruction (Barrangou et al., 2007; Brouns et al., 2008; Marraffini and Sontheimer, 2008; Garneau et al., 2010).

Despite the general immunity stages for all the characterized CRISPR-Cas systems, the Cas proteins and hence the effector complexes vary widely. According to the assortment of *cas* genes and the complexity of their inference complexes, to date, six main types, types I to VI, of CRISPR-Cas systems have been identified and grouped into two classes, classes 1 and 2 (Makarova et al., 2015, 2018; **Table 1**). Systems of class 1, including types I, III, and IV, are defined by multi-Cas proteins, whereas those of class 2, including types II, V, and VI, utilize a single effector Cas protein (**Figure 1A**).

Because of the simplicity of class 2 systems, in which a single Cas protein is sufficient to execute targets binding and cleavage, their effector machineries are relatively easy to be adopted and have been emerged as powerful tools for genome manipulation applications in both prokaryotic and eukaryotic cells. Type II CRISPR-Cas9, as the first identified class 2 system, has been extensively harnessed for genome editing in a wide range of organism, from bacteria to eukaryotic cells, in the past few years (Jinek et al., 2012; Cong et al., 2013; Malina et al., 2013; Jiang et al., 2014). Subsequently, type V CRISPR-Cas12 was characterized and repurposed for genome editing (Zetsche et al., 2015, 2017; Fonfara et al., 2016). These systems have been also engineered for applications beyond genome editing, for example, gene expression regulation via repression or activation, epigenome editing, *in situ* genomic imaging, large-scale genomic screening, and so on (Chen et al., 2013; Cheng et al., 2013; Perez-Pinera et al., 2013; Qi et al., 2013; Shalem et al., 2014; Takei et al., 2017). Type VI CRISPR-Cas13 is the third type in class 2 system, which was demonstrated and developed as a versatile RNA manipulation tool to be used in RNA interference (RNAi), *in vivo* RNA molecule visualization, and nucleic acid detection (Cox et al., 2017; O'Connell, 2019). Recently, several novel single-stranded DNA (ssDNA)-cleaving CRISPR-Cas14 systems belonging to class 2 were identified (Harrington et al., 2018). It is worth to be mentioned that the targeted non-specific ssDNA cleavage activity of Cas14 enabled the system to perform genotyping (Harrington et al., 2018), while it has only about half size of Cas9/Cpf1, thus representing so far the smallest effector nuclease in a single-Cas effector system.

Undoubtedly, class 2 CRISPR-Cas systems have attracted great attention with their fruitful achievements in genome manipulations. However, the engineered targets exhibited an

obvious bias toward eukaryotic cells. One of the reasons could be that, as heterologous large-sized nucleases with intrinsic toxicity, the class 2 Cas effectors are hard to be introduced into prokaryotes, particularly those poorly genetically accessible prokaryotic cells. In one recent study, it failed to yield any colony when introducing Cas9 into *Corynebacterium glutamicum* cells even without a guide RNA (gRNA), suggesting the cytotoxicity of the Cas9 *per se* (Jiang et al., 2017). It was also reported that overexpressing a catalytically dead Cas9 (dCas9) in *Escherichia coli* resulted in abnormal morphology and retarded growth, indicating that the cytotoxicity of Cas9 is not solely caused by DNA cleavage but possibly transient non-specific DNA binding across the genome (Cho et al., 2018). Therefore, using endogenous CRISPR-Cas systems of the host for genome engineering could be an effective way to overcome the restriction (Hidalgo-Cantabrana et al., 2019a). In comparison with the imported class 2 systems, all the protein components of endogenous type I systems are present in the cells, excluding any heterologous nuclease. They naturally produce mature crRNA guides without any heterologous helper, which is with particular convenience to conduct, for example, multiplexed genome editing or simultaneous multiple-gene regulation for metabolic pathway engineering by simply supplying an artificial CRISPR array (Luo et al., 2015; Cheng et al., 2017).

It was reported that class 1 systems, primarily types I and III, with only a few reports added recently of type IV (Crowley et al., 2019; Ozcan et al., 2019; Taylor et al., 2019), are present in more than 90% of sequenced genomes of bacteria and archaea (Makarova et al., 2015). Class 1 endogenous systems are much more abundant than class 2 systems (Grissa et al., 2007) and exist not only in mesophiles but also in extreme thermophiles. This is indicative of a great potential to harness the class 1 endogenous systems for applications across many areas of biology. In fact, using type III system for genome editing has been carried out in *Sulfolobus islandicus* (Li et al., 2016). Because the functions and applications of type III systems have been recently reviewed elsewhere (Liu et al., 2018), we will present here the major progress achieved for type I systems, uncovering mechanisms of action of the type I CRISPR-directed immunity, concerning crRNA processing, effector complex assembly, PAM-directed target recognition, seed sequence-mediated target invasion, and Cas3-executed target cleavage, and briefly discuss their recent practical applications, for example, genome editing, antimicrobials, and gene expression regulation, in their prokaryotic hosts.

MECHANISMS OF INVADING DNA DEFENSE BY TYPE I CRISPR-CAS

Type I CRISPR-Cas systems contain a Cas3 protein as the defining feature of this type with exception for transposon-encoded type I variants (Peters et al., 2017; Klompe et al., 2019; Makarova et al., 2019; Strecker et al., 2019) and are divided into six subtypes, I-A through I-G, with each harboring a specifying Cas8 homolog (**Figure 1B** and **Table 1**; Majumdar et al., 2015; Makarova et al., 2015, 2018; Koonin et al., 2017b).

TABLE 1 | The six types of CRISPR-Cas systems.

Class	Type	Subtype	Spacer acquisition	crRNA biogenesis	Interference crRNP	Type of nucleic acid targets
1	I	A-G	Cas1, Cas2, Cas4	Cas6/Cas5d	Cascade	DNA
	III	A-F	Cas1, Cas2	Cas6	Csm/Cmr	DNA/RNA
	IV	A-C	Unknown	Csf5	Csf	DNA
2	II	A-C	Cas1, Cas2, Cas4/Csn2, Cas9	RNase III Cas9	Cas9	DNA
	V	A-I, K	Cas1, Cas2, Cas4	Cas12	Cas12	DNA
	VI	A-D	Cas1, Cas2	Cas13	Cas13	RNA

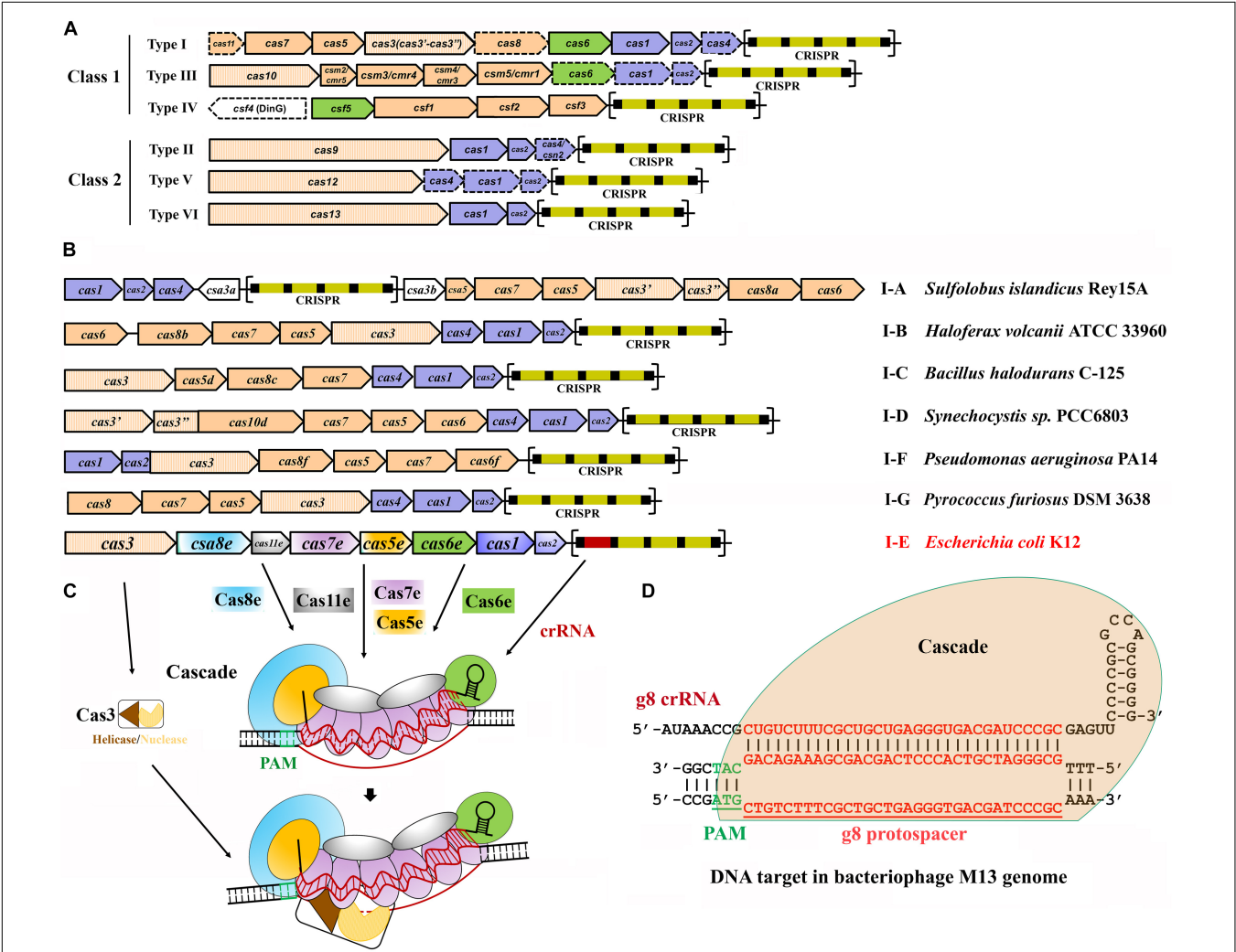


FIGURE 1 | Classification and architecture of CRISPR-Cas systems and interference by type I systems. **(A)** CRISPR-Cas systems are greatly diverse and can be classified into two classes, class 1 and class 2. Class 1 systems encode multisubunit effector complexes; class 2 systems encode single-subunit effectors. Genes that may miss in certain subtypes are indicated with dashed outlines. Genes encoding the components of each interference complex are colored in orange, and those involved in crRNA processing and new spacer acquisition are in green and blue, respectively. The effector nucleases for each subtype are shown with filled vertical lines. CRISPR arrays are indicated, with squares and rectangles representing repeats and spacers, respectively. **(B)** Organization of the CRISPR-Cas loci for the typical type I subtypes. Representative operons for each type are shown, and gene names are indicated. Gene functions are marked with colors the same as shown in **(A)**, except for the subtype I-E of *Escherichia coli* K12. CRISPR arrays are indicated, with squares and rectangles representing repeats and spacers, respectively. **(C)** Schematic of DNA targeting by the representative type I-E of *E. coli* K12. It is composed of a crRNA bound by Cas5 and Cas6 at either end and Cas7 subunits along the guide region, a large subunit (Cas8), and sometimes a small subunit (Cas11). Upon PAM recognition by Cas8, Cascade binding to the target DNA leads to DNA duplex destabilization, allowing crRNA invasion to form a full R-loop. Cas3 is recruited to the R-loop and nicks the replaced strand of the target DNA within the protospacer. **(D)** Schematic showing type I-E Cascade containing a crRNA (g8 crRNA) targeting a sequence on the genome of bacteriophage M13. Sequences of PAM and protospacer are indicated with underlined green and red fonts, respectively [constructed according to Semenova et al. (2011)].

Intensive investigations on model type I CRISPR-Cas systems have revealed molecular mechanisms of multi-Cas CRISPR-based antiviral defense, in respect of crRNA processing, effector complex assembly, PAM recognition and R-loop formation, and Cas3-executed DNA target destruction (**Figures 1C,D**).

crRNA Processing

A mature crRNA is an essential element for an active CRISPR-Cas effector complex, in which it functions to guide the recognition of the cognate targets for destruction. It has been reported that biogenesis of mature crRNAs requires cleavage of long CRISPR transcripts within each repeat. In type I systems, an RNA recognition motif (RRM)-containing protein, either a Cas5d for type I-C (Garside et al., 2012; Nam et al., 2012; Punetha et al., 2014) or a Cas6 homolog for rest type I systems (Przybilski et al., 2011; Sashital et al., 2011; Li et al., 2013; Sokolowski et al., 2014; Majumdar et al., 2015; Taylor et al., 2019), recognizes and catalyzes the crRNA maturation. It should be noted that some type III systems also use Cas6 for crRNA processing (Hale et al., 2009; Majumdar et al., 2015; Peng et al., 2015; Nickel et al., 2019; Wei et al., 2019). Structural analyses of different Cas6/Cas5d-RNA complexes revealed that many repeats formed characteristic stable stem-loop structures. Accordingly, Cas6/Cas5d enzymes have evolved distinct mechanisms to overcome the challenges of binding and catalysis of various RNA molecules (**Figure 2**; Koo et al., 2013; Li, 2014; Shao et al., 2016; Sefcikova et al., 2017).

Mature crRNA production has been reported for each subtype of type I. Repeats of CRISPR arrays from type I-E of *E. coli* and *Thermus thermophilus* and I-F of *Pseudomonas aeruginosa* were reported to form stable canonical stem-loop structures (**Figures 2A–C**; Haurwitz et al., 2010; Sashital et al., 2011; Sternberg et al., 2012). Interestingly, all of the stems and loops greatly vary in both size and sequences, which serve as bases for specific binding of Cas6 and subsequent cleavage. The Cas6 proteins specifically recognize and cleave the pre-crRNAs in a single turnover fashion, forming a stable hairpin structure in each repeat (Haurwitz et al., 2010; Sashital et al., 2011; Sternberg et al., 2012). After cleavage, they remained binding to the cleavage products by associating with the 3' stem-loop structure tightly (Jore et al., 2011). This is consistent with the finding that Cas6 protein is an integrated part of the respective interference complexes (Brouns et al., 2008; Jore et al., 2011; Wiedenheft et al., 2011a,b; Jackson et al., 2014; Mulepati et al., 2014; Zhao et al., 2014). Similarly, repeats of type I-C from *Bacillus halodurans* also formed stable stem-loop structures, which, however, were produced by a unique Cas5 variant (Garside et al., 2012; Nam et al., 2012; Koo et al., 2013; Punetha et al., 2014) [known as Cas5d where the affix “d” refers to “Dvulg” (Haft et al., 2005)], as a *cas6* gene is missing from this system. A 3-bp stem and a tetra-loop included in the hairpin region were illuminated to be a minimal structural requirement for Cas5d recognition and cleavage (Nam et al., 2012).

Differently, CRISPR repeats present in type I-A of *Sulfolobus solfataricus* and type I-B of *Methanococcus maripaludis* usually form mini stem-loop structures (**Figures 2D,E**), instead of showing clear palindromic features (Kunin et al., 2007;

Shao et al., 2016). For instance, in type I-A system, the formed stem-loop is composed of a 3-bp stem and a 5-nt loop, which were specifically recognized and stabilized by SsCas6, a Cas6 homolog. Two base pairs at the base of the stem were essentially required for SsCas6 binding and cleavage, as mutations disrupting the base-pair matching resulted in cleavage inhibition (Shao and Li, 2013). Likewise, a 3-bp stem could be potentially formed by the CRISPR repeats from another type I-B system of *Haloferax volcanii* (Maier et al., 2013), which likely contributes to the binding specificity of the HvCas6. Comparably, type I-G system shares the similar Cas6 homolog protein with coexisting types I-A and III-B systems in *Pyrococcus furiosus* to recognize CRISPR repeats with no obvious stem-loop structure for mature crRNA production (**Figure 2F**; Carte et al., 2010; Elmore et al., 2015).

crRNA processing in a type I-D system is the least known. Processing of CRISPR transcripts of a type I-D system in *Synechocystis* species PCC 6803 involved a Cas6 protein (Cas6-1) (Scholz et al., 2013; Jesser et al., 2019). Depletion of Cas6-1 from the cells largely decreased the crRNA amount, while this deficient phenotype could be restored through expression of Cas6-1 via a plasmid (Scholz et al., 2013). A mini stem-loop was also predicted to be formed in each repeat (Jesser et al., 2019), but whether it serves as the binding signal for Cas6-1 remains uncertain.

Effector Machinery Assembly

Type I CRISPR-Cas systems encode multiple Cas proteins to multi-Cas effector machineries, which is termed the *CRISPR-associated complex for antiviral defense* (Cascade). Cascade was initially used for characterizing the type I-E CRISPR-Cas effector complex of *E. coli* (Brouns et al., 2008). This complex has a molecular weight of approximately 405 kDa and comprises proteins of Cas8e (also known as CasA or Cse1), Cas11 (also known as CasB or Cse2), Cas7 (also known as CasC or Cse4), Cas5 (also known as CasD), and Cas6e (also known as CasE or Cse3), as well as an RNA component, the 61-nt crRNA (Jore et al., 2011). These proteins shape a seahorse-like architecture with a stoichiometry of Cas8e₁-Cas11₂-Cas7₆-Cas5₁-Cas6e₁ (**Figure 1C**; Jore et al., 2011).

Two crystal structures of the type I-E Cascade bound to a crRNA have been solved, offering molecular details in the Cascade complex assembly (**Figure 3A**; Jackson et al., 2014; Zhao et al., 2014). In *E. coli*, as previously mentioned, pre-crRNA is processed by the Cas6e ribonuclease through cleavage of pre-crRNAs within each repeat. After processing, Cas6e remains tight binding to the 3' repeat portion of each crRNA (Jore et al., 2011). At the same time, six Cas7 proteins run along the guide region (spacer) of the crRNA, forming the backbone filament, with the upper most subunit interacting with Cas6e. These Cas7 proteins adopt a right-hand-like shape (Mulepati et al., 2014), and the subunits are connected with one another by interaction between the “thumb” and “fingers” domains of one subunit and its adjacent subunits, respectively (Jackson et al., 2014). The Cas5e protein also exhibits a right-hand-like shape but lacks the “fingers” domain, thus allowing Cas5e to cap the Cas7 filament at the 5' end of the crRNA by undertaking the same interaction of Cas7 with that between Cas7 subunits. In addition, Cas5e protein also holds the first 6 nt of the 5' repeat portion of the crRNA

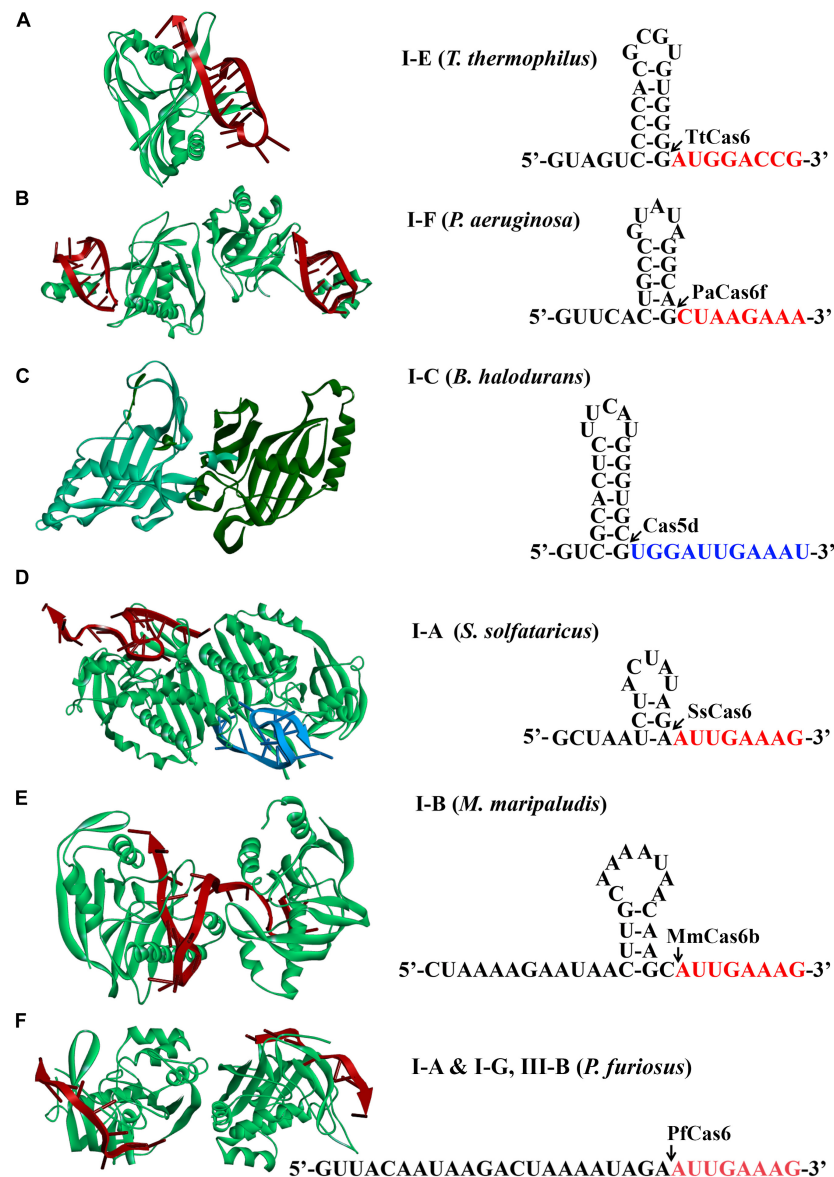


FIGURE 2 | Structures of Cas6 and Cas5d (left) and schematic of CRISPR repeats (right). Structural examples for Cas6 or Cas5d were presented from (A) type I-E of *Thermus thermophilus* (TtCas6, PDB code 2Y8W) (Sashital et al., 2011), (B) type I-F of *Pseudomonas aeruginosa* (PaCas6, PDB code 2XLK) (Haurwitz et al., 2010), (C) type I-C of *Bacillus halodurans* (Cas5d, PDB code 4F3M) (Nam et al., 2012), (D) type I-A of *Sulfolobus solfataricus* (SsCas6, PDB code 4ILL) (Shao and Li, 2013), (E) type I-B of *Methanococcus maripaludis* (MmCas6, PDB code 4Z7K) (Shao et al., 2016), and (F) type I-G of *Pyrococcus furiosus* (PfCas6, PDB code 3PKM) (Wang et al., 2011). The structures of Cas6 are shown in complex with crRNA (red). CRISPR RNAs from type I systems form either stable canonical stem-loop (A–C), mini-stem-loop (D,E), or non-stem-loop (F), structures. The predicted processing sites are indicated by arrows, and sequences are to be present as the 5' handle of a crRNA is shown in red or blue fonts.

(Jackson et al., 2014). In the seahorse-like complex, two Cas11 proteins form a dimer that does not directly interact with crRNA but functions as a bridge to connect the head and tail of the complex. One Cas11 subunit that is proximal to the 5' end of crRNA, along with Cas5e, contacts Cas8 at the bottom of the complex, whereas the other Cas11 subunit interacts with Cas6e on the top (Jackson et al., 2014). Cas8 and Cas11 were identified as the largest and smallest subunits of the Cascade, respectively (Makarova et al., 2011a).

Subsequently, several other type I systems complexes were isolated and characterized (Lintner et al., 2011; Nam et al., 2012; Brendel et al., 2014). Comparison of the overall architectures of these complexes with that of the type I-E Cascade revealed that they share striking architectural similarities and thus being all referred as Cascade (Figure 3B; Reeks et al., 2013). These Cascade complexes show some common features. (1) A core complex of Cas5, Cas7, and/or Cas6 holds a crRNA, each protein possessing at least one RRM motif. (2) Cas7 subunits form the

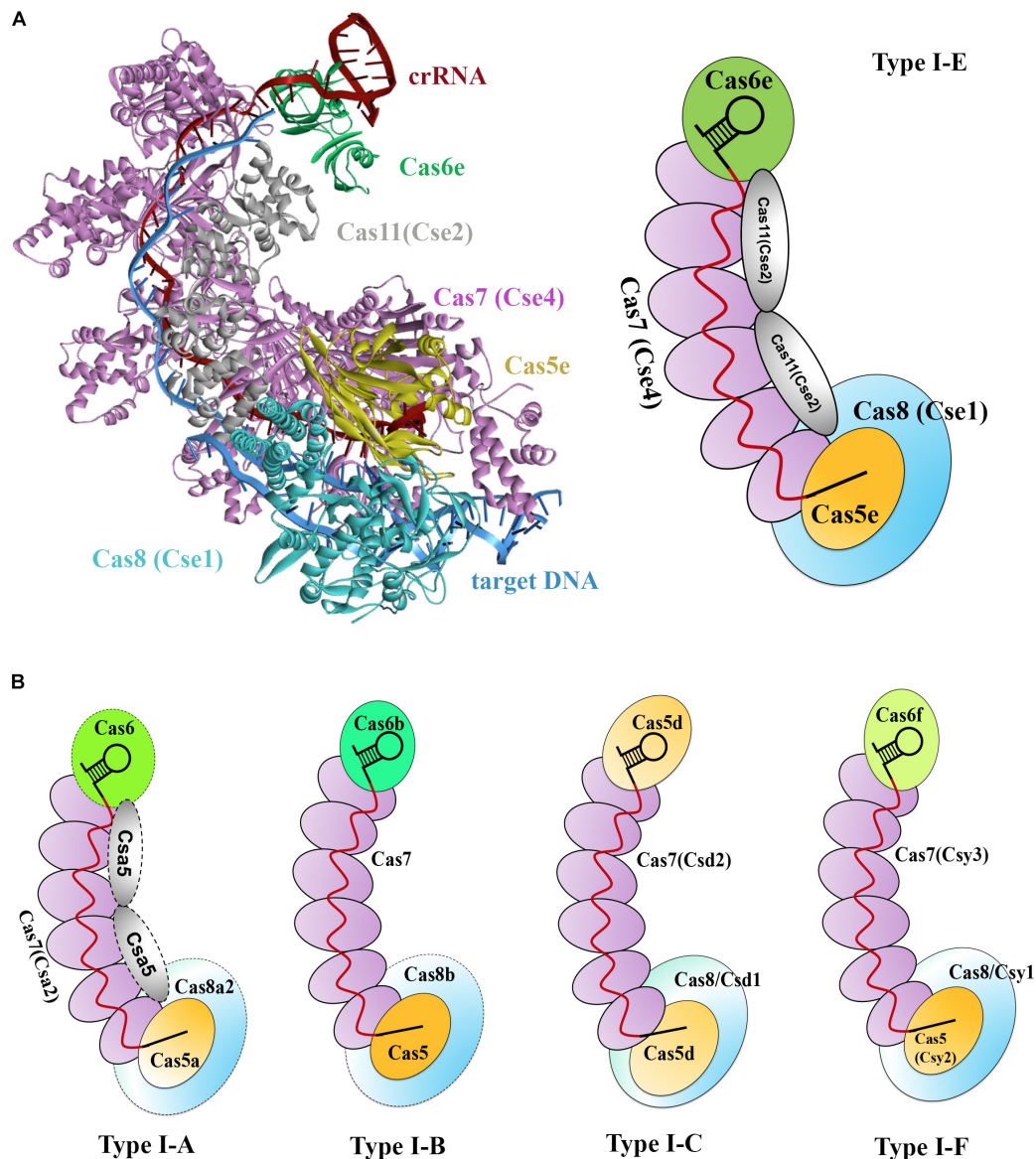


FIGURE 3 | Models of type I Cascade complexes. **(A)** Structure of the type I-E Cascade of *E. coli* binding to a dsDNA target (PDB code: 5H9F, left) and a simulated model according to the structure (right). **(B)** Models for other characterized Cascade complexes of type I systems, including type I-A (Lintner et al., 2011), type I-B (Brendel et al., 2014), type I-C (Nam et al., 2012), and type I-F (Wiedenheft et al., 2011a), showing overall architectural similarities to that of the type I-E. Weakly associated subunits are indicated with dashed outline.

backbone of the complex and are more abundantly present. (3) The large subunit (Cas8) and/or small subunit (Cas11), if present, less tightly associate with the core complex. Thus far, a separate small subunit is only seen in type I-A and I-E systems, that is, Csa5 and Cse2, respectively. This small subunit is absent from the Cascade complexes of type I-B, I-C, and I-F, but the large subunits of these complexes are speculated to have contained a domain that is functionally homologous to the small subunit (Makarova et al., 2011a). Interestingly, the determined Cascade structure of a type I-F variant (I-Fv) lacks both the large and the small subunits, whose functions, however, are replaced by Cas5fv and Cas7fv, respectively (Pausch et al., 2017). The architectural

similarities suggest that these Cascade complexes may use similar mechanisms for complex assembly and DNA interference.

PAM Recognition and R-Loop Formation

The Cascade is directed to an invading DNA molecule solely relying on base pairing between the embedded crRNA and protospacer. An outstanding question would be how crRNA differentiates protospacer from the corresponding spacer that is stored in the genomic CRISPR bank. The evolved mechanisms for these systems to avoid self-CRISPR targeting involve a sequence immediately flanking the protospacer, called a protospacer adjacent motif (PAM), which is essentially required for Cascade

to determine *bona fide* DNA targets. First predicted by Mojica et al. (2009) and experimentally demonstrated for type I-A systems in *Sulfolobus* by Gudbergsson et al. (2011), PAM is typically of two to five base pairs and located at the 5' end of protospacer on the strand matching the spacer.

Protospacer adjacent motif recognition has also been studied in other type I systems. In type I-E system of *E. coli*, a loop structure, named the L1 loop that is located within the N-terminal domain of Cas8, directly contacts with the PAM, mediating specific binding of Cascade to the PAM-containing DNA target (Sashital et al., 2012). Further analyses defined that three structural features, including a glutamine wedge, a glycine loop, and a lysine finger, were required for PAM recognition by Cas8 and specified the interaction of PAMs with the target strand (Hayes et al., 2016). In type I-E Cascade of *Thermobifida fusca*, the Cas8 subunit played the same roles in specifying the PAMs, while through contacting the non-target strand (Xiao et al., 2017). In both cases, PAM sequences were recognized by the Cas8 proteins at the minor groove side, explaining the promiscuity of PAM recognition in these systems. Additionally, the recognition of PAM by Cas8 homologs was also identified in type I-B systems of *H. volcanii* and *Methanothermobacter thermautotrophicus* (Cass et al., 2015). Interestingly, in the reported type I-Fv system, the Cas8 protein is missing. Instead, the existing Cas5f variant (Cas5fv) containing an additional domain may compensate for the roles of Cas8 (Pausch et al., 2017).

Bona fide PAM recognition and base pairing between a crRNA and the cognate protospacer determine a target DNA. Interestingly, in some initial work, researchers found that a few type I CRISPR-Cas systems exhibited tolerance to mismatches between the crRNAs and corresponding protospacers. Impacts of mismatches at different regions of the crRNA on target DNA interference markedly varied. In one of the studies, Wiedenheft et al. (2011b) used isothermal titration calorimetry to investigate DNA-binding affinity of the *P. aeruginosa* type I-F system. The results indicated that an 8-nt ssDNA oligo matching the first 8-nt 5' guide sequence of a crRNA (1–8 nt) showed a high binding affinity of the crRNA, whereas another 8-nt ssDNA oligo complementary to the corresponding 5 to 12 region of the crRNA presented a 4-fold weaker binding affinity. Strikingly, all other tested 8-nt ssDNA oligos that matched the crRNA at a region outside the 1- to 8-nt stretch exhibited no measurable binding affinity. These results indicated that the 1- to 8-nt sequence within the crRNA, immediately adjacent to the PAM, played an essential role in defining an invading DNA as an attacker. This is in analogy to the seed sequence in small RNAs, which functions in target recognition in the RNAi in eukaryotes (Lewis et al., 2003).

Following binding of Cascade to a DNA target upon PAM recognition is the formation of a full R-loop, which was observed in several type I systems. Cascade binding could destabilize the target DNA duplex, allowing crRNA to first pair with the protospacer within the seed region and then throughout the whole matching sequences and thus forming a full R-loop, where the non-target strand is bound by the Cas11 dimer (Hochstrasser et al., 2014; Szczelkun et al., 2014). The existence of an intermediate seed bubble immediately following the PAM recognition but before the full R-loop formation was

recently evidenced. Xiao et al. (2017) captured a structural snapshot of the *T. fusca* type I-E Cascade, showing an 11-bp unwound sequence in the seed region. R-loop formation is accompanied by conformational changes of the small and large subunits that trigger recruitment of Cas3 for target degradation (Hochstrasser et al., 2014).

DNA Target Degradation

As aforementioned, Cascade recruited Cas3 to unwind, cut, and degrade the targets. Cas3 typically comprises an N-terminal HD phosphohydrolase domain and a C-terminal superfamily 2 helicase domain (Makarova et al., 2006). There are also exceptional cases in some type I systems. For example, these two domains are encoded as individual proteins, Cas3' (helicase) and Cas3'' (nuclease), respectively, in type I-A of *S. islandicus* Rey15A (Figure 1B; Guo et al., 2011; Makarova et al., 2011b). It was speculated that the HD domain carried out the divalent ion-dependent catalytic cleavage on ssDNA and/or RNA (Han and Krauss, 2009; Beloglazova et al., 2011; Mulepati and Bailey, 2011; Sinkunas et al., 2011), whereas the helicase domain unwound the DNA/DNA and/or DNA/RNA duplexes in the presence of ATP (Howard et al., 2011; Sinkunas et al., 2011).

The mechanism of target DNA degradation by Cas3 was revealed by structural analyses of type I-E targeting complexes, in which the recruitment of Cas3 strictly required the formation of a full R-loop structure. The ape Cascade and R-loop-forming Cascade present as different conformers and Cas3 only selectively capture the latter (Xiao et al., 2017). This conformational difference might act as signals for triggering Cas3 recruitment and also help the type I systems avoid cleaving partially complementary sequences (off-targeting). Upon the formation of Cas3-Cascade-DNA target complex (Huo et al., 2014), Cas3 nuclease nicked the non-target strand in the 7- to 11-nt region of a protospacer (Hochstrasser et al., 2014). The non-target strand contained a significant bulge structure in the R-loop that was created by the Cascade complex, facilitating its handover from Cascade to the bound Cas3 for nicking (Xiao et al., 2017). This handover was recently confirmed to be essential for type I-E immunity (Xiao et al., 2018). Subsequent exonucleolytic degradation of the DNA target was observed to occur in the direction of 3' to 5' with the need of ATP. Sinkunas et al. (2013) found that Cas3 cleaved only on the displaced strand in the R-loop in absence of ATP, but destroyed both strands when ATP was present. This may indicate that unwinding DNA target by the ATP-dependent Cas3 helicase domain could further provide ssDNA substrates for the nuclease domain of Cas3, or for other host nucleases, leading to degradation of the entire DNA target (Brouns et al., 2008; Mulepati and Bailey, 2013).

A Deduced General Mechanism of Type I DNA Interference

Collectively, as exemplified for the type I-E system in Figure 4A, all known type I CRISPR-Cas systems form a Cascade machinery to perform DNA interference in several steps, consisting of multiple protein components complexed with a mature crRNA molecule. A general mechanism of type I Cascade-mediated DNA

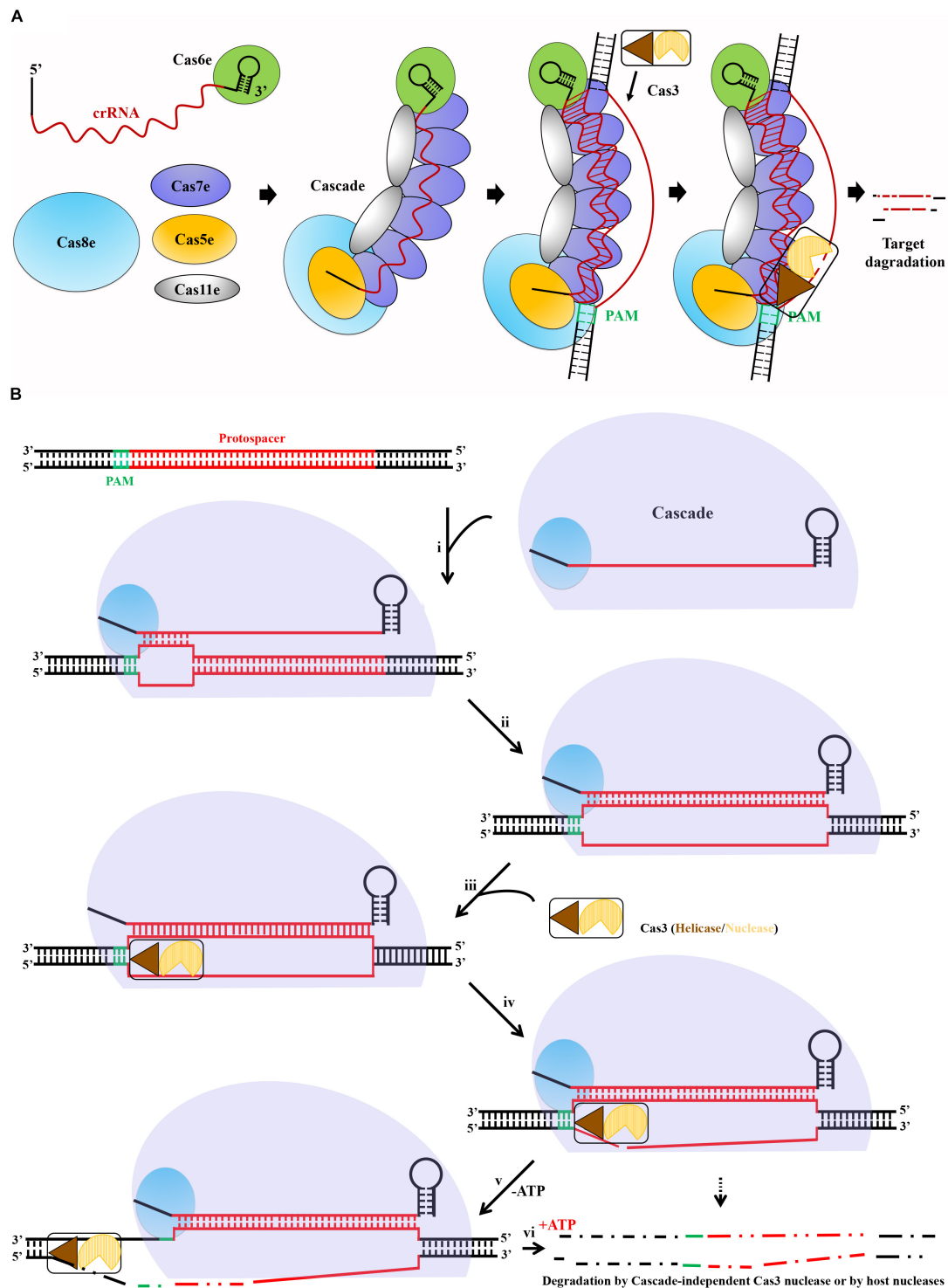


FIGURE 4 | A deduced general mechanism of type I Cascade-mediated DNA interference. **(A)** Schematic showing interference pathway exemplified by the type I-E CRISPR-Cas system of *E. coli*. crRNA produced and bound by Cas6e acts as a scaffold for Cascade assembly. Upon recognition of PAM (green) on the invading DNA, Cascade bound to the target DNA, followed by R-loop formation after crRNA base pairs with the target strand DNA, triggering the recruitment of the endonuclease Cas3. Finally, Cas3 initiates degradation of the non-target strand. **(B)** The crRNA and type I Cas proteins form a Cascade complex. If present, an optimal PAM in a DNA target, Cas3 interacts directly with the PAM, allowing Cascade binding. A primary base pairing between the crRNA and protospacer within the seed (i) is followed by extended base pairing, displacing the non-target strand and forming a full R-loop (ii). Conformational changes caused by target DNA binding trigger Cas3 helicase/nuclease to join in the complex, docking at a Cas8-provided site (iii). In the absence of ATP (-ATP), the nuclease domain cuts the displaced strand within the protospacer (iv), leaving a ssDNA gap in the target (v). In the presence of ATP (+ATP), Cas3 helicase unwinds the dsDNA, and complete degradation of the target DNA is mediated by either the Cascade-independent Cas3 nuclease activity or other host nucleases (vi).

interference could be deduced as described following and shown in **Figure 4B**. The interference begins with the recognition of a suitable PAM by Cas8. Direct interaction between the L1 loop of Cas8 and the PAM (Hochstrasser et al., 2014) locates the Cascade to the DNA target and destabilizes the DNA duplex (Szczytkun et al., 2014). The crRNA base pairs with the protospacer, first within the seed region and then throughout the whole matching sequences, to eventually displace the non-target strand, forming a full R-loop. On the other hand, the initial dsDNA binding induces a major conformational change to the Cascade (Wiedenheft et al., 2011a), which may trigger the recruitment of Cas3 to the Cas8 docking site (Westra et al., 2012; Hochstrasser et al., 2014). It was reported that once the non-target strand is displaced by the crRNA, it is exposed and handed over to the Cas3 nuclease for nicking and successive degrading in the 3' to 5' direction (Sinkunas et al., 2013; Gong et al., 2014). This reaction may generate an intermediate degradation product, as partially ssDNA might not result in complete target DNA degradation. In fact, complete degradation of the target DNA is probably mediated either by the nuclease domain of Cas3 or by other host nucleases with assistance of the ATP-dependent helicase domain of Cas3 to unwind the DNA target (Brouns et al., 2008; Mulepati and Bailey, 2013).

PRACTICAL APPLICATIONS OF TYPE I CRISPR-CAS SYSTEMS

The above mechanistic dissections of type I CRISPR-Cas-based immunity have provided solid theoretical basis for exploiting these systems for a wide range of practical applications in bacterial and archaeal hosts. By simply designing a plasmid-borne artificial mini-CRISPR to express genome-targeting crRNAs, a type I Cascade complex can be readily directed to a genome sequence to accomplish various tasks (**Figure 5A**). These applications can be briefly classified into two classes according to the different activities of these systems. One utilizes the intact DNA interference function of Cascade and Cas3 (**Figure 5B**), for example, genome editing, natural variants selection, and antimicrobials, and the other uses only the target surveillance and binding ability of Cascade alone (without Cas3 nuclease) (**Figure 5C**), for example, gene expression regulation.

Genome Editing

To date, genome editing predominates over other CRISPR applications and remains the best developed, however, overwhelmingly focusing on eukaryotes. In the eukaryotic organisms, double-stranded DNA breaks (DSDBs) introduced by CRISPR-Cas systems at specific locations of the genome could be repaired through either the cellular non-homologous end joining (NHEJ) or the homologous recombination (HR) repair pathways. The NHEJ repair system functions in an error-prone manner that usually generates indels (insertions/deletions) within the vicinity of the target site, leading to frame shifts or gene disruption. In contrast, HR repair system normally creates precise changes at desired positions in the genome when providing engineered DNA templates. Dissimilarly, most

prokaryotic organisms harbor only the HR system. It has to be pointed out that although a bacterial version of NHEJ, involving two proteins, Ku and LigD, was reported (Weller et al., 2002), it occurs only in a very small portion of bacteria. In general, prokaryotes repair the CRISPR-caused DSDBs with relatively much lower efficiencies, which is consistent with the frequently observed CRISPR-mediated lethality when self-targeting crRNAs of active systems were introduced into the prokaryotic cells (Edgar and Qimron, 2010; Vercoe et al., 2013; Goma et al., 2014; Peng et al., 2015). It is reasonable because the invaders would persist to affect the host cells if the cleavage of invading attackers, such as bacteriophages and conjugative plasmids, by Cas nucleases is subsequently repaired. In practical applications, this is the main obstacle that needs to be addressed in harnessing the endogenous type I systems for genome editing.

Via coupling the DNA targeting activity of endogenous type I CRISPR-Cas systems with the DNA-assisted HR mechanism, various genome editing purposes can be achieved, including gene insertion, deletion, replacement, tagging, and nucleotide substitution, as well as multiplexed gene deletion, in their natural hosts. Here, we take our recently published work on type I-F CRISPR-Cas system as an example to introduce the procedure, strategy, and principle of exploiting an endogenous type I system for genome editing in *Zymomonas mobilis* (Zheng et al., 2019). In the study, we first demonstrated the DNA cleavage activity of the endogenous type I-F CRISPR-Cas of *Z. mobilis* and determined the PAM sequences essential for the system through a plasmid invader assay (Peng et al., 2013, 2015). This activity was then directed to genomic locations by crRNAs produced from plasmid-borne artificial CRISPR loci to generate DNA injuries. In addition, donor DNAs were supplied as inserts of the same plasmids for facilitating HR, allowing their multiplication via plasmid replication to ensure effective concentration and stability, which has been evidenced to be an efficient approach for enhancing the HR rate and hence genome editing efficiency (Li et al., 2016; Renaud et al., 2016; Cheng et al., 2017). Using this established type I-F CRISPR-Cas platform, various genome engineering purposes were efficiently achieved with efficiencies of up to 100%, including gene deletion, replacement, *in situ* modifications, particularly large genomic fragment deletion, and simultaneous removal of three genes (**Figure 5D**). Moreover, our work demonstrated that depletion of a DNA restriction-modification (R-M) system could also lead to boosted genome engineering efficiency (Zheng et al., 2019). Considering the widespread of R-M systems (Koonin et al., 2017a) and other DNA interference systems (Doron et al., 2018) in microorganisms, the method could be served as an important reference for the development and deployment of similar CRISPR-Cas toolkits in organisms with low efficiency in the wild-type genetic background.

Endogenous type I CRISPR-based genome editing was first reported in *S. islandicus*, and then other organisms. Gene deletion and site-directed mutagenesis were completed in the Crenarchaeota *S. islandicus* by constitutively expressing its native type I-A system (Peng et al., 2013; Li et al., 2016). After transforming a plasmid bearing both the CRISPR target and donor DNA template into the host cells, almost all the

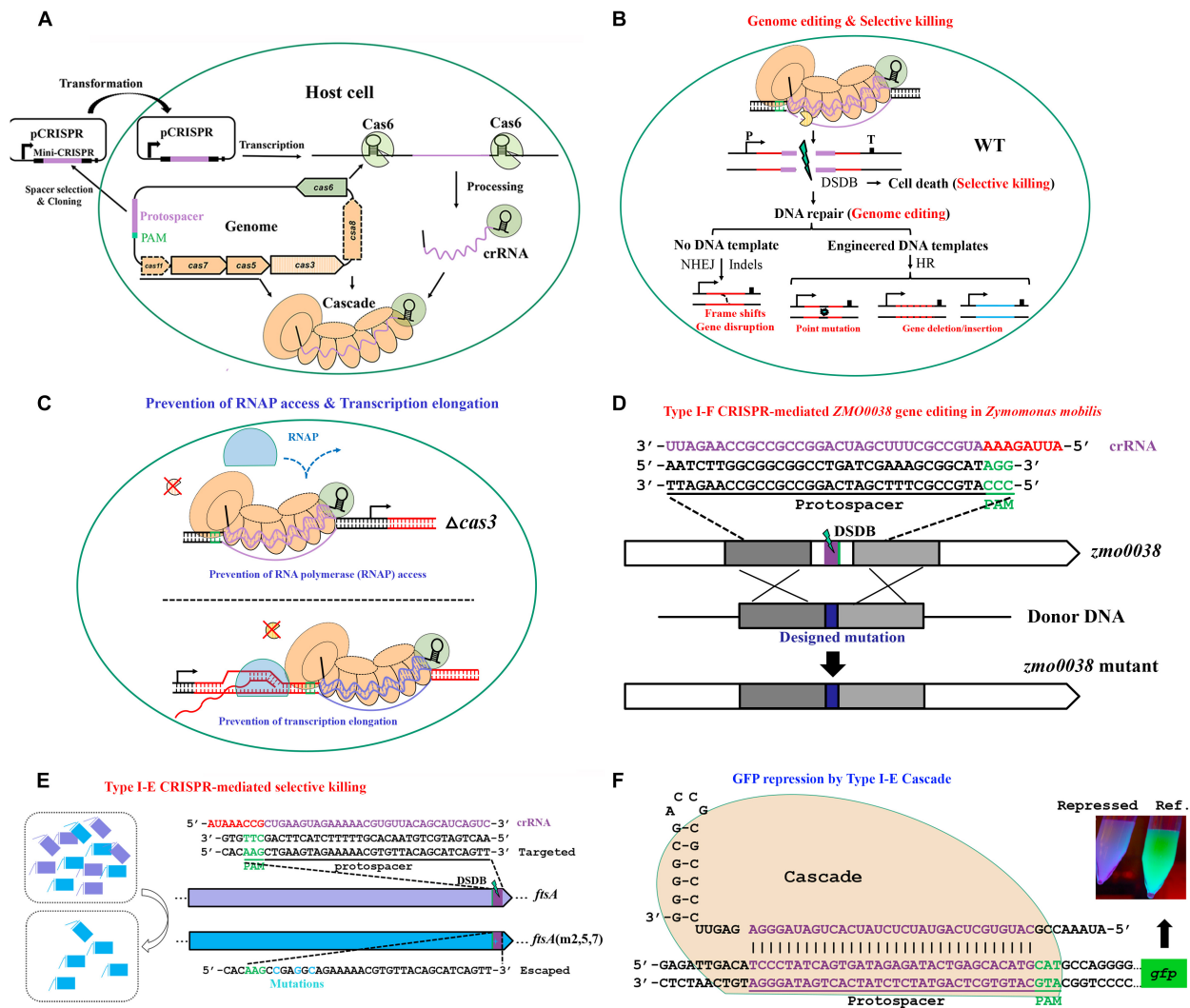


FIGURE 5 | The basic working principle of type I Cascade-based technologies. **(A)** Strategy for native type I Cascade-based applications. A DNA stretch immediately 5' downstream of a PAM is selected for mini-CRISPR construction. crRNA expressed from the plasmid-borne mini-CRISPR array forms the Cascade complex with Cas proteins expressed from the genomic cas operon. **(B)** Architecture of type I Cascade-mediated genome engineering. **(C)** Architecture of type I Cascade-mediated gene expression modulation. The Cascade is directed to the target site in the host genome, either recruiting the Cas3 to generate a double-stranded DNA break (DSDB) in wild-type (WT) cells **(B)** or binding to the target tightly without cleaving it in a *cas3* knockout background **(C)**. **(D)** Schematic showing an example of genome editing by repurposing the type I-F of *Zymomonas mobilis* [constructed according to Zheng et al. (2019)]. **(E)** Schematic showing an example of selective killing by using the type I-E of *E. coli* [constructed according to Goma et al. (2014)]. **(F)** Schematic showing an example of gene expression control by the type I-E Cascade in *E. coli* [modified according to Rath et al. (2015)].

analyzed transformants were found to possess precise changes including deletions and multiple point substitutions as designed (Li et al., 2016). Likewise, the endogenous type I-B system of the halophilic archaeon *Haloarcula hispanica* was also redirected for gene deletion, insertion, point mutations introduction, and simultaneous deletion of two genes (Cheng et al., 2017). Besides, two other type I-B systems from the bacteria *Clostridium tyrobutyricum* and *Clostridium pasteurianum*, respectively, have also been used for genome editing in their native hosts, with an editing efficiency of 100% on gene deletion/insertion (Pyne et al., 2016; Zhang et al., 2018). Strikingly, the native type I-B system of *C. pasteurianum* facilitated more efficient genome

editing of around 4-fold higher than that of the heterologously expressed Cas9 system (Pyne et al., 2016). Very recently, the type I-E system of *Lactobacillus crispatus* was also exploited to perform *in situ* genomic modifications in the host cells (Hidalgo-Cantabrana et al., 2019b).

Targeted DNA integration can also be accomplished using crRNA-guided transposition, which was first proposed by Peters et al. (2017). It was found that a number of CRISPR-Cas systems are carried by transposons belonging to the Tn7 family (Peters, 2014), and they possess a notable feature of lacking a key factor responsible for DNA targeting. Moreover, the CRISPR-Cas systems carried by them are not capable for DNA interference.

This proposed mechanism has been recently experimentally confirmed in *E. coli* by two groups (Klompe et al., 2019; Strecker et al., 2019). In one instance, Klompe et al. (2019) show that a variant type I-F system from *Vibrio cholerae*, where the adaptation module and Cas3 nuclease are missing, could still form a Cascade complex and guide transposition into specific sites 46 to 55 bp downstream of crRNA-matching sequences. Interestingly, the transposition can be done only with the coevolved type I-F variant, as other tested native CRISPR-Cas systems did not work properly (Klompe et al., 2019). Moreover, the authors also found that the Cascade could be copurified with a TniQ protein, an element of the Tn7 system involved in one of the characterized Tn7 transposition pathways (Peters, 2014). More interestingly, this crRNA-guided transposition could be observed only when expressing a fusion of TniQ-Cas6, but not TniQ-Cas8. These observations thus allowed the authors to propose a mechanism that the CRISPR-Cas system could cofunction with the Tn7 system (Klompe et al., 2019). Similarly, Strecker et al. (2019) reported that the Tn7-like system could recruit a type V-K variant from *Scytonema hofmannii*. This mechanism was later further supported by a cryo-EM structure of TniQ-Cascade complex (Halpin-Healy et al., 2019), within which two TniQ subunits form a dimer, with each interacting with Cas6 and the immediately adjacent Cas7 subunit, respectively. Finally, with either system, CRISPR-directed DNA insertion has been attained in a programmable fashion with high frequencies. More importantly, with no requirement for target DNA cleavage, homologous DNA templates, endogenous DNA repair systems, and selective pressure, this strategy is advantageous for genome modification over many other existing tools.

Selective Killing

As aforementioned, reprogramming an active Cascade toward the chromosome without providing a repair template would lead to killing of most, if not all, targeted cells. Two alternative fates might be brought to the targeted cells, including the death of wild-type cells due to CRISPR-mediated chromosomal degradation, or the survival if variants carry mutations in the targeted sequences. This selective killing feature can be adopted to exploit DNA-cleaving CRISPR-Cas systems as screening tools to select for genetic variants from a given population or as novel programmable antimicrobials to selectively remove certain pathogens from a mixed population (Figure 5B).

In an early study, Edgar and Qimron (2010) demonstrated that the native type I-E CRISPR-Cas system of *E. coli* could be used to cure the cells from prophage. The induced endogenous system could lead to killing of more than 98% of the cells in the population when the targeting activity was directed to an integrated lambda prophage. Interestingly, although prophage induction was also lethal to the cells, simultaneously inducing both of the pathways largely enhanced the survival rate. Further analyses showed that the genome of survivors exclusively did not harbor any prophage sequences. According to the observations, the authors suggested that the survived cells were possibly protected by the CRISPR system acting on excised bacteriophages, and most cells that still harbored prophage genes in the genome were killed by DNA targeting

(Edgar and Qimron, 2010). Later, self-targeting by a native type I-F system was reported to result in dramatic changes in the host's genome (Vercoe et al., 2013). Either part of or an entire preexisting pathogenicity island was deleted from the chromosome when targeted by the type I-F CRISPR-Cas system of *Pectobacterium atrosepticum*, a potato phytopathogen. The chromosomal alterations allowed the genetic variants to survive from CRISPR targeting and resulted in strains lacking pathogenicity, which was proposed to be a strong selective pressure for bacterial evolution (Vercoe et al., 2013).

The sequence specificity and selective killing feature of CRISPR-mediated genome targeting have enabled its antimicrobial utilization (Figure 5E), a concept that was put forward by Gomaa et al. (2014). Gomaa and coworkers assessed the genome targeting efficiency of the native type I-E CRISPR-Cas system from *E. coli* through evaluating cell escape rates. It was found that targeting single or multiple sites within coding or non-coding region of essential or non-essential genes on either strand of the genome gave similar outcomes of a dramatically low cell escape rate, demonstrating that the targeting was efficient and specific yet flexible, requiring only the target sequence with an optimal PAM. This specificity and flexibility allowed selective removal of individual or multiple strains, including highly similar ones, from pure or mixed cultures by directing the targeting activity to a unique or shared PAM-flanking genomic sequence (Gomaa et al., 2014). The application of type I-E CRISPR-Cas system of *E. coli* as antimicrobials was echoed in another study, in which Yosef et al. (2015) engineered a lambda prophage to deliver an active CRISPR-Cas system along with an artificial CRISPR that expresses crRNAs targeting antibiotic resistance genes into the *E. coli* host cells. After the delivery, the lysogenized *E. coli* cells were immunized against the corresponding antibiotic resistance gene-housing genetic elements, not only clearing the preexisting resistance determinants to sensitize the antibiotic-resistant bacteria, but also blocking further uptake of the same resistance. Importantly, the sensitized cells were protected by the delivered CRISPR-Cas system against lytic bacteriophages bearing the same targeting sequences, whereas the residual antibiotic-resistant cells would be persistently attacked by such type of bacteriophages, thus bringing out obvious selective benefit to the sensitized cells over the resistant ones. In addition, two endogenous type II CRISPR-Cas systems of *Streptococcus thermophilus* were also proven to be able to selectively remove closely related organisms by targeting unique sequences from a mixed population of microbes (Gomaa et al., 2014). Therefore, potent selective killing can be gained through different endogenous CRISPR-Cas systems. In fact, if provided with an appropriate delivery vehicle, heterologous CRISPR-Cas can be used as a programmable antimicrobial as well. In two parallel works, a heterologous type II CRISPR-Cas system was delivered into *E. coli* by an M13-based phagemid (Citorik et al., 2014) and into *Staphylococcus aureus* by a Φ NM1-based phagemid (Bikard et al., 2014), respectively, to selectively killing the pathogenic host cells.

In all above cases, both types I and II CRISPR self-targeting could give very robust selective pressure, thus obscuring the difference of targeting effect between these two types of

CRISPR-Cas. As illustrated in **Figure 4B**, Cas3 in type I is mainly responsible for target destruction, first nicking and then degrading DNA via its 3'- to 5'' exonuclease activity. In contrast, Cas9 in type II only cuts the target DNA. It would be interesting to evaluate whether DNA degradation contributes to further increased potency of killing through DNA repair prevention. Nevertheless, these CRISPR-based antimicrobials will undoubtedly limit the increasing threat of antimicrobial resistance microorganisms to the global public health.

Gene Expression Modulation

Type I CRISPR-Cas systems use the protein elements of Cascade and Cas3 for DNA interference. Depletion of Cas3 from a native type I system would still allow Cascade to tightly bind to the target DNA but without cleaving it. Thereby, the standalone Cascade becomes a transcriptional barrier to prevent either RNA polymerase access or transcription elongation, thus being capable of gene expression regulation (**Figure 5C**).

The capability of type I CRISPR-Cas systems in transcriptional regulation has been demonstrated for type I-E system of *E. coli* (**Figure 5F**) in two parallel studies, in both of which the Cas3 nuclease was eliminated (Luo et al., 2015; Rath et al., 2015). In *E. coli*, expression of the Cascade operon is largely repressed under laboratory conditions (Pul et al., 2010; Westra et al., 2010). In order to address this issue, Luo et al. (2015) generated a mutant strain, in which the transcription of Cascade operon was modified to be driven by a constitutive promoter, and Rath et al. (2015) exogenously introduced an extra copy of Cascade operon via a plasmid. These strains kept the ability to process the plasmid-borne CRISPR arrays containing either a single spacer or multiple spacers. As expected, the produced crRNA guided the Cascade to the target sites and exhibited strong repression effect on expression of a genome-integrated *gfp* reporter gene, especially when targeting the promoter region. Moreover, simultaneously repressing several genes was also assayed to be effective by taking the advantage that multiple unique mature crRNA molecules could be produced from a single CRISPR array (Luo et al., 2015; Rath et al., 2015).

Stachler and Marchfelder (2016) similarly, used the endogenous type I-B CRISPR-Cas system to perform *in vivo* gene down-regulation in the archaeon *H. volcanii*. Also, the *cas3* gene was either deleted or mutated to disable its catalytic activity to avoid genome cleavage. In addition, the crRNA-producing Cas6 protein was further depleted from the system, such that the genome-encoded CRISPR arrays would not be processed. Instead, the targeting crRNAs were encoded from a plasmid (Stachler and Marchfelder, 2016) and processed into mature crRNAs via a Cas6-independent approach for *H. volcanii* (Maier et al., 2015). This was evidenced to be significant for the interference efficiency, suggestive of competition between the targeting crRNA and internal crRNAs for Cascade and pointing toward the fact that Cascade is a limiting factor of type I silencing in this strain. Based on the strain modifications, efficient gene repression was seen, with the greatest reducing of transcripts by 92% when targeting the promoter region. Strand bias was also observed that Cascade targeting to the template strand showed much higher silencing efficiency than targeting

to the non-template strand (Stachler and Marchfelder, 2016). In our recent work, gene expression repression by an endogenous type I-F system was also successfully achieved for *Z. mobilis* (Zheng et al., 2019).

Aside from repression of independent genes, type I CRISPR interference was coopted for pathway engineering as well. In a pioneering work, the endogenous type I-E system was used to regulate catabolism of four sugars by targeting their respective operons in *E. coli*. All the four targeted sugar catabolism pathways were efficiently silenced by simply expressing a four-spacer CRISPR array (Luo et al., 2015). Subsequently, using the same endogenous system targeting *gltA* gene in *E. coli* also highly repressed the citrate synthase, leading to accumulation of acetate and thus regulation of the metabolic flux of central metabolism (Chang et al., 2016). Recently, Tarasava et al. (2018) applied CRISPR interference strategy to simultaneously alter the expression levels of multiple genes associated with 3-hydroxypropionate (3-PH) production and finally achieved nearly 2-fold increase of 3-PH yield in *E. coli*. In order to controllably utilize the type I-E system for CRISPR interference, the authors replaced the native promoter of Cascade operon with an arabinose-inducible promoter in a *cas3* deletion mutant. Considering that the placement of spacers within the cluster would influence the repression strength (Luo et al., 2015), the effect of different orders of spacer combination on the enhancement of 3-PH production was tested. On the other hand, a combinatorial library of gRNA array targeting six genes was built and subsequently used to screen for highest producing variants in this work, which was estimated to contain approximately 10⁴ unique variants and approximately three orders of magnitude more than that analyzed in the rational design approaches (Lv et al., 2015; Wu et al., 2015). Importantly, this library was proven to be diverse combinatorial as 48 out of 50 sequenced variants were found to be unique to each other. Furthermore, the orders of spacer combination harbored by some outstanding producing variants screened from the library were highly consistent with the rationally engineered variants (Tarasava et al., 2018).

All these studies have paved the way for further development of type I CRISPR-Cas-based *in vivo* gene interference tools in bacteria and archaea. Considering the broad occurrence of diverse type I systems, it is of great interest to see whether other subtypes are able to perform gene silencing in many other bacteria and archaea.

CONCLUSION AND PERSPECTIVES

Based on the extensive studies on characterizing the type I CRISPR-Cas functions, a general mechanism of type I DNA interference can be deduced (**Figure 4B**). The functional demonstrations have contributed great efforts for exploiting the endogenous type I systems as CRISPR toolkits for genome editing, antimicrobials, gene regulation, and so on, in bacteria and archaea. While many successful achievements have already proven type I CRISPR-based technologies to be powerful tools for prokaryotic engineering, they are still in their infancy stage,

leaving many hurdles for their deeper improvements for a wider range of applications.

Hurdles Ahead

To truly exploit the endogenous type I CRISPR-Cas systems, there are several critical obstacles still required to be addressed. First, because of the host-specific property of endogenous CRISPR-Cas systems, each of them must be thoroughly characterized in the host cells, including determination of PAM sequences, demonstration of Cas functions, and identification of mature crRNAs, as well as dissection of its mode of action during foreign DNA defense. Second, low efficiency of exogenous DNA delivery and their low stability in host cells might significantly hamper the repurposing of endogenous CRISPR-Cas. Although there is no need of importing exogenous Cas proteins, other genetic materials, for example, artificial CRISPR arrays, and donor DNA templates during genome editing, are still required to be introduced into the cells with relatively high concentrations. Therefore, efficient delivery systems would help for better performances during the applications. Separately, prokaryotes harbor a collection of innate defense systems, such as R-M (Roberts et al., 2015), BREX (Goldfarb et al., 2015), and so on. Many of these systems are prevalent; for example, approximately 95% of sequenced bacterial genomes encode at least one R-M system (Roberts et al., 2015). Research has shown that destroying such innate defense systems can lead to boosted plasmid transformation rate and hence genome engineering efficiency (Zheng et al., 2019). In addition, because most of prokaryotes use the less efficient HR pathway for repairing the CRISPR-generated DNA injuries, it is always good to maintain a high concentration of introduced donor DNAs to ensure a better performance of genome editing. To this end, several strategies can be used, such as supplying DNA templates as inserts of the vectors to allow their multiplication (Li et al., 2016; Cheng et al., 2017; Zheng et al., 2019). Finally, during the CRISPR-targeting, escape always occurs with various modes, normally due to modifications/alterations in spacer or protospacer, or alternatively mutations in Cas proteins. However, it would be important but troublesome to understand the escape modes and underlying mechanisms, which might provide possibility for further increasing the overall efficiency of genome manipulations.

CRISPR-dCas3 Exploitation

Current applications of type I CRISPR-Cas systems focus mainly on genome editing and gene down-regulation. For the latter,

in most studies, the *cas3* gene was deleted from the system. Actually, a system with a catalytically inactive Cas3 (dCas3) would have further uses. For instance, considering DSDBs are repaired with relatively lower efficiencies in prokaryotic cells, it would be beneficial to use a catalytically inactive Cas protein, for example, dCas9 or dCas3, with the *FokI* endonuclease to generate DSDBs in a manner that can be more easily repaired by the endogenous pathways, hence increasing engineering efficiency (Guilinger et al., 2014; Tsai et al., 2014). In an even efficient manner, single DNA changes within a targeted window can be achieved without introducing DSDBs by using deaminase-dCas9 fusions in *E. coli* (Gaudelli et al., 2017; Banno et al., 2018), where the CRISPR-dCas9 system might be potentially replaced with an endogenous CRISPR-dCas3 system. Additionally, dCas3, together with the Cascade, may enrich a fusing transcription activator to a genomic region and may thus lead to activation of targeted genes, just in parallel with the similar applications of dCas9/dCas12 as reviewed by Yao et al. (2018). In short, attempts of other applications through the endogenous type I CRISPR-dCas3 systems, such as cell imaging that has not been reported in prokaryotes, can be achievable and will further extend the application scope of CRISPR-based technologies.

AUTHOR CONTRIBUTIONS

WP conceived the outline with inputs from all authors. YZ and WP prepared and wrote the manuscript. WP and LY revised the manuscript. JL, BW, JH, YH, SW, XM, SY, and LM conducted the extensive review. All authors contributed to the writing, reading, and approval of the final manuscript.

FUNDING

This work was supported by the National Key Technology Research and Development Program of China (2018YFA090091 and 2018YFD0500203 to LY); the Natural Science Foundation of Hubei Province of China (2017CFB538, to WP); the Scientific Research Program of Hubei Provincial Department of Education (Q20161007, to WP); and the National Science Foundation of China (31870057, to LY and WP). WP and LY also acknowledge the support from the State Key Laboratory of Biocatalysis and Enzyme Engineering.

REFERENCES

- Banno, S., Nishida, K., Arazoe, T., Mitsunobu, H., and Kondo, A. (2018). Deaminase-mediated multiplex genome editing in *Escherichia coli*. *Nat. Microbiol.* 3, 423–429. doi: 10.1038/s41564-017-0102-6
- Barrangou, R., Fremaux, C., Deveau, H., Richards, M., Boyaval, P., Moineau, S., et al. (2007). CRISPR provides acquired resistance against viruses in prokaryotes. *Science* 315, 1709–1712. doi: 10.1126/science.1138140
- Beloglazova, N., Petit, P., Flick, R., Brown, G., Savchenko, A., and Yakunin, A. F. (2011). Structure and activity of the Cas3 HD nuclease MJ0384, an effector enzyme of the CRISPR interference. *EMBO J.* 30, 4616–4627. doi: 10.1038/emboj.2011.377
- Bikard, D., Euler, C. W., Jiang, W., Nussenzweig, P. M., Goldberg, G. W., Duportet, X., et al. (2014). Exploiting CRISPR-Cas nucleases to produce sequence-specific antimicrobials. *Nat. Biotechnol.* 32, 1146–1150. doi: 10.1038/nbt.3043
- Bolotin, A., Quinquis, B., Sorokin, A., and Ehrlich, S. D. (2005). Clustered regularly interspaced short palindrome repeats (CRISPRs) have spacers of extrachromosomal origin. *Microbiology* 151, 2551–2561. doi: 10.1099/mic.0.28048-0
- Brendel, J., Stoll, B., Lange, S. J., Sharma, K., Lenz, C., Stachler, A. E., et al. (2014). A complex of Cas proteins 5, 6, and 7 is required for the biogenesis and stability of clustered regularly interspaced short palindromic repeats (crispr)-derived rnas (crRNAs) in *Haloferax volcanii*. *J. Biol. Chem.* 289, 7164–7177. doi: 10.1074/jbc.M113.508184

- Brouns, S. J., Jore, M. M., Lundgren, M., Westra, E. R., Slijkhuis, R. J., Snijders, A. P., et al. (2008). Small CRISPR RNAs guide antiviral defense in prokaryotes. *Science* 321, 960–964. doi: 10.1126/science.1159689
- Carte, J., Pfister, N. T., Compton, M. M., Terns, R. M., and Terns, M. P. (2010). Binding and cleavage of CRISPR RNA by Cas6. *RNA* 16, 2181–2188. doi: 10.1261/rna.2230110
- Cass, S. D., Haas, K. A., Stoll, B., Alkhnbashi, O. S., Sharma, K., Urlaub, H., et al. (2015). The role of Cas8 in type I CRISPR interference. *Biosci. Rep.* 35:e00197. doi: 10.1042/BSR20150043
- Chang, Y., Su, T., Qi, Q., and Liang, Q. (2016). Easy regulation of metabolic flux in *Escherichia coli* using an endogenous type I-E CRISPR-Cas system. *Microb. Cell Fact.* 15:195. doi: 10.1186/s12934-016-0594-4
- Chen, B., Gilbert, L. A., Cimini, B. A., Schnitzbauer, J., Zhang, W., Li, G. W., et al. (2013). Dynamic imaging of genomic loci in living human cells by an optimized CRISPR/Cas system. *Cell* 155, 1479–1491. doi: 10.1016/j.cell.2013.12.001
- Cheng, A. W., Wang, H., Yang, H., Shi, L., Katz, Y., Theunissen, T. W., et al. (2013). Multiplexed activation of endogenous genes by CRISPR-on, an RNA-guided transcriptional activator system. *Cell Res.* 23, 1163–1171. doi: 10.1038/cr.2013.122
- Cheng, F., Gong, L., Zhao, D., Yang, H., Zhou, J., Li, M., et al. (2017). Harnessing the native type I-B CRISPR-Cas for genome editing in a polyploid archaeon. *J. Genet. Genomics* 44, 541–548. doi: 10.1016/j.jgg.2017.09.010
- Cho, S., Choe, D., Lee, E., Kim, S. C., Palsson, B., and Cho, B. K. (2018). High-level dCas9 expression induces abnormal cell morphology in *Escherichia coli*. *ACS Synth. Biol.* 7, 1085–1094. doi: 10.1021/acssynbio.7b00462
- Citorik, R. J., Mimmee, M., and Lu, T. K. (2014). Sequence-specific antimicrobials using efficiently delivered RNA-guided nucleases. *Nat. Biotechnol.* 32, 1141–1145. doi: 10.1038/nbt.3011
- Cong, L., Ran, F. A., Cox, D., Lin, S., Barretto, R., Habib, N., et al. (2013). Multiplex genome engineering using CRISPR/Cas systems. *Science* 339, 819–823. doi: 10.1126/science.1231143
- Cox, D. B. T., Gootenberg, J. S., Abudayyeh, O. O., Franklin, B., Kellner, M. J., Joung, J., et al. (2017). RNA editing with CRISPR-Cas13. *Science* 358, 1019–1027. doi: 10.1126/science.aag0180
- Crowley, V. M., Catching, A., Taylor, H. N., Borges, A. L., Metcalf, J., Bondy-Denomy, J., et al. (2019). A type IV-A CRISPR-Cas system in *Pseudomonas aeruginosa* mediates RNA-guided plasmid interference in vivo. *CRISPR J.* 2, 434–440. doi: 10.1089/crispr.2019.0048
- Doron, S., Melamed, S., Ofir, G., Leavitt, A., Lopatina, A., Keren, M., et al. (2018). Systematic discovery of antiphage defense systems in the microbial pangenome. *Science* 359:eaar4120. doi: 10.1126/science.aar4120
- Edgar, R., and Qimron, U. (2010). The *Escherichia coli* CRISPR system protects from lambda lysogenization, lysogens, and prophage induction. *J. Bacteriol.* 192, 6291–6294. doi: 10.1128/JB.00644-10
- Elmore, J., Deighan, T., Westpheling, J., Terns, R. M., and Terns, M. P. (2015). DNA targeting by the type I-G and type I-A CRISPR-Cas systems of *Pyrococcus furiosus*. *Nucleic Acids Res.* 43, 10353–10363. doi: 10.1093/nar/gkv1140
- Fonfara, I., Richter, H., Bratovic, M., Le Rhun, A., and Charpentier, E. (2016). The CRISPR-associated DNA-cleaving enzyme Cpf1 also processes precursor CRISPR RNA. *Nature* 532, 517–521. doi: 10.1038/nature17945
- Garneau, J. E., Dupuis, M. E., Villion, M., Romero, D. A., Barrangou, R., Boyaval, P., et al. (2010). The CRISPR/Cas bacterial immune system cleaves bacteriophage and plasmid DNA. *Nature* 468, 67–71. doi: 10.1038/nature09523
- Garside, E. L., Schellenberg, M. J., Gesner, E. M., Bonanno, J. B., Sauder, J. M., Burley, S. K., et al. (2012). Cas5d processes pre-crRNA and is a member of a larger family of CRISPR RNA endonucleases. *RNA* 18, 2020–2028. doi: 10.1261/rna.033100.112
- Gaudelli, N. M., Komor, A. C., Rees, H. A., Packer, M. S., Badran, A. H., Bryson, D. I., et al. (2017). Programmable base editing of A*T to G*C in genomic DNA without DNA cleavage. *Nature* 551, 464–471. doi: 10.1038/nature24644
- Goldfarb, T., Sberro, H., Weinstock, E., Cohen, O., Doron, S., Charpak-Amikam, Y., et al. (2015). BREX is a novel phage resistance system widespread in microbial genomes. *EMBO J.* 34, 169–183. doi: 10.15252/embj.201489455
- Gomaa, A. A., Klumpe, H. E., Luo, M. L., Selle, K., Barrangou, R., and Beisel, C. L. (2014). Programmable removal of bacterial strains by use of genome-targeting CRISPR-Cas systems. *mBio* 5:e00928-13. doi: 10.1128/mBio.00928-13
- Gong, B., Shin, M., Sun, J., Jung, C. H., Bolt, E. L., van der Oost, J., et al. (2014). Molecular insights into DNA interference by CRISPR-associated nuclease-helicase Cas3. *Proc. Natl. Acad. Sci. U.S.A.* 111, 16359–16364. doi: 10.1073/pnas.1410806111
- Grissa, I., Vergnaud, G., and Pourcel, C. (2007). The CRISPRdb database and tools to display CRISPRs and to generate dictionaries of spacers and repeats. *BMC Bioinformatics* 8:172. doi: 10.1186/1471-2105-8-172
- Gudbergdottir, S., Deng, L., Chen, Z., Jensen, J. V., Jensen, L. R., She, Q., et al. (2011). Dynamic properties of the *Sulfolobus* CRISPR/Cas and CRISPR/Cmr systems when challenged with vector-borne viral and plasmid genes and protospacers. *Mol. Microbiol.* 79, 35–49. doi: 10.1111/j.1365-2958.2010.07452.x
- Guilinger, J. P., Thompson, D. B., and Liu, D. R. (2014). Fusion of catalytically inactive Cas9 to FokI nuclease improves the specificity of genome modification. *Nat. Biotechnol.* 32, 577–582. doi: 10.1038/nbt.2909
- Guo, L., Brugger, K., Liu, C., Shah, S. A., Zheng, H., Zhu, Y., et al. (2011). Genome analyses of Icelandic strains of *Sulfolobus islandicus*, model organisms for genetic and virus-host interaction studies. *J. Bacteriol.* 193, 1672–1680. doi: 10.1128/JB.01487-10
- Haft, D. H., Selengut, J., Mongodin, E. F., and Nelson, K. E. (2005). A guild of 45 CRISPR-associated (Cas) protein families and multiple CRISPR/Cas subtypes exist in prokaryotic genomes. *PLoS Comput. Biol.* 1:e60. doi: 10.1371/journal.pcbi.0010060
- Hale, C. R., Zhao, P., Olson, S., Duff, M. O., Graveley, B. R., Wells, L., et al. (2009). RNA-guided RNA cleavage by a CRISPR RNA-Cas protein complex. *Cell* 139, 945–956. doi: 10.1016/j.cell.2009.07.040
- Halpin-Healy, T. S., Klompe, S. E., Sternberg, S. H., and Fernandez, I. S. (2019). Structural basis of DNA targeting by a transposon-encoded CRISPR-Cas system. *Nature* 577, 271–274. doi: 10.1038/s41586-019-1849-0
- Han, D., and Krauss, G. (2009). Characterization of the endonuclease SSO2001 from *Sulfolobus solfataricus* P2. *FEBS Lett.* 583, 771–776. doi: 10.1016/j.febslet.2009.01.024
- Harrington, L. B., Burstein, D., Chen, J. S., Paez-Espino, D., Ma, E., Witte, I. P., et al. (2018). Programmed DNA destruction by miniature CRISPR-Cas14 enzymes. *Science* 362, 839–842. doi: 10.1126/science.aav4294
- Haurwitz, R. E., Jinek, M., Wiedenheft, B., Zhou, K., and Doudna, J. A. (2010). Sequence- and structure-specific RNA processing by a CRISPR endonuclease. *Science* 329, 1355–1358. doi: 10.1126/science.1192272
- Hayes, R. P., Xiao, Y., Ding, F., van Erp, P. B., Rajashankar, K., Bailey, S., et al. (2016). Structural basis for promiscuous PAM recognition in type I-E Cascade from *E. coli*. *Nature* 530, 499–503. doi: 10.1038/nature16995
- Hidalgo-Cantabrana, C., Goh, Y. J., and Barrangou, R. (2019a). Characterization and repurposing of type I and type II CRISPR-Cas systems in bacteria. *J. Mol. Biol.* 431, 21–33. doi: 10.1016/j.jmb.2018.09.013
- Hidalgo-Cantabrana, C., Goh, Y. J., Pan, M., Sanozky-Dawes, R., and Barrangou, R. (2019b). Genome editing using the endogenous type I CRISPR-Cas system in *Lactobacillus crispatus*. *Proc. Natl. Acad. Sci. U.S.A.* 116, 15774–15783. doi: 10.1073/pnas.1905421116
- Hochstrasser, M. L., Taylor, D. W., Bhat, P., Guegler, C. K., Sternberg, S. H., Nogales, E., et al. (2014). CasA mediates Cas3-catalyzed target degradation during CRISPR RNA-guided interference. *Proc. Natl. Acad. Sci. U.S.A.* 111, 6618–6623. doi: 10.1073/pnas.1405079111
- Howard, J. A., Delmas, S., Ivancic-Bace, I., and Bolt, E. L. (2011). Helicase dissociation and annealing of RNA-DNA hybrids by *Escherichia coli* Cas3 protein. *Biochem. J.* 439, 85–95. doi: 10.1042/BJ20110901
- Huo, Y., Nam, K. H., Ding, F., Lee, H., Wu, L., Xiao, Y., et al. (2014). Structures of CRISPR Cas3 offer mechanistic insights into Cascade-activated DNA unwinding and degradation. *Nat. Struct. Mol. Biol.* 21, 771–777. doi: 10.1038/nsmb.2875
- Jackson, R. N., Golden, S. M., van Erp, P. B., Carter, J., Westra, E. R., Brouns, S. J., et al. (2014). Crystal structure of the CRISPR RNA-guided surveillance complex from *Escherichia coli*. *Science* 345, 1473–1479. doi: 10.1126/science.1256328
- Jansen, R., Embden, J. D., Gaastra, W., and Schouls, L. M. (2002). Identification of genes that are associated with DNA repeats in prokaryotes. *Mol. Microbiol.* 43, 1565–1575. doi: 10.1046/j.1365-2958.2002.02839.x
- Jesser, R., Behler, J., Benda, C., Reimann, V., and Hess, W. R. (2019). Biochemical analysis of the Cas6-1 RNA endonuclease associated with the subtype I-D

- CRISPR-Cas system in *Synechocystis* sp. PCC 6803. *RNA Biol.* 16, 481–491. doi: 10.1080/15476286.2018.1447742
- Jiang, W., Yang, B., and Weeks, D. P. (2014). Efficient CRISPR/Cas9-mediated gene editing in *Arabidopsis thaliana* and inheritance of modified genes in the T2 and T3 generations. *PLoS One* 9:e99225. doi: 10.1371/journal.pone.0099225
- Jiang, Y., Qian, F., Yang, J., Liu, Y., Dong, F., Xu, C., et al. (2017). CRISPR-Cpf1 assisted genome editing of *Corynebacterium glutamicum*. *Nat. Commun.* 8:15179. doi: 10.1038/ncomms15179
- Jinek, M., Chylinski, K., Fonfara, I., Hauer, M., Doudna, J. A., and Charpentier, E. (2012). A programmable dual-RNA-guided DNA endonuclease in adaptive bacterial immunity. *Science* 337, 816–821. doi: 10.1126/science.1225829
- Jore, M. M., Lundgren, M., van Duijn, E., Bultema, J. B., Westra, E. R., Waghmare, S. P., et al. (2011). Structural basis for CRISPR RNA-guided DNA recognition by Cascade. *Nat. Struct. Mol. Biol.* 18, 529–536. doi: 10.1038/nsmb.2019
- Klompe, S. E., Vo, P. L. H., Halpin-Healy, T. S., and Sternberg, S. H. (2019). Transposon-encoded CRISPR-Cas systems direct RNA-guided DNA integration. *Nature* 571, 219–225. doi: 10.1038/s41586-019-1323-z
- Koo, Y., Ka, D., Kim, E. J., Suh, N., and Bae, E. (2013). Conservation and variability in the structure and function of the Cas5d endoribonuclease in the CRISPR-mediated microbial immune system. *J. Mol. Biol.* 425, 3799–3810. doi: 10.1016/j.jmb.2013.02.032
- Koonin, E. V., Makarova, K. S., and Wolf, Y. I. (2017a). Evolutionary genomics of defense systems in archaea and bacteria. *Annu. Rev. Microbiol.* 71, 233–261. doi: 10.1146/annurev-micro-090816-093830
- Koonin, E. V., Makarova, K. S., and Zhang, F. (2017b). Diversity, classification and evolution of CRISPR-Cas systems. *Curr. Opin. Microbiol.* 37, 67–78. doi: 10.1016/j.mib.2017.05.008
- Kunin, V., Sorek, R., and Hugenholtz, P. (2007). Evolutionary conservation of sequence and secondary structures in CRISPR repeats. *Genome Biol.* 8:R61. doi: 10.1186/gb-2007-8-4-r61
- Lewis, B. P., Shih, I. H., Jones-Rhoades, M. W., Bartel, D. P., and Burge, C. B. (2003). Prediction of mammalian microRNA targets. *Cell* 115, 787–798. doi: 10.1016/s0092-8674(03)01018-3
- Li, H. (2014). Structural principles of CRISPR RNA processing. *Structure* 23, 13–20. doi: 10.1016/j.str.2014.10.006
- Li, M., Liu, H., Han, J., Liu, J., Wang, R., Zhao, D., et al. (2013). Characterization of CRISPR RNA biogenesis and Cas6 cleavage-mediated inhibition of a provirus in the haloarchaeon *Haloferax mediterranei*. *J. Bacteriol.* 195, 867–875. doi: 10.1128/JB.01688-12
- Li, Y., Pan, S., Zhang, Y., Ren, M., Feng, M., Peng, N., et al. (2016). Harnessing Type I and Type III CRISPR-Cas systems for genome editing. *Nucleic Acids Res.* 44:e34. doi: 10.1093/nar/gkv1044
- Lintner, N. G., Kerou, M., Brumfield, S. K., Graham, S., Liu, H., Naismith, J. H., et al. (2011). Structural and functional characterization of an archaeal clustered regularly interspaced short palindromic repeat (CRISPR)-associated complex for antiviral defense (CASCADE). *J. Biol. Chem.* 286, 21643–21656. doi: 10.1074/jbc.M111.238485
- Liu, T., Pan, S., Li, Y., Peng, N., and She, Q. (2018). Type III CRISPR-Cas system: introduction and its application for genetic manipulations. *Curr. Issues Mol. Biol.* 26, 1–14. doi: 10.21775/cimb.026.001
- Luo, M. L., Mullis, A. S., Leenay, R. T., and Beisel, C. L. (2015). Repurposing endogenous type I CRISPR-Cas systems for programmable gene repression. *Nucleic Acids Res.* 43, 674–681. doi: 10.1093/nar/gku971
- Lv, L., Ren, Y. L., Chen, J. C., Wu, Q., and Chen, G. Q. (2015). Application of CRISPRi for prokaryotic metabolic engineering involving multiple genes, a case study: controllable P(3HB-co-4HB) biosynthesis. *Metab. Eng.* 29, 160–168. doi: 10.1016/j.ymben.2015.03.013
- Maier, L. K., Lange, S. J., Stoll, B., Haas, K. A., Fischer, S., Fischer, E., et al. (2013). Essential requirements for the detection and degradation of invaders by the *Haloferax volcanii* CRISPR/Cas system I-B. *RNA Biol.* 10, 865–874. doi: 10.4161/rna.24282
- Maier, L. K., Stachler, A. E., Saunders, S. J., Backofen, R., and Marchfelder, A. (2015). An active immune defense with a minimal CRISPR (clustered regularly interspaced short palindromic repeats) RNA and without the Cas6 protein. *J. Biol. Chem.* 290, 4192–4201. doi: 10.1074/jbc.M114.617506
- Majumdar, S., Zhao, P., Pfister, N. T., Compton, M., Olson, S., Glover, C. V., et al. (2015). Three CRISPR-Cas immune effector complexes coexist in *Pyrococcus furiosus*. *RNA* 21, 1147–1158. doi: 10.1261/rna.049130.114
- Makarova, K. S., Aravind, L., Wolf, Y. I., and Koonin, E. V. (2011a). Unification of Cas protein families and a simple scenario for the origin and evolution of CRISPR-Cas systems. *Biol. Direct* 6:38. doi: 10.1186/1745-6150-6-38
- Makarova, K. S., Grishin, N. V., Shabalina, S. A., Wolf, Y. I., and Koonin, E. V. (2006). A putative RNA-interference-based immune system in prokaryotes: computational analysis of the predicted enzymatic machinery, functional analogies with eukaryotic RNAi, and hypothetical mechanisms of action. *Biol. Direct* 1:7. doi: 10.1186/1745-6150-1-7
- Makarova, K. S., Haft, D. H., Barrangou, R., Brouns, S. J., Charpentier, E., Horvath, P., et al. (2011b). Evolution and classification of the CRISPR-Cas systems. *Nat. Rev. Microbiol.* 9, 467–477. doi: 10.1038/nrmicro2577
- Makarova, K. S., Wolf, Y. I., Alkhnbashi, O. S., Costa, F., Shah, S. A., Saunders, S. J., et al. (2015). An updated evolutionary classification of CRISPR-Cas systems. *Nat. Rev. Microbiol.* 13, 722–736. doi: 10.1038/nrmicro3569
- Makarova, K. S., Wolf, Y. I., Iranzo, J., Shmakov, S. A., Alkhnbashi, O. S., Brouns, S. J. J., et al. (2019). Evolutionary classification of CRISPR-Cas systems: a burst of class 2 and derived variants. *Nat. Rev. Microbiol.* 18, 67–83. doi: 10.1038/s41579-019-0299-x
- Makarova, K. S., Wolf, Y. I., and Koonin, E. V. (2018). Classification and Nomenclature of CRISPR-Cas Systems: Where from Here? *CRISPR J.* 1, 325–336. doi: 10.1089/crispr.2018.0033
- Malina, A., Mills, J. R., Cencic, R., Yan, Y., Fraser, J., Schippers, L. M., et al. (2013). Repurposing CRISPR/Cas9 for in situ functional assays. *Genes Dev.* 27, 2602–2614. doi: 10.1101/gad.227132.113
- Marraffini, L. A., and Sontheimer, E. J. (2008). CRISPR interference limits horizontal gene transfer in *Staphylococci* by targeting DNA. *Science* 322, 1843–1845. doi: 10.1126/science.1165771
- Mojica, F. J., Diez-Villasenor, C., Garcia-Martinez, J., and Almendros, C. (2009). Short motif sequences determine the targets of the prokaryotic CRISPR defence system. *Microbiology* 155, 733–740. doi: 10.1099/mic.0.023960-0
- Mojica, F. J., Diez-Villasenor, C., Garcia-Martinez, J., and Soria, E. (2005). Intervening sequences of regularly spaced prokaryotic repeats derive from foreign genetic elements. *J. Mol. Evol.* 60, 174–182. doi: 10.1007/s00239-004-0046-3
- Mulepati, S., and Bailey, S. (2011). Structural and biochemical analysis of nuclease domain of clustered regularly interspaced short palindromic repeat (CRISPR)-associated protein 3 (Cas3). *J. Biol. Chem.* 286, 31896–31903. doi: 10.1074/jbc.M111.270017
- Mulepati, S., and Bailey, S. (2013). In vitro reconstitution of an *Escherichia coli* RNA-guided immune system reveals unidirectional, ATP-dependent degradation of DNA target. *J. Biol. Chem.* 288, 22184–22192. doi: 10.1074/jbc.M113.472233
- Mulepati, S., Heroux, A., and Bailey, S. (2014). Crystal structure of a CRISPR RNA-guided surveillance complex bound to a ssDNA target. *Science* 345, 1479–1484. doi: 10.1126/science.1256996
- Nam, K. H., Haitjema, C., Liu, X., Ding, F., Wang, H., DeLisa, M. P., et al. (2012). Cas5d protein processes pre-crRNA and assembles into a cascade-like interference complex in subtype I-C/Dvulg CRISPR-Cas system. *Structure* 20, 1574–1584. doi: 10.1016/j.str.2012.06.016
- Nickel, L., Ulbricht, A., Alkhnbashi, O. S., Forstner, K. U., Cassidy, L., Weidenbach, K., et al. (2019). Cross-cleavage activity of Cas6b in crRNA processing of two different CRISPR-Cas systems in *Methanosarcina mazei* Go1. *RNA Biol.* 16, 492–503. doi: 10.1080/15476286.2018.1514234
- O'Connell, M. R. (2019). Molecular mechanisms of RNA targeting by Cas13-containing Type VI CRISPR-Cas systems. *J. Mol. Biol.* 431, 66–87. doi: 10.1016/j.jmb.2018.06.029
- Ozcan, A., Pausch, P., Linden, A., Wulf, A., Schuhle, K., Heider, J., et al. (2019). Type IV CRISPR RNA processing and effector complex formation in *Aromatoleum aromaticum*. *Nat. Microbiol.* 4, 89–96. doi: 10.1038/s41564-018-0274-8
- Pausch, P., Muller-Esparza, H., Gleditsch, D., Altegoer, F., Randau, L., and Bange, G. (2017). Structural variation of Type I-F CRISPR RNA guided DNA surveillance. *Mol. Cell* 67, 622–632.e4. doi: 10.1016/j.molcel.2017.06.036
- Peng, W., Feng, M., Feng, X., Liang, Y. X., and She, Q. (2015). An archaeal CRISPR type III-B system exhibiting distinctive RNA targeting features and mediating dual RNA and DNA interference. *Nucleic Acids Res.* 43, 406–417. doi: 10.1093/nar/gku1302

- Peng, W., Li, H., Hallstrom, S., Peng, N., Liang, Y. X., and She, Q. (2013). Genetic determinants of PAM-dependent DNA targeting and pre-crRNA processing in *Sulfolobus islandicus*. *RNA Biol.* 10, 738–748. doi: 10.4161/rna.23798
- Perez-Pinera, P., Kocak, D. D., Vockley, C. M., Adler, A. F., Kabadi, A. M., Polstein, L. R., et al. (2013). RNA-guided gene activation by CRISPR-Cas9-based transcription factors. *Nat. Methods* 10, 973–976. doi: 10.1038/nmeth.2600
- Peters, J. E. (2014). Tn7. *Microbiol. Spectr.* 2, 1–20. doi: 10.1128/microbiolspec.MDNA3-0010-2014
- Peters, J. E., Makarova, K. S., Shmakov, S., and Koonin, E. V. (2017). Recruitment of CRISPR-Cas systems by Tn7-like transposons. *Proc. Natl. Acad. Sci. U.S.A.* 114, E7358–E7366. doi: 10.1073/pnas.1709035114
- Pourcel, C., Salvignol, G., and Vergnaud, G. (2005). CRISPR elements in *Yersinia pestis* acquire new repeats by preferential uptake of bacteriophage DNA, and provide additional tools for evolutionary studies. *Microbiology* 151, 653–663. doi: 10.1099/mic.0.27437-0
- Przybilski, R., Richter, C., Gristwood, T., Clulow, J. S., Vercoc, R. B., and Fineran, P. C. (2011). Csy4 is responsible for CRISPR RNA processing in *Pectobacterium atrosepticum*. *RNA Biol.* 8, 517–528. doi: 10.4161/rna.8.3.15190
- Pul, U., Wurm, R., Arslan, Z., Geissen, R., Hofmann, N., and Wagner, R. (2010). Identification and characterization of *E. coli* CRISPR-cas promoters and their silencing by H-NS. *Mol. Microbiol.* 75, 1495–1512. doi: 10.1111/j.1365-2958.2010.07073.x
- Punetha, A., Sivathanu, R., and Anand, B. (2014). Active site plasticity enables metal-dependent tuning of Cas5d nuclease activity in CRISPR-Cas type I-C system. *Nucleic Acids Res.* 42, 3846–3856. doi: 10.1093/nar/gkt1335
- Pyne, M. E., Bruder, M. R., Moo-Young, M., Chung, D. A., and Chou, C. P. (2016). Harnessing heterologous and endogenous CRISPR-Cas machineries for efficient markerless genome editing in *Clostridium*. *Sci. Rep.* 6:25666. doi: 10.1038/srep25666
- Qi, L. S., Larson, M. H., Gilbert, L. A., Doudna, J. A., Weissman, J. S., Arkin, A. P., et al. (2013). Repurposing CRISPR as an RNA-guided platform for sequence-specific control of gene expression. *Cell* 152, 1173–1183. doi: 10.1016/j.cell.2013.02.022
- Rath, D., Amlinger, L., Hoekzema, M., Devulapally, P. R., and Lundgren, M. (2015). Efficient programmable gene silencing by Cascade. *Nucleic Acids Res.* 43, 237–246. doi: 10.1093/nar/gku1257
- Reeks, J., Naismith, J. H., and White, M. F. (2013). CRISPR interference: a structural perspective. *Biochem. J.* 453, 155–166. doi: 10.1042/BJ20130316
- Renaud, J. B., Boix, C., Charpentier, M., De Cian, A., Cochenne, J., Duvernois-Berthet, E., et al. (2016). Improved genome editing efficiency and flexibility using modified oligonucleotides with TALEN and CRISPR-Cas9 nucleases. *Cell Rep.* 14, 2263–2272. doi: 10.1016/j.celrep.2016.02.018
- Roberts, R. J., Vincze, T., Posfai, J., and Macelis, D. (2015). REBASE—a database for DNA restriction and modification: enzymes, genes and genomes. *Nucleic Acids Res.* 43, D298–D299. doi: 10.1093/nar/gku1046
- Sashital, D. G., Jinek, M., and Doudna, J. A. (2011). An RNA-induced conformational change required for CRISPR RNA cleavage by the endonuclease Cse3. *Nat. Struct. Mol. Biol.* 18, 680–687. doi: 10.1038/nsmb.2043
- Sashital, D. G., Wiedenheft, B., and Doudna, J. A. (2012). Mechanism of foreign DNA selection in a bacterial adaptive immune system. *Mol. Cell* 46, 606–615. doi: 10.1016/j.molcel.2012.03.020
- Scholz, I., Lange, S. J., Hein, S., Hess, W. R., and Backofen, R. (2013). CRISPR-Cas systems in the cyanobacterium *Synechocystis* sp. PCC6803 exhibit distinct processing pathways involving at least two Cas6 and a Cmr2 protein. *PLoS One* 8:e56470. doi: 10.1371/journal.pone.0056470
- Sefcikova, J., Roth, M., Yu, G., and Li, H. (2017). Cas6 processes tight and relaxed repeat RNA via multiple mechanisms: a hypothesis. *Bioessays* 39:10.1002/bies.201700019. doi: 10.1002/bies.201700019
- Semenova, E., Jore, M. M., Datsenko, K. A., Semenova, A., Westra, E. R., Wanner, B., et al. (2011). Interference by clustered regularly interspaced short palindromic repeat (CRISPR) RNA is governed by a seed sequence. *Proc. Natl. Acad. Sci. U.S.A.* 108, 10098–10103. doi: 10.1073/pnas.1104144108
- Shalem, O., Sanjana, N. E., Hartenian, E., Shi, X., Scott, D. A., Mikkelsen, T., et al. (2014). Genome-scale CRISPR-Cas9 knockout screening in human cells. *Science* 343, 84–87. doi: 10.1126/science.1247005
- Shao, Y., and Li, H. (2013). Recognition and cleavage of a nonstructured CRISPR RNA by its processing endonuclease Cas6. *Structure* 21, 385–393. doi: 10.1016/j.str.2013.01.010
- Shao, Y., Richter, H., Sun, S., Sharma, K., Urlaub, H., Randau, L., et al. (2016). A non-stem-loop CRISPR RNA is processed by dual binding Cas6. *Structure* 24, 547–554. doi: 10.1016/j.str.2016.02.009
- Sinkunas, T., Gasiunas, G., Fremaux, C., Barrangou, R., Horvath, P., and Siksnys, V. (2011). Cas3 is a single-stranded DNA nuclease and ATP-dependent helicase in the CRISPR/Cas immune system. *EMBO J.* 30, 1335–1342. doi: 10.1038/emboj.2011.41
- Sinkunas, T., Gasiunas, G., Waghmare, S. P., Dickman, M. J., Barrangou, R., Horvath, P., et al. (2013). *In vitro* reconstitution of Cascade-mediated CRISPR immunity in *Streptococcus thermophilus*. *EMBO J.* 32, 385–394. doi: 10.1038/emboj.2012.352
- Sokolowski, R. D., Graham, S., and White, M. F. (2014). Cas6 specificity and CRISPR RNA loading in a complex CRISPR-Cas system. *Nucleic Acids Res.* 42, 6532–6541. doi: 10.1093/nar/gku308
- Stachler, A. E., and Marchfelder, A. (2016). Gene repression in Haloarchaea using the CRISPR (Clustered Regularly Interspaced Short Palindromic Repeats)-Cas I-B system. *J. Biol. Chem.* 291, 15226–15242. doi: 10.1074/jbc.M116.724062
- Sternberg, S. H., Haurwitz, R. E., and Doudna, J. A. (2012). Mechanism of substrate selection by a highly specific CRISPR endonuclease. *RNA* 18, 661–672. doi: 10.1261/rna.030882.111
- Strecker, J., Ladha, A., Gardner, Z., Schmid-Burgk, J. L., Makarova, K. S., Koonin, E. V., et al. (2019). RNA-guided DNA insertion with CRISPR-associated transposases. *Science* 365, 48–53. doi: 10.1126/science.aax9181
- Szczelkun, M. D., Tikhomirova, M. S., Sinkunas, T., Gasiunas, G., Karvelis, T., Pschera, P., et al. (2014). Direct observation of R-loop formation by single RNA-guided Cas9 and Cascade effector complexes. *Proc. Natl. Acad. Sci. U.S.A.* 111, 9798–9803. doi: 10.1073/pnas.1402597111
- Takei, Y., Shah, S., Harvey, S., Qi, L. S., and Cai, L. (2017). Multiplexed Dynamic imaging of genomic loci by combined CRISPR imaging and DNA sequential FISH. *Biophys. J.* 112, 1773–1776. doi: 10.1016/j.bpj.2017.03.024
- Tarasava, K., Liu, R., Garst, A., and Gill, R. T. (2018). Combinatorial pathway engineering using type I-E CRISPR interference. *Biotechnol. Bioeng.* 115, 1878–1883. doi: 10.1002/bit.26589
- Taylor, H. N., Warner, E. E., Armbrust, M. J., Crowley, V. M., Olsen, K. J., and Jackson, R. N. (2019). Structural basis of Type IV CRISPR RNA biogenesis by a Cas6 endonuclease. *RNA Biol.* 16, 1438–1447. doi: 10.1080/15476286.2019.1634965
- Tsai, S. Q., Wyvekens, N., Khayter, C., Foden, J. A., Thapar, V., Reyon, D., et al. (2014). Dimeric CRISPR RNA-guided FokI nucleases for highly specific genome editing. *Nat. Biotechnol.* 32, 569–576. doi: 10.1038/nbt.2908
- Vercoc, R. B., Chang, J. T., Dy, R. L., Taylor, C., Gristwood, T., Clulow, J. S., et al. (2013). Cytotoxic chromosomal targeting by CRISPR/Cas systems can reshape bacterial genomes and expel or remodel pathogenicity islands. *PLoS Genet.* 9:e1003454. doi: 10.1371/journal.pgen.1003454
- Wang, R., Preamplume, G., Terns, M. P., Terns, R. M., and Li, H. (2011). Interaction of the Cas6 ribonuclease with CRISPR RNAs: recognition and cleavage. *Structure* 19, 257–264. doi: 10.1016/j.str.2010.11.014
- Wei, W., Zhang, S., Fleming, J., Chen, Y., Li, Z., Fan, S., et al. (2019). Mycobacterium tuberculosis type III-A CRISPR/Cas system crRNA and its maturation have atypical features. *FASEB J.* 33, 1496–1509. doi: 10.1096/fj.201800557RR
- Weller, G. R., Kysela, B., Roy, R., Tonkin, L. M., Scanlan, E., Della, M., et al. (2002). Identification of a DNA nonhomologous end-joining complex in bacteria. *Science* 297, 1686–1689. doi: 10.1126/science.1074584
- Westra, E. R., Pul, U., Heidrich, N., Jore, M. M., Lundgren, M., Stratmann, T., et al. (2010). H-NS-mediated repression of CRISPR-based immunity in *Escherichia coli* K12 can be relieved by the transcription activator LeuO. *Mol. Microbiol.* 77, 1380–1393. doi: 10.1111/j.1365-2958.2010.07315.x
- Westra, E. R., van Erp, P. B., Kunne, T., Wong, S. P., Staats, R. H., Seegers, C. L., et al. (2012). CRISPR immunity relies on the consecutive binding and degradation of negatively supercoiled invader DNA by Cascade and Cas3. *Mol. Cell* 46, 595–605. doi: 10.1016/j.molcel.2012.03.018

- Wiedenheft, B., Lander, G. C., Zhou, K., Jore, M. M., Brouns, S. J., van der Oost, J., et al. (2011a). Structures of the RNA-guided surveillance complex from a bacterial immune system. *Nature* 477, 486–489. doi: 10.1038/nature10402
- Wiedenheft, B., van Duijn, E., Bultema, J. B., Waghmare, S. P., Zhou, K., Barendregt, A., et al. (2011b). RNA-guided complex from a bacterial immune system enhances target recognition through seed sequence interactions. *Proc. Natl. Acad. Sci. U.S.A.* 108, 10092–10097. doi: 10.1073/pnas.1102716108
- Wu, J., Du, G., Chen, J., and Zhou, J. (2015). Enhancing flavonoid production by systematically tuning the central metabolic pathways based on a CRISPR interference system in *Escherichia coli*. *Sci. Rep.* 5:13477. doi: 10.1038/srep13477
- Xiao, Y., Luo, M., Dolan, A. E., Liao, M., and Ke, A. (2018). Structure basis for RNA-guided DNA degradation by Cascade and Cas3. *Science* 361:eaat0839. doi: 10.1126/science.aat0839
- Xiao, Y., Luo, M., Hayes, R. P., Kim, J., Ng, S., Ding, F., et al. (2017). Structure basis for directional R-loop formation and substrate handover mechanisms in Type I CRISPR-Cas system. *Cell* 170, 48–60.e11 doi: 10.1016/j.cell.2017.06.012.
- Yao, R., Liu, D., Jia, X., Zheng, Y., Liu, W., and Xiao, Y. (2018). CRISPR-Cas9/Cas12a biotechnology and application in bacteria. *Synth. Syst. Biotechnol.* 3, 135–149. doi: 10.1016/j.synbio.2018.09.004
- Yosef, I., Manor, M., Kiro, R., and Qimron, U. (2015). Temperate and lytic bacteriophages programmed to sensitize and kill antibiotic-resistant bacteria. *Proc. Natl. Acad. Sci. U.S.A.* 112, 7267–7272. doi: 10.1073/pnas.1500107112
- Zetsche, B., Gootenberg, J. S., Abudayyeh, O. O., Slaymaker, I. M., Makarova, K. S., Essletzbichler, P., et al. (2015). Cpf1 is a single RNA-guided endonuclease of a class 2 CRISPR-Cas system. *Cell* 163, 759–771. doi: 10.1016/j.cell.2015.09.038
- Zetsche, B., Heidenreich, M., Mohanraju, P., Fedorova, I., Kneppers, J., DeGennaro, E. M., et al. (2017). Multiplex gene editing by CRISPR-Cpf1 using a single crRNA array. *Nat. Biotechnol.* 35, 31–34. doi: 10.1038/nbt.3737
- Zhang, J., Zong, W., Hong, W., Zhang, Z. T., and Wang, Y. (2018). Exploiting endogenous CRISPR-Cas system for multiplex genome editing in *Clostridium tyrobutyricum* and engineer the strain for high-level butanol production. *Metab. Eng.* 47, 49–59. doi: 10.1016/j.ymben.2018.03.007
- Zhao, H., Sheng, G., Wang, J., Wang, M., Bunkoczi, G., Gong, W., et al. (2014). Crystal structure of the RNA-guided immune surveillance Cascade complex in *Escherichia coli*. *Nature* 515, 147–150. doi: 10.1038/nature13733
- Zheng, Y., Han, J., Wang, B., Hu, X., Li, R., Shen, W., et al. (2019). Characterization and repurposing of the endogenous Type I-F CRISPR-Cas system of *Zymomonas mobilis* for genome engineering. *Nucleic Acids Res.* 47, 11461–11475. doi: 10.1093/nar/gkz940

Conflict of Interest: The authors declare that the research was conducted in the absence of any commercial or financial relationships that could be construed as a potential conflict of interest.

Copyright © 2020 Zheng, Li, Wang, Han, Hao, Wang, Ma, Yang, Ma, Yi and Peng. This is an open-access article distributed under the terms of the Creative Commons Attribution License (CC BY). The use, distribution or reproduction in other forums is permitted, provided the original author(s) and the copyright owner(s) are credited and that the original publication in this journal is cited, in accordance with accepted academic practice. No use, distribution or reproduction is permitted which does not comply with these terms.



Multiple Small RNAs Interact to Co-regulate Ethanol Tolerance in *Zymomonas mobilis*

Runhua Han^{1†}, Katie Haning^{1†}, Juan C. Gonzalez-Rivera¹, Yongfu Yang², Runxia Li², Seung Hee Cho³, Ju Huang², Bobi A. Simonsen¹, Shihui Yang² and Lydia M. Contreras^{1,3*}

¹ McKetta Department of Chemical Engineering, The University of Texas at Austin, Austin, TX, United States, ² State Key Laboratory of Biocatalysis and Enzyme Engineering, Hubei Collaborative Innovation Center for Green Transformation of Bio-resources, Environmental Microbial Technology Center of Hubei Province, and School of Life Sciences, Hubei University, Wuhan, China, ³ Institute for Cellular and Molecular Biology, College of Natural Sciences, The University of Texas at Austin, Austin, TX, United States

OPEN ACCESS

Edited by:

Zhanglin Lin,
South China University of Technology,
China

Reviewed by:

Yuanyuan Ma,
Tianjin University, China
Zhen Kang,
Jiangnan University, China

*Correspondence:

Lydia M. Contreras
lcontrer@che.utexas.edu

[†]These authors have contributed
equally to this work

Specialty section:

This article was submitted to
Synthetic Biology,
a section of the journal
Frontiers in Bioengineering and
Biotechnology

Received: 09 November 2019

Accepted: 14 February 2020

Published: 04 March 2020

Citation:

Han R, Haning K,
Gonzalez-Rivera JC, Yang Y, Li R,
Cho SH, Huang J, Simonsen BA,
Yang S and Contreras LM (2020)
Multiple Small RNAs Interact
to Co-regulate Ethanol Tolerance
in *Zymomonas mobilis*.
Front. Bioeng. Biotechnol. 8:155.
doi: 10.3389/fbioe.2020.00155

sRNAs represent a powerful class of regulators that influences multiple mRNA targets in response to environmental changes. However, very few direct sRNA–sRNA interactions have been deeply studied in any organism. *Zymomonas mobilis* is a bacterium with unique ethanol-producing metabolic pathways in which multiple small RNAs (sRNAs) have recently been identified, some of which show differential expression in ethanol stress. In this study, we show that two sRNAs (Zms4 and Zms6) are upregulated under ethanol stress and have significant impacts on ethanol tolerance and production in *Z. mobilis*. We conducted multi-omics analysis (combining transcriptomics and sRNA-immunoprecipitation) to map gene networks under the influence of their regulation. We confirmed that Zms4 and Zms6 bind multiple RNA targets and regulate their expressions, influencing many downstream pathways important to ethanol tolerance and production. In particular, Zms4 and Zms6 interact with each other as well as many other sRNAs, forming a novel sRNA–sRNA direct interaction network. This study thus uncovers a sRNA network that co-orchestrates multiple ethanol related pathways through a diverse set of mRNA targets and a large number of sRNAs. To our knowledge, this study represents one of the largest sRNA–sRNA direct interactions uncovered so far.

Keywords: *Zymomonas mobilis*, small RNA, sRNA interactions, integrated omics, ethanol tolerance

INTRODUCTION

As global controllers of gene expression, small RNAs (sRNAs) represent powerful tools for engineering complex phenotypes (Cho et al., 2015; Leistra et al., 2019). These (typically) non-coding RNAs are 5–500 nucleotide (nt) transcripts that act as regulators of protein expression, mostly by blocking translation or changing mRNA stability (Storz et al., 2011). Although less common, proteins have also been shown to be targets of sRNA regulation (Pichon and Felden, 2007). Traditionally thought of as non-coding RNAs, many have been discovered in intergenic regions (Tsai et al., 2015), although some are now known to produce small peptides (Pichon and Felden, 2007). The majority of well-studied sRNAs act in *trans*, meaning their targets are encoded

elsewhere in the genome; this is in contrast to *cis*-encoded sRNAs, which neighbor their targets on the same or opposite DNA strand (Gottesman and Storz, 2011).

Advances in high-throughput sequencing have enabled discovery of hundreds of sRNAs across bacteria (Tsai et al., 2015; Hor et al., 2018), but characterization lags far behind. As a result, the vast majority of sRNAs have functions completely unknown, especially in non-model organisms. Current approaches take advantage of RNA-seq and proteomics to determine sRNA target networks (Lalaouina and Masse, 2015; Melamed et al., 2016), although a challenge remains to decouple direct vs. indirect interactions. Computational tools such as IntaRNA can be helpful in predicting most favorable sRNA-mRNA interactions and binding sites, although *in vivo* conditions and competition of multiple targets for binding sites cannot be accounted for (Busch et al., 2008). Ultimately, electrophoretic mobility shift assays (EMSAs) and reporter gene systems can complement these approaches in testing direct binding of RNA and protein targets *in vitro* and *in vivo* (Corcoran et al., 2012; Tomasini et al., 2017). Most recent, the mapping of sRNA interfaces that could be available *in vivo* for interactions has also been useful to determine biologically relevant mRNA targets (Vazquez-Anderson et al., 2017; Mihailovic et al., 2018).

Increasingly complex regulatory networks have been discovered, including several direct sRNA-sRNA interactions (Vogel et al., 2003; Lybecker et al., 2014; Miyakoshi et al., 2015; Frohlich et al., 2016). One reported interaction is between sRNAs SraC and SdsR in *Escherichia coli*, which originates from the same intergenic region, encoded in opposite directions (Vogel et al., 2003). However, due to the complete overlap of SdsR in antisense sequence to SraC, the binding of these sRNAs is expected and it results in RNase III-dependent cleaving (Vogel et al., 2003). Although still largely uncharacterized in *E. coli*, the target network of SdsR has been characterized in *Salmonella enterica* and includes stress response regulators (Frohlich et al., 2016). Another known interaction is between sRNA GcvB and the RNA sponge SroC, which represses GcvB in *E. coli* (Miyakoshi et al., 2015). This mRNA cross-talk forms a feed-forward loop in the regulation of ABC transporters and affects growth in different nutrient conditions (Miyakoshi et al., 2015). Additionally, two sRNAs (AsxR and AgvB) have been identified within bacteriophage-derived regions in enterohemorrhagic *E. coli* acting as “anti-sRNAs.” They antagonized the function of two of the genome core regulatory sRNAs, GcvB, and FnrS, by mimicking their mRNA substrate sequences to manipulate bacterial pathogenesis (Tree et al., 2014). However, few studies comprehensively investigate the regulatory effects caused by sRNA-sRNA direct interactions.

An advantage of sRNA regulation is its efficiency compared to protein regulators like transcription factors because they do not require translation and act directly on mRNA transcripts (Shimoni et al., 2007). The dynamic nature and low metabolic burden make sRNAs especially suitable to coordinate stress responses including temperature, nutrient, membrane, oxidative, iron, pH, and anaerobic stresses (Gottesman et al., 2006; Hoe et al., 2013; Gottesman, 2019). Ethanol tolerance represents

a complex phenotype that sRNAs appear to help regulate. For example, sRNA Nc117 in *Synechocystis* sp. PCC 6803 (Pei et al., 2017) as well as OLE RNA in *Bacillus halodurans* C-125 (Wallace et al., 2012) both appear to protect the cells from ethanol toxicity. However, the mRNA and/or protein targets of these sRNAs are unknown (Nc117) or limited in number (OLE RNA). OLE RNA is known to bind to RNase P as well as a protein (aptly named the OLE-associating protein), which associates to the membrane (Ko and Altman, 2007; Block et al., 2011; Wallace et al., 2012). The lack of network characterization in these contexts has precluded advances in understanding alcohol tolerance and in general sRNA function in non-model organisms. Moreover, as it relates to the specific phenotype of ethanol tolerance, these uncharacterized ethanol-related regulatory RNAs have left unanswered questions of the specific pathways that are co-regulated to naturally grant the ethanol resistance phenotype in some organisms.

Zymomonas mobilis is a highly biotechnologically relevant bacterium due to its natural ethanol producing ability up to 12% (v/v) and ethanol tolerance up to 16% (v/v) (Rogers et al., 2007; Franden et al., 2013; Yang et al., 2016a). Over the last 20 years, a variety of *Z. mobilis* strains have been developed through metabolic engineering and directed evolution (Rogers et al., 2007; Yang et al., 2013). The responses of *Z. mobilis* to a variety of stresses, especially ethanol stress, have been explored by transcriptomics and proteomics approaches (Yang et al., 2009, 2013; He et al., 2012a,b; Yi et al., 2015; Zhang et al., 2015). These stress responses are considered a complex phenotype because they trigger the differential expression of large sets of transcripts and proteins with a wide variety of cellular functions. For example, the ethanol stress response has been characterized to include up regulation of protein folding chaperones, DNA repair proteins, and transporters and down regulation of genes related to translation, ribosome biogenesis, and metabolism (He et al., 2012a; Yang et al., 2013; Zhang et al., 2015). These responses are important to the ethanol tolerance in *Z. mobilis* since the ethanol accumulation in cells is toxic, which influences membrane stability, as well as the structure and function of macromolecules such as proteins, nucleic acids, and lipids (Hallsworth et al., 2003). However, regulation mechanisms that cope with these widespread changes remain unclear.

It is likely that these complex phenotypes are made possible by multiple layers of regulation (DNA, RNA, protein) coordinating responses to extracellular environments. Recently, 106 sRNA candidates were identified in *Z. mobilis* by transcriptomics analysis and computationally prediction, where 15 were validated experimentally by Northern blotting analysis and 4 were shown to have differential expression to anaerobic or ethanol stresses (Cho et al., 2014). In this study, we use multiple omics analyses to map the regulatory networks for two of these sRNAs, Zms4 and Zms6, and demonstrate that they have significant impacts on ethanol tolerance and production in *Z. mobilis* through a diverse set of mRNA targets and other sRNA interactions. This work presents the first sRNAs with regulatory binding interactions confirmed in *Z. mobilis* and a large sRNA-sRNA interacting network which has not been widely observed in bacteria.

MATERIALS AND METHODS

Strains and Culture Conditions

The *Z. mobilis* 8b strain, which is an integrant of the ZM4 strain (ATCC 31821), was used in this study. *Z. mobilis* 8b was cultured in RMG media (glucose, 20.0 g/L; yeast extract, 10.0 g/L; KH_2PO_4 , 2.0 g/L; pH 6.0) at 33°C. *E. coli* DH5 α was used for plasmid construction and manipulation, grown in LB media at 37°C. All strains used in this study are listed in **Supplementary Table S1**.

To generate sRNA overexpression strains, each sRNA was cloned into the *NcoI-SalI* site of the pEZ-tet vector (Yang et al., 2016b) to allow for inducible expression under the *P_{tet}* promoter. For sRNA co-immunoprecipitation constructs, synthesized 2MS2BD-Zms4/Zm6/control sequences were cloned into pBBR1MCS2-*P_{gap}* vector (Yang et al., 2014) between *NheI* and *SalI*. All plasmids used in this study are listed in **Supplementary Table S1**. Strains containing pBBR1MCS2-*P_{gap}* plasmids were cultured with 350 $\mu\text{g/mL}$ of kanamycin for *Z. mobilis* and with 50 $\mu\text{g/mL}$ for *E. coli*. Overexpression strains containing pEZ-tet vectors were grown with 200 $\mu\text{g/mL}$ spectinomycin for *Z. mobilis* and 50 $\mu\text{g/mL}$ for *E. coli*.

For deletion strain construction, homologous upstream and downstream fragments (each 1 kb) of the target deletion gene were assembled with the spectinomycin gene *aadA*, flanked by *LoxP* sites, in the middle. Purified PCR product (1 μg) was directly electroporated (200 Ω , 25 μF , 1.6 kV) into *Z. mobilis* competent cells. Electroporated cells were recovered for 6 h and plated onto spectinomycin-containing plates (200 $\mu\text{g/mL}$). Plated cells were incubated anaerobically in a BD GasPakTM container system for 3–4 days at 33°C. Transformants appearing on the selective plates were cultured and screened for correct size using forward primers of upstream homologous and reverse primer of downstream primer and then sequence-verified. All sequences of primers used in this study are listed in **Supplementary Table S2**.

Growth rates of *Z. mobilis* strains were evaluated using the Plate Reader (BioTek, Winooski, VT, United States). Biological triplicates of each strain were distributed in triplicates with appropriate antibiotics into 96-well plates with RMG (with and without 6% ethanol) such that each well had a total volume of 200 μL with initial $\text{OD}_{600\text{nm}}$ of 0.1. 10 $\mu\text{g/mL}$ anhydrotetracycline was added to each strain to induce sRNA expression from the plasmids. The plate reader measured the turbidity (600 nm) every 0.5 h for 24 h as the cultures grew without shaking at 33°C.

For sRNA induction experiments, each strain was initially grown in biological duplicates in 5 mL RMG culture overnight then transferred into 500 mL with initial $\text{OD}_{600\text{nm}}$ of 0.1. Cells were grown anaerobically in sealed flasks containing nitrogen-purged RMG media at 33°C for 4 h to reach $\text{OD}_{600\text{nm}}$ around 0.4. Then, 150 mL of cells were collected for transcriptomics and ethanol assay. When $\text{OD}_{600\text{nm}}$ reached 0.5 (~4.5 h of growth), 10 $\mu\text{g/mL}$ anhydrotetracycline was added to each strain to induce sRNA expression from the plasmids. After 0.5 h's induction (~5 h of growth), 150 mL of cells were collected to compare the gene

expression profile in the middle of exponential phase. In this way, the effect of overexpressing Zms4 and Zms6 on the transcriptome could be confirmed by comparing the samples before and after induction. Final samples were collected during stationary phase (~12 h of growth). Pelleted cells were stored at -80°C before further processing.

Ethanol Assay

Ethanol concentrations were measured using the UV-based ethanol assay kit (R-Biopharm, Darmstadt, Germany) according to the manufacturer's protocol.

MS2-Affinity Purification of sRNAs *in vivo*

To identify *in vivo* sRNA interactions, each sRNA (Zms4 and Zms6) were tagged with a 2-MS2 binding domain (Said et al., 2009) and isolating by affinity purification with maltose binding protein (MBP) fused to the MS2 coat protein and amylose beads. Briefly, total RNA (100 μL at 500 ng/ μL) extracted from *Z. mobilis* strains containing pMS2, pMS2-Zms4, and pMS2-Zms6 was incubated with 10 pmol purified MS2-MBP protein for 1 h at 4°C. Washed amylose beads were incubated with 2MS2BD-Zms4/Zms6/control+MS2-MBP complexes for 2 h at 4°C. Supernatants were removed from the beads by applying a magnet. Beads were washed three times and incubated with 50 μL of elution buffer for 15 min. The elution step was repeated so that 100 μL of each were collected. To precipitate the RNA, equal volumes of isopropanol was added to elution sample and incubated overnight at -20°C . RNA was pelleted at 15,000 rpm for 15 min at 4°C and washed with 1 mL 75% ethanol. The RNA pellets were air-dried then resuspended in 50 μL RNase-free water. RNA samples were stored at -80°C until sequencing.

To find proteins associated with each sRNA *in vivo*, 500 μg of total lysates from *Z. mobilis* strains containing pMS2, pMS2-Zms4, and pMS2-Zms6 were incubated with 10 pmol of purified MS2-MBP protein for 1 h at 4°C. Then, 1 mL Trizol was added to eluted samples for protein purification. After addition of 300 μL of chloroform:isoamyl alcohol mix (v/v 24:1), the samples were inverted for 15 s, and then incubated at 25°C for 3 min. Then, tubes were centrifuged at 13,000 rpm for 10 min. 1.5 mL of isopropanol was then added to the phenol-chloroform layer and mixtures were incubated for 10 min at room temperature and then centrifuged at $12,000 \times g$ for 10 min at 4°C to pellet the protein. Pelleted protein was washed with 2 mL of 0.3 M guanidine hydrochloride in 95% ethanol and incubated for 20 min at room temperature then centrifuged at $7,500 \times g$ for 5 min at 4°C. Washing steps were repeated twice more. Then, 2 mL of 100% ethanol was added to the protein pellets and samples were centrifuged at $7,500 \times g$ for 5 min at 4°C. Air-dried protein pellets were resuspended in 3 \times SDS-loading buffer and run 3 mm into the resolving layer of an SDS-PAGE gel (5% stacking; 10% resolving) to concentrate protein before mass spectrometry. The gel was Coomassie stained and total protein bands were excised and stored in destaining solution at 4°C.

RNA Sequencing and Data Analysis

Total RNA was prepared and purified according to standard methods (DiChiara et al., 2010) for all the growth conditions tested. Prepared RNA was quantified and checked for quality using Bioanalyzer before sequencing. NEBNext® Multiplex RNA Library Prep Set for Illumina® (New England Biolabs Inc.) was used for generating RNA libraries. Sequencing was performed using Illumina® NextSeq 500 with paired-end 2×150 bp runs (Genomic Sequencing and Analysis Facility at the University of Texas at Austin).

Adapter sequences and low-quality ends (phred quality < 30) were trimmed from the raw fastq files with cutadapt (v1.3) and reads shorter than 22 nt were discarded (Mortazavi et al., 2008). FastQC was used to verify good read quality for the trimmed files. Reads were aligned to the *Z. mobilis* ZM4 reference genome (taxonomy ID 264203) with BWA-mem (v0.7.12-r1039) (Langmead and Salzberg, 2012). Aligned reads (33~97 million aligned reads for each sample) were filtered for quality (MAPQ ≥ 10) and sorted by chromosomal coordinates using SAMtools (v0.1.19-44428cd) (Li et al., 2009). The number of reads aligned to each gene was calculated using HTSeq (intersection-non-empty mode for overlaps) (Anders et al., 2015). DESeq2 was used to normalize and identify significantly differentially expressed transcripts between strains (Love et al., 2014). Cytoscape Enrichment Map plugin was used for gene enrichment analysis (Reimand et al., 2019). The experiments for each strain/condition were performed in at least two replicates.

Mass Spectrometry

Polyacrylamide gel bands containing protein were digested with trypsin. To identify proteins, LC-MS/MS was performed using the Dionex Ultimate 3000 RSLCnano LC coupled to the Thermo Orbitrap Elite with a 2 h run time at the ICMB Proteomics Facility using published methods (Shevchenko et al., 2006). Proteins were searched against the Uniprot *Z. mobilis* ATCC ZM4 database (April 27, 2016) using Sequest HT in Proteome Discoverer 1.4. The identifications were validated with Scaffold v4.4.1 (Proteome Software) with greater than 99.0% probability and with a minimum of two peptides at 99.0% peptide probability. In Scaffold, peptide and protein false discovery rates were both calculated as 0.0%. The experiments for each strain/condition were performed in two replicates.

Electromobility Shift Assays

Electromobility shift assays (EMSA) were performed to detect the RNA–RNA interactions *in vitro*. Each RNA of interest was amplified from *Z. mobilis* genomic DNA using the primers listed in **Supplementary Table S2** and *in vitro* transcribed using MEGascript T7 Transcription Kit (ThermoFisher). The RNA binding reaction was performed in a 12 μ L reaction volume containing $1 \times$ binding reaction buffer [20 mM Tris–HCl (pH 8.0), 1 mM MgCl₂, 20 mM KCl, 10 mM Na₂HPO₄ –NaH₂PO₄ (pH 8.0)], 10% glycerol, 5 pmol of ³²P-labeled sRNA and 10–200 pmol of target RNA. This reaction was denatured at 70°C for 5 min, and then incubated at 37°C for 75 min. Samples were mixed with loading dye (10 mM Tris, 50% glycerol, and 0.0001% wt/vol bromophenol blue) and analyzed by electrophoresis in

a 5% non-denaturing polyacrylamide gel (0.5 \times TBE, 5% wt/vol acrylamide-bisacrylamide, 5% glycerol, 0.25% ammonium persulfate, and 0.001% TEMED) with 0.5 \times TBE running buffer at 4°C for 2.5 h. Next, the gel was placed on a sheet of Whatman grade GB004 blotting paper and dried at 80°C for 60 min (Gel Dryer 583, BioRad). Radioactive bands were visualized using a Typhoon FLA 700 (GE Health Life Science) and analyzed using CLIQS (TotalLab). The fraction bound was then calculated based on the ratio of the intensity of the RNA–RNA complex to the total intensity in each lane, and the dissociation constant (K_d) can be calculated as the concentration of the target RNA that showed 50% of binding.

Detection of RNA-5'UTR Regulation *in vivo*

For 5'UTR sequence determination, the core promoter region and transcriptional start site (TSS) of the target gene were predicted using BPROM. The sequence from the predicted TSS to 99-bp downstream of the ATG was cloned as the 5' gene fragment to a shuttle vector of dual fluorescence reporting system (Yang et al., 2019). Briefly, using P_{gap} dual report system as backbone, primers of target fragments were designed to contain 15~20 nucleotides (nts) overlapping regions, which 5' end overlapped with TSS upstream of P_{gap} and 3' end overlapped with ATG downstream of GFP. PCR products of target fragments were separated by gel electrophoresis, followed by gel purification, and subsequently quantified using NanoDrop. Fragments and vector were mixed in a molar ratio of 3:1, 0.5 U T5 exonuclease (New England Biolabs Inc.), 0.5 μ L buffer 4 (New England Biolabs Inc.), and the final volume was set to 5 μ L with ddH₂O. All reagents were mixed and reacted on the ice for 5 min; *E. coli* chemically competent cells were subsequently added. Cells were plated on LB agar plates with spectinomycin and recombinants were selected by colony PCR and then confirmed by Sanger sequencing (Sangon). The dual-reporter plasmids encoding each target gene was then transformed into the wild type 8b strain and the deletion strains for either Zms4 or Zms6. All sequences of primers used are listed in **Supplementary Table S2**.

Strains were grown at 30°C for 6–8 h without shaking before washing with phosphate buffered saline (PBS) twice, and then resuspended into PBS to a final concentration of 10^7 cells/mL. Cells were analyzed by flow cytometry using Beckman CytoFLEX FCM (Beckman Coulter, Inc.) with the PBS as the sheath fluid. The cells fluorescence of Enhanced Green Fluorescent Protein (EGFP) were excited with 488 nm and detected with FITC, mCherry were excited with 561 nm and detected with PC5.5. Compensation was applied to ensure that the EGFP has minimal affection on the detection of mCherry with at least 20,000 events of each sample analyzed. Data were processed via FlowJo software (FlowJo, LLC). The mean fluorescence intensity of triplicates was calculated, then the ratio of 'average EGFP'/average mCherry' was used to analyze the interaction of sRNA and 5'-UTR. In addition, the standard deviation was set as error bars. Each experiment was carried out at duplicates.

To detect if sRNA can exert regulations of the targets through the coding regions, an alternative approach was used by replacing the native promoter of the selected targets in the chromosome

by a P_{tet} inducible *mCherry* reporter system along with an *aadA* gene as the antibiotics selection marker. The *Zms4* and *Zms6* overexpression plasmids were then introduced to these strains using the pEZ-tet vector with kanamycin gene replacing the original spectinomycin gene (pEZ-Kana) (**Supplementary Table S1**). The empty vector was also transformed into these strains as the control. The *mCherry* expression levels of each strain were then measured using the same method as described above.

Northern Blotting Analysis

Northern blotting analysis was performed by standard methods (Cho et al., 2014). Briefly, DNA oligonucleotide probes specific for each sRNA were labeled using 20 pmol of oligonucleotide in a 20 μ L kinase reaction containing 25 μ M γ - P^{32} ATP and 20 units T4 polynucleotide kinase (New England Biolabs Inc.) at 37°C for 1 h. Ladder [Φ X174 DNA/*Hinf*I (Promega)] was labeled in the same manner. Total RNA (50–100 μ g) from deletion and wild type strains were separated on a 10% denaturing polyacrylamide gel that was then transferred to a positively charged membrane (Hybond N+, GE Life Sciences) for blotting. Hybridization was performed using Amersham Rapid-hyb buffer (GE Healthcare), following the recommended protocol with overnight incubation at 42°C. After three washes with washing buffer (5 \times SSC, 0.1% SDS at 30°C for the first wash and 1 \times SSC, 0.1% SDS at 42°C for the second and third washes), membranes were exposed to a phosphor screen overnight. Radioactive bands were visualized using a Typhoon FLA 700 (GE Health Life Science) and analyzed using CLIQS (TotalLab). All probes used in this study are listed in **Supplementary Table S2**.

RESULTS

Zms4 and Zms6 Are Induced by Ethanol and Affect Bacterial Ethanol Tolerance

Four sRNAs (*Zms2*, *Zms4*, *Zms6*, and *Zms18*) were previously shown as differentially expressed under 5% (v/v) ethanol stress and/or anaerobic conditions (Cho et al., 2014), favoring glucose consumption, enabling higher growth rates and ethanol accumulation (Yang et al., 2009). To determine their direct impacts on the ethanol tolerance phenotype, we overexpressed and deleted each sRNA. However, *Zms2* could not be independently overexpressed because it significantly overlaps with its neighboring gene *ZMO1198* and *Zms18* could not be fully deleted due to multiple homologous regions in the genome. As such, we focused our study on the characterization of *Zms4* and *Zms6*.

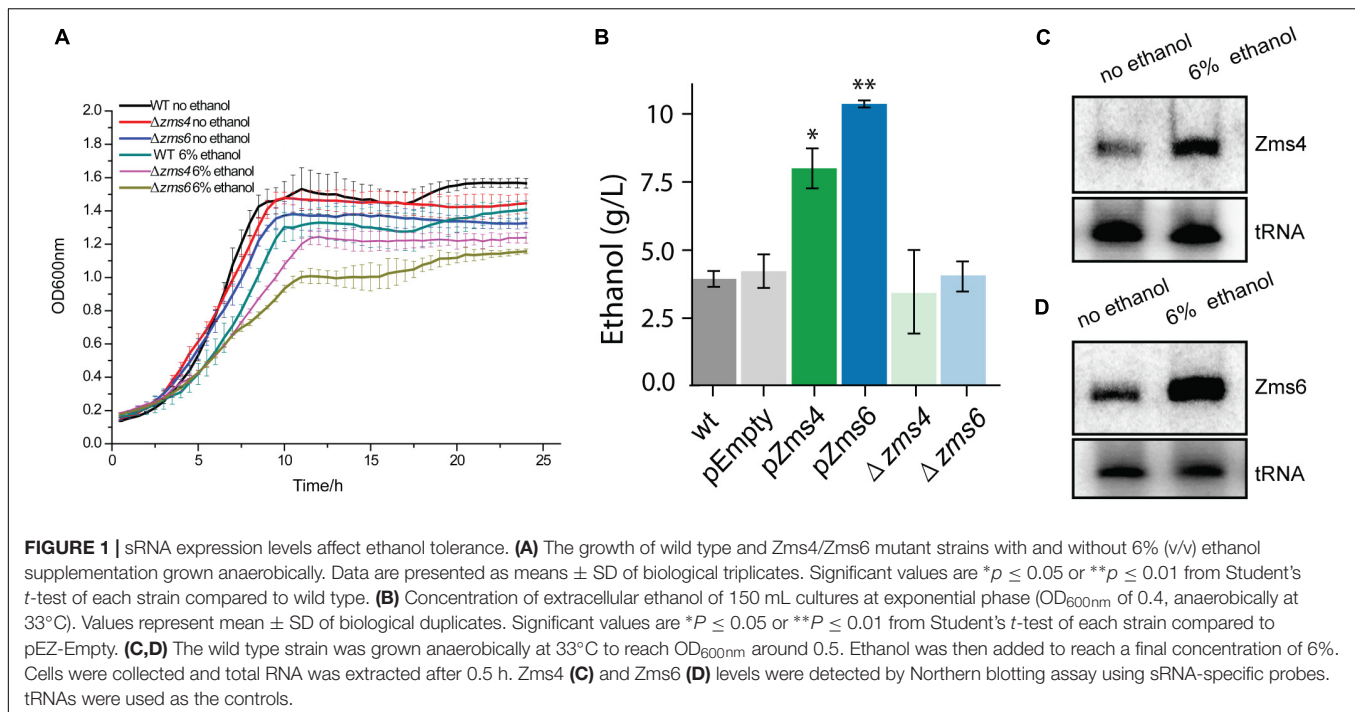
After validation of the sRNA deletion and overexpression strains (**Supplementary Figure S1**), these strains were grown anaerobically in media with and without 6% (v/v) ethanol supplementation to observe the effects of each sRNA on the ethanol survival phenotype. This concentration of 6% (v/v) ethanol was selected to significantly impact cell growth while still maintaining viability (and therefore reproducibility) (Yang et al., 2013). As shown in **Figure 1A**, $\Delta zms4$ and $\Delta zms6$ strains had similar growth to the wild type strain but they

showed significantly reduced growth under 6% ethanol stress. Considering the natural ethanol production of *Z. mobilis* and the tolerance effects, we reasoned that the regulatory contribution of *Zms4* and *Zms6* to the high ethanol tolerance phenotype could also be captured by measuring ethanol production. As shown in **Figure 1B**, *Zms4* and *Zms6* overexpression strains showed significantly higher levels of ethanol production relative to strains expressing an empty plasmid and to the wild type strain (with no plasmid). However, the deletion strains remained the same ethanol production ability as the wild type strain. Interestingly, our results also showed natural upregulation of *Zms4* and *Zms6* when 6% ethanol was added to the media (**Figures 1C,D**), indicating the possibility that their natural differential expression in *Z. mobilis* plays important roles in increasing fitness to ethanol stress.

Transcriptomics Analysis Reveal That Gene Networks Affected by Zms4 and Zms6 Are Associated With Ethanol Stress

As global regulators, sRNAs can interact with multiple mRNA and protein targets to coordinate complex phenotypes. Given that sRNAs can repress or activate gene expression, we expect that altering their stoichiometry will lead to significant changes on the innate levels of their direct or indirect targets. To uncover the networks of targets affected by *Zms4* and *Zms6*, we used an Integrative FourD-Omics (INFO) approach (Sowa et al., 2017), useful for identification of regulated targets and regulatory mechanisms underlying sRNA-driven systems. This integrated analysis (**Figures 2A,B**) included collection of transcriptome and MS2-affinity purification coupled with RNA sequencing (MAPS) profiles evaluated in *Zms4* and *Zms6* overexpression strains.

For these analyses, cells were collected before induction during the exponential-phase (4 h), 0.5-hour post-induction (5 h), and 7 h post-induction in the stationary phase (12 h) (**Figure 2A**). From these samples, RNA was extracted by standard methods and further characterized by RNA-seq in duplicates. 1939 genes and sRNAs (91.77% of 2113 uncovered genes/sRNAs) were detected using DESeq2 and 723 genes and sRNAs (34.22%) were observed to be differentially expressed by at least a twofold increase or decrease upon *Zms4* and *Zms6* induction. From this analysis, 504 genes and 42 sRNAs were significantly affected in a *Zms4*-dependent manner ($p_{adj} < 0.05$); and 418 genes and 35 sRNAs were significantly affected in a *Zms6*-dependent manner ($p_{adj} < 0.05$) (**Supplementary Table S3**). The induction of *Zms4* especially affected expression of transcripts involved in transport and biosynthetic processes (**Figure 2C**) and the induction of *Zms6* especially influenced oxidative stress response, cell motility/flagellum organization, and carbohydrate utilization (**Figure 2D**). Interestingly, more than half of them (249 genes and 27 sRNAs) were influenced by both *Zms4* and *Zms6*, such as translation, hydrogen sulfide biosynthetic processes, sulfate assimilation, and cysteine biosynthetic processes (**Supplementary Table S3** and **Figures 2C,D**). Several transcripts and proteins potentially regulated by *Zms4* and *Zms6* have been previously reported to



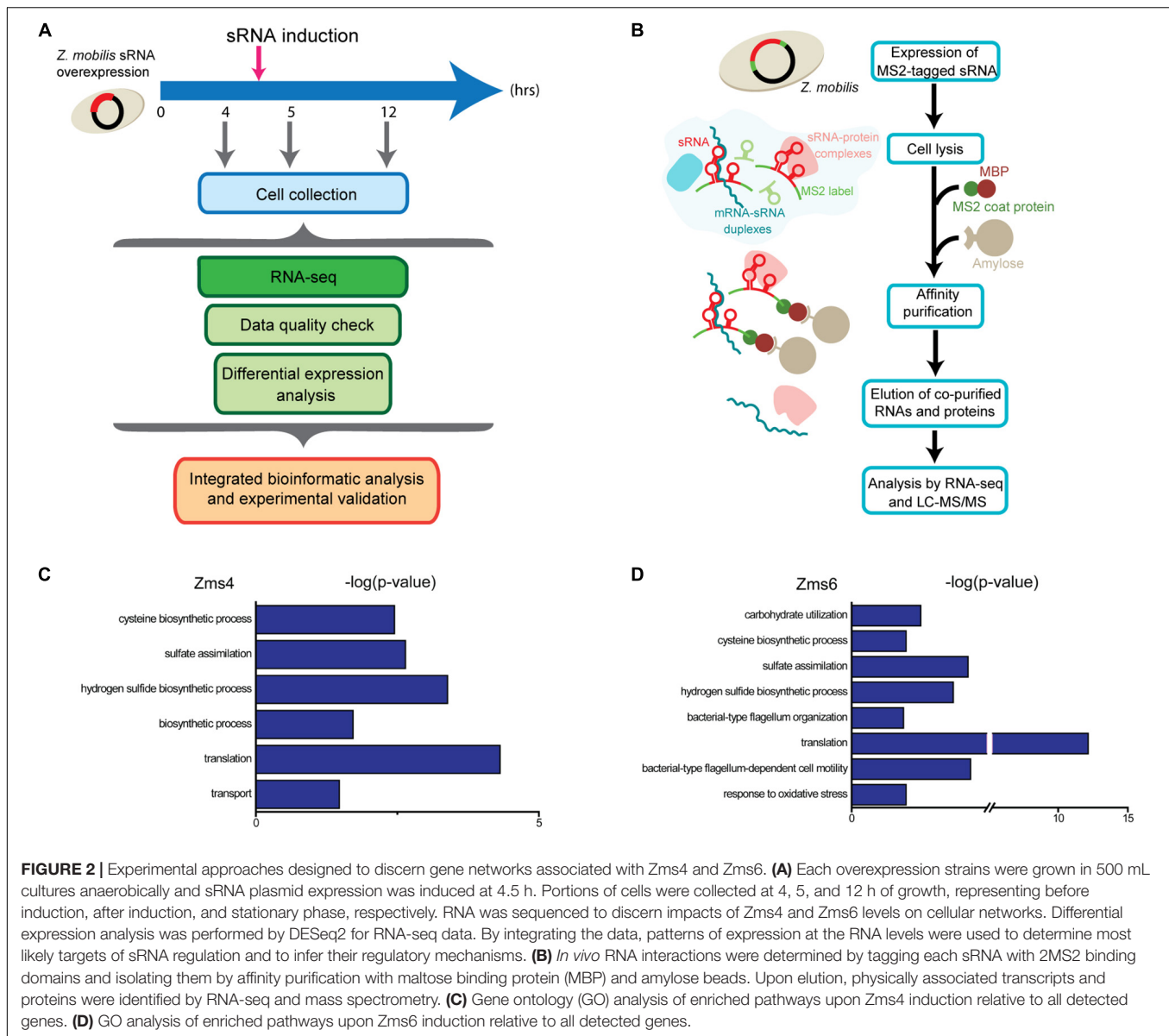
be differentially expressed under ethanol stress (Table 1). Given that Zms4 and Zms6 are naturally up-regulated upon ethanol stress, these observations evidence that many transcripts and proteins associated with cellular levels of Zms4 and Zms6 are tightly linked to ethanol tolerance pathways. In addition, several genes directly involved in ethanol metabolism were also found differentially expressed. For instance, alcohol dehydrogenase 1 (*adhA*), which facilitates the interconversion between alcohols and aldehydes, was significantly upregulated by Zms4 and Zms6 overexpression. The expression of *hfq* gene and its 5'-UTR were also significantly upregulated upon the induction of both Zms4 and Zms6, suggesting that Zms4 and Zms6 may affect these important pathways by modulating the expression of other Hfq-dependent sRNAs (although Hfq has not been yet demonstrated to be functional as an sRNA chaperone in *Z. mobilis*).

Identification of Potential Direct Targets of Zms4 and Zms6

To identify specific transcripts and proteins that *directly* interact *in vivo* with Zms4 and Zms6, we conducted a genome-wide MAPS approach (Figure 2B) (Lalaouna and Masse, 2015). For these experiments, each sRNA was 5' end tagged with a 2-MS2-binding domain (sequences in Supplementary Table S2). The tagged sRNAs were expressed in the wild type strain using the pBBR1MCS2-Pgap vector (Yang et al., 2014). Bound complexes were collected at the exponential phase (OD_{600nm} of 0.6) and isolated using maltose binding protein (MBP) columns. Transcripts and proteins co-precipitated with each sRNA were identified by RNA-sequencing and Mass spectrometry. Transcripts and proteins with at least 1.5-fold enrichment in the pMS2-Zms4 and pMS2-Zms6 strains relative to the pMS2 control

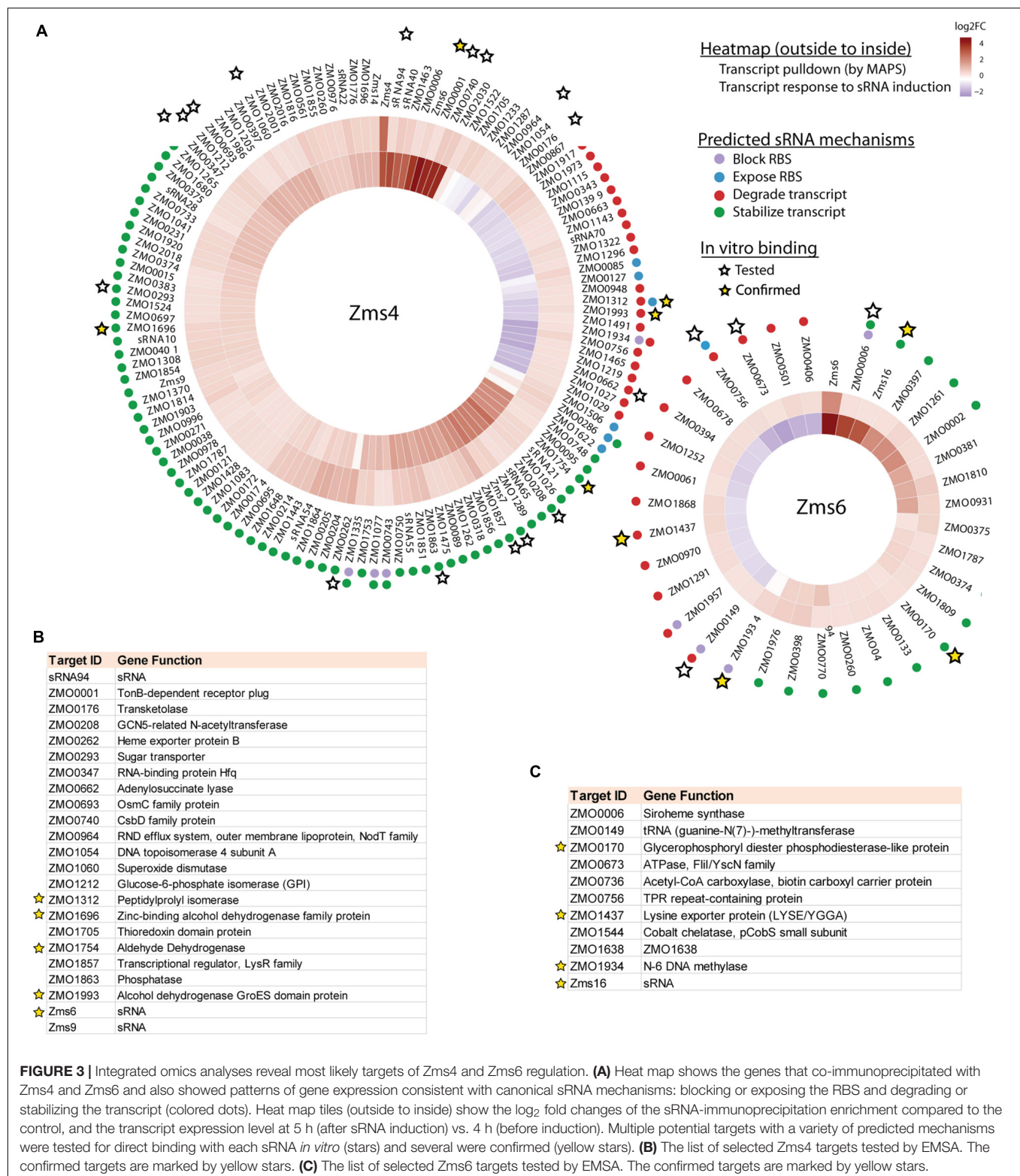
(lacking sRNA expression) were analyzed further as potential sRNA targets (Supplementary Tables S4, S5).

123 and 35 transcripts were pulled down by MS2-MBP-Zms4 and MS2-MBP-Zms6, respectively (Figure 3A and Supplementary Table S4). Based on the observed expression patterns in the transcriptomics data, potential mechanisms of regulation were predicted (Figure 3A). Zms4 was hypothesized to directly repress 33 transcripts by inducing transcript degradation or blocking the ribosome binding site (RBS) sequence and to directly activate 88 genes by transcript stabilization or exposure of the RBS. Similarly, Zms6 was hypothesized to directly up-regulate 16 transcripts and directly down-regulate 20 transcripts by the same corresponding mechanisms. Functionally, these potential targets are involved in differently pathways, including transport, DNA repair, cell motility/flagellum organization and oxidative-reductase stress response. One of our most interesting observations was that the Zms4 and Zms6 pulldowns were enriched for several other sRNAs that were previously identified to naturally respond to ethanol stress in *Z. mobilis* (Cho et al., 2014), which is consistent with our transcriptomic data showing altered expression of several previously identified sRNAs (Cho et al., 2014) by Zms4 and Zms6 induction (Supplementary Table S3). Importantly, Zms6 was also significantly enriched in the Zms4 pulldown, and 26 transcripts were enriched in both Zms4 and Zms6 (Supplementary Table S4). These observations strengthened the possibility that Zms4 and Zms6 interact with each other and subsequently seed a multi-sRNA network. Another observation was the potential that Zms4 and Zms6 have both activation and repression regulatory capabilities, an interesting possibility given the rarer activation role that has been assigned to sRNAs from studies in model bacteria.



To analyze the potential functional dependence of Zms4 and Zms6 on cellular factors (i.e., chaperones, etc.), we also analyzed proteins that were uniquely enriched by co-precipitation with Zms4 and Zms6 relative to the pMS2 control (lacking sRNA expression) ($p < 0.05$, Student's *T*-test, **Supplementary Table S5**). Given that our major focus was to identify mRNA targets, we were most interested in proteins that co-immunoprecipitated with both sRNAs as potential indication of specific cellular co-factors that could play important roles in the biology of sRNAs in *Z. mobilis*. This was especially interesting given the lack of sRNA characterization that has been done in this non-model organism. Given that the transcription termination/antitermination protein (NusA, ZMOB_1083) was co-immunoprecipitated with both sRNAs, it is likely that NusA-dependent transcription processing is relevant to these sRNAs in *Z. mobilis*. The biological significance (if any) of the second

protein enriched in both Zms4 and Zms6 [3-isopropylmalate dehydratase large subunit (LeuC, ZMOB_0723)] is less clear as no RNA interactions are predicted for this protein and no homologs of this protein that have been shown to be regulated by sRNAs in other species. It is also worth noting that the Hfq protein, was not detected to co-precipitate with these sRNAs, indicating the possibility that it is not essential for Zms4 and Zms6 function or that it might not serve as a strong general sRNA-mRNA chaperone in this organism. Although we cannot exclude the possibility that some proteins attached *in vivo* were lost in our purification procedure or difficult to detect by LC-MS/MS (Kaboord et al., 2015), the lack of Hfq binding to these particular sRNAs was also observed *in vitro* (**Supplementary Figure S2A**). The expression of Zms4 and Zms6 was also not affected by the deletion of *hfq* (**Supplementary Figure S2B**), although we showed here that Hfq is essential



for the survival of *Z. mobilis* under both normal condition and 6% ethanol stress (Supplementary Figure S2C). However, our transcriptomics data showed that the expression of *hfq* gene and its 5'UTR was upregulated significantly upon Zms4 and

Zms6 induction (Supplementary Table S3). These data suggest that Zms4 and Zms6 could serve as advanced regulators over other sRNAs through affecting the expression of *hfq*. Overall, our characterization of Hfq interactions indicate that these two

sRNAs function in an Hfq-independent manner but potentially affect a wide range of sRNAs through modulating *hfq* expression indirectly. It is worth noting that no homology of other known sRNA chaperons, like ProQ, has been found in *Z. mobilis*.

Confirmation of Multiple Direct RNA Targets

Given the non-specific interactions that can be captured via pull-down approaches like MAPS (which are likely amplified by the sensitivity of RNA-seq approaches), we next validated physical interactions of the predicted mRNA targets and the corresponding sRNA. We selected 23 target candidates of *Zms4* and 11 target candidates of *Zms6* for *in vitro* testing (marked with a star in **Figure 3A**). We selected our candidates based on their potential relevance to ethanol tolerance as judged by our transcriptomics data and previous omics studies in *Z. mobilis* (Yang et al., 2009; Yi et al., 2015) and by whether they are independently transcribed (whether their 5'-UTRs significantly overlap with neighboring gene coding regions). For these assays, the 5' region (~ -200 to +100 nt relevant to the start codon) of each mRNA target was initially screened for binding with the full sRNA transcript [as previously characterized by RACE analysis (Cho et al., 2014)] using EMSAs with 5 pmol sRNA and excessive targets (100 pmol). We selected these regions given that most sRNAs are found to base pair within the 5'-UTR region of the target they regulate (Gottesman and Storz, 2011). We confirmed interactions for 5 of the 23 RNAs tested as potential *Zms4* targets and for 4 of the 11 RNAs tested as potential *Zms6* targets by EMSA analysis (**Figures 3B,C**, **Table 2**, and **Supplementary Figure S3**). We confirmed two alcohol dehydrogenase genes (*ZMO1696* and *ZMO1993*), a peptidylprolyl isomerase gene (*ZMO1312*) and an aldehyde dehydrogenase gene (*ZMO1934*) as *Zms4* targets, suggesting that both the ethanol synthesis and anabolism pathways are potentially regulated by this sRNA directly. As for *Zms6*, the confirmed targets include an N-6 DNA methylase gene (*ZMO1934*), a lysine exporter encoding gene (*ZMO1437*) and a glycerophosphoryl diester phosphodiesterase encoding gene (*ZMO0170*), which indicates *Zms6* might affect the ethanol related pathways in an indirect manner through these genes. Notably, we also confirmed the binding between *Zms4* and *Zms6* as well as the interaction between *Zms6* and another previously identified sRNA, *Zms16* (Cho et al., 2014). This supports our hypothesis that these sRNAs interplay with each other and form a multi-sRNA network.

To better quantify how strong these interactions are and to exclude the possibility that the observed interactions did not result artificially from excessive usage of RNA targets, we incubated 5 pmol of sRNA with increasing concentrations (0~200 pmol) of various targets and calculated their dissociation constant (**Figures 4A–D** and **Table 2**). Our results demonstrated that *Zms4* formed stable complexes with high affinity (46.8 pmol and 42.8 pmol) with *ZMO1696* and *Zms6*. Interestingly, for these two targets, two distinct complexes were observed, indicating a potential 2:1 binding stoichiometry between *Zms4* and these mRNAs. In contrast, the affinities of RNA complexes between *Zms4* and *ZMO1993*, *ZMO1754* and *ZMO1312* were weaker (107.3 pmol, 117.9 pmol, and 600 pmol). For *Zms6*,

TABLE 1 | List of transcripts and proteins differentially regulated by both ethanol stress and sRNA overexpression in *Z. mobilis*.

Transcripts differentially expressed under both 5% ethanol stress (He et al., 2012a) and *Zms4* over expression

ZMO0265	Aspartyl protease
ZMO0374	Levansucrase (beta-D-fructofuranosyl transferase) (sucrose 6-fructosyl transferase)
ZMO0447	Uncharacterized protein
ZMO0614	Flagellar basal body rod protein FlgB
ZMO0924	Protein translocase subunit SecA
ZMO1045	Phosphate-selective porin O and P
ZMO1055	Diguanylate cyclase/phosphodiesterase
ZMO1065	Phage shock protein C, PspC
ZMO1262	Binding-protein-dependent transport systems inner membrane component
ZMO1285	Glucose-methanol-choline oxidoreductase
ZMO1426	DNA repair protein RadC
ZMO1458	Uncharacterized protein
ZMO1522	TonB-dependent receptor
ZMO1647	Transcription-repair-coupling factor (TRCF)
ZMO1649	Uracil-DNA glycosylase superfamily
ZMO1696	Zinc-binding alcohol dehydrogenase family protein
ZMO1802	Integration host factor subunit beta
ZMO1851	Uncharacterized protein
ZMO1855	Transcriptional regulator, GntR family with aminotransferase domain
ZMO1882	Uncharacterized protein
ZMO1961	Uncharacterized protein
ZMO2030	50S ribosomal protein L32

Transcripts differentially expressed under both 5% ethanol stress (He et al., 2012a) and *Zms6* over expression

ZMO0265	Aspartyl protease
ZMO0374	Levansucrase (Beta-D-fructofuranosyl transferase) (Sucrose 6-fructosyl transferase)
ZMO0899	NAD+ synthetase
ZMO0917	2-nitropropane dioxygenase, NPD
ZMO0952	tRNA (cytidine(34)-2'-O)-methyltransferase (tRNA (cytidine/uridine-2'-O)-methyltransferase TrmL)
ZMO0998	Peptide methionine sulfoxide reductase MsrA (Protein-methionine-S-oxide reductase)
ZMO1012	Uncharacterized protein
ZMO1030	Uncharacterized protein
ZMO1067	Fe-S metabolism associated SufE
ZMO1295	7-carboxy-7-deazaguanine synthase (CDG synthase) (queuosine biosynthesis protein QueE)
ZMO1311	LPS-assembly protein LptD
ZMO1458	Uncharacterized protein
ZMO1473	Uncharacterized protein
ZMO1522	TonB-dependent receptor
ZMO1649	Uracil-DNA glycosylase superfamily
ZMO1697	Zinc-binding alcohol dehydrogenase family protein
ZMO1855	Transcriptional regulator, GntR family with aminotransferase domain
ZMO2034	Conserved hypothetical replication initiator and transcription repressor protein

TABLE 2 | Confirmed targets of Zms4 and Zms6 regulation.

sRNA	Targets	Description	Predicted binding sites	K_d (pmol)
Zms4	ZMO1696	Zinc-binding alcohol dehydrogenase family protein	–11 –1	46.8
	ZMO1754	Aldehyde dehydrogenase	–28 –17	117.9
	ZMO1993	Alcohol dehydrogenase GroES domain protein	–51 –38	107.3
	ZMO1312	Peptidylprolyl isomerase	+40 +53	600.0
Zms6	Zms6	sRNA	99 117	42.8
	ZMO1934	N-6 DNA methylase	–38 +26	20.9
	ZMO0170	Glycerophosphoryl diester phosphodiesterase-like protein	–3 +12	53.2
	ZMO1437	Lysine exporter protein	+28 +75	132.0
	Zms16	sRNA	303 318	27.7

ZMO1934 and Zms16 showed the strongest affinity (20.9 pmol and 27.7 pmol), while the binding of other complexes (ZMO1437 and ZMO0170 mRNAs) was significantly weaker (132 pmol and 53.2 pmol).

We subsequently predicted the binding sites of these confirmed targets using IntaRNA (Supplementary Figure S4). The results showed that the binding sites on the mRNA targets localize in traditional 5'-UTR regions or near the start codon in the coding region. For Zms4 targets, the binding sites with ZMO1696, ZMO1993, and ZMO1754 were predicted to be located in 5'-UTR region, and the binding site with ZMO1312 was predicted to be located in the coding region. In terms of Zms6 targets, the binding site for ZMO1437 was predicted to be located in the coding region, while the binding sites for ZMO0170 and ZMO1934 were predicted to be located in both the 5'-UTR and the coding region. The predicted binding locations of these targets were then mapped to each sRNA's secondary structure inferred from NUPACK (Zadeh et al., 2011). As shown in Figures 4E,F, Zms4 and Zms6 contain multiple functional sites that potentially contribute to multi-tasking in their function. Moreover, these sites are predicted to occupy regions of high and low hybridization efficacy, as identified by the InTherAcc biophysical model (Vazquez-Anderson et al., 2017), which could explain the observed differences in binding affinities. These results also imply that Zms4 and Zms6 could bind and regulate multiple targets simultaneously and efficiently.

Confirmation of the Predicted Binding Sites for Important Targets by Mutagenesis Analysis

To confirm computationally predicted binding sites, we selected some of the important RNA targets that are either confirmed to be

ethanol-relevant or displaying strong affinity, and experimentally confirmed the actual binding site locations of them by EMSAs. For Zms4, we studied ZMO1696, ZMO1993 and Zms6 because they exhibited strong affinities. ZMO1754 was also selected since this gene encodes aldehyde dehydrogenase that converts acetaldehyde, a compound generated from ethanol anabolism, to acetate, and thus directly related to ethanol tolerance. For Zms6, we studied ZMO1934 and Zms16 considering they showed higher affinity than the other two targets and are likely the most important targets of Zms6.

As exemplified in Figure 5, we mutated several nucleotides in the predicted base pairing regions for each target RNA and the ability of mutated targets to form complexes with Zms4 and Zms6 were then tested. The data showed that the complexes of Zms4–ZMO1696mut and Zms4–Zms6mut almost disappeared (Figures 5A,B), while complex formations of ZMO1754mut and ZMO1993mut with Zms4 were completely abolished (Figures 5C,D). These results are consistent with the IntaRNA predictions that these mRNA targets interact with Zms4 though the 5'-UTR regions (Supplementary Figure S4). Through similar testing, the binding sites on ZMO1934 and Zms16 essential for their interactions with Zms6 were also confirmed (Figures 5E,F). Specifically, Zms6 was predicted to interact with the ZMO1934 mRNA through extensive base pairing (over 50 nucleotides), which overlaps with both 5'-UTR and coding regions. We then created three mutations for this target and found that only ZMO1934mut1 failed to interact with Zms6, while the other two are still able to form stable complexes with this sRNA (Figure 5E). However, quantification of the data showed that ZMO1934mut2 and ZMO1934mut3 bind to Zms6 with much lower affinities (39.4 pmol and 44.1 pmol, Supplementary Figure S5), which indicates cooperation between all of the three sites and the region from –38 to –27 nt to be the dominating site. Taken together, these results correlate well with the prediction of the basepairing interactions and suggest that these mRNA targets are potentially regulated by Zms4 or Zms6 through 5'-UTR regions or near the start codon in the coding region.

Detection of sRNA-Target Regulation and sRNA–sRNA Crosstalk *in vivo*

Then we used fluorescent reporter assays to confirm that the sRNAs can exert a regulatory effect on their mRNA targets *in vivo* through the predicted binding sites. In this assay, the 5' UTRs of the RNA targets shown to interact with Zms4 (ZMO1993, ZMO1312, ZMO1696, and ZMO1754) or Zms6 (ZMO1934, ZMO0170, and ZMO1437) *in vitro* were cloned upstream of EGFP and expressed under the constitutive strong promoter P_{gap} in a dual-reporter-gene system (Yang et al., 2019) (Supplementary Figure S6A). The vector also contains *mCherry* under the P_{lacUV5} promoter as a control for the expression level so the specific effect of the sRNA on each gene's 5'-UTR can be observed. The vectors containing the 5'-UTR of targets were transformed into the wild type 8b strain and Zms4/Zms6 deletion strains. Unfortunately, we were only able to test the 5'-UTR of ZMO1993 and ZMO1754 for Zms4 and the 5'-UTR

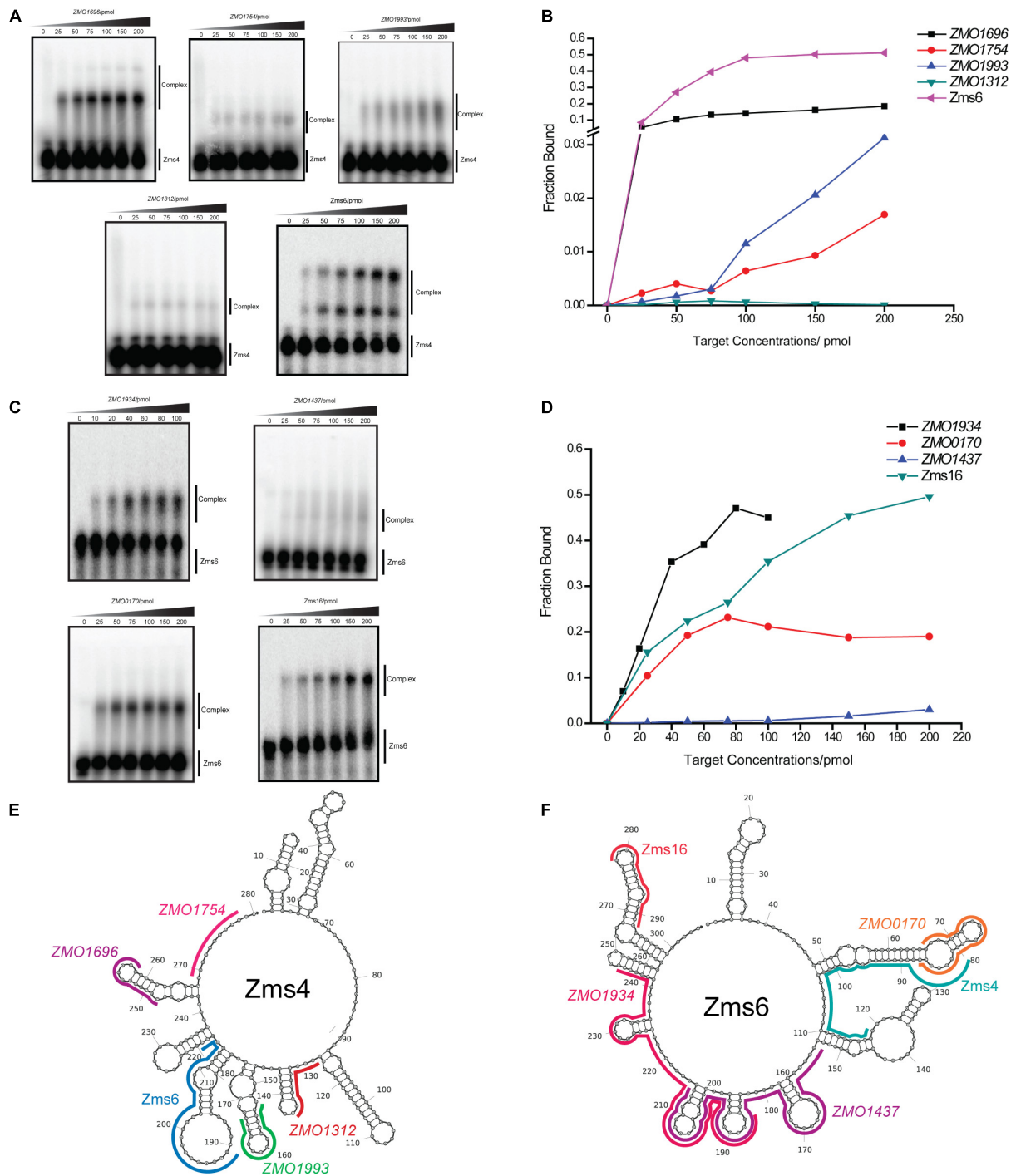


FIGURE 4 | sRNA-target interacting pairs verified by EMSA. The internally labeled Zms4/Zms6 (5 pmol) was incubated with increasing concentrations (0–200 pmol) of target RNAs. ZMO1696, ZMO1754, ZMO1993, ZMO1312, and Zms6 were confirmed to bind to Zms4 *in vitro* (A) with various affinities (B). In the case of Zms6, two complexes were detected. ZMO1934, ZMO1437, ZMO0170, and Zms16 were confirmed to bind to Zms6 *in vitro* (C) with various affinities (D). Binding site locations of the confirmed targets of Zms4 and Zms6 were predicted by IntaRNA and mapped onto the secondary structure of sRNAs inferred by NUPACK (E,F).

of ZMO1934 and ZMO0170 for Zms6 as no fluorescence of ZMO1696, ZMO1312 (for Zms4), and ZMO1437 (for Zms6) could be detected (implying that the reporter system did not work for these constructs).

The relative *EGFP* and *mCherry* expression levels of each strain were then quantified using a flow cytometer. The 5'-UTR of ZMO1993 exhibited a higher relative *EGFP*/*mCherry* fluorescence ratio in Zms4 deletion strain than that of the

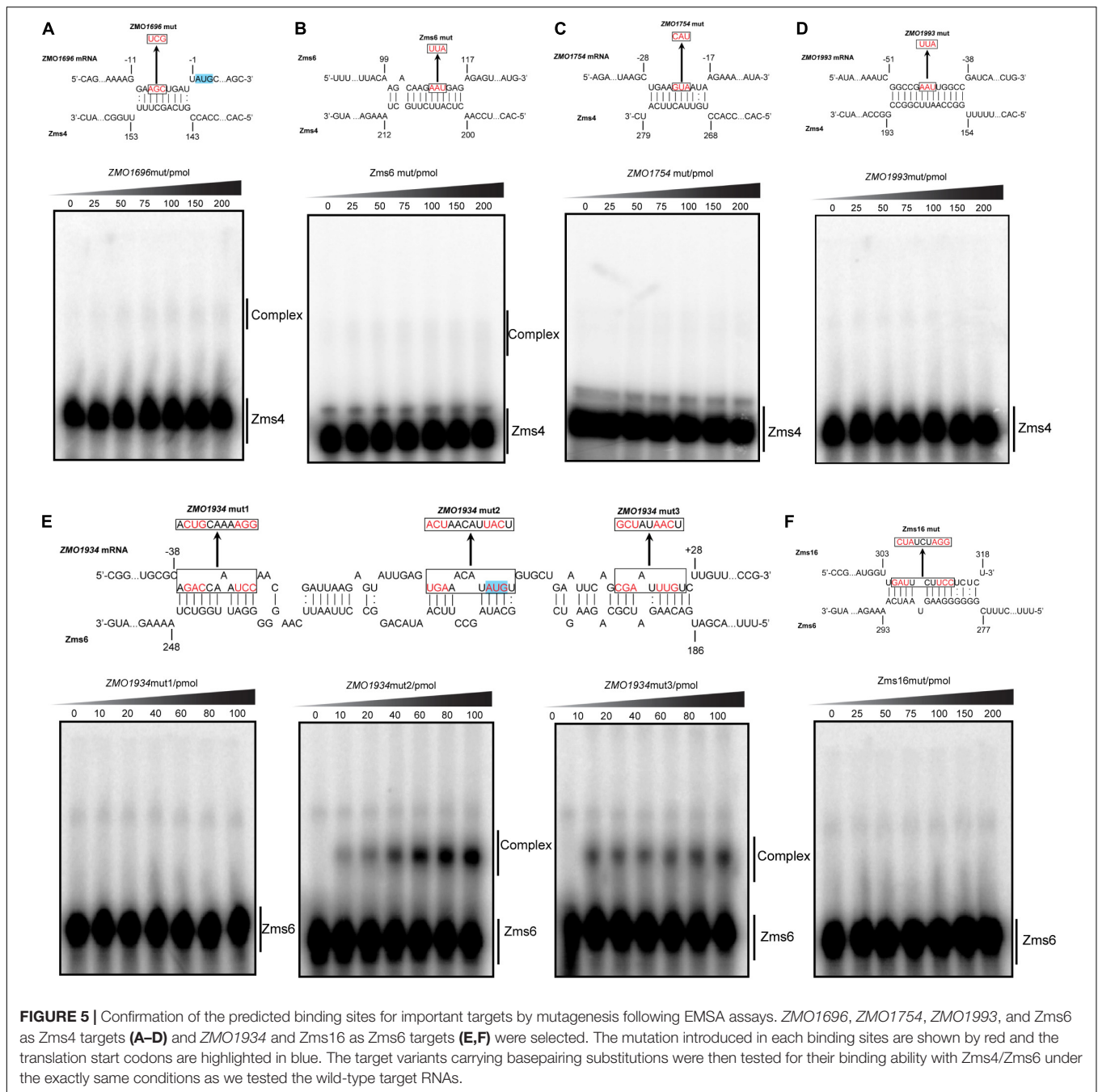


FIGURE 5 | Confirmation of the predicted binding sites for important targets by mutagenesis following EMSA assays. *ZMO1696*, *ZMO1754*, *ZMO1993*, and *Zms6* as *Zms4* targets (**A–D**) and *ZMO1934* and *Zms16* as *Zms6* targets (**E,F**) were selected. The mutation introduced in each binding sites are shown by red and the translation start codons are highlighted in blue. The target variants carrying basepairing substitutions were then tested for their binding ability with *Zms4*/*Zms6* under the exactly same conditions as we tested the wild-type target RNAs.

wild type strain, indicating the potential negative regulatory effect of *Zms4* on *ZMO1993* (Figure 6A). For *ZMO1754*, the deletion of *Zms4* leads to a significant decrease in *EGFP/mCherry* fluorescence ratio relative to the wild type strain (Figure 6A), which suggests that *Zms4* positively regulates *ZMO1754* through interactions with its 5'-UTR. These results are consistent with our hypothesized mechanism by IntaRNA prediction and transcriptomic data that *Zms4* protects *ZMO1754* transcript from degradation while promotes degradation of *ZMO1993* transcript by binding to the 5'-UTR regions of these mRNAs (Figure 3A and Supplementary Figure S4A). *Zms6* appears to

negatively regulate *ZMO1934* *in vivo* through its 5'-UTR, since the *EGFP/mCherry* fluorescence ratio increased in the *Zms6* deletion strain relative to the wild type strain (Figure 6B). However, no significant effect of *Zms6* on the *ZMO0170* 5'-UTR was observed (Figure 6B). This is likely due to the predicted competitive binding of *Zms4* with a higher affinity *in vivo* on the same region where *Zms6*-*ZMO0170* base-pairing locates (Figure 4F).

Since the binding sites on some of the targets also locate in the coding regions (i.e., *ZMO1934* and *ZMO1437*, Supplementary Figure S4B), we used a promoter replacement

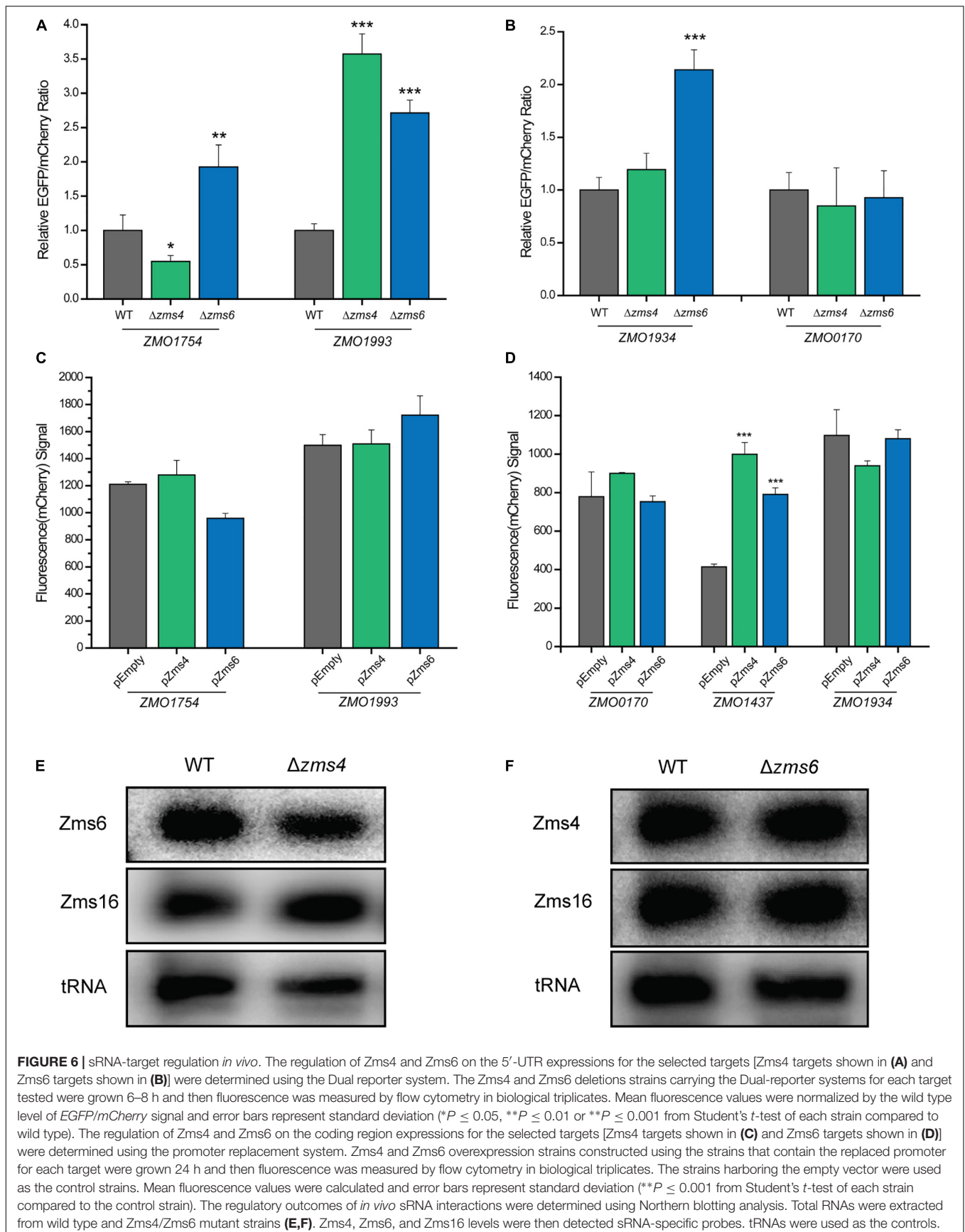


FIGURE 6 | sRNA-target regulation *in vivo*. The regulation of Zms4 and Zms6 on the 5'-UTR expressions for the selected targets [Zms4 targets shown in (A) and Zms6 targets shown in (B)] were determined using the Dual reporter system. The Zms4 and Zms6 deletions strains carrying the Dual-reporter systems for each target tested were grown 6–8 h and then fluorescence was measured by flow cytometry in biological triplicates. Mean fluorescence values were normalized by the wild type level of EGFP/mCherry signal and error bars represent standard deviation (* $P \leq 0.05$, ** $P \leq 0.01$ or *** $P \leq 0.001$ from Student's *t*-test of each strain compared to wild type). The regulation of Zms4 and Zms6 on the coding region expressions for the selected targets [Zms4 targets shown in (C) and Zms6 targets shown in (D)] were determined using the promoter replacement system. Zms4 and Zms6 overexpression strains constructed using the strains that contain the replaced promoter for each target were grown 24 h and then fluorescence was measured by flow cytometry in biological triplicates. The strains harboring the empty vector were used as the control strains. Mean fluorescence values were calculated and error bars represent standard deviation (** $P \leq 0.001$ from Student's *t*-test of each strain compared to the control strain). The regulatory outcomes of *in vivo* sRNA interactions were determined using Northern blotting analysis. Total RNAs were extracted from wild type and Zms4/Zms6 mutant strains (E,F). Zms4, Zms6, and Zms16 levels were then detected sRNA-specific probes. tRNAs were used as the controls.

system (**Supplementary Figure S6B**) to observe the *in vivo* regulation of Zms4 and Zms6 on the coding regions for some of the important targets. The native promoter regions of the confirmed targets (ZMO1993 and ZMO1754 for Zms4, and ZMO1934 and ZMO0170 for Zms6) were replaced by a P_{tet} induced *mCherry* reporter system along with an *aadA* gene. We also selected ZMO1437 because this gene (lysine exporter) was previously reported to improve the tolerance to phenolic aldehydes (Yi et al., 2015) and thus may also play important roles in the Zms6 regulation. The fluorescence signals of *mCherry* were then measured in Zms4 and Zms6 overexpression strains as compared to the signals from the wild type strain carrying the empty vector (the control strain). The signals of ZMO1993 and ZMO1754 in the Zms4 overexpression strain were comparable to the control strain (**Figure 6C**), and the signals from ZMO1934 and ZMO0170 upon Zms6 overexpression were also similar to the signals from the control strains (**Figure 6D**). These are consistent of our predictions and mutagenesis experiments that the binding sites of these targets are in the 5'UTR region instead of the coding regions. On the contrary, the *mCherry* signal of ZMO1437 in the Zms6 overexpression strain were significantly greater than the control strain (**Figure 6D**). From this data, we can infer that Zms6 likely activates the expression of ZMO1437 through the interaction with the coding region, as consistent with our IntaRNA prediction (**Supplementary Figure S4B**). These experiments confirm that binding of Zms4 and Zms6 to their confirmed mRNA targets can exert regulatory effects *in vivo*.

Given the lack of overlap between the confirmed set of direct mRNA targets of Zms4 and Zms6 and the fact that these two sRNAs share some important pathways associated with alcohol tolerance (**Figures 2C,D** and **Supplementary Table S3**), we hypothesized that Zms4 and Zms6 could mediate crosstalk between these targets. In this way, these two sRNAs can link regulation of a broader set of pathways, establishing a wider regulatory network of relevance to a complex phenotype like ethanol tolerance. Thus, we further tested if one sRNA can affect the confirmed targets of the other one. Using the dual reporter system, we observed that the relative *EGFP/mCherry* fluorescence ratios of ZMO1754 and ZMO1993 5'-UTRs were significantly higher in Zms6 deletion strain compared to the wild type strain (**Figure 6A**). In contrast, the relative *EGFP/mCherry* fluorescence ratios of ZMO1934 and ZMO0170 5'-UTRs were comparable than those in the Zms4 deletion strain in comparison with the wild type strain (**Figure 6B**). However, using the promoter replacement system, we found that Zms4 overexpression strain also exhibited a significantly higher fluorescence signal than the control strain (**Figure 6D**), while the coding regions of other targets (ZMO1754, ZMO1993, ZMO1934, and ZMO0170) were not influenced by Zms4 or Zms6 (**Figures 6C,D**). These results showed that the interaction between Zms4 and Zms6 could result in the crosstalk of the regulations on some of their direct targets. More importantly, we found that deletion of Zms4 also did not affect transcript levels of Zms6 and vice versa (**Figures 6D,E**). Similarly, Zms16 levels also didn't shown any obvious change in Zms4 and Zms6 deletion strains (**Figures 6D,E**). This indicates that, unlike the mRNA targets, the sRNA-sRNA interplays (Zms4-Zms6 or Zms6-Zms16 interaction) are probably through

competition binding or structural changes instead of changing the expressions.

Combinatorial Effects of sRNAs on Ethanol Tolerance Show Complex Effect

Considering the interactive network of multiple sRNAs potentially seeded by Zms4 and Zms6 and some pathways specifically mediated by Zms4 or Zms6 (i.e., transport process regulated by Zms4 and hydrogen sulfate biosynthetic process regulated by Zms6), we further investigated the combinatorial effect of sRNAs on ethanol tolerance. For these experiments, strains overexpressing each possible combination pairs of Zms4, Zms6, and Zms16 were developed, as well as a strain expressing all three. As **Supplementary Figure S7** shows, most of the combination strains exhibited growth rates with significantly enhanced growth under ethanol than the wild type strain with empty plasmid in 6% (v/v) ethanol. The strain combination of overexpression of all three (pZms4-6-16 strain) shows the highest growth rate of all the strains tested under ethanol stress, while its growth rate is comparable to the empty vector control under no ethanol condition. These results confirmed the combinatorial importance of these sRNAs to growth on the ethanol stress, and the possibility that sRNAs could work in synergy to co-regulate the ethanol tolerance and confirmed that the interactions between Zms4 and Zms6 could lead to the cross-talk regulations on their targets *in vivo*.

DISCUSSION

The survival of bacteria is highly dependent on their ability to sense and adapt to changes in the environment, which entails a coordinated regulation of large networks of gene/protein expression (Hoe et al., 2013). In this study, two sRNAs, Zms4 and Zms6, that are naturally differentially expressed under ethanol stress in *Z. mobilis* are shown to be key to ethanol tolerance and shown to coordinate a large network of gene regulation that includes sRNA-sRNA interactions. Without these sRNAs, cells are highly sensitive to ethanol stress, and that by manipulating their cellular levels, ethanol tolerance can be improved. To our knowledge, this represents the first large sRNA-sRNA interacting network in bacteria.

In this study, multi-omics analyses play a key role in uncovering the network of sRNAs and their important roles in ethanol stress response (**Figures 2A,B** and **Supplementary Table S3**). Our transcriptomics experiment identified 34.22% of *Z. mobilis* genes involved in a wide range of cellular processes that are differentially regulated by the overexpression of Zms4 and Zms6 (**Supplementary Table S3**). This global level of transcriptional change is not surprising because both Zms4 and Zms6 greatly affect the ethanol tolerance, a complex phenotype (**Figure 1A**), and regulate several global transcriptional regulators or two-component systems. Many of the changed transcripts are associated with translation, hydrogen sulfide biosynthetic process, sulfate assimilation, and cysteine biosynthetic processes. These pathways represent many of the same basal metabolic function that are negatively impacted by ethanol stress and have

therefore been implicated in ethanol toxicity (Yang et al., 2009, 2013; He et al., 2012a,b; Yi et al., 2015; Zhang et al., 2015). Previous studies also showed that accumulation of ethanol inside the cells can also promote changes in membrane composition and affect membrane-related processes such as energy generation and transport (Hallsworth et al., 2003). Correspondingly, we found that a large number of transporters, electron transfer genes, DNA repair genes and membrane associated genes are affected by Zms4 or Zms6, either positively or negatively, which may be important to combat the negative consequences caused by the ethanol accumulation.

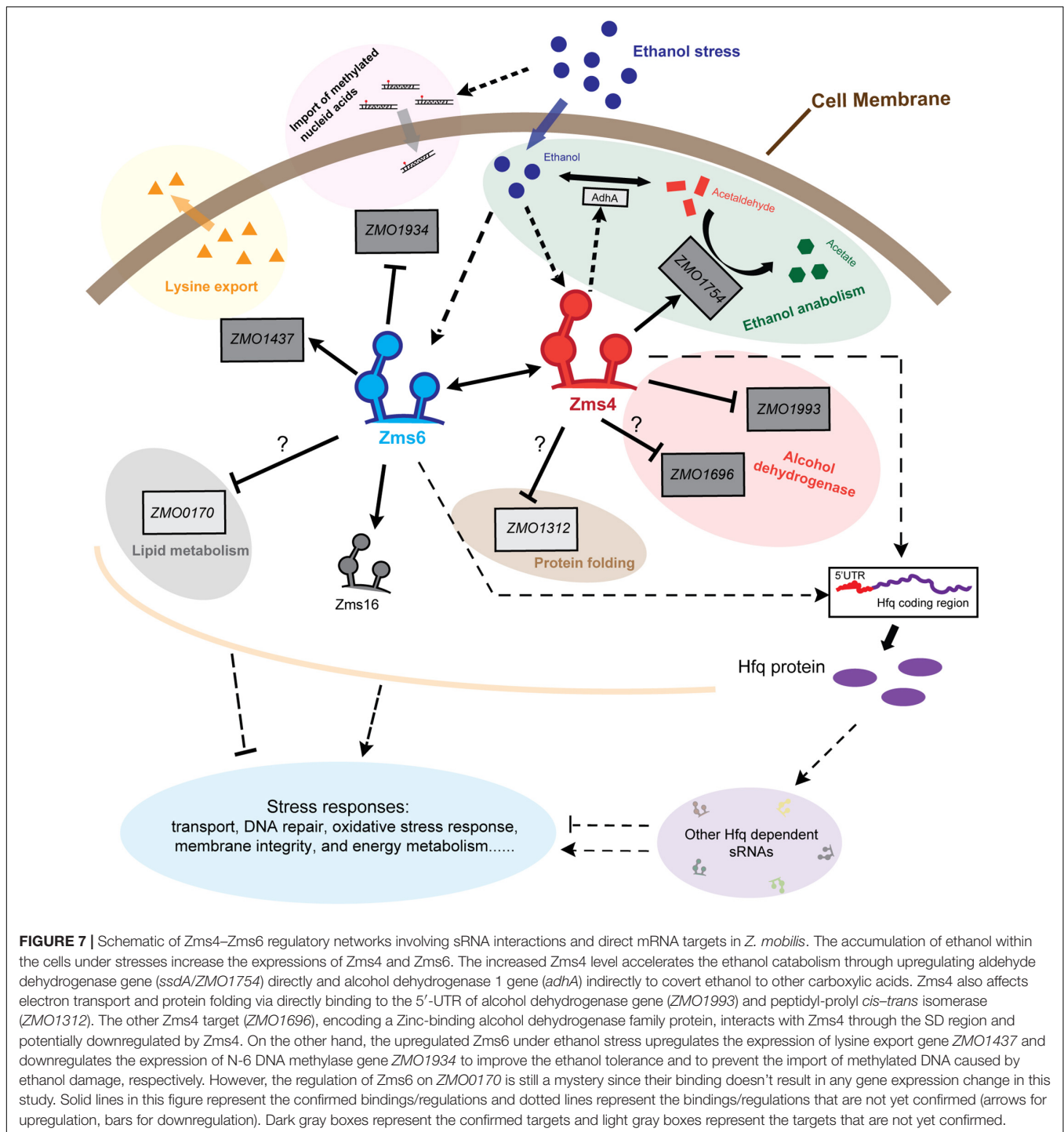
Although several potential mRNA targets were tested, EMSA assays revealed a few mRNAs to form stable complexes with Zms4 and Zms6 (Figures 4A–D). The targets not detected to bind might be highly dependent on the *in vivo* environment and/or bind to other locations of the mRNAs, outside the 5' regions tested in this study. Alternatively, some RNA-binding protein may exist to simulate the formation of multiple RNA–RNA complexes *in vivo* which we didn't include in the EMSA assays. RNA–RNA binding site interactions can be difficult to predict computationally due to the sensitivity of these interactions to structural complexity and *in vivo* variables beyond current modeling capabilities. Interestingly, most of the Zms4 and Zms6 targets occupy different sites on the sRNAs (Figures 4E,F). This observation indicates that the sRNAs could potentially co-regulate multiple targets simultaneously, suggesting flexibility and efficiency of the Zms4 and Zms6 regulation.

Although the inferred mechanisms of Zms4 and Zms6 regulation on all the targets were not specifically validated in this study, the hypothesized mechanisms are consistent with those observed in previous studies about *Z. mobilis* and other organisms. Using *in vivo* reporter systems, we uncovered that Zms4 positively regulates aldehyde dehydrogenase gene *ZMO1754* and represses the expression of alcohol dehydrogenase gene *ZMO1993* through interaction with their 5' UTR regions (Figure 6A). Aldehyde dehydrogenase (*ZMO1754/SsdA*) is responsible for the oxidation of acetaldehyde to acetate and is expressed eightfold higher in xylose-only media compared with glucose-only media (Mohagheghi et al., 2014). In the metabolism, acetaldehyde represents a branching point: converted to either ethanol by *AdhA/B* or acetate by *SsdA* (*ZMO1754*) (Zhang et al., 1995; Edenberg, 2007; Yi et al., 2015). Interestingly, the elevated *adhA* levels were also found by the overexpression of Zms4 in our transcriptomic data. Considering that any of these three compounds cause stress to the cell, one important role of Zms4 could be to shift flux away from ethanol production by stabilizing this particular transcript during stress, and/or to reduce acetaldehyde/ethanol accumulation. *ZMO1993* encodes an alcohol dehydrogenase protein, which is homologous to the *E. coli* *QorA*, known to respond to oxidative stress as part of the electron transport chain (Edwards et al., 1996). Both the transcript and protein of *ZMO1993* were down-regulated in the acetate tolerant mutant *AcR* strain compared to the *ZM4* strain (Yang et al., 2013). In *Clostridium thermocellum*, a mutation to alcohol dehydrogenase improved ethanol tolerance through changing NADH-dependent activity to NADPH-dependent, thus altering the electron transport

chain in the mutant (Brown et al., 2011). These are consistent with our results that Zms4 promotes the degradation of *ZMO1993* transcript through its 5'-UTR, thereby also decrease the protein expression to improve the bacterial ethanol tolerance under stress. Interestingly, another confirmed Zms4 target, *ZMO1696*, also encodes an alcohol dehydrogenase family protein and interacts with Zms4 with high affinity. Even though we failed to discern the regulatory outcomes of Zms4 on this gene, the mutagenesis results showed that Zms4 binds to the *ZMO1696* mRNA through the 5'-UTR region (and through the Shine-Dalgarno (SD) region) (Figure 5A), which probably results instability of this transcript and/or reduced translation. *ZMO1696* is also previously shown to influence the glucose consumption and ethanol production in *Z. mobilis*, which may explain the elevated ethanol levels in the Zms4 overexpression strain (Figure 1B). Additionally, *ZMO1312* interacts with Zms4 but with a relatively low affinity (Figures 4A,B) and there is no clear clue about its contribution to the ethanol metabolism. Thus, we didn't study this target in detail.

In terms of Zms6, *ZMO1934* is the strongest target and negatively regulated by Zms6 *in vivo* (Figure 6B). Interestingly, three binding sites responsible for Zms6–*ZMO1934* interaction were identified by mutagenesis analysis: all the three binding sites are important but only the 5'-UTR region is indispensable (Figure 5E and Supplementary Figure S5), which is supported by the *in vivo* results that Zms6 only influences the expression of the 5'-UTR but has little effect on the coding region (Figures 6B,D). Functionally, *ZMO1934* encodes the methyltransferase subunit of the type I restriction-modification system, which has been linked to lower glucose utilization rate (Kerr et al., 2011). Therefore, the repression of *ZMO1934* by Zms6 could be important in reducing DNA replication in order to conserve energy under ethanol stress but more likely to prevent the ethanol damaged/methylated DNA from entering the cell. The expression of the lysine exporter gene *ZMO1437* shows a lower affinity but is confirmed to be positively affected by Zms6 through the coding region (Figure 6D). The up-regulated expression of *ZMO1437* was previously shown to improve the tolerance to phenolic aldehydes (Yi et al., 2015), and Zms6 potentially stabilizes this transcript based on our results. Therefore, the negative regulation of *ZMO1934* and *ZMO1437* could improve the bacterial ethanol tolerance. However, it is intriguing that the *ZMO0170* level does not change in the Zms6 deletion strain (Figures 6B,D), even though this gene exhibits a high affinity to Zms6 *in vitro* (Figures 4C,D). One cannot be excluded that the Zms6 regulation on this target is not strong enough to detect due to the complex *in vivo* condition. Other factors, like Zms4, might also interfere with this regulation by competing the same region on Zms6 with a higher affinity where Zms6–*ZMO0170* base-pairing locates (Figure 4F).

Importantly, in this study, the co-regulation of various pathways by multiple sRNAs is especially insightful. Notably, we suspect that the mutual interaction between Zms4 and Zms6 leads to cross-talk regulatory effects on the targets. For instance, *ZMO1437*, the target upregulated by Zms6, is also positively influenced by Zms4 (Figure 6D). Some of the Zms4 targets, like *ZMO1993*, also display differential expression in



the Zms6 deletion strain (Figure 6A). Interestingly, abolishing the expression of Zms4 does not affect transcript levels of Zms6 and vice versa (Figures 6E,F). Thus, we hypothesize that the Zms4–Zms6 interaction affects the binding between sRNAs and their targets through competition or structural changes. Furthermore, the interaction between Zms4 and Zms6 allows them to co-regulate a similar set of pathways important to ethanol stress response, especially the pathways related to translation,

hydrogen sulfide biosynthetic process, sulfate assimilation, cysteine biosynthetic process and transport (Figures 2C,D). Nevertheless, several pathways were uniquely regulated by Zms6 overexpression, showing that Zms6 exhibits other regulatory roles instead of only serving as a Zms4 target.

Second, several other uncharacterized sRNAs are also involved in the Zms4–Zms6 regulatory network. In the MAPS assay, 16 other sRNAs were co-purified with Zms4 except for Zms6,

whereas only two sRNAs (sRNA37 and Zms16) were pulled down with Zms6. In addition, our transcriptomic data also discovered a large number of sRNAs differentially expressed upon Zms4/Zms6 induction, including these directly bound sRNA targets (**Supplementary Tables S2, S4**). These changes might result from some regulators or RNA-binding proteins affected by Zms4 or Zms6 in an indirect way. Our previous study identified that the UTR region of *hfq* gene (ZMO0347) is sensitive to ethanol stress and act as a post-transcriptional regulator to increase sensitivity of Hfq protein under lower-level ethanol stress (Cho et al., 2017). In this study, the UTR region of *hfq* gene was found to be one of the targets co-purified with Zms4 (**Figure 3** and **Supplementary Table S4**), but interaction between them was not detected in our study. These indicate that the regulation of Zms4 and Zms6 does not rely on the expression of Hfq, even though Hfq is confirmed to be essential for the fitness of *Z. mobilis* (**Supplementary Figure S2C**). However, our transcriptional analysis showed that both Zms4 and Zms6 positively regulate the expression of *hfq* gene as well as its 5'UTR region (**Supplementary Table S2**). This strongly indicates that these two sRNAs potentially affect a wide range of sRNAs through indirectly modulating Hfq expression.

Moreover, we identified the combinatorial effect of sRNAs on ethanol tolerance by overexpressing them simultaneously, based on the observation that some pathways are specifically regulated by Zms4 or Zms6. We selected Zms16 because it was confirmed to be one of the strongest targets of Zms6, and it is the only sRNA confirmed to directly interplay with Zms4/Zms6 in this study (**Figures 4C,D**). Our results showed that either single or combined sRNA overexpression strains exhibited different growth rate under ethanol stress (**Supplementary Figure S7**). Notably, the combination expression of all three sRNAs (pZms4-6-16) showed the highest growth rate under 6% ethanol. However, the benefits of sRNA expression are not always directly additive in this system as previously reported for three sRNAs involved in *E. coli* acid tolerance (Gaida et al., 2013). For example, the overexpression of single sRNAs (pZms4 and pZms6) showed decreased growth rate under ethanol, whereas the pZms4-6 strain shows the highest growth rate under no ethanol condition, likely due to some metabolic changes of harboring a plasmid overexpressing the two interacting sRNAs (albeit under the same *P_{tet}* promoter) simultaneously. Therefore, this indicates that the network represents a potentially delicate interplay of sRNAs defined by optimal stoichiometric ratios.

Our work thus far proposes a sRNA regulatory network in *Z. mobilis* (**Figure 7**), where two newly uncovered sRNAs, Zms4 and Zms6, interact with each other and collaboratively regulate several mRNA targets *in vivo* that affect ethanol resistance, probably through the competitive binding and/or structural changes. It is worth noting that only Zms4 and Zms6 were specifically characterized in this study, so additional pathways may also be affected given the likelihood that Zms16 and other sRNAs have their own separate targets. Overall, our results strongly suggest that the sRNA regulatory network in *Z. mobilis* is part of general stress response mechanisms, contributing to comprehensive effects on multiple pathways essential to

the ethanol tolerance, such as transport, DNA repair, ethanol anabolism, and energy metabolism.

Taken together, this concept of a sRNA-sRNA interaction regulating bacterial tolerance and fitness under ethanol stress as seen here in *Z. mobilis* is novel and we expect to see the emergence of similar networks in other bacterial species to regulate other complex phenotypes.

DATA AVAILABILITY STATEMENT

High-throughput sequencing datasets have been deposited in NCBI GEO under accession number GSE107219.

AUTHOR CONTRIBUTIONS

LC, RH, and KH conceived and designed the experiments. RH, KH, JG-R, SC, and BS performed the experiments and analyzed the data. SY, YY, RL, and JH conceived and conducted the *in vivo* validation of the sRNA targets using the reporter systems. LC, RH, and KH wrote and revised the manuscript.

FUNDING

This work was supported by the National Science Foundation (DGE-1610403 to KH and CBET-1254754 to LC); the Welch Foundation (F-1756 to LC); the Administrative Department of Science, Technology and Innovation (COLCIENCIAS) of Colombia (to JG-R); the Fulbright Program (479 to JG-R); the Cancer Prevention Research Initiative of Texas (RP110782); and the Undergraduate Research Fellowship Program at the University of Texas at Austin (to BS). Funding for open access charge: National Science Foundation (CBET-1254754). YY, RL, JH, and SY acknowledge the support from State Key Laboratory of Biocatalysis and Enzyme Engineering and Technical Innovation Special Fund of Hubei Province (2018ACA149).

ACKNOWLEDGMENTS

We gratefully appreciate Dr. Zhang Min (National Bioenergy Center, National Renewable Energy Laboratory, United States) for providing us with the *Z. mobilis* 8b strain. We also would like to thank Maria D. Person at the Proteomics Facility of the University of Texas at Austin who performed mass spectrometry analysis and the Genomic Sequencing and Analysis Facility of the University of Texas at Austin who performed next generation sequencing.

SUPPLEMENTARY MATERIAL

The Supplementary Material for this article can be found online at: <https://www.frontiersin.org/articles/10.3389/fbioe.2020.00155/full#supplementary-material>

REFERENCES

- Anders, S., Pyl, P. T., and Huber, W. (2015). HTSeq—a Python framework to work with high-throughput sequencing data. *Bioinformatics* 31, 166–169. doi: 10.1093/bioinformatics/btu638
- Block, K. F., Puerta-Fernandez, E., Wallace, J. G., and Breaker, R. R. (2011). Association of OLE RNA with bacterial membranes via an RNA-protein interaction. *Mol. Microbiol.* 79, 21–34. doi: 10.1111/j.1365-2958.2010.07439.x
- Brown, S. D., Guss, A. M., Karpins, T. V., Parks, J. M., Smolin, N., Yang, S. H., et al. (2011). Mutant alcohol dehydrogenase leads to improved ethanol tolerance in *Clostridium thermocellum*. *Proc. Natl. Acad. Sci. U.S.A.* 108, 13752–13757. doi: 10.1073/pnas.1102444108
- Busch, A., Richter, A. S., and Backofen, R. (2008). IntaRNA: efficient prediction of bacterial sRNA targets incorporating target site accessibility and seed regions. *Bioinformatics* 24, 2849–2856. doi: 10.1093/bioinformatics/btn544
- Cho, S. H., Haning, K., and Contreras, L. M. (2015). Strain engineering via regulatory noncoding RNAs: not a one-blueprint-fits-all. *Curr. Opin. Chem. Eng.* 10, 25–34. doi: 10.1016/j.coche.2015.07.008
- Cho, S. H., Haning, K., Shen, W., Blome, C., Li, R., Yang, S., et al. (2017). Identification and characterization of 5' untranslated regions (5'UTRs) in *Zymomonas mobilis* as regulatory biological parts. *Front. Microbiol.* 8:2432. doi: 10.3389/fmicb.2017.02432
- Cho, S. H., Lei, R., Henninger, T. D., and Contreras, L. M. (2014). Discovery of ethanol-responsive small RNAs in *Zymomonas mobilis*. *Appl. Environ. Microbiol.* 80, 4189–4198. doi: 10.1128/Aem.00429-14
- Corcoran, C. P., Podkaminski, D., Papenfort, K., Urban, J. H., Hinton, J. C., and Vogel, J. (2012). Superfolder GFP reporters validate diverse new mRNA targets of the classic porin regulator, MicF RNA. *Mol. Microbiol.* 84, 428–445. doi: 10.1111/j.1365-2958.2012.08031.x
- DiChiara, J. M., Contreras-Martinez, L. M., Livny, J., Smith, D., McDonough, K. A., and Belfort, M. (2010). Multiple small RNAs identified in *Mycobacterium bovis* BCG are also expressed in *Mycobacterium tuberculosis* and *Mycobacterium smegmatis*. *Nucleic Acids Res.* 38, 4067–4078. doi: 10.1093/nar/gkq101
- Edenberg, H. J. (2007). The genetics of alcohol metabolism: role of alcohol dehydrogenase and aldehyde dehydrogenase variants. *Alcohol Res. Health* 30, 5–13.
- Edwards, K. J., Barton, J. D., Rossjohn, J., Thorn, J. M., Taylor, G. L., and Ollis, D. L. (1996). Structural and sequence comparisons of quinone oxidoreductase, zeta-crystallin, and glucose and alcohol dehydrogenases. *Arch. Biochem. Biophys.* 328, 173–183. doi: 10.1006/abbi.1996.0158
- Franden, M. A., Pilath, H. M., Mohagheghi, A., Pienkos, P. T., and Zhang, M. (2013). Inhibition of growth of *Zymomonas mobilis* by model compounds found in lignocellulosic hydrolysates. *Biotechnol. Biofuels* 6:99. doi: 10.1186/1754-6834-6-99
- Frohlich, K. S., Haneke, K., Papenfort, K., and Vogel, J. (2016). The target spectrum of SdsR small RNA in *Salmonella*. *Nucleic Acids Res.* 44, 10406–10422. doi: 10.1093/nar/gkw632
- Gaida, S. M., Al-Hinai, M. A., Indurthy, D. C., Nicolaou, S. A., and Papoutsakis, E. T. (2013). Synthetic tolerance: three noncoding small RNAs, DsrA, ArcZ and RprA, acting supra-additively against acid stress. *Nucleic Acids Res.* 41, 8726–8737. doi: 10.1093/nar/gkt651
- Gottesman, S. (2019). Trouble is coming: signaling pathways that regulate general stress responses in bacteria. *J. Biol. Chem.* 294, 11685–11700. doi: 10.1074/jbc.REV119.005593
- Gottesman, S., McCullen, C. A., Guillier, M., Vanderpool, C. K., Majdalani, N., Benhammou, J., et al. (2006). Small RNA regulators and the bacterial response to stress. *Cold Spring Harb. Symp. Quant. Biol.* 71, 1–11. doi: 10.1101/sqb.2006.71.016
- Gottesman, S., and Storz, G. (2011). Bacterial small RNA regulators: versatile roles and rapidly evolving variations. *Cold Spring Harb. Perspect. Biol.* 3:a003798. doi: 10.1101/cshperspect.a003798
- Hallsworth, J. E., Prior, B. A., Nomura, Y., Iwahara, M., and Timmis, K. N. (2003). Compatible solutes protect against chaotrope (ethanol)-induced, nonosmotic water stress. *Appl. Environ. Microbiol.* 69, 7032–7034. doi: 10.1128/aem.69.12.7032-7034.2003
- He, M. X., Wu, B., Shui, Z. X., Hu, Q. C., Wang, W. G., Tan, F. R., et al. (2012a). Transcriptome profiling of *Zymomonas mobilis* under ethanol stress. *Biotechnol. Biofuels* 5:75. doi: 10.1186/1754-6834-5-75
- He, M. X., Wu, B., Shui, Z. X., Hu, Q. C., Wang, W. G., Tan, F. R., et al. (2012b). Transcriptome profiling of *Zymomonas mobilis* under furfural stress. *Appl. Microbiol. Biotechnol.* 95, 189–199. doi: 10.1007/s00253-012-4155-4
- Hoe, C. H., Raabe, C. A., Rozhdestvensky, T. S., and Tang, T. H. (2013). Bacterial sRNAs: regulation in stress. *Int. J. Med. Microbiol.* 303, 217–229. doi: 10.1016/j.ijmm.2013.04.002
- Hor, J., Gorski, S. A., and Vogel, J. (2018). Bacterial RNA biology on a genome scale. *Mol. Cell* 70, 785–799. doi: 10.1016/j.molcel.2017.12.023
- Kaboord, B., Smith, S., Patel, B., and Meier, S. (2015). Enrichment of low-abundant protein targets by immunoprecipitation upstream of mass spectrometry. *Methods Mol. Biol.* 1295, 135–151. doi: 10.1007/978-1-4939-2550-6_12
- Kerr, A. L., Jeon, Y. J., Svenson, C. J., Rogers, P. L., and Neilan, B. A. (2011). DNA restriction-modification systems in the ethanologen, *Zymomonas mobilis* ZM4. *Appl. Microbiol. Biotechnol.* 89, 761–769. doi: 10.1007/s00253-010-2936-1
- Ko, J. H., and Altman, S. (2007). OLE RNA, an RNA motif that is highly conserved in several extremophilic bacteria, is a substrate for and can be regulated by RNase P RNA. *Proc. Natl. Acad. Sci. U.S.A.* 104, 7815–7820. doi: 10.1073/pnas.0701715104
- Lalaouna, D., and Masse, E. (2015). Identification of sRNA interacting with a transcript of interest using MS2-affinity purification coupled with RNA sequencing (MAPS) technology. *Genom. Data* 5, 136–138. doi: 10.1016/j.gdata.2015.05.033
- Langmead, B., and Salzberg, S. L. (2012). Fast gapped-read alignment with Bowtie 2. *Nat. Methods* 9, 357–359. doi: 10.1038/nmeth.1923
- Leistra, A. N., Curtis, N. C., and Contreras, L. M. (2019). Regulatory non-coding sRNAs in bacterial metabolic pathway engineering. *Metab. Eng.* 52, 190–214. doi: 10.1016/j.ymben.2018.11.013
- Li, H., Handsaker, B., Wysoker, A., Fennell, T., Ruan, J., Homer, N., et al. (2009). The Sequence Alignment/Map format and SAMtools. *Bioinformatics* 25, 2078–2079. doi: 10.1093/bioinformatics/btp352
- Love, M. I., Huber, W., and Anders, S. (2014). Moderated estimation of fold change and dispersion for RNA-seq data with DESeq2. *Genome Biol.* 15:550. doi: 10.1186/s13059-014-0550-8
- Lybecker, M., Zimmermann, B., Bilusic, I., Tukhtubaeva, N., and Schroeder, R. (2014). The double-stranded transcriptome of *Escherichia coli*. *Proc. Natl. Acad. Sci. U.S.A.* 111, 3134–3139. doi: 10.1073/pnas.1315974111
- Melamed, S., Peer, A., Faigenbaum-Romm, R., Gatt, Y. E., Reiss, N., Bar, A., et al. (2016). Global mapping of small RNA-target interactions in bacteria. *Mol. Cell* 63, 884–897. doi: 10.1016/j.molcel.2016.07.026
- Mihailovic, M. K., Vazquez-Anderson, J., Li, Y., Fry, V., Vimalathas, P., Herrera, D., et al. (2018). High-throughput in vivo mapping of RNA accessible interfaces to identify functional sRNA binding sites. *Nat. Commun.* 9:4084. doi: 10.1038/s41467-018-06207-z
- Miyakoshi, M., Chao, Y. J., and Vogel, J. (2015). Cross talk between ABC transporter mRNAs via a target mRNA-derived sponge of the GcvB small RNA. *EMBO J.* 34, 1478–1492. doi: 10.15252/embj.201490546
- Mohagheghi, A., Linger, J., Smith, J., Yang, S. H., Dowe, N., and Pienkos, P. T. (2014). Improving xylose utilization by recombinant *Zymomonas mobilis* strain 8b through adaptation using 2-deoxyglucose. *Biotechnol. Biofuels* 7:19. doi: 10.1186/1754-6834-7-19
- Mortazavi, A., Williams, B. A., McCue, K., Schaeffer, L., and Wold, B. (2008). Mapping and quantifying mammalian transcriptomes by RNA-Seq. *Nat. Methods* 5, 621–628. doi: 10.1038/nmeth.1226
- Pei, G. S., Sun, T., Chen, S., Chen, L., and Zhang, W. W. (2017). Systematic and functional identification of small non-coding RNAs associated with exogenous biofuel stress in cyanobacterium *Synechocystis* sp PCC 6803. *Biotechnol. Biofuels* 10:57. doi: 10.1186/s13068-017-0743-y
- Pichon, C., and Felden, B. (2007). Proteins that interact with bacterial small RNA regulators. *FEMS Microbiol. Rev.* 31, 614–625. doi: 10.1111/j.1574-6976.2007.00079.x
- Reimand, J., Isserlin, R., Voisin, V., Kucera, M., Tannus-Lopes, C., Rostamianfar, A., et al. (2019). Pathway enrichment analysis and visualization of omics data using g:Profiler, GSEA, Cytoscape and EnrichmentMap. *Nat. Protoc.* 14, 482–517. doi: 10.1038/s41596-018-0103-9
- Rogers, P. L., Jeon, Y. J., Lee, K. J., and Lawford, H. G. (2007). *Zymomonas mobilis* for fuel ethanol and higher value products. *Biotechnol. Biofuels* 108, 263–288. doi: 10.1007/10_2007_060

- Said, N., Rieder, R., Hurwitz, R., Deckert, J., Urlaub, H., and Vogel, J. (2009). In vivo expression and purification of aptamer-tagged small RNA regulators. *Nucleic Acids Res.* 37:e133. doi: 10.1093/nar/gkp719
- Shevchenko, A., Tomas, H., Havlis, J., Olsen, J. V., and Mann, M. (2006). In-gel digestion for mass spectrometric characterization of proteins and proteomes. *Nat. Protoc.* 1, 2856–2860. doi: 10.1038/nprot.2006.468
- Shimoni, Y., Friedlander, G., Hetzroni, G., Niv, G., Altuvia, S., Biham, O., et al. (2007). Regulation of gene expression by small non-coding RNAs: a quantitative view. *Mol. Syst. Biol.* 3:138. doi: 10.1038/msb4100181
- Sowa, S. W., Gelderman, G., Leistra, A. N., Buvaendiran, A., Lipp, S., Pitaktong, A., et al. (2017). Integrative FourD omics approach profiles the target network of the carbon storage regulatory system. *Nucleic Acids Res.* 45, 1673–1686. doi: 10.1093/nar/gkx048
- Storz, G., Vogel, J., and Wassarman, K. M. (2011). Regulation by small RNAs in bacteria: expanding frontiers. *Mol. Cell* 43, 880–891. doi: 10.1016/j.molcel.2011.08.022
- Tomasini, A., Moreau, K., Chicher, J., Geissmann, T., Vandenesch, F., Romby, P., et al. (2017). The RNA targetome of *Staphylococcus aureus* non-coding RNA RsaA: impact on cell surface properties and defense mechanisms. *Nucleic Acids Res.* 45, 6746–6760. doi: 10.1093/nar/gkx219
- Tree, J. J., Granneman, S., McAteer, S. P., Tollervey, D., and Gally, D. L. (2014). Identification of bacteriophage-encoded anti-sRNAs in pathogenic *Escherichia coli*. *Mol. Cell* 55, 199–213. doi: 10.1016/j.molcel.2014.05.006
- Tsai, C. H., Liao, R., Chou, B., Palumbo, M., and Contreras, L. M. (2015). Genome-wide analyses in bacteria show small-RNA enrichment for long and conserved intergenic regions. *J. Bacteriol.* 197, 40–50. doi: 10.1128/Jb.02359-14
- Vazquez-Anderson, J., Mihailovic, M. K., Baldridge, K. C., Reyes, K. G., Haning, K., Cho, S. H., et al. (2017). Optimization of a novel biophysical model using large scale in vivo antisense hybridization data displays improved prediction capabilities of structurally accessible RNA regions. *Nucleic Acids Res.* 45, 5523–5538. doi: 10.1093/nar/gkx115
- Vogel, J., Bartels, V., Tang, T. H., Churakov, G., Slagter-Jager, J. G., Huttenhofer, A., et al. (2003). RNomics in *Escherichia coli* detects new sRNA species and indicates parallel transcriptional output in bacteria. *Nucleic Acids Res.* 31, 6435–6443. doi: 10.1093/nar/gkg867
- Wallace, J. G., Zhou, Z. Y., and Breaker, R. R. (2012). OLE RNA protects extremophilic bacteria from alcohol toxicity. *Nucleic Acids Res.* 40, 6898–6907. doi: 10.1093/nar/gks352
- Yang, S. H., Fei, Q., Zhang, Y. P., Contreras, L. M., Utturkar, S. M., Brown, S. D., et al. (2016a). *Zymomonas mobilis* as a model system for production of biofuels and biochemicals. *Microb. Biotechnol.* 9, 699–717. doi: 10.1111/1751-7915.12408
- Yang, S. H., Mohagheghi, A., Franden, M. A., Chou, Y. C., Chen, X. W., Dowe, N., et al. (2016b). Metabolic engineering of *Zymomonas mobilis* for 2,3-butanediol production from lignocellulosic biomass sugars. *Biotechnol. Biofuels* 9:189. doi: 10.1186/s13068-016-0606-y
- Yang, S. H., Pan, C. L., Hurst, G. B., Dice, L., Davison, B. H., and Brown, S. D. (2014). Elucidation of *Zymomonas mobilis* physiology and stress responses by quantitative proteomics and transcriptomics. *Front. Microbiol.* 5:246. doi: 10.3389/fmicb.2014.00246
- Yang, S. H., Pan, C. L., Tschaplinski, T. J., Hurst, G. B., Engle, N. L., Zhou, W., et al. (2013). Systems biology analysis of *Zymomonas mobilis* ZM4 ethanol stress responses. *PLoS One* 8:e68886. doi: 10.1371/journal.pone.0068886
- Yang, S. H., Tschaplinski, T. J., Engle, N. L., Carroll, S. L., Martin, S. L., Davison, B. H., et al. (2009). Transcriptomic and metabolomic profiling of *Zymomonas mobilis* during aerobic and anaerobic fermentations. *BMC Genomics* 10:34. doi: 10.1186/1471-2164-10-34
- Yang, Y., Shen, W., Huang, J., Li, R., Xiao, Y., Wei, H., et al. (2019). Prediction and characterization of promoters and ribosomal binding sites of *Zymomonas mobilis* in system biology era. *Biotechnol. Biofuels* 12:52. doi: 10.1186/s13068-019-1399-6
- Yi, X., Gu, H. Q., Gao, Q. Q., Liu, Z. L., and Bao, J. (2015). Transcriptome analysis of *Zymomonas mobilis* ZM4 reveals mechanisms of tolerance and detoxification of phenolic aldehyde inhibitors from lignocellulose pretreatment. *Biotechnol. Biofuels* 8:153. doi: 10.1186/s13068-015-0333-9
- Zadeh, J. N., Steenberg, C. D., Bois, J. S., Wolfe, B. R., Pierce, M. B., Khan, A. R., et al. (2011). NUPACK: analysis and design of nucleic acid systems. *J. Comput. Chem.* 32, 170–173. doi: 10.1002/jcc.21596
- Zhang, K., Shao, H. H., Cao, Q. H., He, M. X., Wu, B., and Feng, H. (2015). Transcriptional analysis of adaptation to high glucose concentrations in *Zymomonas mobilis*. *Appl. Microbiol. Biotechnol.* 99, 2009–2022. doi: 10.1007/s00253-014-6342-y
- Zhang, M., Eddy, C., Deanda, K., Finkstein, M., and Picataggio, S. (1995). Metabolic engineering of a pentose metabolism pathway in ethanologenic *Zymomonas-Mobilis*. *Science* 267, 240–243. doi: 10.1126/science.267.5195.240

Conflict of Interest: The authors declare that the research was conducted in the absence of any commercial or financial relationships that could be construed as a potential conflict of interest.

Copyright © 2020 Han, Haning, Gonzalez-Rivera, Yang, Li, Cho, Huang, Simonsen, Yang and Contreras. This is an open-access article distributed under the terms of the Creative Commons Attribution License (CC BY). The use, distribution or reproduction in other forums is permitted, provided the original author(s) and the copyright owner(s) are credited and that the original publication in this journal is cited, in accordance with accepted academic practice. No use, distribution or reproduction is permitted which does not comply with these terms.



The Synergistic Action of Electro-Fenton and White-Rot Fungi in the Degradation of Lignin

Lipeng Hou^{1†}, Dandan Ji^{1,2,3†}, Weifang Dong¹, Lin Yuan¹, Fengshan Zhang², Yan Li⁴ and Lihua Zang^{1*}

¹ College of Environmental Science and Engineering, Qilu University of Technology, Shandong Academy of Science, Jinan, China, ² Huatai Group Corp. Ltd., Dongying, China, ³ Jiangsu Key Laboratory of Anaerobic Biotechnology, Jiangnan University, Wuxi, China, ⁴ Langfang Meihua Biotechnology Development Co. Ltd., Langfang, China

OPEN ACCESS

Edited by:

Shihui Yang,
Hubei University, China

Reviewed by:

Fengxue Xin,
Nanjing Tech University, China
Daochen Zhu,
Jiangsu University, China

*Correspondence:

Lihua Zang
zlh@qlu.edu.cn

[†] These authors have contributed
equally to this work

Specialty section:

This article was submitted to
Bioprocess Engineering,
a section of the journal
Frontiers in Bioengineering and
Biotechnology

Received: 13 September 2019

Accepted: 03 February 2020

Published: 12 March 2020

Citation:

Hou L, Ji D, Dong W, Yuan L,
Zhang F, Li Y and Zang L (2020) The
Synergistic Action of Electro-Fenton
and White-Rot Fungi
in the Degradation of Lignin.
Front. Bioeng. Biotechnol. 8:99.
doi: 10.3389/fbioe.2020.00099

White-rot fungus is a common lignin-degrading fungus. However, compared with those of microorganisms that biodegrade lignin alone, synergistic systems of electro-Fenton processes and white-rot fungi are superior because of their high efficiency, mild conditions, and environmental friendliness. To investigate the details of lignin degradation by a synergistic system comprising electro-Fenton processes and white-rot fungi, lignin degradation was studied at different voltages with three lignin-degrading fungi (*Phanerochaete chrysosporium*, *Lentinula edodes*, and *Trametes versicolor*). The lignin degradation efficiency (82~89%) of the synergistic systems at 4 V was higher than that of a control at 96 h post inoculation. Furthermore, the H₂O₂ produced and phenolic lignin converted in the system can significantly enhance the efficiency of ligninolytic enzymes, so a considerably increased enzyme activity was obtained by the synergistic action of electro-Fenton processes and white-rot fungi. ¹³C NMR spectroscopy revealed that aromatic structure units (103–162 ppm) were effectively degraded by the three fungi. This study shows that the combination of electro-Fenton processes and white-rot fungi treatment significantly improved the lignin degradation efficiency, which established a promising strategy for lignin degradation and valorization.

Keywords: lignin, electron-Fenton, white-rot fungi, synergistic system, lignin-degrading enzyme

INTRODUCTION

In the degradation of lignin by microorganisms, synergistic systems have a more significant degradation effect than have systems without synergy. This is due to the non-specific, complex spatial structure of lignin. The lignin structure is characterized by the substitution of methoxycinnamic and hydroxycinnamic acid in the polymerization of heterogeneous 3D crystal polymers and mainly includes three basic components: guaiacyl units (G), syringyl units (S),

Abbreviations: ABTS, 2,2'-azino-bis-(3-ethylbenzothiazoline-6-sulfonate); ACF, activated carbon fiber; ANOVA, analysis of variance; CCEF, composite cathode electro-Fenton; cDNA, complementary DNA; DC, direct current; H₂O₂, hydrogen peroxide; Lac, laccase; LiP, lignin peroxidase; MnP, manganese peroxidase; mRNA, messenger RNA; NMR, nuclear magnetic resonance; OD, optical density; PDA, potato dextrose agar; PPO, polyphenol oxidase; real-time PCR, real-time polymerase chain reaction; ROS, reactive oxygen species; SPSS, Statistical Product and Service Solutions.

and *p*-hydroxyphenyl units (H) (Ewellyn et al., 2005; Pinto et al., 2012). These structures are interconnected by C–C single bonds (approximately 30%) and C–O bonds (approximately 60–70%) (Chakar et al., 2004; Pandey and Kim, 2011). Lignin macromolecules contain multiple functional groups, such as hydroxyl, methoxy, carbonyl, and aromatic structures (Azimvand, 2014). High-lignin materials have heterogeneity and structural stability, which are due to the formation and fracture modes of chemical bonds between complex chemical groups, conversions between different chemical groups, and various random interactions. These are the reasons considered challenging for the microbial degradation of aromatic compounds (Wen et al., 2013).

White-rot fungi are among the microorganisms in nature that can mineralize lignin into carbon dioxide and water. Lignin is degraded by their unique H_2O_2 production and extracellular enzyme system. The systems involved in lignin degradation mainly include the following. (i) The H_2O_2 production system includes glucose oxidase, glyoxal oxidase, and veratryl alcohol oxidase. These enzymes use a small organic molecule as a substrate, and reduction of molecular oxygen to H_2O_2 starts the peroxidase reaction process. (ii) The lignin oxidase system involves key enzymes for the degradation of lignin by white-rot fungi, which includes laccase (Lac), manganese peroxidase (MnP), and lignin peroxidase (LiP) (Derrien et al., 2017). MnP and LiP require H_2O_2 to trigger their oxidation and activate enzyme cycle reactions. Studies have shown that white-rot fungi are closely connected with the Fenton reaction in the process of lignin degradation. The low-molecular-weight compound, such as organic acids (Galkin et al., 1998), fatty acids (Gutiérrez et al., 2002), Fe^{3+} chelators, and catechol derivatives (Arantes and Milagres, 2006), is secreted by white-rot fungi in the process of wood biodegradation. These substances can reduce Fe^{3+} to Fe^{2+} and generate hydroxyl radicals by the Fenton reaction. The hydroxyl radical is one of the strongest oxidants ($E = 2.8$ V versus normal hydrogen electrode) and can efficiently and non-selectively oxidize various organic compounds (Cisneros et al., 2002). Hydroxyl radicals can convert non-phenolic lignin into phenolic lignin. Then, MnP and Lac can further oxidize phenolic lignin. This mechanism ensures that lignin can be degraded efficiently when the LiP content is low or absent.

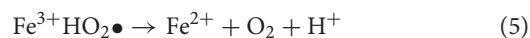
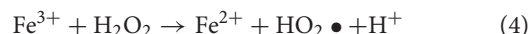
Fe^{3+} -reducing compounds and Fenton reagents are commonly used to degrade lignin phenolic resins and enable non-phenolic lignin reactions, which are known as chelator-mediated Fenton reactions (Arantes et al., 2006). White-rot fungi can reduce the pH of the environment as they grow: a substantial reduction in pH was caused by fungi in liquid cultures through metabolic regulation (Jellison et al., 1992; Humar et al., 2001). This change is attributed to fungi that can secrete and produce many acidic group-containing compounds, such as phenolic acids and other simple organic acids, during metabolism (Jellison et al., 1997).

There are limitations of single-component biodegradation, such as lone reaction time and high environmental requirements, and this study attempted to adopt a synergistic system of biodegradation and electro-Fenton. Electro-Fenton technology

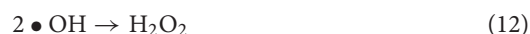
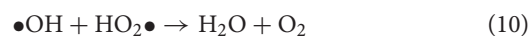
is a new technology of lignin treatment. It is a combination of Fenton oxidation and electrochemical technology, which has unique advantages in the treatment of refractory organic pollutants (Pulgarin and Kiwi, 1996). Composite cathode electro-Fenton (CCEF) technology is an improved electro-Fenton technology that can produce H_2O_2 and Fenton reagents *in situ* without the exogenous addition of Fe^{2+} . Dioxygen in solution is reduced by two electrons at the cathode and protonated to H_2O_2 , which then reacts with Fe^{2+} to produce hydroxyl radicals while Fe^{2+} is oxidized to Fe^{3+} . The newly generated Fe^{3+} can be regenerated on the surface of the electrode to improve the efficiency of the iron catalyst. The cathode reactions are as follows (Eqs 1–3) (Kurt et al., 2007; Ting et al., 2008):



Fe^{3+} can be reduced to Fe^{2+} by reducing substances in the solution or on the cathode surface (Eqs 4–6):



The following side reactions are present in the solution (Eqs 7–12):



This experiment aimed to study the effect of lignin decomposition in a constructed synergistic system. The synergistic system is a lignin fungus culture containing a composite cathode loaded with Fe^0 to which a voltage has been applied. The growth of fungi decreased the pH of the environment and provided acidic conditions for the Fenton reaction. The Fe^0 becomes Fe^{2+} in the composite cathode under an applied potential. At the same time, there was a continuous Fenton reaction between Fe^{2+} and H_2O_2 produced by the composite cathode, and the large number of hydroxyl radicals produced degraded lignin. H_2O_2 can also quickly start LiP and MnP enzymatic hydrolysis reactions to accelerate lignin biodegradation (Mir-Tutusa et al., 2018). In addition, the voltage promoted the growth of fungal cells (Thrash and Coates, 2008; Loghavi et al., 2010b), so that more lignin-degrading enzymes were produced. The effect of lignin degradation in this mutually advantageous synergistic system was also investigated. This is the main content of this paper.

MATERIALS AND METHODS

Materials

Dealkaline lignin, a mixture of different herbaceous plants, such as corn stover, bamboo, and straw, was obtained from Shanghai Chemical Reagent Four Factory (Shanghai, China).

The white-rot fungi medium included dealkaline lignin (500 mg/L), KH_2PO_4 (2 g/L), MgSO_4 (0.25 g/L), CaCl_2 (0.1 g/L), MnSO_4 (5 mg/L), VB_1 (10 mg/L), ammonium tartrate (0.2 g/L), and trace element solution (150 ml/L). The trace element solution included NaCl (1.0 g/L), $\text{FeSO}_4 \cdot 7\text{H}_2\text{O}$ (100 mg/L), $\text{CoSO}_4 \cdot 7\text{H}_2\text{O}$ (100 mg/L), CaCl_2 (100 mg/L), $\text{ZnSO}_4 \cdot 7\text{H}_2\text{O}$ (100 mg/L), $\text{CuSO}_4 \cdot 5\text{H}_2\text{O}$ (10 mg/L), $\text{KAl}(\text{SO}_4)_2$ (100 mg/L), H_3BO_3 (10 mg/L), and Na_2MoO_4 (10 mg/L). All reagents were purchased from Sinopharm Chemical Reagent Co., Ltd., (Beijing, China).

Fabrication of composite electrodes [Fe^0 and Fe_3O_4 /activated carbon fiber (ACF)]: An ACF (3 × 10 cm) was ultrasonically cleaned in water for 10 min and then dried in a blast oven. The pretreated ACF was soaked in 100 ml of solution for 1 h. The solution was an 80% ethanol aqueous solution in which 9.66 g of $\text{FeCl}_3 \cdot 6\text{H}_2\text{O}$ was dissolved. NaBH_4 (3.54 g) was preliminarily dissolved in 100 ml of deionized water, and the NaBH_4 solution was dropwise added to the ACFs in a surface pan at a speed of 0.5 ml/s using a dropper. The whole operation was completed at room temperature. During the drip process, a large number of bubbles were produced, and black fluffy substances were generated on the ACFs. After the completion of 1 h of dropwise addition, residual NaBH_4 on the carbon fiber surface was removed with deionized water and ethanol. Under the protection of argon, infrared light drying was performed, and composite cathodes (Fe^0 and Fe_3O_4 /ACF) were obtained.

A constant current was supplied using a DC power supply (Zhaoxin, China, 0–3 A, 0–5 V).

Fungal Strains and Inoculation

Phanerochaete chrysosporium (CICC14076), *Lentinula edodes* (CICC14019), and *Trametes versicolor* (CICC50001) were purchased from the China Industrial Bacteria Conservation Center.

These strains were preserved on potato dextrose agar (PDA) plates at 4°C. They were inoculated into the white-rot fungi medium with an inoculation loop (1 μl) and incubated for 4 days at 39°C.

Analytical Methods

Lignin Removal Efficiency Determination

The sample was first hydrolyzed for 30 min at room temperature using 72% (w/w) H_2SO_4 . Then it was hydrolyzed a second time for 60 min at 120°C with 4% H_2SO_4 . The solid residue obtained after acid hydrolysis was determined. Ash content was determined in an oven at 550°C over 8 h. Lignin content on free ash basis is the difference between the solid residue and ash (Ballesteros et al., 2004).

The lignin degrading ratio was calculated using the formula $R (\%) = 100 \times (m_0 - m)/m_0$, where R is the degrading ratio for

the sample; m_0 is the initial content of lignin; m is the sampling content of lignin.

Ligninolytic Enzyme Activity

The enzyme activity was determined in 5 g of culture that was suspended in 100 ml of sodium acetate buffer (1 mM) and pH 5 and vigorously blended for 1 min in a Waring blender. The Lac activity was tested in 1 mM of sodium acetate buffer at pH 5 with 0.5 M of 2,2'-azinobis-(3-ethylbenzothiazoline-6-sulfonate) (ABTS) (Bourbonnais et al., 1995) and measured in a microplate reader at 420 nm (ϵ_{420} , 36,000 $\text{M}^{-1} \text{cm}^{-1}$) with a distance of 0.29 cm. The LiP activity was tested in 125 mM of sodium tartrate at pH 3 using 2 mM of hydrogen peroxidase and 0.16 mM of azure B (Archibald, 1992) and measured in a microplate reader at 610 nm (ϵ_{610} , 48,800 $\text{M}^{-1} \text{cm}^{-1}$). The MnP activity was determined in 50 mM of sodium succinate (pH 4.5) and 50 mM of sodium lactate (pH 4.5) using 0.1 mM of MnSO_4 , 0.1 mM of phenol red, and 50 μM of H_2O_2 and measured in a microplate reader at 610 nm (ϵ_{610} , 30,737 $\text{M}^{-1} \text{cm}^{-1}$).

^{13}C NMR

Nuclear magnetic resonance (NMR) spectra of lignin media were acquired at 298 K on an AVANCE III HD 500 MHz instrument (Bruker, Switzerland). The sample (80 mg) was dissolved in 0.5 ml of $\text{DMSO}-d_6$ (99.8%). The parameters were as follows: pulse angle (30°), pulse width (9.2 μs), delay time (1.00 s), and acquired time (3.28 s).

Expression of Lac and Versatile Peroxidase

Transcripts by Real-Time Polymerase Chain Reaction

The total RNA of *P. chrysosporium* and *L. edodes* mycelia growing in different electro-Fenton levels using lignin medium was isolated by TRIzol reagent (Invitrogen, Carlsbad, CA, United States). The RNA concentration was determined by absorbance at 260 nm. Subsequently, 2 μg of RNA was reverse-transcribed in a 50 μl reaction mixture using the iScriptTM complementary DNA (cDNA) synthesis kit (Bio-Rad Laboratories, Hercules, CA, United States). The cDNA samples were stored at −20°C for use.

To determine the mRNA levels of the *LiP*, *MnP*, and *Lac* genes, quantitative real-time PCR was performed with a CFX96 real-time system (Bio-Rad Laboratories, Hercules, CA, United States) and SYBR green I in 96-well plates. The volume of each PCR sample was 20 μl , which included 0.5 μl of PCR reverse primer, 10 μl of SYBR green I, 0.5 μl of PCR forward primer, 5 μl of cDNA, and 4 μl of distilled water (DW). The β -actin gene of *P. chrysosporium* was used as an internal control. The β -tubulin gene of *L. edodes* was used as an internal control. The primer pairs for intergenic regions are shown in Table 1.

RESULTS AND DISCUSSION

Determination of Optimal Voltage for Electro-Fenton Reaction

In a certain range, the applied voltage clearly promoted the growth of the three white-rot fungi (*P. chrysosporium*, *T.*

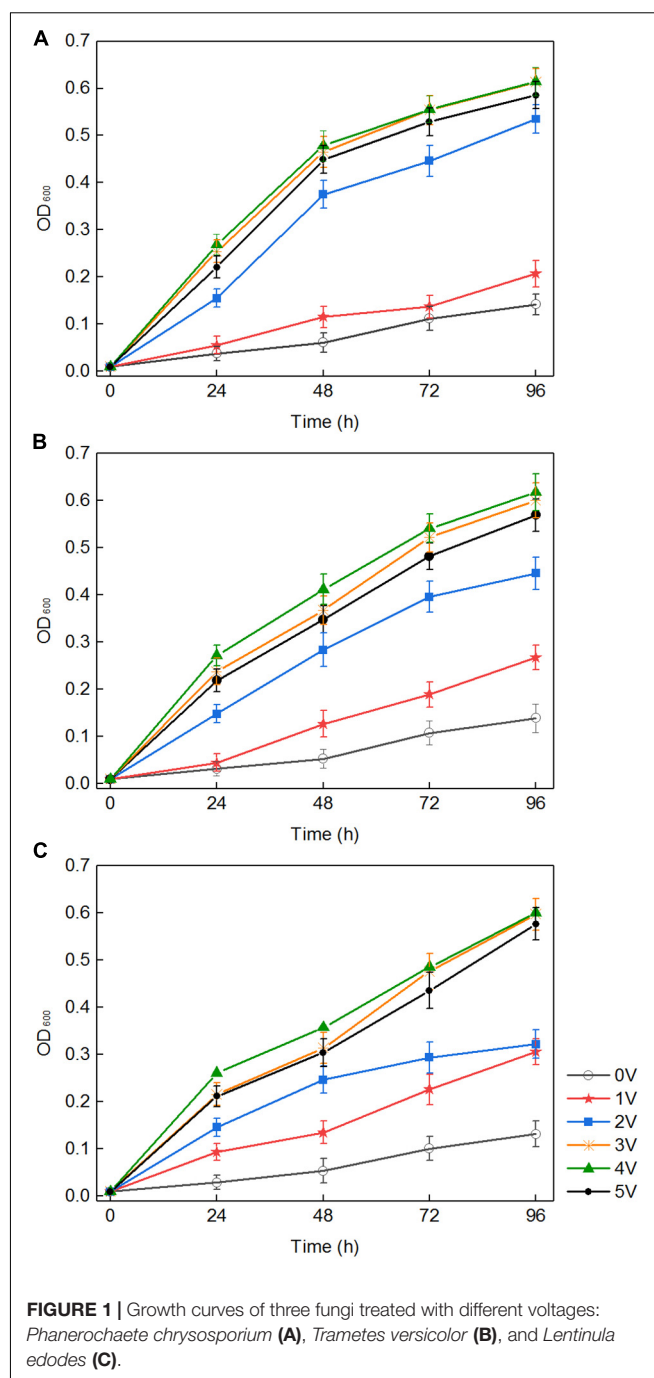
TABLE 1 | Primer pairs of the real-time PCR.

Strain	Gene	Primer pairs
<i>P. chrysosporium</i>	<i>LiP</i>	F: 5'-TTCTTCGTCGAGACTCAG-3' R: 5'-CTTGGACTGGTTGTTGAC-3'
<i>P. chrysosporium</i>	<i>MnP</i>	F: 5'-CTGTGAGTTACGGAATTGG-3' R: 5'-GGAGGAGGAGGAAGTAGA-3'
<i>P. chrysosporium</i>	β -Actin	F: 5'-GCACCACACCTTCTACAA-3' R: 5'-TCATCTTCTCACGGTTAGC-3'
<i>L. edodes</i>	<i>LiP</i>	F: 5'-GACGCCTTTCCCTGCTCTTACTG-3' R: 5'-AGCAGCAGAACGAGCATATTCAGG-3'
<i>L. edodes</i>	<i>MnP</i>	F: 5'-CAATCCTCCGCTGTTACA-3' R: 5'-TCGTTGCTGACCAAGATAA-3'
<i>L. edodes</i>	<i>Lac</i>	F: 5'-CCAACCATTCGTTCTCTA-3' R: 5'-GCAGTCAGCAATAGTAAGC-3'
<i>L. edodes</i>	β -Tubulin	F: 5'-TTCACCGACACATCACT-3' R: 5'-GACATAACAAGGGACACAAG-3'
<i>T. versicolor</i>	<i>LiP</i>	F: 5'-CACGACCTTTCCATCTTC-3' R: 5'-ATGCTTGCTGTTAGTTG-3'
<i>T. versicolor</i>	<i>MnP</i>	F: 5'-GACACGCAGTTCCTCATC-3' R: 5'-CTGGTTGTTGACGAAGGA-3'
<i>T. versicolor</i>	<i>Lac</i>	F: 5'-GCTATCCTCCGCTATGAT-3' R: 5'-GCCGTTGATGAAGAAGT-3'
<i>T. versicolor</i>	β -Actin	F: 5'-TATCCGTCGTGACCTCTA-3' R: 5'-CGATCTTGACCTTCATACTTG-3'

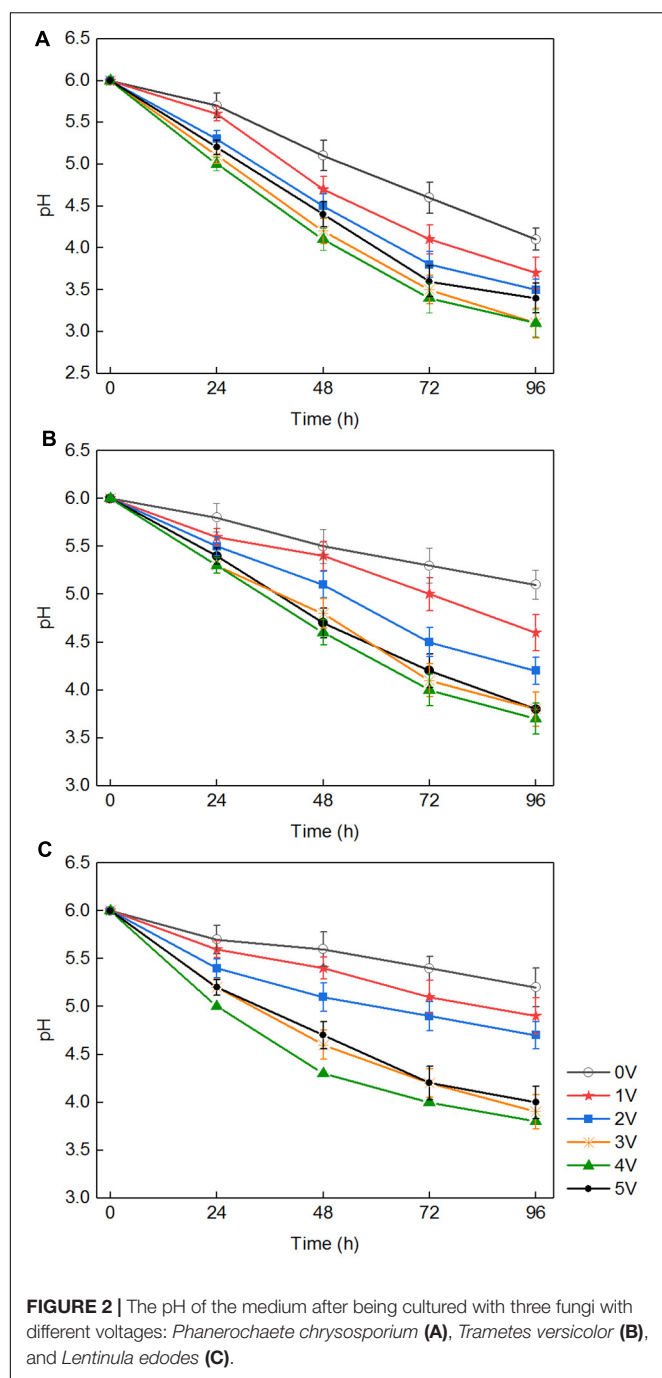
All data were normalized to the internal control, and relative expression was calculated using the 2-DDCt method. The results were analyzed by one-way analysis of variance (ANOVA). Statistical analysis was performed using Statistical Product and Service Solutions (SPSS).

versicolor, and *L. edodes*). As shown in **Figure 1**, in the absence of an applied voltage in the control, white-rot fungi grew slowly, and the highest optical density (OD) of *P. chrysosporium*, *T. versicolor*, and *L. edodes* was only 0.142, 0.132, and 0.139 within 96 h, respectively. However, under an applied voltage, the growth of the three fungi rapidly increased with increasing voltage. The results also showed that different voltages had different effects on the three white-rot fungi; and 1, 2, 3, and 4 V promoted the growth of the three white-rot fungi to varying degrees. The higher the voltage was in the range of 1–4 V, the more obvious the promoting effect. The OD of *P. chrysosporium*, *T. versicolor*, and *L. edodes* reached the highest values (0.615, 0.618, and 0.601, respectively) at 4 V. However, the OD slightly decreased at 5 V, suggesting that 4 V is the best voltage for the growth of these three white-rot fungi.

There were three ways to explain the above phenomenon. First, in the medium with white-rot fungi, the pH dropped rapidly to approximately 3.5 (**Figure 2**). H_2O_2 and Fe^{2+} generated in the composite cathode under an applied voltage reacted to produce hydroxyl radicals, which occurred via the Fenton reaction. The macromolecular groups were converted into small molecules that could be easily used by white-rot fungi (Kai et al., 2018), which was conducive to the transport of nutrients into the cell and promoted the growth and reproduction of white-rot fungi. Second, it was reported that an external voltage can change the cell membrane permeabilization (Loghavi et al., 2010a), which indicates that the permeability of the fungal cell membrane could be improved by application of an appropriate voltage. For cells grown in liquid medium, because



of the diffusion of nutrients in the liquid matrix, the increased membrane permeability promoted the diffusion of nutrients on cell membranes. Third, an applied voltage increased intracellular protein and ATP levels and promoted the metabolic ability of cells to a certain extent (Filipič et al., 2012). Previous studies suggested that temporary, non-lethal membrane permeabilization occurs when cells are subjected to suitable voltage, which is conducive to introducing various exogenous substances into living cells. However, because of the permeability of cell membrane, the growth and metabolism of white-rot fungi could be inhibited



when the applied voltage was over the capacity of microorganism (Loghavi et al., 2010c). This is the reason for the slow growth of white-rot fungi at 5 V.

The Improvement of Lignin Degradation by Electro-Fenton Reaction Analysis of Lignin Degradation Efficiency

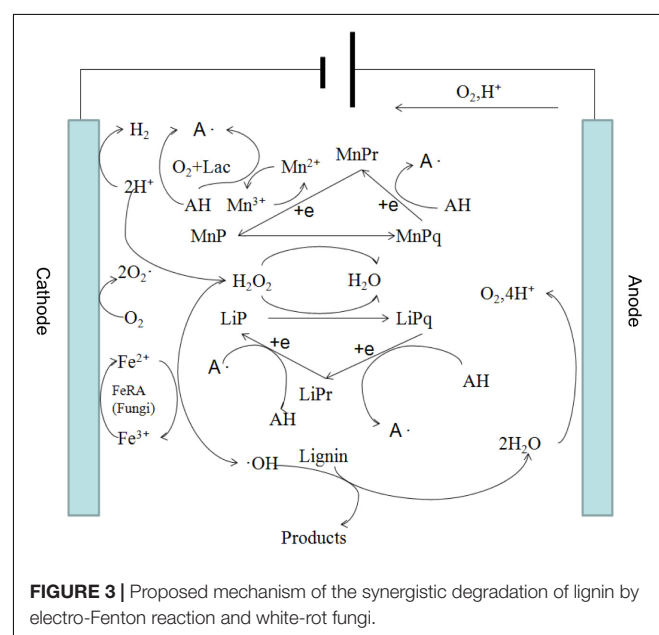
In the medium containing lignin, *P. chrysosporium*, *T. versicolor*, and *L. edodes* were cultured for 96 h. As shown

in Table 2, in the absence of voltage, the degradation rates of lignin for *P. chrysosporium*, *T. versicolor*, and *L. edodes* were 17, 19, and 19%, respectively. The degradation rate of lignin at 4 V was approximately 19% when there was no white-rot fungus. In the presence of white-rot fungus and an applied voltage, the degradation rates of lignin for *P. chrysosporium*, *T. versicolor*, and *L. edodes* at 4 V were 82, 86, and 89%, respectively, which were 65–70% higher than those obtained with white-rot fungi or applied voltage alone.

These results indicate that a synergistic effect on lignin degradation occurred in the presence of white-rot fungi and applied voltage. The reasons for the synergistic effect can be summarized as follows. First, under an appropriate voltage for the electro-Fenton reaction, the pH of the liquid medium decreased rapidly owing to the growth of white-rot fungi (Figure 2) and reached the appropriate acidity required by the Fenton reaction. The Fenton reaction occurred between the H_2O_2 and the Fe^{2+} generated under the applied voltage on the composite cathode. Large numbers of hydroxyl radical ($OH\cdot$) and various functional groups in lignin were degraded by direct oxidation. The degradation of lignin was promoted. Second, in the presence of an

TABLE 2 | Lignin degradation efficiency by three fungi at different voltages.

Strains	Lignin degradation efficiency (%) at different voltages					
	0V	1V	2V	3V	4V	5V
<i>P. chrysosporium</i>	17 ± 1	23 ± 2	50 ± 2	79 ± 3	82 ± 3	78 ± 2
<i>T. versicolor</i>	19 ± 2	28 ± 3	55 ± 2	77 ± 3	86 ± 3	75 ± 2
<i>L. edodes</i>	19 ± 2	34 ± 3	60 ± 3	87 ± 4	89 ± 3	85 ± 3
No fungi	N/A	7 ± 1	12 ± 2	15 ± 1	19 ± 1	22 ± 2



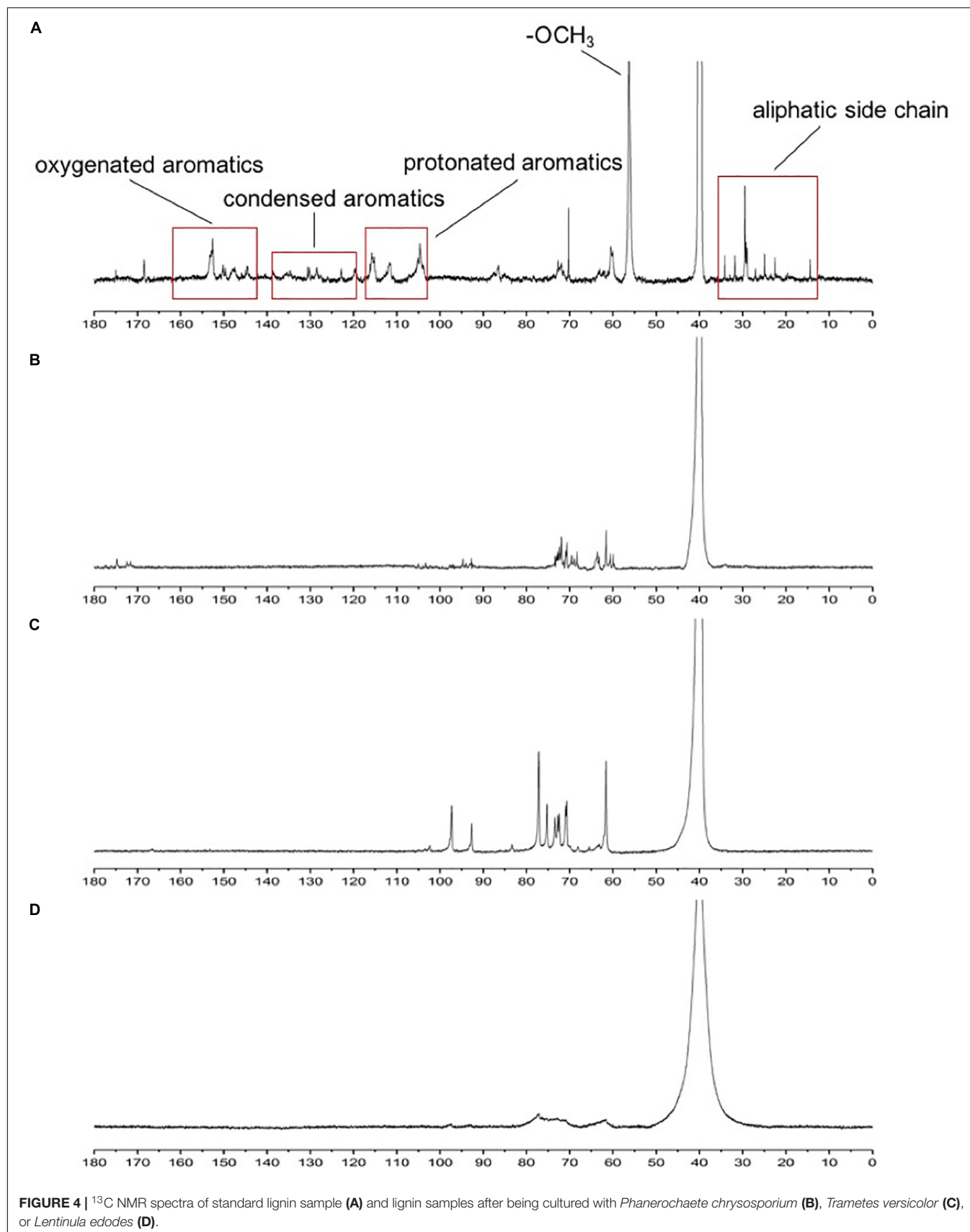


FIGURE 4 | ^{13}C NMR spectra of standard lignin sample (A) and lignin samples after being cultured with *Phanerochaete chrysosporium* (B), *Trametes versicolor* (C), or *Lentinula edodes* (D).

TABLE 3 | Signal assignments of lignin medium samples in the ^{13}C NMR.

δ (ppm)	Assignments	δ (ppm)	Assignments
152.3	C ₃ /C ₅ in S unit	115.6	C ₅ in S unit
150–148	C ₃ in G unit	111.1	C ₂ in G unit
147.0	C ₄ in G unit	104.2	C ₂ /C ₆ in S unit
130.1	C ₂ /C ₆ in pCA unit	62–75	Interunit linkages
128	C ₂ /C ₆ in H unit		(β -5, β - β and β -O-4)
119	C ₆ /C ₅ in G unit	56.5	OCH ₃ in G and S unit

G, guaiacyl unit; S, syringyl unit; H, *p*-hydroxyphenyl unit; pCA, esterified *p*-coumaric acid.

applied voltage, H_2O_2 produced by the composite cathode initiated the enzymatic hydrolysis reactions of LiP and MnP secreted by white-rot fungi (Mir-Tutusa et al., 2018), thus accelerating the lignin biodegradation. The mechanism is shown in Figure 3. Third, the hydroxyl radical produced by the Fenton reaction and LiP synergized to convert non-phenolic lignin into phenolic lignin (Ohashi et al., 2011), which further improved the ability of MnP and Lac to degrade lignin.

The Structure Analysis of Lignin During the Process of Degradation

^{13}C NMR is often used to determine the structural changes in lignin during biodegradation. ^{13}C NMR spectra of lignin were analyzed before and after degradation. In the ^{13}C NMR spectra (Figure 4), the aromatic region (103–162 ppm) of undegraded lignin (Figure 4A) was easily identified by the correlated signals at 104.2, 111.1, 115.6, 119, 128, 130.1, 147.0, 150, and 152.3 ppm, corresponding to the S_{2,6}, G₂, G₅, G_{5,6}, H_{2,6}, pCA_{2,6}, G₄, G₃, and S_{3,5} positions, respectively, as shown in Table 3 (Capanema et al., 2004; Sun et al., 2016; Ying et al., 2018). The signal intensities of the aromatic region (based on the signals at 103–162 ppm) (Ying et al., 2018) in the degraded lignin decreased significantly or even disappeared after degradation by the three white-rot fungi. The changes in the above signals indicated that degradation by *P. chrysosporium*, *L. edodes*, and *T. versicolor* can reduce the aromatic structures in lignin.

Moreover, decreasing signal intensities for $-\text{OCH}_3$ were observed at 56.5 ppm, implying that the degradation of lignin by the three studied white-rot fungi could cause demethoxylation and demethylation. The bands of β -5, β - β , and β -O-4 (62–75 ppm) (Evstigneyev et al., 2018) became weak and narrow in

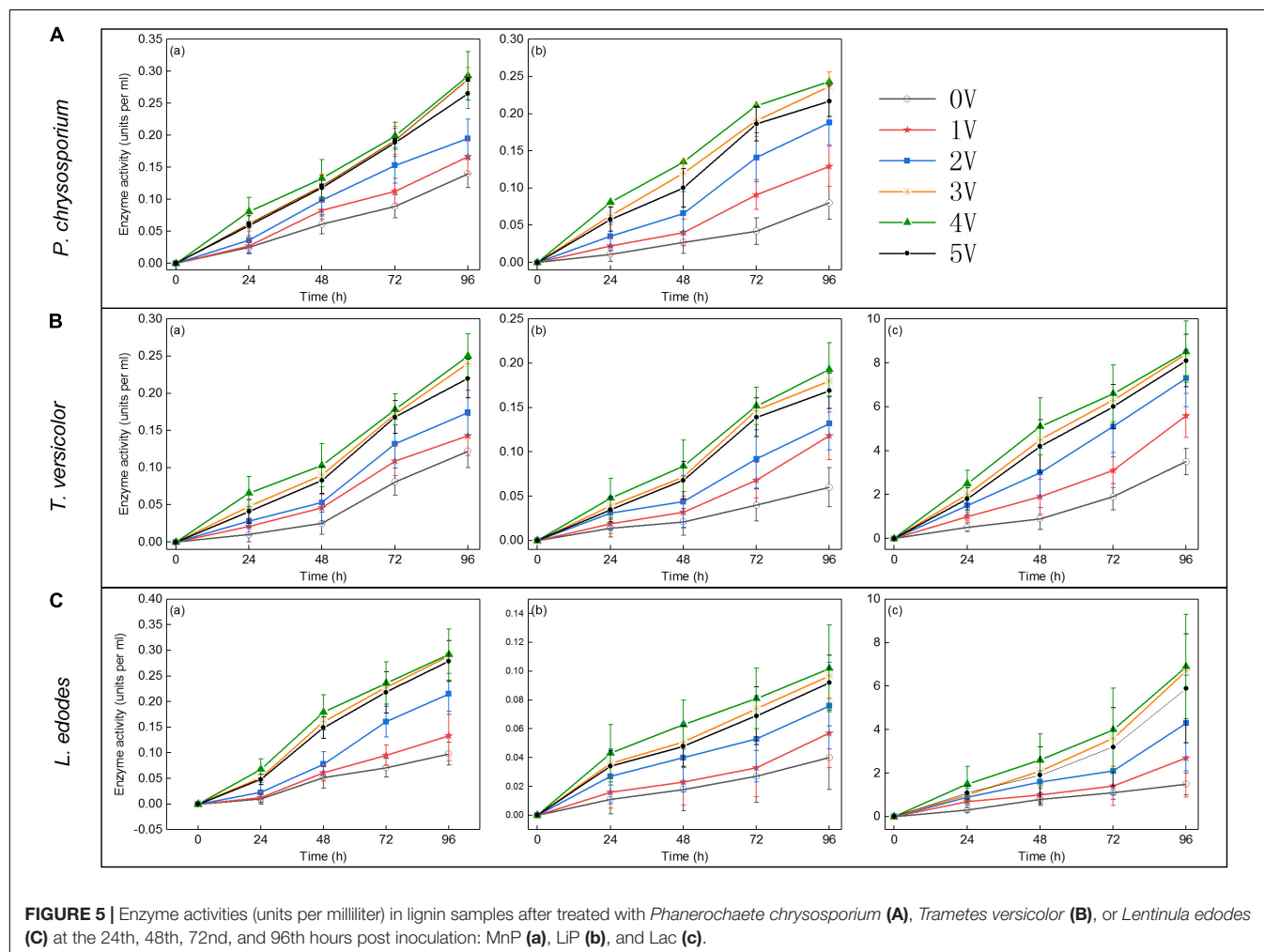


FIGURE 5 | Enzyme activities (units per milliliter) in lignin samples after treated with *Phanerochaete chrysosporium* (A), *Trametes versicolor* (B), or *Lentinula edodes* (C) at the 24th, 48th, 72nd, and 96th hours post inoculation: MnP (a), LiP (b), and Lac (c).

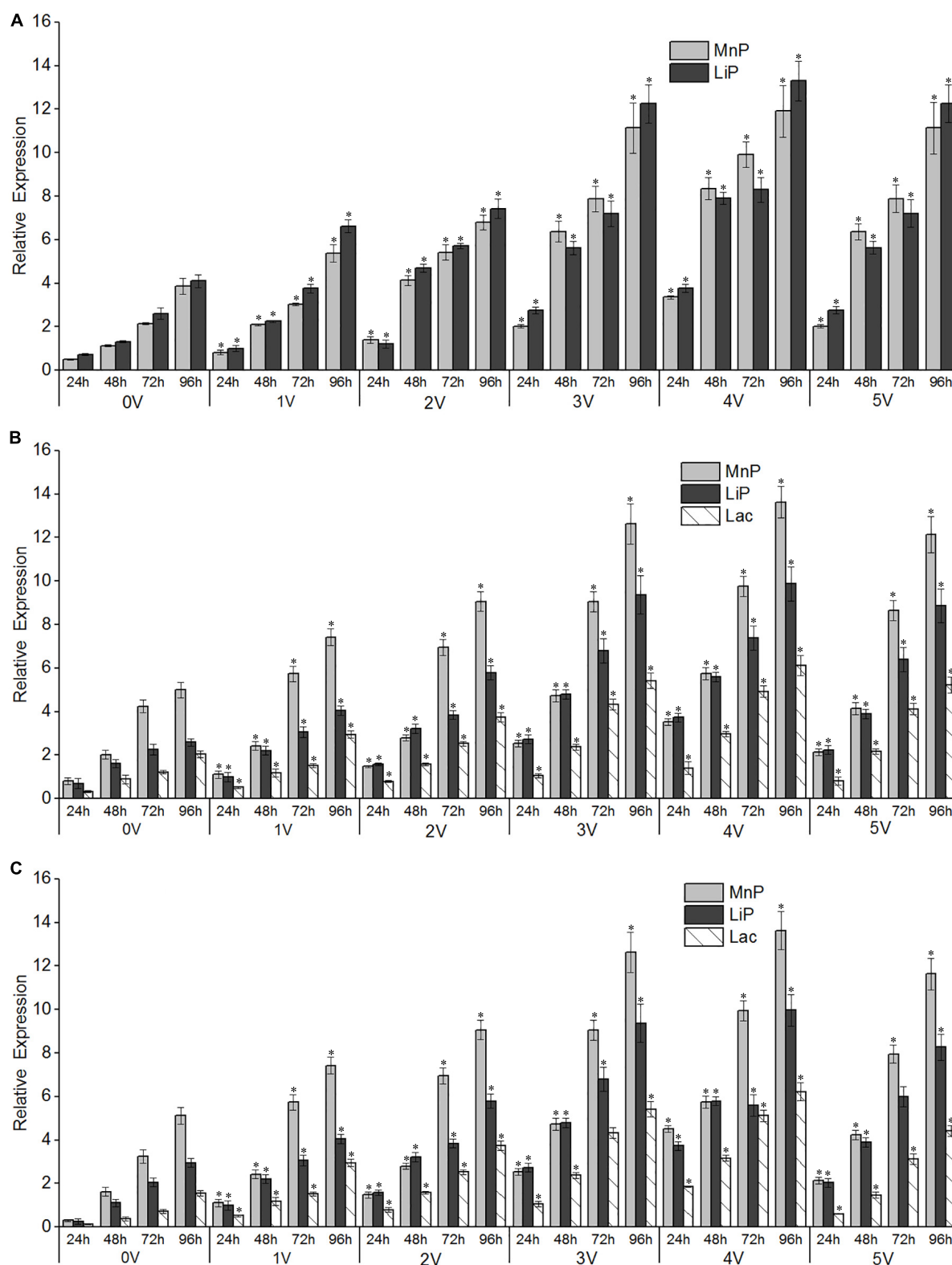


FIGURE 6 | Effects of different electro-Fenton levels on the mRNA expression patterns of lignin-degrading enzymes in *Phanerochaete chrysosporium* (A), *Trametes versicolor* (B), and *Lentinula edodes* (C). Quantitative real-time PCR analysis was performed with samples obtained after 96 h of cultivation of white-rot fungi at varying electro-Fenton concentrations. Asterisk indicates significance at $p < 0.05$. β -Actin (A,C) and β -tubulin (B) were used as internal control genes for normalization.

Figure 4D compared with those in **Figures 4B,C**, implying that *L. edodes* had a more significant influence on lignin during the degradation than the other two fungi (Sun et al., 2016).

Improvement of Lignin-Degrading Enzyme Activity by Electro-Fenton Reaction

Analysis of Lignin-Degrading Enzyme Activity

Lignin hydrolase is a peroxidase that oxidizes lignin during the depolymerization of lignin structure (Tekere et al., 2001). Similar to previous results (Maria et al., 2009), the data showed that significant lignin degradation always accompanied an increase in a lignin-degrading enzyme activity. Lignin degradation was achieved by the synergistic action of various enzymes, and the applied voltage significantly affected the activity of lignin-degrading enzymes. As shown in **Figure 5**, MnP, LiP, and Lac activities increased with increasing voltage within 96 h. The main reason for the above phenomenon was that the biomass of white-rot fungi and the expression of enzyme gene were significantly increased under voltage stimulation (**Figures 1, 6**). Lac activity of *P. chrysosporium* was not detected in this study (**Figure 5A**), which was similar to the results of a previous study (Dong et al., 2013). The activities of three enzymes (MnP, LiP, and Lac) in *T. versicolor* were slightly lower than those in *P. chrysosporium* (**Figure 5B**); that is, the MnP activity was relatively small and the LiP growth rate was low. However, among the three enzymes measured for *L. edodes* (**Figure 5C**), both LiP and Lac had low enzyme activity, and the Lac activity increased rapidly at the 72nd hour. These results differ from those of a previous study (Osma et al., 2011), which revealed that Lac activity remained consistent over time. In the current study, increases in LiP activity may be affected by the color of aromatic compounds or the presence of some inhibitors of veratryl alcohol oxidation, as reported in another study (Maria et al., 2009). Overall, the enzyme activity increased with increasing voltage, and the effect of voltage on a lignin-degrading enzyme activity was significant.

Enzyme Gene Expression

There was a significant correlation between enzyme activity and gene expression, as shown in **Figure 6**, and the relative expression of LiP genes in the three strains increased with increasing treatment time. The voltage had an obvious promoting effect on the expression of LiP genes, and the expression of LiP genes increased with increasing voltage. In *P. chrysosporium*, both LiP and MnP gene expression was induced by electro-Fenton treatment, and the highest expression was observed at the 96th hour at 4 V. In *L. edodes* and *T. versicolor*, the gene expression of LiP, MnP, and Lac was induced by electro-Fenton treatment, and the highest expression was observed at the 96th hour with an applied voltage of 4 V. In *P. chrysosporium* and *L. edodes*, the expression of the LiP gene was the highest, whereas the expression of the MnP gene was the highest in *T. versicolor*.

Lacs are involved in functions such as host–pathogen interactions, stress defenses, and the degradation of lignin and many xenobiotic compounds. Such ligninolytic enzymes are

widely used in biotechnology. Therefore, the regulation of *Lac*, *LiP*, and *MnP* gene expression and the activity of enzymes in the white-rot fungi, *P. chrysosporium*, *T. versicolor*, and *L. edodes*, grown in liquid culture for 96 h with different levels of electro-Fenton treatment, were studied. The result of increased Lac activity at low levels of electro-Fenton treatment was consistent with results of a previous report that showed the stimulatory effects of electro-Fenton treatment on the Lac activity of *P. chrysosporium* and *L. edodes* (Merve and Raziye Ozturk, 2014). The stimulatory effects of electro-Fenton treatment on LiP and MnP activity in *P. chrysosporium* have also been noted (Couto et al., 2005).

In the presence of low concentrations of OH[•], incubation of fungal cultures also led to the depletion of peroxidase (Welinder, 1992). In contrast, lignin-degrading enzyme transcripts were found at high levels in mycelium growth medium receiving electro-Fenton treatments. This result was probably related to the improved antioxidant status of the organism because of the induction of proteins in a stressed reactive oxygen species (ROS) environment, probably through a stress response mechanism. This study showed the highest expression of ligninolytic enzyme genes in all three white-rot fungi. Similar studies have been conducted on the regulation of peroxidases and especially oxidative stress with peptone-containing liquid cultures of *Pleurotus eryngii*. In these cases, the maximal peroxidase messenger RNA (mRNA) content was detected 15 min after the initiation of stress, suggesting a rapid response (Ruiz et al., 2010).

CONCLUSION

Electro-Fenton processes promoted the degradation of lignin by white-rot fungi. For the three white-rot fungi, the lignin degradation rate increased with increased voltage of the electro-Fenton processes within a certain range. The highest degradation rates were 82% for *P. chrysosporium*, 86% for *T. versicolor*, and 89% for *L. edodes*, which were achieved at 4 V. Aromatic structures (103–162 ppm) in lignin were degraded, and *L. edodes* under electro-Fenton treatment exhibited significant delignification activity. The biological characteristics of the three white-rot fungi changed significantly compared with those of the control. Owing to the applied voltage and the accompanying production of H₂O₂ by electro-Fenton processes, the OD, ligninolytic enzyme activity, and the relative expression of ligninolytic enzyme genes were greatly improved. Overall, electro-Fenton processes increased the activity of ligninolytic enzymes and had a synergistic effect with white-rot fungi on lignin degradation.

DATA AVAILABILITY STATEMENT

All datasets generated for this study are included in the article/supplementary material.

AUTHOR CONTRIBUTIONS

LH and LZ designed the research. LZ guided the writing, LH, DJ, and LY performed the research. LH, DJ, WD, and LZ analyzed the data. FZ and LY contributed new reagents and analytic tools. LH and WD wrote the manuscript. All authors have read and approved the final manuscript.

REFERENCES

- Arantes, V., Baldocchi, C., and Milagres, A. M. J. C. (2006). Degradation and decolorization of a biodegradable-resistant polymeric dye by chelator-mediated fenton reactions. *Chemosphere* 63, 1764–1772. doi: 10.1016/j.chemosphere.2005.09.038
- Arantes, V., and Milagres, A. M. F. (2006). Evaluation of different carbon sources for production of iron-reducing compounds by *Wolfiporia cocos* and *Perenniporia medulla-panis*. *Process Biochem.* 41, 887–891. doi: 10.1016/j.procbio.2005.11.008
- Archibald, F. S. (1992). A new assay for lignin-type peroxidases employing the dye azure B. *Appl. Environ. Microbiol.* 58:3110. doi: 10.1128/aem.58.9.3110-3116.1992
- Azimvand, J. (2014). Studying of optical breakdown of DIOXANE lignin as a result of structural changes in the functional groups carbonyl, ether C-O and PHENOLIC hydroxyl with the use of Raman and FT-IR spectroscopy. *Adv. Natural Appl. Sci.* 8, 94–101.
- Ballesteros, M., Negro, J. M. O. J., Manzanares, P., and Ballesteros, I. J. (2004). Ethanol from lignocellulosic materials by a simultaneous saccharification and fermentation process (SFS) with *Kluyveromyces marxianus* CECT 10875. 39, 1843–1848. doi: 10.1016/j.procbio.2003.09.011
- Bourbonnais, R., Paice, M., Reid, I., Lanthier, P., and Yaguchi, M. (1995). Lignin oxidation by laccase isozymes from *Trametes versicolor* and role of the mediator 2,2'-azinobis(3-ethylbenzthiazoline-6-sulfonate) in kraft lignin depolymerization. *Appl. Environ. Microbiol.* 61, 1876–1880. doi: 10.1128/aem.61.5.1876-1880.1995
- Capanema, E. A., Balakshin, M. Y., and Kadla, J. F. (2004). A comprehensive approach for quantitative lignin characterization by NMR spectroscopy. *J. Agric. Food Chem.* 52, 1850–1860. doi: 10.1021/jf035282b
- Chakar, F. S., Ragauskas, A. J., Abaecherli, A., Guran, B., Gosselink, R. J., and Jong, D. D. (2004). Review of current and future softwood kraft lignin process chemistry. *Industr. Crop Products* 20, 131–141. doi: 10.1016/j.indcrop.2004.04.016
- Cisneros, R. L., Espinoza, A. G., and Litter, M. I. (2002). Photodegradation of an azo dye of the textile industry. *Chemosphere* 48:393. doi: 10.1016/s0045-6535(02)00117-0
- Couto, S. R., Sanromán, M., and Gübitz, G. M. J. C. (2005). Influence of redox mediators and metal ions on synthetic acid dye decolorization by crude laccase from *Trametes hirsuta*. *Chemosphere* 58, 417–422. doi: 10.1016/j.chemosphere.2004.09.033
- Derrien, D., Bédu, H., Buée, M., Kohler, A., Goodell, B., and Gelhaye, E. (2017). “Energy balance associated with the degradation of lignocellulosic material by white-rot and brown-rot fungi,” in *Proceedings of the 19th EGU General Assembly, EGU2017, Proceedings from the Conference Held 23-28 April, 2017, Vienna*.
- Dong, X. Q., Yang, J. S., Zhu, N., Wang, E. T., and Yuan, H. L. (2013). Sugarcane bagasse degradation and characterization of three white-rot fungi. *Bioresour. Technol.* 131, 443–451. doi: 10.1016/j.biortech.2012.12.182
- Evstigneyev, E. I., Mazur, A. S., Kalugin, A. V., Pranovich, A. V., and Vasilyev, A. V. (2018). Solid-State ¹³C CP/MAS NMR for Alkyl-O-Aryl bond determination in lignin preparations. *J. Wood Chem. Technol.* 38, 137–148. doi: 10.1080/02773813.2017.1393436
- Ewelyn, A. C., Balakshin, M. Y., and Kadla, J. F. (2005). Quantitative characterization of a hardwood milled wood lignin by nuclear magnetic resonance spectroscopy. *J. Agric. Food Chem.* 53, 9639–9649. doi: 10.1021/jf0515330
- Filipič, J., Kraigher, B., Tepuš, B., Kokol, V., and Mandimulec, I. J. B. T. (2012). Effects of low-density static magnetic fields on the growth and activities of wastewater bacteria *Escherichia coli* and *Pseudomonas putida*. *Bioresour. Technol.* 120, 225–232. doi: 10.1016/j.biortech.2012.06.023
- Galkin, S., Vares, T., Kalsi, M., and Hatakka, A. (1998). Production of organic acids by different white-rot fungi as detected using capillary zone electrophoresis. *Biotechnol. Techniq.* 12, 267–271.
- Gutiérrez, A., del Río, J. C., Martínez-Iñigo, M. J., Martínez, M. J., and Martínez, A. T. (2002). Production of new unsaturated lipids during wood decay by ligninolytic basidiomycetes. *Appl. Environ. Microbiol.* 68, 1344–1350. doi: 10.1128/aem.68.3.1344-1350.2002
- Humar, M., Petrič, M., and Pohleven, F. J. (2001). Changes of the pH value of impregnated wood during exposure to wood-rotting fungi. *Bibliogr. Inform.* 59, 288–293. doi: 10.1007/s001070100207
- Jellison, J., Connolly, J., Goodell, B., Doyle, B., Illman, B., Fekete, F., et al. (1997). The role of cations in the biodegradation of wood by the brown rot fungi. *Int. Biodeterior. Biodegr.* 39, 165–179. doi: 10.1016/s0964-8305(97)00018-8
- Jellison, J., Smith, K. C., and Shortle, W. T. (1992). *Cation Analysis of Wood Degraded by White- and Brown-Rot Fungi*. Rome: FAO.
- Kai, W., Ying, W., Zheng, J. S., Yang, H., and Jing, Y. (2018). Fenton reaction-oxidized bamboo lignin surface and structural modification to reduce nonproductive cellulase binding and improve enzyme digestion of cellulose. *ACS Sustain. Chem. Eng.* 6:3.
- Kurt, U., Apaydin, O., and Gonullu, M. T. (2007). Reduction of COD in wastewater from an organized tannery industrial region by electro-fenton process. *J. Hazard. Mater.* 143, 33–40. doi: 10.1016/j.jhazmat.2006.08.065
- Loghavi, L., Sastry, S. K., and Yousef, A. E. (2010a). Effect of moderate electric field frequency on growth kinetics and metabolic activity of *Lactobacillus acidophilus*. *Biotechnol. Prog.* 24, 148–153. doi: 10.1021/bp070268v
- Loghavi, L., Sastry, S. K., and Yousef, A. E. (2010b). Effect of moderate electric field frequency and growth stage on the cell membrane permeability of *Lactobacillus acidophilus*. *Biotechnol. Prog.* 25, 85–94. doi: 10.1002/btpr.84
- Loghavi, L., Sastry, S. K., Yousef, A. E. (2010c). Effect of moderate electric field on the metabolic activity and growth kinetics of *Lactobacillus acidophilus*. *Biotechnol. Prog.* 98, 872–881. doi: 10.1002/bit.21465
- Maria, J. D., Rui, M. F. B., Fernando, N., Albino, A. D., Cristina, V. G., Luís, M. M. F., et al. (2009). Modification of wheat straw lignin by solid state fermentation with white-rot fungi. *Bioresour. Technol.* 100, 4829–4835. doi: 10.1016/j.biortech.2009.04.036
- Merve, A., and Raziye Ozturk, U. J. P. B. (2014). Extracellular ligninolytic enzymes production by *Pleurotus eryngii* on agroindustrial wastes. 44, 772–781. doi: 10.1080/10826068.2013.867870
- Mir-Tutusa, J. A., Baccar, R., Caminal, G., and Sarra, M. J. W. R. (2018). Can white-rot fungi be a real wastewater treatment alternative for organic micropollutants removal? A review. *Water Res.* 138, 137–151. doi: 10.1016/j.watres.2018.02.056
- Ohashi, Y., Uno, Y., Amirta, R., Watanabe, T., Honda, Y., and Watanabe, T. (2011). Alkoxy- and carbon-centered radicals as primary agents for degrading non-phenolic lignin-substructure model compounds. *Organ. Biomol. Chem.* 9:2481. doi: 10.1039/c0ob00797h
- Osma, J. F., Moilanen, U., Tocaherrera, J. L., and Rodríguezcouto, S. (2011). Morphology and laccase production of white-rot fungi grown on wheat bran flakes under semi-solid-state fermentation conditions. *FEMS Microbiol. Lett.* 318, 27–34. doi: 10.1111/j.1574-6968.2011.02234.x
- Pandey, M. P., and Kim, C. S. (2011). Lignin depolymerization and conversion: a review of thermochemical methods. *Chem. Eng. Technol.* 34, 29–41. doi: 10.1002/ceat.201000270

FUNDING

This work was supported by the Project of Green Manufacturing system, the Open Subject of Jiangsu Key Laboratory of Anaerobic Biotechnology (JKLAB201605), and the Young Doctorate Cooperation Fund Project of Advanced Materials Institute, Shandong Academy of Science (2018QNHZ04).

- Pinto, P. C. R., Silva, E. A. B. D., and Rodrigues, A. E. (2012). *Lignin as Source of Fine Chemicals: Vanillin and Syringaldehyde*. Berlin: Springer.
- Pulgarin, C., and Kiwi, J. (1996). Overview on photocatalytic and electrocatalytic pretreatment of industrial non-biodegradable pollutants and pesticides. *Chimia* 50, 50–55.
- Ruiz, D. F., Martinez, M. J., and Martínez, A. T. (2010). Molecular characterization of a novel peroxidase isolated from the ligninolytic fungus *Pleurotus eryngii*. *Mol. Microbiol.* 31, 223–235. doi: 10.1046/j.1365-2958.1999.01164.x
- Sun, S. L., Huang, Y., Sun, R. C., and Tu, M. (2016). Strong association of condensed phenolic moieties in isolated lignins with their inhibition of enzymatic hydrolysis. *Green Chem.* 18:4286.
- Tekere, M., Mswaka, A. Y., Zvauya, R., and Read, J. S. (2001). Growth, dye degradation and ligninolytic activity studies on Zimbabwean white rot fungi. *Enzym. Microb. Technol.* 28, 420–426. doi: 10.1016/s0141-0229(00)00343-4
- Thrash, J. C., and Coates, J. D. (2008). Review: direct and indirect electrical stimulation of microbial metabolism. *Environ. Sci. Technol.* 42, 3921–3931. doi: 10.1021/es702668w
- Ting, W. P., Lu, M. C., and Huang, Y. H. (2008). The reactor design and comparison of Fenton, electro-Fenton and photoelectro-Fenton processes for mineralization of benzene sulfonic acid (BSA). *J. Hazard. Mater.* 156, 421–427. doi: 10.1016/j.jhazmat.2007.12.031
- Welinder, K. G. (1992). Superfamily of plant, fungal and bacterial peroxidases. *Curr. Opin. Struct. Biol.* 2, 388–393. doi: 10.1016/0959-440x(92)90230-5
- Wen, J. L., Xue, B. L., Sun, S. L., and Sun, R. C. (2013). Quantitative structural characterization and thermal properties of birch lignins after autocatalyzed organosolv pretreatment and enzymatic hydrolysis. *J. Chem. Technol. Biotechnol.* 88, 1663–1671. doi: 10.1002/jctb.4017
- Ying, W., Shi, Z., Yang, H., Xu, G., Zheng, Z., and Jing, Y. (2018). Effect of alkaline lignin modification on cellulase–lignin interactions and enzymatic saccharification yield. *Biotechnol. Biofuels* 11:214. doi: 10.1186/s13068-018-1217-6

Conflict of Interest: DJ and FZ were employed by company Huatai Group Corp. Ltd. YL was employed by company Langfang Meihua Biotechnology Development Co. Ltd.

The remaining authors declare that the research was conducted in the absence of any commercial or financial relationships that could be construed as a potential conflict of interest.

Copyright © 2020 Hou, Ji, Dong, Yuan, Zhang, Li and Zang. This is an open-access article distributed under the terms of the Creative Commons Attribution License (CC BY). The use, distribution or reproduction in other forums is permitted, provided the original author(s) and the copyright owner(s) are credited and that the original publication in this journal is cited, in accordance with accepted academic practice. No use, distribution or reproduction is permitted which does not comply with these terms.



Molecular Mechanism Associated With the Impact of Methane/Oxygen Gas Supply Ratios on Cell Growth of *Methylobacterium buryatense* 5GB1 Through RNA-Seq

OPEN ACCESS

Edited by:

Hao Song,
Tianjin University, China

Reviewed by:

Song Yang,
Qingdao Agricultural University, China
Jianping Yu,
National Renewable Energy
Laboratory (DOE), United States

*Correspondence:

Shihui Yang
Shihui.Yang@hubu.edu.cn
Qiang Fei
feiqiang@xjtu.edu.cn

[†] These authors have contributed
equally to this work

Specialty section:

This article was submitted to
Synthetic Biology,
a section of the journal
Frontiers in Bioengineering and
Biotechnology

Received: 14 January 2020

Accepted: 13 March 2020

Published: 07 April 2020

Citation:

Hu L, Yang Y, Yan X, Zhang T,
Xiang J, Gao Z, Chen Y, Yang S and
Fei Q (2020) Molecular Mechanism
Associated With the Impact
of Methane/Oxygen Gas Supply
Ratios on Cell Growth
of *Methylobacterium buryatense*
5GB1 Through RNA-Seq.
Front. Bioeng. Biotechnol. 8:263.
doi: 10.3389/fbioe.2020.00263

Lizhen Hu^{1†}, Yongfu Yang^{2†}, Xin Yan³, Tianqing Zhang¹, Jing Xiang¹, Zixi Gao¹,
Yunhao Chen², Shihui Yang^{2*} and Qiang Fei^{1,4*}

¹ School of Chemical Engineering and Technology, Xi'an Jiaotong University, Xi'an, China, ² State Key Laboratory of Biocatalysis and Enzyme Engineering, Environmental Microbial Technology Center of Hubei Province, and School of Life Sciences, Hubei University, Wuhan, China, ³ Key Laboratory of Agricultural Environmental Microbiology, Ministry of Agriculture, College of Life Sciences, Nanjing Agricultural University, Nanjing, China, ⁴ Shaanxi Key Laboratory of Energy Chemical Process Intensification, Xi'an Jiaotong University, Xi'an, China

The methane (CH₄)/oxygen (O₂) gas supply ratios significantly affect the cell growth and metabolic pathways of aerobic obligate methanotrophs. However, few studies have explored the CH₄/O₂ ratios of the inlet gas, especially for the CH₄ concentrations within the explosion range (5~15% of CH₄ in air). This study thoroughly investigated the molecular mechanisms associated with the impact of different CH₄/O₂ ratios on cell growth of a model type I methanotroph *Methylobacterium buryatense* 5GB1 cultured at five different CH₄/O₂ supply molar ratios from 0.28 to 5.24, corresponding to CH₄ content in gas mixture from 5% to 50%, using RNA-Seq transcriptomics approach. In the batch cultivation, the highest growth rate of 0.287 h⁻¹ was achieved when the CH₄/O₂ supply molar ratio was 0.93 (15% CH₄ in air), and it is crucial to keep the availability of carbon and oxygen levels balanced for optimal growth. At this ratio, genes related to methane metabolism, phosphate uptake system, and nitrogen fixation were significantly upregulated. The results indicated that the optimal CH₄/O₂ ratio prompted cell growth by increasing genes involved in metabolic pathways of carbon, nitrogen and phosphate utilization in *M. buryatense* 5GB1. Our findings provided an effective gas supply strategy for methanotrophs, which could enhance the production of key intermediates and enzymes to improve the performance of bioconversion processes using CH₄ as the only carbon and energy source. This research also helps identify genes associated with the optimal CH₄/O₂ ratio for balancing energy metabolism and carbon flux, which could be candidate targets for future metabolic engineering practice.

Keywords: methanotroph, *Methylobacterium buryatense*, CH₄/O₂ gas supply ratio, transcriptomics, methane metabolism, nitrogen fixation

INTRODUCTION

As climate change and global warming become severe, much attention has been given to explore more efficient and economical approaches to utilize the GHGs. Methane (CH_4) as one of the major GHGs has a much greater global warming potential than CO_2 . Currently, more than 50% of the CH_4 emission is contributed by natural gas from energy extractions and biogas from agricultures and enteric fermentations (Opio et al., 2013). Because of the development of horizontal drilling and hydraulic fracturing techniques, the unconventional natural gas (shale gas and tight gas) is produced at a surplus globally in last decade. The tremendous increase in shale gas also caused a huge amount gas flared annually at extraction sites around the world. Therefore, it is urgent to capture CH_4 and fulfill the value of this feedstock.

Methanotrophic bacteria are a subset of methylotrophs, which are capable of using CH_4 as the sole carbon source for cell growth and biosynthesis of metabolites. Thus, the biological conversion of CH_4 has been gathering more and more interest as a key role in global carbon cycle. So far, significant efforts have been undertaken to utilize CH_4 as the substrate to produce biofuels and biochemicals by methanotrophs.

Methylobacterium buryatense 5GB1 is a type I methanotroph that assimilates CH_4 to methanol using methane monooxygenase (pMMO) first, and then metabolizes methanol mainly through RuMP pathway for pyruvate production and cell growth (Fu et al., 2017). Recently, *M. buryatense* 5GB1 has been proved as a promising industrial strain due to its robust growth as well as the established genetics and synthetic biology approaches for strain engineering. A series of genetic constructions and metabolic engineering works of *M. buryatense* 5GB1 have been carried out to enhance the carbon flux for the production of biomass, lipids, lactic acid, fatty acids, etc. (Dong et al., 2017; Fu et al., 2017; Hu et al., 2017; Garg et al., 2018). The highest lipid productivity of 45 mg/L/h along with the growth rate of 0.22 h^{-1} and DCW of 21 g/L has been achieved by knocking out glycogen biosynthesis genes of *M. buryatense* 5GB1 in batch cultures (Fei et al., 2018). The flux balance model of *M. buryatense* 5GB1 also suggests that the maximum carbon conversion efficiency (CCE) can be as high as 60~70% on molar basis. Garg et al. (2018) have successfully improved the CCE 50 times by using suitable promoters and RBS combinations for lactic acid production by *M. buryatense* 5GB1.

Abbreviations: ANOVA, analysis of variance; CCE, carbon conversion efficiency; CH_4 , methane; ClpX, ATPase and specificity subunit of ClpX-ClpP ATP-dependent serine protease; DCW, dry cell weight; DEGs, differentially expressed genes; DraG, ADP-ribosylhydrolase; DraT, ADP-ribosyltransferase; Fbp, fructose-1,6-bisphosphatase; GHGs, greenhouse gases; Glk, glucokinase; GlnG, response regulator; GlnK, nitrogen assimilation regulatory protein; GlnL, sensory histidine kinase; MoxF, methanol dehydrogenase [cytochrome c] subunit 1; NifA, Nif-specific regulatory protein; NifD, nitrogenase molybdenum-iron protein alpha chain; NifH, nitrogenase iron protein; NifHDK, nitrogenase; NifK, nitrogenase molybdenum iron protein beta chain; NifL, anti-activator of NifA; NMS, nitrate mineral salt; OadG, putative oxaloacetate decarboxylase gamma chain; OD, optical density; PhoB, DNA-binding response regulator in two-component regulatory system with PhoR; PhoU, phosphate uptake regulator; pMMOs, particulate methane monooxygenases; Por, pyruvate-ferredoxin/flavodoxin oxidoreductase; PstA, high-affinity phosphate transport protein membrane subunit; PstB, high-affinity phosphate transporter ATP-binding subunit; PstC, high-affinity phosphate transport protein membrane subunit; PstS, periplasmic phosphate-binding protein; PstS1a, ABC-type phosphate transport system; RBS, ribosome-binding site; RuMP, ribulose-monophosphate.

Methylobacterium buryatense 5GB1 is an aerobic obligate methanotroph, and the oxygen supply is an essential factor influencing cell growth, electron transfer, and energy supply. It has been projected that the growth rate is associated with the consumption rates of CH_4 and O_2 , which may be caused by the differences of NADH production via oxidative phosphorylation. Similar phenomenon has been observed in cultures of *M. buryatense* 5GB1 with two different CH_4/O_2 ratios of inlet gas mixtures. It was found that a better growth and gas update rate were obtained in the cultures with CH_4/O_2 ratios of 4.4 on mole basis, compared with that of 0.14 (Zhu et al., 2017).

Moreover, transcriptomic studies suggested that the expression of several key genes associated with NADH formation (formaldehyde to carbon dioxide) was changed dramatically under O_2 -limited conditions (Gilman et al., 2015). Akberdin et al. (2018) also demonstrated that *Methylobacterium alcaliphilum* 20Z cultured under aerobic or micro-aerobic conditions affected the formation of pyruvate and biomass significantly. It has also been shown that *M. buryatense* 5GB1 exhibited a complex metabolism under O_2 starvation (Gilman et al., 2017). These findings suggest that under different CH_4/O_2 gas supply ratios, the expression of certain genes can be regulated between aerobic methanotrophic growth and denitrification phases, which is important for industrial applications of methanotrophs.

Although applying optimal CH_4/O_2 ratios of the inlet gas exhibits significant effects on the overall CCE of metabolic pathways related to cell growth, carbon flux, reducing power and energy generation, few studies have thoroughly explored the CH_4/O_2 ratios of the inlet gas, especially for the CH_4 concentrations within the explosion range (5~15% of CH_4 in air), which is mainly due to the safety concerns. We have already developed an automatic control system with CH_4 alarm and cut-off device along with gas mass flow meters to keep operation running smoothly and safely (Fei and Pienkos, 2018). From the standpoint of revealing the influence of the inlet gas ratio of CH_4/O_2 on cell growth, nutrients utilization and energy consumption, it is desirable to understand the effects of various inlet gas ratios of CH_4/O_2 on methanotrophic metabolism using a lab-scale, safe bioconversion system (Fei and Pienkos, 2018).

To explore the changes at transcriptional levels globally, many researchers have applied transcriptomics to their studies. Recently, Fu et al. (2019) reported significant differences between growth on CH_4 and methanol by transcriptional analysis in *M. buryatense* 5GB1. Similarly, a comparative transcriptome analysis was utilized in *Methylobacterium* sp. DH-1 to explore the roles of secondary metabolite pathways during growth on CH_4 and methanol (Nguyen et al., 2019). However, there is no systematical research on *M. buryatense* 5GB1 under different CH_4/O_2 ratios.

In this study, five different inlet gas ratios of CH_4/O_2 (including three ratios within explosion range for the first time) were investigated in methanotrophic cultivation with continuous supply of CH_4 and O_2 in bioreactors. Cell growth and key metabolites were measured to analyze the impact of different CH_4/O_2 ratios on *M. buryatense* 5GB1, and transcriptomics study was performed to identify genes differentially expressed under these conditions to help elucidate the impact of CH_4/O_2 ratio

on cell growth and metabolism of *M. buryatense* 5GB1. The effective gas supply ratio identified in this study could help enable the production of key intermediate such as pyruvate, which is an important precursor for various downstream biochemical biosynthesis, and therefore offers a potentially efficient path to produce biochemicals using CH₄ as the only carbon source by improving nutrient utilization and energy supply.

MATERIALS AND METHODS

Strain and Culture Conditions

Methylobacterium buryatense 5GB1 obtained from Prof. Mary Lidstrom was revived on NMS agar medium for 5 days, while seed culture was prepared in a gas cylinder filled with gas mixture of 20% CH₄ in air at 30°C. The medium composition of NMS used in batch cultures was mentioned previously (Fei et al., 2018). Aerobic fermentation was carried out in a 3 L fermentation cylinder (BaoXing Bio-engineering Equipment, Shanghai, China) containing 2 L of modified NMS2 (8 g/liter KNO₃ and 2 × trace elements) medium by mass-flow gas meter controlling mixed gas content with reliable explosion-proof equipment and good ventilated condition. The composition of the gas blends used in this experiment was as follows: 0.28 (#1, 5% CH₄ in air), 0.58 (#2, 10% CH₄ in air), 0.93 (#3, 15% CH₄ in air), 1.31 (#4, 20% CH₄ in air), and 5.24 (#5, 50% CH₄ in air).

Cell Growth and Metabolite Measurements

Optical density of cell was measured at 600 nm with a spectrophotometer (TU-1810, PERSEE, Beijing, China). As for DCW, sampling was performed every 12 h. 10 mL bacterial solution was placed in a 15-mL centrifuge tube each time and centrifuged at 7,000 rpm for 15 min. The supernatant was discarded, and cells were then resuspended with 5 mL deionized water. Centrifugation step was repeated once. Cells were preserved in the −80°C refrigerator for 4 h, which was then dried by a lyophilizer for 36–48 h before measuring the dry weight of the cells. Statistical analysis was performed in Microsoft Excel 2007, and *P*-values with statistical significance of *P* < 0.05 and *P* < 0.01 were obtained.

Total protein and pyruvate were determined using kits from Beyotime and Suzhou Comin Biotechnology. The total protein was measured using the Bradford Protein Assay Kit (Beyotime, Shanghai, China). Briefly, 1 mL bacterial culture was transferred to the 1.5 mL microcentrifuge tubes for cell lysis. The absorbance values of the samples diluted with water at 595 nm were measured by UV-spectrophotometry (TU-1810, PERSEE, Beijing, China). Pyruvate was measured by Pyruvate Content Determination kit (Suzhou Comin Biotechnology Inc, Suzhou, China) following the manual. The supernatant was removed by centrifugation, and the precipitate was resuspended with extracting solution before cell lysis using the ultrasonic cell breaker (YH-1000Y, Ningbo, China). The procedure also involved in adding a single working reagent for pyruvate determination at 520 nm by UV-spectrophotometry.

Enzymatic Assays

Particulate methane monooxygenase activity was measured using propene epoxidation assay as described before (Miyaji et al., 2002). The intracellular NADH and NAD⁺ concentrations were measured by the enzyme cycling method (He et al., 2016). Briefly, 1-mL bacterial liquid was transferred to the 1.5-mL microcentrifuge tubes for NADH or NAD⁺ extraction. After centrifugation, cell pellets were resuspended with 300 μL 0.2 M NaOH for NADH quantification or 300 μL 0.2 M HCl for NAD⁺ determination. The samples are bathed in 50°C for 10 min and immediately placed in iced water. The cell lysate was neutralized by adding the same volume of HCl or NaOH. The supernatants were stored at −20°C and used to detect the NADH and NAD⁺ activity after centrifuging at 15,000 rpm for 5 min. The solution (total volume was 0.6 mL) contained 0.1 mL of each of followings: 1.0 M Bicine buffer (pH 8.0), absolute ethanol, 40 mM EDTA (pH 8.0), 4.2 mM MTT (thiazolyl blue), and 0.2 mL of 16.6 mM PES (phenazine methosulfate). 50 μL extract, 0.3 mL ddH₂O, 0.6 mL mixture and 50 μL alcohol dehydrogenase (500 U/mL) were then mixed to start the reaction, and the absorbance at 570 nm was measured with the spectrophotometer (TU-1810, PERSEE, Beijing, China) for 5 min. Commercial NADH and NAD⁺ (Meryer Chemical Technology, Shanghai, China) were used to make the standard curves.

Transcriptomic Analysis

Transcriptomics study was carried out following the method described in previous reports (He et al., 2018; Yang et al., 2018). Briefly, cell culture samples were collected within 24 h fermentation duration with different CH₄/O₂ gas mixture ratios. RNA-Seq were performed using the paired-end sequencing technology according to standard Illumina protocols by GENEWIZ, Inc. (Suzhou, China). The quality of RNA-Seq fastq data was checked using FastQC program¹. Data passing the quality control were imported into CLC Genomics Workbench (version 11.0) for RNA-Seq analysis to get the RPKM values with the reference genome from the MicroScope database². Gene expression normalization, ONE-WAY ANOVA analysis, and hierarchical clustering analysis were conducted using JMP Genomics (version 9.0) to identify differentially expressed genes at different conditions. Genes were determined to be significantly differentially expressed with a selection threshold of *P*-value ≤ 0.01 and log₂-fold change ≥ 1 (significant induction) or ≤ −1 (significant repression). Duplicate samples were used for each condition.

RESULTS AND DISCUSSION

CH₄/O₂ Ratios Affected Cell Growth Especially on Logarithmic Phase

Cell growth using various gas mixtures with different CH₄/O₂ ratios (from 0.28 to 5.24 mole/mole) were evaluated in 3-L bioreactors in duplicate. Three ratios within the CH₄ explosion

¹<http://www.bioinformatics.babraham.ac.uk/projects/fastqc/>

²<http://www.genoscope.cns.fr/agc/microscope>

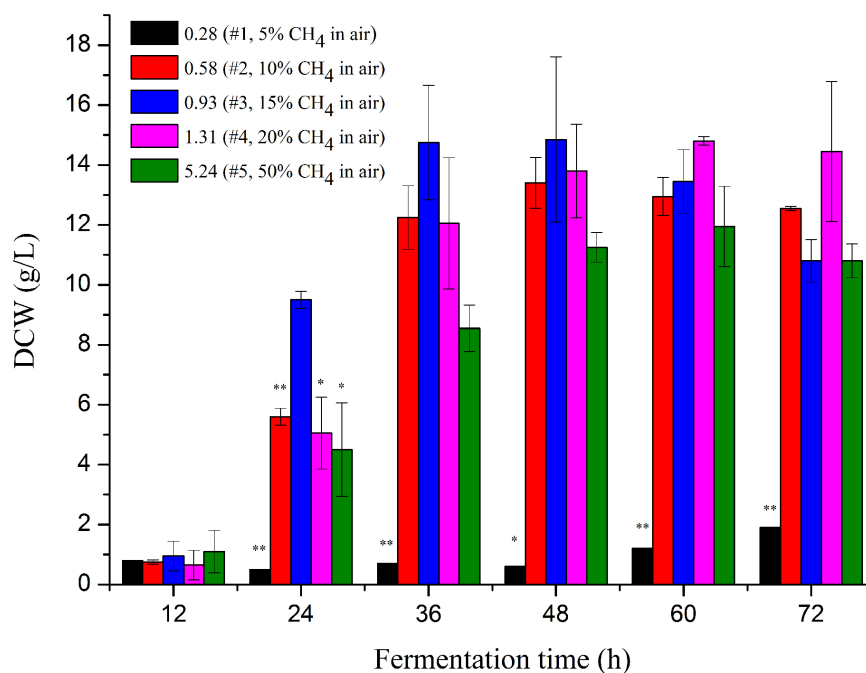


FIGURE 1 | Cell mass of *M. buryatense* 5GB1 in the cultures using different CH₄/O₂ ratios of 0.28, 0.58, 0.93, 1.31, and 5.24 at different time points of 12, 24, 36, 48, 60, and 72 h post inoculation, respectively. The * and ** indicated this ratio exhibited significant difference compared to that under the CH₄/O₂ ratio of 0.93 with statistical significance of $P < 0.05$ and $P < 0.01$, respectively. DCW, dry cell weight.

range (5~15% in air) of 0.28, 0.58, and 0.93 were explored for the first time by using a safety-proof control system in the lab (Fei and Pienkos, 2018). As shown in **Figure 1**, cells grew the best with a gas mixture ratio of 0.93, which provided the highest specific growth rate of 0.287 h^{-1} , followed by 0.219 h^{-1} and 0.198 h^{-1} for gas mixture ratios of 1.31 and 0.58, respectively (**Supplementary Table S1**).

The highest specific growth rate of *M. buryatense* 5GB1 reported before was 0.231 h^{-1} obtained in cultures with CH₄/O₂ of 1.31 (20% CH₄ in air) (Puri et al., 2015). Our result, for the first time exhibited that the CH₄/O₂ ratio of 0.93 is optimal for cell growth of 5GB1, providing a DCW of 15 g/L along with a productivity of 0.3 g/L/h at the time point of 48 h. More importantly, *M. buryatense* 5GB1 exhibited a good state of growth on logarithmic phase, since the biomass at the time points of 24, 36, and 48 h especially the first two time points with the ratio of 0.93 was higher than those with other ratios. It is clear that the growth was significantly limited when cultured under the condition of 5% CH₄ in the air, which is mainly due to the insufficient carbon source of CH₄ during cultivation. However, higher CH₄ supply (e.g., 50% CH₄ with the ratio of 5.5) did not provide the best cell growth neither (**Figure 1** and **Supplementary Figure S1**). Although cell grew better than that using lower carbon source in cultures under the gas ratio of 0.28, they grew poorly compared with other three conditions with 10~20% CH₄, which could be due to limited electron acceptor O₂ in the gas mixture.

Our findings thus demonstrated the importance of CH₄/O₂ ratios in the gas mixtures for balanced cell growth and production

cost. The molar ratio of 0.93 was the best among all ratios, which can reach an OD value two-fold of other conditions within 24 h post-inoculation and had the highest OD value within 36~48 h fermentation time. The shorter time cells took to reach its highest growth and the lower CH₄ in the gas mixture could mean a higher productivity with less carbon supplied for economic biochemical production.

Different CH₄/O₂ Ratios of Inlet Gas Affected the Accumulation of Key Metabolites and the Level of Reducing Power

Since CH₄/O₂ ratios affected cell growth and the ratio of carbon and oxygen was crucial for balanced cell growth, the impact of different CH₄/O₂ ratios on the redox and the production of metabolite intermediates were investigated. Several key metabolites and enzymes during CH₄ oxidation and metabolism were analyzed as shown in **Table 1**, when *M. buryatense* 5GB1 was cultured with different gas supply ratios. It is obvious that the highest values of pyruvate and pMMO activity were observed in cultures with the gas ratio of 0.93. The higher values of pyruvate amount and pMMO activity were also observed in cultures with the gas ratio of 0.93, which is consistent with the result of growth rate in the same condition. These findings could be due to the fact that some key metabolites were not sufficiently synthesized when either CH₄ or O₂ was not supplied sufficiently under other conditions. Higher pyruvate (key precursor for TCA cycle) produced in cultures with gas ratio of 0.93 was

TABLE 1 | Quantification of the amount of total protein, pyruvate, NADH, and MMO activity under different CH₄/O₂ ratio conditions at time point 24 h post inoculation.

CH ₄ /O ₂ ratio (mol)	0.58 (#2)	0.93 (#3)	1.31 (#4)	5.24 (#5)
Protein (g/L)	1.18 ± 0.07	1.00 ± 0.07	0.75 ± 0.05	0.88 ± 0.00
Pyruvate (mg/g protein)	1.13 ± 0.35	2.91 ± 0.33	1.03 ± 0.26	2.23 ± 0.49
NADH/NAD ⁺	0.94 ± 0.10	1.28 ± 0.05	1.61 ± 0.32	0.89 ± 0.02
pMMO (ug/min/g protein)	6.04 ± 1.25	7.0 ± 0.05	4.65 ± 0.40	6.75 ± 1.68

corresponding with the higher DCW, which is in good agreement with previous report showing that TCA cycle is essential for the production of both cell mass and reducing power in 5GB1 (Fu et al., 2017).

The changes of CH₄/O₂ ratios could affect NADH/NAD⁺ ratio, which determined the fluxes of metabolic pathways as well as the transcriptional level of many genes (Zhou et al., 2011). In this work, under the gas ratios of 1.31 and 0.93, the values of NADH/NAD⁺ ratio were higher, and the highest value was 1.61, almost double that under the gas ratio of 5.24 (Table 1). This could be due to the different content of metabolite accumulation and the complicated metabolism in *M. buryatense* 5GB1 with different gas ratios. This process was accompanied by changes of many genes at transcriptional level, so genomic and transcriptomic analyses could help further identify gene and metabolic pathways differentially expressed at different CH₄/O₂ ratios.

Identification of Differentially Expressed Genes at Different Gas Supply Conditions

Transcriptomic study was further carried out to investigate the impact of different CH₄/O₂ ratios on global gene expression and the underlying mechanism of CH₄/O₂ ratio on cell growth and metabolism. As shown in Figure 1, the cell growth under the gas ratio of 0.93 exhibited obvious difference over other gas conditions at 24 h, so we adopted the samples for transcriptome analyses. Since different CH₄/O₂ ratios significantly influenced the cell growth and central metabolism, which result in different phenotypes, the relationship of five conditions with different CH₄/O₂ ratios were analyzed by hierarchical clustering using significantly differentially expressed genes based on the RNA-Seq result (Figure 2).

The result demonstrated that these samples can be divided into three groups: #3, #2, and #1, which not only indicates that the metabolism of #3 was different from others, but also suggests that the metabolism in cells was different under #2, #4, and #5 conditions despite that they exhibited similar growth (Figure 2A and Supplementary Figure S1). There were total of 1429, 733, and 592 DEGs by comparing #3 with other three conditions of #2, #4, and #5, respectively (Figure 2B and Supplementary Table S2). The DEGs of #3 versus #2, #4 or #5 were analyzed, and the result indicated that 337 common genes were significantly differentially expressed (log₂fold change ≥ 1, *p*-value ≤ 0.01) with 160 down-regulated and 177 up-regulated ones (Supplementary Table S3). Among

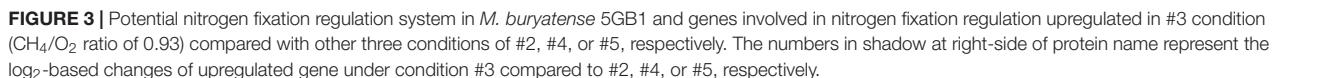
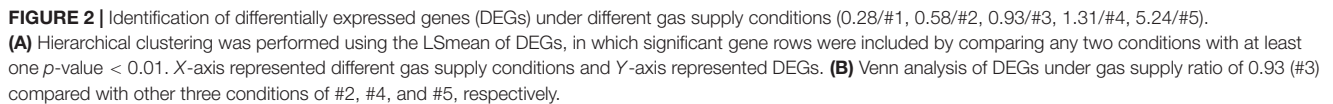
these significantly differentially expressed genes, the function of 106 genes was unknown (Supplementary Table S3), which needs further studies to confirm.

Our results also demonstrated that different CH₄/O₂ ratios affected both carbon and energy metabolism of *M. buryatense* 5GB1 at transcriptional level (Supplementary Figure S2). Genes up-regulated were mainly involved in signal transduction, membrane transport, cell process, carbohydrate and energy metabolism, while genes down-regulated were majorly involved in metabolism of cofactors and vitamins, nucleotide metabolism and amino acid metabolism. This result indicated that the different phenotypes at condition of 0.93 compared with others were possibly ascribed to the function and expression levels of DEGs involved in carbon and nitrogen utilization, although further investigation is needed.

Genes Involved in Nitrogen Fixation and Utilization Upregulated to Supply Sufficient Nitrogen for Enhanced Growth

Methylobacterium buryatense 5GB1 has been reported to use nitrate, ammonia, and urea as nitrogen sources (Kaluzhnaya et al., 2001). Some methane-oxidizing bacteria (methanotrophs) are known to be capable of expressing nitrogenase and utilizing N₂ as the nitrogen source (Auman et al., 2001; Matsen et al., 2013). From the genome annotation and metabolic modeling, *M. buryatense* 5GB1 was also predicted to be able to assimilate N₂ into ammonia, which can be used as a nitrogen source (de la Torre et al., 2015; Garg et al., 2018). The intriguing discovery from our transcriptomic analysis was that thirty-four nitrogen assimilation related genes were significantly up-regulated in the #3 condition compared with other conditions, including nitrogen fixation structural genes molybdenum nitrogenase genes (*nifHDK*), nitrogenase MoFe maturation genes (*NifPZ*), cofactor biosynthesis genes (*nifBEMNXQTUVY*), ferredoxin genes (*fdxBCD*), as well as genes involved in electron supply (*rnfCH*, *nifF*, *rsxABDEG*), nitrogen fixation regulation (*nifLA*, *glnGLK*), and post-translational modification (*draTG*) (Figure 3 and Supplementary Table S2).

In *P. stutzeri* A1501, the nitrogen regulatory cascade, AmtB-GlnK-NtrBC, senses the nitrogen signal and controls the expression of *nif*-specific regulatory proteins NifLA, in which the NifA is an activator and the NifL is an anti-activator to control the expression of all other *nif* genes (Lin et al., 2015). In our RNA-Seq result, genes encoding PII protein GlnK, *nif*-specific regulatory protein NifLA, as well as GlnLG homologous to NtrBC were up-regulated under the optimal CH₄/O₂ ratio condition #3. The upregulation of nitrogen fixation regulatory genes indicated that the *nif* gene expression in 5GB1 may be tightly regulated at the transcriptional level. Correspondingly, the nitrogenase genes *nifHDK* were up-regulated triggered by this regulatory network under the CH₄/O₂ ratio of 0.93, which shown enhanced DCW (Figure 1). These findings in physiological and transcriptional levels may suggest that extra nitrogen source from N₂ can be assimilated supporting cell growth and metabolic activities after the nitrate source was exhausted, although further study is needed in the future.



the higher expression of nitrogen assimilation related genes, which indicated that 5GB1 likely shifted its metabolic flux to overcome the energy barrier for nitrogen fixation. Meanwhile, the nitrogenase post-translational genes (*draTG*), which can switch off or on the nitrogenase activity through adding or removing

ADP-ribose group to a specific arginine residue on nitrogenase (Moure et al., 2015), were also up-regulated in response to quickly modulating the activity of nitrogenase when the environmental ammonium concentration was suddenly changed (Masepohl and Hallenbeck, 2010). Additionally, *RsxABCDGE* genes are essential for nitrogen fixation, which are involved in transferring electrons to nitrogenase (Schmehl et al., 1993; Koo et al., 2003). The upregulation of *RsxA*, *RsxB*, *RsxD*, *RsxE*, and *RsxG* (Figure 3) suggested a high nitrogenase activity achieved under #3 condition, which could then facilitate the use of N_2 as nitrogen source for cell growth. Although higher activity of nitrogenase from #3 condition would promote the nitrogen assimilation, which in turn enhanced the cell growth, the intensive electron cost during nitrogen fixation process could cost cellular energy (Hoffman et al., 2014; Inomura et al., 2018). Unfortunately, research on balancing the N_2 assimilation and energy supply is still very limited.

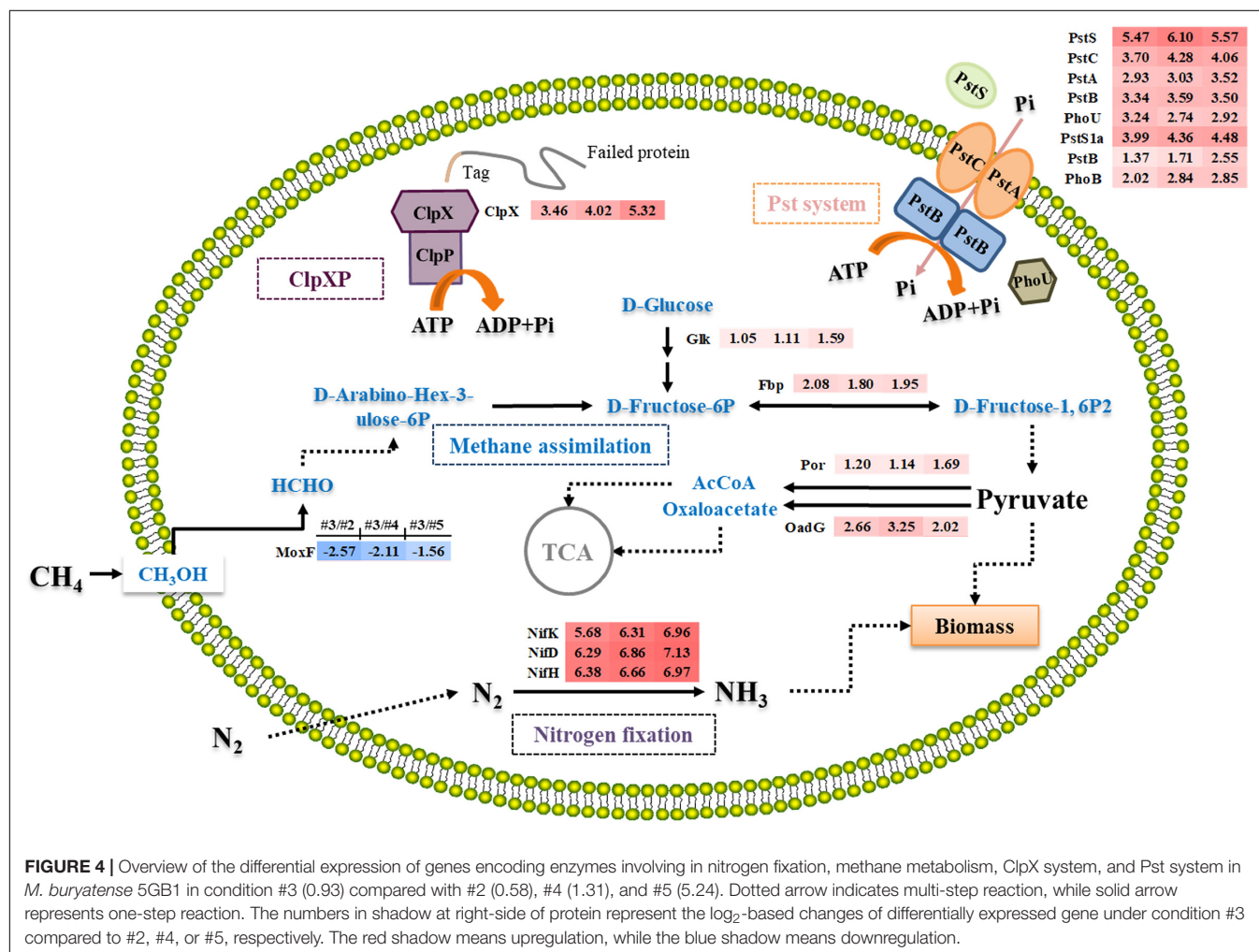
It has been reported that higher CH_4/O_2 ratio can significantly affect nitrite removal in aerobic methanotrophs, and the highest denitrifying activity correlated with two nitrite reductases (NirK and NirS) was also observed when the molar ratio of CH_4/O_2 was 4.4 (Zhu et al., 2017). However, nitrite reductase (NirB)

of *M. buryatense* 5GB1 did not show significant differential expression, which may be due to the low CH_4/O_2 ratio (0.93) used in the #3 condition.

The Upregulation of Methane Metabolism Genes Boosted Cell Growth

As an aerobic obligate methanotroph, *M. buryatense* 5GB1 can oxidize CH_4 to methanol and formate in the beginning before flowing into RuMP and/or serine pathway for assimilations, providing energy for cell growth and metabolic processes at the same time (Trotsenko and Murrell, 2008). It has been reported that the major pathway for pyruvate production in Group I methanotrophic bacteria is the glycolysis pathway (Kalyuzhnaya et al., 2013). Since cell grew better in #3 condition, carbon flux to glycolysis could be enhanced considering the fact that genes related to glycolysis pathway were also upregulated in #3 condition, which is consistent with our result that the expression of *fbp* (MBURv2_60345) was up-regulated greater than two folds (Figure 4).

Fructose-1,6-bisphosphatase is an essential enzyme in glycolysis pathway to hydrolyze D-fructose-1,6-bisphosphate to D-fructose-6-phosphate (Rittmann et al., 2003). Previous



study confirmed that Fbp regulated the level of fructose-1,6-bisphosphate, one of the most important intermediates associating with the ATP generation (Li et al., 2013). Besides, Rittmann et al. (2003) investigated the relationship between *fbp* gene and cell growth by deleting it from the chromosome, and discovered that *C. glutamicum* WTΔ*fbp* could not grow as well as the wild-type strain. Although Entner–Doudoroff pathway was suggested to be a potential solution to increase carbon flux for methanotrophic bacteria (Kalyuzhnaya et al., 2015), our result suggests that the enhanced expression of *fbp* gene under the optimal CH₄/O₂ ratio can accelerate the conversion of CH₄ into pyruvate and NADH in *M. buryatense* 5GB1.

Genes Involved in Key Intermediate Synthesis Upregulated for Enhancing Precursor Supply to TCA Cycle

In both aerobic and anaerobic microorganisms, ATP is an important energy source to sustain microbial growth (Khmelena et al., 2011). Aerobic microorganisms mainly rely on TCA cycle and oxidative phosphorylation, which provide 95% ATP (Khmelena et al., 2011). Comparing the transcriptional analysis of #3 with other conditions, two genes (*por* and *oadG*) involved in Acetyl-CoA (AcCoA) and oxaloacetate synthesis were up-regulated (Figure 4), which encode putative oxidoreductase and putative oxaloacetate decarboxylase gamma chain, respectively. Pyruvate was converted to oxaloacetate and AcCoA, which then entered into TCA cycle. The higher production of DCW and NADH observed in #3 condition was therefore consistent with the previous prediction that TCA cycle is responsive for both biomass synthesis and reducing power generation in *M. buryatense* 5GB1 (Fu et al., 2017). This result is also in agreement with previous study reporting the additional NADH input can support the direct coupling between methane oxidation and methanol oxidation for better cell growth (de la Torre et al., 2015).

Genes Involved in Phosphate Transport System Upregulated to Maintain Optimal Phosphate Pools for Enhanced Growth

The phosphate uptake systems, which are highly depended on the phosphate transport system (Pst), significantly influence cell growth. Therefore, an efficient Pst system can ensure an enhanced cell mass production (Luz et al., 2012). As shown in Figure 4, six genes (*PstSCAB* and *PstS1a*) belonging to the Pst system were up-regulated under #3 condition comparing with #2, #4, and #5. Additionally, two key regulator genes, *phoB* and *phoU*, encoding phosphate regulon transcriptional regulatory protein (DNA-binding response regulator) and phosphate signaling complex protein (phosphate uptake regulator), respectively, were also upregulated under #3 condition. It was proposed that there was a dynamic equilibrium between active and inactive PstSCAB in response to local internal fluctuations in phosphate concentrations, which was modulated by PhoU (diCenzo et al., 2017). PhoU rapidly responds to elevated phosphate levels by significantly decreasing the phosphate transport of PstSCAB, thereby preventing phosphate toxicity

and cell death (diCenzo et al., 2017). It has been known that phosphate is an indispensable compound for cell growth, whereas high concentration phosphate can still be toxic to cell. Therefore, these aforementioned up-regulated genes related to phosphate uptake system may guarantee the rapid response to switch on or off the inorganic phosphate transport system according to cell growth.

Under #3 condition, high cell growth rate probably reflected the high expression level of these genes related to phosphate uptake system that maintains the intracellular Pi pool for optimal growth. Although the mechanism of this system is still elusive and needs more work in the future, our findings provided a new insight into the manipulation of the level of phosphate uptake for enhancing cell growth of methanotrophs, which is possible by controlling CH₄/O₂ ratios during the cultivation.

Genes Involved in ClpX Upregulated to Promote Cell Growth by Controlling ATP Hydrolysis for Energy Supply

As a AAA + protease (ATPase associated with a variety of cellular activities), ClpX hydrolyses ATP to provide energy for targeting the misfolded protein for subsequent degradation during protein synthesis in cell growth process (Keiler et al., 1996; Gottesman et al., 1998; Moore and Sauer, 2007). In addition, the energy produced by hydrolysis of ATP is the main energy source of the ClpXP protease complex in protein degradation. Therefore, upregulated ClpX activated more energy supporting in protein synthesis during cell growth under the #3 condition. Previous studies in *Bacillus subtilis* showed that the cells were damaged readily with the corresponding decrease of the growth rate in the absence of either ClpX or ClpP under stressful environmental conditions (Zhang and Zuber, 2007), which suggests the upregulation of ClpX could be beneficial for protecting cells from damage and promoting the cell growth as what we observed under #3 condition in this study.

CONCLUSION

In this work, the impact of different CH₄/O₂ ratios on the growth and global gene expression of *M. buryatense* 5GB1 was investigated, and our result indicated that the CH₄/O₂ mole ratio of 0.93 is optimal for cell growth, pyruvate accumulation, nutrient utilization and energy supply. Meanwhile, genes related to nitrogen fixation and methane metabolism were significantly up-regulated, which suggest that *M. buryatense* 5GB1 is capable of utilizing N₂ as the nitrogen source to reduce the production cost. In addition, by controlling CH₄/O₂ ratios during the cultivation, the level of phosphate uptake for enhancing cell growth of methanotrophs was improved to maintain an optimal intracellular Pi pool for growth. Our work thus provides novel insights in terms of the influences of CH₄/O₂ ratios of gas supply on transcriptional level of key genes in methanotrophic bacteria, and candidate gene targets for future metabolic engineering in this promising industrial methanotrophic microorganism.

DATA AVAILABILITY STATEMENT

The authors declare that all the data supporting the findings of this study are available within the manuscript and its **Supplementary Information** files from the corresponding author on request. The RNA-Seq raw data was deposited at Sequence Read Archive (SRA) database with the BioProject accession number PRJNA597286.

AUTHOR CONTRIBUTIONS

QF and SY conceived the work, and provided conceptual advice with inputs from all authors. LH designed and performed the experiments, analyzed the data, and wrote the manuscript. YY handled and analyzed the transcriptomic data with help from YC. XY provided conceptual advice. LH, YY, QF, and SY wrote the manuscript, and prepared figures and tables. All authors contributed to data analyses, read, revised and approved the final manuscript.

FUNDING

This work was supported by the National Key R&D Programs of China (2018YFA0901500) and National Natural Science Foundation of China (21878241, 21978071, and U1932141). This

work was also supported by Technical Innovation Special Fund of Hubei Province (2019AHB055 and 2018ACA149), and the Open Project Funding of State Key Laboratory of Biocatalysis and Enzyme Engineering of Hubei University.

SUPPLEMENTARY MATERIAL

The Supplementary Material for this article can be found online at: <https://www.frontiersin.org/articles/10.3389/fbioe.2020.00263/full#supplementary-material>

FIGURE S1 | Growth curve of *M. buryatense* 5GB1 under different CH₄/O₂ ratios of 0.28, 0.58, 0.93, 1.31, and 5.24, respectively.

FIGURE S2 | KEGG enrichment of differentially expressed genes (DEGs) in *M. buryatense* 5GB1 by comparing 0.93/#3 with 0.58/#2, 1.31/#4, and 5.24/#5. **(a)** Common up-regulated genes in KEGG pathway; **(b)** common down-regulated genes in KEGG pathway.

TABLE S1 | Log₂OD growth data for specific growth rate under different CH₄/air ratio conditions.

TABLE S2 | Differentially expressed genes of #3 (15% CH₄ in air) compared with #2 (10% CH₄ in air), #4 (20% CH₄ in air), and #5 (50% CH₄ in air).

TABLE S3 | Differentially expressed genes of #3 (15% CH₄ in air) versus #2 (10% CH₄ in air), #4 (20% CH₄ in air), and #5 (50% CH₄ in air). 337 genes were significantly changed (log₂fold change ≥ 1, *p*-value ≤ 0.01) among these comparisons including 160 down-regulated and 177 up-regulated genes.

REFERENCES

- Akberdin, I. R., Thompson, M., Hamilton, R., Desai, N., Alexander, D., Henard, C. A., et al. (2018). Methane utilization in *Methylobacterium alcaliphilum* 20Z(R): a systems approach. *Sci. Rep.* 8:2512. doi: 10.1038/s41598-018-20574-z
- Auman, A. J., Speake, C. C., and Lidstrom, M. E. (2001). nifH sequences and nitrogen fixation in type I and type II methanotrophs. *Appl. Environ. Microbiol.* 67, 4009–4016. doi: 10.1128/aem.67.9.4009-4016.2001
- Bebout, B. M., Fitzpatrick, M. W., and Paerl, H. W. (1993). Identification of the sources of energy for nitrogen fixation and physiological characterization of nitrogen-fixing members of a marine microbial mat community. *Appl. Environ. Microbiol.* 59, 1495–1503. doi: 10.1128/aem.59.5.1495-1503.1993
- de la Torre, A., Metivier, A., Chu, F., Laurens, L. M., Beck, D. A., Pienkos, P. T., et al. (2015). Genome-scale metabolic reconstructions and theoretical investigation of methane conversion in *Methylobacterium buryatense* strain 5G(B1). *Microb. Cell Fact.* 14:188. doi: 10.1186/s12934-015-0377-373
- diCenzo, G. C., Sharthiya, H., Nanda, A., Zamani, M., and Finan, T. M. (2017). PhoU allows rapid adaptation to high phosphate concentrations by modulating PstSCAB transport rate in *Sinorhizobium meliloti*. *J. Bacteriol.* 199:e00143-17. doi: 10.1128/JB.00143-117
- Dong, T., Fei, Q., Genelot, M., Smith, H., Laurens, L. M. L., Watson, M. J., et al. (2017). A novel integrated biorefinery process for diesel fuel blendstock production using lipids from the methanotroph, *Methylobacterium buryatense*. *Energ. Convers. Manag.* 140, 62–70. doi: 10.1016/j.enconman.2017.02.075
- Fei, Q., and Pienkos, P. T. (2018). "Bioconversion of methane for value-added products," in *Extremophilic Microbial Processing of Lignocellulosic Feedstocks to Biofuels, Value-Added Products, and Usable Power*, eds R. K. Sani and N. Krishnaraj Rathinam (Cham: Springer International Publishing), 145–162. doi: 10.1007/978-3-319-74459-9_8
- Fei, Q., Puri, A. W., Smith, H., Dowe, N., and Pienkos, P. T. (2018). Enhanced biological fixation of methane for microbial lipid production by recombinant *Methylobacterium buryatense*. *Biotechnol. Biofuels* 11:129. doi: 10.1186/s13068-018-1128-1126
- Fu, Y., He, L., Reeve, J., Beck, D. A. C., and Lidstrom, M. E. (2019). Core metabolism shifts during growth on methanol versus methane in the methanotroph *Methylobacterium buryatense* 5GB1. *mBio* 10, 1–14. doi: 10.1128/mBio.00406-419
- Fu, Y., Li, Y., and Lidstrom, M. (2017). The oxidative TCA cycle operates during methanotrophic growth of the Type I methanotroph *Methylobacterium buryatense* 5GB1. *Metab. Eng.* 42, 43–51. doi: 10.1016/j.ymben.2017.05.003
- Garg, S., Clomburg, J. M., and Gonzalez, R. (2018). A modular approach for high-flux lactic acid production from methane in an industrial medium using engineered *Methylobacterium buryatense* 5GB1. *J. Ind. Microbiol. Biotechnol.* 45, 379–391. doi: 10.1007/s10295-018-2035-2033
- Gilman, A., Fu, Y., Hendershott, M., Chu, F., Puri, A. W., Smith, A. L., et al. (2017). Oxygen-limited metabolism in the methanotroph *Methylobacterium buryatense* 5GB1C. *PeerJ* 5:e3945. doi: 10.7717/peerj.3945
- Gilman, A., Laurens, L. M., Puri, A. W., Chu, F., Pienkos, P. T., and Lidstrom, M. E. (2015). Bioreactor performance parameters for an industrially-promising methanotroph *Methylobacterium buryatense* 5GB1. *Microb. Cell Fact.* 14:182. doi: 10.1186/s12934-015-0372-378
- Gottesman, S., Roche, E., Zhou, Y., and Sauer, R. T. (1998). The ClpXP and ClpAP proteases degrade proteins with carboxy-terminal peptide tails added by the SsrA-tagging system. *Genes Dev.* 12, 1338–1347. doi: 10.1101/gad.12.9.1338
- He, A. Y., Yin, C. Y., Xu, H., Kong, X. P., Xue, J. W., Zhu, J., et al. (2016). Enhanced butanol production in a microbial electrolysis cell by *Clostridium beijerinckii* IB4. *Bioprocess Biosyst. Eng.* 39, 245–254. doi: 10.1007/s00449-015-1508-1502
- He, Q., Yang, Y., Yang, S., Donohoe, B. S., Van Wychen, S., Zhang, M., et al. (2018). Oleaginity of the yeast strain *Saccharomyces cerevisiae* D5A. *Biotechnol. Biofuels* 11:258. doi: 10.1186/s13068-018-1256-z
- Hoffman, B. M., Lukoyanov, D., Yang, Z. Y., Dean, D. R., and Seefeldt, L. C. (2014). Mechanism of nitrogen fixation by nitrogenase: the next stage. *Chem. Rev.* 114, 4041–4062. doi: 10.1021/cr400641x
- Hu, L., Wang, J., Yuan, B., Zhu, F., Fei, Q., and Fu, R. (2017). Production of biofuels and chemicals from C1 gases by microorganisms: status and prospects. *Chin. J. Bioproc. Eng.* 15, 17–25.

- Inomura, K., Bragg, J., Riemann, L., and Follows, M. J. (2018). A quantitative model of nitrogen fixation in the presence of ammonium. *PLoS One* 13:e0208282. doi: 10.1371/journal.pone.0208282
- Kaluzhnaya, M., Khmelenina, V., Eshinimaev, B., Suzina, N., Nikitin, D., Solonin, A., et al. (2001). Taxonomic characterization of new alkaliphilic and alkali-tolerant methanotrophs from soda lakes of the Southeastern Transbaikalian region and description of *Methylobacterium buryatense* sp. nov. *Syst. Appl. Microbiol.* 24, 166–176. doi: 10.1078/0723-2020-2028
- Kalyuzhnaya, M. G., Puri, A. W., and Lidstrom, M. E. (2015). Metabolic engineering in methanotrophic bacteria. *Metab. Eng.* 29, 142–152. doi: 10.1016/j.ymben.2015.03.010
- Kalyuzhnaya, M. G., Yang, S., Rozova, O. N., Smalley, N. E., Clubb, J., Lamb, A., et al. (2013). Highly efficient methane biocatalysis revealed in a methanotrophic bacterium. *Nat. Commun.* 4:2785. doi: 10.1038/ncomms3785
- Keiler, K. C., Waller, P. R., and Sauer, R. T. (1996). Role of a peptide tagging system in degradation of proteins synthesized from damaged messenger RNA. *Science* 271, 990–993. doi: 10.1126/science.271.5251.990
- Khmelenina, V. N., Rozova, O. N., and Trotsenko, Y. A. (2011). Characterization of the recombinant pyrophosphate-dependent 6-phosphofructokinases from *Methylobacterium alcaliphilum* 20Z and *Methylococcus capsulatus* Bath. *Methods Enzymol.* 495, 1–14. doi: 10.1016/B978-0-12-386905-0.00001-2
- Koo, M. S., Lee, J. H., Rah, S. Y., Yeo, W. S., Lee, J. W., Lee, K. L., et al. (2003). A reducing system of the superoxide sensor SoxR in *Escherichia coli*. *EMBO J.* 22, 2614–2622. doi: 10.1093/emboj/cdg252
- Li, H., Wang, J., Xu, H., Xing, R., Pan, Y., Li, W., et al. (2013). Decreased fructose-1,6-bisphosphatase-2 expression promotes glycolysis and growth in gastric cancer cells. *Mol. Cancer* 12:110. doi: 10.1186/1476-4598-12-110
- Lin, M., Yan, Y., Lu, W., Zhan, Y., and Zhang, Y. (2015). “Regulatory coupling of nitrogen and carbon metabolism in nitrogen-fixing *Pseudomonas stutzeri* A1501,” in *Biological Nitrogen Fixation*, ed. F. J. D. Bruijn (Hoboken, NJ: John Wiley & Sons, Inc), 109–119.
- Luz, D. E., Nepomuceno, R. S., Spira, B., and Ferreira, R. C. (2012). The Pst system of *Streptococcus mutans* is important for phosphate transport and adhesion to abiotic surfaces. *Mol. Oral Microbiol.* 27, 172–181. doi: 10.1111/j.2041-1014.2012.00641.x
- Masepohl, B., and Hallenbeck, P. C. (2010). Nitrogen and molybdenum control of nitrogen fixation in the phototrophic bacterium *Rhodospirillum rubrum*. *Adv. Exp. Med. Biol.* 675, 49–70. doi: 10.1007/978-1-4419-1528-3_4
- Matsen, J. B., Yang, S., Stein, L. Y., Beck, D., and Kalyuzhnaya, M. G. (2013). Global molecular analyses of methane metabolism in methanotrophic Alphaproteobacterium, *Methylobacterium trichosporium* OB3b. part i: transcriptomic study. *Front. Microbiol.* 4:40. doi: 10.3389/fmicb.2013.00040
- Miyaji, A., Kamachi, T., and Okura, I. (2002). Improvement of the purification method for retaining the activity of the particulate methane monooxygenase from *Methylobacterium trichosporium* OB3b. *Biotechnol. Lett.* 24, 1883–1887. doi: 10.1023/A:1020963112179
- Moore, S. D., and Sauer, R. T. (2007). The tmRNA system for translational surveillance and ribosome rescue. *Annu. Rev. Biochem.* 76, 101–124. doi: 10.1146/annurev.biochem.75.103004.142733
- Moure, V. R., Costa, F. F., Cruz, L. M., Pedrosa, F. O., Souza, E. M., Li, X. D., et al. (2015). Regulation of nitrogenase by reversible mono-ADP-ribosylation. *Curr. Top. Microbiol. Immunol.* 384, 89–106. doi: 10.1007/82_2014_380
- Nguyen, A. D., Kim, D., and Lee, E. Y. (2019). A comparative transcriptome analysis of the novel obligate methanotroph *Methylobacterium* sp. DH-1 reveals key differences in transcriptional responses in C1 and secondary metabolite pathways during growth on methane and methanol. *BMC Genomics* 20:130. doi: 10.1186/s12864-019-5487-5486
- Opio, C., Gerber, P., Mottet, A., Falcucci, A., Tempio, G., MacLeod, M., et al. (2013). *Greenhouse Gas Emissions from Ruminant Supply Chains - A Global Life Cycle Assessment*. Rome: Food and Agriculture Organization of the United Nations (FAO).
- Puri, A. W., Owen, S., Chu, F., Chavkin, T., Beck, D. A., Kalyuzhnaya, M. G., et al. (2015). Genetic tools for the industrially promising methanotroph *Methylobacterium buryatense*. *Appl. Environ. Microbiol.* 81, 1775–1781. doi: 10.1128/AEM.03795-3714
- Rittmann, D., Schaffer, S., Wendisch, V. F., and Sahm, H. (2003). Fructose-1,6-bisphosphatase from *Corynebacterium glutamicum*: expression and deletion of the fbp gene and biochemical characterization of the enzyme. *Arch. Microbiol.* 180, 285–292. doi: 10.1007/s00203-003-0588-586
- Schmehl, M., Jahn, A., Meyer zu Vilsendorf, A., Hennecke, S., Masepohl, B., Schuppler, M., et al. (1993). Identification of a new class of nitrogen fixation genes in *Rhodospirillum rubrum*: a putative membrane complex involved in electron transport to nitrogenase. *Mol. Gen. Genet.* 241, 602–615. doi: 10.1007/bf00279903
- Trotsenko, Y. A., and Murrell, J. C. (2008). Metabolic aspects of aerobic obligate methanotrophy. *Adv. Appl. Microbiol.* 63, 183–229. doi: 10.1016/S0065-2164(07)00005-6
- Yang, S., Vera, J. M., Grass, J., Savvakis, G., Moskvina, O. V., Yang, Y., et al. (2018). Complete genome sequence and the expression pattern of plasmids of the model ethanologen *Zymomonas mobilis* ZM4 and its xylose-utilizing derivatives 8b and 2032. *Biotechnol. Biofuels* 11:125. doi: 10.1186/s13068-018-1116-x
- Zhang, Y., and Zuber, P. (2007). Requirement of the zinc-binding domain of ClpX for Spx proteolysis in *Bacillus subtilis* and effects of disulfide stress on ClpXP activity. *J. Bacteriol.* 189, 7669–7680. doi: 10.1128/JB.00745-747
- Zhou, Y., Wang, L., Yang, F., Lin, X., Zhang, S., and Zhao, Z. K. (2011). Determining the extremes of the cellular NAD(H) level by using an *Escherichia coli* NAD(+)-auxotrophic mutant. *Appl. Environ. Microbiol.* 77, 6133–6140. doi: 10.1128/AEM.00630-611
- Zhu, J., Xu, X., Yuan, M., Wu, H., Ma, Z., and Wu, W. (2017). Optimum O₂:CH₄ ratio promotes the synergy between aerobic methanotrophs and denitrifiers to enhance nitrogen removal. *Front. Microbiol.* 8:1112. doi: 10.3389/fmicb.2017.01112

Conflict of Interest: The authors declare that the research was conducted in the absence of any commercial or financial relationships that could be construed as a potential conflict of interest.

Copyright © 2020 Hu, Yang, Yan, Zhang, Xiang, Gao, Chen, Yang and Fei. This is an open-access article distributed under the terms of the Creative Commons Attribution License (CC BY). The use, distribution or reproduction in other forums is permitted, provided the original author(s) and the copyright owner(s) are credited and that the original publication in this journal is cited, in accordance with accepted academic practice. No use, distribution or reproduction is permitted which does not comply with these terms.



Enhanced Bacitracin Production by Systematically Engineering S-Adenosylmethionine Supply Modules in *Bacillus licheniformis*

Dongbo Cai¹, Bowen Zhang¹, Jiang Zhu¹, Haixia Xu¹, Pei Liu¹, Zhi Wang², Junhui Li³, Zhifan Yang^{1*}, Xin Ma¹ and Shouwen Chen^{1*}

¹ State Key Laboratory of Biocatalysis and Enzyme Engineering, Environmental Microbial Technology Center of Hubei Province, College of Life Sciences, Hubei University, Wuhan, China, ² Key Laboratory of Fermentation Engineering (Ministry of Education), Hubei Provincial Key Laboratory of Industrial Microbiology, School of Food and Biological Engineering, Hubei University of Technology, Wuhan, China, ³ Lifecome Biochemistry Co., Ltd., Nanping, China

OPEN ACCESS

Edited by:

Mingjie Jin,
Nanjing University of Science
and Technology, China

Reviewed by:

Xixian Xie,
Tianjin University of Science
and Technology, China
Zhen Chen,
Tsinghua University, China

*Correspondence:

Zhifan Yang
sailiangzhf@hubei.edu.cn
Shouwen Chen
mel212@126.com

Specialty section:

This article was submitted to
Bioprocess Engineering,
a section of the journal
Frontiers in Bioengineering and
Biotechnology

Received: 04 February 2020

Accepted: 20 March 2020

Published: 07 April 2020

Citation:

Cai D, Zhang B, Zhu J, Xu H,
Liu P, Wang Z, Li J, Yang Z, Ma X and
Chen S (2020) Enhanced Bacitracin
Production by Systematically
Engineering S-Adenosylmethionine
Supply Modules in *Bacillus*
licheniformis.
Front. Bioeng. Biotechnol. 8:305.
doi: 10.3389/fbioe.2020.00305

Bacitracin is a broad-spectrum veterinary antibiotic that widely used in the fields of veterinary drug and feed additive. S-Adenosylmethionine (SAM) is a critical factor involved in many biochemical reactions, especially antibiotic production. However, whether SAM affects bacitracin synthesis is still unknown. Here, we want to analyze the relationship between SAM supply and bacitracin synthesis, and then metabolic engineering of SAM synthetic pathway for bacitracin production in *Bacillus licheniformis*. Firstly, our results implied that SAM exogenous addition benefited bacitracin production, which yield was increased by 12.13% under the condition of 40 mg/L SAM addition. Then, SAM synthetases and Methionine (Met) synthetases from *B. licheniformis*, *Corynebacterium glutamicum*, and *Saccharomyces cerevisiae* were screened and overexpressed to improve SAM accumulation, and the combination of SAM synthetase from *S. cerevisiae* and Met synthetase from *B. licheniformis* showed the best performance, and 70.12% increase of intracellular SAM concentration (31.54 mg/L) and 13.08% increase of bacitracin yield (839.54 U/mL) were achieved in resultant strain DW2-KE. Furthermore, Met transporters MetN and MetP were, respectively, identified as Met exporter and importer, and bacitracin yield was further increased by 5.94% to 889.42 U/mL via deleting *metN* and overexpressing *metP* in DW2-KE, attaining strain DW2-KENP. Finally, SAM nucleosidase gene *mtnN* and SAM decarboxylase gene *speD* were deleted to block SAM degradation pathways, and bacitracin yield of resultant strain DW2-KENPND reached 957.53 U/mL, increased by 28.97% compared to DW2. Collectively, this study demonstrated that SAM supply served as the critical role in bacitracin synthesis, and a promising strain *B. licheniformis* DW2-KENPND was attained for industrial production of bacitracin.

Keywords: bacitracin, S-Adenosylmethionine, *Bacillus licheniformis*, methionine, metabolic engineering

Abbreviations: BCAAs, branched chain amino acid; GC, gas chromatography; HPLC, high performance liquid chromatography; Lys, lysine; Met, methionine; NRPS, non-ribosomal polypeptide synthetases; Orn, ornithine; SAM, S-Adenosylmethionine.

INTRODUCTION

Bacitracin, an important peptide antibiotic that consists of 11 kinds of amino acids, is mainly produced by *B. licheniformis* and *Bacillus subtilis*. Bacitracin biosynthetase gene cluster in *B. licheniformis* spans over 45 kd of DNA, which containing four genes, *bacT*, *bacA*, *bacB* and *bacC*. Gene *bacT* encodes thioesterase, and the relationship between bacitracin synthesis with *bacT* is unclear. *BacA* is responsible for activating and polymerizing five kinds of amino acids (Ile, Cys, Leu, D-Glu, and Ile) at bacitracin tail, *BacB* and *BacC* are responsible for activating and polymerizing seven kinds of amino acids in heptapeptide loop (Wang D. et al., 2017). Bacitracin owns the advantages of wide antimicrobial spectrum, rapid excretion rate, low absorption of livestock and poultry, not easy to produce resistance etc., and it inhibits the synthesis of cell wall of most gram-positive and a few of gram-negative bacteria, thus, bacitracin is widely used as the feed additive in feed industry, however, the low-yield has hindered its application (Fang et al., 2017).

With the development of synthetic biology and metabolic engineering, many elements and strategies have been developed for antibiotic metabolic engineering breeding (Zhou et al., 2017). The Leu-responsive regulatory protein Lrp has been engineered to improve erythromycin and actinorhodin production in *Streptomyces* (Liu et al., 2017), and deletion of phosphorus metabolism regulator gene *phop* was proven to be beneficial for avermectin, pimaricin, etc., production (Sola-Landa et al., 2003; Martin et al., 2017; Mendes et al., 2007). In addition, precursor supply served as the critical role in secondary metabolite synthesis (Wohlleben et al., 2012). Branched chain amino acid (BCAA) served as the critical role in erythromycin production, and strengthening BCAA supplies led to a 41% increase of erythromycin yield, via deleting *lrp* and overexpressing BCAA transporter SACE_5387 (Liu et al., 2017). Moreover, acetyl-CoA carboxylase was overexpressed to improve malonyl-CoA supply, which further led to a 43% increase of surfactin production, reached 13.37 g/L (Wang et al., 2019). In addition, efficient use of substrate is also critical for metabolite production. Previously, maltose ABC transporter MalEFG was strengthened to improve utilization rate of corn starch, resulting in a 3.3-fold increase of ivermectin production in *Streptomyces* (Li et al., 2010). Generally, S-adenosylmethionine (SAM) served as the critical role in antibiotic biosynthesis, and strengthening SAM supply has been proven as an efficient strategy for lincomycin, avermectin, novobiocin, cephalosporin, etc., production (Zhao et al., 2010). However, whether SAM supply affects bacitracin synthesis has not been investigated in *Bacillus*.

S-Adenosylmethionine is one of the most widely used cofactor for group transfer reactions that involved in various metabolic processes, and it serves as the main methyl donor for DNA methylation, protein and secondary metabolite syntheses (Ruan et al., 2019), and SAM-dependent methylation is also the critical step for metabolite production. In addition, SAM addition improves antibiotic synthesis might via activating the transcription of pathway-specific regulatory genes or increasing the auto-phosphorylation of regulatory kinase (Kim et al., 2003). Generally, SAM is synthesized from aspartate, which generated

from glucose via glycolytic and tricarboxylic acid (TCA) cycle, and methionine (Met) serves as the direct precursor for SAM biosynthesis (Ruan et al., 2019). Recently, several strategies have been conducted to improve SAM production, including: (i) enhancing activity of SAM synthetase, (ii) deleting cystathionin- β -synthase, (iii) releasing the feedback inhibitions of SAM to SAM synthetase and methylenetetrahydrofolate reductase (Chu et al., 2013). In addition, SAM titer was significantly enhanced via coupling SAM synthetic pathway with TCA cycle in *Bacillus amyloliquefaciens* (Ruan et al., 2019).

Bacillus licheniformis DW2 is an industrial strain for bacitracin production (Cai et al., 2019b), and several metabolic engineering approaches have been developed to improve bacitracin production. The synthetic pathways of Lysine (Lys) and Ornithine (Orn) were strengthened, which led to 28.95 and 16.5% increases of bacitracin yields, respectively (Wu et al., 2019; Yu et al., 2019). BCAA transporters BrnQ and YdhG were engineered to improve intracellular BCAA accumulations for bacitracin synthesis (Li et al., 2018; Zhu et al., 2018). Additionally, the main regulators in carbon, nitrogen and phosphorus metabolisms were engineered, which led to a 35.72% increase of bacitracin yield (Cai et al., 2019b). Due to the importance of SAM supply on antibiotic synthesis, in this study, we want to improve bacitracin production via rewiring SAM synthetic pathways, including in SAM synthetic, degradation and Met transportation pathways. Our results demonstrated that SAM supply served as a critical role on bacitracin synthesis, and this study provided a promising strain for industrial production of bacitracin.

MATERIALS AND METHODS

Strains, Plasmids and Cultivation Conditions

The strains and plasmids used in this research were listed in **Table 1**. *B. licheniformis* DW2 acted as the original strain for constructing recombinants (Zhu et al., 2019), and *Escherichia coli* DH5 α served as the host for vector construction. The plasmid T2(2)-Ori was applied for gene deletion, promoter replacement and gene integration in *B. licheniformis*, pHY300PLK was applied for constructing gene expression vector. All primers used in this research were provided in **Supplementary Table S1**.

Luria-Bertani (LB) medium was served as the basic medium for strain cultivation, and corresponding antibiotics (20 mg/L kanamycin, 20 mg/L tetracycline or 50 mg/L ampicillin) were added when necessary. The seed culture was inoculated in a 250 mL flask containing 20 mL LB medium for 6 h, and transferred (1 mL) into bacitracin production medium (10% soybean meal, 4.5% corn starch, 0.1% (NH₄)₂SO₄, 0.6% CaCO₃, natural pH), and then cultivated at 37°C, 230 r/min for 48 h. In order to analyze the function roles of Met transporters MetN and MetP, ME medium (20 g/L glucose, 20 g/L sodium glutamate, 10 g/L sodium citrate, 7 g/L NH₄Cl, 0.5 g/L K₂HPO₄ 3H₂O, 0.5 g/L MgSO₄ 7H₂O, 0.04 g/L FeCl₃·6H₂O, 0.104 g/L MnSO₄·4H₂O, 0.15 g/L CaCl₂ 2H₂O, pH 7.2) was applied (Birrer et al., 1994). All the fermentation experiments were repeated at least three times.

TABLE 1 | The strains and plasmids used in this research.

Strains and plasmids	Relevant properties	Source of references
Strains		
<i>Escherichia coli</i> DH5 α	<i>supE44</i> Δ <i>lacU169</i> (f 80 <i>lacZ</i> Δ M15) <i>hsd</i> R17 <i>recA1</i> <i>gyrA96</i> <i>thi1</i> <i>relA1</i>	This study
<i>Bacillus licheniformis</i> DW2	Wide-type CCTCC M2011344	CCTCC
DW2/pHY-metK _{BI}	DW2 harboring SAM synthetase MetK expression vector pHY-metK _{BI}	This study
DW2/pHY-metK _{Cg}	DW2 harboring SAM synthetase MetK _{Cg} expression vector pHY-metK _{Cg}	This study
DW2/pHY-SAM2	DW2 harboring SAM synthetase SAM2 expression vector pHY-SAM2	This study
DW2/pHY-300	DW2 harboring pHY300PLK, as the control strain	This study
DW2-K	SAM synthetase SAM2 integrated overexpression strain, based on strain DW2	This study
DW2-K/pHY-metH _{BI}	DW2-K harboring Met synthetase MetH expression vector pHY-metH _{BI}	This study
DW2-K/pHY-metH _{Cg}	DW2-K harboring Met synthetase MetH expression vector pHY-metH _{Cg}	This study
DW2-K/pHY-Met6	DW2-K harboring Met synthetase Met6 expression vector pHY-Met6	This study
DW2-KE	Met synthetase MetH overexpression strain via promoter replacement, based on strain DW2-K	This study
DW2/pHY-metN	DW2 harboring Met transporter MetN expression vector pHY-metN	This study
DW2/pHY-metP	DW2 harboring Met transporter MetP expression vector pHY-metP	This study
DW2 Δ metN	Deletion of <i>metN</i> in DW2	This study
DW2 Δ metP	Deletion of <i>metP</i> in DW2	This study
DW2-KEN	Deletion of <i>metN</i> in DW2-KE	This study
DW2-KENP	Overexpression of <i>metP</i> in DW2-KEN	This study
DW2-KENP Δ mtnN	Deletion of <i>mtnN</i> in DW2-KENP	This study
DW2-KENP Δ speD	Deletion of <i>speD</i> in DW2-KENP	This study
DW2-KENPND	Deletion of <i>mtnN</i> and <i>speD</i> in DW2-KENP	This study
Plasmids		
pHY300PLK	<i>E. coli</i> and <i>B. s</i> shuttle vector; Amp ^r , Tet ^r	Lab collection
T ₂ (2)-Ori	<i>Bacillus</i> knockout vector; Kan ^r	Lab collection
pHY-metK _{BI}	SAM synthetase MetK _{BI} expression vector, based on pHY300PLK	This study
pHY-metK _{Cg}	SAM synthetase MetK _{Cg} expression vector, based on pHY300PLK	This study
pHY-SAM2	SAM synthetase SAM2 expression vector, based on pHY300PLK	This study
pHY-MetH _{BI}	Met synthetase MetH _{BI} expression vector, based on pHY300PLK	This study
pHY-metH _{Cg}	Met synthetase MetH _{Cg} expression vector, based on pHY300PLK	This study
pHY-Met6	Met synthetase Met6 expression vector, based on pHY300PLK	This study
pHY-metN	Met transporter MetN expression vector, based on pHY300PLK	This study
pHY-metP	Met transporter MetP expression vector, based on pHY300PLK	This study
T ₂ :-SAM2	T ₂ (2)-Ori-SAM2(A+SAM2+B); to overexpress SAM2	This study
T ₂ -PbacA-PmethH	T ₂ (2)-Ori-PmethH(A+PbacA+B); to replace the promoter of <i>metH</i> by PbacA	This study
T ₂ -metN	T ₂ (2)-Ori-metN(A+B); to delete <i>metN</i>	This study
T ₂ -metP	T ₂ (2)-Ori-metP(A+B); to delete <i>metP</i>	This study
T ₂ -PbacA-PmetP	T ₂ (2)-Ori-PmetP(A+PbacA+B); to replace the promoter of <i>metP</i> by PbacA	This study
T ₂ -mtnN	T ₂ (2)-Ori-mtnN(A+B); to delete <i>mtnN</i>	This study
T ₂ -speD	T ₂ (2)-Ori-speD(A+B); to delete <i>speD</i>	This study

Construction of Gene Expression Vector

The gene expression vector was constructed according to our previous research (Zhu et al., 2019), based on pHY300PLK, and SAM synthetase MetK from *B. licheniformis* expression vector pHY-metK_{BI} was served as an example. Briefly, P43 promoter from *B. subtilis* 168, gene *metK* and *amyL* terminator from *B. licheniformis* DW2 were amplified by corresponding primers (Supplementary Table S1), and fused by Splicing Overlap Extension (SOE)-PCR. The fused fragment was inserted into pHY300PLK at restriction sites *EcoRI/XbaI*, diagnostic PCR and DNA sequence confirmed that gene expression vector was constructed successfully, named as pHY-metK_{BI}. Similarly, other gene expression vectors were attained by the same method.

Gene Deletion in *B. licheniformis*

The method for gene deletion in *B. licheniformis* was referred to our previously reported research (Cai et al., 2019b), and Met transporter gene *metN* deletion strain was served as an example. In brief, the upstream and downstream homology arms of *metN* were amplified from *B. licheniformis* DW2, and fused by SOE-PCR. The fused fragment was inserted into T₂(2)-Ori at restriction sites *SacI/XbaI*, diagnostic PCR and DNA sequence confirmed that gene deletion vector was constructed successfully, named T2-metN. Then, T2-metN was transferred into *B. licheniformis* DW2 via electroporation, and the positive transformants were cultivated in LB medium with 20 mg/L kanamycin at 45°C, and sub-cultured for three generations.

Then, transferred into LB medium and sub-cultured for six generations at 37°C. The gene *metN* deletion strain was attained via homologous double crossover, diagnostic PCR and DNA sequence confirmed that *metN* deletion strain was constructed successfully, named as DW2Δ*metN*.

Gene Integrated Expression in *B. licheniformis*

To construct the strain which overexpressing SAM synthetase SAM2 from *Saccharomyces cerevisiae*, gene SAM2 mediated by P43 promoter was integrated into the chromosome of *B. licheniformis* DW2, following to previously reported protocol (Cai et al., 2018), diagnostic PCR and DNA sequence confirmed that the gene integrated overexpression strain was constructed successfully.

Promoter Replacement in *B. licheniformis*

The method for gene promoter replacement in *B. licheniformis* was referred to our previously reported research (Wu et al., 2019), and the procedure for promoter of Met synthetase MetH replaced by P*bacA*, a strong promoter that has been proven in our previous research (Shi et al., 2019), was served as an example. Briefly, the upstream and downstream homology arms of P*metH*, promoter P*bacA*, were amplified to form T2-P*bacA*-P*metH*, and promoter P*metH* was replaced by P*bacA* via homologous double crossover, which procedure was the same as that of gene deletion.

Analytical Methods

Bacitracin yield was measured by Agilent 1260 high performance liquid chromatography (HPLC), equipped with C18 column (ZORBAX SB-C18). Cell biomass was determined by dilution coating method (Cai et al., 2019a). SAM concentration was determined by HPLC (Ruan et al., 2019), and concentrations of intracellular and extracellular amino acids were measured by gas chromatography (GC), according to our previously reported research (Cai et al., 2019b). The transcriptional levels of bacitracin synthetase gene cluster were determined by RT-qPCR, and gene *16S rDNA* was served as the reference for data normalization (Cai et al., 2017).

Statistical Analysis

All data were conducted to analyze the variance at $P < 0.05$ and $P < 0.01$, and a *t*-test was applied to compare the mean values using the software package Statistica 6.0, and bars represented the standard deviations, * $P < 0.05$; and ** $P < 0.01$ indicated the significance levels between recombinant strains and control (Cai et al., 2018).

RESULTS

Exogenous SAM Addition Benefited Bacitracin Production

Previously, SAM was proven to own the critical role in the syntheses numerous kinds of antibiotic (Zhao et al., 2010),

however, whether SAM supply affect bacitracin synthesis has not been clarified in *Bacillus*. Here, different concentrations of SAM was, respectively, added into bacitracin production medium at 24 h (The beginning period of bacitracin synthesis), and our results in **Figure 1A** implied that exogenous SAM addition benefited bacitracin production, and the maximum bacitracin yield (832.45 U/mL) was attained under the condition of 40 mg/L SAM addition, increased by 12.13% compared to control (742.43 U/mL). Transcriptional levels of bacitracin synthetase genes *bacT*, *bacA*, *bacB* and *bacC* were measured under optimal condition, and our results implied that SAM addition improved transcription of bacitracin synthetase, increased by 1.43-, 1.34-, 1.31-, and 1.29-fold, respectively (**Figure 1B**). In addition, our results demonstrated that SAM addition have no effects on cell biomass (**Supplementary Figure S1**). Moreover, the concentrations of intracellular SAM and Met were determined before (24 h) and after (36 h) SAM addition. Our results implied that the concentrations of intracellular SAM was 7.54 mg/L at 24 h, and which was increased to 17.29 mg/L at 30 h when SAM addition, increased by 53.69% compared to the control group (11.25 mg/L). While, Met concentrations showed no significant differences between two groups (**Supplementary Figure S2**). Taken together, these above results demonstrated that SAM served as the key role in bacitracin synthesis, and strengthening SAM supply was conducive to bacitracin production.

Overexpressing SAM Synthetase Improved SAM Accumulation and Bacitracin Yield

S-Adenosylmethionine synthetase served as the key role in SAM formation from Met and ATP (Kanai et al., 2017), and overexpression of SAM synthetase benefited SAM production (Ruan et al., 2019). The SAM synthetic pathway of *B. licheniformis* was showed in **Figure 2**, here, SAM synthetases from *B. licheniformis*, *Corynebacterium glutamicum*, *S. cerevisiae* were strengthened in *B. licheniformis* DW2, attaining recombinant strains DW2/pHY-MetK_{Bl}, DW2/pHY-MetK_{Cg} and DW2/pHY-SAM2, respectively.

Then, all these recombinant strains were cultivated in bacitracin production medium, as well as controls DW2 and DW2/pHY300. Based on our results of **Figure 3A**, bacitracin yields produced by DW2/pHY-MetK_{Bl}, DW2/pHY-MetK_{Cg} and DW2/pHY-SAM2 were 724.32 U/mL, 743.42 U/mL and 765.31 U/mL, increased by 8.40, 11.24, and 14.51% compared with that of DW2/pHY300 (668.27 U/mL). In addition, cell biomasses of these strains showed no significant differences, and bacitracin produced by per cell were 1.95×10^{-8} U/CFU, 2.00×10^{-8} U/CFU and 2.05×10^{-8} U/CFU, 7.97%, 10.46 and 13.43% higher than that of DW2/pHY300 (1.81×10^{-8} U/CFU), respectively. Furthermore, SAM2 expression cassette was inserted into chromosome of DW2, attaining SAM2 integrated overexpression strain DW2-K. Based on the results of **Figure 3B**, bacitracin yield of DW2-K reached 795.42 U/mL, increased by 7.14% compared to DW2 (742.43 U/mL). The

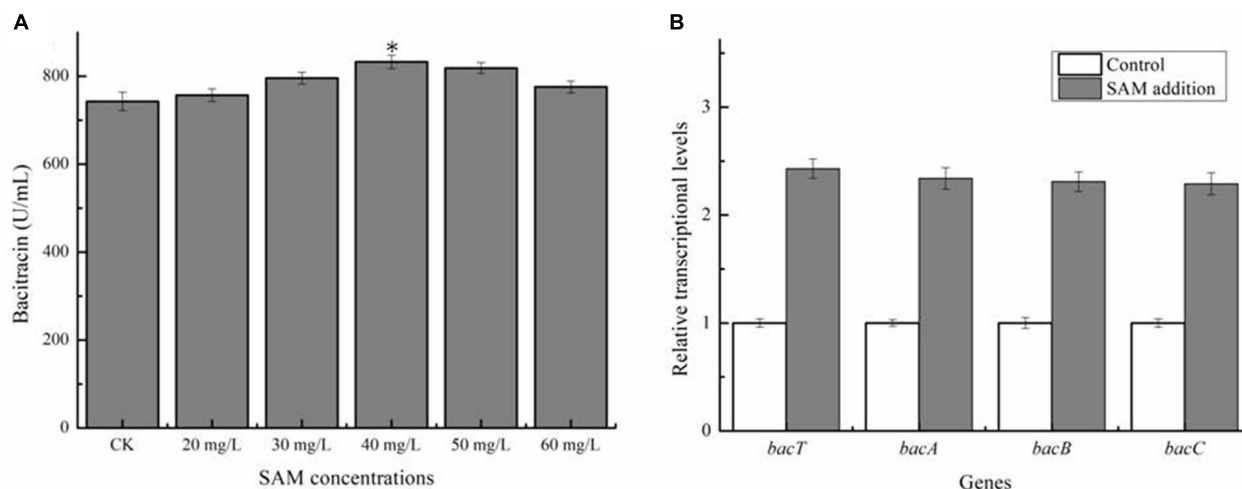


FIGURE 1 | Effects of exogenous SAM addition on bacitracin production. **(A)** Effects of different concentrations of SAM (20, 30, 40, 50, and 60 mg/L) additions on bacitracin yield. **(B)** Effects of SAM addition on the transcriptional levels of bacitracin synthetase genes *bacT*, *bacA*, *bacB*, and *bacC*. * $P < 0.05$ and ** $P < 0.01$ indicate the significance levels between recombinant strains and control strain.

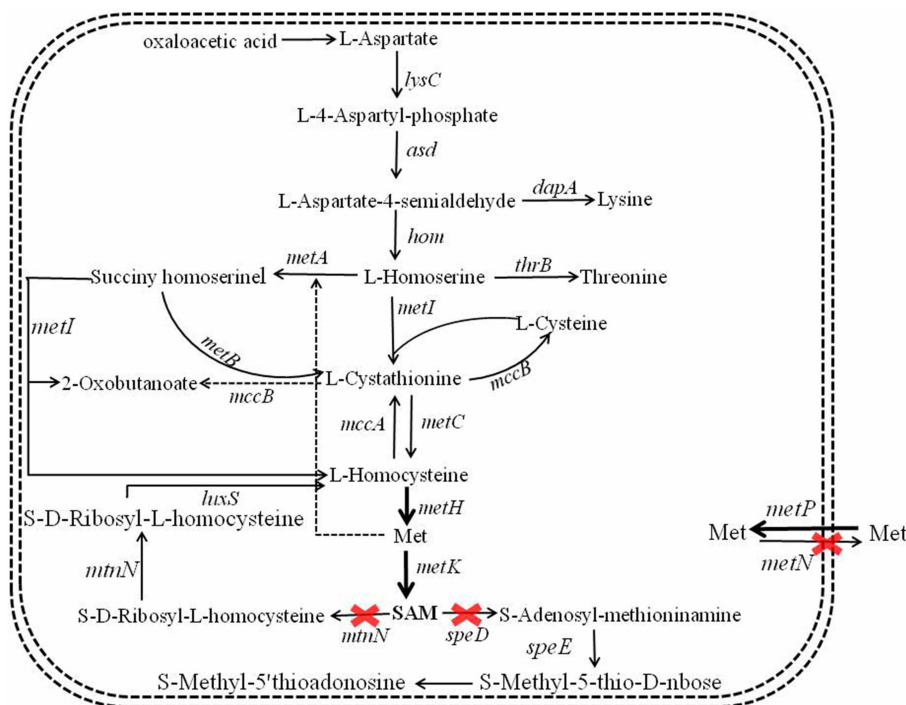


FIGURE 2 | Metabolic engineering of SAM synthetic and degradation, Met transportation pathways for SAM accumulation and bacitracin synthesis in *B. licheniformis*.

bacitracin produced by per cell was 1.98×10^{-8} U/CFU, increased by 6.30% (1.84×10^{-8} U/CFU). The concentration of intracellular SAM (36 h) in DW2-K was 26.32 mg/L, 41.96% higher than that of DW2 (18.54 mg/L). Additionally, transcriptional levels of genes *bacT*, *bacA*, *bacB* and *bacC* were also increased significantly (Figure 3C), as the increase of SAM accumulation in DW2-K.

Strengthening Precursor Met Supply Benefited SAM Accumulation and Bacitracin Production

Acting as the precursor for SAM synthesis, Met supply might affect the synthetic efficiency of SAM, which further affect bacitracin production. Here, Met synthetases from

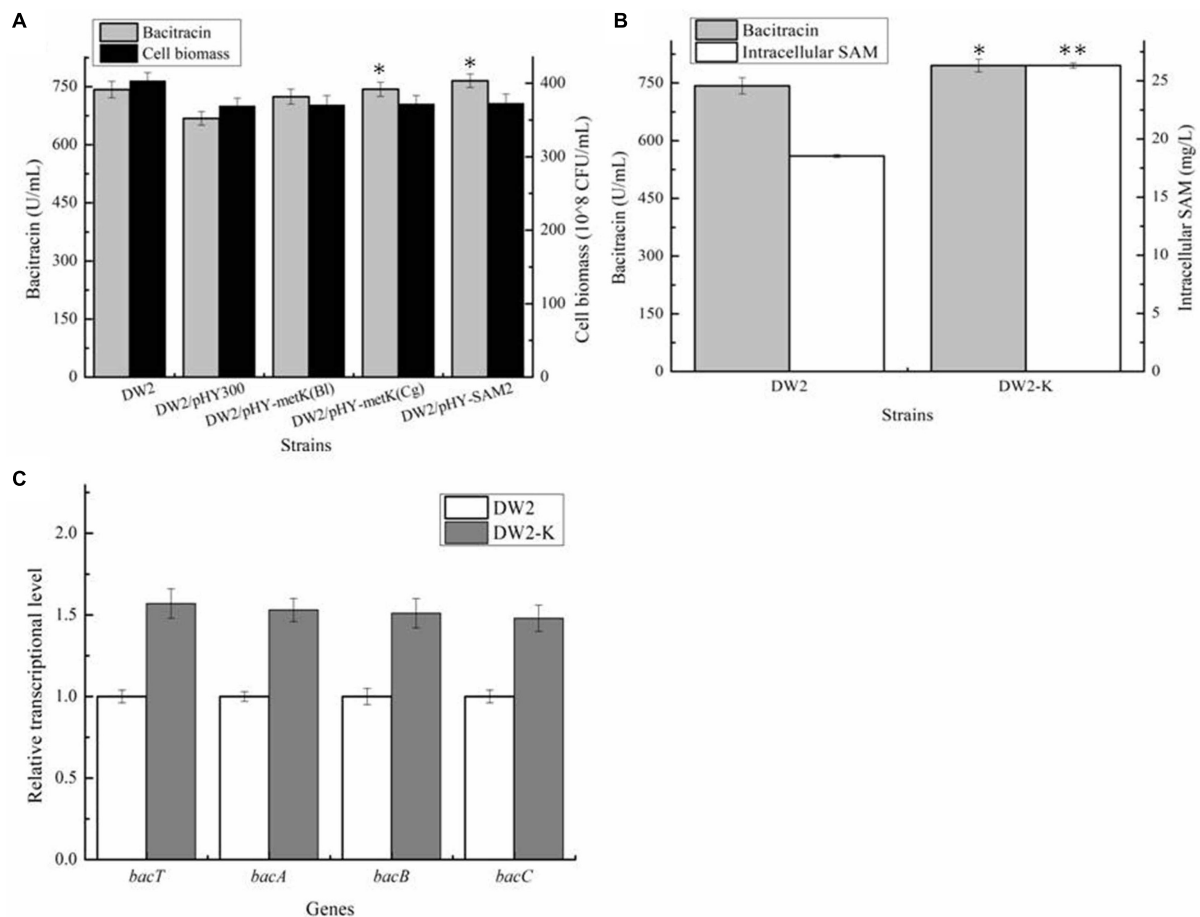


FIGURE 3 | Effects of strengthening SAM synthetase expression on SAM accumulation and bacitracin production. **(A)** Effects of SAM synthetase overexpression on bacitracin yield and cell biomass, **(B)** Effects of integrated overexpression of SAM2 from *S. cerevisiae* on bacitracin yield, cell biomass and SAM accumulation, **(C)** Effects of SAM2 overexpression on the transcriptional levels of bacitracin synthetase genes *bacT*, *bacA*, *bacB*, and *bacC*. * $P < 0.05$ and ** $P < 0.01$ indicate the significance levels between recombinant strains and control strain.

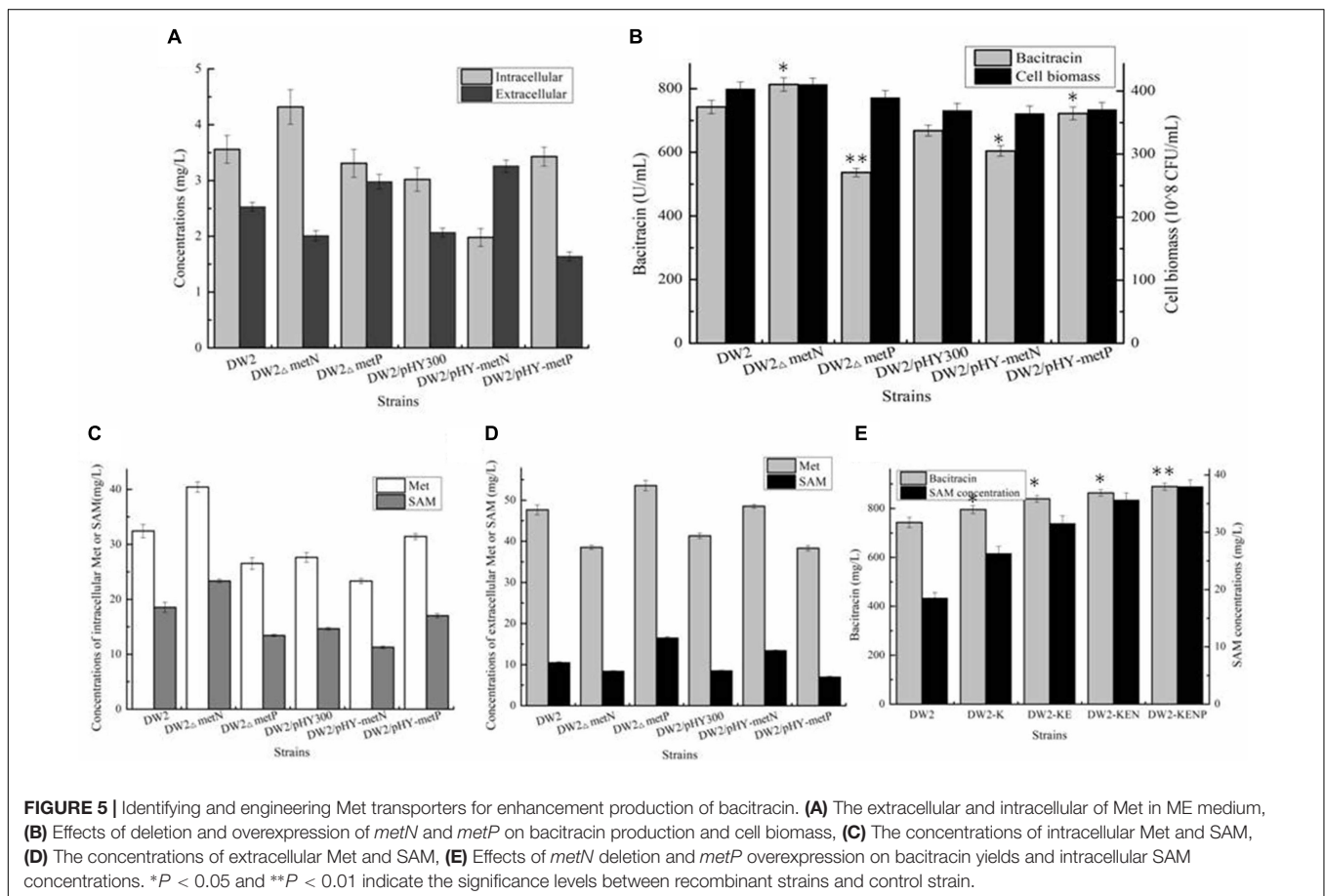
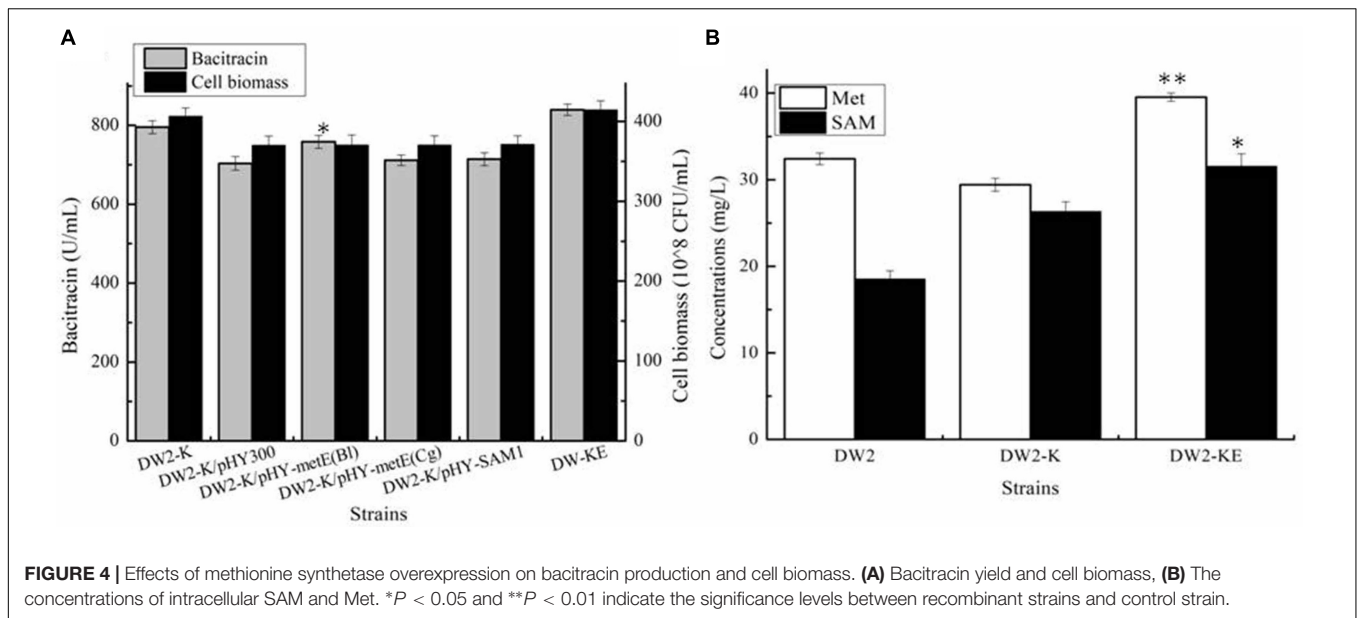
B. licheniformis (MetH), *C. glutamicum* (MetH), *S. cerevisiae* (Met6) were strengthened in DW2-K, attaining strains DW2-K/pHY-MetH_{BI}, DW2-K/pHY-MetH_{Cg} and DW2-K/pHY-Met6, respectively. Our results implied that overexpression of MetH from *B. licheniformis* benefited bacitracin synthesis, however, strengthening Met synthetases from *C. glutamicum* and *S. cerevisiae* has no positive effect on bacitracin production. After that, the promoter of *metH* of DW2-K was replaced by bacitracin synthetase cluster promoter P_{bacA}, a proven strong promoter that has been confirmed in our previous research (Shi et al., 2019), attaining MetH overexpression strain DW2-KE. Based on our results, bacitracin produced by DW2-KE reached 839.54 U/mL, increased by 5.55 and 13.08% compared to DW2-K and DW2, respectively. Bacitracin produced by per cell was 2.03×10^{-8} U/mL, increased by 11.89 and 3.51% (Figure 4A). In addition, the intracellular Met and SAM concentrations (36 h) were 39.54 mg/L and 31.54 mg/L, increased by 34.40 and 19.83% compared with those of DW2-K (29.42 mg/L and 26.32 mg/L), respectively (Figure 4B). Taken together, all these above results demonstrated that strengthening

Met synthetic pathway benefited SAM accumulation and bacitracin production.

Identification and Engineering Met Transporters MetN and MetP Improved SAM Supply and Bacitracin Yield

Apart from metabolic pathway, engineering transportation pathway is also regarded as an efficient approach to improve target metabolite production. Previously, amino acid transporters LysE, BrnFE, and TcyP have been identified and engineered for Lys, Val and Cys production (Chen et al., 2015; Ohtsu et al., 2015; Dong et al., 2016), and deleting Lys transporter LysE and BCAA permease YhdG were also proven to be beneficial for bacitracin syntheses (Li et al., 2018; Wu et al., 2019). Here, MetN and MetP were annotated as Met transporters in *B. licheniformis* DW2, however, transportation modules of them have not been clarified, nor their roles on bacitracin production.

To elucidate the transportation modes of these two transporters, genes *metN* and *metP* were deleted and



overexpressed in DW2, attaining DW2 Δ metN, DW2 Δ metP, DW2/pHY-MetN and DW2/pHY-MetP, respectively. Then, these strains were cultivated in ME medium, and the concentrations of intracellular and extracellular Met were measured after 24 h

cultivation. Based on the results of **Figure 5A**, strengthening MetP expression benefited Met import, while the concentration of intracellular Met was dropped significantly in MetN overexpression strain, and vice versa. Collectively, these

above results suggested that MetN and MetP might act as the Met exporter and importer in *B. licheniformis* DW2, respectively.

Then, all these strains were cultivated in bacitracin production medium, and further results implied that *metN* deletion and *metP* overexpression benefited bacitracin production, which yields were increased by 9.55 and 8.05%, meanwhile, bacitracin yields were decreased by 9.58 and 27.73% in *metN* overexpression and *metP* deletion strains, compared to DW2 and DW2/pHY300, respectively (Figure 5B). Moreover, the intracellular Met concentrations were increased by 24.71 and 13.71% in DW2 Δ metN and DW2/pHY-MetP, which concentrations were dropped by 18.17 and 15.59% in DW2 Δ metP and DW2/pHY-MetN, indicated that *metN* deletion and MetP overexpression benefited intracellular Met accumulation (Figures 5C,D). Since Met served as the critical role in SAM synthesis and accumulation, the transporters MetN and MetP were confirmed to act as Met exporter and importer, respectively.

To further improve bacitracin synthesis capability of DW2-KE, gene *metN* was deleted to attain DW2-KEN, and *metP* was further overexpressed via promoter replacement, attaining strain DW2-KENP. Bacitracin fermentation results implied that 889.42 U/mL bacitracin was produced by DW2-KENP, increased

by 19.80 and 5.94%, compared to DW2 and DW2-KE, and the specific bacitracin yield of DW2-KENP were increased by 20.31 and 5.71%, respectively. Meanwhile, the intracellular SAM concentration was increased to 37.98 mg/L, increased by 104.85 and 20.42%, respectively (Figure 5E).

Blocking SAM Degradation Pathways Improved Bacitracin Synthesis

In the above work, although concentration of intracellular SAM was enhanced significantly, the accumulated SAM might also be transformed into byproducts S-D-Ribosyl-L-homocysteine and S-Adenosyl-methioninamine, under the catalyses of SAM nucleosidase MtnN and SAM decarboxylase SpeD, respectively, which was not conducive to SAM accumulation. Here, genes *mtnN* and *speD* were deleted in DW2-KENP, resulting in DW2-KENP Δ mtnN and DW2-KENP Δ speD, respectively. As shown in Figure 6, deletion of *mtnN* and *speD* were beneficial for intracellular SAM accumulation, and bacitracin yields were also enhanced in gene deletion strains. Furthermore, the strain DW2-KENPND was attained via deleting *mtnN* and *speD* simultaneously, and bacitracin yield of DW2-KENPND reached

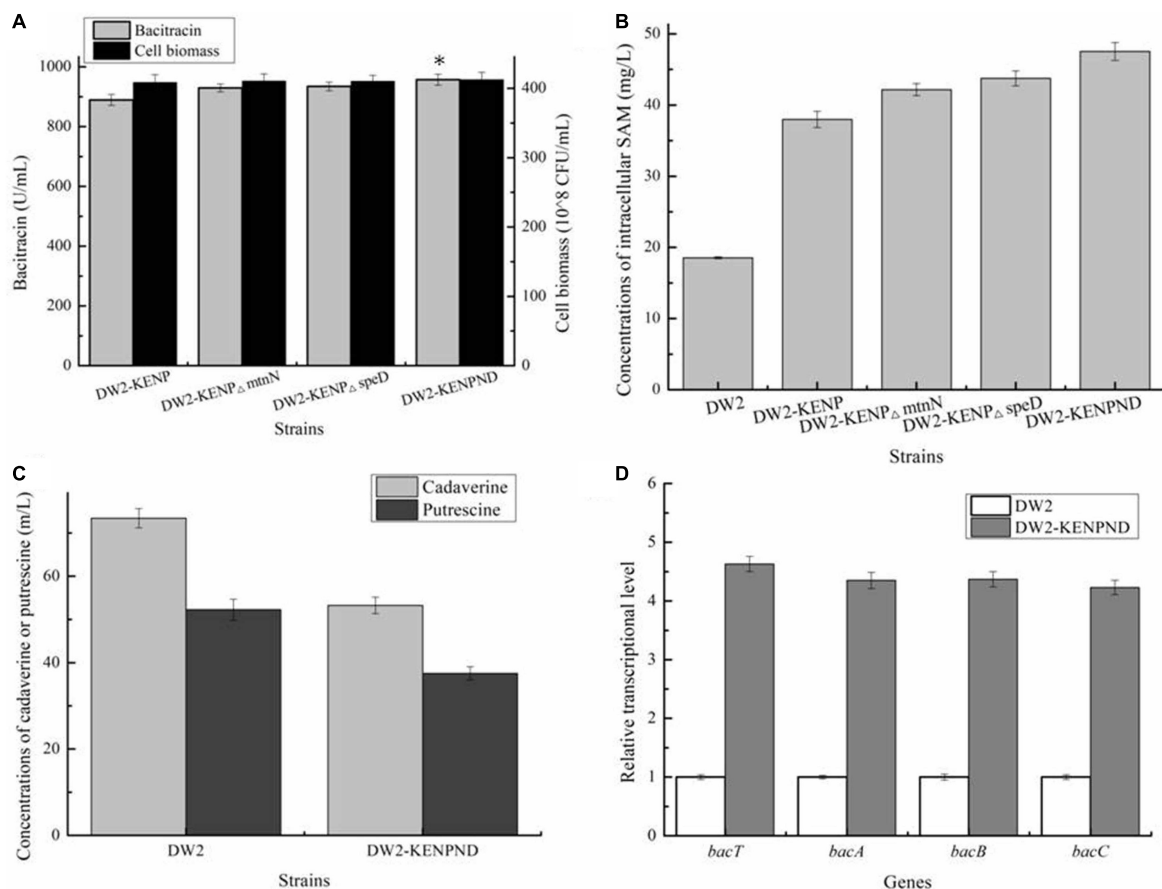
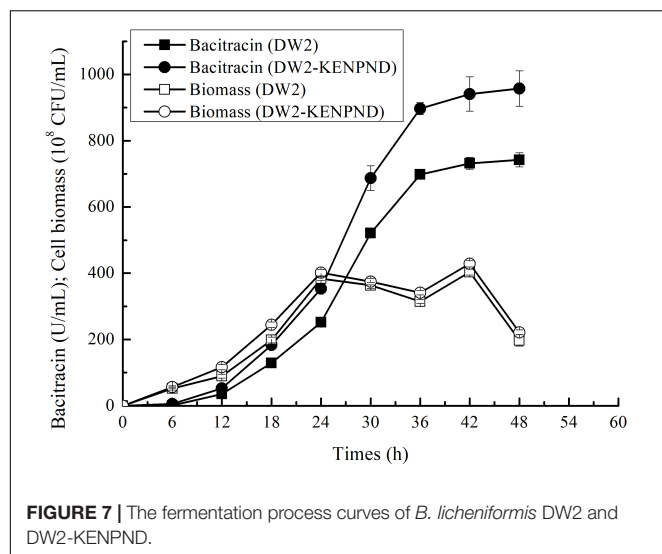


FIGURE 6 | Effects of *mtnN* and *speD* deletion on bacitracin production. **(A)** Bacitracin yield and cell biomass, **(B)** The concentration of intracellular SAM, **(C)** The concentrations of cadaverine and putrescine, **(D)** Transcriptional level analysis. * $P < 0.05$ and ** $P < 0.01$ indicate the significance levels between recombinant strains and control strain.



957.25 U/mL, increased by 28.93 and 7.63% compared to DW2 and DW2-KENP, respectively (Figure 6A). The intracellular SAM concentration of DW2-KENPND was 47.53 mg/L, increased by 1.56-fold compared to DW2 (Figure 6B). In addition, the harmful by-products during bacitracin production, cadaverine and putrescine, produced by DW2-KENPND were 53.24 and 37.52 mg/L, decreased by 27.50 and 37.04% compared with those of DW2 (73.43 mg/L and 52.25 mg/L), as the weakened expression of amino acid decarboxylase (Figure 6C). Moreover, the transcriptional levels of *bacT*, *bacA*, *bacB* and *bacC* were increased by 3.63-, 3.35-, 3.37-, and 3.23-fold, respectively (Figure 6D).

The Fermentation Processes of *B. licheniformis* DW2 and DW2-KENPND

Furthermore, the fermentation curves of *B. licheniformis* DW2 and DW2-KENPND were measured, and cell biomass and bacitracin yields were determined during fermentation process. Based on the results of Figure 7, bacitracin was synthesized from 12 h, and bacitracin yields of DW2-KENPND were higher than those of DW2 throughout the whole fermentation process, and the maximum yield produced by DW2-KENPND reached 957.53 U/mL, increased by 28.97%. In addition, the maximum cell biomass of DW2-KENPND was 428.54×10^8 CFU/mL, increased by 6.22% compared to DW2 (403.43×10^8 CFU/mL). The bacitracin produced by per cell was 2.23×10^{-8} U/CFU, 21.42% higher than that of DW2 (1.84×10^{-8} U/CFU).

DISCUSSION

Bacitracin is a widely used veterinary antibiotic that mainly produced by *Bacillus*, and low production efficiency limits its promotion and application. SAM is an important cofactor in cell metabolism, which serves as the critical roles in syntheses of multiple antibiotics (Zhao et al., 2010). However, whether SAM affects antibiotic synthesis in *Bacillus*, especially for bacitracin,

is still unknown. In this study, our results confirmed that strengthening intracellular SAM accumulation was beneficial for bacitracin production, and a metabolic engineered strain *B. licheniformis* DW2-KENPND with bacitracin yield of 957.53 U/mL was attained, via rewiring SAM synthetic and Met transportation pathways.

Acting as a critical methyl donor, SAM serves as the important role in the biosynthesis of multiple antibiotics (Zhang et al., 2008), in addition, SAM could increase the transcription of pathway-specific regulatory genes or auto-phosphorylation of regulatory kinase (Berney et al., 2015), therefore, strengthening SAM supply has been proven to be beneficial for production of lincomycin (Pang et al., 2015; Xu et al., 2018), avermectin (Tian et al., 2017), erythromycin (Wang et al., 2007), actinorhodin (Kim et al., 2003), etc. Moreover, SAM is not only involved in the transfer of sulfonyl and ribosyl groups, but also regulates intracellular metabolites that involved in primary and second metabolisms (Ruan et al., 2019). In this research, bacitracin is produced by Non-Ribosomal Polypeptide Synthetases (NRPS) in *B. licheniformis* (Rietkotter et al., 2008), different from those of above antibiotics (Polyketide Synthase) that which were mainly produced by *Streptomyces*, moreover, our results implied that strengthening SAM supply increased the transcription of bacitracin synthetase gene cluster, and transcriptional levels of genes *bacT*, *bacA*, *bacB*, and *bacC* were enhanced all under the condition of SAM addition. In addition, the transcriptional level of regulator gene *abrB* was decreased by 32.54% (Supplementary Figure S3). Since regulator *AbrB* has been proven as the negative regulator of bacitracin synthetase cluster *bacTABC* (Wang D. et al., 2017), our results suggested that additional SAM attenuated the inhibitory effect of *AbrB* on bacitracin synthase, and then improved bacitracin synthesis. Nevertheless, more work needs to be done to resolve the relationship between SAM and bacitracin synthetase.

Based on the previous researches, Met yield produced by microbial is generally at a high level (Huang et al., 2018), while SAM yield is quite low (Chu et al., 2013; Wendisch, 2019), indicating the low efficiency of SAM synthetic and transportation capabilities. Here, several SAM synthetases from *B. licheniformis*, *C. glutamicum* and *S. cerevisiae* were tested, and SAM2 from *S. cerevisiae* showed the best performances on SAM accumulation and bacitracin synthesis, consistent with the previous results of our group (Ruan et al., 2019). Along with developments of metabolic engineering and synthetic biology, various strategies have been conducted to improve SAM accumulation, including in strengthening SAM synthetic pathways (Zhang et al., 2008), coupling with TCA cycle (Ruan et al., 2019), increasing ATP level (Kanai et al., 2017), etc. In this research, the SAM synthetic and degradation pathways, Met transportation pathways were engineered to improve intracellular SAM accumulation for bacitracin production, and SAM concentration was increased to 47.53 mg/L by 1.56-fold, which led to a 28.97% increase of bacitracin yield. Based on the previous researches, the corresponding SAM transporters have been identified in *E. coli*, *Streptomyces coelicolor* etc., (Lee et al., 2012; Yang et al., 2014; Husna et al., 2018), also, the intracellular SAM concentration at 30 h was increased by 53.69% after SAM addition, suggested that

additional SAM could be imported by amino acid transporter, thus, we suggested that SAM transporter is also present in *B. licheniformis* DW2, although it has not been identified or annotated. In addition, SAM decarboxylase gene *speD* was deleted to block synthetic pathway of byproduct, meantime, based on our results, two other harmful by-products, cadaverine and putrescine (Li et al., 2019), were also decreased by 27.50 and 37.04%, due to the weakening of amino acid decarboxylase (**Figure 6C**), and this result was positively correlated with our previous research (Wu et al., 2019). Furthermore, since SAM synthetase catalyzed the formation of SAM from Met and ATP, as well as the critical role of ATP supply in physiological metabolism (Cai et al., 2018), the ATP pool of DW2-KENPND should be enhanced in our future work.

Engineering transporter has been proven as an efficiency tactic for enhancement production of metabolite. Overexpression of ABC transporter AvtAB benefited avermectin secretion, and further led to the 50% increase of avermectin production (Qiu et al., 2011). Lys transporter LysE has been overexpressed to improve Lys production in *C. glutamicum* (Dong et al., 2016). However, bacitracin transporter in *Bacillus* has not been identified until now, although much work has been done on bacitracin microbial breeding and regulation (Fang et al., 2017; Wang D. et al., 2017; Shu et al., 2018). Here, two Met transporters MetN and MetP were screened, identified and engineered for bacitracin production at the first time. Based on our results, transporter MetN acted as Met exporter and MetP functioned as Met importer, and both of them served as the critical roles in Met distribution and bacitracin synthesis. Since soybean meal contains Met (Wang Q. et al., 2017), overexpression of MetP improved the accumulation of intracellular Met, which further benefit bacitracin production. Meantime, several other amino acid transporters (YdhG, BrnQ, and LysE) have also been engineered for bacitracin production (Li et al., 2018; Zhu et al., 2018; Wu et al., 2019), indicated that engineering amino acid transporter was an efficient strategy for bacitracin production. Similar to Met transportation, several other amino acids also have multiple corresponding transporters. Such as, transporters YdhG, BrnQ, YvbW, and BraB were responsible for BCAAs transportation (Cai et al., 2019b), LysE, LysP and YvsH for lysine transportation (Wu et al., 2019), TcyP and YdeD for cysteine transportation (Ohtsu et al., 2015). The synergy of multiple transporters benefited the relative stability of intracellular and extracellular amino acids.

CONCLUSION

S-Adenosylmethionine served as the critical role in antibiotic production, however, whether it affects bacitracin synthesis is

still unknown. Here, our results confirmed that exogenous SAM addition benefited bacitracin production, and a metabolic engineered strain *B. licheniformis* DW2-KENPND was attained via rewiring SAM synthetic and degradation, Met transportation pathways. Based on our results, SAM synthetase SAM2 from *S. cerevisiae* and Met synthetase MetH from *B. licheniformis* showed the best performance on SAM accumulation and bacitracin syntheses, and Met transporters MetN and MetP were identified as Met exporter and importer in *B. licheniformis* DW2, respectively. Finally, The concentration of intracellular SAM of DW2-KENPND was 47.53 U/mL, increased by 1.56-fold compared to DW2, and bacitracin yield reached 957.53 U/mL, increased by 28.97%. Taken together, this research demonstrated that SAM served as the critical role in bacitracin synthesis, and a promising strain *B. licheniformis* DW2-KENPND was attained for industrial production of bacitracin.

DATA AVAILABILITY STATEMENT

The datasets generated for this study are available on request to the corresponding author.

AUTHOR CONTRIBUTIONS

DC and SC designed the study. DC, BZ, JZ, and HX carried out the molecular biology studies and construction of engineering strains. DC, BZ, JZ, and PL carried out the fermentation studies. DC, ZW, JL, ZY, XM, and SC analyzed the data and wrote the manuscript. All authors read and approved the final manuscript.

FUNDING

This work was supported by the National Key Research and Development Program of China (2018YFA0900300), the Technical Innovation Special Fund of Hubei Province (2018ACA149), the Natural Science Foundation of Hubei Province of China (2019CFB319), the China Postdoctoral Science Foundation (2018M642802), and the Open Funding Project of State Key Laboratory of Biocatalysis and Enzyme Engineering (SKLBEE2018005).

SUPPLEMENTARY MATERIAL

The Supplementary Material for this article can be found online at: <https://www.frontiersin.org/articles/10.3389/fbioe.2020.00305/full#supplementary-material>

REFERENCES

- Berney, M., Berney-Meyer, L., Wong, K. W., Chen, B., Chen, M., Kim, J., et al. (2015). Essential roles of methionine and S-adenosylmethionine in the autarkic lifestyle of *Mycobacterium tuberculosis*. *Proc. Natl. Acad. Sci. U.S.A.* 112, 10008–10013. doi: 10.1073/pnas.1513033112
- Birrer, G. A., Cromwick, A. M., and Gross, R. A. (1994). Gamma-poly(glutamic acid) formation by *Bacillus licheniformis* 9945a: physiological and biochemical studies. *Int. J. Biol. Macromol.* 16, 265–275. doi: 10.1016/0141-8130(94)90032-9
- Cai, D., Chen, Y., He, P., Wang, S., Mo, F., Li, X., et al. (2018). Enhanced production of Poly-gamma-glutamic acid by improving ATP supply in metabolically

- engineered *Bacillus licheniformis*. *Biotechnol. Bioeng.* 115, 2541–2553. doi: 10.1002/bit.26774
- Cai, D., Wang, H., He, P., Zhu, C., Wang, Q., Wei, X., et al. (2017). A novel strategy to improve protein secretion via overexpression of the SppA signal peptide peptidase in *Bacillus licheniformis*. *Microb. Cell Fact.* 16:70. doi: 10.1186/s12934-017-0688-7
- Cai, D., Zhang, B., Rao, Y., Li, L., Zhu, J., Li, J., et al. (2019a). Improving the utilization rate of soybean meal for efficient production of bacitracin and heterologous proteins in the aprA-deficient strain of *Bacillus licheniformis*. *Appl. Microbiol. Biotechnol.* 103, 4789–4799. doi: 10.1007/s00253-019-09804-0
- Cai, D., Zhu, J., Zhu, S., Lu, Y., Zhang, B., Lu, K., et al. (2019b). Metabolic engineering of main transcription factors in carbon, nitrogen, and phosphorus metabolisms for enhanced production of bacitracin in *Bacillus licheniformis*. *ACS Synth. Biol.* 8, 866–875. doi: 10.1021/acssynbio.9b00005
- Chen, C., Li, Y., Hu, J., Dong, X., and Wang, X. (2015). Metabolic engineering of *Corynebacterium glutamicum* ATCC13869 for L-valine production. *Metab. Eng.* 29, 66–75. doi: 10.1016/j.ymben.2015.03.004
- Chu, J., Qian, J., Zhuang, Y., Zhang, S., and Li, Y. (2013). Progress in the research of S-adenosyl-L-methionine production. *Appl. Microbiol. Biotechnol.* 97, 41–49. doi: 10.1007/s00253-012-4536-8
- Dong, X., Zhao, Y., Hu, J., Li, Y., and Wang, X. (2016). Attenuating L-lysine production by deletion of *ddh* and *lysE* and their effect on L-threonine and L-isoleucine production in *Corynebacterium glutamicum*. *Enzyme Microb. Technol.* 93–94, 70–78. doi: 10.1016/j.enzmictec.2016.07.013
- Fang, C., Nagy-Staron, A., Grafe, M., Heermann, R., Jung, K., Gebhard, S., et al. (2017). Insulation and wiring specificity of BceR-like response regulators and their target promoters in *Bacillus subtilis*. *Mol. Microbiol.* 104, 16–31. doi: 10.1111/mmi.13597
- Huang, J. F., Shen, Z. Y., Mao, Q. L., Zhang, X. M., Zhang, B., Wu, J. S., et al. (2018). Systematic analysis of bottlenecks in a multibranched and multilevel regulated pathway: the molecular fundamentals of L-methionine biosynthesis in *Escherichia coli*. *ACS Synth. Biol.* 7, 2577–2589. doi: 10.1021/acssynbio.8b00249
- Husna, A. U., Wang, N., Cobbold, S. A., Newton, H. J., Hocking, D. M., Wilksch, J. J., et al. (2018). Methionine biosynthesis and transport are functionally redundant for the growth and virulence of *Salmonella Typhimurium*. *J. Biol. Chem.* 293, 9506–9519. doi: 10.1074/jbc.RA118.002592
- Kana, M., Mizunuma, M., Fujii, T., and Iefuji, H. (2017). A genetic method to enhance the accumulation of S-adenosylmethionine in yeast. *Appl. Microbiol. Biotechnol.* 101, 1351–1357. doi: 10.1007/s00253-017-8098-7
- Kim, D. J., Huh, J. H., Yang, Y. Y., Kang, C. M., Lee, I. H., Hyun, C. G., et al. (2003). Accumulation of S-adenosyl-L-methionine enhances production of actinorhodin but inhibits sporulation in *Streptomyces lividans* TK23. *J. Bacteriol.* 185, 592–600. doi: 10.1128/jb.185.2.592-600.2003
- Lee, S. K., Mo, S., and Suh, J. W. (2012). An ABC transporter complex containing S-adenosylmethionine (SAM)-induced ATP-binding protein is involved in antibiotics production and SAM signaling in *Streptomyces coelicolor* M145. *Biotechnol. Lett.* 34, 1907–1914. doi: 10.1007/s10529-012-0987-3
- Li, L., Zou, D., Ruan, L., Wen, Z., Chen, S., Xu, L., et al. (2019). Evaluation of the biogenic amines and microbial contribution in traditional Chinese sausages. *Front. Microbiol.* 10:872. doi: 10.3389/fmicb.2019.00872
- Li, M., Chen, Z., Zhang, X., Song, Y., Wen, Y., and Li, J. (2010). Enhancement of avermectin and ivermectin production by overexpression of the maltose ATP-binding cassette transporter in *Streptomyces avermitilis*. *Bioresour. Technol.* 101, 9228–9235. doi: 10.1016/j.biortech.2010.06.132
- Li, Y., Wu, F., Cai, D., Zhan, Y., Li, J., Chen, X., et al. (2018). [Enhanced production of bacitracin by knocking out of amino acid permease gene *yhdG* in *Bacillus licheniformis* DW2]. *Sheng Wu Gong Cheng Xue Bao* 34, 916–927. doi: 10.13345/j.cjb.170500
- Liu, J., Chen, Y., Wang, W., Ren, M., Wu, P., Wang, Y., et al. (2017). Engineering of an Lrp family regulator *SACE_Lrp* improves erythromycin production in *Saccharopolyspora erythraea*. *Metab. Eng.* 39, 29–37. doi: 10.1016/j.ymben.2016.10.012
- Martin, J. F., Rodriguez-Garcia, A., and Liras, P. (2017). The master regulator PhoP coordinates phosphate and nitrogen metabolism, respiration, cell differentiation and antibiotic biosynthesis: comparison in *Streptomyces coelicolor* and *Streptomyces avermitilis*. *J. Antibiot.* 70, 534–541. doi: 10.1038/ja.2017.19
- Mendes, M. V., Tunca, S., Anton, N., Recio, E., Sola-Landa, A., Aparicio, J. F., et al. (2007). The two-component *phoR-phoP* system of *Streptomyces natalensis*: inactivation or deletion of *phoP* reduces the negative phosphate regulation of pimaricin biosynthesis. *Metab. Eng.* 9, 217–227. doi: 10.1016/j.ymben.2006.10.003
- Ohtsu, I., Kawano, Y., Suzuki, M., Morigasaki, S., Saiki, K., Yamazaki, S., et al. (2015). Uptake of L-cystine via an ABC transporter contributes defense of oxidative stress in the L-cystine export-dependent manner in *Escherichia coli*. *PLoS One* 10:e0120619. doi: 10.1371/journal.pone.0120619
- Pang, A. P., Du, L., Lin, C. Y., Qiao, J., and Zhao, G. R. (2015). Co-overexpression of *lmbW* and *metK* led to increased lincomycin A production and decreased byproduct lincomycin B content in an industrial strain of *Streptomyces lincolnensis*. *J. Appl. Microbiol.* 119, 1064–1074. doi: 10.1111/jam.12919
- Qiu, J., Zhuo, Y., Zhu, D., Zhou, X., Zhang, L., Bai, L., et al. (2011). Overexpression of the ABC transporter AvtAB increases avermectin production in *Streptomyces avermitilis*. *Appl. Microbiol. Biotechnol.* 92, 337–345. doi: 10.1007/s00253-011-3439-4
- Rietkotter, E., Hoyer, D., and Mascher, T. (2008). Bacitracin sensing in *Bacillus subtilis*. *Mol. Microbiol.* 68, 768–785. doi: 10.1111/j.1365-2958.2008.06194.x
- Ruan, L., Li, L., Zou, D., Jiang, C., Wen, Z., Chen, S., et al. (2019). Metabolic engineering of *Bacillus amyloliquefaciens* for enhanced production of S-adenosylmethionine by coupling of an engineered S-adenosylmethionine pathway and the tricarboxylic acid cycle. *Biotechnol. Biofuels* 12:211. doi: 10.1186/s13068-019-1554-0
- Shi, J., Zhan, Y., Zhou, M., He, M., Wang, Q., Li, X., et al. (2019). High-level production of short branched-chain fatty acids from waste materials by genetically modified *Bacillus licheniformis*. *Bioresour. Technol.* 271, 325–331. doi: 10.1016/j.biortech.2018.08.134
- Shu, C. C., Wang, D., Guo, J., Song, J., Chen, S., Chen, L., et al. (2018). Analyzing AbrB-knockout effects through genome and transcriptome sequencing of *Bacillus licheniformis* DW2. *Front. Microbiol.* 9:307. doi: 10.3389/fmicb.2018.00307
- Sola-Landa, A., Moura, R. S., and Martin, J. F. (2003). The two-component PhoR-PhoP system controls both primary metabolism and secondary metabolite biosynthesis in *Streptomyces lividans*. *Proc. Natl. Acad. Sci. U.S.A.* 100, 6133–6138. doi: 10.1073/pnas.0931429100
- Tian, P., Cao, P., Hu, D., Wang, D., Zhang, J., Wang, L., et al. (2017). Comparative metabolomics reveals the mechanism of avermectin production enhancement by S-adenosylmethionine. *J. Ind. Microbiol. Biotechnol.* 44, 595–604. doi: 10.1007/s10295-016-1883-y
- Wang, D., Wang, Q., Qiu, Y., Nomura, C. T., Li, J., and Chen, S. (2017). Untangling the transcription regulatory network of the bacitracin synthase operon in *Bacillus licheniformis* DW2. *Res. Microbiol.* 168, 515–523. doi: 10.1016/j.resmic.2017.02.010
- Wang, Q., Zheng, H., Wan, X., Huang, H., Li, J., Nomura, C. T., et al. (2017). Optimization of inexpensive agricultural by-products as raw materials for bacitracin production in *Bacillus licheniformis* DW2. *Appl. Biochem. Biotechnol.* 183, 1146–1157. doi: 10.1007/s12010-017-2489-1
- Wang, M., Yu, H., and Shen, Z. (2019). Antisense RNA-based strategy for enhancing surfactin production in *Bacillus subtilis* TS1726 via overexpression of the unconventional biotin carboxylase II to enhance ACCase activity. *ACS Synth. Biol.* 8, 251–256. doi: 10.1021/acssynbio.8b00459
- Wang, Y., Wang, Y., Chu, J., Zhuang, Y., Zhang, L., and Zhang, S. (2007). Improved production of erythromycin A by expression of a heterologous gene encoding S-adenosylmethionine synthetase. *Appl. Microbiol. Biotechnol.* 75, 837–842. doi: 10.1007/s00253-007-0894-z
- Wendisch, V. F. (2019). Metabolic engineering advances and prospects for amino acid production. *Metab. Eng.* 58, 17–34. doi: 10.1016/j.ymben.2019.03.008
- Wohlleben, W., Mast, Y., Muth, G., Rottgen, M., Stegmann, E., and Weber, T. (2012). Synthetic biology of secondary metabolite biosynthesis in actinomycetes: engineering precursor supply as a way to optimize antibiotic production. *FEBS Lett.* 586, 2171–2176. doi: 10.1016/j.febslet.2012.04.025
- Wu, F., Cai, D., Li, L., Li, Y., Yang, H., Li, J., et al. (2019). Modular metabolic engineering of lysine supply for enhanced production of bacitracin in *Bacillus licheniformis*. *Appl. Microbiol. Biotechnol.* 103, 8799–8812. doi: 10.1007/s00253-019-10110-y
- Xu, Y., Tan, G., Ke, M., Li, J., Tang, Y., Meng, S., et al. (2018). Enhanced lincomycin production by co-overexpression of *metK1* and *metK2* in *Streptomyces*

- lincolnensis*. *J. Ind. Microbiol. Biotechnol.* 45, 345–355. doi: 10.1007/s10295-018-2029-1
- Yang, J., Sun, B., Huang, H., Jiang, Y., Diao, L., Chen, B., et al. (2014). High-efficiency scarless genetic modification in *Escherichia coli* by using lambda red recombination and I-SceI cleavage. *Appl. Environ. Microbiol.* 80, 3826–3834. doi: 10.1128/AEM.00313-14
- Yu, W., Li, D., Jia, S., Liu, Z., Nomura, C. T., Li, J., et al. (2019). Systematic metabolic pathway modification to boost L-ornithine supply for bacitracin production in *Bacillus licheniformis* DW2. *Appl. Microbiol. Biotechnol.* 103, 8383–8392. doi: 10.1007/s00253-019-10107-7
- Zhang, X., Fen, M., Shi, X., Bai, L., and Zhou, P. (2008). Overexpression of yeast S-adenosylmethionine synthetase *metK* in *Streptomyces actuosus* leads to increased production of nosiheptide. *Appl. Microbiol. Biotechnol.* 78, 991–995. doi: 10.1007/s00253-008-1394-5
- Zhao, X. Q., Gust, B., and Heide, L. (2010). S-Adenosylmethionine (SAM) and antibiotic biosynthesis: effect of external addition of SAM and of overexpression of SAM biosynthesis genes on novobiocin production in *Streptomyces*. *Arch. Microbiol.* 192, 289–297. doi: 10.1007/s00203-010-0548-x
- Zhou, S., Ding, R., Chen, J., Du, G., Li, H., and Zhou, J. (2017). Obtaining a panel of cascade promoter-5'-UTR complexes in *Escherichia coli*. *ACS Synth. Biol.* 6, 1065–1075. doi: 10.1021/acssynbio.7b00006
- Zhu, J., Cai, D., Xu, H., Liu, Z., Zhang, B., Wu, F., et al. (2018). Enhancement of precursor amino acid supplies for improving bacitracin production by activation of branched chain amino acid transporter BrnQ and deletion of its regulator gene *lrp* in *Bacillus licheniformis*. *Synth. Syst. Biotechnol.* 3, 236–243. doi: 10.1016/j.synbio.2018.10.009
- Zhu, S., Cai, D., Liu, Z., Zhang, B., Li, J., Chen, S., et al. (2019). Enhancement of bacitracin production by NADPH generation via overexpressing glucose-6-phosphate dehydrogenase *Zwf* in *Bacillus licheniformis*. *Appl. Biochem. Biotechnol.* 187, 1502–1514. doi: 10.1007/s12010-018-2894-0

Conflict of Interest: JL was employed by Lifecome Biochemistry Co., Ltd., in China.

The remaining authors declare that the research was conducted in the absence of any commercial or financial relationships that could be constructed as a potential conflict of interest.

Copyright © 2020 Cai, Zhang, Zhu, Xu, Liu, Wang, Li, Yang, Ma and Chen. This is an open-access article distributed under the terms of the Creative Commons Attribution License (CC BY). The use, distribution or reproduction in other forums is permitted, provided the original author(s) and the copyright owner(s) are credited and that the original publication in this journal is cited, in accordance with accepted academic practice. No use, distribution or reproduction is permitted which does not comply with these terms.



Production of Terpenoids by Synthetic Biology Approaches

Caizhe Zhang and Kui Hong*

Key Laboratory of Combinatorial Biosynthesis and Drug Discovery, Ministry of Education, School of Pharmaceutical Sciences, Wuhan University, Wuhan, China

OPEN ACCESS

Edited by:

Shihui Yang,
Hubei University, China

Reviewed by:

Jifeng Yuan,
Xiamen University, China
Zhihua Zhou,
Shanghai Institutes for Biological
Sciences (CAS), China
Lee Seung-Goo,
Korea Research Institute
of Bioscience and Biotechnology
(KRIBB), South Korea

*Correspondence:

Kui Hong
kuihong31@whu.edu.cn

Specialty section:

This article was submitted to
Synthetic Biology,
a section of the journal
Frontiers in Bioengineering and
Biotechnology

Received: 21 December 2019

Accepted: 30 March 2020

Published: 24 April 2020

Citation:

Zhang C and Hong K (2020)
Production of Terpenoids by Synthetic
Biology Approaches.
Front. Bioeng. Biotechnol. 8:347.
doi: 10.3389/fbioe.2020.00347

Terpenoids are a large family of natural products with remarkable diverse biological functions, and have a wide range of applications as pharmaceuticals, flavors, pigments, and biofuels. Synthetic biology is presenting possibilities for sustainable and efficient production of high value-added terpenoids in engineered microbial cell factories, using *Escherichia coli* and *Saccharomyces cerevisiae* which are identified as well-known industrial workhorses. They also provide a promising alternative to produce non-native terpenes on account of available genetic tools in metabolic engineering and genome editing. In this review, we summarize the recent development in terpenoids production by synthetic biology approaches.

Keywords: terpenoids, synthetic biology, metabolic engineering, *Escherichia coli*, *Saccharomyces cerevisiae*

INTRODUCTION

Terpenoids, also known as terpenes or isoprenoids, are a large family of natural products. More than 80,000 different terpenoids have been found in almost all life forms. Structural diversity of terpenoids makes them a wide range of applications as pharmaceutical, biofuels, and flavors. The skeletons of terpenoids are derived by condensation of multiple units of isopentenyl diphosphate (IPP) and its isomer dimethylallyl diphosphate (DMAPP), which are naturally generated by either mevalonate (MVA) pathway in eukaryotes and methylerythritol-phosphate (MEP) pathway in prokaryotes and plant plastids. In addition to these natural routes, synthetic routes for non-natural precursors have also been reported (Kang et al., 2016; Chatzivasileiou et al., 2019; Clomburg et al., 2019). Core structures of terpenes are then post-modified by cytochromes P450s (P450s) that play a vital role in endowing various bioactivities to terpenoids.

Production of terpenoids from natural resources may encounter technical challenges. For instance, ginsenoside Rh2, a potent candidate for cancer therapy, is a triterpenoid saponin derived from *Panax* species (Wong et al., 2015). Its content in dried *Panax* ginseng roots is less than 0.01% (Wang et al., 2019). Using the synthetic biology approach in engineered yeast, the yield of ginsenoside Rh2 has reached 2.25 g/L in fed-batch fermentation (Wang et al., 2019). This result provides an excellent case for improving cell factories to produce plant rare natural products. The rapid advances in synthetic biology suggest an alternative sustainable approach to achieve the industrial scale of terpenoids production (Bian et al., 2017; Clomburg et al., 2017; Wang et al., 2018). However, several significant challenges remain in microbial biosynthesis as a general approach for the supply of valuable terpenoids, including (i) the biological parts for genetic circuits construction have not been sufficiently characterized; (ii) the post-modifications of terpenoids remains inefficient; and (iii) the toxic accumulation of intermediate products and insufficient supply of precursors. Therefore, a platform that can provide available genetic tools and a comprehensive understanding of its metabolism is urgently needed. In this purpose, *Escherichia*

coli and *Saccharomyces cerevisiae* have been used as ideal platform hosts for various creative explorations (Table 1). In this review, we focus on recently developed strategies specific to address challenges that in the pathway efficiencies optimization, gene circuits construction and regulation, pathway programing, subcellular engineering and co-culture strategy of terpenoids biosynthesis using synthetic biology approaches.

GENETIC CIRCUITS AND DYNAMIC CONTROL

As the basic genetic elements of biosynthetic pathways, biological parts (e.g., promoter, terminator, ribosome-binding site (RBS), regulatory protein, etc.) should be well-characterized and optimized for synthetic biology. Constitutive or inducible promoters with different strengths are always the major theme in synthetic biology. Their efficiency are also affected by the combination of terminators and RBS.

Comparing to constitutive promoters, inducible promoters possess a strong capacity to start gene expression only under specific culture conditions. For example, the glucose-sensing promoter *HXT1*(*P_{HXT1}*) is strong at high glucose concentrations and weak at low glucose concentrations. Using glucose-responsive promoters also avoids the need for expensive repressors or inducers (Scalcinati et al., 2012; Xie et al., 2015; Zhao et al., 2017; Cheng et al., 2019). By using *P_{HXT1}*, the competing gene farnesyl diphosphate synthase (*ERG20*) for the consumption of precursors IPP and DMAPP was inhibited, and the carbon flux was reallocated from the growth pathway to the limonene synthetic pathway, and the limonene titer reached 917.7 mg/L in fed-batch fermentation (Cheng et al., 2019). When each of MVA pathway enzymes was transcribed from high-expression galactose-regulated promoters (*P_{GAL1}* or *P_{GAL10}*), an amorpho-4,11-diene yield of more than 40 g/L was resulted (Westfall et al., 2012). FPP (farnesyl diphosphate) is the intermediate of MVA pathway, but exhibits toxicity when it accumulates in *E. coli* (Martin et al., 2003). Whole-genome transcript arrays identified an FPP-responsive promoter answering to the accumulation of FPP (Dahl et al., 2013). Using IPP/FPP-responsive promoter in *E. coli*, Shen et al. (2016) coordinated the expression of all genes of the MVA pathway from *S. cerevisiae* using the tunable intergenic regions to increase the availability of FPP. The dynamically regulated MVA pathway prevented the toxic accumulation of IPP/FPP, and the titer of zeaxanthin reached 722.46 mg/L in fed-batch fermentation (Supplementary Figure S1A). *P_{ERG1}* represents an ergosterol-sensitive promoter, was shown to restrict squalene synthase (*ERG9*) expression levels efficiently (Yuan and Ching, 2015). Callari et al. (2018) replaced the promoter regions of *ERG20* and *ERG9* with *P_{HXT1}* and *P_{ERG1}* to redirect the flux from FPP and sterols, generated a titer of 108.5 mg/L of casbene.

Clustered regularly interspaced short palindromic repeats interference (CRISPRi) uses a catalytically-inactive Cas9 protein (dCas9) and a single guide RNA (gRNA) to repress the expression of targeted genes by blocking transcription (Qi et al., 2013). Kim et al. (2016) established a dynamic regulation CRISPRi

system to coordinate the metabolic flux between cell growth and IPP/DMAPP accumulation. An L-rhamnose-inducible promoter was used to control the expression of dCas9. During the production phase, L-rhamnose was removed to restore gene expression, and the production of lycopene and α -bisabolol increased. Lian et al. (2017) developed a CRISPR-AID system using three orthogonal CRISPR proteins combines. When *HMG1* was overexpressed, down-regulation of *ERG9* and deletion of *ROX1* could significantly increase the production of β -carotene in *S. cerevisiae*. These genes were chosen as the targets for CRISPRa (transcriptional activation), CRISPRi, and CRISPRd (gene deletion), respectively (Supplementary Figure S1B).

The modular pathway engineering group multiple genes into modules to reduce regulatory complexities and help to unlock the potential of the multi-gene pathway for the production of terpenoid products (Ajikumar et al., 2010; Supplementary Figure S1C). Keasling's group tuned the expression of multiple genes within operons by generating libraries of tunable intergenic regions and balancing the expression of MVA pathway, which resulted in a 7-fold increase in mevalonate production (Pfleger et al., 2006). Zhang et al. (2018b) reported a multidimensional heuristic process for astaxanthin production. Astaxanthin biosynthesis pathway was grouped into four modules, that each module controlled by different promoter of pre-determined strength, and get a yield of 320 mg/L in *E. coli*. Through screening of combinations of promoters and terminators, valencene synthase expression cassette was optimized to reach a titer of 539.3 mg/L (Chen et al., 2019). When Shukal et al. (2019) introduced viridiflorol synthase (VS) from *Agrocybe aegerita* to *E. coli*, three T7 promoter variants were characterized for different pathway expression, and RBS libraries that covered a broad range of translational initiation rates were optimized. The yield of viridiflorol was increased to 25.7 g/L in fed-batch fermentation.

PATHWAY ENZYME DESIGN

Directed evolution and rational protein design have been used to engineer enzymes in heterologous pathways (Eriksen et al., 2014; Niu et al., 2018; Hong et al., 2019; Supplementary Figure S1E). Monoterpenes are synthesized from geranyl diphosphate (GPP), which is also the precursor for the biosynthesis of FPP. Therefore, preventing the consumption of GPP by restricting FPP formation is profitable to produce monoterpenes. Mendez-Perez et al. (2017) introduced a mutation (Ser81 to Phe) in native FPP synthase of *E. coli*, resulting in an enzyme that preferentially synthesizes GPP instead of FPP, and the engineered strains yielded 653 mg/L of 1,8-cineole and 505 mg/L of linalool, which are 30- and 5-fold improvement, respectively. Jiang et al. (2017) demonstrated that two essential amino acid residues Y436 and D501 located in active pocket of the key enzyme geraniol synthase are critical for the key step of dephosphorylation. By overexpression of truncated 3-hydroxy-3-methylglutaryl-coenzyme reductase (tHMGR) and isopentenyl diphosphate isomerase (IDI), the highest titer of 1.68 g/L geraniol was achieved in fed-batch fermentation in *S. cerevisiae*.

TABLE 1 | Strategies for production of various terpenoids in *S. cerevisiae* and *E. coli*

Product	Strategy and features	Culture conditions	Titer or Improvement	References
<i>S. cerevisiae</i>				
8-hydroxygeraniol	Mitochondrial compartmentalization by targeting the geraniol biosynthetic pathway to the mitochondria	Fed-batch fermentation	227 mg/L	Yee et al., 2019
Geraniol	Protein structure analysis, site-directed mutation, overexpression of tHMGR and IDI	Fed-batch fermentation	1.68 g/L	Jiang et al., 2017
Limonene	Regulation of ERG20 by P _{HXT1} promoter (glucose-sensitive)	Fed-batch fermentation	917.7 mg/L 6-fold	Cheng et al., 2019
	N-degron-mediated destabilization of ERG20	Batch fermentation	76 mg/L	Peng et al., 2018
Amorpha-4,11-diene	Optimization of [NADPH]/[NADP ⁺] ratios by introducing mutations into phosphofructokinase (PFK) along with overexpression of ZWF1	Shake flasks	497 mg/L	Kwak et al., 2019
	Mitochondria compartmentalization by targeting the whole FPP pathway together with Amorpha-4,11-diene synthase (ADS) into mitochondria	Shake flasks	427 mg/L	Yuan and Ching, 2016
Zerumbone	Regulation of ERG9 by P _{HXT1} promoter	Fed-batch fermentation	40 mg/L	Zhang et al., 2018a
Farnesene	Increase the availability of acetyl-CoA by removing the native source of cytosolic acetyl-CoA ($\Delta RHR2$) and overexpressing xPK, PTA, ADA and NADH-HMGr	Fed-batch fermentation	2.24 g/L/h > 130 g/L	Meadows et al., 2016
Oxygenated taxanes	<i>E. coli</i> - <i>S. cerevisiae</i> co-culture by dividing the synthetic pathway for the acetylated diol paclitaxel precursor into two modules	Co-culture in bioreactor	33 mg/L	Zhou et al., 2015
Nerolidol	Minimizing competition for FPP by destabilizing squalene synthase, degrade ER membrane-integrating protein.	Two-phase flask	4–5.5 g/L	Peng et al., 2017
Casbene	Regulation of ERG20 and ERG9 by P _{HXT1} and P _{ERG1} promoters	Deepwell microplate	108.5 mg/L	Callari et al., 2018
Jolkinol C	Optimize soluble expression of Cbsp using protein tagging strategies, codon-optimization of CYPs	Milliliter plates	800 mg/L	Wong et al., 2018
Carotenoid	Colorimetric-based promoter strength comparison system; inducer/repressor-free sequential control strategy by combining a modified GAL regulation system and a P _{HXT1} -controlled squalene synthetic pathway	Fed-batch fermentation	1156 mg/L	Xie et al., 2015
Lycopene	Lipid engineering; Improve triacylglycerol metabolism	Fed-batch fermentation	2.37 g/L	Ma et al., 2019
	Scaffold-free enzyme assemblies (IDI and CrTE);	Fed-batch fermentation	2.3 g/L	Kang W. et al., 2019
Medicagenic acid	Endoplasmic reticulum (ER) engineering; expand the ER by disrupting the phosphatidic acid phosphatase	Tube cultures	27.1 mg/L 6-fold	Arendt et al., 2017
β -Carotene	Tri-functional CRISPR system combines transcriptional activation, transcriptional interference, and gene deletion	Tube cultures	2.8-fold	Lian et al., 2017
Squalene	ER engineering; expand the ER by overexpressing a key ER size regulatory factor, INO2.	Shake flasks	634 mg/L	Kim J.E. et al., 2019
<i>E. coli</i>				
Total monoterpenoids	Non-natural route to isoprenoid biosynthesis (isoprenoid alcohol pathway/IPA)	Shake flasks	0.6 g/L	Clomburg et al., 2019
Pinene	Adaptive laboratory evolution for improving pinene tolerance; <i>E. coli</i> co-culture system; whole-cell biocatalysis	Shake flasks	166.5 mg/L	Niu et al., 2018
	Cell-free enzyme systems for production of monoterpenes from glucose	Glass vials	14.9 g/L	Korman et al., 2017
Limonene	Cell-free enzyme systems	Glass vials	12.5 g/L	Korman et al., 2017

(Continued)

TABLE 1 | Continued

Product	Strategy and features	Culture conditions	Titer or Improvement	References
Geranyl acetate	Two-phase system; convert monoterpenoid geraniol to its acetyl ester to avoid geraniol toxicity	Fed-batch fermentation	4.8 g/L	Chacón et al., 2019
Viridiflorol	Promoters and RBSs engineering	Fed-batch fermentation	25.7 g/L	Shukal et al., 2019
α-Bisabolol	CRISPRi-guided balancing of MVA pathway	Shake flasks	25 mg/L	Kim et al., 2016
	FPP-resistant mevalonate kinase 1; lower MVA pathway; Optimization of inducer concentration, aeration and enzymatic cofactor	Fed-batch fermentation	8.5 g/L	Kim S. et al., 2019
Oxygenated taxanes	Modular engineering (MEP, cyclase, and P450 module), promoters engineering	Fed-batch fermentation	570 mg/L	Biggs et al., 2016
Longifolene	Codon optimization of longifolene synthase, investigate into different FPP synthases	Fed-batch fermentation	382 mg/L	Cao et al., 2019
Ophiobolin F	Ophiobolin synthase with SUMO tag; phylogenetics based mutation	Shake flasks	150.5 mg/L	Yuan et al., 2019
Carotenoids	Scaffold-free enzyme assemblies (IDI and CrtE)	Fed-batch fermentation	276.3 mg/L 5.7-fold	Kang A. et al., 2019
Astaxanthin	Promoters and RBSs engineering; multidimensional heuristic process (MHP)	Fed-batch fermentation	320 mg/L	Zhang et al., 2018b
	CRISPR-mediated morphology and oxidative stress engineering	Shake flasks	11.92 mg/g DCW	Lu and Liu, 2019
Zeaxanthin	Dynamic control of MVA pathway by IPP/FPP-responsive promoter.	Fed-batch fermentation	722.46 mg/L	Shen et al., 2016
Lycopene	CRISPRi-guided balancing of MVA pathway	Shake flasks	71.4 mg/L	Kim et al., 2016
	Optimization of the lycopene biosynthetic; Overexpressing the MEP pathway	Shake flasks	448 mg/g DCW	Coussement et al., 2017

Protein tagging strategies are effective means for enzyme engineering. A truncated gene encoding casebene synthase from *Jatropha curcas* with various protein tags was integrated into a geranylgeranyl diphosphate (GGPP)-producing strain, which yields 160 mg/L of casbene (Wong et al., 2018). Using a small ubiquitin-like modifier (SUMO) fusion tag and phylogenetics based mutations, ophiobolin synthase solubility and activity were improved. The yield of sesterterpene ophiobolin F was increased to 150.51 mg/L in *E. coli* (Yuan et al., 2019). Endoplasmic reticulum-associated protein degradation decreased cellular levels of ERG9, and increased the titer of sesquiterpene nerolidol to 100 mg/L (Peng et al., 2017). Also, N-degron-mediated destabilization of ERG20 improved the production of monoterpenes of 18 mg/L linalool or 76 mg/L limonene in *S. cerevisiae* (Peng et al., 2018). To decrease the concentration of pivotal enzyme, a synthetic degradation has been established based on *Mesoplasma florum* tmRNA system (Cameron and Collins, 2014). Based on the CRISPRi and the N-end rule for protein stability, Martínez et al. (2017) described a genome editing approach by changing the rates of both RNA synthesis and protein degradation. Synthetic protein scaffolds provide precise control of metabolic flux by preventing the loss of intermediates to diffusion or competing pathways (Dueber et al., 2009). However, scaffolded enzyme assemblies have different limitations, as enzymes fused in large structures may encounter a decrease or complete loss of the activity (Jia et al., 2014). Recently, Kang W. et al. (2019) developed a scaffold-free modular enzyme assembly by employing a pair of short peptide tags. The GGPP synthase and IDI were modularly assembled, which increased carotenoid production by 5.7-folds in *E. coli* and yielded a titer of 2.3 g/L lycopene in *S. cerevisiae*.

REPROGRAMING AND DESIGN NEW PRECURSOR BIOSYNTHETIC PATHWAYS

High intracellular levels of the essential intermediate IPP, may cause growth inhibition, reduce cell viability and plasmid instability (Martin et al., 2003; George et al., 2014, 2018). To explore more efficient and practical terpenoids biosynthetic pathways, non-natural pathways were developed. Kang et al. reported an alternative IPP-bypass MVA pathway by utilizing promiscuous activities of phosphomevalonate decarboxylase and an *E. coli* endogenous phosphatase, which successfully decoupled isopentenol production from IPP generation, and remarkably improved isoprenol titer to 3.7 g/L in batch cultures (Kang et al., 2016; Kang A. et al., 2019). Clomburg et al. (2019) constructed an isoprenoid alcohol pathway (IPA) for terpenoids synthesis, which could convert isoprenoid precursors through a minimal number of steps, and less ATP consumption. Chatzivasileiou et al. (2019) established an isopentenol utilization pathway (IUP) for bioconversion of isopentenols, isoprenol, or prenol to IPP or DMAPP. The IUP is composed of choline kinase (from *S. cerevisiae*), isopentenyl phosphate kinase, and isopentenyl-pyrophosphate delta isomerase and requires ATP as its sole

co-factor, whereas much more straightforward than the current MVA or MEP alternatives.

Acetyl-CoA is also the critical branch-point precursor for terpenoids biosynthesis. However, in *S. cerevisiae*, acetyl-CoA is compartmentalized that mainly derived from pyruvate in mitochondria and fatty acids degradation in the peroxisome (Hammer and Avalos, 2017). Meadows et al. (2016) rewired the central carbon metabolism of *S. cerevisiae* to improve redox balance and enable biosynthesis of cytosolic acetyl-CoA with a reduced ATP requirement. The engineered strains produced 25% more farnesene while requiring 75% less oxygen, and sustaining stable yield for 2 weeks that reaches >130 g/L farnesene. This system has provided a reference for all terpenoids and other acetyl-CoA-derived compounds. Lu et al. (2019) constructed a synthetic acetyl-CoA pathway, in which, the catalytic activity of glyceraldehyde synthase was improved by directed evolution. Then the acetyl-phosphate synthase was selected based on the phylogenetic tree of PKs, which converts glyceraldehyde into acetyl-phosphate (AcP). AcP could be used to generate acetyl-CoA by the phosphate acetyltransferase. It is the shortest pathway from formaldehyde to acetyl-CoA.

In *S. cerevisiae*, NADPH production highly depends on the oxidative pentose phosphate pathway (Minard and McAlister-Henn, 2005). Kwak et al. (2019) engineered mutated phosphofructokinase (PFK) along with overexpression of glucose-6-phosphate dehydrogenase to reduce glycolytic metabolic fluxes, resulted in substantial increases of [NADPH]/[NADP⁺] ratios. Moreover, amorpha-4,11-diene was overproduced in *S. cerevisiae* achieved a titer of 497 mg/L with a 3.7-fold increase compared to the parental strain.

SUBCELLULAR ENGINEERING AND CELL FREE SYSTEM

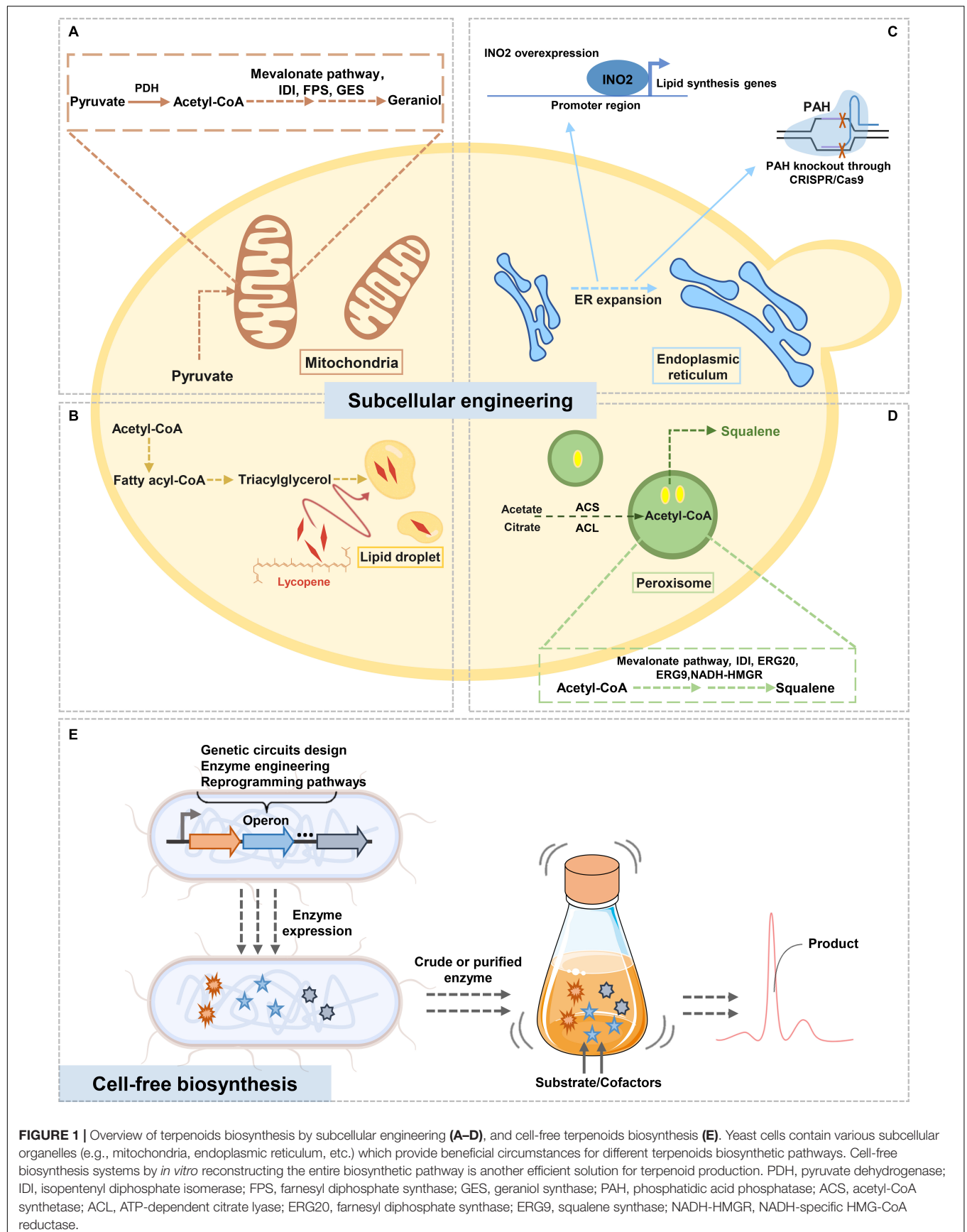
Compared with cytosol, mitochondria provide a compartmentalized environment with higher reducing redox potential. There is a growing interest in utilizing the acetyl-CoA pool in mitochondria for the biosynthesis of value-added compounds. By transplanting the whole FPP pathway together with amorpha-4,11-diene synthase into yeast mitochondria, the yield of amorpha-4,11-diene in engineered strain reached 427 mg/L (Yuan and Ching, 2016). Yee et al. (2019) targeted the geraniol biosynthetic pathway to the *S. cerevisiae* mitochondria to protect the GPP pool from consumption by the cytosolic ergosterol pathway. The production of geraniol in mitochondrial was 6-fold increase compared to cytosolic producing strains (Figure 1A). Lipid droplets (LDs) are ubiquitous organelles that store metabolic energy in the form of neutral lipids. Ma et al. (2019) established a lipophilic lycopene production strategy in *S. cerevisiae* by using LDs accumulation. A non-oleaginous *S. cerevisiae* for triacylglycerols production was combined with their composition adjustment and LDs size regulation. Therefore, lycopene accumulated continuously to 2.37 g/L in 5 days (Figure 1B). Expansion of the endoplasmic reticulum (ER) could increase yeast metabolic capacity. Arendt et al. (2017) reported that the disruption of the phosphatidic acid

phosphatase (PAH) resulted in the expansion of the ER, which stimulated the production of triterpene biosynthesis enzymes and increased triterpenoid and triterpene saponin accumulation. Kim J.E. et al. (2019) engineered *S. cerevisiae* to expand the ER by overexpressing a key ER size regulatory factor, INO2. The production of squalene was increased by 71-fold, with the titer of 634 mg/L in shake flask fermentation (Figure 1C). Liu et al. (2020) compartmentalized yeast peroxisome as a subcellular factory for squalene biosynthesis. Hybridization of the cytoplasm- and peroxisome-engineered strains was constructed, and squalene with a titer of 11.0 g/L was reached in two-stage fed-batch fermentation (Figure 1D).

On the other hand, cell free biosynthesis (CFB) systems are easy to use multiple enzyme pathways sourced from various organisms, and also overcome the challenges of precursor supply and products toxicity. The purified enzyme system and crude cell extract system are common application forms of CFB systems (Dudley et al., 2015; Li et al., 2018; Figure 1E). CFB systems designed by Korman et al. (2017) converted glucose into monoterpenes and can be self-sustaining for long periods. The platform contains 27 enzymes and using glycolysis reconstituted to generates both ATP, NADPH, and acetyl-CoA, resulting in the production of 12.5 g/L limonene and 14.9 g/L pinene. In addition, CFB systems provide great flexibility for biochemical pathways study. Chen et al. (2017) utilized *in vitro* metabolic engineering to reveal the regulatory network of a reconstituted amorpha-4,11-diene synthetic pathway, and identified the inhibition of ATP on both FPP synthase and amorpha-4,11-diene synthase.

CYTOCHROMES P450 AND POST-MODIFICATIONS OF TERPENOID

Cytochromes P450 (P450s) play a crucial role in yielding final terpenoid products with wide chemical diversity and bioactivities. *S. cerevisiae* is a favored host for expressing P450s on account of advanced protein expression mechanism, abundant intracellular membranes and the inherent benefits of large-scale microbial fermentation (Paddon et al., 2013; Gold et al., 2018; Wong et al., 2018; Zhang et al., 2018a). It is generally deemed that the ability to express soluble P450s in *E. coli* is limited. The main challenge is the lack of an endomembrane system for attachment of the eukaryotic P450s, as they have a helical hydrophobic transmembrane domain containing 20–30 amino acid residues at their N-terminal ends. Transmembrane domain truncation and N-terminal replacement are vastly used for heterologous expression of eukaryotic P450s. Ichinose and Wariishi (2013) performed extensive heterologous expression of fungal P450s in *E. coli* using 304 of P450 isoforms and identified N-terminal amino acid sequences that can significantly improve chimeric P450s expression levels. They revealed that the choice of combinations of N-terminal and catalytic domains is critical for high-level expression. Biggs et al. (2016) demonstrated *E. coli* could be a feasible host for P450-mediated terpenoid biosynthesis. In their study, the first module, “MEP,” was comprised of the rate-limiting enzymes of the IPP-producing MEP pathway. The second “cyclase” module was comprised of



taxadiene synthase (TxS) and GGPP synthase. The relatively low expression of a five-copy plasmid with a weak promoter was essential for P450 and CPR functionality. Besides, with reductase partner interactions and N-terminal modifications, a record yield of 570 mg/L of oxygenated taxanes was achieved in *E. coli*.

The important post-modifications of terpenoids also include hydroxylation by P450s and glycosylation by glycosyltransferases. Gold et al. (2018) showed a platform for the production of steviol glucosides (SGs) in *S. cerevisiae*. Two P450s of kaurene oxidase (KO) and kaurenoic acid hydroxylase (KAH) are required in succession in the conversion of kaurene into steviol. By optimizing the copy number modulation of KO-KAH-CPR combinations, the conversion was maximized. Wang et al. (2015, 2019) established a series of cell factories to produce ginsenoside Rh2 by optimizing UDP-glycosyltransferase bioparts expression. Combined with precursor (protopanaxadiol) supply optimization, the titer of ginsenoside Rh2 reached 2.25 g/L in fed-batch fermentation.

CO-CULTURE OF ENGINEERED STRAINS

A newly approach of co-culture engineering to enhance terpenoids production was developed. In some conditions, a single host cell cannot provide an optimal environment for functioning all pathway enzymes, and metabolic burdens from overexpression of complex pathways may reduce biosynthetic efficiency (Zhang et al., 2015; Wang et al., 2020). By dividing the acetylated diol paclitaxel precursor synthetic route into two modules, expressed in either *S. cerevisiae* or *E. coli*, a stable co-culture was achieved in the bioreactor. The engineered *E. coli* strain accomplishes the biosynthesis of the intermediate taxadiene. Meanwhile, *S. cerevisiae* is the preferred host for cytochrome P450 (P450s) expression, using this two-component system, oxygenated taxanes with a titer of 33 mg/L was overproduced (Zhou et al., 2015; **Supplementary Figure 1D**). Similarly, Niu et al. (2018) constructed an *E. coli* - *E. coli* co-culture system for pinene biosynthesis. The MEV pathway and heterologous pathway (the GPP synthase and pinene synthase) were engineered in different pinene tolerance *E. coli* strains, respectively. The optimization of whole-cell biocatalysis, which could separate cell growth and production phase, improved pinene production to 166.5 mg/L.

REFERENCES

- Ajikumar, P. K., Xiao, W. H., Tyo, K. E. J., Wang, Y., Simeon, F., Leonard, E., et al. (2010). Isoprenoid pathway optimization for Taxol precursor overproduction in *Escherichia coli*. *Science* 330, 70–74. doi: 10.1126/science.1191652
- Arendt, P., Miettinen, K., Pollier, J., de Rycke, R., Callewaert, N., and Goossens, A. (2017). An endoplasmic reticulum-engineered yeast platform for overproduction of triterpenoids. *Metab. Eng.* 40, 165–175. doi: 10.1016/j.ymben.2017.02.007
- Bian, G., Deng, Z., and Liu, T. (2017). Strategies for terpenoid overproduction and new terpenoid discovery. *Curr. Opin. Biotechnol.* 48, 234–241. doi: 10.1016/j.copbio.2017.07.002

CONCLUSION

Over the last few decades, biological engineers achieved grand developments in synthetic biology. The enormous potential of *E. coli* and *S. cerevisiae* as platform strains has been confirmed with various successes. However, as synthetic biology targets are progressively more complicated, there remain some challenges to engineering industrial hosts because of the lack of knowledge of complex biochemical and cellular metabolism and its regulation. With the fast development of synthetic biology tools such as CRISPR-Cas9, adaptive laboratory evolution (ALE) combine with next-generation sequencing and high-throughput screening, it promises to reach a deeper understanding of cellular metabolism. The capacity of DNA synthesis has been made great progressed over the past decade, and it is conventional to synthesize the large gene cluster for terpenoids biosynthesis. In addition, new DNA assembly methods facilitate the speedy construction of different genetic part combinations or to replace genetic parts in a single step. Besides, dynamic control, compartmentalization, module design, or cell-free system are practical methods to enhance the overall reaction efficiency of multi-enzyme pathways.

AUTHOR CONTRIBUTIONS

Both authors conceived the review, wrote and reviewed the manuscript.

FUNDING

This research work was financially supported by the National Key R&D Program of China (No. 2018YFC0311001), National Natural Science Foundation of China (Grant No. 81741153), and the Fundamental Research Funds for the Central Universities granted to KH.

SUPPLEMENTARY MATERIAL

The Supplementary Material for this article can be found online at: <https://www.frontiersin.org/articles/10.3389/fbioe.2020.00347/full#supplementary-material>

- Biggs, B. W., Lim, C. G., Sagliani, K., Shankar, S., Stephanopoulos, G., de Mey, M., et al. (2016). Overcoming heterologous protein interdependency to optimize P450-mediated Taxol precursor synthesis in *Escherichia coli*. *Proc. Natl. Acad. Sci. U.S.A.* 113, 3209–3214. doi: 10.1073/pnas.1515826113
- Callari, R., Meier, Y., Ravasio, D., and Heider, H. (2018). Dynamic control of ERG20 and ERG9 expression for improved casbene production in *Saccharomyces cerevisiae*. *Front. Bioeng. Biotechnol.* 6:160. doi: 10.3389/fbioe.2018.00160
- Cameron, D. E., and Collins, J. J. (2014). Tunable protein degradation in bacteria. *Nat. Biotechnol.* 32, 1276–1281. doi: 10.1038/nbt.3053
- Cao, Y., Zhang, R., Liu, W., Zhao, G., Niu, W., Guo, J., et al. (2019). Manipulation of the precursor supply for high-level production of longifolene by metabolically engineered *Escherichia coli*. *Sci. Rep.* 9:95. doi: 10.1038/s41598-018-36495-w

- Chacón, M. G., Marriott, A., Kendrick, E. G., Styles, M. Q., and Leak, D. J. (2019). Esterification of geraniol as a strategy for increasing product titre and specificity in engineered *Escherichia coli*. *Microb. Cell Fact.* 18:105. doi: 10.1186/s12934-019-1130-0
- Chatzivasilieiou, A. O., Ward, V., Edgar, S. M., and Stephanopoulos, G. (2019). Two-step pathway for isoprenoid synthesis. *Proc. Natl. Acad. Sci. U.S.A.* 116, 506–511. doi: 10.1073/pnas.1812935116
- Chen, H., Zhu, C., Zhu, M., Xiong, J., Ma, H., Zhuo, M., et al. (2019). High production of valencene in *Saccharomyces cerevisiae* through metabolic engineering. *Microb. Cell Fact.* 1:195. doi: 10.1186/s12934-019-1246-2
- Chen, X., Zhang, C., Zou, R., Stephanopoulos, G., and Too, H. P. (2017). *In vitro* metabolic engineering of amorpho-4,11-diene biosynthesis at enhanced rate and specific yield of production. *ACS Synth. Biol.* 6, 1691–1700. doi: 10.1021/acssynbio.6b0037
- Cheng, S., Liu, X., Jiang, G., Wu, J., Zhang, J., Lei, D., et al. (2019). Orthogonal engineering of biosynthetic pathway for efficient production of limonene in *Saccharomyces cerevisiae*. *ACS Synth. Biol.* 8, 968–975. doi: 10.1021/acssynbio.9b00135
- Clomburg, J. M., Crumbley, A. M., and Gonzalez, R. (2017). Industrial biomanufacturing: the future of chemical production. *Science* 355:aag0804. doi: 10.1126/science.aag0804
- Clomburg, J. M., Qian, S., Tan, Z., Cheong, S., and Gonzalez, R. (2019). The isoprenoid alcohol pathway, a synthetic route for isoprenoid biosynthesis. *Proc. Natl. Acad. Sci. U.S.A.* 116, 12810–12815. doi: 10.1073/pnas.1821004116
- Coussemment, P., Bauwens, D., Maertens, J., and de Mey, M. (2017). Direct combinatorial pathway optimization. *ACS Synth. Biol.* 6, 224–232. doi: 10.1021/acssynbio.6b00122
- Dahl, R. H., Zhang, F., Alonso-Gutierrez, J., Baidoo, E., Batth, T. S., Redding-Johanson, A. M., et al. (2013). Engineering dynamic pathway regulation using stress-response promoters. *Nat. Biotechnol.* 31, 1039–1046. doi: 10.1038/nbt.2689
- Dudley, Q. M., Karim, A. S., and Jewett, M. C. (2015). Cell-free metabolic engineering: biomanufacturing beyond the cell. *Biotechnol. J.* 10, 69–82. doi: 10.1002/biot.201400330
- Dueber, J. E., Wu, G. C., Malmirchegini, G. R., Moon, T. S., Petzold, C. J., Ullal, A. V., et al. (2009). Synthetic protein scaffolds provide modular control over metabolic flux. *Nat. Biotechnol.* 27, 753–759. doi: 10.1038/nbt.1557
- Eriksen, D. T., Lian, J., and Zhao, H. (2014). Protein design for pathway engineering. *J. Struct. Biol.* 185, 234–242. doi: 10.1016/j.jsb.2013.03.011
- George, K. W., Chen, A., Jain, A., Batth, T. S., Baidoo, E. E. K., Wang, G., et al. (2014). Correlation analysis of targeted proteins and metabolites to assess and engineer microbial isopentenol production. *Biotechnol. Bioeng.* 111, 1648–1658. doi: 10.1002/bit.25226
- George, K. W., Thompson, M. G., Kim, J., Baidoo, E. E. K., Wang, G., Benites, V. T., et al. (2018). Integrated analysis of isopentenyl pyrophosphate (IPP) toxicity in isoprenoid-producing *Escherichia coli*. *Metab. Eng.* 47, 60–72. doi: 10.1016/j.ymben.2018.03.004
- Gold, N. D., Fossati, E., Cetti Hansen, C., DiFalco, M., Douchin, V., and Martin, V. J. J. (2018). A Combinatorial Approach to study cytochrome P450 enzymes for de novo production of steviol glucosides in baker's yeast. *ACS Synth. Biol.* 7, 2918–2929. doi: 10.1021/acssynbio.8b00470
- Hammer, S. K., and Avalos, J. L. (2017). Harnessing yeast organelles for metabolic engineering. *Nat. Chem. Biol.* 13, 823–832. doi: 10.1038/nchembio.2429
- Hong, J., Park, S. H., Kim, S., Kim, S. W., and Hahn, J. S. (2019). Efficient production of lycopene in *Saccharomyces cerevisiae* by enzyme engineering and increasing membrane flexibility and NAPDH production. *Appl. Microbiol. Biotechnol.* 103, 211–223. doi: 10.1007/s00253-018-9449-8
- Ichinose, H., and Wariishi, H. (2013). High-level heterologous expression of fungal cytochrome P450s in *Escherichia coli*. *Biochem. Biophys. Res. Commun.* 438, 289–294. doi: 10.1016/j.bbrc.2013.07.057
- Jia, F., Narasimhan, B., and Mallapragada, S. (2014). Materials-based strategies for multi-enzyme immobilization and co-localization: a review. *Biotechnol. Bioeng.* 111, 209–222. doi: 10.1002/bit.25136
- Jiang, G.-Z., Yao, M.-D., Wang, Y., Zhou, L., Song, T.-Q., Liu, H., et al. (2017). Manipulation of GES and ERG20 for geraniol overproduction in *Saccharomyces cerevisiae*. *Metab. Eng.* 41, 57–66. doi: 10.1016/j.ymben.2017.03.005
- Kang, A., George, K. W., Wang, G., Baidoo, E., Keasling, J. D., and Lee, T. S. (2016). Isopentenyl diphosphate (IPP)-bypass mevalonate pathways for isopentenol production. *Metab. Eng.* 34, 25–35. doi: 10.1016/j.ymben.2015.12.002
- Kang, A., Mendez-Perez, D., Goh, E.-B., Baidoo, E. E. K., Benites, V. T., Beller, H. R., et al. (2019). Optimization of the IPP-bypass mevalonate pathway and fed-batch fermentation for the production of isoprenol in *Escherichia coli*. *Metab. Eng.* 56, 85–96. doi: 10.1016/j.ymben.2019.09.003
- Kang, W., Ma, T., Liu, M., Qu, J., Liu, Z., Zhang, H., et al. (2019). Modular enzyme assembly for enhanced cascade biocatalysis and metabolic flux. *Nat. Commun.* 10:4248. doi: 10.1038/s41467-019-12247-w
- Kim, J. E., Jang, I. S., Son, S. H., Ko, Y. J., Cho, B. K., Kim, S. C., et al. (2019). Tailoring the *Saccharomyces cerevisiae* endoplasmic reticulum for functional assembly of terpene synthesis pathway. *Metab. Eng.* 56, 50–59. doi: 10.1016/j.ymben.2019.08.013
- Kim, S., Kim, S. K., Seong, W., Woo, S., Lee, H., Yeom, S., et al. (2019). Enhanced (-)- α -bisabolol productivity by efficient conversion of mevalonate in *Escherichia coli*. *Catalysts* 9:432. doi: 10.3390/catal9050432
- Kim, S. K., Han, G. H., Seong, W., Kim, H., Kim, S.-W., Lee, D.-H., et al. (2016). CRISPR interference-guided balancing of a biosynthetic mevalonate pathway increases terpenoid production. *Metab. Eng.* 38, 228–240. doi: 10.1016/j.ymben.2016.08.006
- Korman, T. P., Opgenorth, P. H., and Bowie, J. U. (2017). A synthetic biochemistry platform for cell free production of monoterpenes from glucose. *Nat. Commun.* 8:15526. doi: 10.1038/ncomms15526
- Kwak, S., Yun, E. J., Lane, S., Oh, E. J., Kim, K. H., and Jin, Y. (2019). Redirection of the glycolytic flux enhances isoprenoid production in *Saccharomyces cerevisiae*. *Biotechnol. J.* 15:1900173. doi: 10.1002/biot.201900173
- Li, J., Zhang, L., and Liu, W. (2018). Cell-free synthetic biology for in vitro biosynthesis of pharmaceutical natural products. *Synth. Syst. Biotechnol.* 3, 83–89. doi: 10.1016/j.synbio.2018.02.002
- Lian, J., Hamedirad, M., Hu, S., and Zhao, H. (2017). Combinatorial metabolic engineering using an orthogonal tri-functional CRISPR system. *Nat. Commun.* 8:1688. doi: 10.1038/s41467-017-01695-x
- Liu, G.-S., Li, T., Zhou, W., Jiang, M., Tao, X.-Y., Liu, M., et al. (2020). The yeast peroxisome: a dynamic storage depot and subcellular factory for squalene overproduction. *Metab. Eng.* 57, 151–161. doi: 10.1016/j.ymben.2019.11.001
- Lu, Q., and Liu, J. Z. (2019). Enhanced astaxanthin production in *Escherichia coli* via morphology and oxidative stress engineering. *J. Agric. Food Chem.* 67, 11703–11709. doi: 10.1021/acs.jafc.9b05404
- Lu, X., Liu, Y., Yang, Y., Wang, S., Wang, Q., Wang, X., et al. (2019). Constructing a synthetic pathway for acetyl-coenzyme A from one-carbon through enzyme design. *Nat. Commun.* 10:1378. doi: 10.1038/s41467-019-09095-z
- Ma, T., Shi, B., Ye, Z., Li, X., Liu, M., Chen, Y., et al. (2019). Lipid engineering combined with systematic metabolic engineering of *Saccharomyces cerevisiae* for high-yield production of lycopene. *Metab. Eng.* 52, 134–142. doi: 10.1016/j.ymben.2018.11.009
- Martin, V. J. J., Pitera, D. J., Withers, S. T., Newman, J. D., and Keasling, J. D. (2003). Engineering a mevalonate pathway in *Escherichia coli* for production of terpenoids. *Nat. Biotechnol.* 21, 796–802. doi: 10.1038/nbt833
- Martinez, V., Lauritsen, I., Hobel, T., Li, S., Nielsen, A. T., and Nørholm, M. H. H. (2017). CRISPR/Cas9-based genome editing for simultaneous interference with gene expression and protein stability. *Nucleic Acids Res.* 45, e171. doi: 10.1093/nar/gkx797
- Meadows, A. L., Hawkins, K. M., Tsegaye, Y., Antipov, E., Kim, Y., Raetz, L., et al. (2016). Rewriting yeast central carbon metabolism for industrial isoprenoid production. *Nature* 537, 694–697. doi: 10.1038/nature19769
- Mendez-Perez, D., Alonso-Gutierrez, J., Hu, Q., Molinas, M., Baidoo, E. E. K., Wang, G., et al. (2017). Production of jet fuel precursor monoterpenoids from engineered *Escherichia coli*. *Biotechnol. Bioeng.* 114, 1703–1712. doi: 10.1002/bit.26296
- Minard, K. I., and McAlister-Henn, L. (2005). Sources of NADPH in yeast vary with carbon source. *J. Biol. Chem.* 280, 39890–39896. doi: 10.1074/jbc.m509461200
- Niu, F.-X., He, X., Wu, Y.-Q., and Liu, J.-Z. (2018). Enhancing production of pinene in *Escherichia coli* by using a combination of tolerance, evolution, and modular co-culture engineering. *Front. Microbiol.* 9:1623. doi: 10.3389/fmicb.2018.01623

- Paddon, C. J., Westfall, P. J., Pitera, D. J., Benjamin, K., Fisher, K., McPhee, D., et al. (2013). High-level semi-synthetic production of the potent antimalarial artemisinin. *Nature* 496, 528–532. doi: 10.1038/nature12051
- Peng, B., Nielsen, L. K., Kampranis, S. C., and Vickers, C. E. (2018). Engineered protein degradation of farnesyl pyrophosphate synthase is an effective regulatory mechanism to increase monoterpene production in *Saccharomyces cerevisiae*. *Metab. Eng.* 47, 83–93. doi: 10.1016/j.ymben.2018.02.005
- Peng, B., Plan, M. R., Chrysanthopoulos, P., Hodson, M. P., Nielsen, L. K., and Vickers, C. E. (2017). A squalene synthase protein degradation method for improved sesquiterpene production in *Saccharomyces cerevisiae*. *Metab. Eng.* 39, 209–219. doi: 10.1016/j.ymben.2016.12.003
- Pfleger, B. F., Pitera, D. J., Smolke, C. D., and Keasling, J. D. (2006). Combinatorial engineering of intergenic regions in operons tunes expression of multiple genes. *Nat. Biotechnol.* 24, 1027–1032. doi: 10.1038/nbt1226
- Qi, L. S., Larson, M. H., Gilbert, L. A., Doudna, J. A., Weissman, J. S., Arkin, A. P., et al. (2013). Repurposing CRISPR as an RNA-guided platform for sequence-specific control of gene expression. *Cell* 152, 1173–1183. doi: 10.1016/j.cell.2013.02.022
- Scalcinati, G., Knuf, C., Partow, S., Chen, Y., Maury, J., Schalk, M., et al. (2012). Dynamic control of gene expression in *Saccharomyces cerevisiae* engineered for the production of plant sesquiterpene α -santalene in a fed-batch mode. *Metab. Eng.* 14, 91–103. doi: 10.1016/j.ymben.2012.01.007
- Shen, H., Cheng, B., Zhang, Y., Tang, L., Li, Z., Bu, Y.-F., et al. (2016). Dynamic control of the mevalonate pathway expression for improved zeaxanthin production in *Escherichia coli* and comparative proteome analysis. *Metab. Eng.* 38, 180–190. doi: 10.1016/j.ymben.2016.07.012
- Shukal, S., Chen, X., and Zhang, C. (2019). Systematic engineering for high-yield production of viridiflorol and amorphadiene in auxotrophic *Escherichia coli*. *Metab. Eng.* 55, 170–178. doi: 10.1016/j.ymben.2019.07.007
- Wang, C., Liwei, M., Park, J. B., Jeong, S. H., Wei, G., Wang, Y., et al. (2018). Microbial platform for terpenoid production: *Escherichia coli* and Yeast. *Front. Microbiol.* 9:2460. doi: 10.3389/fmicb.2018.02460
- Wang, P., Wei, W., Ye, W., Li, X., Zhao, W., Yang, C., et al. (2019). Synthesizing ginsenoside Rh2 in *Saccharomyces cerevisiae* cell factory at high-efficiency. *Cell Discov.* 5:5. doi: 10.1038/s41421-018-0075-5
- Wang, P., Wei, Y., Fan, Y., Liu, Q., Wei, W., Yang, C., et al. (2015). Production of bioactive ginsenosides Rh2 and Rg3 by metabolically engineered yeasts. *Metab. Eng.* 29, 97–105. doi: 10.1016/j.ymben.2015.03.003
- Wang, R., Zhao, S., Wang, Z., and Koffas, M. A. (2020). Recent advances in modular co-culture engineering for synthesis of natural products. *Curr. Opin. Biotechnol.* 62, 65–71. doi: 10.1016/j.copbio.2019.09.004
- Westfall, P. J., Pitera, D. J., Lenihan, J. R., Eng, D., Woolard, F. X., Regentin, R., et al. (2012). Production of amorphadiene in yeast, and its conversion to dihydroartemisinic acid, precursor to the antimalarial agent artemisinin. *Proc. Natl. Acad. Sci. U.S.A.* 109, 111–118. doi: 10.1073/pnas.1110740109
- Wong, A. S. T., Che, C.-M., and Leunga, K.-W. (2015). Recent advances in ginseng as cancer therapeutics: a functional and mechanistic overview. *Nat. Prod. Rep.* 32, 256–272. doi: 10.1039/c4np00080c
- Wong, J., de Rond, T., d'Espaux, L., van der Horst, C., Dev, I., Rios-Solis, L., et al. (2018). High-titer production of lathyrane diterpenoids from sugar by engineered *Saccharomyces cerevisiae*. *Metab. Eng.* 45, 142–148. doi: 10.1016/j.ymben.2017.12.007
- Xie, W., Ye, L., Lv, X., Xu, H., and Yu, H. (2015). Sequential control of biosynthetic pathways for balanced utilization of metabolic intermediates in *Saccharomyces cerevisiae*. *Metab. Eng.* 28, 8–18. doi: 10.1016/j.ymben.2014.11.007
- Yee, D. A., DeNicola, A. B., Billingsley, J. M., Creso, J. G., Subrahmanyam, V., and Tang, Y. (2019). Engineered mitochondrial production of monoterpenes in *Saccharomyces cerevisiae*. *Metab. Eng.* 55, 76–84. doi: 10.1016/j.ymben.2019.06.004
- Yuan, J., and Ching, C. B. (2015). Dynamic control of ERG9 expression for improved amorpho-4,11-diene production in *Saccharomyces cerevisiae*. *Microb. Cell Fact.* 14:38. doi: 10.1186/s12934-015-0220-x
- Yuan, J., and Ching, C.-B. (2016). Mitochondrial acetyl-CoA utilization pathway for terpenoid productions. *Metab. Eng.* 38, 303–309. doi: 10.1016/j.ymben.2016.07.008
- Yuan, W., Lv, S., Chen, L., Zhao, Y., Deng, Z., and Hong, K. (2019). Production of sesterterpene ophiobolin by a bifunctional terpene synthase in *Escherichia coli*. *Appl. Microbiol. Biotechnol.* 103, 8785–8797. doi: 10.1007/s00253-019-10103-x
- Zhang, C., Liu, J., Zhao, F., Lu, C., Zhao, G.-R., and Lu, W. (2018a). Production of sesquiterpenoid zerumbone from metabolic engineered *Saccharomyces cerevisiae*. *Metab. Eng.* 49, 28–35. doi: 10.1016/j.ymben.2018.07.010
- Zhang, C., Seow, V. Y., Chen, X., and Too, H. P. (2018b). Multidimensional heuristic process for high-yield production of astaxanthin and fragrance molecules in *Escherichia coli*. *Nat. Commun.* 9:1858. doi: 10.1038/s41467-018-04211-x
- Zhang, H., Pereira, B., Li, Z., Stephanopoulos, G., and Demain, A. L. (2015). Engineering *Escherichia coli* coculture systems for the production of biochemical products. *Proc. Natl. Acad. Sci. U.S.A.* 112, 8266–8271. doi: 10.1073/pnas.1506781112
- Zhao, J., Li, C., Zhang, Y., Shen, Y., Hou, J., and Bao, X. (2017). Dynamic control of ERG20 expression combined with minimized endogenous downstream metabolism contributes to the improvement of geraniol production in *Saccharomyces cerevisiae*. *Microb. Cell Fact.* 16:17. doi: 10.1186/s12934-017-0641-9
- Zhou, K., Qiao, K., Edgar, S., and Stephanopoulos, G. (2015). Distributing a metabolic pathway among a microbial consortium enhances production of natural products. *Nat. Biotechnol.* 33, 377–383. doi: 10.1038/nbt.3095

Conflict of Interest: The authors declare that the research was conducted in the absence of any commercial or financial relationships that could be construed as a potential conflict of interest.

Copyright © 2020 Zhang and Hong. This is an open-access article distributed under the terms of the Creative Commons Attribution License (CC BY). The use, distribution or reproduction in other forums is permitted, provided the original author(s) and the copyright owner(s) are credited and that the original publication in this journal is cited, in accordance with accepted academic practice. No use, distribution or reproduction is permitted which does not comply with these terms.



Exploring a Highly D-Galactose Specific L-Arabinose Isomerase From *Bifidobacterium adolescentis* for D-Tagatose Production

Guoyan Zhang^{1†}, Yingfeng An^{2†}, Amreesh Parvez¹, Hossain M. Zabed¹, Junhua Yun¹ and Xianghui Qi^{1*}

¹ School of Food and Biological Engineering, Jiangsu University, Zhenjiang, China, ² College of Biosciences and Biotechnology, Shenyang Agricultural University, Shenyang, China

OPEN ACCESS

Edited by:

Min Jiang,
Nanjing Tech University, China

Reviewed by:

Fengxue Xin,
Nanjing Tech University, China
Wenjing Cui,
Jiangnan University, China

*Correspondence:

Xianghui Qi
qxh@ujs.edu.cn

[†] These authors have contributed
equally to this work

Specialty section:

This article was submitted to
Synthetic Biology,
a section of the journal
Frontiers in Bioengineering and
Biotechnology

Received: 09 February 2020

Accepted: 06 April 2020

Published: 29 April 2020

Citation:

Zhang G, An Y, Parvez A,
Zabed HM, Yun J and Qi X (2020)
Exploring a Highly D-Galactose
Specific L-Arabinose Isomerase From
Bifidobacterium adolescentis
for D-Tagatose Production.
Front. Bioeng. Biotechnol. 8:377.
doi: 10.3389/fbioe.2020.00377

D-Galactose-specific L-arabinose isomerase (L-AI) would have much potential for the enzymatic conversion of D-Galactose into D-tagatose, while most of the reported L-AIs are L-arabinose specific. This study explored a highly D-Galactose-specific L-AI from *Bifidobacterium adolescentis* (BAAI) for the production of D-tagatose. In the comparative protein-substrate docking for D-Galactose and L-arabinose, BAAI showed higher numbers of hydrogen bonds in D-Galactose-BAAI bonding site than those found in L-arabinose-BAAI bonding site. The activity of BAAI was 24.47 U/mg, and it showed good stability at temperatures up to 65°C and a pH range 6.0–7.5. The K_m , V_{max} , and K_{cat}/K_m of BAAI were found to be 22.4 mM, 489 U/mg and $9.3 \text{ mM}^{-1} \text{ min}^{-1}$, respectively for D-Galactose, while the respective values for L-arabinose were 40.2 mM, 275.1 U/mg, and $8.6 \text{ mM}^{-1} \text{ min}^{-1}$. Enzymatic conversion of D-Galactose into D-tagatose by BAAI showed 56.7% conversion efficiency at 55°C and pH 6.5 after 10 h.

Keywords: *Bifidobacterium adolescentis*, L-arabinose isomerase, D-tagatose, sweetener, probiotic bacteria

INTRODUCTION

D-tagatose is a rare ketohexose in nature found mostly in gums and lichens, which is widely used as a low caloric sweetener and substitute of sucrose for its 92% sweetness of sucrose in a 10% aqueous solution with only one-third calories of sucrose (Guo et al., 2018). It is also known for its prebiotic action, capability of reducing cholesterol, preventing colon cancer, treatment of type II diabetes, and so on (Lu et al., 2008). It is widely used in many food and pharmaceuticals preparations, including drinks, yogurt, diabetes-specific foods, diet foods, cereals, meat products, candies, cough syrups, anti-adhesives for fixed dentures and oral disinfectants (Kim, 2004; Marylane et al., 2017).

D-tagatose can be produced either by chemical or biological method, where the former is mainly based on the isomerization of D-Galactose into D-tagatose by a chemical catalyst, such as soluble alkali metal salt or an alkaline earth metal salt or potassium aluminate. In spite of its maturity

and application on large scale, chemical method has some drawbacks, including production of by-products, requirement of an extensive purification step, and responsibility to environmental pollution (Oh, 2007). In contrast, biological method offers an eco-friendly conversion approach, in which L-arabinose isomerase (L-AI, EC 5.3.1.4) is used for isomerizing D-Galactose into D-tagatose (Zhang et al., 2017, 2019).

To achieve a sustainable bioconversion process for D-tagatose production, utilization of cheap substrate and efficient enzyme are utmost important. In this context, milk industry wastes, particularly whey powder rich in lactose, would be an attractive source of substrates, which provides galactose upon hydrolysis of lactose (Zhang et al., 2020). As attempts to obtain potential source of L-AIs with a high efficiency, more than 30 L-AIs have been reported thus far from various natural or engineered microorganisms, such as *Escherichia coli* (Wu et al., 2020), *Clostridium hylemonae* (Nguyen et al., 2018), *Bacillus subtilis* (Kim et al., 2010), *Bacillus coagulans* (Mei et al., 2016), *Lactobacillus plantarum* (Chouayekh et al., 2007), *Lactobacillus brevis* (Guo et al., 2018), *Geobacillus thermodenitrificans* (Kim and Oh, 2005), *Enterococcus faecium* (Marylane et al., 2017) and *Bifidobacterium longum* (Salonen et al., 2012). However, almost all of these L-AIs showed higher specificity to L-arabinose than the specificity to D-Galactose (Xu et al., 2018). This has indicated that existing L-AIs might not be as efficient for valorizing milk whey powder as desired. Therefore, screening and characterization of highly galactose-specific L-AIs should receive significant research priority. Furthermore, D-tagatose produced from D-Galactose derived from whey powder requires hydrolysis of its lactose, which need to be carried out under acidic condition (Zhan et al., 2014; Zhang et al., 2020).

In this study, we report a highly D-Galactose-specific L-AI from *Bifidobacterium adolescentis* (BAAI) for the first time, which worked under acidic condition. This enzyme was structurally and biochemically characterized after cloning and expressing its relevant gene (*araA*) in *E. coli* BL21(DE3). The purified enzyme was studied to determine the optimum conditions for obtaining its maximum activity and to evaluate its substrate specificities. Subsequently, structural homology and protein-substrate docking of the BAAI were analyzed to explain the basis of substrate specificity. Finally, enzymatic conversion of D-Galactose into D-tagatose was carried out using the purified BAAI for evaluating its conversion efficiency.

MATERIALS AND METHODS

Bacterial Strains and Materials

B. adolescentis CICC 6178 strain was obtained from the China Center of Industrial Culture Collection (CICC), Beijing, China. It was cultivated anaerobically in TPY fluid Medium at 37°C without agitation. pANY1 plasmid was obtained from Shenyang Agricultural University, China (Gao et al., 2018; Liu et al., 2018), which was used as the expression vector. *E. coli* BL21(DE3) was obtained from the Stratagene (California, United States). Q5 DNA Polymerase

and Restriction Endonucleases were bought from the New England Biolab (NEB) (Beijing, China). ClonExpress® One-Step Cloning Kit, FastPure Plasmid Mini Kit, and FastPure Gel DNA Extraction Mini Kit were purchased from Vazyme (Nanjing, China). Solubilization and Refolding Kit was bought from the TIANDZ (Beijing, China). All other chemicals and reagents were purchased from the Sinopharm (Beijing, China).

Cloning of *araA* From *B. adolescentis*

Gene of BAAI (*araA*) was amplified by PCR from the genomic DNA of *B. adolescentis* CICC 6178 using the forward primer P1 (5'-GGGGGATCCACTAGTAGGCCTATG GCAATGGAAAAC-3') and reverse primer P2 (5'-AGCAGCC AACTGCAGGAGCTCTCAGTGACGGTTGTT-3') containing the restriction endonucleases sites *SacI* and *StuI* (underlined), respectively, and then cloned into pANY1 using the Cloning Kit. Recombinant pANY1-*araA* vector was then transformed into *E. coli* BL21(DE3) competent cells by heat shock method. Transformed strains were grown in LB medium at 37°C for 1 h, and the culture was then transferred to LB plate supplemented with kanamycin (50 µg/mL). Positive colonies were screened by PCR and confirmed by sequencing.

Phylogenetic Analysis and Multiple Sequence Alignment

Protein sequences of other L-AIs were retrieved from the UniPort. Phylogenetic tree of BAAI was constructed using the neighbor-joining algorithm in MEGA7 (Version 7.0.26). Multiple Sequence Alignment (MSA) of BAAI with structurally characterized L-AIs was done using the Clustal Omega server of EMBL (Sievers et al., 2011), which provided information about conservation of active site residues of L-AIs. The alignment of these proteins was represented by BoxShade 3.21 web server.

Expression and Purification of Recombinant BAAI

E. coli B21(DE3)-*araA* was grown in LB broth at 37°C and 200 rpm until OD₆₀₀ value reached to 0.4–0.6. Then, 1.0 mM of IPTG was added to it for inducing the expression of gene, and incubated for further 10 h at 25°C and 120 rpm (Yun et al., 2018). Due to strong expression and misfolding of BAAI during induction process, recombinant BAAI formed inclusion bodies as also reported for L-AI of *C. hylemonae* (Nguyen et al., 2018). To dissolve inclusion bodies and get BBAI in soluble form, cells were harvested by centrifugation at 8,000 rpm (4°C) for 15 min and washed twice with 100 mM sodium phosphate buffer (pH 7.4) as described earlier (Qi et al., 2016; Zhang et al., 2018). Thereafter, cells were re-suspended in the lysis buffer (50 mM Tris-Cl, 100 mM NaCl, 1% Triton X) and disrupted by sonication (350 W; 1.5 s working time, 2 s interval, for 20 mins, at 4°C), and centrifuged at 10,000 rpm (4°C) for 10 min (Qi et al., 2017). Finally, insoluble BAAI contained in precipitate was dissolved and renatured as per the instruction of the Kit for obtaining soluble and active BAAI for further analysis.

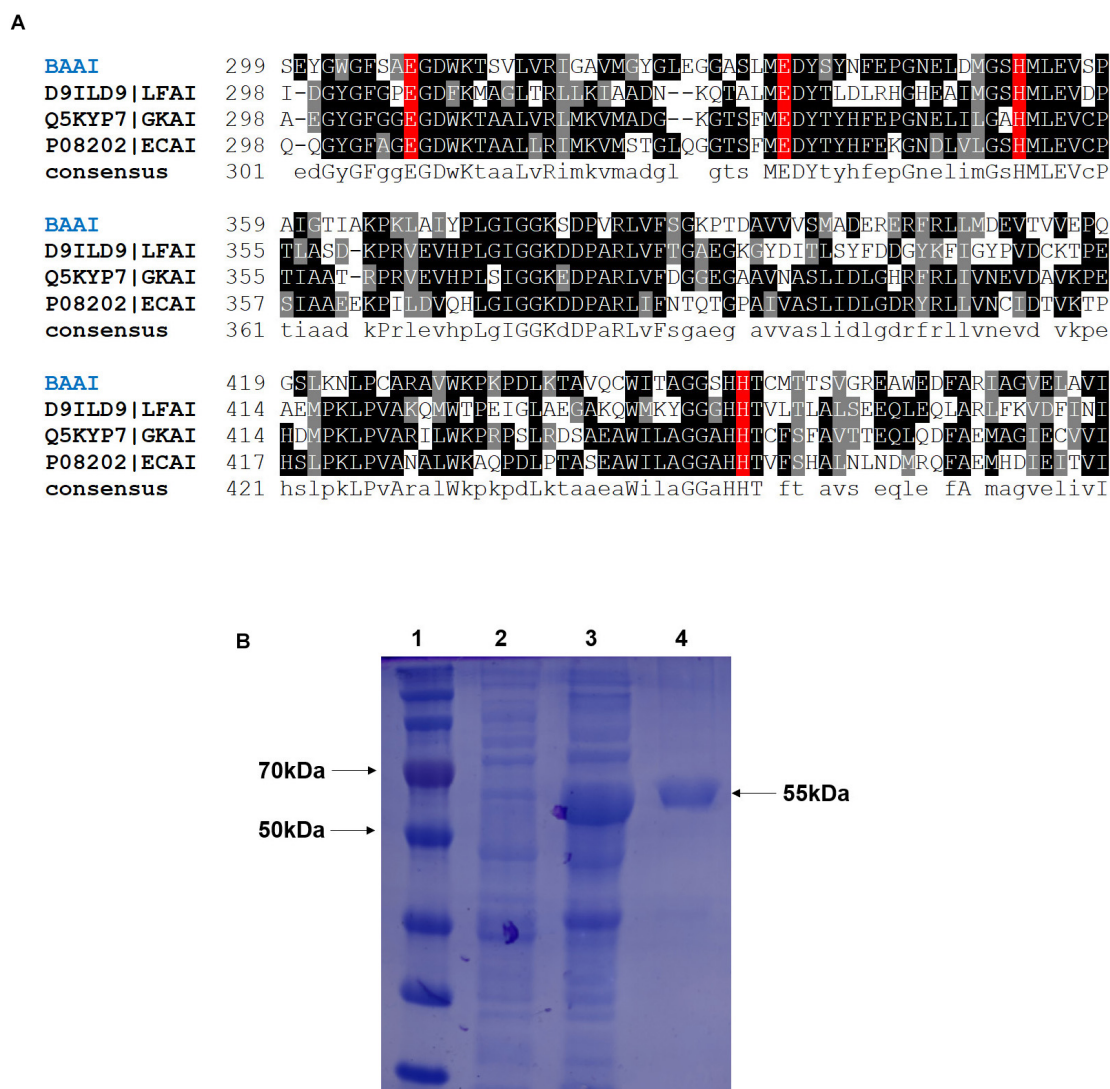


FIGURE 1 | (A) Multiple sequence alignment of L-arabinose isomerase (L-AIs) amino acid sequences from *B. adolescentis* (BAAI), *L. fermentum* (LFAI), *G. kaustophilus* (GKAI), *E. coli* (ECAI). The strongly and weakly conserved amino acid residues are indicated by dark and light black, respectively. The amino acids involved in the catalytic activity are shown by the red box. **(B)** SDS-PAGE of the L-arabinose isomerase expressed in *E. coli* BL21(DE3) from *B. adolescentis* CICC 6178 (BAAI). Lane 1, molecular marker; Lane 2, *E. coli* BL21(DE3)/pANY1-araA without IPTG induction; Lane 3, *E. coli* BL21(DE3)/pANY1-araA with IPTG induction; Lane 4, purified BAAI.

Quantification of Protein and Determination of Enzyme Activity

Protein concentration was measured by the Bradford method using bovine serum albumin as the standard (Bradford, 1976). Activity of BAAI was determined based on the amount of D-tagatose produced during reaction with D-Galactose under the standard conditions. Reaction mixture consisted of 0.5 mg BAAI enzyme, 0.5 M D-Galactose, and 10 mM $MnCl_2$ (pH 7.0). Enzymatic reaction was done at 60°C for 1 h using the method described by Chouayekh et al. (2007). Thereafter, reaction was stopped by adding 0.5 M HCl to the reaction mixture. D-tagatose produced was determined by the cysteine carbazole sulfuric-acid method (Dische and Borenfreund, 2007).

Determination of Optimum Conditions for Maximum Activity and Stability of BAAI

Experiments were done at various temperatures (45, 50, 55, 58, 60, 62, 65, 68, and 70°C) to determine the optimum temperature for maximum BAAI activity. Thermal stability of BAAI was determined by conducting reactions at 50–80°C for 120 min. Experiments were also carried out under various pH (3–10) conditions at 60°C for 1 h. Target pH was adjusted by using three different buffer systems, namely sodium acetate buffer (pH 3.0–5.0), phosphate buffer (pH 6.0–8.0), and glycine-sodium hydroxide buffer (pH 9.0–10.0). Stability of BAAI at pH was determined by conducting reactions at pH 5–8 for 24 h. Effects

of metal ions on the enzyme activity was determined by doing experiments in the presence of various metal ions (FeSO_4 , ZnCl_2 , CoSO_4 , MnCl_2 , NiCl_2 , CaCl_2 , CuCl_2 , EDTA) with 1 mM concentration each. To determine the optimum concentrations of Mn^{2+} , reactions were performed under various concentrations of Mn^{2+} , ranging from 1 to 10 mM.

Substrate Specificity and Kinetic Properties of BAAI

Substrate specificity of BAAI was determined under the optimum reaction conditions using 0.5 M of various aldoses (L-arabinose, D-Galactose, D-xylose, D-glucose, and D-mannose). Kinetic parameters of BAAI were determined by conducting reactions in sodium phosphate buffer (100 mM, pH 6.5) at 55°C for 20 min using 10–500 mM of D-Galactose and L-arabinose without adding any metal ions. Kinetic parameters (K_m , V_{\max} , and K_{cat}/K_m) were estimated using the non-linear regression software namely GraphPad Prism (Version 6.0, San Diego, CA, United States).

Structural Homology and Protein-Substrate Docking of BAAI

Homology model was constructed for BAAI with the L-AI of *E. coli* (ECAI) (PDB ID: 4F2D) as a template by SWISS-MODEL (Waterhouse et al., 2018) using default parameters. The Ramachandra plot of model was examined by PROCHECK (Laskowski et al., 1993) to ensure the amino acid residues were not situated in unfavorable region. Protein-substrate docking of BAAI with various substrates were performed using AutoDock Vina software (Trott and Olson, 2009). The interacting amino acid residues of BAAI with ligands were visualized and highlighted using PyMOL software (DeLano, 2002) and Discovery Studio visualizer (Version 17.2.0.16349, San Diego Dassault Systems).

Bioconversion of D-Galactose Into D-Tagatose

Enzymatic synthesis of D-tagatose from D-Galactose was carried out at 50, 55, 60°C for 10 h. The reaction mixture contained 100 mM of D-Galactose, 6 mM MnCl_2 and 0.5 mg of the purified enzyme in 100 mM PBS buffer (pH 6.5). Samples were collected every 2 h and D-tagatose was quantified in the high-performance liquid chromatography (HPLC; Shimadzu, GL, Japan; LC-20AT), equipped with a refractive index detector (RID, 40°C) and a Sugar-Ca column (Welch, Shanghai, China; 5mm, $7.8 \times 300\text{mm}$). Column was eluted at 85°C with pure water at a flow rate of 0.7 mL/min.

Statistical Analysis

Each experiment was repeated in triplicate. Origin 9.0 software (OriginLab Inc., Northampton, MA, United States) was used to perform statistical analysis and data were expressed as mean value \pm standard deviation. Data were compared by one-way analysis of variance (ANOVA) considering the least significant difference test (LSD) as *post hoc* test at $p < 0.05$ level.

RESULTS AND CONCLUSION

Cloning, Sequence Analysis, and Structural Homology of BAAI

PCR-amplified product of *araA* from *B. adolescentis* was cloned and sequenced. The sequence of the BAAI gene was submitted to the GenBank database (Accession No.: MK929561). The open reading frame (ORF) of *araA* encoding BAAI was found to be 1515 bp long and encoded a polypeptide with 504 amino acids. LC-MS/MS analysis revealed that molecular weight and isoelectric point of BAAI were 55.85 kDa and 5.06, respectively. The phylogenetic analysis of BAAI with the other L-AIs demonstrated that it had closeness with *B. longum* (I3ZR32), *Thermoanaerobacter mathranii* (Q70G56), and *Thermoanaerobacterium saccharolyticum* (K7SW59). Within the phylogenetic tree, other L-AIs were clustered independently in different groups, while BAAI displayed low identity with those L-AIs. The results of sequence analysis of BAAI using PDB BLAST demonstrated 47% identity with L-AI of *Geobacillus Kaustophilus* (Q5KYP7), 45% with L-AI of *E. coli* (P08202), and 39% with L-AI of *Lactobacillus fermentum* (D9ILD9). Despite amino acid sequence identity of BAAI was slightly higher with L-AI of *G. Kaustophilus* (GKAI) than that found with the L-AI of *E. coli* (ECAI), the latter was used to in the model considering the cofactor (manganese/ Mn^{2+}), where GKAI did not have the cofactor in its crystal structure. Although the amino acid sequence identity between BAAI with other L-AIs were between 40 and 47%, the MSA of BAAI with the other L-AIs disclosed that amino acid residues at catalytic site were highly conserved. **Figure 1A** represents MSA of several L-AIs and amino acid residues present in catalytic site (E308, E335, H352, and H452 in BAAI), which were conserved in these L-AIs.

Expression, Purification, and Activity of BAAI

The cloned and expressed BAAI was purified from inclusion bodies using refolding kit to get the purified and soluble BAAI. Molecular weight of the purified BAAI was around 55 kDa (**Figure 1B**), which was similar to the molecular weight of other reported L-AIs, like L-AIs of *T. saccharolyticum* (Hung et al., 2014), *L. plantarum* (Chang et al., 2016; Zhang et al., 2020), and *B. longum* (Salonen et al., 2012).

Activity of the purified BAAI was found to be 24.47 U/mg. Previous studies reported varying activities of L-AIs depending on the source strains. Except a high activity of L-AI reported from the pathogenic bacterium, *E. coli* (63 U/mg) (Kim et al., 2001), activity of the most L-AIs reported for other bacteria ranged between 0.44 and 26.4 U/mg (Kim and Oh, 2005; Cheng et al., 2010; Li et al., 2011; Hung et al., 2014; Nguyen et al., 2018). L-AI obtained from *Anoxybacillus flavithermus* showed the highest enzyme activity thus far (26.4 U/mg). However, *A. flavithermus* is a major contaminant of milk powder and gelatin, and hence, it would not be a good source for producing D-tagatose. Therefore, highly active L-AI derived

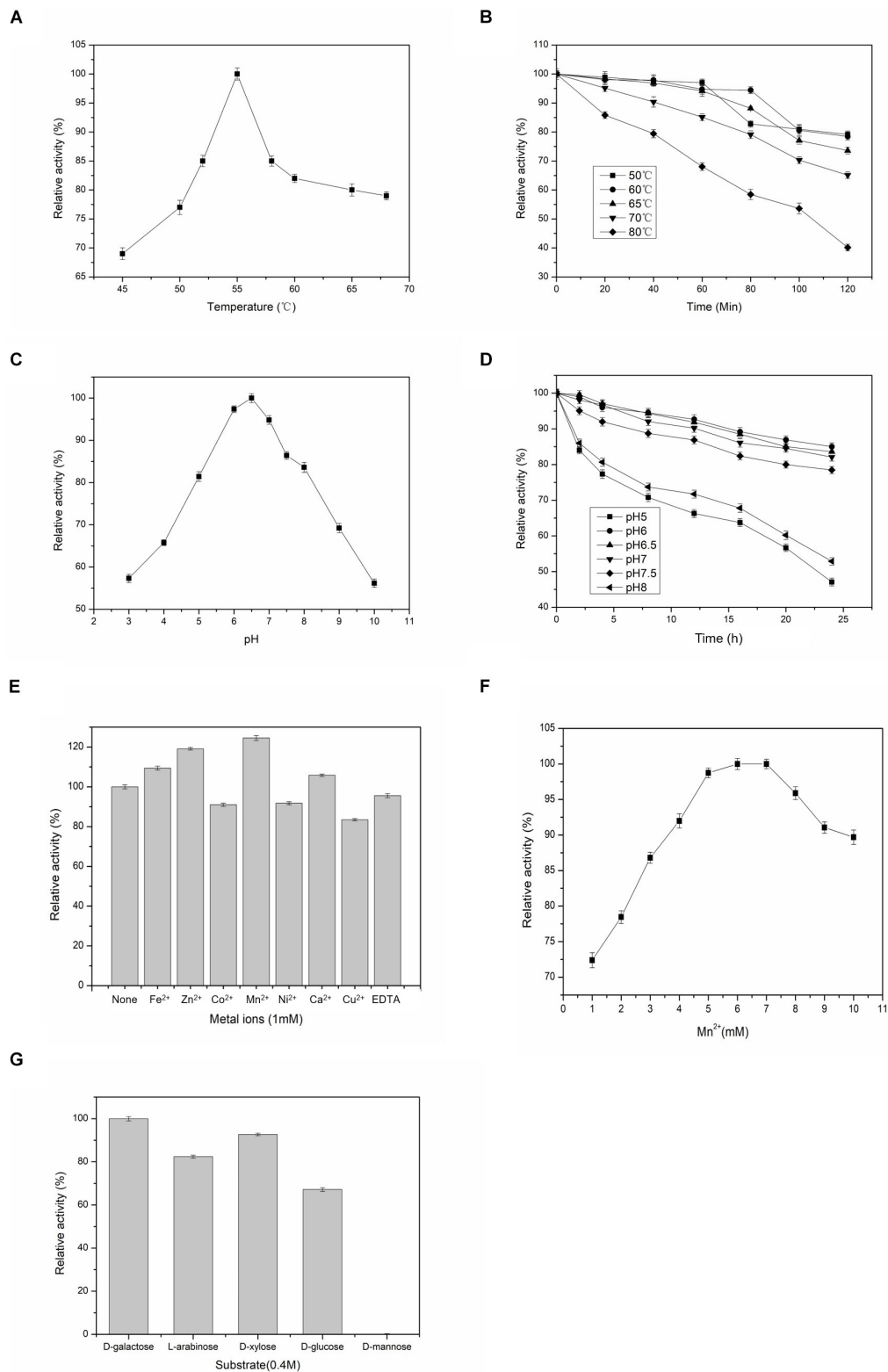
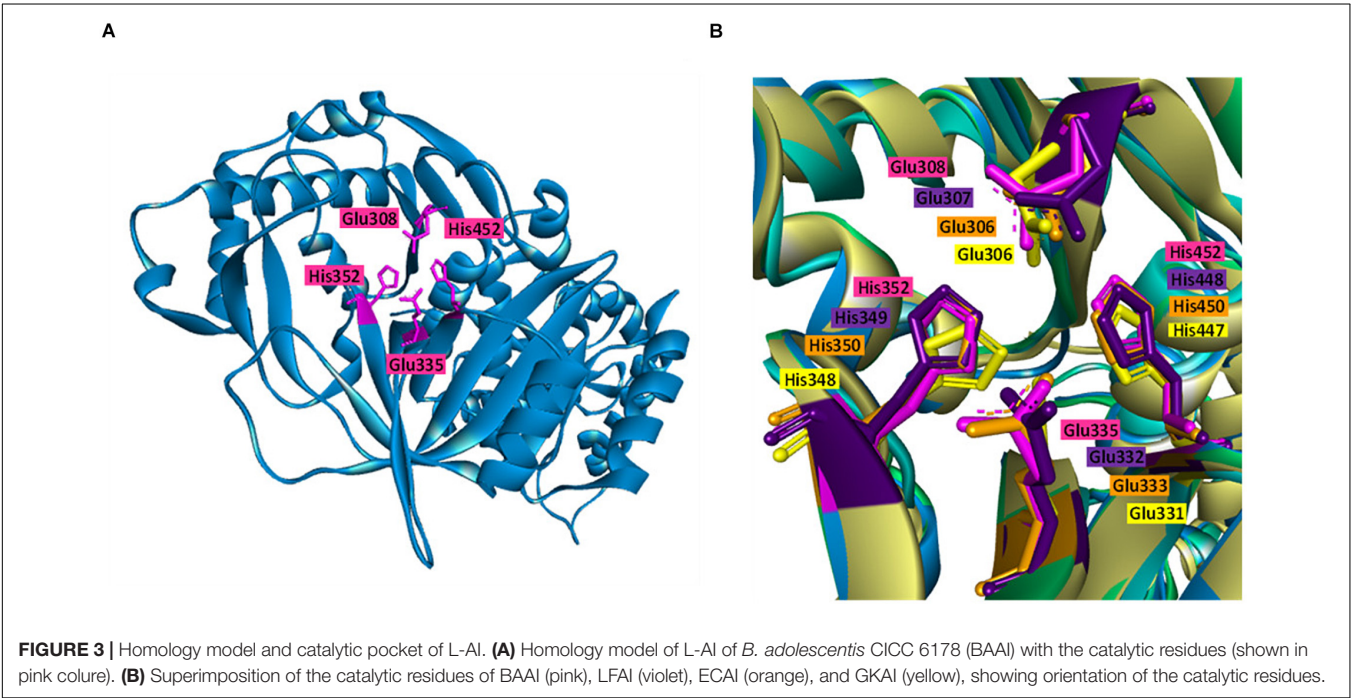


FIGURE 2 | Effects of temperatures, pH, metal ions on the activity and substrate specificities of BAAI. **(A)** activity at various temperature, **(B)** stability at various temperature, **(C)** activity at various pH, and **(D)** stability at various pH. **(E)** Effect of the metal ions on the activity of L-arabinose isomerase of *B. adolescentis* CICC 6178 (BAAI). Activity measured without adding any metallic ion is the control and it represents 100% activity. **(F)** Effects of Mn²⁺ concentrations on the activity of L-arabinose isomerase of *B. adolescentis* CICC 6178 (BAAI). Activities at the optimal Mn²⁺ concentration was defined as 100%. **(G)** Substrate specificities of the L-arabinose isomerase from *B. adolescentis* CICC 6178(BAAI).

TABLE 1 | Comparative kinetic characteristics of L-AIs obtained from various microbial species determined for D-Galactose and L-arabinose as the substrates.

Microorganisms	Temperature (°C)	pH	Metal ions	K_m (mM)		K_{cat}/K_m (mM ⁻¹ min ⁻¹)		References
				D-Gal	L-Ara	D-Gal	L-Ara	
<i>A. Flavithermus</i>	95	9.5–10.5	Ni ²⁺	25.2	78.5	5.2	0.67	Li et al., 2011
<i>G. stearotherophilus</i> DSM 22	70	7.0–7.5	Mn ²⁺ , Mg ²⁺	117	63	4.3	32.5	Lee et al., 2005
<i>G. kaustophilus</i>	60	7.5	Mg ²⁺ , Ca ²⁺	86.1	11.3	NR	NR	Choi et al., 2016
<i>G. thermodenitrificans</i>	70	8.5	Mn ²⁺	408	142	0.5	48	Kim and Oh, 2005
<i>B. subtilis</i> str. 168	32	7.5	Mn ²⁺	NR	NR	NR	121	Kim et al., 2010
<i>E. coli</i>	40	8.0	Mn ²⁺ , Fe ²⁺	NR	NR	NR	NR	Yoon et al., 2003
<i>B. longum</i> NRRL B-41409	55	6.0–6.5	Ca ²⁺ , Mg ²⁺	590	120	0.72	48	Salonen et al., 2012
<i>T. mathranii</i> DSM 11426	65	8.0	Mn ²⁺	120	80	NR	NR	Jørgensen et al., 2004
<i>T. saccharolyticus</i> NT0U1	70	7.0–7.5	Mn ²⁺ , Co ²⁺	122	NR	2.41	NR	Hung et al., 2014
<i>B. licheniformis</i> ATCC 14580	50	7.5	Mn ²⁺	NR	369	NR	34	Prabhu et al., 2008
<i>Pediococcus pentosaceus</i> PC-5	50	6.0	Mn ²⁺ , Co ²⁺	66	NR	2.9	NR	Men et al., 2014
<i>L. fermentum</i> CGMCC 2921	65	6.5	Mn ²⁺ , Co ²⁺	60	NR	9.0	19	Xu et al., 2011
<i>L. plantarum</i> NC8	60	7.5	Mn ²⁺	69.7	43.4	1.6	15.5	Chouayekh et al., 2007
<i>B. adolescentis</i> CICC 6178	55	6.5	Mn ²⁺ , Zn ²⁺	22.4	40.2	9.3	8.6	This study

NR, Not Reported.



from probiotic strain might have potential for the food-grade D-tagatose production.

Effects of Temperature and pH on the Enzyme Activity and Stability

Experiments were done at different temperatures ranged between 45 and 70°C to determine the effects of this important factor on the activity of BAAI that varied significantly among the temperatures ($p < 0.001$). As shown in **Figure 2A**, optimum temperature for the maximum activity of BAAI was found to be 55°C. Similar temperature was also reported as the

optimum temperature for L-AI of *B. longum* (Salonen et al., 2012). At 50–65°C, activity of BAAI was stable until 60 min (almost no change), while as much as 80% of the activity retained after 120 min (**Figure 2B**). On the other hand, a higher temperature above the optimum temperature, particularly at 80°C, activity of BAAI decreased over time (**Figure 2B**). This might be due to the denaturation of the enzyme at high temperatures and over time, in addition to the generation of unwanted by-products under such conditions. L-AI from the thermophilic and hyper thermophilic microbes, such as L-AI of *Thermotoga maritima*, are highly thermostable and require high temperatures (Lee et al., 2004), which is not

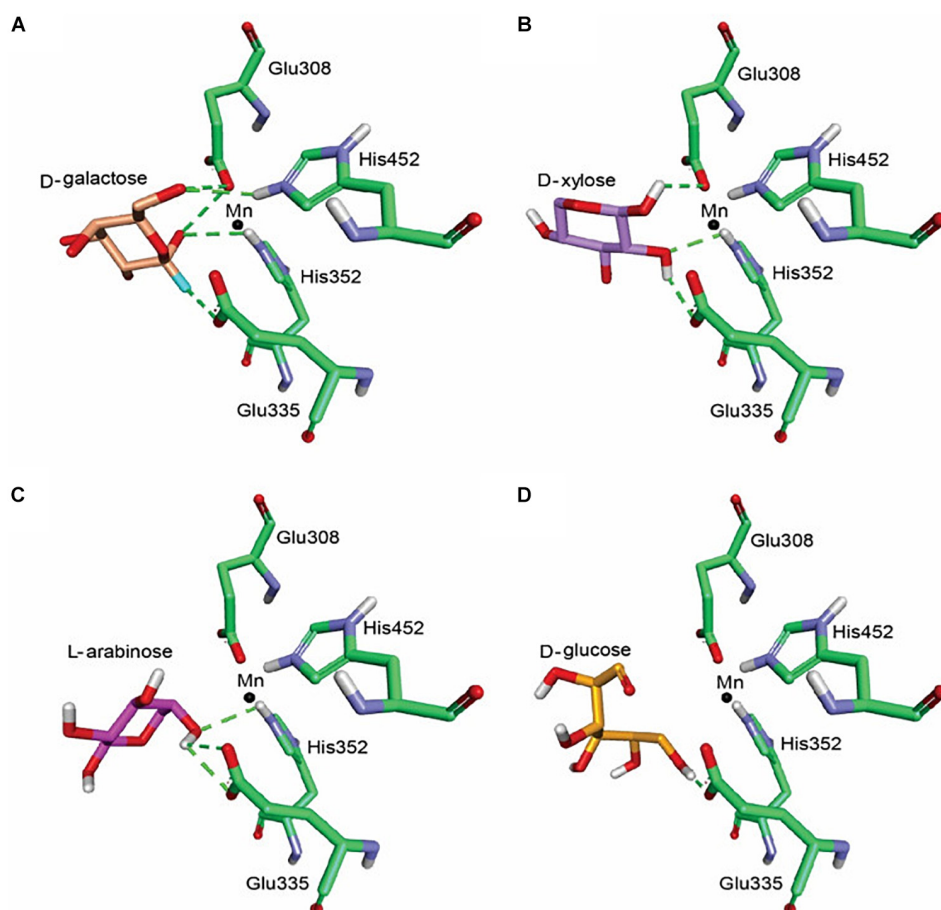


FIGURE 4 | Molecular docking of BAAI for the active sites that interact with D-Galactose (A), D-xylose (B), L-arabinose (C), and D-glucose (D). The green dotted line denotes the H-bonds between the substrates and the active sites of BAAI.

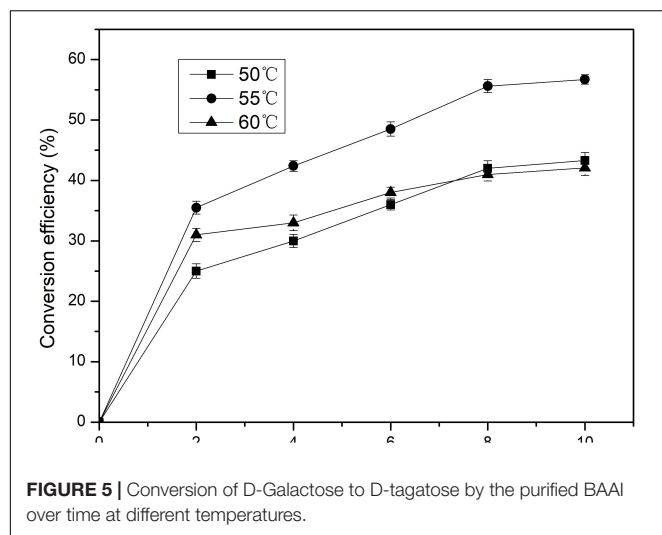
viable for the production of D-tagatose on industrial scale. On the other hand, L-AIs from the mesophilic microorganisms, including *L. plantarum* NC8 (Chouayekh et al., 2007) and *L. fermentum* CGMCC2921 (Xu et al., 2011), also showed excellent thermostability, but they were effective at relatively lower temperatures compared to those of thermophilic bacteria. In particular, BAAI showed higher stability than the L-AI of *B. longum* (Salonen et al., 2012).

Effects of pH on the activity of BAAI were determined by conducting experiments at pH 3–10, in which activity varied significantly among the pH conditions ($p < 0.001$). BAAI showed its maximum activity under slightly acidic condition at pH 6.5 (Figure 2C), while more than 90% activity was found at pH 6.0–7.0. Activity of BAAI was stable at a broad range of pH varied from 6.0 to 7.0 until 24 h (Figure 2D). Earlier it was reported that a slightly acidic condition is important for industrial applications of L-AI to minimize by-products formation (Xu et al., 2018). On the other hand, lactose hydrolysis by β -galactosidase for generating D-Galactose was also affected by the acid pH (Zhan et al., 2014). Similar requirement would make the co-production based on β -galactosidase and L-AI from lactose to D-tagatose more efficient. However, most of the reported L-AIs displayed

maximal activity of this enzyme at neutral or alkaline pH (Xu et al., 2018). Therefore, thermostable BAAI with optimum activity at a slightly acid pH could hold great potential for D-tagatose production.

Effects of Metallic Ions on the Activity of BAAI

Activities of most of L-AIs are dependent on divalent metal ions, especially Co^{2+} and Mn^{2+} significantly play important roles on the activity of L-AI (Xu et al., 2018). Compared to the control (without any metal ions), BAAI showed its higher catalytic activity in the presence of Fe^{2+} , Zn^{2+} , Mn^{2+} ($p < 0.05$), and Ca^{2+} , where maximum activity was provided by Mn^{2+} (Figure 2E). On the other hand, Co^{2+} , Ni^{2+} , Cu^{2+} , and EDTA reduced the activity of BAAI to around 80% compared with the activity of the control (Figure 2E). Considering the obtainment of maximum activity with Mn^{2+} , experiments were done under various concentrations of this metal ion (Figure 2F). Maximum activity was obtained for 6 mM of Mn^{2+} . Above 6 mM of Mn^{2+} , enzyme activity was found to be plateaued or even decreased. Possible reasons for such findings could be due to the fact



that excessive ions inhibited the enzyme activity to increase the apparent K_m , which had led to a decrease in the enzyme activity.

Substrate Specificity of BAAI

L-AIs can bind and act on various aldoses as the substrates. Therefore, substrate specificity of BAAI was determined by conducting experiments with five aldose sugars and results are shown in **Figure 2G**. Specificity of BAAI varied significantly among the substrates ($p < 0.01$). BAAI showed its maximum specificity to D-Galactose among aldoses tested at a relative activity of 100%, while no conversion was observed for D-mannose. Specificities of BAAI to the other three substrates were found to be 67.2% for D-glucose, 82.4% for L-arabinose, and 92.7% for D-xylose. Earlier, almost all of the reported L-AIs showed specificities with both L-arabinose and D-Galactose, in which higher specificities were recorded with L-arabinose than D-Galactose (Xu et al., 2018). For example, L-AIs of *Acidothermus cellulolyticus* ATCC 43068 (Cheng et al., 2010), *Bacillus stearothermophilus* US100 (Rhimi and Bejar, 2006), and *Lactobacillus reuteri* (Petra et al., 2014) showed maximum specificities with L-arabinose. Specially, L-AIs of *B. subtilis* str. 168 (Kim et al., 2010) and *Pseudoalteromonas haloplanktis* ATCC 14393 (Xu et al., 2016) showed specificity only to L-arabinose and could not convert D-Galactose into D-tagatose.

Kinetic Parameters of BAAI

Non-linear regression fitting of Michaelis–Menten equation was determined for two major substrates, namely D-Galactose and L-arabinose under the optimum conditions (55°C, pH 6.5). Initial velocities were determined in the standard assay mixture. D-Galactose and L-arabinose had hyperbolic saturation curves, and the corresponding double-reciprocal plot was linear. The K_m values of BAAI for D-Galactose and L-arabinose were 22.4 mM (V_{max} , 489 U/mg) and 40.2 mM (V_{max} , 275.1 U/mg), respectively. Interestingly, K_m for L-arabinose was almost twofolds higher than that of D-Galactose, while V_{max} was twofolds lower for the former than for the latter. The K_{cat}/K_m values for D-Galactose

and L-arabinose were found to be $9.3 \text{ mM}^{-1} \text{ min}^{-1}$ and $8.6 \text{ mM}^{-1} \text{ min}^{-1}$, respectively. The higher V_{max} , and K_{cat}/K_m of BAAI with D-Galactose indicated a higher catalytic efficiency of BAAI with D-Galactose, which were compared and summarize in **Table 1** with other L-AIs.

Structural Homology and Protein-Substrate Docking

Biochemical and sequence analyses of BAAI displayed substrate specificity with four different type of substrates and conservation of catalytic active site with other L-AIs. For further analysis of substrates interaction and structural compression, homology model was generated and docked with the substrates. Homology model of BAAI was generated using ECAI (4F2D) as a template by SWISS-MODEL (**Figure 3A**). This model contained 99.8% of the total amino acid residues in the favorable and allowed regions, whereas only 0.2% of residues in the disallowed regions. MSA analysis of the protein revealed that high conservation was located at the catalytic sites, which was structurally superimposed as determined by the discovery studio visualizer (**Figure 3B**). The superimposed structures of the proteins showed similar orientation of the catalytic amino acids (**Figure 3B**).

BAAI demonstrated substrate specificities with D-Galactose, D-xylose, L-arabinose, and D-glucose in the biochemical assay (**Figure 2G**). Further investigation on the interaction of BAAI with these substrates were revealed by docking with 3-D homology model. Among the substrates, D-Galactose exhibited interaction with all four catalytic residues through five H-bonds (**Figure 4A**), whereas D-xylose and L-arabinose showed three H-bonds (**Figures 4B,C**). On the other hand, D-glucose could bind loosely with the active site of BAAI due to a single H-bond (**Figure 4D**). These results could explain the reasons for varying specificity of BAAI to different substrates that were solely for the difference in the interaction of these substrates with BAAI. Based on the biochemical and docking analyses, D-Galactose would be the best substrate for BAAI, followed by D-xylose, L-arabinose, and D-glucose.

Enzymatic Conversion for D-Tagatose Production

Isomerization reaction of D-Galactose to D-tagatose by BAAI was further investigated at different temperature (50, 55, and 60°C) and pH 6.5 for 10 h. The maximum conversion of D-Galactose into D-tagatose reached after 8 h (**Figure 5**). Conversion efficiency of D-Galactose to D-tagatose reaction were nearly 40% at 50 and 60°C, which was 56.7% at 55°C. Conversion efficiency increased with time at 55°C and reached to the maximum after 8 h. This maximum conversion efficiency of BAAI was higher than the efficiency reported for several other L-AIs earlier, such as L-AI of *L. plantarum* NC8 (30%, 6 h, at 60°C) (Chouayekh et al., 2007), and L-AI from *A. cellulolyticus* (53%, 12 h at 75°C) (Cheng et al., 2010). This study showed that the probiotic-derived BAAI has good potential for the production of D-tagatose, which suggested that the intestinal bacteria *Bifidobacterium* and lactic acid bacteria, could be good sources of L-AI.

CONCLUSION

This study elucidates the biochemical and structural features of BAAI for the first time, with revealing its efficiency to convert D-Galactose into D-tagatose. The comparative structural analysis of the characterized BAAI and other L-AIs had similar amino acid residues conservation at the catalytic sites. The protein-ligand docking of BAAI identified a strong interaction between the residues of catalytic site and D-Galactose (preferred substrate). Subsequent bioconversion of D-Galactose into D-tagatose with the purified BAAI provided 56.7% conversion efficiency after 10 h at 55°C, which is excellently comparable with the efficiencies of other L-AIs reported thus far.

DATA AVAILABILITY STATEMENT

All datasets generated for this study are included in the article/supplementary material.

REFERENCES

- Bradford, M. M. (1976). A rapid and sensitive method for the quantitation of microgram quantities of protein utilizing the principle of protein-dye binding. *Anal. Biochem.* 72, 248–254. doi: 10.1016/0003-2697(76)90527-3
- Chang, X., Ying, B., Zhang, Y., Cao, H., Zhou, T., Zhong, P., et al. (2016). The Study of Food-grade induced expression and enzymatic properties of L-arabinose Isomerase from *Lactobacillus plantarum* WU14 with High D-Tagatose yield. *Food Nutr. Sci.* 7, 320–337. doi: 10.4236/fns.2016.74034
- Cheng, L., Mu, W., Zhang, T., and Jiang, B. (2010). An L-arabinose isomerase from *Acidothermus cellulolyticus* ATCC 43068: cloning, expression, purification, and characterization. *Appl. Microbiol. Biot.* 86, 1089–1097. doi: 10.1007/s00253-009-2322-z
- Choi, J. M., Lee, Y. J., Cao, T. P., Shin, S. M., Park, M. K., Lee, H. S., et al. (2016). Structure of the thermophilic L-arabinose isomerase from *Geobacillus kaustophilus* reveals metal-mediated intersubunit interactions for activity and thermostability. *Arch. Biochem. Biophys.* 596, 51–62. doi: 10.1016/j.abb.2016.02.033
- Chouayekh, H., Bejar, W., Rhimi, M., Jelleli, K., Mseddi, M., and Bejar, S. (2007). Characterization of an L-arabinose isomerase from the *Lactobacillus plantarum* NC8 strain showing pronounced stability at acidic pH. *FEMS Microbiol. Lett.* 277, 260–267. doi: 10.1111/j.1574-6968.2007.00961.x
- DeLano, W. L. (2002). Pymol: an open-source molecular graphics tool. *NEWSL. Protein Crystallogr* 40, 82–92.
- Dische, Z., and Borenfreund, E. (2007). A new spectrophotometric method for the detection and determination of hexo sugars and trioses. *J. Biol. Chem.* 67, 14–21.
- Gao, H., Qi, X., Hart, D. J., Gao, S., Wang, H., Xu, S., et al. (2018). Three Novel *Escherichia coli* vectors for convenient and efficient molecular biological manipulations. *J. Agr. Food Chem.* 66, 6123–6131. doi: 10.1021/acs.jafc.8b01960
- Guo, Q., An, Y., Yun, J., Yang, M., Magocha, T. A., Zhu, J., et al. (2018). Enhanced D-tagatose production by spore surface-displayed L-arabinose isomerase from isolated *Lactobacillus brevis* PC16 and biotransformation. *Bioresour. Technol.* 247, 940–946. doi: 10.1016/j.biortech.2017.09.187
- Hung, X. G., Tseng, W. C., Liu, S. M., Tzou, W. S., and Fang, T. Y. (2014). Characterization of a thermophilic L-arabinose isomerase from *Thermoanaerobacterium saccharolyticum* NT0U1. *Biochem. Eng. J.* 83, 121–128. doi: 10.1016/j.bej.2013.04.026
- Jørgensen, F., Hansen, O. C., and Stougaard, P. (2004). Enzymatic conversion of D-Galactose to D-tagatose: heterologous expression and characterisation of a thermostable L-arabinose isomerase from *Thermoanaerobacter mathranii*. *Appl. Microbiol. Biot.* 64, 816–822. doi: 10.1007/s00253-004-1578-6
- Kim, H. J., and Oh, D. K. (2005). Purification and characterization of an L-arabinose isomerase from an isolated strain of *Geobacillus thermodenitrificans* producing D-tagatose. *J. Biotechnol.* 120, 162–173. doi: 10.1016/j.jbiotec.2005.06.004
- Kim, J. H., Prabhu, P., Jeya, M., Tiwari, M. K., Moon, H. J., Singh, R. K., et al. (2010). Characterization of an L-arabinose isomerase from *Bacillus subtilis*. *Appl. Microbiol. Biot.* 85, 1839–1847. doi: 10.1007/s00253-009-2210-6
- Kim, P. (2004). Current studies on biological tagatose production using L-arabinose isomerase: a review and future perspective. *Appl. Microbiol. Biot.* 65, 243–249. doi: 10.1007/s00253-004-1665-8
- Kim, P., Yoon, S. H., Roh, H. J., and Choi, J. H. (2001). High production of D-tagatose, a potential sugar substitute, using immobilized L-arabinose isomerase. *Biotechnol. Progr.* 17, 208–210. doi: 10.1021/bp000147u
- Laskowski, R. A., MacArthur, M. W., Moss, D. S., and Thornton, J. M. (1993). PROCHECK: a program to check the stereochemical quality of protein structures. *J. Appl. Crystallogr.* 26, 283–291. doi: 10.1107/s0021889892009944
- Lee, D. W., Choe, E. A., Kim, S. B., Eom, S. H., Hong, Y. H., Lee, S. J., et al. (2005). Distinct metal dependence for catalytic and structural functions in the L-arabinose isomerases from the mesophilic *Bacillus halodurans* and the thermophilic *Geobacillus stearothermophilus*. *Arch. Biochem. Biophys.* 434, 333–343. doi: 10.1016/j.abb.2004.11.004
- Lee, D. W., Jang, H. J., Choe, E. A., Kim, B. C., Lee, S. J., Kim, S. B., et al. (2004). Characterization of a Thermostable L-arabinose (D-Galactose) isomerase from the hyperthermophilic eubacterium *Thermotoga maritima*. *Appl. Environ. Microb.* 70, 1397–1404. doi: 10.1128/AEM.70.3.1397-1404.2004
- Li, Y., Zhu, Y., Liu, A., and Sun, Y. (2011). Identification and characterization of a novel L-arabinose isomerase from *Anoxybacillus flavithermus* useful in D-tagatose production. *Extremophiles* 15, 441–450. doi: 10.1007/s00792-011-0375-2
- Liu, X., Li, T., Hart, D. J., Gao, S., Wang, H., Gao, H., et al. (2018). A universal mini-vector and an annealing of PCR products (APP)-based cloning strategy for convenient molecular biological manipulations. *Biochem. Bioph. Res.* 497, 978–982. doi: 10.1016/j.bbrc.2018.02.099
- Lu, Y., Levin, G. V., and Donner, T. W. (2008). Tagatose, a new antidiabetic and obesity control drug. *Diabetes Obes. Metab.* 10, 109–134. doi: 10.1111/j.1463-1326.2007.00799.x
- Marylana, D. S., Ricardo, M. M., José, L. G., Enrique, J. M., Luciana, R. B. G., and Benevides, C. P. (2017). Engineering the L-arabinose isomerase from *Enterococcus faecium* for D-Tagatose synthesis. *Molecules* 22:2164. doi: 10.3390/molecules22122164
- Mei, W., Wang, L., Zang, Y., Zheng, Z., and Ouyang, J. (2016). Characterization of an L-arabinose isomerase from *Bacillus coagulans* NL01 and its application for D-tagatose production. *BMC Biotechnol.* 16:55. doi: 10.1186/s12896-016-0286-5

AUTHOR CONTRIBUTIONS

XQ, GZ, and YA designed the study. GZ performed all the experiments, analyzed the data, and drafted the manuscript. AP assisted in the docking studies. JY assisted in the recombinant strain construction and protein purification. HZ and XQ helped to revise the manuscript. All authors have read and approved the manuscript.

FUNDING

This work was supported by the National Natural Science Foundation of China (Grant Nos. 31950410550, 31972042, and 31571806), China Postdoctoral Science Foundation (Grant Nos. 2019T120402 and 2017M621657), High-level talents project of Six Talent Peaks in Jiangsu Province (Grant No. SWYY-018), and National Key R&D Program of China (Grant No. 2017YFC1600806).

- Men, Y., Zhu, Y., Zhang, L., Kang, Z., Izumori, K., Sun, Y., et al. (2014). Enzymatic conversion of D-Galactose to D-tagatose: cloning, overexpression and characterization of L-arabinose isomerase from *Pediococcus pentosaceus* PC-5. *Microbiol. Res.* 169, 171–178. doi: 10.1016/j.micres.2013.07.001
- Nguyen, T. K., Hong, M. G., Chang, P. S., Lee, B. H., and Yoo, S. H. (2018). Biochemical properties of L-arabinose isomerase from *Clostridium hylemonae* to produce D-tagatose as a functional sweetener. *PLoS One* 13:1–12. doi: 10.1371/journal.pone.0196099
- Oh, D. K. (2007). Tagatose: properties, applications, and biotechnological processes. *Appl. Microbiol. Biotechnol.* 76, 1–8. doi: 10.1007/s00253-007-0981-1
- Petra, S., Dietmar, H., and Peterbauer, C. K. (2014). L-arabinose Isomerase and D-Xylose Isomerase from *Lactobacillus reuteri*: characterization, Co-expression in the food grade host *Lactobacillus plantarum*, and application in the conversion of D-Galactose and D-Glucose. *J. Agr. Food Chem.* 62, 1617–1624. doi: 10.1021/jf404785m
- Prabhu, P., Kumar Tiwari, M., Jeya, M., Gunasekaran, P., Kim, I. W., and Lee, J. K. (2008). Cloning and characterization of a novel L-arabinose isomerase from *Bacillus licheniformis*. *Appl. Microbiol. Biot.* 81, 283–290. doi: 10.1007/s00253-008-1652-6
- Qi, X., Yun, J., Qi, Y., Zhang, H., Wang, F., Guo, Q., et al. (2016). Expression and characterization of a novel 1,3-Propanediol Dehydrogenase from *Lactobacillus brevis*. *Appl. Biochem. Biotech.* 179, 959–972. doi: 10.1007/s12010-016-2043-6
- Qi, X., Zhang, H., Magocha, T. A., An, Y., Yun, J., Yang, M., et al. (2017). Improved xylitol production by expressing a novel D-arabitol dehydrogenase from isolated *Gluconobacter* sp. JX-05 and co-biotransformation of whole cells. *Bioresour. Tech.* 235, 50–58. doi: 10.1016/j.biortech.2017.03.107
- Rhimi, M., and Bejar, S. (2006). Cloning, purification and biochemical characterization of metallic-ions independent and thermoactive L-arabinose isomerase from the *Bacillus stearothermophilus* US100 strain. *Biochim. Biophys. Acta* 1760, 191–199. doi: 10.1016/j.pnucene.2007.08.008
- Salonen, N., Nyssölä, A., Salonen, K., and Turunen, O. (2012). *Bifidobacterium longum* L-arabinose isomerase overexpression in *Lactococcus lactis*, purification, and characterization. *Appl. Biochem. Biotech.* 168, 392–405. doi: 10.1007/s12010-012-9783-8
- Sievers, F., Andreas, W., David, D., Toby, J. G., Kevin, K., Wei, L., et al. (2011). Fast, scalable generation of high-quality protein multiple sequence alignments using Clustal Omega. *Mol. Syst. Biol.* 7:539. doi: 10.1038/msb.2011.75
- Trott, O., and Olson, A. J. (2009). AutoDock Vina: improving the speed and accuracy of docking with a new scoring function, efficient optimization, and multithreading. *J. Comput. Chem.* 12, 455–461. doi: 10.1002/jcc.21334
- Waterhouse, A., Bertoni, M., Bienert, S., Studer, G., Tauriello, G., Gumienny, R., et al. (2018). SWISS-MODEL: homology modelling of protein structures and complexes. *Nucleic Acids Res.* 46, 296–303. doi: 10.1093/nar/gky427
- Wu, H., Huang, J., Deng, Y., Zhang, W., and Mu, W. (2020). Production of L-ribose from L-arabinose by co-expression of L-arabinose isomerase and D-lyxose isomerase in *Escherichia coli*. *Enzyme Microb. Tech.* 132:109443. doi: 10.1016/j.enzymictec.2019.109443
- Xu, W., Fan, C., Zhang, T., Jiang, B., and Mu, W. (2016). Cloning, expression, and characterization of a novel L-arabinose isomerase from the psychrotolerant bacterium *Pseudoalteromonas haloplanktis*. *Mol. Biotechnol.* 58, 695–706. doi: 10.1007/s12033-016-9969-3
- Xu, W., Zhang, W. L., Zhang, T., Jiang, B., and Mu, W. M. (2018). L-arabinose isomerases: characteristics, modification, and application. *Trends Food Sci. Tech.* 78, 25–33. doi: 10.1016/j.tifs.2018.05.016
- Xu, Z., Qing, Y., Li, S., Feng, X., Xu, H., and Ouyang, P. (2011). A novel L-arabinose isomerase from *Lactobacillus fermentum* CGMCC2921 for D-tagatose production: gene cloning, purification and characterization. *J. Mol. Catal. B-Enzym.* 70, 1–7. doi: 10.1016/j.molcatb.2011.01.010
- Yoon, S. H., Kim, P., and Oh, D. K. (2003). Properties of L-arabinose isomerase from *Escherichia coli* as biocatalyst for tagatose production. *World J. Microbiol. Biot.* 19, 47–51. doi: 10.1023/A:1022575601492
- Yun, J., Yang, M., Magocha, T. A., Zhang, H., Xue, Y., Zhang, G., et al. (2018). Production of 1,3-propanediol using a novel 1,3-propanediol dehydrogenase from isolated *Clostridium butyricum* and co-biotransformation of whole cells. *Bioresour. Tech.* 247, 838–843. doi: 10.1016/j.biortech.2017.09.180
- Zhan, Y., Xu, Z., Li, S., Liu, X., Xu, L., Feng, X., et al. (2014). Coexpression of β -D-galactosidase and L-arabinose isomerase in the production of D-tagatose: a functional sweetener. *J. Agr. Food Chem.* 62, 2412–2417. doi: 10.1021/jf4042485
- Zhang, G., An, Y., Zayed, H., Guo, Q., Yang, M., Yuan, J., et al. (2019). *Bacillus subtilis* spore surface display technology: a review of its development and applications. *J. Microbiol. Biotechnol.* 29, 179–190. doi: 10.4014/jmb.1807.06066
- Zhang, G., Zayed, H., Yun, J., Yuan, J., Zhang, Y., Wang, Y., et al. (2020). Two-stage biosynthesis of D-tagatose from milk whey powder by an engineered *Escherichia coli* strain expressing L-arabinose isomerase from *Lactobacillus plantarum*. *Bioresour. Tech.* 305:123010. doi: 10.1016/j.biortech.2020.123010
- Zhang, H., Yun, J., Zayed, H., Yang, M., Zhang, G., Qi, Y., et al. (2018). Production of xylitol by expressing xylitol dehydrogenase and alcohol dehydrogenase from *Gluconobacter thailandicus* and co-biotransformation of whole cells. *Bioresour. Tech.* 257, 223–228. doi: 10.1016/j.biortech.2018.02.095
- Zhang, Y., Fan, Y., Hu, H., Yang, H., Luo, X., Li, Z., et al. (2017). D-Tagatose production by *Lactococcus lactis* NZ9000 Cells Harboring *Lactobacillus plantarum* L-arabinose Isomerase. *Indian J. Pharm. Educ.* 51, 288–294. doi: 10.5530/ijper.51.2.34

Conflict of Interest: The authors declare that the research was conducted in the absence of any commercial or financial relationships that could be construed as a potential conflict of interest.

Copyright © 2020 Zhang, An, Parvez, Zayed, Yun and Qi. This is an open-access article distributed under the terms of the Creative Commons Attribution License (CC BY). The use, distribution or reproduction in other forums is permitted, provided the original author(s) and the copyright owner(s) are credited and that the original publication in this journal is cited, in accordance with accepted academic practice. No use, distribution or reproduction is permitted which does not comply with these terms.



High-Efficiency Secretion and Directed Evolution of Chitinase BcChiA1 in *Bacillus subtilis* for the Conversion of Chitinaceous Wastes Into Chitooligosaccharides

Sijia Wang^{1,2}, Gang Fu^{3,4}, Jinlong Li^{3,5}, Xunfan Wei⁶, Huan Fang^{3,4}, Dawei Huang^{1,6*}, Jianping Lin^{3,5,7*} and Dawei Zhang^{3,4*}

OPEN ACCESS

Edited by:

Thomas Bartholomäus Brück,
Technical University of Munich,
Germany

Reviewed by:

Wolfram Brück,
University of Applied Sciences
and Arts of Western Switzerland,
Switzerland
Christopher John Brigham,
Wentworth Institute of Technology,
United States

*Correspondence:

Dawei Huang
huangdw@ioz.ac.cn
Jianping Lin
jianpinglin@nankai.edu.cn
Dawei Zhang
zhang_dw@tib.cas.cn

Specialty section:

This article was submitted to
Bioprocess Engineering,
a section of the journal
Frontiers in Bioengineering and
Biotechnology

Received: 18 February 2020

Accepted: 15 April 2020

Published: 07 May 2020

Citation:

Wang S, Fu G, Li J, Wei X,
Fang H, Huang D, Lin J and Zhang D
(2020) High-Efficiency Secretion
and Directed Evolution of Chitinase
BcChiA1 in *Bacillus subtilis*
for the Conversion of Chitinaceous
Wastes Into Chitooligosaccharides.
Front. Bioeng. Biotechnol. 8:432.
doi: 10.3389/fbioe.2020.00432

¹ Key Laboratory of Zoological Systematics and Evolution, Institute of Zoology, Chinese Academy of Sciences, Beijing, China, ² University of Chinese Academy of Sciences, Beijing, China, ³ Tianjin Institute of Industrial Biotechnology, Chinese Academy of Sciences, Tianjin, China, ⁴ Key Laboratory of Systems Microbial Biotechnology, Chinese Academy of Sciences, Tianjin, China, ⁵ Biodesign Center, Tianjin Institute of Industrial Biotechnology, Chinese Academy of Sciences, Tianjin, China, ⁶ College of Life Sciences, Nankai University, Tianjin, China, ⁷ College of Pharmacy, Nankai University, Tianjin, China

Limitations of enzyme production and activity pose a challenge for efficient degradation of chitinaceous wastes. To solve this problem, we engineered a system for high-yielding extracellular secretion of chitinase A1 from *Bacillus circulans* (BcChiA1) in *B. subtilis*. Furthermore, an innovative chitinase high-throughput screening method based on colloidal chitin stained with Remazol Brilliant Blue R (CC-RBB) was established and used to identify three mutants with improved chitinase activity: Y10A/R301A/E327A (Mu1), Y10A/D81A/E327A (Mu2), and F38A/K88A/R301A (Mu3). Their highest specific activity reached 1004.83 ± 0.87 U/mg, representing a 16.89-fold increase in activity compared to native BcChiA1. Additionally, we found that there is a synergistic effect between BcChiA1 and a lytic polysaccharide monooxygenase from *Bacillus atrophaeus* (BatLPMO10), which increased the chitin processing efficiency by 50% after combining the two enzymes. The yield of chitooligosaccharide (COS) production using the mutant Mu1 and BatLPMO10 reached 2885.25 ± 2.22 mg/L. Taken together, the results indicated that the CC-RBB high-throughput screening method is a useful tool for chitinase screening, and evolution of BcChiA1 in collaboration with BatLPMO10 has tremendous application potential in the biological treatment of chitinaceous wastes for COS production.

Keywords: chitin, chitinase, BcChiA1, high-throughput screening, synergistic effect, BatLPMO10, chitooligosaccharide

INTRODUCTION

Chitin is an insoluble, linear, high molecular weight polymer composed of β -1,4 linked N-acetylglucosamine (GlcNAc) units, and is one of the most ubiquitous polysaccharides in nature, second only to cellulose (Singh et al., 2017). It is the major structural component of a wide range of organisms, most notably fungi and arthropods, including species of shrimp and

other seafood (Kumar et al., 2018). It has been reported that the worldwide seafood industry generates approximately 6–8 million tons of shell-waste annually (Gao et al., 2016). However, there is a limited scope of commercial applications of chitin despite its great quantity and notable biochemical characteristics, mainly due to its high crystallinity and insolubility which make processing a challenge (Kumar et al., 2018). Since the degradation of chitin is a time-consuming and arduous task, disposal of chitin-containing waste has become an environmental challenge and is on the verge of becoming a crisis for many countries. Therefore, it is imperative to find an effective and environmentally friendly means to degrade chitinous wastes, and preferably valorize it for use in valuable products. Chito oligosaccharides (COS) are chitin derivatives with a low degree of polymerization (≤ 20) that have great value due to their improved solubility (Liang et al., 2018). Moreover, they are highly biocompatible and non-toxic, and possess reported antiviral, antibacterial, antifungal, immunoregulatory, and antioxidant activities (Liaquat and Eltem, 2018). Hence, COSs have multiple promising applications in various fields such as food processing, biomedicine, agriculture, water purification, and cosmetics (Naveed et al., 2019).

Enzymatic hydrolysis of chitin is a good substitute for chemical treatments. As specific enzymes that convert chitin into COS, chitinases (EC 3.2.1.14) play a pivotal role in chitin biodegradation by catalyzing the hydrolysis of the β -1,4-glycosidic bonds that form chitin. Several chitinases have been isolated and characterized from various sources. *Bacillus circulans* WL-12 was found to secrete at least six chitinases, among which chitinase A1 (BcChiA1) exhibited the highest affinity and hydrolytic activity toward crystalline chitin (Watanabe et al., 2001; Ferrandon, 2003). More importantly, the catalytic mechanism of BcChiA1 has been thoroughly studied (Nakamura et al., 2018), which lays a solid theoretical foundation for follow-up research that can explore the evolution and optimization of BcChiA1.

However, the practical application of these enzymes remains challenging due to the low levels of production and weak activity of chitinases in wild type strains, which limits efforts to break down crystalline chitin. Heterologous expression is an effective strategy to increase the production of target proteins. As one of the most widely used expression systems, *B. subtilis* possesses many advantages such as a high growth rate, short fermentation period, easy genetic manipulation, and superior secretion capacity of recombinant proteins (Cui et al., 2018; Gu et al., 2018; Cai et al., 2019). Moreover, as one of the most widespread and powerful strategies for protein design, directed evolution plays a key role in enhancing the activity of target enzymes through the construction of mutant libraries and high-throughput screening (Porter et al., 2016). For example, the catalytic efficiency of a chitinase from *Beauveria bassiana* was enhanced 2.7-fold (Fan et al., 2007), while that of an improved chitinase from *Bacillus licheniformis* was 2.7-fold higher than that of the wild type (Songsiriritthigul et al., 2009). Despite these promising early efforts, the current methods of directed evolution have not yielded optimal results in chitinases, and there is still much room for innovation and improvement.

Therefore, we created a new screening method based on using colloidal chitin stained with Remazol Brilliant Blue R (CC-RBB) as a substrate to probe chitinase activity. Furthermore, we found explanations for the evolved mutants of BcChiA1 by computing high-energy intermediate (HEI) states, in that the states observed in computational simulations can reflect the catalytic activity of enzyme variants (Bolon and Mayo, 2001; Hermann et al., 2006; Nanda and Koder, 2010; Grisewood et al., 2013; London et al., 2015). Bell and Koshland (1971) demonstrated that covalent enzyme-substrate intermediates participate in enzymatic reactions. The covalent intermediate state is a high-energy or transition state between the ground state and the product state. Lahiri et al. (2003) found that the stabilization of HEI states along the reaction trajectory is the crucial determinant behind the catalytic ability of enzymes.

Improving substrate pretreatment efficiency is also a vital prerequisite to biocatalytic processes. Recent studies have revealed that lytic polysaccharide monoxygenases (LPMOs) can oxidize polysaccharides with high degrees of crystallinity at diverse carbon positions to increase substrate accessibility to glycoside hydrolases (Vaaje-Kolstad et al., 2010; Isaksen et al., 2014). Some studies have shown that the pretreatment of chitin with LPMOs led to increases in product yields between 2.49- and 3-fold compared with chitinase treatment alone (Manjeet et al., 2013; Yang et al., 2017). Here, BatLPMO10, which was identified from a screen of fermented food, was used for chitin pretreatment to maximize the contact between the chitin substrate and BcChiA1, and to further enhance the production of COS.

In this study, we sought to overcome the limitations of catalytic activity and production of wild-type BcChiA1 by establishing a heterologous expression system in *B. subtilis* and performing directed evolution of this enzyme. In addition to optimizing the properties of BcChiA1 itself, we wanted to understand whether there is a synergistic effect between BcChiA1 and BatLPMO10 in the biodegradation of chitin. Thus, our objective is not only to achieve the highly efficient degradation of chitinous wastes, but also to obtain valuable COS products with high yield.

MATERIALS AND METHODS

Bacterial Strains, Plasmids and Culture Conditions

The bacterial strains and plasmids used in this study are listed in the **Supplementary Material**. *E. coli* DH5 α was used for molecular cloning and plasmid construction, while *B. subtilis* 1A751 served as the expression host for BcChiA1 and BatLPMO10. All the bacterial strains were cultured in Luria-Bertani medium at 37°C and 220 rpm. The plasmid pMATE (Yue et al., 2017) was used as the expression vector for BcChiA1 and BatLPMO10.

Plasmid Construction

The primers and the signal peptides used in this study are listed in the **Supplementary Material**. The genes encoding BcChiA1 from *Bacillus circulans* (GenBank: AAA81528.1) and

BatLPMO10 from *Bacillus atrophaeus* (GenBank: ADP32663.1), both without the native signal peptide and with a C-terminal his-tag, were codon optimized and synthesized by GENEWIZ (Suzhou, China). The plasmid backbone of pMATE including the promoter P_{malA} is from our laboratory. SP_{phoD} , SP_{lipA} , SP_{ywbN} , SP_{nprE} , SP_{sacB} , and SP_{yvcE} (SP: signal peptide) were obtained by PCR using the genome of *B. subtilis* 168 as the template. All the DNA fragments were amplified using PrimeSTAR polymerase (Takara, Dalian, China). Construction of the recombinant plasmids was entirely in accordance with the operating instructions of the ClonExpress® II One Step Cloning Kit (Vazyme Biotech Co., Ltd, Nanjing, China). The basic molecular cloning techniques were described in the literature (Spizizen, 1958; Sambrook et al., 1989; Smith, 1991). Based on the resistance markers on the plasmids, the transformants were selected on Luria-Bertani agar plates containing 100 µg/mL ampicillin for *E. coli* or 20 µg/mL kanamycin for *B. subtilis*.

Shake-Flask Fermentation Experiments and SDS-PAGE Analysis

The recombinant strains were streaked onto Luria-Bertani agar plates containing 20 µg/mL kanamycin and cultivated overnight at 37°C. Then, a single colony was used to inoculate fresh Luria-Bertani medium as the seed for further fermentation. The resulting seed cultures were transferred at 1% inoculum size into 30 mL of 2 × SR medium (30 g/L tryptone, 50 g/L yeast extract and 6 g/L K_2HPO_4 , pH 7.2) with 50 µg/mL kanamycin in 250 mL shake flasks, and cultivated at 37°C and 220 rpm for 48 h. After inoculation, 30 g/L final concentration of maltose was added from a 500 g/L stock solution as inducer immediately.

After 48 h of fermentation, the supernatant components of the samples were collected by centrifugation (4°C, 14,000 g, 10 min). The cell precipitate was resuspended in 50 µl lysis buffer (50 mM Tris-HCl, 2.5 mM EDTA, pH 8.0) per one unit of OD₆₀₀. After adding 1:5 volume of 5 × SDS-PAGE sample loading buffer [250 mM Tris-HCl, 10% (v/v) SDS, 0.5% (w/v) bromophenol blue, 50% (v/v) glycerol, and 5% (w/v) β-mercaptoethanol, pH 6.8], the samples were boiled for 20 min. SDS-PAGE was carried out on NuPAGE 10% Bis-Tris protein gels (Invitrogen Life Technologies, CA, United States) to investigate the expression of BcChiA1 and BatLPMO10. The gels were stained with Coomassie Brilliant Blue R-250 (Solarbio life sciences, Beijing, China), and ColorMixed Prestained Protein Marker (Solarbio Life Sciences, Beijing, China) was used to evaluate the approximate molecular weight of the target proteins.

Enzyme Purification and Chitinase Activity Assay

The purification of BcChiA1 and BatLPMO10 was conducted at 4°C. After shake-flask fermentation, the crude enzymes were collected by centrifugation at 18,693 × g for 20 min and subsequently loaded onto the affinity columns (1.5 × 8 cm) containing 5 ml Ni NTA Beads 6FF (Solarbio Life Sciences, Beijing, China) and allowed to bind for 2 h. The beads were washed with buffer A (50 mM sodium phosphate, pH 7.6), followed by a gradient of buffer B (50 mM Tris-HCl, 500 mM

NaCl, 50–300 mM imidazole) to wash out the impurities and weakly bound proteins. BcChiA1 and BatLPMO10 were eluted with buffer C (50 mM Tris-HCl, 500 mM imidazole and 500 mM NaCl) and the volume was reduced to 2 ml by ultrafiltration through 10 kDa and 3 kDa molecular weight cutoff membranes (Millipore, United States), respectively. The two purified enzymes were verified by SDS-PAGE and their concentrations were determined using the BCA Protein Quantitation Kit (Solarbio Life Sciences, Beijing, China).

A sensitive and simple method based on the substrate CC-RBB was used to evaluate the chitinase activity as described previously (Gómez Ramírez et al., 2004). A mixture comprising 1 ml of the enzyme solution and 1 ml of 40% (w/v) CC-RBB suspension was incubated at 50°C for 1 h. Enzymes deactivated by boiling in a water bath for 10 min were used as negative controls. All the tubes were centrifuged at 12396 × g for 5 min, and the absorption of the supernatants was measured at 595 nm. One unit (U) of chitinase activity was defined as the amount of enzyme that causes an increase of 0.01 in the absorbance under the above conditions. The protein concentrations of the enzyme samples were determined as described above.

Microstructure Analysis of Chitin Treated With BcChiA1

The morphology of the treated chitin was analyzed by scanning electron microscopy (SEM) using a HT7700 Exalens (Hitachi, Tokyo, Japan). Samples were dehydrated using the critical point drying method and fastened to a metal stub using conductive carbon tape. The chitin was sprayed with a platinum film (Pt coated) and observed at an acceleration voltage of 15 kV (Huang et al., 2018).

Fourier Transform Infrared Spectroscopy (FT-IR) was carried out on a Nicolet IS5 670 (Nicolet Tech, Wisconsin, United States) within a range of 4000 cm⁻¹ to 400 cm⁻¹ based on the attenuated total reflection method (Zhang et al., 2018).

The X-ray diffraction (XRD) measurements were conducted on a Bruker D8 Advance diffractometer (Bruker, Karlsruhe, Germany) with Cu Kα radiation ($\lambda = 1.5418 \text{ \AA}$). The data on the X-ray powder diffraction of chitin was obtained in a range of 2θ from 5° to 60° in steps of 0.02°. The crystallinity index (I_{CR}) of the chitin samples was calculated according to the formula $I_{CR} (\%) = (I_{110} - I_{am}) / I_{110} \times 100\%$, where I_{110} refers to the peaks at $2\theta \approx 20^\circ$, corresponding to the maximum intensity, and I_{am} represents the intensity of the amorphous diffraction at $2\theta \approx 16^\circ$, as described before (Zhang et al., 2018).

Synergistic Effects of BcChiA1 and BatLPMO10 on the Degradation of Chitin

To determine the synergistic action of BcChiA1 and BatLPMO10, samples comprising 500 µl of purified BatLPMO10 (9, 18, 36, 72, 144, or 288 nmol), 1 ml of 40% CC-RBB in sodium phosphate buffer (50 mM, pH 7.0) and 1 mM ascorbic acid were incubated at 50°C for 1 h. Enzymes deactivated by boiling in a water bath for 10 min were used as negative controls. Then, 500 µl of purified BcChiA1 (9 nmol) was added and the mixtures were incubated for another 1 h at 50°C. All the enzyme reactions were

conducted under constant shaking at 200 rpm. After that, the reaction mixture was centrifuged at $12396 \times g$ for 5 min, and the absorbance of the supernatants was measured at 595 nm. All reactions were performed in triplicate.

High-Performance Liquid Chromatography

The degradation products of chitin were analyzed via HPLC on a Waters 600 instrument (Waters Corp., Milford, MA, United States) equipped with an NH₂ Column (5 μ m, 4.6 mm \times 250 mm; Shimadzu, Kyoto, Japan) and an ultraviolet detector set at 195 nm. A reaction system containing 1U purified chitinase and 1 ml 20% CC-RBB solution was incubated at 50°C and 200 rpm for 24 h. The samples were filtered through a 0.22 μ m pore-size membrane. The mobile phase was composed of acetonitrile and water (70:30, v/v) at a flow rate of 0.5 ml/min, and the injection volumes was 10 μ l. The products were quantified by comparing to standard curves made using standard COS samples with degrees of polymerization 1-6 (BZ Oligo Biotech Co. Ltd, Qingdao, China).

Directed Evolution of BcChiA1

Error-prone PCR was applied to introduce random mutations into the BcChiA1 gene (1.9 kb) using the Adjustable Error-prone PCR kit (Tiandz, Beijing, China). PrimeSTAR polymerase was used to clone the vector backbone of the pMATE plasmid. The DNA multimer was produced by prolonged overlap extension PCR (POE-PCR) with PrimeSTAR polymerase based on two DNA templates containing 3' and 5' overlapping termini of 40-50 bp. Finally, the multimers were used to transform competent *B. subtilis* 1A751. The transformants were screened on Luria-Bertani agar plates containing 20 μ g/mL kanamycin. Individual bacterial colonies from the mutant library were seeded into 96 deep-well plates containing 0.5 mL Luria-Bertani medium with 20 μ g/mL kanamycin, 2% CC-RBB (w/v) and 1% maltose per well. The plates were cultivated at 37°C and 800 rpm for 24 h on a Microtron 28759 shaker (Infors, Bottmingen, Switzerland), and then centrifuged on a JXN-26 centrifuge (Beckman, CA, United States) at $18923 \times g$ for 30 min. The culture supernatants were transferred to corresponding wells of 96-well ELISA plates by an RV-3S-S11 Automatic Liquid Handling Workstation (Caliper Life Sciences, Boston, United States) and the absorbance at 595 nm was recorded for each well.

Molecular Dynamic Simulations

Since chitin is a high-molecular-weight polymer with poor solubility, which presents difficulties in docking simulations with chitinase, we chose octa-*N*-acetyl-chitooctaose, (GlcNAc)₈, as the substrate to reflect the real-life conditions as closely as possible. (GlcNAc)₈ was used to simulate the chitin hydrolysis reaction based on a published crystal structure (PDB ID: 1E1B) (Papanikolaou et al., 2001). A HEI state substrate (Bolon and Mayo, 2001; Hermann et al., 2006; Hermann et al., 2007; Grisewood et al., 2013), designated as HEI8 (Figure 1), was generated according to the reaction mechanism (Nakamura et al., 2018). The initial wild-type (WT) complex was constructed using

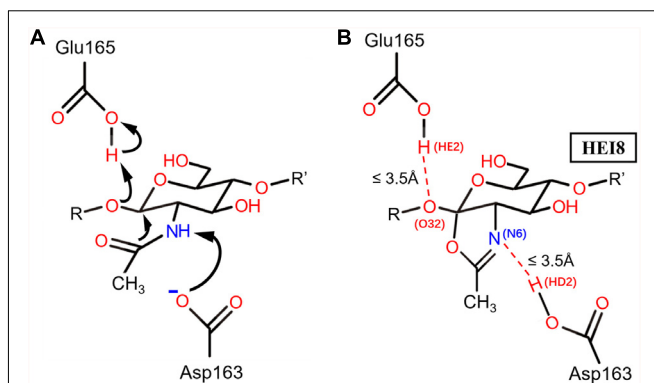


FIGURE 1 | The catalytic mechanism of BcChiA1 and the HEI state of the substrate bound to BcChiA1. R and R' represent the (GlcNAc)s that connect to the O atoms on C1 and C4, respectively. **(A)** Proposed mechanism of substrate-assisted catalysis by BcChiA1. **(B)** The HEI state of (GlcNAc)₈, designated as HEI8. The red dotted line indicates the distance of proton transfer, which forms a new pentacyclic structure.

the glide module with ligand sampling refine only in Schrödinger software, with restriction between BcChiA1 and HEI8. The 3D complex models of Mu1, Mu2, and Mu3 were built based on the WT complex using ROSETTA3 enzyme design (Leaver-Fay et al., 2011; Richter et al., 2011), and the detailed parameters are shown in the **Supplementary Material**. AMBER16 was used for the energy minimization of the constructed model and molecular dynamics (MD) simulation of the final model using the ff14SB.redq force field. The constrained MD simulations with the HEI state of WT-HEI8, Mu1-HEI8, Mu2-HEI8 and Mu3-HEI8 as initial input were conducted for 10 ns (Case et al., 2016). Finally, 100 ns MD simulations were performed without any restriction. The complete simulation methodology used in this work is available in the supporting information. The MD trajectories were applied for further analysis and used to determine relevant binding poses.

RESULTS AND DISCUSSION

Efficient Secretory Expression of BcChiA1 and BatLMPO10 in *B. subtilis*

In this study, *B. subtilis* 1A751 was used as the expression host and plasmid pMATE was used for the expression of BcChiA1 and BatLMPO10. We verified the effect of six different signal peptides (SP_{phoD}, SP_{lipA}, SP_{ywbN}, SP_{nprE}, SP_{sacB}, and SP_{yvcE}) from *B. subtilis*, as well as a construct without a signal peptide (noSP) on the secretion of the two enzymes. After 48 h of shake-flask fermentation, bands corresponding to the target proteins were clearly visible on SDS-PAGE gels (Figure 2A). The apparent molecular weights of BcChiA1 and BatLMPO10 in this study were approximately 73 and 20 kDa, which was in agreement with previous reports (Watanabe et al., 1990; Yu et al., 2016). The results indicated that all signal peptides led to successful BcChiA1 secretion, but the noSP group performed best. For BatLMPO10, the noSP group

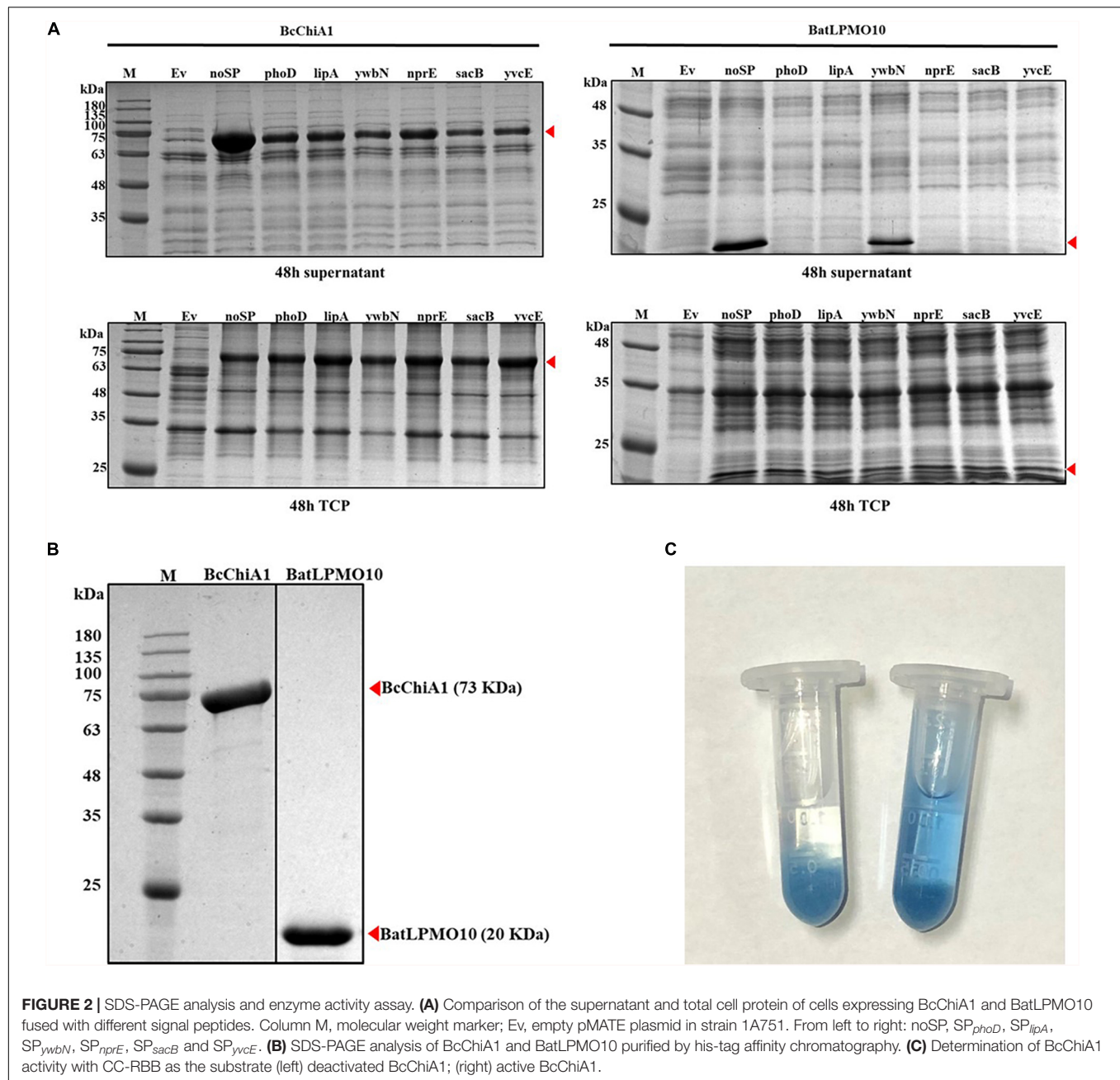
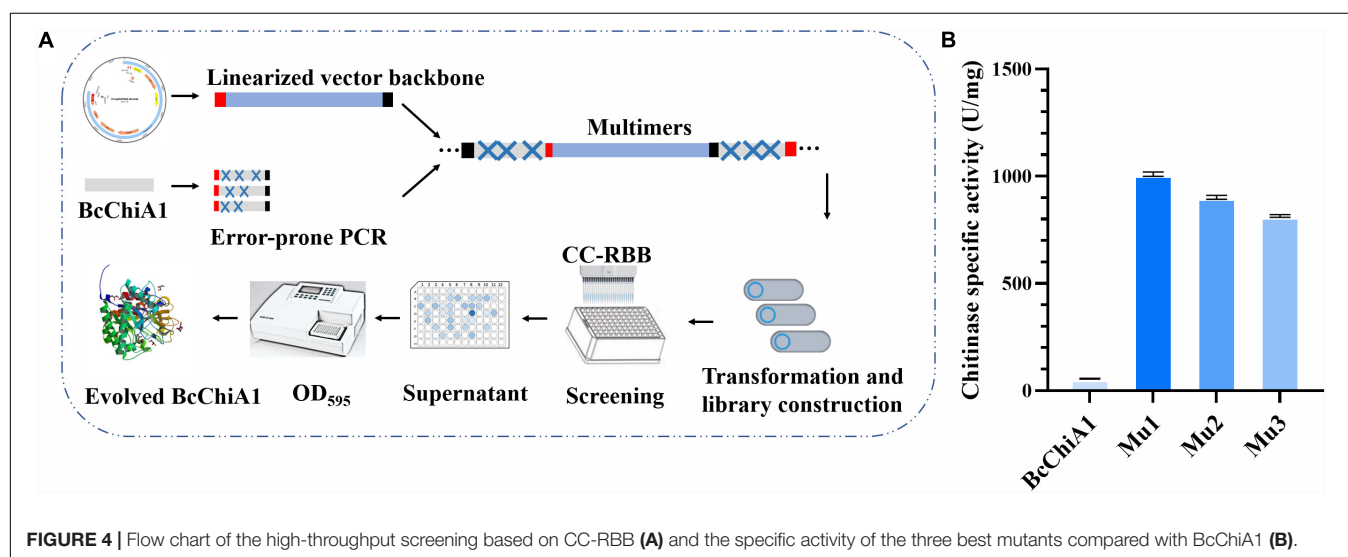
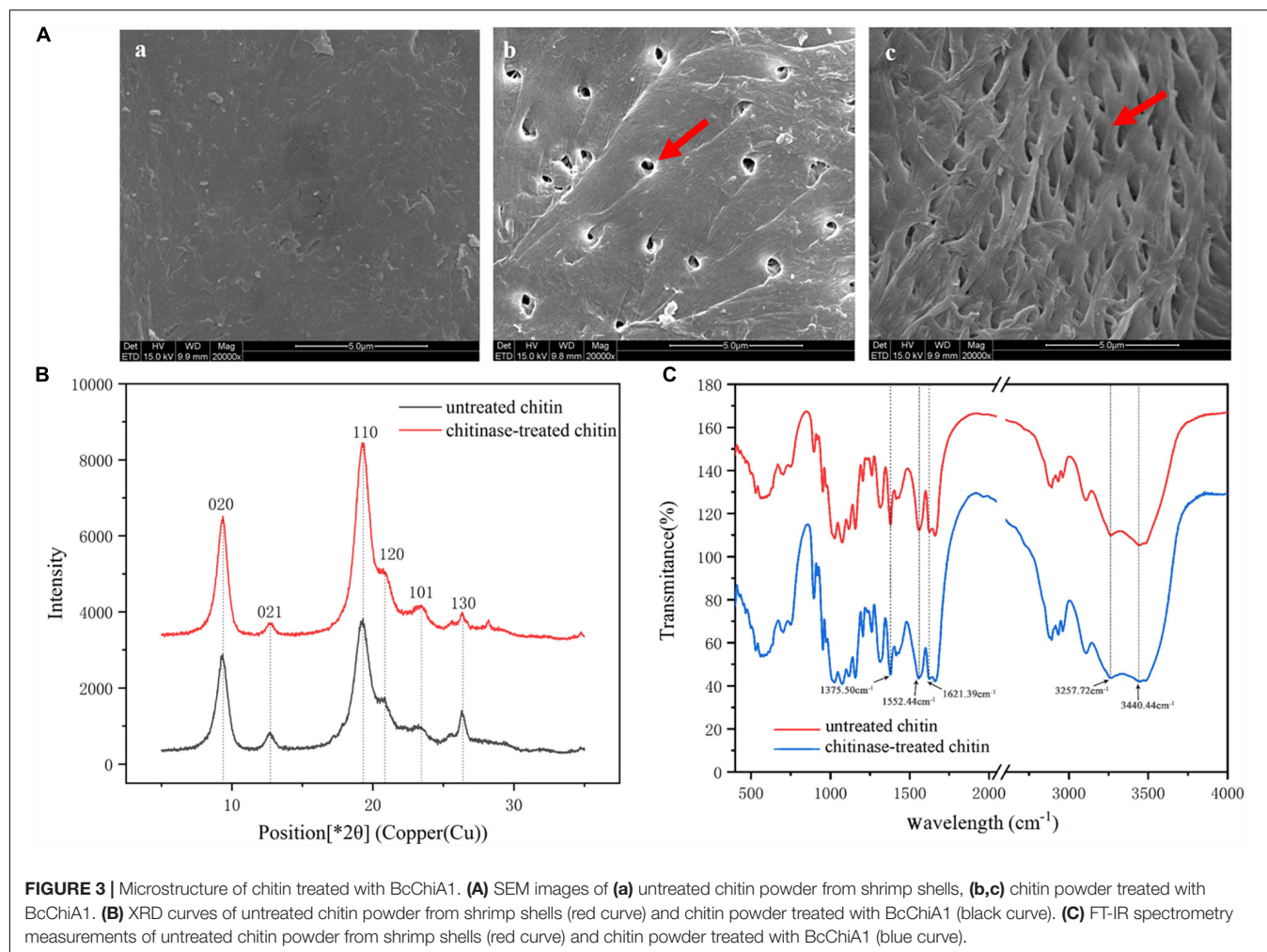


FIGURE 2 | SDS-PAGE analysis and enzyme activity assay. **(A)** Comparison of the supernatant and total cell protein of cells expressing BcChiA1 and BatLPMO10 fused with different signal peptides. Column M, molecular weight marker; Ev, empty pMATE plasmid in strain 1A751. From left to right: noSP, SP_{phoD}, SP_{lipA}, SP_{ywbN}, SP_{nprE}, SP_{sacB} and SP_{yvcE}. **(B)** SDS-PAGE analysis of BcChiA1 and BatLPMO10 purified by his-tag affinity chromatography. **(C)** Determination of BcChiA1 activity with CC-RBB as the substrate (left) deactivated BcChiA1; (right) active BcChiA1.

had the best performance, followed by SP_{ywbN}, while little or no BatLPMO10 secretion was observed with the other tested signal peptides. In general, signal peptides are crucial for the transport and secretion of target proteins. Nevertheless, an inappropriate signal peptide can have a negative influence on the yield and secretion of target proteins (Nguyen et al., 2018). Fortunately, we achieved highly efficient secretion of both target proteins without extensive signal peptide screening. In addition, *B. subtilis* has an intrinsically superior secretion capacity, which makes the subsequent process of separation and purification much simpler.

Enzyme Purification and Activity Assay

BcChiA1 and BatLPMO10 were purified from the culture supernatant via affinity chromatography on Ni-NTA columns and the purity was confirmed by SDS-PAGE (Figure 2B). The molecular weights of the two purified enzymes were consistent with the fermentation results. The specific activity of BcChiA1 with CC-RBB as substrate was 56.16 ± 0.92 U/mg (Figure 2C), which was much higher than the results obtained with other chitinases in previous studies. For example, PbChi70 from *Paenibacillus barengoltzii* displayed a specific activity of 30.3 U/mg (Yang et al., 2016), Chit42 from *Trichoderma*



harzianum 5.2 U/mg (Kidibule et al., 2018), and Pa-Chi from *Vibrio parahaemolyticus* 1.5 U/mg (Kadokura et al., 2007).

Analysis of Changes in Chitin Micro-Structure

The morphology of chitin powder from shrimp shells before and after chitinase treatment was studied by SEM, as shown in **Figure 3A**. There was a significant change in the surface topography of chitin powder following chitinase treatment. A rough surface without any interstice could be observed in the untreated chitin powder samples (**Figure 3Aa**), while the morphology of the samples treated with BcChiA1 showed a porous structure (**Figure 3Ab**) and high-density fibers (**Figure 3Ac**). The SEM results indicated that efficient enzymatic degradation of crystalline chitin was achieved via BcChiA1 treatment.

The XRD spectrum of the chitin powder after chitinase treatment was investigated to determine crystal structure and crystallinity (**Figure 3B**). The position and relative intensity of all the diffraction peaks of the chitinase-treated samples were consistent with the standard XRD pattern of chitin. Moreover, the crystal-reflection peaks of the samples treated with BcChiA1 were lower than those of the untreated chitin powder, which meant the I_{CR} of chitin clearly decreased after chitinase treatment. It was calculated that the crystallinity of chitin decreased by 11.84%.

The FT-IR spectra of the chitin powder after chitinase treatment presented in **Figure 3C** shows characteristic spectral bands of α -chitin at 1660 cm^{-1} and 1625 cm^{-1} (amide I, intra-chain hydrogen bonds with NH groups and inter-chain hydrogen bonds with the primary OH, respectively), 1558 cm^{-1} (amide II), 3266 cm^{-1} (N-H stretching vibrations), and 3443 cm^{-1} (O-H-stretching band) (Xu et al., 2018). The absorption bands of chitin powder were similar to those of the chitinase-treated samples, which meant that the enzymatic degradation did not cause chitin deacetylation.

Synergistic Effect of BcChiA1 and BatLPMO10 on Chitin Degradation

Recent studies have revealed that LPMOs are active on crystalline polysaccharides and have a synergistic effect with hydrolytic enzymes to stimulate the degradation of crystalline biopolymers (Courtade and Achmann, 2019). To investigate the influence of BatLPMO10 on the chitin-degradation efficiency of BcChiA1, different concentrations of purified BatLPMO10 were added to preprocess the substrate, and purified BcChiA1 was added to the reaction mixture later (the group without BcChiA1 served as a control). We concluded that BatLPMO10 has practically no ability to degrade chitin wastes independently, as the absorbance at 595 nm barely increased compared with other groups, and was essentially the same as the blank control (with no addition of enzymes). Moreover, the results showed that there was a conspicuous positive correlation between the added amount of BatLPMO10 and the amount of RBB released (absorbance at 595 nm), which confirmed that BatLPMO10 was effective in substrate pretreatment and made the chitin more accessible to degradation by BcChiA1. In the presence of

$192\text{ }\mu\text{M}$ BatLPMO10, $4.5\text{ }\mu\text{M}$ BcChiA1 showed the maximum degradation efficiency, which was improved by 50% (shown in the **Supplementary Material**). The optimum ratio of BcChiA1 and BatLPMO10 for the synergistic effect offers a theoretical basis for the treatment of chitin waste and the production of COS.

Directed Evolution of BcChiA1

To further improve the efficacy of BcChiA1, directed evolution *in vitro* was applied to the ORF of the BcChiA1 gene without a native signal peptide (**Figure 4A**). The most important factors in determining the capacity of the mutant library are the quantity of DNA templates, PCR cycle numbers, and the reagent concentration of the Adjustable Error-prone PCR kit. We determined that the optimal conditions encompass 300 ng DNA template, 60 PCR thermal cycles, and $1\text{ }\mu\text{M}$ MnCl_2 . Under these conditions, three rounds of error-prone PCR were conducted, and finally a BcChiA1 mutant library with 12000 clones was constructed. Sixty transformants were randomly selected from the mutagenesis library for DNA sequencing, which revealed an average mutation rate of 0.2%, corresponding to an average of three nucleotide changes within the BcChiA1 gene.

There are three main approaches to chitinase screening in the literature. One relies on transparent zones surrounding colonies on colloidal chitin, the second uses fluorescence based on p-nitrobenzene or 4-methylumbelliferone, and the third is the 3,5-dinitrosalicylic acid (DNS) method. Because all have certain limitations such as low accuracy, low throughput, high cost, poor universality, or cumbersome steps (Fan et al., 2007; Songsiririthigul et al., 2009; Pan et al., 2019), we established a rapid and sensitive high-throughput screening method based on the substrate CC-RBB, which is non-toxic to microorganisms and can be added directly to growth medium. Using this method, the screening process was greatly shortened. In addition, this method is not restricted by chitinase type and is widely applicable to exo- and endo-chitinases, as well as N-acetylglucosaminidases.

After initial high-throughput screening and confirmation via shake-flask fermentation, the three mutants (Mu1, Mu2, and Mu3) were selected, with specific activities of 1004.83 ± 0.87 , 906.9 ± 0.55 , and $809.36 \pm 0.16\text{ U/mg}$, respectively. These activities corresponded to 16.89-, 15.15-, and 13.41-fold increases in activity compared with the wild type (**Figure 4B**).

Molecular Dynamic Simulations of the HEI State

Based on the catalytic mechanism of BcChiA1 (Nakamura et al., 2018), Asp163 and Glu165 participate in proton transfer while stabilizing the substrate to complete the catalytic process. Asp163 abstracts a proton from the N atom of the sugar-ring amide, while the carbonyl of the amide attacks the C1 of the sugar ring and forms a pentacyclic structure. At the same time, the O atom attaches to the former sugar ring on the substrate and captures the proton of Glu165 (**Figure 1A**). Asp163 captures the proton of the substrate, after which the carbonyl attacks the sugar ring. Thus, we retained the newly formed 5-membered ring, the protonated state of Glu165, and

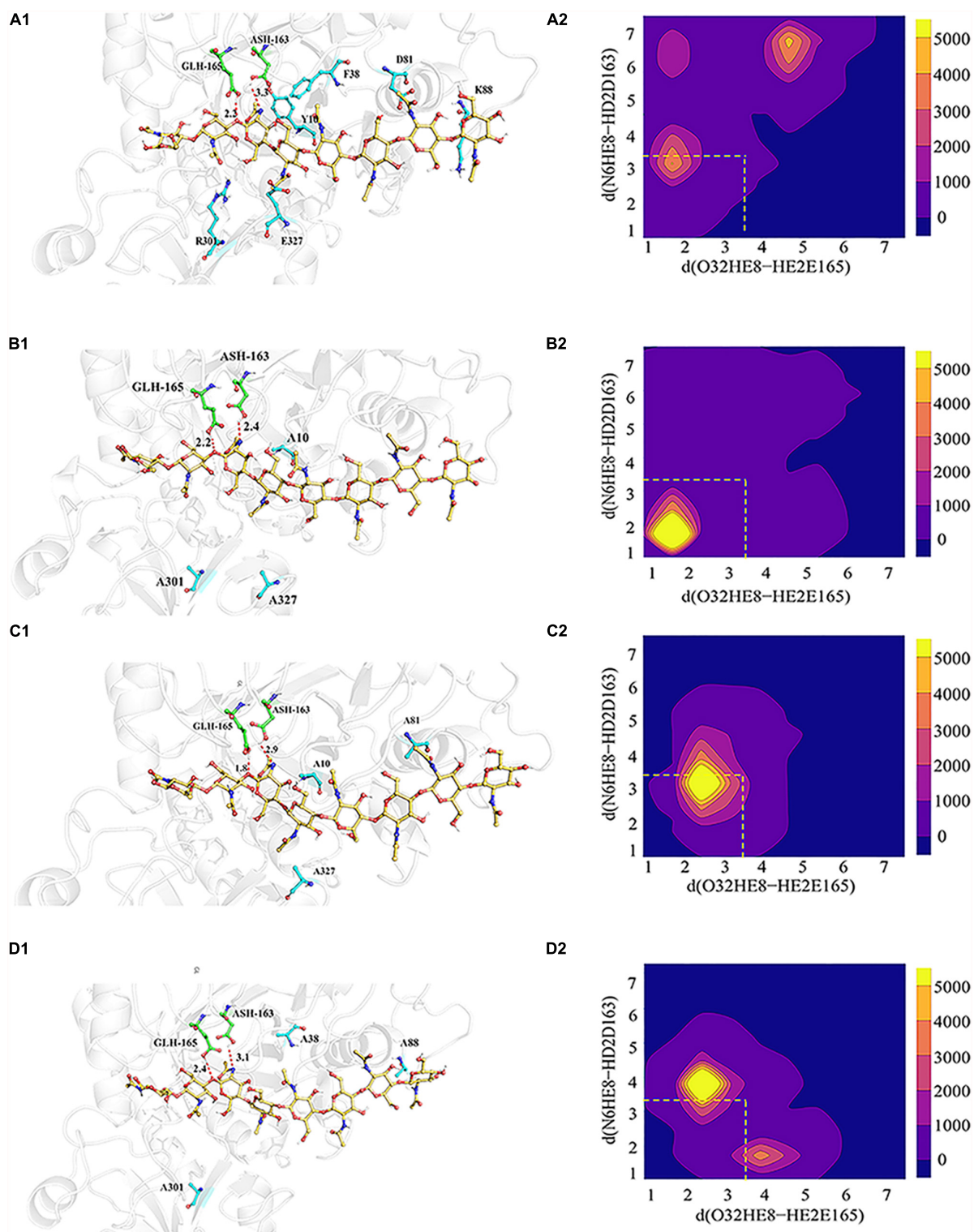


FIGURE 5 | 3D model showing the interrelationships between the substrate (yellow), catalytic residues (green) and mutant residues (blue), as well as the statistical distribution of the HEI states throughout the kinetic process. **(A₁–D₁)** Signify relative positions of the substrate (yellow), catalytic residues (green) and mutant residues (blue) in WT-HEI8, Mu1, Mu2 and Mu3, respectively. The red dotted line represents the distance of the H atom from two catalytic residues and the O atom and N atom involved in proton transfer, d (O32HE8-HE2E165) and d (N6HE8-HD2D163). **(A₂–D₂)** Signify the distributions of these two distances in WT-HEI8, Mu1, Mu2, and Mu3, respectively. Yellow indicates that the occupied frame number in this area is greater than or equal to 5000. For every color change from yellow to blue, the number range of distribution decreases by 1000, whereby pure blue indicates 0. The red dotted box indicates the distribution of the two distances within 3.5 Å.

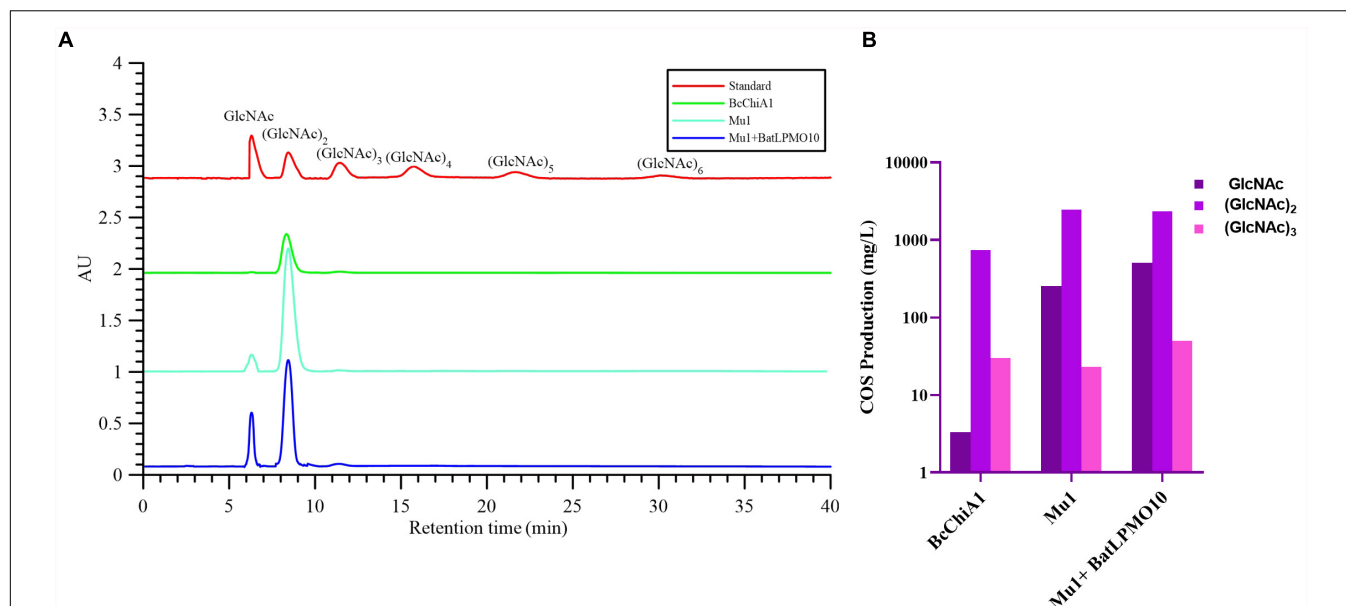


FIGURE 6 | HPLC analysis (A) and the yields of GlcNAc, (GlcNAc)₂, (GlcNAc)₃ (B) of the products of chitin hydrolysis by BcChiA1 and its best mutant Mu1, alone and in combination with BatLPMO10.

the connection of oxygen and C1 of the previous GlcNAc, simulating a transition state before the new bond breaks, as the HEI state (the substrate designated as HEI8, **Figure 1B**). We constructed the complex between the HEI state of the substrate and BcChiA1 (PDB ID: 1ITX) (Matsumoto et al., 1999) using a restrictive docking method based on the transfer of protons by the substrate and catalytic residues (**Figure 1B**). Docking studies using the Glide module (Schrödinger, 2018-1) were performed with wild-type bound to HEI8 as the substrate. The structure with $d(N6HE8-HD2D163) \leq 3.5 \text{ \AA}$ and $d(O32HE8-HE2E165) \leq 3.5 \text{ \AA}$ (**Figure 1B**) could be used to represent the start of the hydride transfer process. Therefore, a conformation that satisfies these two constraints can be considered as a sign of the HEI state.

In order to explore the possible reasons for the enhanced catalytic activity of mutants Mu1, Mu2, and Mu3, MD simulations were performed to evaluate the propensity of the bound substrate to enter the HEI state before and after mutation using ROSETTA3 based on the WT-HEI8 complex. The orientation of HEI8 was observed in the stable HEI states of WT-HEI8 and all the mutants (**Figure 5**). However, it was difficult to sustain a HEI state of WT-HEI8 (**Figure 5A2**). Remarkably, the proportions of “catalytic” conformations with both $d(N6HE8-HD2D163) \leq 3.5 \text{ \AA}$ and $d(O32HE8-HE2E165) \leq 3.5 \text{ \AA}$ were 79.32, 52.14, and 23.22% in Mu1, Mu2, and Mu3, respectively (**Figure 5**). Moreover, the frequency of the best mutant, Mu1, was more than ten times that observed in WT-HEI8 (7.28%). These results illustrate that the three mutants with significantly improved activity have active-site structures that are more favorable for the formation of HEI states, which was consistent with the trend of enhanced catalytic activity.

HPLC Analysis of the Products of Chitin Hydrolysis by BcChiA1

HPLC was used to detect the degradation products of chitin using COS standards as references, including GlcNAc, (GlcNAc)₂, (GlcNAc)₃, (GlcNAc)₄, (GlcNAc)₅, and (GlcNAc)₆, with respective retention times of 6.303, 8.442, 11.433, 15.742, 21.655, and 30.094 min (**Figure 6A**). After treatment with BcChiA1, the degradation products GlcNAc, (GlcNAc)₂, and (GlcNAc)₃ were detected, while the higher degree of polymerization forms of GlcNAc were not detectable. The HPLC results revealed that (GlcNAc)₂ was the major product, with a content of $741.90 \pm 2.78 \text{ mg/L}$, followed by (GlcNAc)₃ and GlcNAc (**Figure 6B**). According to the results, BcChiA1 displayed a stochastic catalytic mode of action on chitin, with a high production of (GlcNAc)₂. The accumulation of (GlcNAc)₂ means that BcChiA1 can hydrolyze the second glycoside bond. In this regard, this property of BcChiA1 is similar to those of previously investigated GH family 18 endochitinases from bacteria, such as those from *Paenibacillus barengoltzii* (Yang et al., 2016) and *Streptomyces albolongus* (Gao et al., 2018), as well as a fungal enzyme from *Myrothecium verrucaria* (Vidhate et al., 2019). The best mutant obtained by the directed evolution of BcChiA1, Mu1, was also investigated. The contents of GlcNAc, (GlcNAc)₂, and (GlcNAc)₃ after Mu1 treatment were $253.91 \pm 0.64 \text{ mg/L}$, $2444.21 \pm 4.12 \text{ mg/L}$, and $23.05 \pm 0.65 \text{ mg/L}$, respectively (**Figure 6B**). These values were 76.39-, 3.29-, and 0.77-fold higher than the corresponding values of the wild type. In pursuit of a higher yield of COS, the optimum combination of Mu1 and BatLPMO10 was chosen to degrade chitin synergistically. As the results of HPLC analysis show (**Figure 6B**), the contents of GlcNAc, (GlcNAc)₂, and

(GlcNAc)₃ were 152.96-, 3.14-, and 1.66-fold higher than those obtained after BcChiA1 treatment alone. The HPLC results therefore confirmed a significant increase in chitinase productivity after optimization. The COS yield of Mu1 and BatLPMO10 in this study was 2.89 g/L, which was nearly 3.25-fold higher than the reported yield obtained using the chitinase from *Bacillus* sp. DAU101 (0.89 g/L) (Pan et al., 2019). In addition, the yield of (GlcNAc)₂ obtained using Mu1 was approximately 2.44 g/L, which was a 20 percent improvement compared with an optimized cocktail of chitinolytic enzymes from *Serratia marcescens* (SmChiA-M, SmChiB, and SmChiC) (Chu et al., 2019). Thus, the combination of evolved BcChiA1 with BatLPMO10 has great practical value.

CONCLUSION

BcChiA1 was cloned and its secretory expression was achieved in *B. subtilis* with high efficiency. Furthermore, three improved variants of BcChiA1 were obtained by directed evolution based on an innovative CC-RBB high-throughput screening technique. In addition to the successful optimization of expression level and catalytic activity of BcChiA1 itself, we also found that there is synergy between BcChiA1 and BatLPMO10 during chitin degradation. After directed evolution and optimized combination conditions, the specific activity of the mutant Mu1 reached 1004.83 ± 0.87 U/mg and COS production by a combination of Mu1 and BatLPMO10 was improved up to 2.89 g/L. Most importantly, this study created a novel method for high-throughput screening of chitinase efficiency and provides a new strategy of chitinous waste biodegradation in a green and sustainable way.

REFERENCES

- Bell, R. M., and Koshland, D. E. Jr. (1971). Covalent enzyme-substrate intermediates. *Science* 172, 1253–1256. doi: 10.1126/science.172.3989.1253
- Bolon, D. N., and Mayo, S. L. (2001). Enzyme-like proteins by computational design. *Proc. Natl. Acad. Sci. U.S.A.* 98, 14274–14279. doi: 10.1073/pnas.251553998
- Cai, D., Rao, Y., Zhan, Y., Wang, Q., and Chen, S. (2019). Engineering *Bacillus* for efficient production of heterologous protein: current progress, challenge and prospect. *J. Appl. Microbiol.* 126, 1632–1642. doi: 10.1111/jam.14192
- Case, D., Betz, R., Cerutti, D., Cheatham, T. I., Darden, T., Duke, R., et al. (2016). *AMBER 16*. San Francisco, CA: University of California.
- Chu, F., Wang, D., Liu, T., Han, H., Yu, Y., and Yang, Q. (2019). An optimized cocktail of chitinolytic enzymes to produce N,N'-diacetylchitobiose and N-acetyl-d-glucosamine from defatted krill by-products. *Int. J. Biol. Macromol.* 133, 1029–1034. doi: 10.1016/j.jbiomac.2019.04.114
- Courtade, G., and Aachmann, F. L. (2019). Chitin-Active Lytic Polysaccharide Monoxygenases. *Adv. Exp. Med. Biol.* 1142, 115–129. doi: 10.1007/978-981-13-7318-3_6
- Cui, W., Han, L., Suo, F., Liu, Z., Zhou, L., and Zhou, Z. (2018). Exploitation of *Bacillus subtilis* as a robust workhorse for production of heterologous proteins and beyond. *World J. Microbiol. Biotechnol.* 34:145. doi: 10.1007/s11274-018-2531-7
- Fan, Y., Fang, W., Xiao, Y., Yang, X., Zhang, Y., Bidochka, M. J., et al. (2007). Directed evolution for increased chitinase activity. *Appl. Microbiol. Biotechnol.* 76, 135–139. doi: 10.1007/s00253-007-0996-7

DATA AVAILABILITY STATEMENT

All datasets generated for this study are included in the article/Supplementary Material.

AUTHOR CONTRIBUTIONS

SW participated in investigation, data curation, writing and original draft preparation. GE, HE, and XW contributed to project administration. JLL and JpL were responsible for methodology, software and formal analysis. DH and DZ took charge of conceptualization and funding acquisition. All authors provided critical advice for the final manuscript.

FUNDING

This work was financially supported by the National Key R&D Program of China (2018YFA0900302, 2018YFA0901600, and 2018YFD0901001), the National Natural Science Foundation of China (NSFC 31830084, 31800086, and 31900052), the Tianjin Science Fund for Distinguished Young Scholars (17JCQJC45300), and the Science and Technology Service Network (STS) Initiative of the Chinese Academy of Sciences (CAS) (KFJ-STZ-ZDTP-065).

SUPPLEMENTARY MATERIAL

The Supplementary Material for this article can be found online at: <https://www.frontiersin.org/articles/10.3389/fbioe.2020.00432/full#supplementary-material>

- Ferrandon, S. (2003). A single surface tryptophan in the chitin-binding domain from *Bacillus circulans* chitinase A1 plays a pivotal role in binding chitin and can be modified to create an elutable affinity tag. *Biochim. Biophys. Acta Gen. Subj.* 1621, 31–40. doi: 10.1016/s0304-4165(03)00029-1
- Gao, L., Sun, J., Secundo, F., Gao, X., Xue, C., and Mao, X. (2018). Cloning, characterization and substrate degradation mode of a novel chitinase from *Streptomyces albolongus* ATCC 27414. *Food Chem.* 261, 329–336. doi: 10.1016/j.foodchem.2018.04.068
- Gao, X., Chen, X., Zhang, J., Guo, W., Jin, F., and Yan, N. (2016). Transformation of chitin and waste shrimp shells into acetic acid and pyrrole. *ACS Sustain. Chem. Eng.* 4, 3912–3920. doi: 10.1021/acssuschemeng.6b00767
- Gómez Ramírez, M., Rojas Avelizapa, L. I., Rojas Avelizapa, N. G., and Cruz Camarillo, R. (2004). Colloidal chitin stained with Remazol Brilliant Blue R®, a useful substrate to select chitinolytic microorganisms and to evaluate chitinases. *J. Microbiol. Methods* 56, 213–219. doi: 10.1016/j.mimet.2003.10.011
- Grisewood, M. J., Gifford, N. P., Pantazes, R. J., Li, Y., Cirino, P. C., Janik, M. J., et al. (2013). OptZyme: computational enzyme redesign using transition state analogues. *PLoS One* 8:e75358. doi: 10.1371/journal.pone.0075358
- Gu, Y., Xu, X., Wu, Y., Niu, T., Liu, Y., Li, J., et al. (2018). Advances and prospects of *Bacillus subtilis* cellular factories: from rational design to industrial applications. *Metab. Eng.* 50, 109–121. doi: 10.1016/j.ymben.2018.05.006
- Hermann, J. C., Ghanem, E., Li, Y., Raushel, F. M., Irwin, J. J., and Shoichet, B. K. (2006). Predicting substrates by docking high-energy intermediates to enzyme structures. *J. Am. Chem. Soc.* 128, 15882–15891. doi: 10.1021/ja065860f

- Hermann, J. C., Marti-Arbona, R., Fedorov, A. A., Fedorov, E., Almo, S. C., Shoichet, B. K., et al. (2007). Structure-based activity prediction for an enzyme of unknown function. *Nature* 448, 775–779. doi: 10.1038/nature05981
- Huang, W. C., Zhao, D., Guo, N., Xue, C., and Mao, X. (2018). Green and facile production of chitin from crustacean shells using a natural deep eutectic solvent. *J. Agric. Food Chem.* 66, 11897–11901. doi: 10.1021/acs.jafc.8b03847
- Isaksen, T., Westereng, B., Aachmann, F. L., Agger, J. W., Kracher, D., Kittl, R., et al. (2014). A C4-oxidizing lytic polysaccharide monooxygenase cleaving both cellulose and cello-oligosaccharides. *J. Biol. Chem.* 289, 2632–2642. doi: 10.1074/jbc.M113.530196
- Kadokura, K., Rokutani, A., Yamamoto, M., Ikegami, T., Sugita, H., Itoi, S., et al. (2007). Purification and characterization of *Vibrio parahaemolyticus* extracellular chitinase and chitin oligosaccharide deacetylase involved in the production of heterodisaccharide from chitin. *Appl. Microbiol. Biotechnol.* 75, 357–365. doi: 10.1007/s00253-006-0831-6
- Kidibule, P. E., Santos-Moriano, P., Jimenez-Ortega, E., Ramirez-Escudero, M., Limon, M. C., Remacha, M., et al. (2018). Use of chitin and chitosan to produce new chitooligosaccharides by chitinase Chit42: enzymatic activity and structural basis of protein specificity. *Microb. Cell. Fact.* 17:47. doi: 10.1186/s12934-018-0895-x
- Kumar, M., Brar, A., Vivekanand, V., and Pareek, N. (2018). Bioconversion of chitin to bioactive chitooligosaccharides: amelioration and coastal pollution reduction by microbial resources. *Mar. Biotechnol.* 20, 269–281. doi: 10.1007/s10126-018-9812-x
- Lahiri, S. D., Zhang, G., Dunaway-Mariano, D., and Allen, K. N. (2003). The pentacovalent phosphorus intermediate of a phosphoryl transfer reaction. *Science* 299:2067. doi: 10.1126/science.1082710
- Leaver-Fay, A., Tyka, M., Lewis, S. M., Lange, O. F., Thompson, J., Jacak, R., et al. (2011). ROSETTA3: an object-oriented software suite for the simulation and design of macromolecules. *Methods Enzymol.* 487, 545–574. doi: 10.1016/b978-0-12-381270-4.00019-6
- Liang, S., Sun, Y., and Dai, X. (2018). A review of the preparation, analysis and biological functions of chitooligosaccharide. *Int. J. Mol. Sci.* 19:2197. doi: 10.3390/ijms19082197
- Liaquat, F., and Eltem, R. (2018). Chitooligosaccharides and their biological activities: a comprehensive review. *Carbohydr. Polym.* 184, 243–259. doi: 10.1016/j.carbpol.2017.12.067
- London, N., Farelli, J. D., Brown, S. D., Liu, C., Huang, H., Korczynska, M., et al. (2015). Covalent docking predicts substrates for haloalkanoate dehalogenase superfamily phosphatases. *Biochemistry* 54, 528–537.
- Manjeet, K., Purushotham, P., Neeraja, C., and Podile, A. R. (2013). Bacterial chitin binding proteins show differential substrate binding and synergy with chitinases. *Microbiol. Res.* 168, 461–468. doi: 10.1016/j.micres.2013.01.006
- Matsumoto, T., Nonaka, T., Hashimoto, M., Watanabe, T., and Mitsui, Y. (1999). Three-dimensional structure of the catalytic domain of chitinase A1 from *Bacillus circulans* WL-12 at a very high resolution. *Proc. Jpn. Acad. Ser. B Phys. Biol. Sci.* 75, 269–274. doi: 10.2183/pjab.75.269
- Nakamura, A., Okazaki, K.-I., Furuta, T., Sakurai, M., and Iino, R. (2018). Processive chitinase is Brownian monorail operated by fast catalysis after peeling rail from crystalline chitin. *Nat. Commun.* 9:3814. doi: 10.1038/s41467-018-06362-3
- Nanda, V., and Koder, R. (2010). Designing artificial enzymes by intuition and computation. *Nature chemistry* 2, 15–24. doi: 10.1038/nchem.473
- Naveed, M., Phil, L., Sohail, M., Hasnat, M., Baig, M., Ihsan, A. U., et al. (2019). Chitosan oligosaccharide (COS): an overview. *Int. J. Biol. Macromol.* 129, 827–843. doi: 10.1016/j.ijbiomac.2019.01.192
- Nguyen, H. Q., Vu, V. H., Le, P. D., and Chu, H. M. (2018). High-level expression, purification and properties of an Endochitinase gene without signal peptide from *Lecanicillium lecanii* 43H in *Pichia pastoris*. *Mol. Biol. Rep.* 45, 1067–1075. doi: 10.1007/s11033-018-4256-y
- Pan, M., Xu, X., Liu, Y., Li, J., Lu, X., Du, G., et al. (2019). [Directed evolution of chitinase Chisb and biosynthesis of chitooligosaccharides]. *Sheng Wu Gong Cheng Xue Bao* 35, 1787–1796. doi: 10.13345/j.cjb.190069
- Papanikolaou, Y., Prag, G., Tavlak, G., Vorgias, C. E., Oppenheim, A. B., and Petratos, K. (2001). High resolution structural analyses of mutant chitinase A complexes with substrates provide new insight into the mechanism of catalysis. *Biochemistry* 40, 11338–11343. doi: 10.1021/bi010505h
- Porter, J. L., Rusli, R. A., and Ollis, D. L. (2016). Directed Evolution of Enzymes for Industrial Biocatalysis. *ChemBiochem* 17, 197–203. doi: 10.1002/cbic.201500280
- Richter, F., Leaver-Fay, A., Khare, S. D., Bjelic, S., and Baker, D. (2011). De novo enzyme design using Rosetta3. *PLoS One* 6:e19230. doi: 10.1371/journal.pone.0019230
- Sambrook, J., Fritsch, E. F., and Maniatis, T. (1989). *Molecular Cloning: A Laboratory Manual*. Cold Spring Harbor, NY: Cold Spring Harbor Laboratory Press.
- Singh, R., Shitiz, K., and Singh, A. (2017). Chitin and chitosan: biopolymers for wound management. *Int. Wound J.* 14, 1276–1289. doi: 10.1111/iwj.12797
- Smith, M. C. M. (1991). Molecular biological methods for *Bacillus*. *FEBS Lett.* 287:227.
- Songsiriuthigul, C., Pesatcha, P., Eijsink, V. G., and Yamabhai, M. (2009). Directed evolution of a *Bacillus chitinase*. *Biotechnol. J.* 4, 501–509. doi: 10.1002/biot.200800258
- Spizizen, J. (1958). Transformation of biochemically deficient strains of *Bacillus subtilis* by deoxyribonucleate. *Proc. Natl. Acad. Sci. U.S.A.* 44, 1072–1078.
- Vaaje-Kolstad, G., Westereng, B., Horn, S. J., Liu, Z., Zhai, H., Sorlie, M., et al. (2010). An oxidative enzyme boosting the enzymatic conversion of recalcitrant polysaccharides. *Science* 330, 219–222. doi: 10.1126/science.1192231
- Vidhate, R. P., Bhide, A. J., Gaikwad, S. M., and Giri, A. P. (2019). A potent chitin-hydrolyzing enzyme from *Myrothecium verrucaria* affects growth and development of *Helicoverpa armigera* and plant fungal pathogens. *Int. J. Biol. Macromol.* 141, 517–528. doi: 10.1016/j.ijbiomac.2019.09.031
- Watanabe, T., Ishibashi, A., Ariga, Y., Hashimoto, M., Nikaidou, N., Sugiyama, J., et al. (2001). Trp122 and Trp134 on the surface of the catalytic domain are essential for crystalline chitin hydrolysis by *Bacillus circulans* chitinase A1. *FEBS Lett.* 494:74.
- Watanabe, T., Suzuki, K., Oyanagi, W., Ohnishi, K., and Tanaka, H. (1990). Gene cloning of chitinase A1 from *Bacillus circulans* WL-12 revealed its evolutionary relationship to *Serratia chitinase* and to the Type III homology units of fibronectin. *J. Biol. Chem.* 265, 15659–15665.
- Xu, P., Wu, X.-L., Guo, X.-X., Tang, J., Zong, M.-H., and Lou, W.-Y. (2018). Double-chitinase hydrolysis of crab shell chitin pretreated by ionic liquid to generate chito-oligosaccharide. *ACS Sustain. Chem. Eng.* 7, 1683–1691. doi: 10.1021/acssuschemeng.8b05447
- Yang, S., Fu, X., Yan, Q., Guo, Y., Liu, Z., and Jiang, Z. (2016). Cloning, expression, purification and application of a novel chitinase from a thermophilic marine bacterium *Paenibacillus barengoltzii*. *Food Chem.* 192, 1041–1048. doi: 10.1016/j.foodchem.2015.07.092
- Yang, Y., Li, J., Liu, X., Pan, X., Hou, J., Ran, C., et al. (2017). Improving extracellular production of *Serratia marcescens* lytic polysaccharide monooxygenase CBP21 and *Aeromonas veronii* B565 chitinase Chi92 in *Escherichia coli* and their synergism. *AMB Express* 7:170. doi: 10.1186/s13568-017-0470-6
- Yu, M. J., Yoon, S. H., and Kim, Y. W. (2016). Overproduction and characterization of a lytic polysaccharide monooxygenase in *Bacillus subtilis* using an assay based on ascorbate consumption. *Enzyme Microb. Technol.* 93–94, 150–156. doi: 10.1016/j.enzmictec.2016.08.014
- Yue, J., Fu, G., Zhang, D., and Wen, J. (2017). A new maltose-inducible high-performance heterologous expression system in *Bacillus subtilis*. *Biotechnol. Lett.* 39, 1237–1244. doi: 10.1007/s10529-017-2357-7
- Zhang, A., Wei, G., Mo, X., Zhou, N., Chen, K., and Ouyang, P. (2018). Enzymatic hydrolysis of chitin pretreated by bacterial fermentation to obtain pure N-acetyl-d-glucosamine. *Green Chem.* 20, 2320–2327. doi: 10.1039/c8gc00265g

Conflict of Interest: The authors declare that the research was conducted in the absence of any commercial or financial relationships that could be construed as a potential conflict of interest.

Copyright © 2020 Wang, Fu, Li, Wei, Fang, Huang, Lin and Zhang. This is an open-access article distributed under the terms of the Creative Commons Attribution License (CC BY). The use, distribution or reproduction in other forums is permitted, provided the original author(s) and the copyright owner(s) are credited and that the original publication in this journal is cited, in accordance with accepted academic practice. No use, distribution or reproduction is permitted which does not comply with these terms.



Recent Development of Extremophilic Bacteria and Their Application in Biorefinery

Daochen Zhu^{1,2*†}, Wasiu Adewale Adebisi^{1†}, Fiaz Ahmad¹, Sivasamy Sethupathy¹, Blessing Danso¹ and Jianzhong Sun^{1*}

¹ Biofuels Institute, School of the Environment and Safety Engineering, Jiangsu University, Zhenjiang, China, ² State Key Laboratory of Applied Microbiology Southern China, Guangdong Provincial Key Laboratory of Microbial Culture Collection and Application, Guangdong Open Laboratory of Applied Microbiology, Guangdong Institute of Microbiology, Guangzhou, China

OPEN ACCESS

Edited by:

Mingjie Jin,
Nanjing University of Science and
Technology, China

Reviewed by:

Zhi-Hua Liu,
Texas A & M University, United States
Xinqing Zhao,
Shanghai Jiao Tong University, China

*Correspondence:

Daochen Zhu
dczhucn@hotmail.com
Jianzhong Sun
jzsun1002@ujs.edu.cn

[†] These authors have contributed
equally to this work

Specialty section:

This article was submitted to
Synthetic Biology,
a section of the journal
Frontiers in Bioengineering and
Biotechnology

Received: 20 January 2020

Accepted: 27 April 2020

Published: 12 June 2020

Citation:

Zhu D, Adebisi WA, Ahmad F,
Sethupathy S, Danso B and Sun J
(2020) Recent Development of
Extremophilic Bacteria and Their
Application in Biorefinery.
Front. Bioeng. Biotechnol. 8:483.
doi: 10.3389/fbioe.2020.00483

The biorefining technology for biofuels and chemicals from lignocellulosic biomass has made great progress in the world. However, mobilization of laboratory research toward industrial setup needs to meet a series of criteria, including the selection of appropriate pretreatment technology, breakthrough in enzyme screening, pathway optimization, and production technology, etc. Extremophiles play an important role in biorefinery by providing novel metabolic pathways and catalytically stable/robust enzymes that are able to act as biocatalysts under harsh industrial conditions on their own. This review summarizes the potential application of thermophilic, psychrophilic alkaliphilic, acidophilic, and halophilic bacteria and extremozymes in the pretreatment, saccharification, fermentation, and lignin valorization process. Besides, the latest studies on the engineering bacteria of extremophiles using metabolic engineering and synthetic biology technologies for high-efficiency biofuel production are also introduced. Furthermore, this review explores the comprehensive application potential of extremophiles and extremozymes in biorefinery, which is partly due to their specificity and efficiency, and points out the necessity of accelerating the commercialization of extremozymes.

Keywords: biofuel, biorefinery, extremophiles, extremozymes, synthetic biology

BACKGROUND

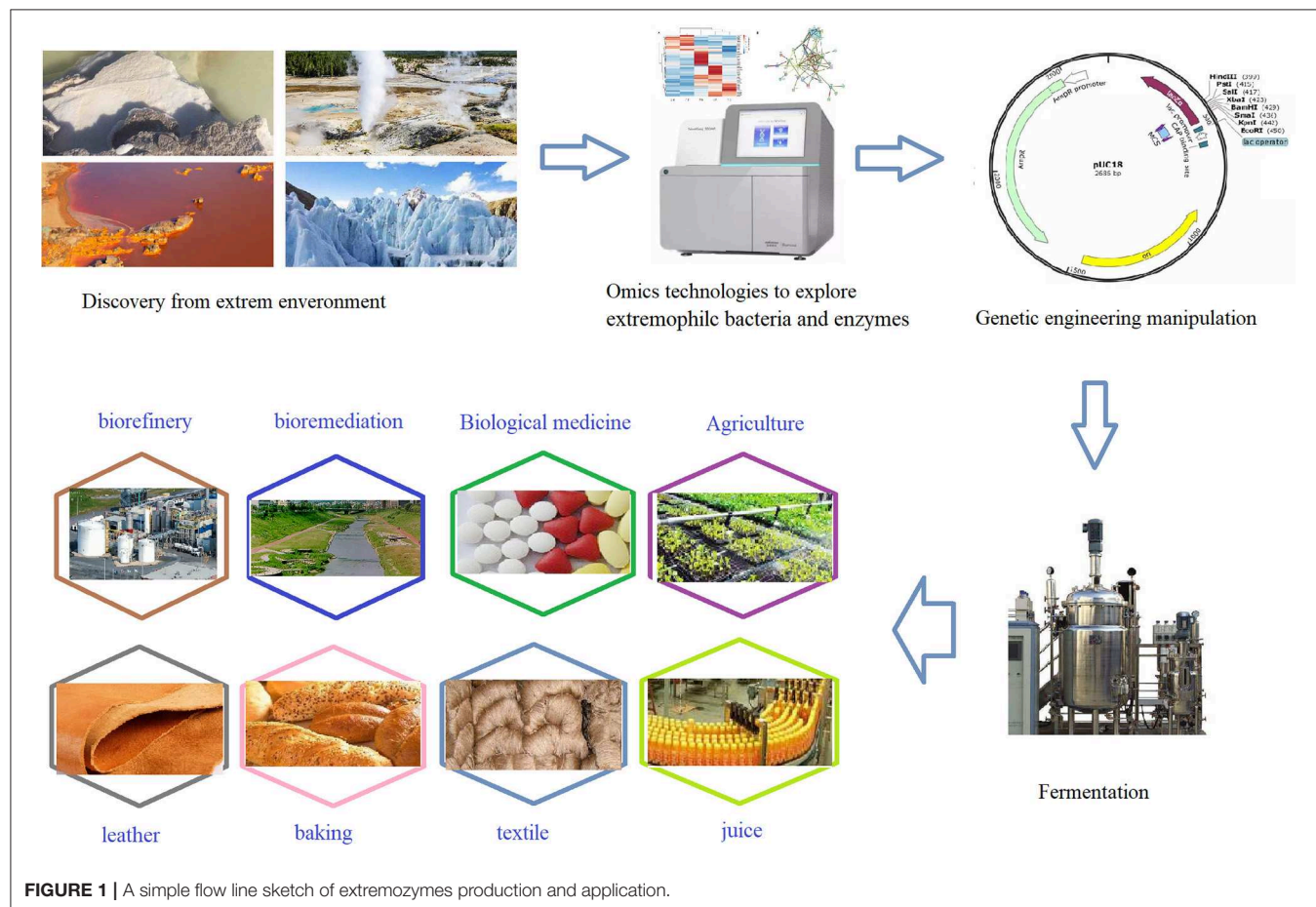
Extremophiles are a group of organisms that thrive under extreme environmental conditions (e.g., high/low temperature, pH, salinity, and pressure) that most life forms find it difficult to survive in. However, most of the earth's crust is covered by extreme environmental conditions in terms of temperatures that can range from -89°C in the Antarctic/Arctic regions to 400°C at the deep seafloor (doi: 10.1016/j.biotechadv.2015.11.001). It is thus not surprising that extremophiles have evolved and developed promising strategies and mechanisms to survive best in extreme conditions of pH, temperature, pressure, and other life-supporting conditions (Navanietha Krishnaraj and Sani, 2017; Singh et al., 2019b).

Extremophiles are comprised of animals, plants, insects, fungi, and bacteria. However, in this review, we only deal with extremophile bacteria with special reference to biofuel and bioenergy (if there is no special explanation, extremophile refers to extremophilic bacteria in the following

text). Extremophilic bacteria could be described as acidophilic (optimally thrive at low pH), alkaliphilic (optimally thrive at high pH), halophilic (thrive well in high concentrations of salt), thermophilic (optimally thrive at high temperature), hyperthermophilic (optimally survive extreme high temperature usually above 80°C), psychrophilic (thrive well at low temperature), piezophilic/barophilic (optimized growth at high pressure), oligotrophic (grow in nutrient deficient environments), endolithic (grow within rock spaces), and xerophilic (thrives in a dry area). Besides, polyextremophiles and extremotolerant microorganisms are also present in various extreme ecological niches (Dumorné et al., 2017; Gundala and Chinthala, 2017; Singh et al., 2019b). Researchers are interested in understanding their metabolic cycles to utilize them for potential industrial use due to their high stability at elevated temperatures, favoring of the good solubility of substrates, high mass transfer rate, and their lowering of the risk of pollution during industrial processes (Chen and Jiang, 2018).

Recently, extremophiles have gained immense interest owing to their ability to catalyze reactions and potential industrial applications under severe conditions (Gupta et al., 2014; Dumorné et al., 2017; Geng et al., 2018). Though extremozymes were identified several decades ago, researchers are still

concentrating more on genetic engineering of existing enzymes to potentiate their activity and the screening of novel enzymes from various sources to obtain the necessary characteristics amenable for industrial and biotechnological applications (Figure 1). Many research groups and companies around the world are committed to engineering microorganisms genetically with desirable industrial characteristics suitable for their industrial operations (Hermann et al., 2018). Many common commercial enzymes cannot meet the industrial requirements, such as being able to withstand industrial requirements with high reproducibility in different pH, temperature, and aeration conditions. Therefore, extremozymes have received increased attention as a strategy of industry process and biorefining (Espliego et al., 2018). Novozymes and Genesco have commercialized cold-adapted amylases and proteases that can eliminate starch stains (Dumorné et al., 2017). Industrial enzymes, such as those used in biorefinery, are considered as technical enzymes, and they were valued for more than \$ 1 billion in 2010 and are expected to grow to \$5.0 billion in 2021 at a rate of 4.0% per year (Kuila and Sharma, 2017). This was surpassed earlier, as they reached \$5.5 billion in 2018 and are now projected to reach \$7.0 billion by 2023 by several research associations (Freedonia, 2018; Research



Biotechnology, 2018; Silveira et al., 2018). Also, a report pointed out that the global market for special enzymes (including extremozymes) reached \$4.0 billion in 2018. This opens a new window for researchers to meet the ever-growing global market demand, and extremozymes are the best candidates for consideration (Dumorné et al., 2017).

The term “Bioenergy” refers to solid, liquid, and/or gaseous substances that have tended to be used as an energy source (e.g., bio-ethanol, butanol, biodiesel, and biomethane) (Fatih Demirbas, 2009; Arevalo-Gallegos et al., 2017; Moreno and Olsson, 2017). A biorefinery, a widely used concept, is a facility that permits the full, integrated use of biomass generated into a spectrum of bio-based products and bioenergy (Cherubini, 2010). Lignocellulose is the main structural component of plants that contains cellulose, hemicellulose, and lignin as its constituents. Lignocelluloses are the best candidate feedstocks for bioenergy production because of their high mass availability, relatively low price, and lack of competition with food provision (Sánchez and Cardona, 2008; Zhang Z. et al., 2016; Arevalo-Gallegos et al., 2017). However, the recalcitrance of lignocelluloses caused by lignin is the key hindrance in the utilization of this valuable resource (Moreno and Olsson, 2017; Geng et al., 2018). Therefore, the effective delignification of the biomass will play an important role in the economic feasibility of biofuel processing (Menon and Rao, 2012; Arevalo-Gallegos et al., 2017). There seems to be a bright future in the study of the delignification and utilization of the lignocellulosic biomass for bioenergy production using the most appropriate extremophilic organism (Amoozegar et al., 2019). In addition, the efficiency of hydrolysis of lignocellulose by enzyme complexes (celluloses, hemicellulose, and accessory proteins) is still a key limiting step of biorefinery (Klein-Marcuschamer et al., 2012). Therefore, it is necessary to develop an improved biorefinery cellulase that has higher catalytic efficiency, higher temperature stability, certain pH stability, and tolerance to the inhibition of the end product.

Pretreatment is the key operation unit of a biorefinery, and its purpose is to improve the accessibility of carbohydrates for biodegradation by delignification, expand the accessible surface area of biomass, and reduce the crystallinity of cellulose (Kumari and Singh, 2018). Extremophiles and their ligninolytic enzymatic systems have been used as single biological pretreatment methods or combined with other pre-treatment technologies to improve the hydrolysis performance of biomass (Ragauskas et al., 2006; Moreno et al., 2015). The process of bioenergy production depends on the utilization of severe reaction conditions, such as high temperature or low temperature and extremes in pH and salinity. The cost of these biotechnology applications can be reduced by using microorganisms with special capabilities, and extremophiles and their enzymes would thus provide a better choice for biofuel production. In this context, this review is essentially focused on the past and current situation of extremophiles and extremozymes application in biorefineries as well as the potential technical methods for the production of low-cost bioenergy from biomass in the foreseeable future.

EXTREMOPHILES AND EXTREMOZYMES

Many extremophiles and enzymes have been isolated and have seen attempted use for biomass processing, including genus *Acidithiobacillus*, *Arthrobacter*, *Bacillus*, *Caldicellulosiruptor*, *Clostridium*, *Coprothermobacter*, *Enterobacter*, *Geobacillus*, *Micrococcus*, *Paenibacillus*, *Penicillium*, *Picrophilus*, *Pseudoalteromonas*, and *Thermobifida*. The enzymes they secreted include α -amylase, subtilase, β -galactosidase, xylanase, β -glucosidase, decarboxylase, endoglucanase, dehydrogenase, tetrathionate hydrolase, etc. These enzymes and extremophiles are summarized in Table 1.

Thermophiles and Thermostable Enzymes

Thermophiles are organisms that thrive at 41–122°C with optimum growth temperatures between 60 and 108°C. These organisms have attracted great attention among extremophiles due to their being the main source of industrially important thermostable enzymes (Singh et al., 2011). Thermophiles can generally be divided into moderate thermophiles (T_{opt} : 50–60°C), extreme thermophiles (T_{opt} : 60–80°C), and hyperthermophiles (T_{opt} : 80–110°C) (Singh et al., 2011). For example, it has been reported that the hyperthermophiles *Methanopyrus kandleri* 116 can even grow at 122°C, which has broad application prospects in industrial processes (Su et al., 2013).

The use of thermostable enzymes in the biorefining process gives substrates properties of better solubility, easier mixing, having a reduced the risk of contamination, and higher conversion efficiency. Thermophilic bacteria are often considered one of the sources of industrially relevant thermostable enzymes (Rigoldi et al., 2018). Generally, an enzyme or protein is considered to be thermostable when it has a high defined unfolding (transition) temperature (T_m) or a long half-life at a selected high temperature (Böhme et al., 2019). These unique characteristics of thermostable enzymes pave a way for their widespread applications in industries. For example, thermostable enzymes obtained from thermophilic bacilli have found a plethora of commercial applications due to their robustness in catalytic activity and their ability to withstand the heat generated in various biotechnological and industrial processes (Margaryan et al., 2018). Thus, thermophilic enzymes can be used to catalyze high-temperature chemical processes that are difficult for normal-temperature enzymes. By far the most successful extremozyme is “Taq polymerase,” which was isolated by F.C. Lowry from thermophilic bacteria “*Thermus aquaticus*.” Similarly, thermophilic *Geobacillus* spp. and *Geobacillus* sp. Iso5 were isolated, characterized from thermal springs, and were shown to produce hyper thermostable α -amylase with an optimum enzyme activity at 90 and 140°C, respectively; they are thus extremely promising for biorefinery application (Nazina et al., 2000, 2001; Gurumurthy and Neelagund, 2012).

It has been reported that a variety of thermophilic bacteria and their secreted enzymes have great application potential in bioenergy production and anaerobic fermentation, and these include *Caldicellulosiruptor bescii*, *Geobacillus proteiniphilus*,

TABLE 1 | Applications of extremophiles and extremozymes in industry.

Species	Source	Enzyme	Optimum reaction temperature (°C)	Use (potential)	References
<i>Bacillus mojavensis</i> SO-10	No information	α -amylase	70	Biorefinery, food, detergent	Ozdemir et al., 2018
Thermophilic <i>Anoxybacillus</i> sp. GXS-BL	Hot spring	α -amylase	60	Food, pharmaceuticals, textile, detergent and bioenergy industries	Liao et al., 2019
<i>Anoxybacillus thermarum</i> FRM-RBK02	Hot spring	α -amylase	80	Biorefinery, food, detergent	Mantiri et al., 2019
<i>Erwinia</i> sp. E602	Frozen soil	Cold-adapted β -galactosidase	40	Dairy industry	Xia et al., 2018
<i>Anoxybacillus flavithermus</i> <i>Bacillus licheniformis</i>	Hot spring	β -galactosidase	60	Food, bioremediation, biosensor	Rani et al., 2019
<i>Alteromonas</i> sp. ML117	Marine	β -galactosidase	10	Food	Yao et al., 2019
<i>Bacillus tequilensis</i> ARMAT1	Feces soil	Thermo-alkali stable xylanase	60	Biorefinery, food	Khusro et al., 2016
<i>Bacillus subtilis</i> Lucky9	No information	Alkali tolerant xylanase	60	Biofuel and food	Chang et al., 2017
<i>Dictyoglomus turgidum</i>	No information	Thermostable β -glucosidase	80	Biorefinery, food	Fusco et al., 2018
<i>Exiguobacterium antarcticum</i> B7	Antarctica soil	Cold-adapted β -glucosidase	30	Biorefinery, ethanol	Crespim et al., 2016
<i>Micrococcus antarcticus</i>	Antarctica	Psychrophilic β -glucosidase	35	Detergents, textiles, bioremediation	Miao et al., 2016
Metagenome	Marine	Thermoactive endoglucanase	115	Biorefinery	Suleiman et al., 2019
<i>Cellulomonas fimi</i> ATCC484	Soil	Thermostable endoglucanase	65	Biorefinery	Saxena et al., 2018
<i>Bacillus cereus</i> FT 1	Soil	Alkaline protease	35	Detergents, pharmaceutical, leather, food, bioremediation	Asha and Palaniswamy, 2018
<i>Janibacter</i> sp. strain R02	Antarctic soil	Thermophilic and halophilic esterase	80	Detergents, pharmaceutical, leather, food, bioremediation	Castilla et al., 2017
Thermophilic <i>Anoxybacillus</i> sp. HBB16	Hot spring	Alkaline lipase	50	Organic synthesis, detergent, wastewater treatment, biodiesel	Burcu Bakir and Metin, 2017
<i>Paenibacillus barengoltzii</i>	Marine	Chitinase	55	Conversion of cellulose to ethanol	Yang et al., 2016

Thermoanaerobacterium, *Pyrococcus*, and *Caldicellulosiruptor* (Jiang et al., 2018; Williams-Rhaesa et al., 2018; Semenova et al., 2019; Straub et al., 2019; Hoffmann et al., 2020). Thermophilic *Clostridium* has been successfully used as green biologics to produce biobutanol using corn stock as a substrate (Zhang and Jia, 2018). The inoculation of *Consortium* TC-5 in digested sludge was reported to significantly increase the methane production rate by 36.6% under thermophilic conditions, which is conducive to the sustainable development of the industrial economy (Kong, 2018). Most recently, a glycocin biosynthetic gene cluster from a thermophilic *Aeribacillus pallidus* 8 was expressed heterologously in *E. coli* as a good tool for the production of hypothetical glycocin, which holds the potential application in biofuel production (Arnoldas Kaunietis et al., 2019). In a recent study, a butanol-producing *Clostridium* sp. strain WST was introduced via the bioaugmentation process, which significantly improved the butanol yield and up to 0.54 g/g by 98-fold. This breakthrough offers an eco-friendly way to efficiently use lignocellulose to produce biofuels and bioenergy, which in turn reduces the production cost (Shanmugam et al., 2019). Generally, thermophiles and their enzymes/proteins have potential usage in biomass pretreatment and biofuels production. However, the disadvantages of using thermophilic bacteria to

produce biofuels include the lack of both scientific understanding of thermophilic bacteria and of appropriate genetic manipulation tools. Recently, an efficient and rapid gene knock-out/knock-in system was established by using the thermosensitive replicon and a heterologous *pyrE* gene of *Geobacillus kaustophilus* as the counter-selection marker, which enabled its use in thermophilic bacilli as a considerable improved metabolic engineering tool (Sheng et al., 2017). Another challenge is that a biorefinery needs a whole enzyme platform, and it is difficult for a single thermostable enzyme to integrate into the conventional enzyme system. A single enzyme will lead to a synergistic effect and affect the application of the enzyme system in biorefineries (Broeker et al., 2018). Therefore, building a whole enzyme platform of the thermostable enzyme system may be one of the important research directions in the future. The current challenge is the construction of chassis cells using a synthetic biology approach and the integration of extremophile-derived enzymes to maximize their industrial application.

Psychrophiles and Psychrotolerant Bacteria

So-called psychrophilic or psychrotolerant organisms are usually found in niche, low-temperature areas of the world, including

the Antarctic or Arctic, freezing appliances, glaciers, shallow underground areas, deep oceans, high-altitude atmospheres, and so on or in plants and animals living in cold regions (Cavicchioli et al., 2009). According to Gounot, cold-adapted bacteria can be classified as psychrophilic (permanently cold) and psychrotrophic (seasonally cold or where temperature fluxes into mesophilic range) (Gounot, 1986). Variations in the soil microbial community structure of mountainous regions have been shown to be associated with altitude level, and the relative abundance and diversity of bacteria were reported to be decreased with an increase in altitude level (Zhang et al., 2009; Margesin and Miteva, 2010; Martin and McMinn, 2017). In the marine ecosystem, psychrophilic bacteria are dominant due to prevailing temperatures ($<5^{\circ}\text{C}$); the deep sea and most of the cold-adapted microbes isolated from the fluctuating land environment are considered to be psychrotolerant (Bölter, 2004).

In recent years, numerous psychrophilic microorganisms with promising industrial application have been isolated and identified from various extreme environments. A novel psychrotolerant *Sanguibacter gelidistatuariae* was isolated from an ice sculpture in Antarctica, and it was found to grow at 3°C (Pikuta et al., 2017). An alkaliphilic and psychrotolerant novel species *Carnobacterium antarcticum* CP1 was isolated from sandy soil near the Davis Station in Antarctica (Zhu S. et al., 2018). Appropriate genetic manipulation tools are very important for the application of psychrophilic bacteria. Four plasmids were identified in *Psychrobacter* sp. DAB_AL43B, and they can be developed as genetic manipulation tools for the construction of *Escherichia coli*-*Psychrobacter* spp. shuttle vectors (Lasek et al., 2017). The exopolysaccharides (EPS) were synthesized as a strategy of psychrophilic bacteria to resist the extreme conditions; they can be used in biomedicine and the food industry as well as for biomaterials, casting, and electrospinning. However, although many biological processes have been developed to produce EPS, the efficiency of EPS production by extremophiles is very low compared with medium and moderate neutral EPS-production bacteria (De Carvalho, 2019). How to use synthetic biology to develop metabolic and genetic engineering strategies for the enhancing yield of EPS is of great significance to the elimination of obstacles in the industrialization of novel EPS.

The “cold-adaptive” enzymes, termed psychrozymes, can thrive at very low temperatures (typically below 15°C). Their cold-activity characteristics give them many advantages in biotechnology due to the high K_{cat} at low to moderate temperatures in biofuels and energy production (Wierzbicka-Woś et al., 2011; Martin and McMinn, 2017). The advantage of psychrophilic bacteria and their cold-adapted enzymes is that they can treat and digest lignocellulose at low temperatures. This greatly reduces the energy input required to heat the bioreactor and avoids chemical side-effects that can occur at higher temperatures and the generation of adverse byproducts. In addition, the mild temperatures of the industrial conditions were better for preventing the denaturation of thermosensitive substrates. Mild temperature will make the industrial operation more convenient and safer, which is the developmental trend of traditional industry (Hamid et al., 2014). Moreover, cold-active enzymes have advantage for the *in-situ* bioremediation

or bioaugmentation of chemical or oil-contaminated cold environments (Alpine soils, the temperate zone, and the frigid zone) and cold-adapted cellulose-degrading enzymes have practical significance for solving the problem of slow decomposition of straw residue in the straw incorporation (Kavitha, 2016). Many psychrozymes have been isolated from the psychrophiles of deep sea and the polar regions, such as amylase, protease, lipase, pectinase, xylanase, cellulase, β -galactosidase, β -glucosidase, chitinase, etc. These can find potential application on an industrial scale (Pooja et al., 2009; Feller, 2013; Siddiqui, 2015). Cold-active endoglucanase (CelX) from psychrotrophic *Pseudoalteromonas* sp. DY3 and β -galactosidase enzyme produced by *Enterobacter ludwigii* are regarded as possible and economically attractive alternatives to hydrolyze lignocellulose at refrigerated temperatures (Zeng et al., 2006; Alikunju et al., 2016; Alikunju et al., 2018). These psychrophilic endocellulases can also be used as detergents in laundry as well as to produce biofuels and chemicals (Yuan et al., 2018). Benefits from the latest advances in synthetic biology, metabolic engineering, X-ray crystallography, structural modeling, protein engineering and biophysical research facilitates the identification, characterizations and optimization of reaction conditions of new psychrozymes from psychrophiles for biomass treatment and bioenergy production.

Alkaliphiles and Acidophiles

Alkaliphiles are a class of extremophiles that survive in alkaline environments (i.e., pH 8.5–11 with optimal growth at pH 9), such as in soda lakes, hydrothermal vents, hind-gut of insects, deep-sea sediments, and carbonate-rich soils (Preiss et al., 2015). Conversely, acidophiles or acidophilic organisms tend to grow well in acidic conditions (i.e., pH 1–5 with optimum growth below pH 3), and these are mainly present in sulfuric pools, solfataric fields, and coal and sulfur mines (Johnson and Schippers, 2017).

Enzymes from alkaliphiles with high thermostability, alkaline activity, and substrate specificity have added more advantage for biofuels production under harsh industrial conditions (Annamalai et al., 2016). Published in 1971, the first report concerning alkaline enzyme was an alkaline cellulase produced by *Bacillus* species (Horikoshi et al., 2011). An alkaliphilic *Bacillus ligniniphilus* L1 was isolated from the South China Sea. It grows well at 30°C and a pH of 9.0, and it has a potential application value in the lignin valorizations (Zhu et al., 2013; Zhu D. et al., 2017). A glycoside hydrolase (GH5)-encoding gene from *Thermobifida halotolerans* YIM 90462^T was expressed in *E. coli*, and its biochemical characterization showed it could be a good candidate enzyme for the application of cellulose degradation (Zhang et al., 2015). In addition, alkaliphilic xylanase was used in the bleaching process of kraft and soda pulps without adjusting the pH, which improved the economic feasibility (Weerachavangkul et al., 2012). It is more economical and energy saving to use alkaline hemicellulase in hemicellulose biorefinery because hemicellulose has better solubility and higher hydrolysis efficiency at high pH, and the direct enzymatic hydrolysis of alkali extracted hemicellulose to monomeric sugars at high pH avoided time-consuming and corrosive pH regulation (Mamo,

2019). In order to meet the demands of a biorefinery, it is an important research goal to improve the pH and thermostability of alkaline xylanase by site-directed mutation and directed evolution (Bai et al., 2016; Li et al., 2019; Xiang et al., 2019).

The unique structures and functions of acidophilic bacteria, such as membrane potential reversal, high membrane impermeability, and the presence of secondary transporters, make them have a broad application prospect in the biological industry. A xylanase produced by acidophilic bacteria *Penicillium oxalicum* GZ-2 has been shown to be useful in biofuels, animal feed, and food industries (Liao et al., 2012), and, more importantly, utilization of acid-tolerant xylanase pulp bleaching at low pH levels is more advantageous than normal processes (Michaux et al., 2010). An Acidophilic *Stenotrophomonas maltophilia* was isolated and was found to be useful in biodegradation of polycyclic aromatic hydrocarbons (Patel et al., 2005; Arulazhagan et al., 2017).

Halophiles and Halotolerant

Halophiles are extremophilic microorganisms that can grow optimally in saline and hypersaline environments, such as deep-sea sediments, saline lakes, salt pans, saline soils, and sea water (Kumar and Khare, 2012), whereas halotolerant microbes are able to survive in high-salt environments and also grow well under normal conditions. These inherent characteristics of halophilic and halotolerant microorganisms and the demand for salt tolerance depends on environmental and nutritional factors. They are therefore one of the best choices for biofuel production and other industrial processes (Singh et al., 2019c). It is worth mentioning that the enzymes for biofuel production, such as cellulase, xylanase, laccase etc., from halophilic and halotolerant microorganisms are relatively more stable than those of a terrestrial origin. It has been reported that a halotolerant *Haloarcula* sp. Strain LLSG7 with high cellulolytic activity from the saline soil of Yuncheng Salt Lake, China, produced five different extracellular endoglucanases with an outstanding stability in the presence of organic solvents. The enzymatic hydrolysate of crude cellulase produced by strain LLSG7 was used as a substrate for bioethanol fermentation by *S. cerevisiae* yielded 10.7 g/L of ethanol, which was much higher when compared with those reported from other cellulases (Li and Yu, 2013). In addition, the polyextremotolerant cellulases from *Paenibacillus tarimensis* L88 showed its optimum activity at 80°C and broad pH range (3.0 to 10.5) in the presence of a high salt concentration (Raddadi et al., 2013). A halophilic bacterium *Nesterenkonia* sp. F can tolerate organic solvents and produce α -amylase, and it is the only wild bacterium that can produce butanol and ethanol except *Clostridia* (Amiri et al., 2016). Many enzymes, such as α -amylase, β -amylase, glucoamylase, lipase, esterase, hemicellulose, and ligninase of a halophilic and halotolerant bacterial origin hold potential industrial applications, such as bioethanol, biodiesel, or fatty acids production using renewable resources (Schreck and Grunden, 2014; Elmansy et al., 2018; Amoozegar et al., 2019). Moreover, in order to improve the performance of halophilic bacteria for industrial application, researchers are currently committed to developing various genetic tools and using synthetic biology and genetic modification technology to

accelerate cell growth and enzyme production (Chen and Jiang, 2018). Through PCR-based site-saturation mutagenesis, the activity of mutant halophilic α -amylase (threonine was replaced by aspartic acid) was increased 14.6 times compared with that of natural enzyme under salt-free conditions (Pan et al., 2020).

Defense Mechanism of Extremophiles Under Various Conditions

In order to survive in the adverse environment, extremophiles have developed a variety of strategies to cope with the harsh environment (Figure 2). The heat above the physiological temperature readily lead to the unfolding and denaturation of proteins, as it destroys the intracellular bonds that are harmful to organisms. Thermophilic microorganisms are able to restore their protein structure and function by producing chaperones or thermosomes under extreme condition to resist the destruction of protein by high temperature (Annamalai et al., 2016). In order to resist the protein unfolding caused by high temperature, thermophilic bacteria have developed special hydrogen bonds that can interact with hydrophobicity. Meanwhile, thermophilic bacterial enzymes are rich in salt bridges and/or extra disulfide bridges to make its structure more stable (Chakravorty et al., 2017). In addition, other thermo-resistance factors, including structural compactness, oligomerization, glycosylation, and hydrophobic interactions between subunits, are crucial for stability (Chakravorty et al., 2017). Synthetic biology, including site-directed mutagenesis and directed evolution of enzymes, has been used to improve the thermal stability of target proteins/enzymes, which is essential for their application in bioenergy industry (Adesioye et al., 2018).

In contrast to thermophiles, psychrophiles are able to live in extreme cold conditions, and this is mainly due to their cellular cold-adaptability mechanisms: the regulation of cold-shock proteins, small RNA-binding proteins, and extracellular polymeric substances to protect the cells against mechanical disruption to the cell membrane caused exerted by low temperature. In addition, the genome of psychrophiles contain higher G+C-rich regions encoding tRNAs, elongation factors, and RNA polymerases, and the presence of plasmids, transposable/mobile genetic elements related to the biosynthesis of unsaturated fatty acids improves their cold adaptability. Furthermore, psychrophiles with high translational and post-translational processing capacity may be essential for their growth at low temperatures (De Maayer et al., 2014). In order to adapt to cold environment, psychrophilic enzymes usually have higher structural flexibility, lower thermal stability, and higher specific activity.

Acidophiles use a variety of homeostatic pH mechanisms that involve restricting/passive proton entry into the cytoplasmic membrane and purging off protons (Mirete et al., 2017). They also have a highly impermeable cell membrane to restrict the proton influx into the cytoplasm by active proton pumping (Zhang X. et al., 2016). The well-studied *Picrophilus oshinae* is a typical example that is capable of thriving at pH 0.7 despite its internal pH being 5 (Madigan, 2000). In alkaliphiles like

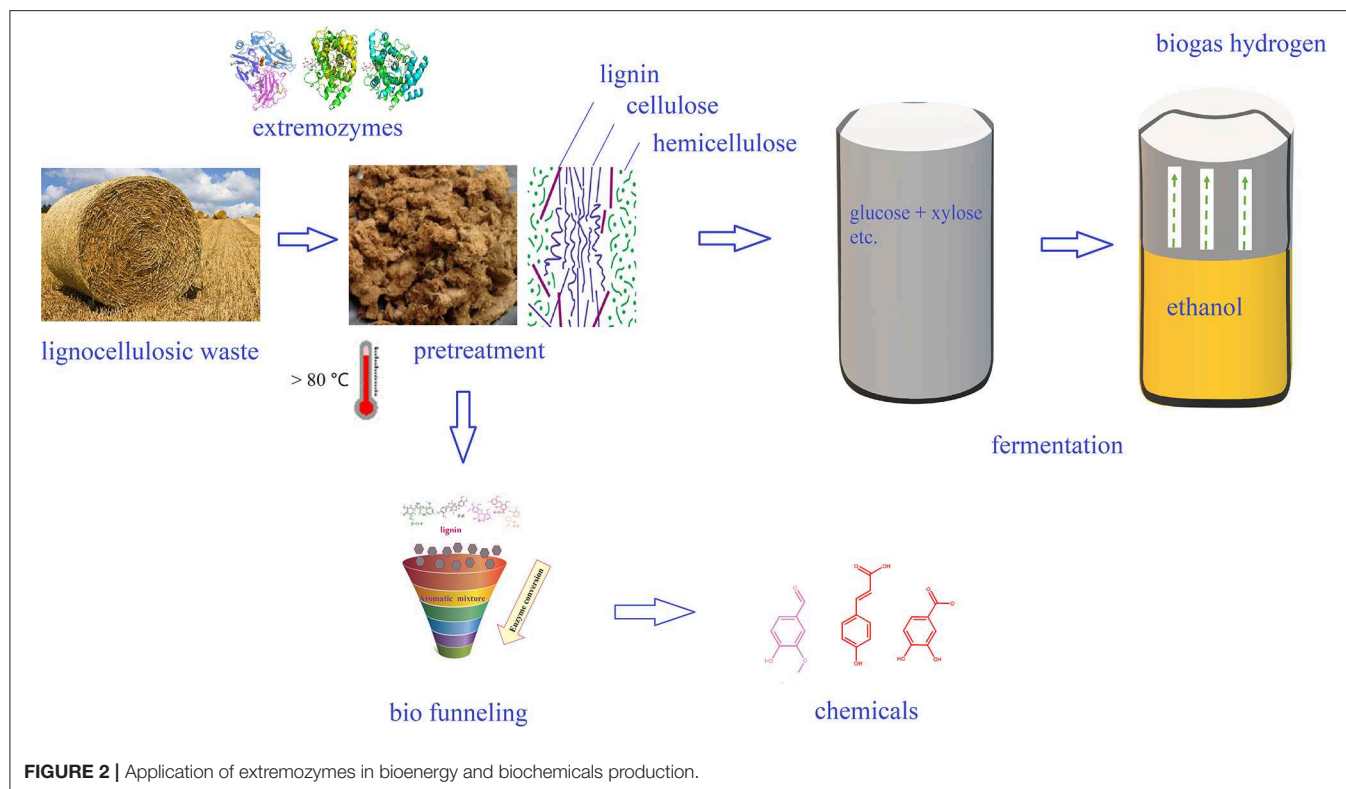


FIGURE 2 | Application of extremozymes in bioenergy and biochemicals production.

Natronobacterium gregoryi, for example, the ions are pumped inside the cells to maintain the cytoplasmic pH at near neutrality (Abe and Horikoshi, 2000).

In order to survive in the high-saline environment, halophiles developed strategies to keep the osmotic balance between intracellular with the environment to prevent water loss. One such strategy is the intracellular synthesis or accumulation of compatible solutes/osmolytes, such as ectoine, trehalose, proline, dimethylsulfoniopropionate K-glutamate, betaine, and carnitine (Zhu et al., 2008; Vauclare et al., 2014). For example, ectoine-mediated homeostasis maintenance mechanism enables halophiles to withstand and grown in the hypersaline environment (Zhu et al., 2010; Babu et al., 2015). Halophile-derived solutes such as ectoine are used in bio-industry for biofuel production. Supplementation of ectoine in the growth medium of *Zymomonas mobilis* has been shown to improve the ethanol production (Zhang et al., 2008).

Challenges of Application of Extremophiles and Extremozymes in Biorefinery

Despite the fascinating prospect of extremophiles and extremozymes, there are still obstacles in large-scale industrial application. It is difficult to cultivate extremophiles on a large scale due to harsh culture conditions. For example, using halophilic bacteria to produce Polyhydroxyalkanoate (PHA) requires a high-salt medium, but high salt concentration resulted in frequent and expensive maintenance of equipment. In addition, the process of extracting PHA from a high-salt culture is complex and costly, and the treatment of high-salinity

wastewater is also a challenge (Zhang et al., 2018; Liu et al., 2019). The lack of suitable genetic tools makes it difficult to improve the efficiency of hydrolysis and increase the product yield of extremophiles by metabolic engineering. It is still difficult for the genetic manipulation of *Halomonas*, the suicide plasmid-mediated homologous recombination system is a time-consuming, low-efficiency method for the engineering of *Halomonas bluephagenesis* TD01 (Fu et al., 2014). Although many extremophiles were culturable, the number was still very tiny compared to uncultured extremophiles. At present, most of the extremophiles were difficult to isolate and identify by the existing culture methods. It was recently estimated that the average number of uncultured microorganisms in the genus level was 7.3×10^{29} , of which 81% of the microbial cells were distributed in terrestrial, underground, and high-salt environments as well as marine sediments, hot springs, and hydrothermal vents (Lloyd et al., 2018). The huge technological gap between producing enzymes in laboratory conditions and obtaining the final commercial product is a challenge when developing extremozymes. It can be seen that a large number of extremozyme-related papers are published every year, but they rarely achieved industrialization (Di Donato et al., 2018; Jin et al., 2019; Varrella et al., 2020). In recent years, more and more scientists have devoted themselves to these issues affecting the application of extremophiles in the field of biorefinery, and they have obtained many achievements. The CRISPR/Cas9 system was developed for the genome editing of extremophiles and is expected to be used for metabolic engineering applications (Mougiakos et al., 2017). Schiraldi et al. designed a bioreactor for

the production of β -glucosidase from thermophilic *Sulfolobus solfataricus* based on a microfiltration hollow-fiber module inside of a traditional bioreactor; it enhanced the cell density from 2 to 35 g/L (Schiraldi et al., 1999). In order to solve the corrosion issue of high salt concentrations to the bioreactor, new materials were developed to replace all of the stainless-steel parts of bioreactor and autoclavable materials, such as Polyether ether ketone (Pandey et al., 2017).

POTENTIAL INDUSTRIAL APPLICATIONS OF EXTREMOZYMES

Extremozymes as biocatalysts possess extraordinary properties, such as thermostability, cold adaptivity, and osmotic allowance, to permit them using in biorefinery, agriculture, chemical industry, bioremediation, biomedicine, and environment pollution control. In this part, we focus on the potential of extreme enzymes in lignocellulose treatment, biofuel production, and high-value utilization of lignin.

Pretreatment of Lignocellulosic Biomass With Extremozymes

Lignocellulosic raw materials come from a wide range of natural sources and are considered an abundant renewable resource for the production of biofuels and value-added chemicals. In recent years, the preparation of fuel ethanol from lignocellulose has attracted much attention due to its eco-friendly nature (Zabed et al., 2016). The development of lignocellulosic energy technology is a “win-win” model for reducing costs and protecting the environment, which is conducive for the sustainable development of biorefinery based economy (Birch, 2019). At present, the cost of biofuel production from plant fiber is still high, and it has thus turned out to be one of the research hotspots to ease the process of biofuel preparation as well as to develop the cost-effective pretreatment method. In recent years, enzymes from microbial origin play a leading role in the biofuel production. When compared with chemical methods, the application of enzymes in industrial bioprocesses reduces the risk of pollution, hence they are therefore considered to be better substitutes for lignocellulose pretreatment (Ummalyma et al., 2019). Owing to the stability and robust catalytic activity of extremozymes, further development of methods involving extreme pH and temperature conditions is much needed research input to accelerate the industrial processes.

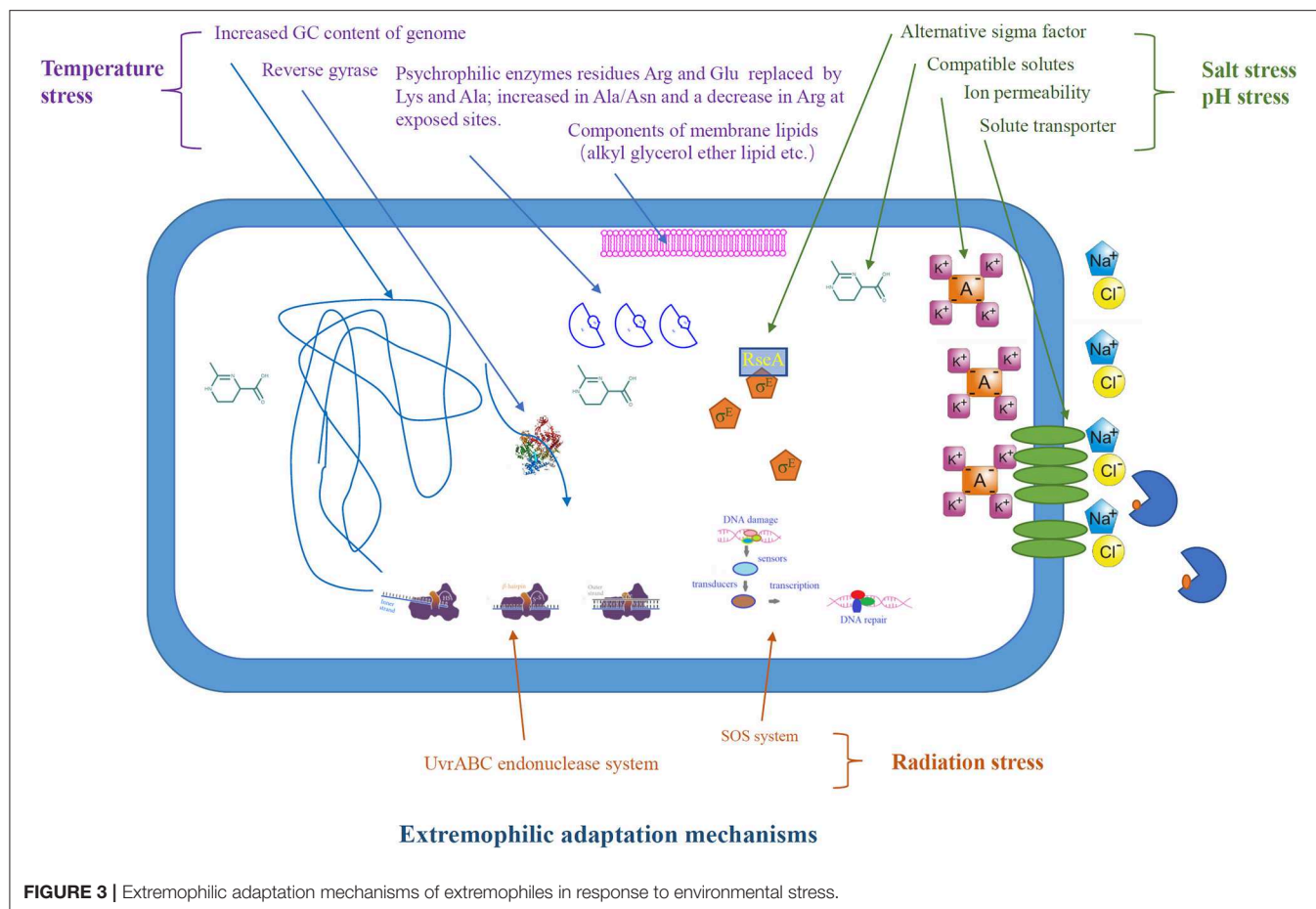
Lignocellulose is decomposed into three different polymers, such as lignin, hemicellulose, and cellulose by pretreatment, and cellulose is then converted into a monosaccharide by cellulase. Biofuel (bioethanol) is then produced by fermentation. The acid- and alkali-tolerant nature of extremozymes are helpful for pretreatment as well as the complete hydrolysis of cellulose/hemicellulose at high temperature. Lignocellulose hydrolase is limited by many factors, including crystallinity and polymerization degree, water expansion, water content, surface area, and lignin content. Lignocellulose pretreatment at industrial scale should be potent enough to overcome the complex physicochemical, structural, and compositional barriers

that inhibit the biomass digestion and improve the hydrolysis rate of lignocellulosic materials (Karimi and Taherzadeh, 2016). Hence, the combination of different pretreatment technologies are currently being employed, for example, a hydrothermal-assisted enzyme degradation process is one of the effective and widely used pretreatment methods (Kirsch et al., 2011). The advantages of this combination of multiple pretreatment processes include energy saving by omitting the cooling step and better operability at high temperatures, such as improving the accessibility of the substrate while reducing viscosity (Bhalla et al., 2013).

Biological pretreatment method involving laccase, along with other pretreatment methods, have been reported to significantly improve the delignification of lignocellulose (Moreno et al., 2015). During removal of lignin from biomass using chemical process, hemicellulose and cellulose can be partially degraded. However, biological pretreatment of biomass with extremophiles and lignin decomposition enzymes reduces the amount of the degradation products as well as time required for the pretreatment. In addition, the combination of chemical and biological pretreatment processes of eucalyptus, wheat straw, pine, and corn straw have increased the delignification efficiency (Moreno et al., 2015). Meanwhile, the high cost of enzymes makes it the most skilled but also the most expensive means in the second generation of biorefinery concept. How to further reduce the production cost of extreme enzymes and improve their activity and stability is a challenge. Further research is needed to break these obstacles and improve the pretreatment methods, and the delignification of extreme enzymes is an amazing and attractive choice for the future biorefinery.

Utilization of Extremophiles and Enzymes in Liquid Biofuels Production

Among all the biofuels, bioethanol is often regarded as the most promising alternative and/or additive for gasoline. In China, gasoline stations in many provinces utilize ethanol as an additive. The production of bioethanol from lignocellulosic biomass, named “second generation bioethanol,” includes four main steps: biomass pretreatment, enzymatic hydrolysis, fermentation, and distillation (Indira et al., 2018). The production of bioethanol from lignocellulosic raw materials is beneficial to environment and helps sustainable development, but the second-generation technology still have problems of high cost, and there are several areas of production technology that still require improvement to cut down the cost. Because of the unique characteristics, extremophiles are resistant to the adverse conditions involved in bioethanol production, and they thus harbor more advantages than terrestrial microorganisms. In particular, thermophiles and their enzymes have great potential for the bioconversion of lignocellulose into bioethanol (Figure 3). Certain thermophilic bacteria are known to produce both cellulase and xylanase, which can completely hydrolyze biomass at high temperature. For example, treatment of biomass using a thermostable cellulase produced by thermophilic *Geobacillus* sp. R7 has been shown to yield a hydrolysate that was readily fermented by *Saccharomyces cerevisiae* ATCC 24860^T to produce 0.45–0.50 g ethanol/g



glucose with a 99% utilization rate of glucose (Zambare et al., 2011). Thermophilic *Caldicellulosiruptor bescii* and *Clostridium thermocellum* have been reported for its potential to use cellulose, hemp, as well as pretreated lignocellulosic biomass as a substrate to yield bioethanol (Olson et al., 2012). In addition, thermophiles *Thermoanaerobacterium thermosaccharolyticum* M18 is able to directly utilize cellulose and xylan for the production of bioethanol (Ábrego et al., 2017).

Although thermophilic bacteria have many advantages and utilize a broad spectrum of degradable carbohydrates and the fermentation of hexose and pentose and offer a low risk of pollution, the problems associated with the low G+C content, the formation of endospores, and the low permeability of plasma membrane increase the difficulty in the genetic engineering of thermophilic bacteria (Jiang et al., 2017). In order to rectify these issues, therefore, recent advancements in synthetic biology are expected to play a crucial role in the near future to construct better strains that would pave a way for consolidated bioprocessing (CBP) model to produce hydrolase, degrade polysaccharides, and ferment all derived sugars into ethanol (Lin and Xu, 2013). CBP, as a promising strategy for ethanol production, integrates enzyme production, saccharification, and fermentation into a one-step process. Strain *Clostridium thermocellum* ATCC 31924, with consolidated

bioprocessing, significantly enhanced the cellulosic ethanol production up to 20% with crystalline cellulose as a substrate (Singh et al., 2018). A partially consolidated bioprocessing (PCBP) approach, including a non-isothermal simultaneous pretreatment and saccharification step using laccase and holocellulase by a co-fermentation of a mixture of *Ricinus communis*, *Saccharum officinarum*, and *Saccharum spontaneum* biomass, obtained a maximum ethanol concentration of 62.01 g/L (Althuri et al., 2017).

When compared with ethanol, biobutanol's lower volatility, lower heat of vaporization, higher viscosity, and higher energy density make it as a potential alternative to ethanol as a gasoline additive. In addition, butanol is more suitable for the existing oil transportation infrastructure due to its non-corrosiveness and poor hygroscopicity. The production and utilization of biological butanol has been studied for several decades, but there are still many challenges, including the low butanol production efficiency, toxicity to the production strain, multiple end-products, high energy consumption during recovery process of bio butanol, etc. (Wang et al., 2017). Therefore, it is an important goal to isolate more butanol producing extremophiles to further enhance the production level. Green Biologics company has developed a technology of producing bio butanol using corn raw materials by thermophilic *Clostridium* strains (Coker, 2016). In

addition, *Thermoanaerobacterium*, *Pyrococcus*, and *Aeropyrum* were isolated, which showed great industrial production potential of biobutanol (De Vrije, 2002). In recent years, the metabolic engineering tools have already been used to for biobutanol production. In order to conquer the intractable gene operation of *Clostridium*, a series of methods were developed to improve the efficiency of electroporation, such as increasing the dissolution of cell membrane by adding solvent, weakening the cell wall by glycine or lysozyme, and optimizing the operation parameters of electroporation (Pyne et al., 2014). CRISPR-Cas tools have also been successfully applied to the genetic transformation of *Clostridium*. For example, the application of *Streptococcus pyogenes* II CRISPR-Cas9 system for the genome editing in *Clostridium acetobutylicum* DSM792^T has promoted it to utilize both glucose and xylose (Bruder et al., 2016). The TargeTron gene-editing technique, which depends on the mobility of group-II introns, was also found to be suitable for genetic manipulations in *Clostridium*. In addition, mesophilic-TargeTron and thermo-TargeTron technology was used for metabolic engineering and identification of functional genes (Wen et al., 2019).

In recent years, bio-jet fuel has attracted huge interest, and hence industries and scientists are currently working on technologies for converting biomass-based sustainable feedstocks into bio-jet fuels. Although most of the current bio-jet fuel technologies focus on chemistry methods, a considerable amount of research on the biotransformation of feedstocks into bio-jet fuel has also made a breakthrough in recent years. Researchers from the Chalmers University of Technology have developed a method to modify the enzyme fatty acid synthase for the synthesis of medium chain fatty acids and methyl ketones for jet fuel and biodiesel production (Zhu Z. et al., 2017). A research report has pointed out that the use of acetogenic bacteria that do not produce carbon dioxide by-products during fermentation can achieve high hydrocarbon biofuel production (330 L/t feedstock) (Crawford et al., 2016). It is one of the important directions of bio-jet fuel to isolate or construct microorganisms using synthetic biology approaches to convert sugar into alkanes efficiently. Cyanobacteria and oleaginous yeasts are considered to be the most suitable microorganisms for the production of alkanes (Jiménez-Díaz et al., 2017). It is a strategic priority to find out extremophiles with enhanced alkane production capabilities from extreme environmental niches could aid in the production of alkanes.

Oleaginous microorganisms, such as *Cryptococcus curvatus*, *Lipomyces starkeyi*, *Rhodospiridium toruloides*, *Rhodococcus opacus*, etc., can accumulate lipids using biomass as substrates (Tsigie et al., 2011). The accumulated lipids can be used as biodiesel feedstock for lignocellulosic biorefineries. Therefore, extremophiles could be a promising source to explore further for lipid production from the lignocellulosic hydrolysates as potential feedstock complement (Poontawee et al., 2017). The use of lignocellulosic biomass to synthesize PHAs by halophilic microorganisms has recently attracted much attention. Although the yield is not high, it is still possible to obtain better results through genetic engineering of the target strains. Although the production of PHA from lignocellulose is still in the research stage, the result reported so far using this technology is promising

as more and more extreme microorganisms gain an important position in biorefinery.

For the second generation of biorefining, enzymes are still the most proficient and expensive means. The use of extreme microorganisms and their enzymes to improve biorefinery processes has great potential. For example, the enzyme secreted by thermophilic bacteria exhibits higher activity and thermal stability at high temperatures, which was more effectively to depolymerize lignocellulose.

Extremophiles and Lignin Valorization

Lignin is the most abundant natural aromatic compound in nature, accounting for 15 to 40% of the dry weight of plants. However, lignin was not fully utilized in the first-generation cellulose biofuel project. Although the research on lignin has a history of several decades, it still fails to develop an industrial technology that can realize the high-value utilization of lignin (Galkin and Samec, 2016). Recent studies have found that some microorganisms have evolved metabolic pathways, which can convert these aromatic substances into central intermediates through the “upper pathway,” and were then converted into central carbon metabolism through the “lower pathway.” This process is known as “Biological funneling.” “Biological funneling” provides a direct biological solution for the high-value utilization of lignin to overcome the heterogeneity problem in the lignin appreciation of modern biological refineries (Galkin and Samec, 2016). Screening ideal microorganisms and realizing the conversion of lignin flow to specific aromatic compounds are the hot research directions at present. Among them, extreme microorganisms and their enzymes are the focus of attention. Several extremophiles have shown their potential for high-value utilization of lignin, such as the halotolerant and alkalophilic bacterium *Bacillus ligniniphilus* L1, which is able to significantly degrade lignin at the optimal pH 9 and produces aromatic compounds, including vanillic acid, vanillin, etc. (Zhu D. et al., 2017). A thermophilic strain *Bacillus* sp. B1 was isolated from decayed wood bark can degrade cinnamic acid, ferulic acid, and coumaric acid into catechol, protocatechuic acid, and gentisic acid (Peng et al., 2003). In addition, a few thermo and halotolerant laccase were obtained from *Bacillus* sp. SS4, *Thermobifida fusca*, and *Trametes troglia*, and these laccase with their laccase-mediator systems (LMS) have potential applications for lignin valorization due to LMS being able to depolymerize lignin into low-molecular weight phenolics and aromatics (Chen et al., 2013; Christopher et al., 2014; Singh et al., 2019a; Yang et al., 2020). Therefore, the use of extremozymes to convert lignin into platform chemicals is one of the breakthrough applications of lignin valorization in the future.

Recent Advancements in Extremozymes Discovery With Multi-Omics Approaches

In recent time, the term “omics,” including meta-genomics, meta-proteomics, meta-transcriptomics, or metabolomics, plays an important role in the discovery of new enzymes for biorefinery with improved activity. In addition, bioinformatics and algorithms play an irreplaceable role in design the *in situ* mutagenesis and gene shuffling to improve the stability of protein

for potential industrial biorefinery purposes (Annamalai et al., 2016). These techniques have proved to be very useful for the development of extremozymes for biotechnology. Since more than 99% of microorganisms in the environment belongs to unculturable microorganisms, the current accessible techniques cannot obtain the target enzyme from the vast enzyme resource pool in nature. Therefore, “omics” technology has provided a powerful tool for the discovery of new enzymes from nature (Juerges and Hansjürgens, 2018).

In the last two decades, whole genome sequencing technology has been of great help to the understanding of the survival strategies of extremophiles in extreme environments. It promotes the understanding and application of the metabolic pathways, substrate biotransformation, transport mechanism, and enzymatic mechanism of extremophiles. Genomics research helps us to better understand the mechanism of robust enzymes and convey information about the three-dimensional structure of extreme enzymes. Based on the annotation and analysis of the genomic data of *Comamonas* SP 35, and combined with the metabolic analysis using GC-MS, the lignin degradation pathways were elucidated, and at least five metabolic pathways of lignin were speculated (Zhu D. et al., 2018). This is of practical significance for genetic transformation of chassis cells to achieve high-value utilization of lignin. Through the bioinformatics analysis of the whole genome sequence of psychrotolerant extremophile *Pseudomonas* sp. MPC6, the metabolism mechanism of toxic aromatic compounds was revealed, and the synthetase system of natural PHAs were identified. It was considered that *Pseudomonas* sp. MPC6 can be exploited as a biopolymer factory (Orellana-Saez et al., 2019). In recent years, the combination of computational and structure-based analysis with evolutionary driven methods (including directed evolution or synthetic biology) has been significantly enhanced by identifying novel extreme enzymes with high industrial application potential (Acevedo-Rocha et al., 2013; Ibrahim et al., 2016).

With the establishment of a large public database of genomic information, sequence-based methods, such as metagenomics, meta-transcriptomics, and meta-proteomics, have greatly increased the discovery of new biological systems (Naba et al., 2016; Caspi et al., 2019). Genomic data for more than 120 thermophilic bacteria are available in public database, and the genomes of *Pyrococcus*, *Anaerobranca*, *Thermotoga*, *Thermoplasma*, and *Thermus* genera have been studied in detail and provide enzymes appropriate for biorefinery industrial application (Counts et al., 2017). In addition, the “omics” technologies could resolve the bottleneck of research on unculturable microorganisms and find new high activity enzymes and metabolic pathways that can be used in biorefinery, which is the driving force to achieve sustainable biofuel production.

Transcriptomics approaches will help the study of the organism's total content of ribonucleic acid transcripts in a cell, including coding and non-coding RNAs, which can provide genome-wide data and information on gene functions to reveal molecular mechanisms related to specific biological processes. RNA sequencing technology has deepened researchers' understanding of RNA-based gene regulation and has become

one of the areas of great concern in the post-genomic era. Transcriptome analysis of extremophiles is helpful to reveal the dynamic changes of gene expression in harsh environments and a more comprehensive understanding of the functional and regulating networks of microorganisms adapting to the living environments (Manzoni et al., 2016; Jorquera et al., 2019). A multi-omics analysis revealed that the thermal adaptation strategies of *Thermus filiformis*, including oxidative stress induced by high temperature, which lead to the inhibition of genes involved in glycolysis and tricarboxylic acid cycle; glucose metabolism is achieved mainly through the pentose phosphate pathway, or the glycolysis pathway, and the accumulation of oxaloacetic acid, α -ketoglutarate, and antioxidant enzymes related to free radical scavenging (Mandelli et al., 2017). Based on the transcriptome analysis of the digestive system of termites, it was revealed that more than 14 kinds of auxiliary oxidoreductases and glycosyl hydrolase genes (12 of them came from intestinal microorganisms) may be involved in the decomposition of lignin components and their redox networks during the process of biomass pretreatment. These finding suggested that the termites have a unique digestive system and provided new insights for biorefinery (Geng et al., 2018). In many studies, transcriptional engineering has been shown to be a powerful tool to improve recombinant bacteria. It will change the pH value, ion demand, and product specificity of wild-type strains and provide higher enzyme activity (Harman-Ware et al., 2017). The mutant α -amylase, as observed from the halophilic thermotolerant *Bacillus* strains cu-48, has brought better industrial applications (Bibra et al., 2017).

The proteomic analysis of extremophiles has paid more and more attention to the revelation of its special resistance to severe climate and environmental conditions. Proteome technology provides enough knowledge for exploring the survival mechanism of extremophiles and promoted the further application of extremophiles in the field of bioenergy (Blachowicz et al., 2019). A research study comparing the proteome of *Bacillus ligniniphilus* L1 with lignin as a substrate revealed that there are more than 30 kinds of upregulated enzymes involved in lignin degradation, such as peroxiredoxin, cytochrome oxidase, oxidoreductase, ferredoxin, etc. Many environmental response factors were also found, including repressor LexA, the DNA integrity scanning protein, the catabolite repression HPr-like protein, the central glycolytic genes regulator, and the transcriptional regulator, which positively regulates lignin as a substrate (Zhu D. et al., 2017). An LC-MS/MS shotgun proteomics analysis revealed that the obligate hydrocarbon-degrading psychrophile *Oleispira antarctica* RB-8 expressed a n-alkane oxidation pathway, including two alkane monooxygenases, two alcohol dehydrogenases, two aldehyde dehydrogenases, a fatty-acid-CoA ligase, and a fatty acid desaturase. When grown on tetradecane (n-C₁₄), the synthesis of these proteins increased 3- to 21-fold compared with the control group (Gregson et al., 2020). However, compared to the existing methods, proteomics can better understand the characteristics of the enzyme, which are more advantageous for their industrial application. For example, the application of proteomics and gene-recombinant protein modification technologies helps to

improve the characteristics of enzymes, such as thermal stability, higher activity, specificity, pH, solvent tolerance, etc. (Antikainen and Martin, 2005; Tesei et al., 2019). The information provided by genomics, proteomics, and transcriptome technologies can be used to identify new targets and metabolic engineering for the production of strains in the biorefinery industry. In this way, the metabolic regulations and the pathways can be extensively studied by multi-omics technologies to further improve the production and the performance of strains (Brugger et al., 2014; Furubayashi et al., 2014).

Role Synthetic Biology in Extremophiles for Biorefinery

In the past two decades, synthetic biology has evolved as an important interdisciplinary research that integrates the genetic and metabolic engineering to customize genetic circuits to synthesize desired products using *E. coli* and *S. cerevisiae*. Henceforth, most of the synthetic biology research has been carried out using *E. coli* and *S. cerevisiae* (Adams et al., 2016). However, in recent years, researchers have begun to use several extremophiles, for example, *Deinococcus* spp, *Geobacillus* spp, *Halomonas* spp, *Pyrococcus* spp, *Thermococcus* spp, *Thermus* spp, etc., to develop industrially important strains. Synthetic biology approaches are handy in scheming organisms to thrive under modified/required conditions and to produce various bioactive molecules, which are of industrial and pharmaceutical importance through synthetic genetic circuits (Li et al., 2019). Synthesis of artemisinic acid, a precursor of artemisinin in *S. cerevisiae*, is one of the breaks through developments in synthetic biology maximizes the production and reduces the cost of artemisinin (Paddon et al., 2013). In case of biofuel and bioenergy, production of branched-chain higher alcohols from renewable resources using synthetic non-fermentative genetic circuit in *E. coli* (Atsumi et al., 2008) is a notable contribution of synthetic biology. Though significant development has been achieved in terms of lignin valorization, several bottle neck conditions have arisen that are attributable to high recalcitrance and the heterogeneous nature of lignin (Liu et al., 2019). High-value bioconversion of lignin is a three-step process that includes depolymerization, aromatics degradation, and synthesis of the required end product. Hence, system-level identification of mechanisms and pathways using integrated (meta)genomics, (meta)transcriptomics, (meta)proteomics, (meta) secretomics, and metabolomics approaches has paved a way to create lignin conversion synthetic genetic circuits, and metabolically engineered ligninolytic strains are amenable hosts for high-value lignin bioconversion. In addition, metabolic engineering and conventional adaptation methods are useful in development of strains with an ability to grow well in the presence of high concentration of aromatic compounds aroused from lignin depolymerization, which often hampers the growth of microorganisms. Lin et al. have developed a *Pseudomonas putida* strain (A514) capable of producing PHA using insoluble kraft lignin as the sole carbon source through peroxidase-based depolymerization, the metabolism of aromatic byproducts, followed by rechanneling of β -oxidation products (Lin et al.,

2016). Metabolic versatility and stability of *Thermoacidophilic Sulfolobus* species has attracted researchers to use it as one of the promising platforms for synthetic biology and metabolic engineering (Schocke et al., 2019). The availability of whole genome sequences, the construction of marker-free in-frame deletion mutants, and the homologs expression of proteins via ectopic integration of foreign genes in *Sulfolobus acidocaldarius* and *Sulfolobus islandicus* allows the modulation of the regulatory mechanisms and rechanneling of metabolic pathways to improve the production (Wagner et al., 2014).

The *S. cerevisiae* INVSc1 strain, equipped with a synthetic genetic circuit containing heat shock protein and superoxide dismutase from *Thermus thermophilus* HB8 and *Thermoanaerobacter tengcongensis* MB4, respectively, can grow well at 42°C and produces significantly more ethanol than its wild type (Sun et al., 2017). It is noteworthy to mention that alcohol dehydrogenases from extremophiles have been proved to be an excellent catalyst to produce butanol using cell-free systems (Karim et al., 2019). Wu et al. (2017) have developed a method that includes chemical depolymerization of alkali lignin into vanillin and syringate and their bioconversion into cis, cis-muconic acid, and pyrogallol, respectively, by means of metabolically engineered *E. coli* strains. In an investigation, Kohlstedt et al. (2018) metabolically engineered *P. putida* KT2440 MA-9 to produce cis and cis-muconic acid by using hydrothermally depolymerized lignin aromatics as a source, which is hydrogenated to form adipic acid and finally polymerized into nylon.

Deletion of vanillin dehydrogenase from the industrially important strains has been shown to enhance the production of vanillin from lignocellulose biomass (Linger et al., 2014). Alternatively, a thermo regulated-genetic system, i.e., the heterologous expression of two key enzymes, such as feruloyl-CoA synthetase (Fcs) and enoyl-CoA hydratase/aldolase (Ech) of thermophilic actinomycete *Amycolatopsis thermoflava* N1165 in *E. coli*, can also be used. This system allows *E. coli* to produce vanillyl alcohol using ferulic acid as a source at 30°C and subsequent conversion of vanillyl alcohol into vanillin at 50°C by the enzymatic activities of Fcs and Ech (Ni et al., 2018a). The abovementioned synthetic pathway is, however, effective in terms of function for the synthesis of vanillin from lignin-derived aromatic compounds affected by the requirement of high energy. Hence, phenolic acid decarboxylase (Pad) and aromatic dioxygenase (Ado), a Coenzyme-Free enzymatic pathway, was introduced into *E. coli*, which, in turn, allows it to the conversion of lignin derived aromatic compounds to vanillin and 4-vinylphenol (Ni et al., 2018b). Utilization of renewable sources for the production of biofuels and bioenergy is a much-needed industrial sector to cope with global warming and draining of fossil fuels. Recent advancements in multi-omics technologies, the discovery of highly efficient lignin-degrading enzymes, the integration of physical, chemical, and biological methods in lignin depolymerization, and the need for economically viable and eco-friendly production of biofuel and bioenergy necessitates researchers to engineer industrially important microorganisms through a synthetic biology approach.

CONCLUSION AND FUTURE PERSPECTIVES

In the past two decades, many countries around the world have invested a lot of money into basic research and the technological development of first- and second-generation biofuels and bioenergy, respectively. In order to deal with the reduction of fossil energy reserves and the requirements of environmental protection, many biorefinery methods have been developed by researchers, but most of them stay in the laboratory or pilot stage; only a few have entered in industries for successful production. Though biofuel industries based on different technical routes have been built around the world, they still have to manage huge limitations in the form of production cost, maintenance, and technology development issues as well as an insufficient maturity of technology, high cost, and the lack of commercial competitiveness. Reports have shown that the pretreatment takes about 40% of the total biomass processing cost (Sindhu et al., 2016). At present, one of the biggest problems in biorefinery is that it has not yet achieved the full utilization of lignin, cellulose, and hemicellulose. One of the key bottlenecks in the green revolution is difficulties associated with biodegradation of lignin. These problems have to be addressed in a scientific, eco-friendly, and cost-effective way, which in turn will boost the industrial processes for sustainable production of biofuel.

Extremophiles and extremozymes bring the dawn of success for biorefinery owing to their specificity, robustness in action, and high tolerance to the adverse conditions of the biorefinery process. It is expected that more extreme bacteria and their enzymes/proteins will provide more competitive chassis cells and catalysts for the production of biofuels in an efficient way. Of course, the realization of all these goals necessitates

the assistance of available traditional and modern cutting edge molecular biological tools. However, the production cost of extreme enzyme is still much higher than that of conventional enzyme preparation. For example, 8,000 units of endo-1,4- β -xylanase cost 177 euros from *Thermotoga maritima* but only 149 euros from *Trichoderma viride* (Ebaïd et al., 2019). In addition, the high-density fermentation of halophilic bacteria requires more than 10% salt content in the culture medium, which requires better corrosion resistance of the production equipment as well as the high cost of environmental protection brought by hypersaline wastewater. Therefore, the chassis cells derived from extremophiles were transformed by synthetic biological methods, the highly active extremophiles were screened based on histochemistry technology, and new metabolic pathways were explored to optimize the technical route. The development of artificial intelligence and nanomaterial technology brings the innovation of production equipment and improves the competitiveness of bioenergy plants.

AUTHOR CONTRIBUTIONS

DZ conceived and designed the manuscript. JS supervised the manuscript. DZ and WA wrote the manuscript. FA, SS, and BD revised the manuscript.

FUNDING

This project was support of the National Key R&D Program of China (Grant No. 2018YFE0107100); the National Natural Science Foundation of China (Grant No. 31772529); and the Priority Academic Program Development of Jiangsu Higher Education Institutions.

REFERENCES

- Abe, F., and Horikoshi, K. (2000). Tryptophan permease gene TAT2 confers high-pressure growth in *Saccharomyces cerevisiae*. *Mol. Cell. Biol.* 20, 8093–8102. doi: 10.1128/MCB.20.21.8093-8102.2000
- Ábrego, U., Chen, Z., and Wan, C. (2017). "Chapter Three - consolidated bioprocessing systems for cellulosic biofuel production," in *Advances in Bioenergy*, eds Y. Li and X. Ge (Amsterdam: Elsevier), 143–182. doi: 10.1016/bs.aibe.2017.01.002
- Acevedo-Rocha, C. G., Hoesl, M. G., Nehring, S., Royter, M., Wolschner, C., Wilttschi, B., et al. (2013). Non-canonical amino acids as a useful synthetic biological tool for lipase-catalysed reactions in hostile environments. *Catalysis Sci. Technol.* 3, 1198–1201. doi: 10.1039/c3cy20712a
- Adams, R. L., Terry, L. J., and Wente, S. R. (2016). A novel *Saccharomyces cerevisiae* FG nucleoporin mutant collection for use in nuclear pore complex functional experiments. *G3: Genes, Genomes, Genet.* 6, 51–58. doi: 10.1534/g3.115.023002
- Adesioye, F. A., Makhallanyane, T. P., Vikram, S., Sewell, B. T., Schubert, W. D., and Cowan, D. A. (2018). Structural characterization and directed evolution of a novel acetyl xylan esterase reveals thermostability determinants of the carbohydrate esterase 7 family. *Appl. Environ. Microbiol.* 84, e02695–e02617. doi: 10.1128/AEM.02695-17
- Alikunju, A. P., Sainjan, N., Silvester, R., Joseph, A., Rahiman, M., Antony, A. C., et al. (2016). Screening and characterization of cold-active β -galactosidase producing psychrotrophic *Enterobacter ludwigii* from the sediments of Arctic Fjord. *Appl. Biochem. Biotechnol.* 180, 477–490. doi: 10.1007/s12010-016-2111-y
- Alikunju, A. P., Joy, S., Salam, J. A., Silvester, R., Antony, A. C., Rahiman, K. M. M., et al. (2018). Functional characterization of a new cold-adapted β -galactosidase from an arctic fjord sediment bacteria *Enterobacter ludwigii* MCC 3423. *Catal. Lett.* 148, 3223–3235. doi: 10.1007/s10562-018-2504-3
- Althuri, A., Gujjala, L. K. S., and Banerjee, R. (2017). Partially consolidated bioprocessing of mixed lignocellulosic feedstocks for ethanol production. *Bioresour. Technol.* 245, 530–539. doi: 10.1016/j.biortech.2017.08.140
- Amiri, H., Azarbaijani, R., Yeganeh, L. P., Fazeli, A. S., Tabatabaei, M., Salekdeh, G. H., et al. (2016). *Nesterenkonia* sp. strain F, a halophilic bacterium producing acetone, butanol and ethanol under aerobic conditions. *Sci. Rep.* 6, 1–10. doi: 10.1038/srep18408
- Amoozgar, M. A., Safarpour, A., Akbari Noghabi, K., Bakhtiary, T., and Ventosa, A. (2019). Halophiles and their vast potential in biofuel production. *Front. Microbiol.* 10:1895. doi: 10.3389/fmicb.2019.01895
- Annamalai, N., Rajeswari, M. V., and Balasubramanian, T. (2016). "Chapter 9 - Thermostable and alkaline cellulases from marine sources," in *New and Future Developments in Microbial Biotechnology and Bioengineering*, ed V. K. Gupta (Amsterdam: Elsevier), 91–98. doi: 10.1016/B978-0-444-63507-5.00009-5
- Antikainen, N. M., and Martin, S. F. (2005). Altering protein specificity: techniques and applications. *Bioorg. Med. Chem.* 13, 2701–2716. doi: 10.1016/j.bmc.2005.01.059
- Arevalo-Gallegos, A., Ahmad, Z., Asgher, M., Parra-Saldivar, R., and Iqbal, H. M. N. (2017). Lignocellulose: a sustainable material to produce value-added

- products with a zero waste approach—A review. *Int. J. Biol. Macromol.* 99, 308–318. doi: 10.1016/j.ijbiomac.2017.02.097
- Arnoldas Kaunietis, A. B., Donaldas, J., Citavičius and Oscar, P. (2019). Heterologous biosynthesis and characterization of a glycosin from a thermophilic bacterium. *Nat. Commun.* 10:1115. doi: 10.1038/s41467-019-09065-5
- Arulazhagan, P., Al-Shekri, K., Huda, Q., Godon, J.-J., Basahi, J. M., and Jeyakumar, D. (2017). Biodegradation of polycyclic aromatic hydrocarbons by an acidophilic *Stenotrophomonas maltophilia* strain AJH1 isolated from a mineral mining site in Saudi Arabia. *Extremophiles* 21, 163–174. doi: 10.1007/s00792-016-0892-0
- Asha, B., and Palaniswamy, M. (2018). Optimization of alkaline protease production by *Bacillus cereus* FT 1 isolated from soil. *J. Appl. Pharm. Sci.* 8, 119–127. doi: 10.7324/JAPS.2018.8219
- Atsumi, S., Cann, A. F., Connor, M. R., Shen, C. R., Smith, K. M., Brynildsen, M. P., et al. (2008). Metabolic engineering of *Escherichia coli* for 1-butanol production. *Metab. Eng.* 10, 305–311. doi: 10.1016/j.ymben.2007.08.003
- Babu, P., Chandel, A. K., and Singh, O. V. (2015). “Survival mechanisms of extremophiles,” in *Extremophiles and Their Applications in Medical Processes* (Cham: Springer International Publishing), 9–23. doi: 10.1007/978-3-319-12808-5_2
- Bai, W., Cao, Y., Liu, J., Wang, Q., and Jia, Z. (2016). Improvement of alkalophilicity of an alkaline xylanase Xyn11A-LC from *Bacillus* sp. SN5 by random mutation and Glu135 saturation mutagenesis. *BMC Biotechnol.* 16:77. doi: 10.1186/s12896-016-0310-9
- Bhalla, A., Bansal, N., Kumar, S., Bischoff, K. M., and Sani, R. K. (2013). Improved lignocellulose conversion to biofuels with thermophilic bacteria and thermostable enzymes. *Bioresour. Technol.* 128, 751–759. doi: 10.1016/j.biortech.2012.10.145
- Bibra, M., Navanietha Krishnaraj, R., and Sani, R. K. (2017). “An overview on extremophilic chitinases,” in *Extremophilic Enzymatic Processing of Lignocellulosic Feedstocks to Bioenergy*, eds R. K. Sani and R. N. Krishnaraj (Cham: Springer International Publishing), 225–247. doi: 10.1007/978-3-319-54684-1_12
- Birch, K. (2019). “Background to emerging bio-economies,” in *Neoliberal Bio-Economies?* (New York, NY: Springer), 45–77. doi: 10.1007/978-3-319-91424-4_3
- Blachowicz, A., Chiang, A. J., Elsaesser, A., Kalkum, M., Ehrenfreund, P., Stajich, J. E., et al. (2019). Proteomic and metabolomic characteristics of extremophilic fungi under simulated mars conditions. *Front. Microbiol.* 10:1013. doi: 10.3389/fmicb.2019.01013
- Böhme, B., Moritz, B., Wendler, J., Hertel, T., Ihling, C., Brandt, W., et al. (2019). Enzymatic activity and thermoresistance of improved microbial transglutaminase variants. *Amino Acids* 52:313–26. doi: 10.1007/s00726-019-02764-9
- Bölter, M. (2004). Ecophysiology of psychrophilic and psychrotolerant microorganisms. *Cell. Mol. Biol.* 50, 563–573.
- Broeker, J., Mechelke, M., Baudrexel, M., Mennerich, D., Hornburg, D., Mann, M., et al. (2018). The hemicellulose-degrading enzyme system of the thermophilic bacterium *Clostridium stercoarum*: comparative characterisation and addition of new hemicellulolytic glycoside hydrolases. *Biotechnol. Biofuels* 11:229. doi: 10.1186/s13068-018-1228-3
- Bruder, M. R., Pyne, M. E., Moo-Young, M., Chung, D. A., and Chou, C. P. (2016). Extending CRISPR-Cas9 technology from genome editing to transcriptional engineering in the genus *Clostridium*. *Appl. Environ. Microbiol.* 82, 6109–6119. doi: 10.1128/AEM.02128-16
- Brugger, D., Krondorfer, I., Zahma, K., Stoisser, T., Bolivar, J. M., Nidetzky, B., et al. (2014). Convenient microtiter plate-based, oxygen-independent activity assays for flavin-dependent oxidoreductases based on different redox dyes. *Biotechnol. J.* 9, 474–482. doi: 10.1002/biot.201300336
- Burcu Bakir, Z., and Metin, K. (2017). Production and characterization of an alkaline lipase from thermophilic *Anoxybacillus* sp. HBB16. *Chem. Biochem. Eng. Q.* 31, 303–312. doi: 10.15255/CABEQ.2016.99
- Caspi, R., Billington, R., Fulcher, C. A., Keseler, I. M., Kothari, A., Krummenacker, M., et al. (2019). BioCyc: a genomic and metabolic web portal with multiple omics analytical tools. *FASEB J.* 33, 473.472–473.472.
- Castilla, A., Panizza, P., Rodriguez, D., Bonino, L., Díaz, P., Irazoqui, G., et al. (2017). A novel thermophilic and halophilic esterase from *Janibacter* sp. R02, the first member of a new lipase family (Family XVII). *Enzyme Microbial Technol.* 98, 86–95. doi: 10.1016/j.enzymtec.2016.12.010
- Cavicchioli, R., Saunders, N., and Thomas, T. (2009). “Cold-shock response in microorganisms,” in: *Extremophiles-volume II* (EOLSS Publications Oxford), 122–143.
- Chakravorty, D., Khan, M. F., and Patra, S. (2017). Multifactorial level of extremostability of proteins: can they be exploited for protein engineering? *Extremophiles* 21, 419–444. doi: 10.1007/s00792-016-0908-9
- Chang, S., Guo, Y., Wu, B., and He, B. (2017). Extracellular expression of alkali tolerant xylanase from *Bacillus subtilis* Lucky9 in *E. coli* and application for xylooligosaccharides production from agro-industrial waste. *Int. J. Biol. Macromol.* 96, 249–256. doi: 10.1016/j.ijbiomac.2016.11.032
- Chen, C.-Y., Huang, Y.-C., Wei, C.-M., Meng, M., Liu, W.-H., and Yang, C.-H. (2013). Properties of the newly isolated extracellular thermo-alkali-stable lactase from thermophilic actinomycetes, *Thermobifida fusca* and its application in dye intermediates oxidation. *AMB Express* 3:49. doi: 10.1186/2191-0855-3-49
- Chen, G. Q., and Jiang, X. R. (2018). Next generation industrial biotechnology based on extremophilic bacteria. *Curr. Opin. Biotechnol.* 50, 94–100. doi: 10.1016/j.copbio.2017.11.016
- Cherubini, F. (2010). The biorefinery concept: using biomass instead of oil for producing energy and chemicals. *Energy Convers. Manage.* 51, 1412–1421. doi: 10.1016/j.enconman.2010.01.015
- Christopher, L. P., Yao, B., and Ji, Y. (2014). Lignin biodegradation with laccase-mediator systems. *Front. Energy Res.* 2:12. doi: 10.3389/fenrg.2014.00012
- Coker, J. A. (2016). Extremophiles and biotechnology: current uses and prospects. *F1000Research* 5, F1000 Faculty Rev-1396. doi: 10.12688/f1000research.7432.1
- Counts, J. A., Zeldes, B. M., Lee, L. L., Straub, C. T., Adams, M. W., and Kelly, R. M. (2017). Physiological, metabolic and biotechnological features of extremely thermophilic microorganisms. *Wiley Interdisc. Rev.* 9:e1377. doi: 10.1002/wsbm.1377
- Crawford, J. T., Shan, C. W., Budsberg, E., Morgan, H., Bura, R., and Gustafson, R. (2016). Hydrocarbon bio-jet fuel from bioconversion of poplar biomass: techno-economic assessment. *Biotechnol. Biofuels* 9:141. doi: 10.1186/s13068-016-0545-7
- Crespim, E., Zanthorlin, L. M., De Souza, F. H., Diogo, J. A., Gazolla, A. C., Machado, C. B., et al. (2016). A novel cold-adapted and glucose-tolerant GH1 β -glucosidase from *Exiguobacterium antarcticum* B7. *Int. J. Biol. Macromol.* 82, 375–380. doi: 10.1016/j.ijbiomac.2015.09.018
- De Carvalho, C. C. (2019). Marine exopolysaccharides provide protection in extreme environments. *Enzymatic Technol. Mar. Polysaccharides* 95:5. doi: 10.1201/9780429058653-5
- De Maayer, P., Anderson, D., Cary, C., and Cowan, D. A. (2014). Some like it cold: understanding the survival strategies of psychrophiles. *EMBO Rep.* 15, 508–517. doi: 10.1002/embr.201338170
- de Vrije, T., de Haas, G. G., Tan, G. B., Keijsers, E. R. P., and Claassen, P. A. M. (2002). Pretreatment of Miscanthus for hydrogen production by *Thermotoga elfii*. *Int. J. Hydrogen Energy* 27, 11–12. doi: 10.1016/S0360-3199(02)00124-6
- Di Donato, P., Buono, A., Poli, A., Finore, I., Abbamondi, G. R., Nicolaus, B., et al. (2018). Exploring marine environments for the identification of extremophiles and their enzymes for sustainable and green bioprocesses. *Sustainability* 11, 1–20. doi: 10.3390/su11010149
- Dumorné, K., Camacho Córdova, D., Astorga-Eló, M., and Renganathan, P. (2017). Extremozymes: a potential source for industrial applications. *J. Microbiol. Biotechnol.* 27, 649–659. doi: 10.4014/jmb.1611.11006
- Ebaid, R., Wang, H., Sha, C., Abomohra, A. E.-F., and Shao, W. (2019). Recent trends in hyperthermophilic enzymes production and future perspectives for biofuel industry: a critical review. *J. Cleaner Prod.* 2019:117925. doi: 10.1016/j.jclepro.2019.117925
- Elmansy, E. A., Asker, M. S., El-Kady, E. M., Hassanein, S. M., and Fawka, M. (2018). Production and optimization of α -amylase from thermo-halophilic bacteria isolated from different local marine environments. *Bullet. Natl. Res. Centre* 42:31. doi: 10.1186/s42269-018-0033-2
- Espliego, J. M. E., Saiz, V. B., Torregrosa-Crespo, J., Luque, A. V., Carrasco, M. L. C., Pire, C., et al. (2018). “Extremophile enzymes and biotechnology,” in *Extremophiles* (Boca Raton, FL: CRC Press), 227–248. doi: 10.1201/9781315154695-11

- Fatih Demirbas, M. (2009). Biorefineries for biofuel upgrading: a critical review. *Appl. Energy* 86, S151–S161. doi: 10.1016/j.apenergy.2009.04.043
- Feller, G. (2013). Psychrophilic enzymes: from folding to function and biotechnology. *Scientifica* 2013:28. doi: 10.1155/2013/512840
- Freedonia (2018). *Global Industrial Enzymes - Demand and Sales Forecasts, Market Share, Market Size, Market Leaders*. Freedonia. Available online at: www.freedoniagroup.com/World-Enzymes.html (accessed May 01, 2018).
- Fu, X.-Z., Tan, D., Aibaidula, G., Wu, Q., Chen, J.-C., and Chen, G.-Q. (2014). Development of Halomonas TD01 as a host for open production of chemicals. *Metab. Eng.* 23, 78–91. doi: 10.1016/j.ymben.2014.02.006
- Furubayashi, M., Ikezumi, M., Kajiwar, J., Iwasaki, M., Fujii, A., Li, L., et al. (2014). A high-throughput colorimetric screening assay for terpene synthase activity based on substrate consumption. *PLoS ONE* 9:e93317. doi: 10.1371/journal.pone.0093317
- Fusco, F. A., Fiorentino, G., Pedone, E., Contursi, P., Bartolucci, S., and Limauro, D. (2018). Biochemical characterization of a novel thermostable β -glucosidase from *Dictyoglomus turgidum*. *Int. J. Biol. Macromol.* 113, 783–791. doi: 10.1016/j.ijbiomac.2018.03.018
- Galkin, M. V., and Samec, J. S. (2016). Lignin valorization through catalytic lignocellulose fractionation: a fundamental platform for the future biorefinery. *ChemSusChem* 9, 1544–1558. doi: 10.1002/cssc.201600237
- Geng, A., Cheng, Y., Wang, Y., Zhu, D., Le, Y., Wu, J., et al. (2018). Transcriptome analysis of the digestive system of a wood-feeding termite (*Coptotermes formosanus*) revealed a unique mechanism for effective biomass degradation. *Biotechnol. Biofuels* 11:24. doi: 10.1186/s13068-018-1015-1
- Gounot, A.-M. (1986). Psychrophilic and psychrotrophic microorganisms. *Experientia* 42, 1192–1197. doi: 10.1007/BF01946390
- Gregon, B. H., Metodiev, G., Metodiev, M. V., Golyshin, P. N., and Mckew, B. A. (2020). Protein expression in the obligate hydrocarbon-degrading psychrophile *Oleispira antarctica* RB-8 during alkane degradation and cold tolerance. *Environ. Microbiol.* 22, 1870–1883. doi: 10.1111/1462-2920.14956
- Gundala, P. B., and Chinthala, P. (2017). “Extremophilic Pectinases,” in *Extremophilic Enzymatic Processing of Lignocellulosic Feedstocks to Bioenergy*, eds R. K. Sani and R. N. Krishnaraj (Cham: Springer International Publishing), 155–180. doi: 10.1007/978-3-319-54684-1_9
- Gupta, D. G., Srivastava, D. S., Khare, S., and Prakash, V. (2014). Extremophiles: an overview of microorganism from extreme environment. *Int. J. Agric. Environ. Biotechnol.* 7, 371–380. doi: 10.5958/2230-732X.2014.00258.7
- Gurumurthy, D., and Neelagund, S. (2012). Molecular characterization of industrially viable extreme thermostable novel alpha-amylase of *geobacillus* sp Iso5 Isolated from geothermal spring. *Pure Appl. Microbiol.* 6, 1759–1773.
- Hamid, B., Rana, R. S., Chauhan, D., Singh, P., Mohiddin, F. A., Sahay, S., et al. (2014). Psychrophilic yeasts and their biotechnological applications-a review. *African J. Biotechnol.* 13:13644. doi: 10.5897/AJB2014.13644
- Harman-Ware, A. E., Happs, R. M., Davison, B. H., and Davis, M. F. (2017). The effect of coumaryl alcohol incorporation on the structure and composition of lignin dehydrogenation polymers. *Biotechnol. Biofuels* 10:281. doi: 10.1186/s13068-017-0962-2
- Hermann, A. T. V., Gonçalves, A. L., Velasco, J., Oliva, B., Da Silva Lima, A., França, B. A., et al. (2018). “Chapter 3 - the use of synthetic biology tools in biorefineries to increase the building blocks diversification,” in *Advances in Sugarcane Biorefinery*, eds A. K. Chandel and M. H. Luciano Silveira (Amsterdam: Elsevier), 41–72. doi: 10.1016/B978-0-12-804534-3.00003-3
- Hoffmann, M., Gau, E., Braun, S., Pich, A., and Elling, L. (2020). Enzymatic synthesis of 2-(β -galactosyl)-ethyl methacrylate by β -galactosidase from *Pyrococcus woesei* and application for glycopolymer synthesis and lectin studies. *Biomacromolecules* 21, 974–987. doi: 10.1021/acs.biomac.9b01647
- Horikoshi, K., Nakao, M., Kurono, Y., and Sashihara, N. (2011). Cellulases of an alkalophilic *Bacillus* strain isolated from soil. *Can. J. Microbiol.* 30, 774–779. doi: 10.1139/m84-118
- Ibrahim, A. S., El-Toni, A. M., Al-Salamah, A. A., Almaary, K. S., El-Tayeb, M. A., Elbadawi, Y. B., et al. (2016). Development of novel robust nanobiocatalyst for detergents formulations and the other applications of alkaline protease. *Bioprocess Biosyst. Eng.* 39, 793–805. doi: 10.1007/s00449-016-1559-z
- Indira, D., Das, B., Balasubramanian, P., and Jayabalan, R. (2018). “Sea water as a reaction medium for bioethanol production,” in *Microbial Biotechnology* (New York, NY: Springer), 171–192. doi: 10.1007/978-981-10-7140-9_9
- Jiang, Y., Guo, D., Lu, J., Dürre, P., Dong, W., Yan, W., et al. (2018). Consolidated bioprocessing of butanol production from xylan by a thermophilic and butanogenic *Thermoanaerobacterium* sp. M5. *Biotechnol. Biofuels* 11:89. doi: 10.1186/s13068-018-1092-1
- Jiang, Y., Xin, F., Lu, J., Dong, W., Zhang, W., Zhang, M., et al. (2017). State of the art review of biofuels production from lignocellulose by thermophilic bacteria. *Bioresour. Technol.* 245, 1498–1506. doi: 10.1016/j.biortech.2017.05.142
- Jiménez-Díaz, L., Caballero, A., Pérez-Hernández, N., and Segura, A. (2017). Microbial alkane production for jet fuel industry: motivation, state of the art and perspectives. *Microbial Biotechnol.* 10, 103–124. doi: 10.1111/1751-7915.12423
- Jin, M., Gai, Y., Guo, X., Hou, Y., and Zeng, R. (2019). Properties and applications of extremozymes from deep-sea extremophilic microorganisms: a mini review. *Mar. Drugs* 17:656. doi: 10.3390/md17120656
- Johnson, D. B., and Schippers, A. (2017). Recent advances in acidophile microbiology: fundamentals and applications. *Front. Microbiol.* 8:428. doi: 10.3389/fmicb.2017.00428
- Jorquera, M. A., Graether, S. P., and Maruyama, F. (2019). Bioprospecting and biotechnology of extremophiles. *Front. Bioeng. Biotechnol.* 7:204. doi: 10.3389/fbioe.2019.00204
- Juerges, N., and Hansjürgens, B. (2018). Soil governance in the transition towards a sustainable bioeconomy—A review. *J. Cleaner Prod.* 170, 1628–1639. doi: 10.1016/j.jclepro.2016.10.143
- Karim, A. S., Dudley, Q. M., Juminaga, A., Yuan, Y., Crowe, S. A., Heggstad, J. T., et al. (2019). *In vitro* prototyping and rapid optimization of biosynthetic enzymes for cellular design. *bioRxiv*, 685768.
- Karimi, K., and Taherzadeh, M. J. (2016). A critical review of analytical methods in pretreatment of lignocelluloses: composition, imaging, and crystallinity. *Bioresour. Technol.* 200, 1008–1018. doi: 10.1016/j.biortech.2015.11.022
- Kavitha, M. (2016). Cold active lipases—an update. *Front. Life Sci.* 9, 226–238. doi: 10.1080/21553769.2016.1209134
- Khusro, A., Kaliyan, B. K., Al-Dhabi, N. A., Arasu, M. V., and Agastian, P. (2016). Statistical optimization of thermo-alkali stable xylanase production from *Bacillus tequilensis* strain ARMAT1. *Electr. J. Biotechnol.* 22, 16–25. doi: 10.1016/j.ejbt.2016.04.002
- Kirsch, C., Zetzl, C., and Smirnova, I. (2011). Development of an integrated thermal and enzymatic hydrolysis for lignocellulosic biomass in fixed-bed reactors. *Holzforschung*, 65, 483–489. doi: 10.1515/hf.2011.061
- Klein-Marcuschamer, D., Oleskowicz-Popiel, P., Simmons, B. A., and Blanch, H. W. (2012). The challenge of enzyme cost in the production of lignocellulosic biofuels. *Biotechnology* 109, 1083–1087. doi: 10.1002/bit.24370
- Kohlstedt, M., Starck, S., Barton, N., Stolzenberger, J., Selzer, M., Mehlmann, K., et al. (2018). From lignin to nylon: cascaded chemical and biochemical conversion using metabolically engineered *Pseudomonas putida*. *Metab. Eng.* 47, 279–293.
- Kong, X. (2018). Enhanced methane production from wheat straw with the assistance of lignocellulolytic microbial consortium TC-5. *Bioresour. Technol.* 263, 7–39. doi: 10.1016/j.biortech.2018.04.079
- Kuila, A., and Sharma, V. (2017). *Lignocellulosic Biomass Production and Industrial Applications*. Hoboken, NJ: John Wiley and Sons. doi: 10.1002/9781119323686
- Kumar, S., and Khare, S. K. (2012). Purification and characterization of maltotoligosaccharide-forming α -amylase from moderately halophilic *Marinobacter* sp. EMB8. *Bioresour. Technol.* 116, 247–251. doi: 10.1016/j.biortech.2011.11.109
- Kumari, D., and Singh, R. (2018). Pretreatment of lignocellulosic wastes for biofuel production: a critical review. *Renew. Sustain. Energy Rev.* 90, 877–891. doi: 10.1016/j.rser.2018.03.111
- Lasek, R., Dziewit, L., Ciok, A., Decewicz, P., Romaniuk, K., Jedrys, Z., et al. (2017). Genome content, metabolic pathways and biotechnological potential of the psychrophilic Arctic bacterium *Psychrobacter* sp. DAB_AL43B, a source and a host of novel Psychrobacter-specific vectors. *J. Biotechnol.* 263, 64–74. doi: 10.1016/j.jbiotec.2017.09.011
- Li, Q., Wu, T., Duan, Y., Pei, J., and Zhao, L. (2019). Improving the thermostability and pH stability of *Aspergillus niger* xylanase by site-directed mutagenesis. *Appl. Biochem. Microbiol.* 55, 136–144. doi: 10.1134/S0003683819020108
- Li, X., and Yu, H.-Y. (2013). Halostable cellulase with organic solvent tolerance from *Haloarcula* sp. LLSG7 and its application in bioethanol fermentation

- using agricultural wastes. *J. Industr. Microbiol. Biotechnol.* 40, 1357–1365. doi: 10.1007/s10295-013-1340-0
- Liao, H., Xu, C., Tan, S., Wei, Z., Ling, N., Yu, G., et al. (2012). Production and characterization of acidophilic xylanolytic enzymes from *Penicillium oxalicum* GZ-2. *Bioresour. Technol.* 123, 117–124. doi: 10.1016/j.biortech.2012.07.051
- Liao, S.-M., Liang, G., Zhu, J., Lu, B., Peng, L.-X., Wang, Q.-Y., et al. (2019). Influence of calcium ions on the thermal characteristics of α -amylase from thermophilic *Anoxybacillus* sp. *GXS-BL. Protein Peptide Lett.* 26, 148–157. doi: 10.2174/0929866526666190116162958
- Lin, L., Cheng, Y., Pu, Y., Sun, S., Li, X., Jin, M., et al. (2016). Systems biology-guided biodesign of consolidated lignin conversion. *Green Chem.*, 18, 5536–5547. doi: 10.1039/C6GC01131D
- Lin, L., and Xu, J. (2013). Dissecting and engineering metabolic and regulatory networks of thermophilic bacteria for biofuel production. *Biotechnol. Adv.* 31, 827–837. doi: 10.1016/j.biotechadv.2013.03.003
- Linger, J. G., Vardon, D. R., Guarnieri, M. T., Karp, E. M., Hunsinger, G. B., Franden, M. A., et al. (2014). Lignin valorization through integrated biological funneling and chemical catalysis. *Proc. Natl. Acad. Sci.* 111, 12013–12018. doi: 10.1073/pnas.1410657111
- Liu, C., Baffoe, D. K., Zhang, M., Li, Y., Zhan, Y., and Zhang, G. (2019). Halophile, an essential platform for bioproduction. *J. Microbiol. Methods* 2019:105704. doi: 10.1016/j.mimet.2019.105704
- Lloyd, K. G., Steen, A. D., Ladau, J., Yin, J., and Crosby, L. (2018). Phylogenetically novel uncultured microbial cells dominate earth microbiomes. *mSystems* 3, e00055-18. doi: 10.1128/mSystems.00055-18
- Madigan, M. T. (2000). Extremophilic bacteria and microbial diversity. *Ann. Missouri Bot. Garden* 87, 3–12. doi: 10.2307/2666205
- Mamo, G. (2019). Alkaline active hemicellulases. *Adv. Biochem. Eng. Biotechnol.* 1–47. doi: 10.1007/10_2019_101
- Mandelli, F., Couger, M., Paixão, D., Machado, C., Carnielli, C., Aricetti, J., et al. (2017). Thermal adaptation strategies of the extremophile bacterium *Thermus filiformis* based on multi-omics analysis. *Extremophiles* 21, 775–788. doi: 10.1007/s00792-017-0942-2
- Mantiri, F., Rumende, R., and Sudewi, S. (2019). “Identification of α -amylase gene by PCR and activity of thermostable α -amylase from thermophilic *Anoxybacillus* thermarum isolated from Remboken hot spring in Minahasa, Indonesia,” in *IOP Conference Series: Earth and Environmental Science* (Bristol: IOP Publishing). doi: 10.1088/1755-1315/217/1/012045
- Manzoni, C., Kia, D. A., Vandrovicova, J., Hardy, J., Wood, N. W., Lewis, P. A., et al. (2016). Genome, transcriptome and proteome: the rise of omics data and their integration in biomedical sciences. *Brief. Bioinformatics* 19, 286–302. doi: 10.1093/bib/bbw114
- Margaryan, A., Shahinyan, G., Hovhannisyan, P., Panosyan, H., Birkeland, N.-K., and Trchounian, A. (2018). “Geobacillus and *Anoxybacillus* spp. from terrestrial geothermal springs worldwide: diversity and biotechnological applications,” in *Extremophiles in Eurasian Ecosystems: Ecology, Diversity, and Applications*, eds D. Egamberdieva, N.-K. Birkeland, H. Panosyan, and W.-J. Li (Singapore: Springer Singapore), 119–166. doi: 10.1007/978-981-13-0329-6_5
- Margesin, R., and Miteva, V. (2010). Diversity and ecology of psychrophilic microorganisms. *Res. Microbiol.* 162, 346–361. doi: 10.1016/j.resmic.2010.12.004
- Martin, A., and McMin, A. (2017). Sea ice, extremophiles and life on extra-terrestrial ocean worlds. *Int. J. Astrobiol.* 17, 1–16. doi: 10.1017/S1473550416000483
- Menon, V., and Rao, M. (2012). Trends in bioconversion of lignocellulose: biofuels, platform chemicals and biorefinery concept. *Prog. Energy Combust. Sci.* 38, 522–550. doi: 10.1016/j.pecs.2012.02.002
- Miao, L.-L., Hou, Y.-J., Fan, H.-X., Qu, J., Qi, C., Liu, Y., et al. (2016). Molecular structural basis for the cold adaptedness of the psychrophilic β -glucosidase BglU in *Micrococcus antarcticus*. *Appl. Environ. Microbiol.* 82, 2021–2030. doi: 10.1128/AEM.03158-15
- Michaux, C., Pouyez, J., Mayard, A., Vandurm, P., Housen, I., and Wouters, J. (2010). Structural insights into the acidophilic pH adaptation of a novel endo-1, 4- β -xylanase from *Scytalidium acidophilum*. *Biochimie* 92, 1407–1415. doi: 10.1016/j.biochi.2010.07.003
- Mirete, S., Morgante, V., and González-Pastor, J. E. (2017). “Acidophiles: diversity and mechanisms of adaptation to acidic environments,” in *Adaption of Microbial Life to Environmental Extremes* (New York, NY: Springer), 227–251. doi: 10.1007/978-3-319-48327-6_9
- Moreno, A. D., Ibarra, D., Alvira, P., Tomás-Pejó, E., and Ballesteros, M. (2015). A review of biological delignification and detoxification methods for lignocellulosic bioethanol production. *Critic. Rev. Biotechnol.* 35, 342–354. doi: 10.3109/07388551.2013.878896
- Moreno, A. D., and Olsson, L. (2017). “Pretreatment of lignocellulosic feedstocks,” in *Extremophilic Enzymatic Processing of Lignocellulosic Feedstocks to Bioenergy*, eds R. K. Sani and R. N. Krishnaraj (Cham: Springer International Publishing), 31–52. doi: 10.1007/978-3-319-54684-1_3
- Mougiakos, I., Mohanraju, P., Bosma, E. F., Vrouwe, V., Bou, M. F., Naduthodi, M. I., et al. (2017). Characterizing a thermostable Cas9 for bacterial genome editing and silencing. *Nat. Commun.* 8, 1–11. doi: 10.1038/s41467-017-01591-4
- Naba, A., Clauser, K. R., Ding, H., Whittaker, C. A., Carr, S. A., and Hynes, R. O. (2016). The extracellular matrix: tools and insights for the “omics” era. *Matrix Biol.* 49, 10–24. doi: 10.1016/j.matbio.2015.06.003
- Navanietha Krishnaraj, R., and Sani, R. K. (2017). “Introduction to extremozymes,” in *Extremophilic Enzymatic Processing of Lignocellulosic Feedstocks to Bioenergy*, eds R. K. Sani and R. N. Krishnaraj (Cham: Springer International Publishing), 1–4. doi: 10.1007/978-3-319-54684-1_1
- Nazina, T., Tourova, T., Poltarau, A., Novikova, E., Grigoryan, A., Ivanova, A., et al. (2001). Taxonomic study of aerobic *Thermophilic bacilli*: descriptions of *Geobacillus subterraneus* gen. nov., sp. nov. and *Geobacillus uzenensis* sp. nov. from petroleum reservoirs and transfer of *Bacillus stearothermophilus*, *Bacillus thermocatenulatus*, *Bacillus thermoleovorans*, *Bacillus kaustophilus*, *Bacillus thermodenitrificans* to *Geobacillus* as the new combinations *G. stearothermophilus*. *Int. J. Syst. Evol. Microbiol.* 51, 433–446. doi: 10.1099/00207713-51-2-433
- Nazina, T. N., Tourova, T. P., Poltarau, A. B., Novikova, E. V., Ivanova, A. E., Grigoryan, A. A., et al. (2000). Physiological and phylogenetic diversity of thermophilic spore-forming hydrocarbon-oxidizing bacteria from oil fields. *Microbiology* 69, 96–102. doi: 10.1007/BF020757264
- Ni, J., Gao, Y. Y., Tao, F., Liu, H. Y., and Xu, P. (2018a). Temperature-directed biocatalysis for the sustainable production of aromatic aldehydes or alcohols. *Angew. Chem. Int. Ed.* 57, 1214–1217. doi: 10.1002/anie.201710793
- Ni, J., Wu, Y. T., Tao, F., Peng, Y., and Xu, P. (2018b). A coenzyme-free biocatalyst for the value-added utilization of lignin-derived aromatics. *J. Am. Chem. Soc.* 140, 16001–16005. doi: 10.1021/jacs.8b08177
- Olson, D. G., McBride, J. E., Shaw, A. J., and Lynd, L. R. (2012). Recent progress in consolidated bioprocessing. *Curr. Opin. Biotechnol.* 23, 396–405. doi: 10.1016/j.copbio.2011.11.026
- Orellana-Saez, M., Pacheco, N., Costa, J. I., Mendez, K. N., Miossec, M. J., Meneses, C., et al. (2019). In-depth genomic and phenotypic characterization of the antarctic psychrotolerant strain *Pseudomonas* sp. MPC6 reveals unique metabolic features, plasticity, and biotechnological potential. *Front. Microbiol.* 10:1154. doi: 10.3389/fmicb.2019.01154
- Ozdemir, S., Fincan, S. A., Karakaya, A., and Enez, B. (2018). A novel raw starch hydrolyzing thermostable α -amylase produced by newly isolated *Bacillus mojavensis* SO-10: purification, characterization and usage in starch industries. *Brazil. Arch. Biol. Technol.* 61:399. doi: 10.1590/1678-4324-2018160399
- Paddon, C. J., Westfall, P. J., Pitera, D. J., Benjamin, K., Fisher, K., McPhee, D., et al. (2013). High-level semi-synthetic production of the potent antimalarial artemisinin. *Nature*, 496, 528–532. doi: 10.1038/nature12051
- Pan, S., Yao, T., Du, L., and Wei, Y. (2020). Site-saturation mutagenesis at amino acid 329 of *Klebsiella pneumoniae* halophilic α -amylase affects enzymatic properties. *J. Biosci. Bioeng.* 129, 155–159. doi: 10.1016/j.jbiosc.2019.09.002
- Pandey, A., Larroche, C., and Soccol, C. R. (2017). *Current Developments in Biotechnology and Bioengineering: Current Advances in Solid-State Fermentation*. Amsterdam: Elsevier.
- Patel, M. A., Ou, M. S., Ingram, L. O., and Shanmugam, K. (2005). Simultaneous saccharification and co-fermentation of crystalline cellulose and sugar cane bagasse hemicellulose hydrolysate to lactate by a thermotolerant acidophilic *Bacillus* sp. *Biotechnol. Prog.* 21, 1453–1460. doi: 10.1021/bp0400339
- Peng, X., Misawa, N., and Harayama, S. (2003). Isolation and characterization of thermophilic bacilli degrading cinnamic, 4-coumaric, and ferulic acids. *Appl. Environ. Microbiol.* 69, 1417–1427. doi: 10.1128/AEM.69.3.1417-1427.2003
- Pikuta, E. V., Lyu, Z., Williams, M. D., Patel, N. B., Liu, Y., Hoover, R. B., et al. (2017). *Sanguibacter gelidistaturiae* sp. nov., a novel psychrotolerant anaerobe

- from an ice sculpture in Antarctica, and emendation of descriptions of the family Sanguibacteraceae, the genus Sanguibacter and species *S. antarcticus*, *S. inulinus*, *S. kedieii*, *S. marinus*, *S. soli* and *S. suarezii*. *Int. J. Syst. Evol. Microbiol.* 67, 1442–1450. doi: 10.1099/ijsem.0.001838
- Pooja, G., Alam, S. L., Sunita, B., and Lokendra, S. (2009). Bacterial diversity of soil samples from the western Himalayas, India. *Can. J. Microbiol.* 55, 564–577. doi: 10.1139/W09-011
- Poontawee, R., Yongmanitchai, W., and Limtong, S. (2017). Efficient oleaginous yeasts for lipid production from lignocellulosic sugars and effects of lignocellulose degradation compounds on growth and lipid production. *Process Biochem.* 53, 44–60. doi: 10.1016/j.procbio.2016.11.013
- Preiss, L., Hicks, D. B., Suzuki, S., Meier, T., and Krulwich, T. A. (2015). Alkaliphilic bacteria with impact on industrial applications, concepts of early life forms, and bioenergetics of ATP synthesis. *Front. Bioeng. Biotechnol.* 3:75. doi: 10.3389/fbioe.2015.00075
- Pyne, M. E., Bruder, M., Moo-Young, M., Chung, D. A., and Chou, C. P. (2014). Technical guide for genetic advancement of underdeveloped and intractable *Clostridium*. *Biotechnol. Adv.* 32, 623–641. doi: 10.1016/j.biotechadv.2014.04.003
- Raddadi, N., Cherif, A., Daffonchio, D., and Fava, F. (2013). Halo-alkalitolerant and thermostable cellulases with improved tolerance to ionic liquids and organic solvents from *Paenibacillus tarimensis* isolated from the Chott El Fejej, Sahara desert, Tunisia. *Bioresour. Technol.* 150, 121–128. doi: 10.1016/j.biortech.2013.09.089
- Ragauskas, A. J., Williams, C. K., Davison, B. H., Britovsek, G., Cairney, J., Eckert, C. A., et al. (2006). The path forward for biofuels and biomaterials. *Science* 311:484. doi: 10.1126/science.1114736
- Rani, V., Sharma, P., and Dev, K. (2019). Characterization of thermally stable β galactosidase from *Anoxybacillus flavithermus* and *Bacillus licheniformis* isolated from tattapani hot spring of North Western Himalayas, India. *Int. J. Curr. Microbiol. App. Sci.* 8, 2517–2542. doi: 10.20546/ijcma.2019.801.266
- Research Biotechnology (2018). *Global Markets for Enzymes in Industrial Applications*. Available online at: <https://www.bccresearch.com/market-research/biotechnology/global-markets-for-enzymes-in-industrial-applications-bio030k.html>
- Rigoldi, F., Donini, S., Redaelli, A., Parisini, E., and Gautieri, A. (2018). Engineering of thermostable enzymes for industrial applications. *APL Bioeng.* 2:011501. doi: 10.1063/1.4997367
- Sánchez, Ó. J., and Cardona, C. A. (2008). Trends in biotechnological production of fuel ethanol from different feedstocks. *Bioresour. Technol.* 99, 5270–5295. doi: 10.1016/j.biortech.2007.11.013
- Saxena, H., Hsu, B., De Asis, M., Zierke, M., Sim, L., Withers, S. G., et al. (2018). Characterization of a thermostable endoglucanase from *Cellulomonas fimi* ATCC484. *Biochem. Cell Biol.* 96, 68–76. doi: 10.1139/bcb-2017-0150
- Schiraldi, C., Marulli, F., Di Lernia, I., Martino, A., and De Rosa, M. (1999). A microfiltration bioreactor to achieve high cell density in *Sulfolobus solfataricus* fermentation. *Extremophiles* 3, 199–204. doi: 10.1007/s007920050117
- Schocke, L., Bräsen, C., and Siebers, B. (2019). Thermoacidophilic *Sulfolobus* species as source for extremozymes and as novel archaeal platform organisms. *Curr. Opin. Biotechnol.* 59, 71–77. doi: 10.1016/j.copbio.2019.02.012
- Schreck, S. D., and Grunden, A. M. (2014). Biotechnological applications of halophilic lipases and thioesterases. *Appl. Microbiol. Biotechnol.* 98, 1011–1021. doi: 10.1007/s00253-013-5417-5
- Semenova, E. M., Sokolova, D. S., Grouzdev, D. S., Poltarau, A. B., Vinokurova, N. G., Tourova, T. P., et al. (2019). *Geobacillus proteiniphilus* sp. nov., a thermophilic bacterium isolated from a high-temperature heavy oil reservoir in China. *Int. J. Syst. Evol. Microbiol.* 69, 3001–3008. doi: 10.1099/ijsem.0.03486
- Shanmugam, S., Sun, C., Chen, Z., and Wu, Y.-R. (2019). Enhanced bioconversion of hemicellulosic biomass by microbial consortium for biobutanol production with bioaugmentation strategy. *Bioresour. Technol.* 279, 149–155. doi: 10.1016/j.biortech.2019.01.121
- Sheng, L., Kovács, K., Winzer, K., Zhang, Y., and Minton, N. P. (2017). Development and implementation of rapid metabolic engineering tools for chemical and fuel production in *Geobacillus thermoglucosidarius* NCIMB 11955. *Biotechnol. Biofuels* 10:5. doi: 10.1186/s13068-016-0692-x
- Siddiqui, K. S. (2015). Some like it hot, some like it cold: temperature dependent biotechnological applications and improvements in extremophilic enzymes. *Biotechnol. Adv.* 33, 1912–1922. doi: 10.1016/j.biotechadv.2015.11.001
- Silveira, M. H. L., Vanelli, B. A., and Chandel, A. K. (2018). “Chapter 6 - second generation ethanol production: potential biomass feedstock, biomass deconstruction, and chemical platforms for process valorization,” in *Advances in Sugarcane Biorefinery*, eds A. K. Chandel and M. H. Luciano Silveira (Amsterdam: Elsevier), 135–152. doi: 10.1016/B978-0-12-804534-3.0006-9
- Sindhu, R., Binod, P., and Pandey, A. (2016). Biological pretreatment of lignocellulosic biomass—An overview. *Bioresour. Technol.* 199, 76–82. doi: 10.1016/j.biortech.2015.08.030
- Singh, G., Singh, S., Kaur, K., Arya, S. K., and Sharma, P. (2019a). Thermo and halo tolerant laccase from *Bacillus* sp. SS4: evaluation for its industrial usefulness. *J. Gen. Appl. Microbiol.* 65, 26–33. doi: 10.2323/jgam.2018.04.002
- Singh, N., Mathur, A. S., Gupta, R. P., Barrow, C. J., Tuli, D., and Puri, M. (2018). Enhanced cellulosic ethanol production via consolidated bioprocessing by *Clostridium thermocellum* ATCC 31924? *Bioresour. Technol.* 250, 860–867. doi: 10.1016/j.biortech.2017.11.048
- Singh, P., Jain, K., Desai, C., Tiwari, O., and Madamwar, D. (2019b). “Chapter 18 - microbial community dynamics of extremophiles/extreme environment,” in *Microbial Diversity in the Genomic Era*, eds S. Das and H. R. Dash (Cambridge, MA: Academic Press), 323–332.
- Singh, P., Jain, K., Desai, C., Tiwari, O., and Madamwar, D. (2019c). “Microbial community dynamics of extremophiles/extreme environment,” in *Microbial Diversity in the Genomic Era* (Amsterdam: Elsevier), 323–332. doi: 10.1016/B978-0-12-814849-5.00018-6
- Singh, S., Shukla, L., Nain, L., and Khare, S. (2011). Detection and characterization of new thermostable endoglucanase from *Aspergillus awamori* strain F 18. *J. Mycol. Plant Pathol.* 41, 97–103.
- Straub, C. T., Khatibi, P. A., Wang, J. P., Conway, J. M., Williams-Rhaesa, A. M., Peszlen, I. M., et al. (2019). Quantitative fermentation of unpretreated transgenic poplar by *Caldicellulosiruptor bescii*. *Nat. Commun.* 10, 1–6. doi: 10.1038/s41467-019-11376-6
- Su, A. A., Tripp, V., and Randau, L. (2013). RNA-Seq analyses reveal the order of tRNA processing events and the maturation of C/D box and CRISPR RNAs in the hyperthermophile *Methanopyrus kandleri*. *Nucleic Acids Res.* 41, 6250–6258. doi: 10.1093/nar/gkt317
- Suleiman, M., Schröder, C., Klippel, B., Schäfers, C., Krüger, A., and Antranikian, G. (2019). Extremely thermoactive archaeal endoglucanase from a shallow marine hydrothermal vent from Vulcano Island. *Appl. Microbiol. Biotechnol.* 103, 1267–1274. doi: 10.1007/s00253-018-9542-z
- Sun, H., Jia, H., Li, J., Feng, X., Liu, Y., Zhou, X., et al. (2017). Rational synthetic combination genetic devices boosting high temperature ethanol fermentation. *Synthetic and Syst. Biotechnol.* 2, 121–129. doi: 10.1016/j.synbio.2017.04.003
- Tesei, D., Sterflinger, K., and Marzban, G. (2019). “Global proteomics of extremophilic fungi: mission accomplished?” in *Fungi in Extreme Environments: Ecological Role and Biotechnological Significance* (New York, NY: Springer), 205–249. doi: 10.1007/978-3-030-19030-9_12
- Tsigie, Y. A., Wang, C.-Y., Truong, C.-T., and Ju, Y.-H. (2011). Lipid production from *Yarrowia lipolytica* Polg grown in sugarcane bagasse hydrolysate. *Bioresour. Technol.* 102, 9216–9222. doi: 10.1016/j.biortech.2011.06.047
- Ummalyma, S. B., Supriya, R. D., Sindhu, R., Binod, P., Nair, R. B., Pandey, A., et al. (2019). “Biological pretreatment of lignocellulosic biomass—Current trends and future perspectives,” in *Second and Third Generation of Feedstocks* (Amsterdam: Elsevier), 197–212. doi: 10.1016/B978-0-12-815162-4.00007-0
- Varella, S., Tangherlini, M., and Corinaldesi, C. (2020). Deep hypersaline anoxic basins as untapped reservoir of polyextremophilic prokaryotes of biotechnological interest. *Mar. Drugs* 18:91. doi: 10.3390/md18020091
- Vauclare, P., Madern, D., Girard, E., Gabel, F., Zaccari, G., and Franzetti, B. (2014). New insights into microbial adaptation to extreme saline environments. *BIO Web Conf.* 2:02001. doi: 10.1051/bioconf/20140202001
- Wagner, M., Wagner, A., Ma, X., Kort, J. C., Ghosh, A., Rauch, B., et al. (2014). Investigation of the malE promoter and MalR, a positive regulator of the maltose regulon, for an improved expression system in *Sulfolobus acidocaldarius*. *Appl. Environ. Microbiol.* 80, 1072–1081. doi: 10.1128/AEM.03050-13

- Wang, Y., Ho, S.-H., Yen, H.-W., Nagarajan, D., Ren, N.-Q., Li, S., et al. (2017). Current advances on fermentative biobutanol production using third generation feedstock. *Biotechnol. Adv.* 35, 1049–1059. doi: 10.1016/j.biotechadv.2017.06.001
- Weerachavangkul, C., Laothanachareon, T., Boonyapakron, K., Wongwilaiwalin, S., Nimchua, T., Eurwilaichitr, L., et al. (2012). Alkaliphilic endoxylanase from lignocellulolytic microbial consortium metagenome for biobleaching of eucalyptus pulp. *Microbiol. Biotechnol.* 22, 1636–1643. doi: 10.4014/jmb.1206.06044
- Wen, Z., Lu, M., Ledesma-Amaro, R., Li, Q., Jin, M., and Yang, S. (2019). TargeTron technology applicable in solventogenic clostridia: revisiting 12 years' advances. *Biotechnol. J.* 2019:1900284. doi: 10.1002/biot.201900284
- Wierzbicka-Woś, A., Cieslinski, H., Wanarska, M., Kozłowska-Tylingo, K., Hildebrandt, P., and Kur, J. (2011). A novel cold-active β -D-galactosidase from the *Paracoccus* sp. 32d - gene cloning, purification and characterization. *Microbial Cell Factories* 10:108. doi: 10.1186/1475-2859-10-108
- Williams-Rhaesa, A. M., Rubinstein, G. M., Scott, I. M., Lipscomb, G. L., Poole, F. L., Kelly, R. M., et al. (2018). Engineering redox-balanced ethanol production in the cellulolytic and extremely thermophilic bacterium, *Caldicellulosiruptor bescii*. *Metab. Eng. Commun.* 7:e00073. doi: 10.1016/j.mec.2018.e00073
- Wu, W., Dutta, T., Varman, A. M., Eudes, A., Manalansan, B., Loqué, D., et al. (2017). Lignin valorization: two hybrid biochemical routes for the conversion of polymeric lignin into value-added chemicals. *Sci. Rep.* 7, 1–13. doi: 10.1038/s41598-017-07895-1
- Xia, Y., He, L., Mao, J., Fang, P., Ma, X., and Wang, Z. (2018). Purification, characterization, and gene cloning of a new cold-adapted β -galactosidase from *Erwinia* sp. E602 isolated in northeast China. *J. Dairy Sci.* 101, 6946–6954. doi: 10.3168/jds.2018-14605
- Xiang, L., Lu, Y., Wang, H., Wang, M., and Zhang, G. (2019). Improving the specific activity and pH stability of xylanase XynHBN188A by directed evolution. *Bioresour. Bioprocess.* 6:25. doi: 10.1186/s40643-019-0262-8
- Yang, S., Fu, X., Yan, Q., Guo, Y., Liu, Z., and Jiang, Z. (2016). Cloning, expression, purification and application of a novel chitinase from a thermophilic marine bacterium *Paenibacillus barengoltzii*. *Food Chem.* 192, 1041–1048. doi: 10.1016/j.foodchem.2015.07.092
- Yang, X., Wu, Y., Zhang, Y., Yang, E., Qu, Y., Xu, H., et al. (2020). A thermo-active laccase isoenzyme from *Trametes troglia* and its potential for dye decolorization at high temperature. *Front. Microbiol.* 11:241. doi: 10.3389/fmicb.2020.00241
- Yao, C., Sun, J., Wang, W., Zhuang, Z., Liu, J., and Hao, J. (2019). A novel cold-adapted β -galactosidase from *Alteromonas* sp. ML117 cleaves milk lactose effectively at low temperature. *Process Biochem.* 82, 94–101. doi: 10.1016/j.procbio.2019.04.016
- Yuan, X., Zhang, P., Jiao, S., Du, Y., and Li, J.-J. (2018). Overexpression and biochemical characterization of a recombinant psychrophilic endocellulase from *Pseudoalteromonas* sp. DY3. *Int. J. Biol. Macromol.* 116, 100–105. doi: 10.1016/j.ijbiomac.2018.05.017
- Zabed, H., Sahu, J., Boyce, A. N., and Faruq, G. (2016). Fuel ethanol production from lignocellulosic biomass: an overview on feedstocks and technological approaches. *Renew. Sustain. Energy Rev.* 66, 751–774. doi: 10.1016/j.rser.2016.08.038
- Zambare, V. P., Bhalla, A., Muthukumarappan, K., Sani, R. K., and Christopher, L. P. (2011). Bioprocessing of agricultural residues to ethanol utilizing a cellulolytic extremophile. *Extremophiles* 15:611. doi: 10.1007/s00792-011-0391-2
- Zeng, R., Xiong, P., and Wen, J. (2006). Characterization and gene cloning of a cold-active cellulase from a deep-sea psychrotrophic bacterium *Pseudoalteromonas* sp. DY3. *Extremophiles* 10, 79–82. doi: 10.1007/s00792-005-0475-y
- Zhang, F., Zhang, X.-M., Yin, Y.-R., and Li, W.-J. (2015). Cloning, expression and characterization of a novel GH5 exo/endoglucanase of *Thermobifida halotolerans* YIM 90462T by genome mining. *J. Biosci. Bioeng.* 120, 644–649. doi: 10.1016/j.jbiosc.2015.04.012
- Zhang, J., and Jia, B. (2018). Enhanced butanol production using *Clostridium beijerinckii* SE-2 from the waste of corn processing. *Biomass Bioenergy* 115, 260–266. doi: 10.1016/j.biombioe.2018.05.012
- Zhang, L., Lang, Y., Wang, C., and Nagata, S. (2008). Promoting effect of compatible solute ectoine on the ethanol fermentation by *Zymomonas mobilis* CICC10232. *Proc. Biochem.* 43, 642–646. doi: 10.1016/j.procbio.2008.02.003
- Zhang, L.-M., Wang, M., Prosser, J. I., Zheng, Y.-M., and He, J.-Z. (2009). Altitude ammonia-oxidizing bacteria and archaea in soils of Mount Everest. *FEMS Microbiol. Ecol.* 70, 208–217. doi: 10.1111/j.1574-6941.2009.00775.x
- Zhang, X., Lin, Y., and Chen, G. Q. (2018). Halophiles as chassis for bioproduction. *Adv. Biosyst.* 2:1800088. doi: 10.1002/adbi.201800088
- Zhang, X., Liu, X., Liang, Y., Fan, F., Zhang, X., and Yin, H. (2016). Metabolic diversity and adaptive mechanisms of iron-and/or sulfur-oxidizing autotrophic acidophiles in extremely acidic environments. *Environ. Microbiol. Rep.* 8, 738–751. doi: 10.1111/1758-2229.12435
- Zhang, Z., Hu, S., Chen, D., and Zhu, B. (2016). An analysis of an ethanol-based, whole-crop refinery system in China. *Chin. J. Chem. Eng.* 24, 1609–1618. doi: 10.1016/j.cjche.2016.05.036
- Zhu, D., Cui, S., and Nagata, S. (2008). Isolation and characterization of salt-sensitive mutants of the moderately halophilic bacterium *Salinivibrio costicola* subsp. *yaniae*. *Biosci. Biotechnol. Biochem.* 72, 1977–1982. doi: 10.1271/bbb.70652
- Zhu, D., Li, P., Tanabe, S.-H., and Sun, J. (2013). Genome sequence of the alkaliphilic bacterial strain *Bacillus ligninosis* L1, a novel degrader of lignin. *Genome Announce.* 1:e0004213. doi: 10.1128/genomeA.00042-13
- Zhu, D., Si, H., Zhang, P., Geng, A., Zhang, W., Yang, B., et al. (2018). Genomics and biochemistry investigation on the metabolic pathway of milled wood and alkali lignin-derived aromatic metabolites of *Comamonas serinivorans* SP-35. *Biotechnol. Biofuels* 11:338. doi: 10.1186/s13068-018-1341-3
- Zhu, D., Zhang, P., Xie, C., Zhang, W., Sun, J., Qian, W.-J., et al. (2017). Biodegradation of alkaline lignin by *Bacillus ligniniphilus* L1. *Biotechnol. Biofuels* 10:44. doi: 10.1186/s13068-017-0735-y
- Zhu, D., Zhang, W., Zhang, Q., and Nagata, S. (2010). Accumulation and role of compatible solutes in fast-growing *Salinivibrio costicola* subsp. *Yaniae*. *Can. J. Microbiol.* 56, 1020–1027. doi: 10.1139/W10-092
- Zhu, S., Lin, D., Xiong, S., Wang, X., Xue, Z., Dong, B., et al. (2018). *Carnobacterium antarcticum* sp. nov., a psychrotolerant, alkaliphilic bacterium isolated from sandy soil in Antarctica. *Int. J. Syst. Evol. Microbiol.* 68, 1672–1677. doi: 10.1099/ijsem.0.002727
- Zhu, Z., Zhou, Y. J., Krivoruchko, A., Grininger, M., Zhao, Z. K., and Nielsen, J. (2017). Expanding the product portfolio of fungal type I fatty acid synthases. *Nat. Chem. Biol.* 13, 360–362. doi: 10.1038/nchembio.2301

Conflict of Interest: The authors declare that the research was conducted in the absence of any commercial or financial relationships that could be construed as a potential conflict of interest.

Copyright © 2020 Zhu, Adebisi, Ahmad, Sethupathy, Danso and Sun. This is an open-access article distributed under the terms of the Creative Commons Attribution License (CC BY). The use, distribution or reproduction in other forums is permitted, provided the original author(s) and the copyright owner(s) are credited and that the original publication in this journal is cited, in accordance with accepted academic practice. No use, distribution or reproduction is permitted which does not comply with these terms.



Intracellular Redox Perturbation in *Saccharomyces cerevisiae* Improved Furfural Tolerance and Enhanced Cellulosic Bioethanol Production

Chen-Guang Liu^{1*†}, Kai Li^{1†}, Ke-Yi Li¹, Chularat Sakdaronnarong², Muhammad Aamer Mehmood^{1,3*}, Xin-Qing Zhao¹ and Feng-Wu Bai¹

¹ State Key Laboratory of Microbial Metabolism, Joint International Research Laboratory of Metabolic and Developmental Sciences, School of Life Sciences and Biotechnology, Shanghai Jiao Tong University, Shanghai, China, ² Department of Chemical Engineering, Faculty of Engineering, Mahidol University, Nakhon Pathom, Thailand, ³ Department of Bioinformatics and Biotechnology, Government College University Faisalabad, Faisalabad, Pakistan

OPEN ACCESS

Edited by:

Mingjie Jin,
Nanjing University of Science and
Technology, China

Reviewed by:

Jin Hou,
Shandong University, China
Jiangfeng Ma,
Nanjing Tech University, China

*Correspondence:

Muhammad Aamer Mehmood
draamer@gcuf.edu.pk
Chen-Guang Liu
cg.liu@sjtu.edu.cn

[†]These authors have contributed
equally to this work

Specialty section:

This article was submitted to
Synthetic Biology,
a section of the journal
Frontiers in Bioengineering and
Biotechnology

Received: 20 March 2020

Accepted: 20 May 2020

Published: 23 June 2020

Citation:

Liu C-G, Li K, Li K-Y,
Sakdaronnarong C, Mehmood MA,
Zhao X-Q and Bai F-W (2020)
Intracellular Redox Perturbation in
Saccharomyces cerevisiae Improved
Furfural Tolerance and Enhanced
Cellulosic Bioethanol Production.
Front. Bioeng. Biotechnol. 8:615.
doi: 10.3389/fbioe.2020.00615

Furfural is a major toxic byproduct found in the hydrolysate of lignocellulosic biomass, which adversely interferes with the growth and ethanol fermentation of *Saccharomyces cerevisiae*. The current study was focused on the impact of cofactor availability derived intracellular redox perturbation on furfural tolerance. Here, three strategies were employed in cofactor conversion in *S. cerevisiae*: (1) heterologous expression of NADH dehydrogenase (*NDH*) from *E. coli* which catalyzed the NADH to NAD⁺ and increased the cellular sensitivity to furfural, (2) overexpression of *GLR1*, *OYE2*, *ZWF1*, and *IDP1* genes responsible for the interconversion of NADPH and NADP⁺, which enhanced the furfural tolerance, (3) expression of NAD(P)⁺ transhydrogenase (*PNTB*) and NAD⁺ kinase (*POS5*) which showed a little impact on furfural tolerance. Besides, a substantial redistribution of metabolic fluxes was also observed with the expression of cofactor-related genes. These results indicated that NADPH-based intracellular redox perturbation plays a key role in furfural tolerance, which suggested single-gene manipulation as an effective strategy for enhancing tolerance and subsequently achieving higher ethanol titer using lignocellulosic hydrolysate.

Keywords: *Saccharomyces cerevisiae*, redox perturbation, furfural, stress tolerance, ethanol fermentation

INTRODUCTION

Bioethanol is considered as one of the most promising liquid alternatives to fossil fuels, which can be either blended with gasoline or can directly be used as fuel in dedicated engines (Kuhad et al., 2016; Xu and Lin, 2018). The first-generation (1G) ethanol is being produced predominately from starch-based feedstocks. Despite its potential, it cannot be produced from the food-crops-based sugars due to the enormous demands of food supply for the increasing population. Therefore, the production of cellulosic ethanol from lignocellulosic biomass “2G fuel ethanol” has attracted significant attention. However, there are several bottlenecks in the biological transformation of cellulosic biomass to fuel ethanol which includes tedious pretreatments, pretreatment-derived toxic compounds, and inefficient enzymatic hydrolysis. Hence, it is required to develop robust strains to achieve the economic efficiency of 2G fuel production. Along with other problems, the presence of toxic by-products produced during the pretreatment of lignocellulosic biomass is a

major feedstock-derived problem, which substantially compromises the growth and fermentation of the yeast (Martín et al., 2018).

Furfural, a representative furan derivative, is present in the biomass hydrolysate (Liu et al., 2004; Wang et al., 2011). It acts as a direct inhibitor of the key enzymes in several pathways, including alcohol dehydrogenase, pyruvate dehydrogenase, acetaldehyde dehydrogenase, etc. (Banerjee et al., 1981), which consequently compromises the normal cell growth and fermentation. Furfural also leads to the accumulation of reactive oxygen species (ROS) in cells (Allen et al., 2010; Benjaphokee et al., 2012; Qiu and Jiang, 2017), which damages cellular components such as lipids, proteins, and DNA. Glutathione and glutaredoxin family are usual antioxidant systems to fight against ROS. NADPH is the only cofactor capable of catalyzing oxidized glutathione (GSSG) to reduced glutathione (GSH) (Almeida et al., 2007). Thus, furfural substantially disturbs the intracellular redox homogeneity either through hindering the synthesis of intracellular reducing power NAD(P)H or accelerating their degradation. It is a common approach to overexpress alcohol or acetaldehyde reductases to enhance *S. cerevisiae* and other industrial microorganisms furfural tolerance because these enzymes promote the conversion of furfural to its less-toxic form, furfuryl alcohol (Moon and Liu, 2012; Hasunuma et al., 2014; Li et al., 2015; Zhong et al., 2016). Besides, some researches focused on improving furfural tolerance by bioprocess engineering or adaptive laboratory evolution. For instance, Wang et al. (2020) applied biochar as a matrix for cell immobilization and as a nutrient supply to improve cell furfural tolerance. Hicks et al. (2020) developed a sequential batch culturing process to increase growth rates and reduced lag time under furfural stress. Previously, we enhanced the furfural tolerance of yeast by extracellular redox regulation under precise air control (Li et al., 2019).

Cofactor engineering to regulate the availability of NADH/NAD⁺ and NADPH/NADP⁺ has demonstrated its role in modulating metabolic networks, signal transduction, material transport, and physiological functions (Liu et al., 2013; Wang et al., 2017a). Therefore, changes in intracellular redox levels propose a theoretical solution to enhance the yeast cell tolerance to furfural. The current study was meant to evaluate the impact of

redox perturbation on furfural tolerance. Three types of enzymes were expressed to manipulate the levels of NADH/NAD⁺ and NADPH/NADP⁺ in the cytosol or mitochondria of *S. cerevisiae*. (1), NADH related-genes: *FDH* gene encoding the formate dehydrogenase which catalyzes the NAD⁺ dependent oxidation of formate anion to carbon dioxide (Serov et al., 2002), and *NDH* gene encoding NADH dehydrogenase that catalyzes the transfer of electrons from NADH to the quinone pool in the cytoplasmic membrane of *Escherichia coli* (Salewski et al., 2016). (2), NADPH related-genes: *GLR1* gene encoding cytosolic and mitochondrial glutathione oxidoreductase which reduces the glutathione (Outten and Culotta, 2004), *OYE2* gene encoding NADPH dehydrogenase (Zhao et al., 2017), *ZWF1* gene encoding glucose-6-phosphate dehydrogenase which catalyzes the first step of the pentose phosphate pathway (Cunha et al., 2015), and *IDP1* gene encoding mitochondrial NADP-specific isocitrate dehydrogenase which catalyzes the oxidation of isocitrate to alpha-ketoglutarate (Qin et al., 2015). (3), genes responsible for the interconversion of NADH and NADPH: *POS5* gene localizing in the mitochondria encoding a functional NADH kinase (Shianna et al., 2006), and *PNTB* gene encoding the pyridine nucleotide transhydrogenase of *E. coli* (Clarke et al., 1986). Accordingly, the effects of intracellular redox perturbation caused by cofactor availability on furfural tolerance along with the underlying mechanism, were elucidated.

MATERIALS AND METHODS

Strains and Fermentation

All strains and plasmids used in this study are shown in **Table 1**. *S. cerevisiae* BY4741 was used as an initial strain to construct the cofactor engineered strains. The *E. coli* DH5α was used for vector construction and propagation. Yeast strains were cultured in 250 mL flasks containing 100 mL YPD medium (yeast extract 10 g/L, peptone 20 g/L, glucose 20 g/L) in a shaking incubator set at 30°C and 150 rpm. In the mid-log phase (around 18 h), cells were inoculated at 10% inoculum into a 2.5 L fermenter containing 1 L fermentation medium (yeast extract 3 g/L, peptone 4 g/L, glucose 100 g/L) supplemented with 4 g/L furfural. The temperature, pH, and rotation rate were set at 30°C, pH 4.5, and 150 rpm, respectively.

TABLE 1 | The strains and selected oxidoreductase genes used in this study along with their sources and physiological roles.

Strain	Source	Description	Function
BY-FDH*	<i>S. cerevisiae</i>	Formate dehydrogenase	formate + NAD ⁺ = CO ₂ + NADH
BY-NDH*	<i>E. coli</i>	NADH dehydrogenase	NADH + ubiquinone + 5 H ⁺ = NAD ⁺ + ubiquinol + 4 H ⁺
BY-GLR1**	<i>S. cerevisiae</i>	Glutathione-disulfide reductase	glutathione disulfide + NADPH + H ⁺ = glutathione + NADP ⁺
BY-OYE2**	<i>S. cerevisiae</i>	NADPH dehydrogenase	NADPH + H ⁺ + acceptor = NADP ⁺ + reduced acceptor
BY-ZWF1**	<i>S. cerevisiae</i>	Glucose-6-phosphate dehydrogenase	D-glucose 6-phosphate + NADP ⁺ = D-glucono-1,5-lactone 6-phosphate + NADPH + H ⁺
BY-IDP1**	<i>S. cerevisiae</i>	Isocitrate dehydrogenase	isocitrate + NADP ⁺ = 2-oxoglutarate + CO ₂ + NADPH + H ⁺
BY-POS5***	<i>S. cerevisiae</i>	NADH kinase	ATP + NAD ⁺ = ADP + 2 H ⁺ + NADP ⁺
BY-PNTB***	<i>E. coli</i>	Pyridine nucleotide transhydrogenase	NADH + H ⁺ + NADP ⁺ = NAD ⁺ + NADPH + H ⁺

*NADH related genes, **NADPH related genes, ***NADH to NADPH related genes.

E. coli was cultivated in Luria–Bertani (LB) medium (yeast extract 5 g/L, tryptone 10 g/L, NaCl 10 g/L), a final concentration of 100 µg/L ampicillin was maintained to select the transformants in a 150 mL flask incubated at 37°C, under the constant shaking speed of 200 rpm.

Genetic Manipulations

DNA sequences of the selected oxidoreductase genes namely, *FDH*, *GLR1*, *OYE2*, *ZWF1*, *IDP1*, and *POS5* were amplified by polymerase chain reaction (PCR) from the genomic DNA of the BY4741. Whereas, the gene sequences of *NDH* and *PNTB* were amplified from the genomic DNA of *E. coli* DH5α. Primers used in this study are shown in the **Table S1**. The amplified genes were subcloned into the integration plasmid pHO to obtain overexpression plasmids. Yeast transformation was performed by the LiAc method (Gietz and Schiestl, 2007). The plasmids were transformed into *S. cerevisiae* strains BY4741. Then, the transformants were selected from the YPD agar plates containing 300 µg/mL Geneticin (Sigma-Aldrich, USA).

Biomass and Metabolites Analyses

A 2 mL of sample was collected from the fermentation broth after every 12 h. Cell growth was measured through optical density at 600 nm (OD600) using a Multiscan Go spectrophotometer (Thermo Scientific, US). After removing cells by centrifugation (10,000 × g for 5 min), the supernatant was subjected to glucose, ethanol, glycerol, and acetate concentrations, and the fermentation broth was analyzed by HPLC system equipped with RI- and UV detectors (Waters e2695, Waters, MA, USA). The Aminex HPX-87H Ion Exclusion Column (Bio-Rad, Hercules, USA) was used to separate the components. Where, 4 mM H₂SO₄ was used as a mobile phase at a flow rate of 0.6 mL/min, and the detection temperature of 50°C was used for RI-detector and 65°C for the column. Samples were analyzed in triplicate, and the mean values were calculated.

Intracellular ROS Content

The sensitive probe 2',7'-dichlorodihydrofluorescein diacetate (DCFH-DA) was used to measure the intracellular ROS level of cells. Cells were harvested by centrifugation from the 2 mL sample collected after 48 h of the inoculation, washed with phosphate buffer (PBS), and re-suspended in 500 µL PBS supplemented with 40 µL DCFH-DA and incubated at 30°C, 200 rpm for 1 h in darkness. The cells were then collected, washed twice using PBS, re-suspended in 500 µL PBS. From the suspension, a 200 µL mixture was added into each well of a 96-well microplate (black background), and fluorescence intensity was measured by Tecan Infinite 200 microplate reader (Mannedorf, Switzerland) with excitation at λ485 nm and emission at λ535 nm. The relative fluorescence unit was normalized according to the optical density of the cell culture (Allen et al., 2010).

Intracellular GSH, NADH, and NADPH

NADPH/NADP⁺ and/or NADH/NAD⁺ were estimated based on the role of cofactors in the overexpressed enzymes. The cells (2 mL) were harvested by centrifugation at 48 h after the

inoculation, washed twice with PBS and then re-suspended in 1.0 mL of either 0.2 mol/L HCl (for NAD⁺) or 0.2 mol/L NaOH (for NADH) before ultrasonic decomposition. The suspensions were boiled for 5 min, rapidly quenched in an ice bath, and then 500 µL sample was mixed with 500 µL 0.2 mol/L NaOH (for NAD⁺) or 0.2 mol/L HCl (for NADH). Cell debris was removed by centrifugation at 10,000 g for 10 min, and the supernatant was used to determine the amounts of NAD⁺ and NADH following the protocol of the NADH qualification kit (Qiao Suo Co., Ltd., Shanghai, China) as described previously (Wang et al., 2017b). A similar method was used for NAD⁺ and NADH quantification.

GSH and GSSG were detected using GSH and GSSG Assay Kit (Beyotime Biotechnology, Nantong, China) according to the manufacturer's protocol. Cells (2 × 10⁵ /mL) were seeded into 6-well plates and treated with different BQ concentrations (0, 10, and 20 µmol/L) for 24 h. The cells were washed with PBS, and the protein removal agent was added. The samples were frozen and thawed twice with liquid nitrogen in a water bath at 37°C. The cells were centrifuged at 10,000 × g for 10 min at 4°C. The supernatant was used for GSH and GSSG determination. Absorbance was measured at λ450 nm using a microplate reader.

ATP Measurement

Cells (2 mL) were harvested by centrifugation, washed twice with PBS and then re-suspended in 1 mL cell lysis buffer. From this suspension, 10 µL of the sample was added into 200 µL assay buffer, the mixture was transferred into a 96-well microplate (black background) and fluorescence intensity was measured by Tecan Infinite 200 microplate reader (Mannedorf, Switzerland). The ATP concentration was then calculated according to the ATP standard curve and normalized based on the protein concentration.

Stress Tolerance Assay

Stress tolerance of yeast cells was evaluated using both plate spot assay and liquid culture assay. For plate spot assay, the strains were cultivated at 30°C in the YPD medium. After overnight culture, OD600 of the broth was adjusted to ~1.0 with distilled water. Ten-fold diluted suspensions were spotted on the YPD plates. Inhibitory compound tested was either acetic acid (4 g/L), furfural (4 g/L), or ethanol (100 g/L). For the heat tolerance test, the plates were incubated at 40°C. The size of the colony was used to evaluate the stress tolerance. For liquid culture assay, strains with initial OD600 of 0.1 were inoculated in 100 mL YPD medium containing 4 g/L furfural in 250 mL flasks. The culturing was performed at 30°C and without pH adjustment. Cell growth (OD600) was measured every 12 h, where higher growth was considered as an indicator of stress tolerance.

Real-Time Quantitative PCR

Total RNA was isolated from yeast cells and then reversely transcribed into cDNA using a PrimeScript RT Reagent Kit (TaKaRa, Dalian, China) following the instructions of the manufacturer. Real-time quantitative PCR (RT-qPCR) was performed using SYBR Green qPCR Master Mix (TaKaRa, Dalian, China) on a Real-Time PCR Detection System (Bio-Rad, USA). Relative expression levels were calculated by the 2-ΔΔCt

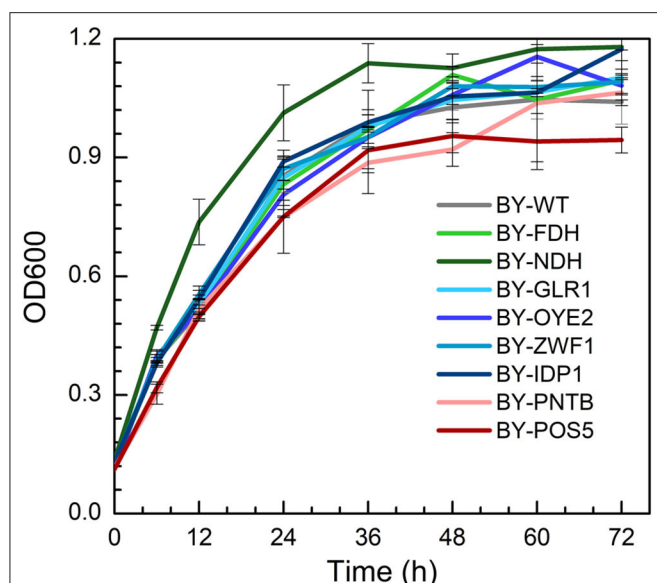


FIGURE 1 | The growth profiles of wild type (BY4741) and engineered strains expressing selected oxidoreductase genes.

method (Zhang et al., 2015) using *ALG9* as the reference gene. The sequences of the forward/reverse primers for the analysis were listed in Table S2.

Heatmap Clustering Analysis and Ternary Plot Analysis

Heatmap clustering analysis was generated using Heml software (<http://hemi.biocuckoo.org/down.php>), where yields of ethanol, glycerol, and acetate were used as input. Euclidean distance metrics and group clustering were used based on group averages (average linkage). The Ternary plot generated by OriginPro 8 software indicated yields of ethanol, glycerol, and acetate in triangular coordinates with scaled values, which were normalized to restrict the range of values between 0 and 1, for example ethanol yield:

scaled value =

$$\frac{\log_{10}(\text{ethanol yield} \times 100)}{\log_{10}(\text{ethanol yield} \times 100) + \log_{10}(\text{acetate yield} \times 100) + \log_{10}(\text{glycerol yield} \times 100)}$$

RESULTS AND DISCUSSION

Cell Growth of Recombinant Yeast

The growth of engineered strains was compared with wild type in the YPD medium containing no furfural (Figure 1). It was found that the strain expressing NADH dehydrogenase (BY-NDH) had the best cell growth when compared to wild type and other mutants because the NADH dehydrogenase might have enhanced the respiratory flux of the strain. Conversely, the expression of both *POS5* and *PNTB* had a little negative impact on the growth of the strains. As an NADH kinase, *POS5*

transforms NADH to NADPH by consuming ATP, which would have constrained the growth due to a lack of enough energy supply. However, as a pyridine nucleotide transhydrogenase, *PNTB* directly transforms NADH to NADPH without ATP consumption. Thus, intracellular imbalance of NADH and NADPH might have resulted in undesirable yeast growth. The other strains overexpressing the *FDH*, *GLR1*, *OYE2*, *ZWF1*, and *IDP1* genes did not show any influence on cell growth when compared to growth profiles of the wild type.

The yields of ethanol, glycerol, and acetic acid are shown in Table S3. The expression of NADH kinase (*POS5*) or pyridine nucleotide transhydrogenase (*PNTB*) increased the glycerol yield but decreased the yield of acetic acid. Whereas, the expression of NADH dehydrogenase (*NDH*) decreased glycerol yield. On the other hand, BY-ZWF1 and BY-GLR1 showed higher ethanol and glycerol yields when compared to the wild type. It might have provided excessive GSH, which helped the cells to build a more reduceable intracellular environment.

Tolerance of Recombinant Yeast With NADH/NAD⁺ Ratio Change

In the YPD medium containing furfural (4 g/L), the wild type strain BY showed a lag phase spanning over 36 h (Figure 2A), whereas the engineered strain BY-NDH was unable to grow although it had a good performance in the inhibitor-free medium (Figure 1) and it neither consumed any sugar nor produced ethanol under furfural stress. However, the strain BY-FDH, which was overexpressing formate dehydrogenase, exhibited a similar growth curve as that of the wild type strain in the presence of furfural. The glucose consumption of the wild type BY strain and the engineered BY-FDH strain showed a rapid decline after 36 h leaving 37 g/L residual glucose after 72 h (Figure 2A). This was consistent with the previous results that there is no noticeable difference in FDH strain without formate addition (Hou et al., 2010). Formate is a necessary substrate for formate dehydrogenase to produce NADH. However, because formate acts as a toxic carboxylic acid, and it would have interfered with the assessment of furfural tolerance, it was not supplemented into the medium in this study.

To further explain the phenomenon, the ratios of NADH/NAD⁺ and ROS content were measured in BY and BY-FDH. Unfortunately, BY-NDH did not grow under furfural stress, and resultantly produced too little biomass to perform the subsequent analyses. Figure 2B showed there was no substantial difference in NADH/NAD⁺ between wild type and BY-FDH. As discussed above, without extra formate addition, the yeast endogenous formate was too little to maintain the supply required for FDH to accumulate excessive NADH.

ROS are often appeared in universal stress response (Allen et al., 2010). Thus, intracellular ROS content might be an indicator of furfural stress. In consideration of the same performance of growth, ethanol, glucose, and the ratio of NADH/NAD⁺, it was not surprising to see that ROS in BY and BY-FDH had no significant differences. Generally, cell tolerance to furfural can be enhanced by increasing the intracellular NADH ratio, but in this study, it was observed that two engineered

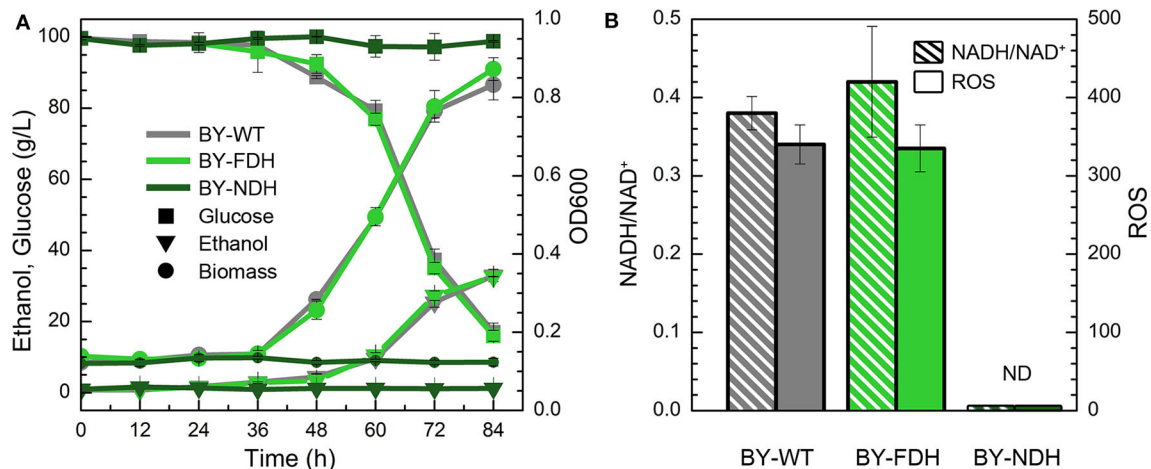


FIGURE 2 | Effect of NADH-related genes expression on yeast cell under the furfural stress (4 g/L). **(A)** Biomass, ethanol, and residual glucose; **(B)** Ratio of NADH/NAD⁺ and ROS content. ND, not detectable.

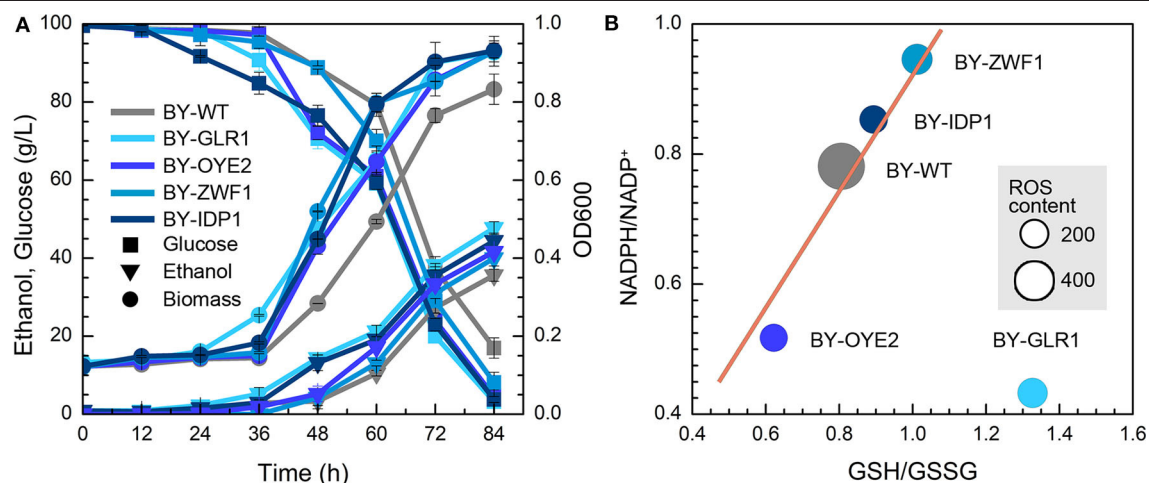


FIGURE 3 | Effect of NADPH-related genes expression on yeast cell under the furfural stress (4 g/L). **(A)** Biomass, ethanol, and residual glucose; **(B)** Content of ROS and ratio of NADPH/NAD⁺ and GSH/GSSG. The size of circles reflects the ROS fluorescence intensity.

strain BY-FDH and BY-NDH did not improve the yeast tolerance to furfural due to shortage of formate and showed significantly poor growth.

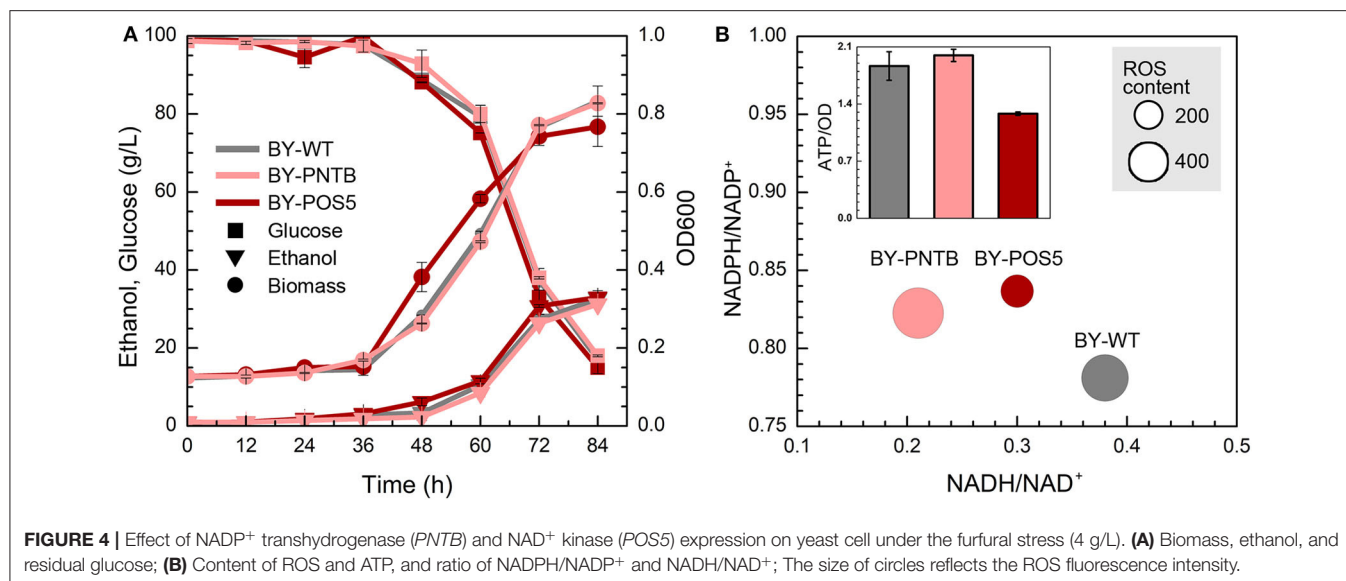
Tolerance of Recombinant Yeast With NADPH/NADP⁺ Ratio Change

The impact of NADPH availability in furfural tolerance was further investigated due to no improvement in strains after overexpression of NADH-related genes. However, both BY-GLR1 and BY-OYE2 showed better growth compared to the wild type in the presence of furfural (Figure 3A). BY-GLR1 even shortened the lag period to 12 h when compared to the wild type. Although BY-OYE2 had the same lag phase with BY, it showed better growth after 36 h. Moreover, BY-OYE2 and BY-GLR1 consumed glucose much quickly, leaving the lower content of residual glucose after 72 h than wild type. Correspondingly, the ethanol

production curves of BY-GLR1 and BY-OYE2 were similar and better than the control.

Both strains BY-GLR1 and BY-OYE2 maintained a lower ratio of NADPH/NADP⁺, which was about 80 and 51% of the wild type strain BY (Figure 3B) because the enzymes encoded by *GLR1* and *OYE2* genes consumed NADPH in cells. The glutathione reductase (*GLR1*) converts oxidized glutathione to reduced glutathione by using NADPH. An NADPH oxidoreductase called old yellow enzyme (*OYE2*) catalyzes geraniol into citronellol by consuming NADPH (Zhao et al., 2017).

Figure 3B combined the data of NADPH/NADP⁺, GSH/GSSG, and ROS in recombinant strains and showed their correlation. The linear relationship between NADPH/NADP⁺ and GSH/GSSG can be found in strains BY-ZWF1, BY-IDP1, BY-OYE2, and BY-WT, which reflected that an increase of



NADPH caused the accumulation of reduced form of GSH. On the other hand, both BY-IDP1 and BY-ZWF1 had higher ratios of NADPH/NADP⁺ because they encoded glucose-6-phosphate dehydrogenase and isocitrate dehydrogenase. Furthermore, intracellular accumulation of NADPH was also beneficial for the intracellular regeneration of GSH. That is why these two strains (BY-IDP1 and BY-ZWF1) showed higher GSH/GSSG ratios when compared to the wild type and BY-OYE2. However, GLR1 encoded the glutathione reductase, which reduced glutathione by consuming NADPH. Accordingly, the highest ratio of GSH/GSSG was observed in the strain overexpressing *GLR1*, which was a unique plot due to its reaction. Moreover, it was interesting to see that the wild type strain had the highest ROS content when compared to any of the four recombinant strains, which strengthen the hypothesis that more intracellular NADPH produced more intracellular GSH, which conferred a better tolerance to furfural. Interestingly, in previous studies, the extracellular ORP regulation had also enhanced cell growth in the presence of furfural. Cells under ORP regulation had shown a faster GSH generation when compared to the cells with no ORP regulated condition (Li et al., 2019). These results are in accordance with another study, which was meant to improving yeast oxidative stress tolerance by adding redox reagent in the medium (Li et al., 2020). So, both extracellular and intracellular redox perturbation can improve furfural tolerance by increasing intracellular GSH content. To increase intracellular GSH content, more NADPH is needed.

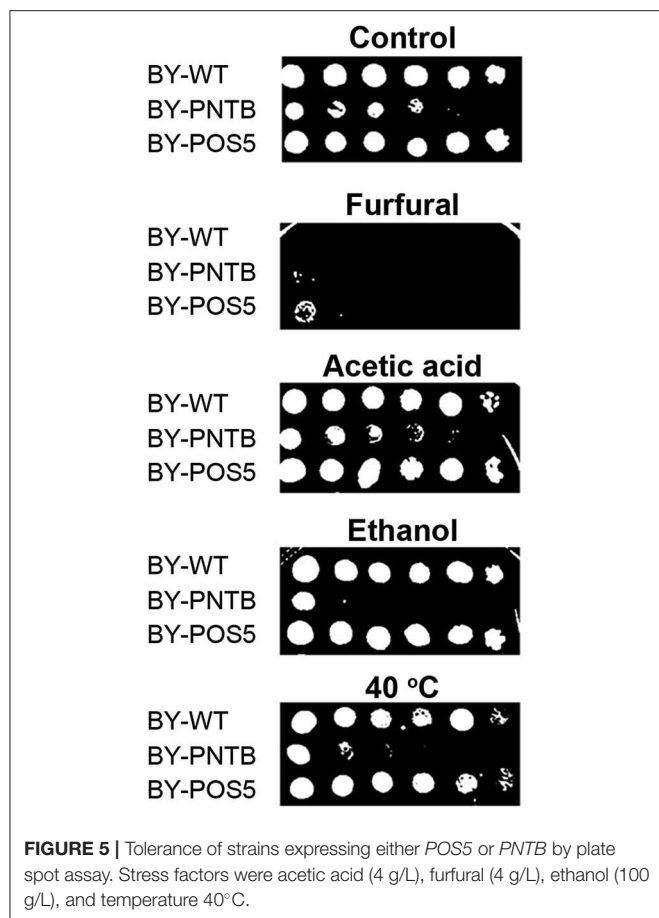
Tolerance of Recombinant Yeast With NADH-NADPH Transformation

Since NADPH manipulation had a positive effect on yeast tolerance to furfural, the NAD⁺ transhydrogenase and NAD⁺ kinase were overexpressed in the BY to increase the NADPH pool. The NADPH-NADP⁺ and NADH-NAD⁺ systems are separated in yeasts due to the absence of enzymatically catalyzed pyridine nucleotide transhydrogenation and NAD(H) kinase

activity (Anderlund et al., 1999). The lack of pyridine nucleotide transhydrogenation has shown considerable consequences for the redox balances of the NAD(H) and NADP(H) coenzyme systems in yeasts (Dijken and Scheffers, 1986). NADH can be transformed to NADPH by the transhydrogenase (*PNTB*) or NADH kinase (*POS5*).

Although the expression of both *PNTB* and/or *POS5* genes weaken the cell growth in the YPD medium (Figure 1). Both engineered strains showed similar growth like the wild type in the presence of furfural (Figure 4A), of which BY-*POS5* had a slightly better performance. It has been reported that *POS5* enzyme is required as a cellular factor for protection from oxidative stress in *S. cerevisiae* (Outten et al., 2005). Ratios of NADH/NAD⁺, NADPH/NADP⁺, and ROS content are shown in Figure 4B. Since *PNTB* and *POS5* catalyzed NADPH formation via consuming NADH; these two enzymes increased the NADPH availability at the cost of decreasing intracellular NADH. Besides, ROS content was significantly decreased in the strain overexpressing the *POS5* gene, which was consistent with cell growth (Figure 4A). However, the ROS content of the strain overexpressing the *PNTB* gene showed almost no difference with the ROS content of wild type strain. The ATP content further demonstrated that *POS5* expression involved the consumption of ATP in NADH to NADPH conversion. *PNTB* expression did not influence the intracellular ATP content (Figure 4B). These phenomena confirmed the function of these two genes.

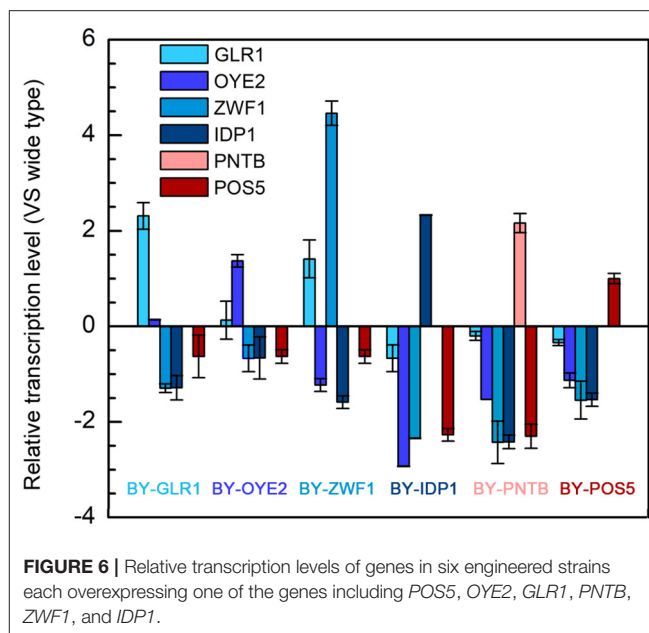
Since *POS5* and *PNTB* could have an impact on cell growth and furfural tolerance, and it was further detected if these two genes have an impact on other stress tolerance. It was found that the expression of the *PNTB* gene defected the cell growth in both solid and liquid YPD medium, and the expression of the *POS5* gene defected the cell growth in the liquid YPD medium but showed no significant difference in the solid medium when compared to the wild type (Figure 5). However, both strains enhanced tolerance against furfural, which was consistent with the cells in the liquid medium. Unfortunately, these two genes



did not confer tolerance against any other stresses. Especially the expression of the *PNTB* gene adversely affected the cell growth under ethanol, acetic acid, or heat (40°C) stress. A possible reason is that NADPH is more important than NADH for furfural stress but not for other stresses.

Relative Transcription Levels of Genes in Engineered Strains

As discussed in section Tolerance of Recombinant Yeast With NADPH/NADP⁺ Ratio Change and Tolerance of Recombinant Yeast With NADH-NADPH Transformation, since the NADPH-related genes enhanced the furfural tolerance in yeast, the transcription level of these genes, including *POS5*, *PNTB*, *GLR1*, *OYE2*, *ZWF1*, and *IDP1* were analyzed (Figure 6). At first, the successful expression of these genes was confirmed because almost every gene in the recombinant strain was up-regulated individually. Moreover, it was interesting to see that overexpression of any gene led to significant depression of the other NADPH-related genes. However, the transcription level of the *GLR1* gene was shown to be significantly enhanced in the strain overexpressing *ZWF1* gene, possibly due to the reason that glutathione oxidoreductase encoded by *GLR1* would have reduced glutathione by using NADPH while glucose-6-phosphate dehydrogenase encoded by *ZWF1* is the main source



of NADPH generation. Similarly, the *ZWF1* and *GLR1* were shown to be upregulated under furfural and HMF stress (Liu and Ma, 2020). This result indicated that all genes related to NADPH might own a tight connection; thus manipulation of one gene can change the expression of multiple genes.

Effect of Cofactor Perturbation on Metabolic Flux

The importance of redox perturbation was further studied for ethanol production by analyzing metabolic flux. A relationship was established among the yields of ethanol, glycerol, and acetic acid in the presence of furfural (Figure 7). The wild type BY strain showed both the lowest ethanol and glycerol yields but had a higher oxidized product yield (acetic acid). However, with the overexpression of glutathione oxidoreductase (*GLR1*), the highest ethanol yield and the lowest acetic acid yields were observed due to excessive GSH, which produced a more reduceable cellular environment. At the same time, the strains overexpressing *IDP1* or *ZWF1* genes showed a lower acetic acid yield. Similarly, the yields of acetic acid, ethanol, or glycerol showed antagonistic relationships under cofactor disturbed conditions (Bloem et al., 2016). Interestingly, although BY-PNTB showed negative growth in normal medium, yet it had the highest yields of glycerol. In a previous study, the *PNTB* expression had also increased glycerol and acetate content in *S. cerevisiae* (Anderlund et al., 1999).

The cluster analysis showed that BY-GLR1 and BY-ZWF1 belonged to one group though they catalyze different reactions because *GLR1* consumes NADPH, but *ZWF1* produces NADPH. Additionally, bubbles representing the strains overexpressing *ZWF1* and *GLR1* strains also showed a close relationship when compared to the other strains, which was also seen in the Ternary plot, which was based on the yields of ethanol, acetate, and

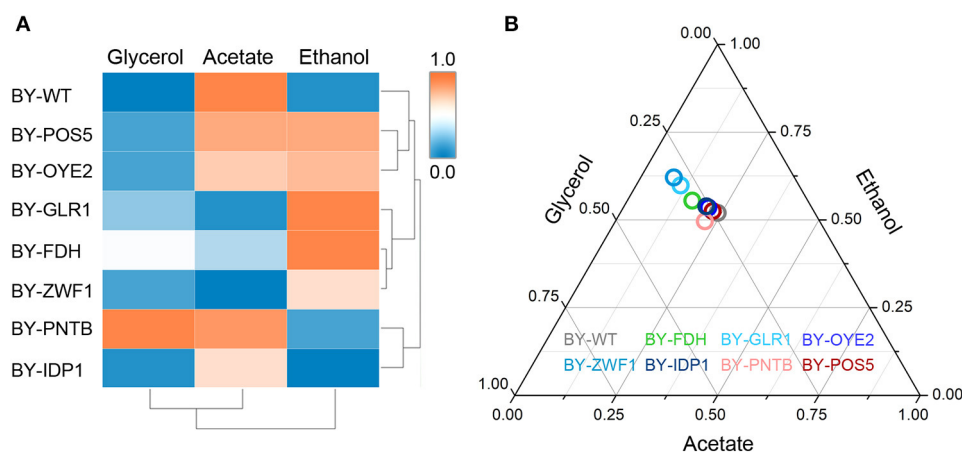


FIGURE 7 | Influence of cofactor-related genes expression on the yield of main products in yeast. **(A)** Heatmap for cluster analysis; **(B)** Ternary plot analysis. All data have been normalized to the range between 0 and 1.

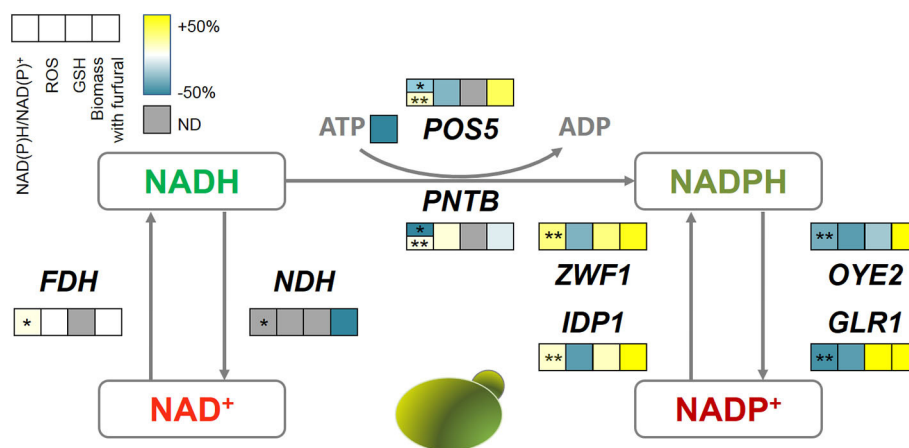


FIGURE 8 | The correlations among oxidoreductases, intracellular redox perturbation, and furfural tolerance. The color bar reflects the improvement defined as (GM-WT)/WT, GM, gene-modified strain; WT, wild type strain. The first square with * shows the NADH/NAD⁺ and with ** shows NADPH/NADP⁺. ND, not detectable.

glycerol (Figure 7). These two strains exhibited a higher ethanol yield but lower glycerol and acetate yield. Both strains are related to GSH synthesis. *GLR1* encoded glutathione oxidoreductase, converted oxidized glutathione to reduced glutathione directly. *ZWF1* encoded glucose-6-phosphate dehydrogenase, catalyzed the first step of the pentose phosphate pathway, which was the main source of intracellular NADPH and indirectly enhanced GSH production. Therefore, these two strains showed an increasing ethanol yield when compared to the other strains in the presence of furfural.

Mechanism of Redox Perturbation During Furfural Tolerance

To elucidate the role of intracellular redox perturbation in conferring the furfural tolerance to yeast, the data of redox change, ROS removal, GSH generation, and biomass production under furfural stress, were compared (Figure 8). It clearly showed that the manipulation of oxidoreductases is capable

of causing redox perturbation according to their defined bioreaction (Table 1), except for FDH and NDH. Formate dehydrogenase (FDH) produces NADH by consuming formate, which is a trace chemical normally involved in the yeast metabolism (Puig-Castellví et al., 2015). But formate as a carboxylic acid is also a kind of inhibitor that is not supplemented into the medium for evaluation of furfural tolerance to avoid false results. Thus, this enzyme did not substantially contribute to the transformation of NADH, which consequently led to the unchanged ROS accumulation and cell growth under furfural stress. The strain overexpressing NDH did not survive when exposed to 4 g/L furfural, but the details of NADH/NAD⁺ and ROS are not available as well due to the unavailability of the biomass for the required analyses.

Interestingly, almost all genes related to NADPH metabolism benefited furfural tolerance, though some of them have contradictory reaction directions. Because POS5, ZWF1, and IDP1 acted as producers of NADPH, which assisted the

anti-oxidative system such as GSH in removing ROS, and thus increased the biomass under furfural stress. Despite causing the depletion of NADPH, the NADPH dehydrogenases (encoded by *OYE2* and *GLR1*) helped the cells to manage a lower ROS content. *OYE2* gene encodes old yellow enzyme that is believed to be involved in sterol metabolism, oxidative stress response, and programmed cell death (Odat et al., 2007). *GLR1* encodes glutathione reductase that directly converts oxidized glutathione (GSSG) to reduced glutathione (GSH) for ROS removal (Heer et al., 2009). It should be noted that PNTB and NDH were heterologously expressed from *E. coli* in yeast. Where, NDH causes cell death under 4 g/L furfural, and PNTB neither influenced the ROS nor the furfural tolerance.

In this study, the improvement of the furfural tolerance of yeast by the redox perturbation through expressing NADH-related genes was not successful. But it did not mean that the change of NADH is invalid for improving furfural tolerance (Wang et al., 2017b). Whereas, the redox perturbation caused by NADPH-related genes has shown promising improvement in furfural tolerance.

CONCLUSION

In this study, the importance of cofactor in furfural tolerance by expressing genes related to NADH or NADPH was examined. Where, it was shown that after the heterologous expression of *NDH* gene (an NADH related gene), the strain became extremely sensitive to furfural and was unable grow in medium containing 4 g/L of furfural, while the strain overexpressing *FDH* gene had similar growth when compared to the wild type due to lack of formate as a substrate. The overexpression of NADPH related genes, all five engineered strains, namely BY-POS5, BY-ZWF1, BY-IDP1, BY-GLR1, and BY-OYE2, showed better performance under furfural stress when compared to the wild type strain. This indicated that NADPH is more critical to improve yeast furfural tolerance than NADH because of its role in regenerating antioxidant, which can clear the ROS produced under furfural stress. But here, a different way was followed to encounter the ROS. The enzymes encoded by

POS5, ZWF1, IDP1 replenished the supply of reducing power NADPH, but *GLR1* and *OYE2* directly eliminated ROS by using NADPH. Moreover, the metabolic flux analysis revealed that cofactor perturbation switched the metabolic flux to improve fermentation performance. Furfural induced the accumulation of ROS in the cell, and effective redox perturbation cleared up the ROS, which helped the cells to cope with the furfural stress. This study provided a novel perspective to improve the cellular tolerance through intracellular redox perturbations by a single-gene manipulation.

DATA AVAILABILITY STATEMENT

The raw data supporting the conclusions of this article will be made available by the authors, without undue reservation.

AUTHOR CONTRIBUTIONS

KL and C-GL conceived the study, wrote the manuscript, and prepared figures and tables. KL and K-YL performed experiments and data analysis. X-QZ, MM, CS, and F-WB discussed and revised the manuscript. All authors read and approved the final manuscript.

FUNDING

The authors appreciate the financial support from National Key R&D Program of China from Ministry of Science and Technology of the People's Republic of China [Grant number 2018YFB1501401], National Natural Science Foundation of China [Grant number 21978167], and the Natural Science Foundation of Shanghai [Grant number 18ZR1420700, 19160745300].

SUPPLEMENTARY MATERIAL

The Supplementary Material for this article can be found online at: <https://www.frontiersin.org/articles/10.3389/fbioe.2020.00615/full#supplementary-material>

REFERENCES

- Allen, S. A., Clark, W., McCaffery, J. M., Zhen, C., Lancot, A., Slininger, P. J., et al. (2010). Furfural induces reactive oxygen species accumulation and cellular damage in *Saccharomyces cerevisiae*. *Biotechnol. Biofuels* 3:2. doi: 10.1186/1754-6834-3-2
- Almeida, J. R., Modig, T., Petersson, A., Hahn-Hägerdal, B., Lidén, G., and Gorwa-Grauslund, M. F. (2007). Increased tolerance and conversion of inhibitors in lignocellulosic hydrolysates by *Saccharomyces cerevisiae*. *J. Chem. Technol. Biot.* 82, 340–349. doi: 10.1002/jctb.1676
- Anderlund, M., Nissen, T. L., Nielsen, J., Villadsen, J., Rydstr, M. J., Hahn-Hägerdal, B., et al. (1999). Expression of the *Escherichia coli* pntA and pntB genes, encoding nicotinamide nucleotide transhydrogenase, in *Saccharomyces cerevisiae* and its effect on product formation during anaerobic glucose fermentation. *Appl. Environ. Microb.* 65, 2333–2340. doi: 10.1128/AEM.65.6.2333-2340.1999
- Banerjee, N., Bhatnagar, R., and Viswanathan, L. (1981). Inhibition of glycolysis by furfural in *Saccharomyces cerevisiae*. *Eur. J. Appl. Microbiol. Biot.* 11, 226–228. doi: 10.1007/BF00505872
- Benjaphokee, S., Hasegawa, D., Yokota, D., Asvarak, T., Auesukaree, C., Sugiyama, M., et al. (2012). Highly efficient bioethanol production by a *Saccharomyces cerevisiae* strain with multiple stress tolerance to high temperature, acid and ethanol. *New Biotechnol.* 29, 379–386. doi: 10.1016/j.nbt.2011.07.002
- Bloem, A., Sanchez, I., Dequin, S., and Camarasa, C. (2016). Metabolic impact of redox cofactor perturbations on the formation of aroma compounds in *Saccharomyces cerevisiae*. *Appl. Environ. Microb.* 82, 174–183. doi: 10.1128/AEM.02429-15
- Clarke, D. M., Loo, T. W., Gillam, S., and Bragg, P. D. (1986). Nucleotide sequence of the pntA and pntB genes encoding the pyridine nucleotide transhydrogenase of *Escherichia coli*. *FEBS J.* 158, 647–653. doi: 10.1111/j.1432-1033.1986.tb09802.x
- Cunha, J. T., Aguiar, T. Q., Romani, A., Oliveira, C., and Domingues, L. (2015). Contribution of PRS3, RPB4 and ZWF1 to the resistance of industrial *Saccharomyces cerevisiae* CCUG53310 and PE-2 strains to lignocellulosic hydrolysate-derived inhibitors. *Bioresour. Technol.* 191, 7–16. doi: 10.1016/j.biortech.2015.05.006

- Dijken, J. P. V., and Scheffers, W. A. (1986). Redox balances in the metabolism of sugars by yeasts. *Fems Microbiol. Lett.* 32, 199–224. doi: 10.1111/j.1574-6968.1986.tb01194.x
- Gietz, R. D., and Schiestl, R. H. (2007). High-efficiency yeast transformation using the LiAc/SS carrier DNA/PEG method. *Nat. Protoc.* 2, 31–34. doi: 10.1038/nprot.2007.13
- Hasunuma, T., Ismail, K. S. K., Nambu, Y., and Kondo, A. (2014). Co-expression of TAL1 and ADH1 in recombinant xylose-fermenting *Saccharomyces cerevisiae* improves ethanol production from lignocellulosic hydrolysates in the presence of furfural. *J. Biosci. Bioeng.* 117, 165–169. doi: 10.1016/j.jbiosc.2013.07.007
- Heer, D., Heine, D., and Sauer, U. (2009). Resistance of *Saccharomyces cerevisiae* to high concentrations of furfural is based on NADPH-dependent reduction by at least two oxiredutases. *Appl. Environ. Microbiol.* 75, 7631–7638. doi: 10.1128/AEM.01649-09
- Hicks, R. H., Sze, Y., and Chuck, C. J. (2020). Enhanced inhibitor tolerance and increased lipid productivity through adaptive laboratory evolution in the oleaginous yeast *Metschnikowia pulcherrima*. *bioRxiv*. [Preprint]. doi: 10.1101/2020.02.17.952291
- Hou, J., Scalcinati, G., Oldiges, M., and Vemuri, G. (2010). Metabolic impact of increased NADH availability in *Saccharomyces cerevisiae*. *Appl. Environ. Microb.* 76, 851–859. doi: 10.1128/AEM.02040-09
- Kuhad, R. C., Deswal, D., Sharma, S., Bhattacharya, A., Jain, K. K., Kaur, A., et al. (2016). Revisiting cellulase production and redefining current strategies based on major challenges. *Renew. Sust. Energ. Rev.* 55, 249–272. doi: 10.1016/j.rser.2015.10.132
- Li, K., Xia, J., Mehmood, M. A., Zhao, X. Q., Liu, C. G., and Bai, F. W. (2019). Extracellular redox potential regulation improves yeast tolerance to furfural. *Chem. Eng. Sci.* 196, 54–63. doi: 10.1016/j.ces.2018.11.059
- Li, K., Zhang, J. W., Liu, C. G., Mehmood, M. A., and Bai, F. W. (2020). Elucidating the molecular mechanism of TEMPOL-mediated improvement on tolerance under oxidative stress in *Saccharomyces cerevisiae*. *Chem. Eng. Sci.* 211:115306. doi: 10.1016/j.ces.2019.115306
- Li, X., Yang, R., Ma, M., Wang, X., Tang, J., Zhao, X., et al. (2015). A novel aldehyde reductase encoded by YML131W from *Saccharomyces cerevisiae* confers tolerance to furfural derived from lignocellulosic biomass conversion. *Bioenerg. Res.* 8, 119–129. doi: 10.1007/s12155-014-9506-9
- Liu, C. G., Xue, C., Lin, Y. H., and Bai, F. W. (2013). Redox potential control and applications in microaerobic and anaerobic fermentations. *Biotechnol. Adv.* 31:257. doi: 10.1016/j.biotechadv.2012.11.005
- Liu, Z. L., and Ma, M. (2020). Pathway-based signature transcriptional profiles as tolerance phenotypes for the adapted industrial yeast *Saccharomyces cerevisiae* resistant to furfural and HMF. *Appl. Microbiol. Biot.* 104, 3473–3492. doi: 10.1007/s00253-020-10434-0
- Liu, Z. L., Slininger, P. J., Dien, B. S., Berhow, M. A., Kurtzman, C. P., and Gorsich, S. W. (2004). Adaptive response of yeasts to furfural and 5-hydroxymethylfurfural and new chemical evidence for HMF conversion to 2,5-bis-hydroxymethylfuran. *J. Ind. Microbiol. Biot.* 31:345. doi: 10.1007/s10295-004-0148-3
- Martín, C., Wu, G., Wang, Z., Stagg, S., and Jönsson, L. J. (2018). Formation of microbial inhibitors in steam-explosion pretreatment of softwood impregnated with sulfuric acid and sulfur dioxide. *Bioresour. Technol.* 262, 242–250. doi: 10.1016/j.biortech.2018.04.074
- Moon, J., and Liu, Z. L. (2012). Engineered NADH-dependent GRE2 from *Saccharomyces cerevisiae* by directed enzyme evolution enhances HMF reduction using additional cofactor NADPH. *Enzyme Microb. Tech.* 50, 115–120. doi: 10.1016/j.enzmictec.2011.10.007
- Odat, O., Matta, S., Khalil, H., Kampranis, S. C., Pfau, R., Tschlis, P. N., et al. (2007). Old yellow enzymes, highly homologous FMN oxidoreductases with modulating roles in oxidative stress and programmed cell death in yeast. *J. Biol. Chem.* 282, 36010–36023. doi: 10.1074/jbc.M704058200
- Outten, C. E., and Culotta, V. C. (2004). Alternative start sites in the *Saccharomyces cerevisiae* GLR1 gene are responsible for mitochondrial and cytosolic isoforms of glutathione reductase. *J. Biol. Chem.* 279, 7785–7791. doi: 10.1074/jbc.M312421200
- Outten, C. E., Falk, R. L., and Culotta, V. C. (2005). Cellular factors required for protection from hyperoxia toxicity in *Saccharomyces cerevisiae*. *Biochem. J.* 388, 93–101. doi: 10.1042/BJ20041914
- Puig-Castellví, F., Alfonso, I., Piña, B., and Tauler, R. (2015). A quantitative ¹H NMR approach for evaluating the metabolic response of *Saccharomyces cerevisiae* to mild heat stress. *Metabolomics* 11, 1612–1625. doi: 10.1007/s11306-015-0812-9
- Qin, J., Zhou, Y. J., Krivoruchko, A., Huang, M., Liu, L., Khoomrung, S., et al. (2015). Modular pathway rewiring of *Saccharomyces cerevisiae* enables high-level production of L-ornithine. *Nat. Commun.* 6, 1–11. doi: 10.1038/ncomms9224
- Qiu, Z., and Jiang, R. (2017). Improving *Saccharomyces cerevisiae* ethanol production and tolerance via RNA polymerase II subunit Rpb7. *Biotechnol. Biofuels*. 10:125. doi: 10.1186/s13068-017-0806-0
- Salewski, J., Batista, A. P., Sena, F. V., Millo, D., Zebger, I., Pereira, M. M., et al. (2016). Substrate-protein interactions of type II NADH: quinone oxidoreductase from *Escherichia coli*. *Biochemistry* 55, 2722–2734. doi: 10.1021/acs.biochem.6b00070
- Serov, A. E., Popova, A. S., Fedorchuk, V. V., and Tishkov, V. I., (2002). Engineering of coenzyme specificity of formate dehydrogenase from *Saccharomyces cerevisiae*. *Biochem. J.* 367, 841–847. doi: 10.1042/bj20020379
- Shianna, K. V., Marchuk, D. A., and Strand, M. K. (2006). Genomic characterization of POS5, the *Saccharomyces cerevisiae* mitochondrial NADH kinase. *Mitochondrion* 6, 94–101. doi: 10.1016/j.mito.2006.02.003
- Wang, G. S., Lee, J. W., Zhu, J. Y., and Jeffries, T. W. (2011). Dilute acid pretreatment of corn cob for efficient sugar production. *Appl. Biochem. Biotech.* 163, 658–668. doi: 10.1007/s12010-010-9071-4
- Wang, M., Chen, B., Fang, Y., and Tan, T. (2017a). Cofactor engineering for more efficient production of chemicals and biofuels. *Biotechnol. Adv.* 35, 1032–1039. doi: 10.1016/j.biotechadv.2017.09.008
- Wang, S., He, Z., and Yuan, Q. (2017b). Xylose enhances furfural tolerance in *Candida tropicalis* by improving NADH recycle. *Chem. Eng. Sci.* 158, 37–40. doi: 10.1016/j.ces.2016.09.026
- Wang, W., Dai, L., and Wu, B. (2020). Biochar-mediated enhanced ethanol fermentation (BMEEF) in *Zymomonas mobilis* under furfural and acetic acid stress. *Biotech. Biofuel.* 13, 1–10. doi: 10.1186/s13068-020-1666-6
- Xu, B., and Lin, B. (2018). Assessing the development of China's new energy industry. *Energ. Econ.* 70, 116–131. doi: 10.1016/j.eneco.2018.01.001
- Zhang, M. M., Zhao, X. Q., Cheng, C., and Bai, F. W. (2015). Improved growth and ethanol fermentation of *Saccharomyces cerevisiae* in the presence of acetic acid by overexpression of SET5 and PPR1. *Biotechnol. J.* 10, 1903–1911. doi: 10.1002/biot.201500508
- Zhao, J., Li, C., Zhang, Y., Shen, Y., Hou, J., and Bao, X. (2017). Dynamic control of ERG20 expression combined with minimized endogenous downstream metabolism contributes to the improvement of geraniol production in *Saccharomyces cerevisiae*. *Microb. Cell Fact.* 16:17. doi: 10.1186/s12934-017-0641-9
- Zhong, Z., Hu, Q., Fu, Z., Wang, R., Xiong, Y., Zhang, Y., et al. (2016). Increased expression of aldehyde dehydrogenase 2 reduces renal cell apoptosis during ischemia/reperfusion injury after hypothermic machine perfusion. *Artif. Organs* 40, 596–603. doi: 10.1111/aor.12607

Conflict of Interest: The authors declare that the research was conducted in the absence of any commercial or financial relationships that could be construed as a potential conflict of interest.

Copyright © 2020 Liu, Li, Li, Sakdaronnarong, Mehmood, Zhao and Bai. This is an open-access article distributed under the terms of the Creative Commons Attribution License (CC BY). The use, distribution or reproduction in other forums is permitted, provided the original author(s) and the copyright owner(s) are credited and that the original publication in this journal is cited, in accordance with accepted academic practice. No use, distribution or reproduction is permitted which does not comply with these terms.



Engineering the Effector Domain of the Artificial Transcription Factor to Improve Cellulase Production by *Trichoderma reesei*

Qing-Shan Meng¹, Fei Zhang¹, Wei Wang², Chen-Guang Liu¹, Xin-Qing Zhao^{1*} and Feng-Wu Bai¹

¹ State Key Laboratory of Microbial Metabolism, Joint International Research Laboratory of Metabolic and Developmental Sciences, School of Life Sciences and Biotechnology, Shanghai Jiao Tong University, Shanghai, China, ² State Key Lab of Bioreactor Engineering, East China University of Science and Technology, Shanghai, China

OPEN ACCESS

Edited by:

Jean Marie François,
Institut Biotechnologique de Toulouse
(INSA), France

Reviewed by:

Fernando Segato,
University of São Paulo, Brazil
Mingfeng Cao,
University of Illinois
at Urbana-Champaign, United States

*Correspondence:

Xin-Qing Zhao
xqzhao@sjtu.edu.cn

Specialty section:

This article was submitted to
Synthetic Biology,
a section of the journal
Frontiers in Bioengineering and
Biotechnology

Received: 01 March 2020

Accepted: 01 June 2020

Published: 25 June 2020

Citation:

Meng Q-S, Zhang F, Wang W,
Liu C-G, Zhao X-Q and Bai F-W
(2020) Engineering the Effector
Domain of the Artificial Transcription
Factor to Improve Cellulase
Production by *Trichoderma reesei*.
Front. Bioeng. Biotechnol. 8:675.
doi: 10.3389/fbioe.2020.00675

Filamentous fungal strains of *Trichoderma reesei* have been widely used for cellulase production, and great effort has been devoted to enhancing their cellulase titers for the economic biorefinery of lignocellulosic biomass. In our previous studies, artificial zinc finger proteins (AZFPs) with the Gal4 effector domain were used to enhance cellulase biosynthesis in *T. reesei*, and it is of great interest to modify the AZFPs to further improve cellulase production. In this study, the endogenous activation domain from the transcription activator Xyr1 was used to replace the activation domain of Gal4 of the AZFP to explore impact on cellulase production. The cellulase producer *T. reesei* TU-6 was used as a host strain, and the engineered strains containing the Xyr1 and the Gal4 activation domains were named as *T. reesei* QS2 and *T. reesei* QS1, respectively. Compared to *T. reesei* QS1, activities of filter paper and endoglucanases in crude cellulase produced by *T. reesei* QS2 increased 24.6 and 50.4%, respectively. Real-time qPCR analysis also revealed significant up-regulation of major genes encoding cellulase in *T. reesei* QS2. Furthermore, the biomass hydrolytic performance of the cellulase was evaluated, and 83.8 and 97.9% more glucose was released during the hydrolysis of pretreated corn stover using crude enzyme produced by *T. reesei* QS2, when compared to the hydrolysis with cellulase produced by *T. reesei* QS1 and the parent strain *T. reesei* TU-6. As a result, we proved that the effector domain in the AZFPs can be optimized to construct more effective artificial transcription factors for engineering *T. reesei* to improve its cellulase production.

Keywords: *Trichoderma reesei*, cellulase production, artificial transcription factors, effector domain, lignocellulosic biomass

INTRODUCTION

Lignocellulosic biomass is abundantly available as a renewable resource, which is mainly composed of cellulose, hemicelluloses, and lignin. Degradation of the cellulose component by cellulase into glucose to produce biofuels and biobased chemicals has attracted extensive research attention (De Bhowmick et al., 2018). However, high production cost of cellulase makes the bioconversion process

too expensive for practical applications, which ultimately limits the utilization of lignocellulosic biomass for biorefinery (Klein-Marcuschamer et al., 2012).

Filamentous fungi are commonly used as cellulase producers, among which *Trichoderma reesei* has been widely studied for cellulase production (Liu et al., 2013). Without doubt, enhancing cellulase production by *T. reesei* is of great importance for developing lignocellulosic biorefinery.

The cellulase enzymatic complex of *T. reesei* has been shown to consist of at least two cellobiohydrolases (CBHs), eight endo- β -1,4-glucanases (EGs), and seven β -glucosidases (BGLs) that act synergistically upon insoluble cellulose substrate (Druzhinina and Kubicek, 2017). The synthesis of these cellulase components is strictly controlled by various regulators, including at least six positive transcriptional activators (Xyr1, Ace2, Ace3, Vib1, BglR, and the Hap2/3/5 complex) as well as three repressors (Ace1, Rce1, and the carbon catabolite repressor Cre1) (Aro et al., 2001, 2003; Cao et al., 2017; Zhang F. et al., 2018). Recently, great effort has been made to genetically modify these endogenous transcription factors to reprogram the transcriptional regulation network to improve cellulase production in *T. reesei* (Derntl et al., 2013; Lv et al., 2015; Zhang et al., 2017; Rassinger et al., 2018; Wang et al., 2019). On the other hand, artificial transcription factors (ATFs) have also been studied to genetically engineer cellulase production. For example, the repressor Cre1 could be changed to transcriptional activator for cellulases gene expression by replacement of the VP₁₆ activation domain (AD) (Zhang J. et al., 2018). In the previous studies, a library of artificial zinc finger proteins (AZFPs) was explored for expression in bacteria and yeast (Park et al., 2003; Ma et al., 2015), and screened for mutants with changed phenotypes. The AZFPs were designed to be composed of four zinc fingers as a DNA-binding domain (DBD) followed by an AD of Gal4p (Gal4_{AD}). We have modified the library and successfully obtained mutants with enhanced cellulase production in *T. reesei* Rut-C30 (Zhang et al., 2016). However, Gal4_{AD} in the AZFPs originates from budding yeast *Saccharomyces cerevisiae*, and it remains unknown whether exogenous transcriptional regulation domains can efficiently recruit protein complex to initiate transcription. Therefore, it is of great interest to investigate the effect of endogenous effector domains in the AZFPs on regulation of cellulase production in *T. reesei*.

In *T. reesei*, Xyr1 is the Gal4 family transcription activator that is essential for cellulase/hemicellulase gene transcription (Dos Santos Castro et al., 2016). We therefore designed a new transcription factor AZFP_{M2}-Xyr1_{AD} harboring the native effector domain of Xyr1 in this study. Production of cellulase, transcription of key genes related to cellulase biosynthesis, and degradation of lignocellulosic biomass in the recombinant strain carrying AZFP_{M2}-Xyr1_{AD} were compared with the parent strain and the control strain with the exogenous Gal4_{AD}. The results provide basis for further optimizing the effector domains of AZFPs to enhance their stimulating effects on cellulase production by *T. reesei*.

MATERIALS AND METHODS

Strains, Culture Media, and Culture Conditions

Escherichia coli GB05-dir was used for vector construction and propagation, which was cultivated in lysogeny broth (LB) medium with 4 μ g/mL tetracycline (Wang et al., 2016).

T. reesei TU-6 (ATCC MYA-256), a non-homologous end joining pathway deficient, uridine auxotrophic derivative of QM9414 (Gruber et al., 1990), was used as the parent strain in this study. The strain and its derivatives were cultured on PDA plate for 5–7 days at 28°C to produce conidia. For fermentation experiment, *T. reesei* strains were inoculated with 10⁶ spores/mL into 250 mL Erlenmeyer flasks containing 50 mL minimal medium (MM) supplemented with 0.1% uridine, 0.2% peptone, and 2% glucose at 28°C and 200 rpm for 48 h. Then, mycelia were harvested by filtration and washed twice with MM solution without any carbon source. Equal amounts (0.4 g cell wet weight) of mycelia were transferred into 250 mL Erlenmeyer flask containing 50 mL MM supplemented with 2% (w/v) microcrystalline cellulose and 2% (w/v) wheat bran, and were cultivated at 28°C, shaking at 200 rpm. The composition of the MM solution is described in the previous report (Liu et al., 2016).

Plasmid Construction and Fungal Transformation

Firstly, the AD of Xyr1 was amplified from *T. reesei* TU-6 cDNA and fused with the AZFP_{M2}-Gal4 DBD amplified from *T. reesei* M2 genomic DNA by overlap extension PCR using primers AZFP-F and Xyr1-R, generating *Azfp*_{M2}-*xyr1*_{AD} coding sequence. To overexpress the AZFPs (*Azfp*_{M2}-*gal4*_{AD} and *Azfp*_{M2}-*xyr1*_{AD}) at the *xyn3* loci in *T. reesei* TU-6, the *Azfp*_{M2}-*gal4*_{AD} coding sequence was amplified from *T. reesei* M2 genomic DNA, and then the two AZFPs coding sequences were ligated into the *Nco* I and *Xba* I sites of pCB303 (Zhang et al., 2016) to obtain the plasmids pCB310 and pCB311, respectively. Subsequently, the two AZFPs (AZFP_{M2}-Gal4_{AD} and AZFP_{M2}-Xyr1_{AD}) expression cassettes which contained the AZFPs coding sequence and the terminator *TtrpC* were amplified from pCB310 and pCB311, respectively. Additionally, Two DNA fragments containing approximately 1.5 kb of up- and downstream the *xyn3* non-coding region and the *pyr4* selection marker cassette were amplified from *T. reesei* QM9414 genomic DNA, respectively. Finally, five fragments including the AZFP (AZFP_{M2}-Gal4_{AD} or AZFP_{M2}-Xyr1_{AD}) expression cassette, the *pyr4* expression cassette, the up- and downstream *xyn3* non-coding region, and the pUG6 fragment amplified from the pUG6 vector were joined into the pUG6-AZFP_{M2}-Gal4_{AD} or pUG6-AZFP_{M2}-Xyr1_{AD} vector by RecET direct cloning technology (Wang et al., 2016). All primers used in this study were listed in **Supplementary Table S1**.

The protoplast transformation protocol follows previous report (Derntl et al., 2015). Transformants were cultivated and screened on MM plates containing 2% glucose without uridine. Southern blot was performed to verify the correct mutants. *T. reesei* QS1 and QS2 strain are the engineered strains

overexpression *Azfp_{M2}-gal4_{AD}* and *Azfp_{M2}-xyn1_{AD}* at the *xyn3* loci, respectively.

Southern-Blot Analysis

Chromosomal DNA was isolated from mycelia by grinding in liquid nitrogen as described previously (Derntl et al., 2015). For analysis of *T. reesei* QS1 and QS2 genome, *Nde* I was used as the restriction endonuclease for genome digestion. Probes were amplified from the genomic DNA with the primers *xyn3*-probe-F/R in **Supplementary Table S1**. Then, the *Nde* I-digested genomic DNA was hybridized by the probe. Finally, the probe-hybridized DNA fragments were detected and visualized with the DIG high prime DNA Labeling and Detection Starter kit I (Roche Diagnostics, Mannheim, Germany), respectively.

Western Blot Analysis

The conidia of the parent strain *T. reesei* TU-6 and the transformants were cultivated in MM medium containing 2% cellulose as a carbon source and 0.1% uridine to support growth. The mycelia at 72 h were collected by filtration and used to extract intracellular protein after grinding in liquid nitrogen. For detection of the His-tagged AZFP, 30 µg cell protein extracts were separated in 12% SDS-PAGE, and then the proteins were electro-transferred to PVDF membrane (Millipore, United States). An anti-His antibody (GenScript, Nanjing, China) was used to incubate with the membrane, washed, and subsequently incubated with HRP-conjugated goat anti-rabbit IgG as a secondary antibody. Bands on the blotting membrane were visualized using the DAB kit (CWBIO, Shanghai, China) according the manufacturer's instructions.

Biochemical Assays

The activities of filter paper (FPase), endo-β-glucanase (CMCase), exo-β-glucanase (pNPCase), β-glucosidase (pNPGase), and Xylanase were determined as described elsewhere (Wood and Bhat, 1988; Gao et al., 2017). Total extracellular proteins were assayed using the BCA Kit (Beyotime, Shanghai, China).

Transcription Analysis by RT-qPCR

The *T. reesei* strains were cultured, and harvested at 24 and 48 h. Total RNA was extracted using the Spin Column Plant Total RNA Purification Kit (Sangon Biotech, China), and 1 µg RNA was reverse transcribed to cDNA using the PrimeScript® RT Reagent Kit with gDNA Eraser (Takara Japan). RT-qPCR analysis was carried out with iQ SYBR Green Supermix Kit (Bio-Rad, United States) and the CFX Connect Real-Time PCR Detection 96 System (Bio-Rad, United States) using the primers listed in **Supplementary Table S2**. Three biological replicates for all reactions were carried out, and the relative transcription of genes was calculated according to the $2^{-\Delta\Delta CT}$ method using the reference gene *tef1* for normalization (Livak and Schmittgen, 2001; Steiger et al., 2010).

Saccharification of Pretreated Lignocellulosic Biomass

Alkaline-pretreated corn stover (APCS) and Jerusalem artichoke stalk (APJAS) were used as substrates in the saccharification process and the chemical compositions of APCS and APJAS were described before (Meng et al., 2018). The crude enzyme was placed in 30 mL citrate buffer (50 mM, pH4.8) containing 5% (W/V) substrate and the reaction mixture was incubated at 150 rpm, 50°C. Enzyme loading was adjusted to the same protein dosage (30 mg/g substrate). Glucose released was detected by HPLC at interval of 12 h. Cellulose conversion was calculated as follows:

Cellulose conversion

$$= \frac{\text{Glucose yields (mg)}}{\text{Substrate weight (mg)} \times \text{Cellulose content (\%)}} \times 0.9 \times 100\%$$

RESULTS

Construction of the Recombinant *T. reesei* Containing the Novel Artificial Transcription Factor AZFP_{M2}-Xyr1_{AD}

In our previous work, transformants containing AZFPs coding sequences driven by the constitutive promoter *pki* were screened (Zhang et al., 2016), and one hyper-cellulolytic mutant *T. reesei* M2 was selected by detecting FPase activity during liquid fermentation for cellulase production in flasks (Meng et al., 2020). Subsequently, the AZFP coding sequence in *T. reesei* M2 was amplified and analyzed. As shown in **Supplementary Figure S1**, the AZFP coding sequence is composed of four zinc fingers acting as a DBD, followed by a Gal4_{AD}, and was named AZFP_{M2}-Gal4_{AD}. Considering the heterologous origin of Gal4_{AD}, we are interested in whether cellulase production could be further improved when Gal4_{AD} was replaced by the endogenous Xyr1_{AD}. In addition, the *pki* promoter was changed to a relatively stronger promoter of *xyn3*. Therefore, a new artificial transcription factor AZFP_{M2}-Xyr1_{AD} was constructed, and was constitutively expressed at the *xyn3* locus in *T. reesei* TU-6, yielding the strain *T. reesei* QS2. For comparison purposes, the AZFP_{M2}-Gal4_{AD} was also inserted in the same locus, and the resultant strain was named *T. reesei* QS1 (**Figure 1A**). Southern blot analysis confirmed correct integration at the *xyn3* locus in *T. reesei* QS1 and QS2 strains, respectively (**Figures 1B,C**). On the other hand, the expression of AZFPs in the cell lysate of *T. reesei* QS1 and QS2 mutants was confirmed by Western blot analysis (**Figure 1D**), indicating the observed phenotypic changes of transformants in cellulase production were resulted from the expression of the integrated AZFPs.

Influence of AZFP_{M2}-Xyr1_{AD} Overexpression on Cellulolytic Activity

The corresponding activities of cellulolytic enzymes from *T. reesei* QS2, QS1, and the parent strain *T. reesei* TU-6 were further

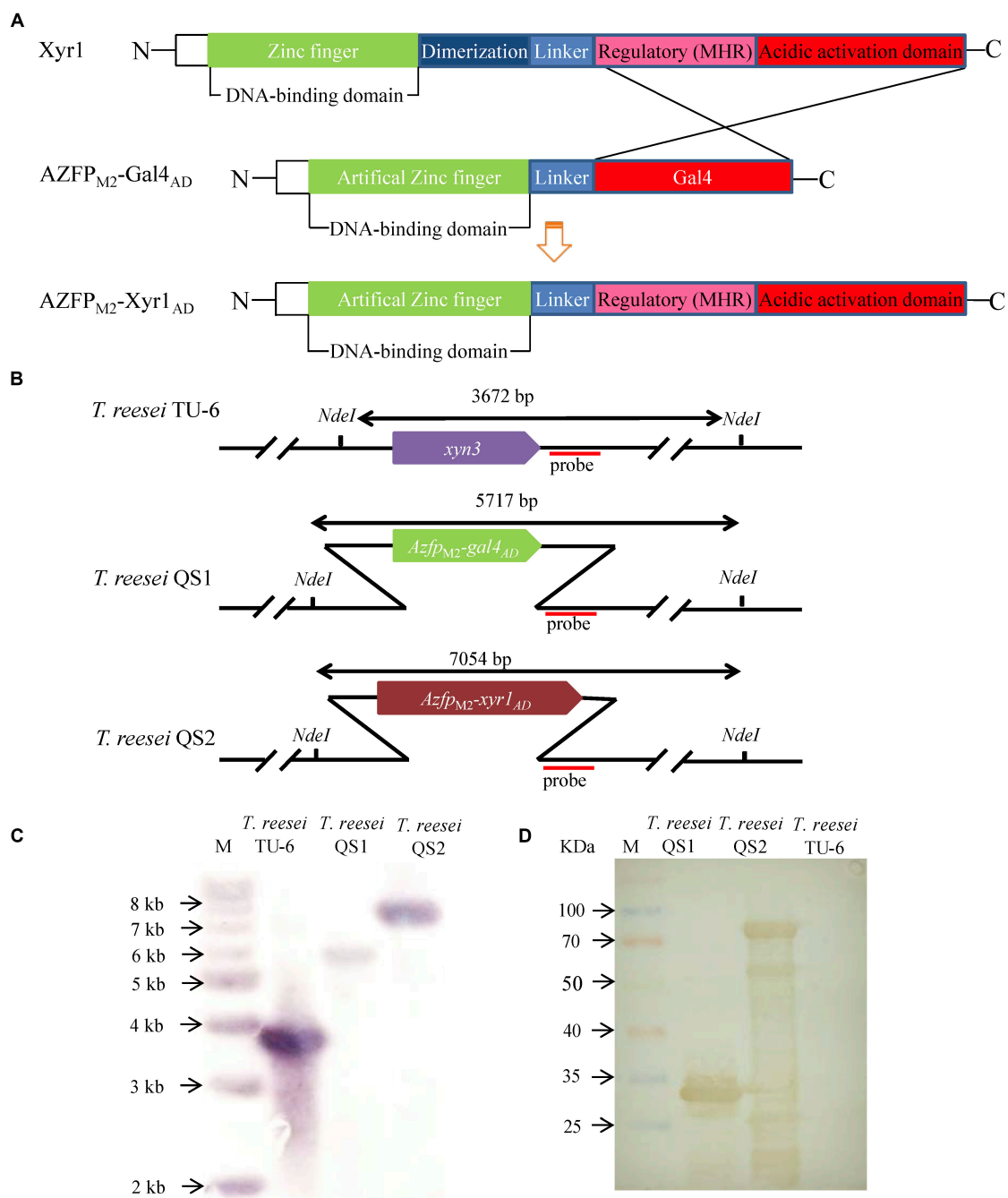


FIGURE 1 | Construction of fusion transcription factor AZFP_{M2}-Xyr1_{AD} in *T. reesei*. **(A)** Schematic map of AZFP_{M2}-Xyr1_{AD}. **(B)** Schematic diagram of Southern blot analysis. **(C)** Southern blot analysis of transformants QS1 and QS2 with AZFPs at *xyn3* loci, respectively. Southern blot analysis of the genome digested with *Nde* I. A fragment of 3.7 kb is present in the parent strain, and the 5.7 and 7.1 kb bands are shown in the mutant strains QS1 and QS2, respectively. **(D)** Western blot analysis for AZFP_{M2}-Gal4_{AD}/Xyr1_{AD} in *T. reesei* QS1 and QS2, respectively. *T. reesei* TU-6 represent the parent strain.

evaluated. As shown in **Figure 2A**, *T. reesei* QS2 displayed the highest cellulase activity (FPase) of 2.4 IU/mL at the 5th day among these strains, 24.2 and 73.7% higher than that secreted by *T. reesei* QS1 and the parent strain TU-6, respectively. In addition, the endoglucanase activity (CMCase) of *T. reesei* QS2 improved 50.4 and 132.4%, respectively, compared to that

of *T. reesei* QS1 and TU-6 strain (**Figure 2B**). In case of exoglucanase activity, *T. reesei* QS2 produced a pNPCase activity of 0.68 IU/mL, which displayed a 25.8 and 52.0% increase compared to the respective strains. However, we found that the activity of β -glucosidase (pNPGase) varied among these strains (**Figure 2C**). Surprisingly, *T. reesei* QS2 exhibited an obviously

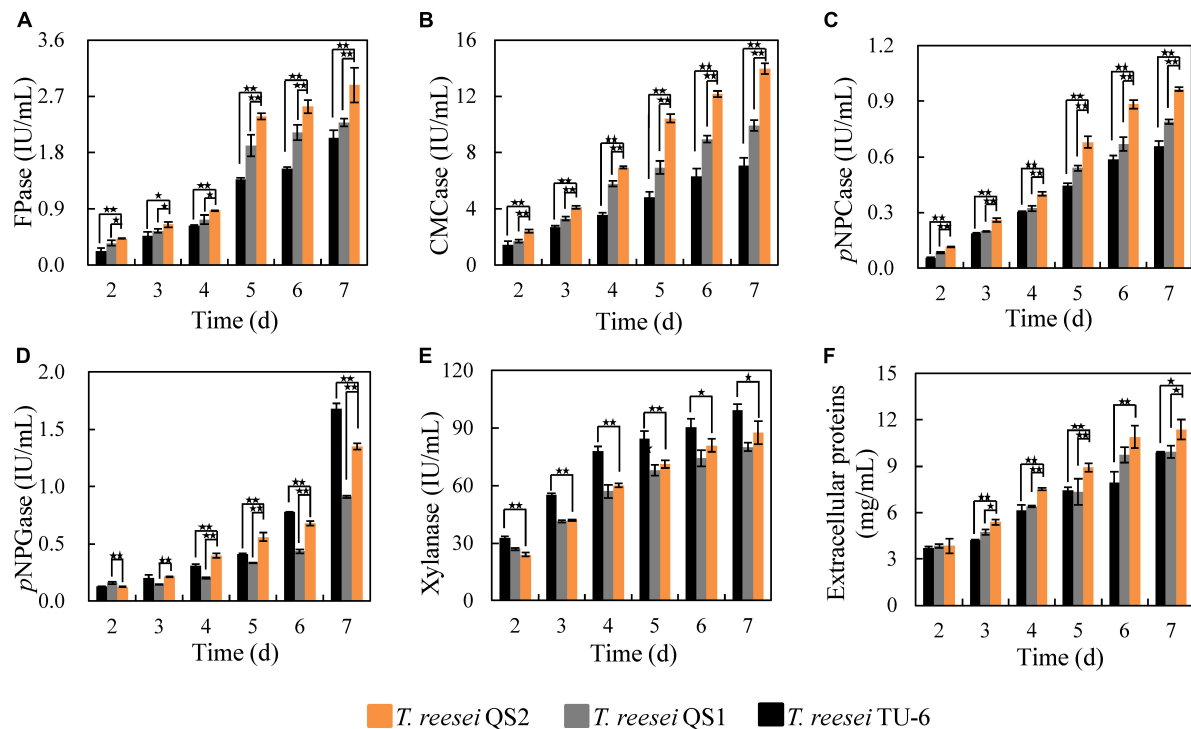


FIGURE 2 | Cellulase production by *T. reesei* QS2, QS1 and TU-6. (A–E) The activities for FPase, CMCase, pNPCase, pNPGase and xylanase, respectively. (F) Total extracellular proteins content. The strains were cultured at 28°C and 180 rpm in flasks using minimal medium supplemented with 2% cellulose and 2% wheat bran as carbon source. Error bar denotes the standard deviations (SD) of three replicates (**p* < 0.05, ***p* < 0.01).

48.4% higher β -glucosidase activity than *T. reesei* QS1 mutant, while 24.4% lower β -glucosidase activity than that of the parent strain TU-6 at the 7th day fermentation in flask (Figure 2D). To compare the roles of the two AZFPs in regulation of cellulase synthesis, the *xyn3* gene locus was chosen for insertion of the AZFPs. As expected, xylanase produced by *T. reesei* QS2 was similar to that of *T. reesei* QS1, but lower than that of the parent strain (Figure 2E), which was caused by the disruption of *xyn3* ORF in these two mutants. However, the extracellular proteins secreted by *T. reesei* QS2 showed a 21.5 and 20.2% increase in comparison with that of *T. reesei* QS1 and TU-6 strain, respectively (Figure 2F). These results suggest that optimization of artificial transcription factors with endogenous ADs is a viable strategy for increasing cellulase production.

Influence of AZFP_{M2}-Xyr1_{AD} Overexpression on Transcript Levels of Cellulase Encoding Genes

To gain further insight into how the overexpression of AZFP_{M2}-Xyr1_{AD} influences the regulation of the cellulase biosynthesis in *T. reesei* QS2, the transcriptional levels of major cellulase and related transcription factor genes were measured. For *T. reesei* QS2, higher expression of the major cellulase genes (*cbh1*, *cbh2*, *egl1*, *egl2*, and *bgl1*), 2.3-, 2.9-, 2.5-, 2.4-, and 3.2-folds compared with that of *T. reesei* QS1, was observed early at 24 h, which may consequently lead to more efficient production

of cellulase characterized by the increased FPase activity. In addition, the expression of cellulolytic enzyme genes (*cbh2*, *egl1*, *egl2*, and *bgl1*) was also significantly up-regulated and a dramatic down-regulation of *xyn2* at 24 h was observed in *T. reesei* QS2 compared with the parent strain *T. reesei* TU-6, which was in accordance with the activities of cellulolytic enzymes produced by *T. reesei* QS2 (Figure 3A). On the other hand, the transcription of accessory protein encoding genes in *T. reesei* QS2 also exhibited significant elevation when compared with *T. reesei* QS1 and the parent strain (Figure 3B). Among these genes, the transcription of *cel61a* and *cip2* in *T. reesei* QS2 were 4.1- and 2.7-fold as well as 19.7- and 2.3-fold higher than that from *T. reesei* QS1 and TU-6 at 24 h, respectively, suggesting that the crude enzyme secreted by *T. reesei* QS2 is more suitable for further hydrolysis of lignocellulosic biomass.

In addition to the enzyme-encoding genes mentioned above, the transcriptional levels of the most known cellulase transcription factor genes were also significantly altered in both *T. reesei* QS1 and QS2 (Figure 3C). Among these transcription factor genes, *xyl1*, which encodes the major transcriptional activator for cellulase biosynthesis (Stricker et al., 2006), was significantly up-regulated by 3.8- and 2.9- fold in *T. reesei* QS2 at 24 compared with that of *T. reesei* QS1 and the parent strain, respectively. Similar trend was observed at 48 h. Even more, an enhanced expression of another transcription activator gene *ace3*, approximately 5.0- and 9.2-folds in *T. reesei* QS2 compared with that of *T. reesei* QS1 and the parent strain,

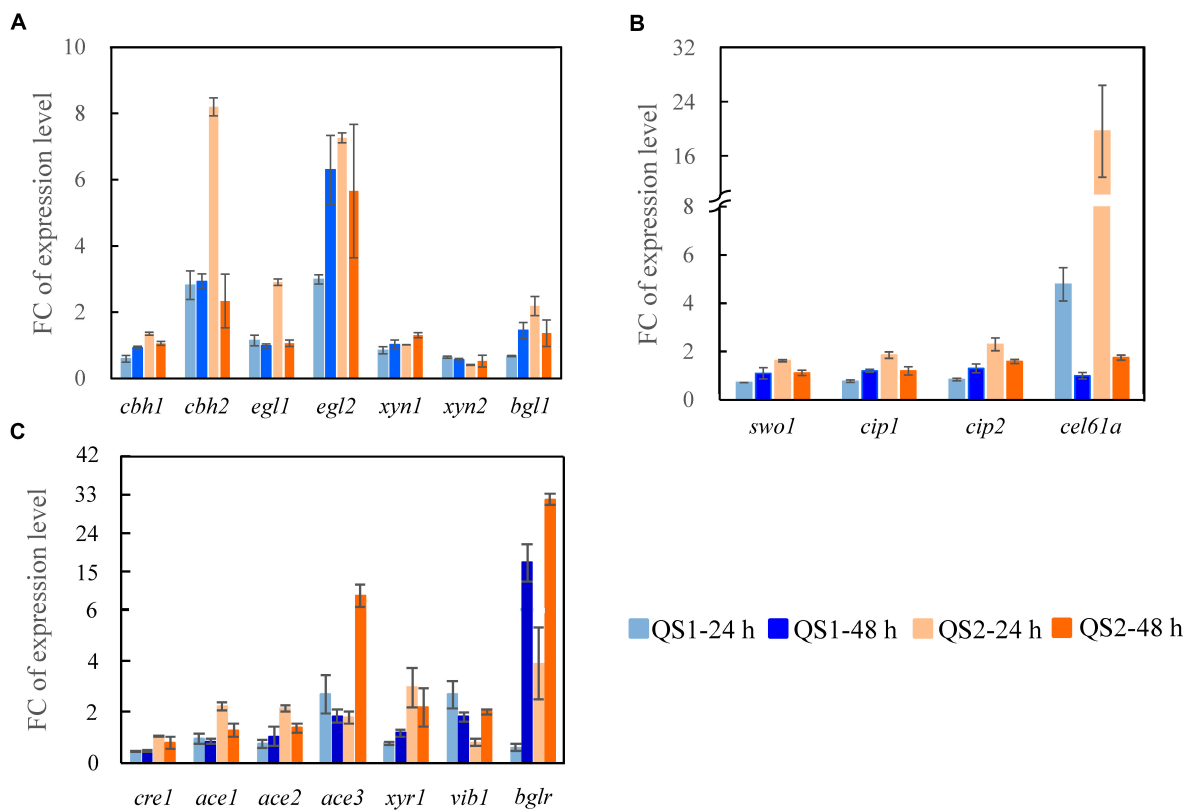


FIGURE 3 | Transcription analysis of genes encoding major cellulolytic enzymes and regulators. Genes encoding (A) cellulolytic enzymes, (B) regulators, and (C) accessory proteins were analyzed for *T. reesei* QS1 and QS2 mutants with *T. reesei* TU-6 as the reference strain. Strains were cultured at 28°C and 180 rpm in flasks using minimal medium supplemented with 2% cellulose and 2% wheat bran as a carbon source for 24 and 48 h, respectively. Expression levels of the reference gene *tef1* were used as an endogenous control. The value is the mean of three biological replicates with SD as the error bars. FC represents fold change of the transcription levels with targeted genes detected in the mutants over that detected in the control.

was also observed at 48 h, indicating that the production of cellulase might be specifically regulated by these transcription factors. As for *bglr* encoding an activator specific for regulating β -glucosidases except *bgl1*, its expression in *T. reesei* QS2 was substantially enhanced to 6.5-folds at the early stage of 24 h, and then attenuated to 1.9-folds at 48 h compared with that of *T. reesei* QS1. Whereas, *T. reesei* QS2 and QS1 showed highly similar transcription profile across the tested genes in comparison to the parent strain, but the magnitude of gene expression change was more pronounced in *T. reesei* QS2. Conclusively, we assume that the AZFP_{M2}-Xyr1_{AD} is more advantageous for regulation of cellulase biosynthesis in *T. reesei* than the AZFP_{M2}-Gal4_{AD}.

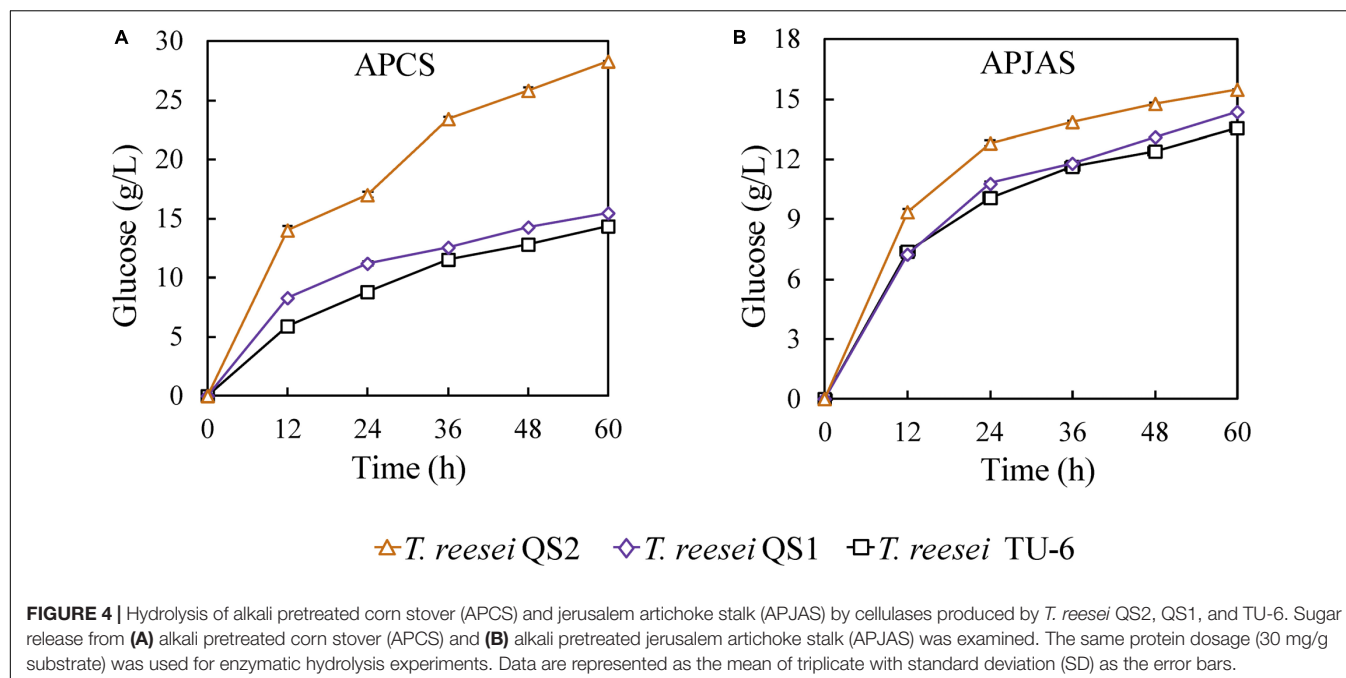
Saccharification of Lignocellulosic Substrates by Cellulolytic Enzyme Preparations From the *T. reesei* Strains

In order to evaluate the hydrolysis ability of the cellulase produced by the *T. reesei* strains on lignocellulosic biomass, the crude enzyme complexes were used to saccharify APCS and APJAS. At the same enzyme loading (30 mg/g substrate), the glucose release (28.3 g/L corresponding to 86.9% cellulose conversion) using the *T. reesei* QS2 enzyme in the saccharification

of APCS increased 83.8 and 97.9% compared with that from *T. reesei* QS1 (15.4 g/L corresponding to 47.3% cellulose conversion) and TU-6 (14.3 g/L corresponding to 43.9% cellulose conversion) at 60 h (Figure 4A). In contrast, similar as described in the previous reports, less glucose was released using APJAS as a substrate, and less difference was observed using crude enzymes from different strains, which would be caused by different composition and structure of APCS and APJAS (Meng et al., 2018). However, we still found slightly more glucose release by cellulase produced with *T. reesei* QS2 among the three strains. The glucose concentrations are 15.5, 14.4, and 13.6 g/L (corresponding to 58.7, 54.5, and 51.4% cellulose conversion), for *T. reesei* QS2, QS1 and the parent strain, respectively (Figure 4B). These results revealed that the optimized enzyme system of *T. reesei* QS2 benefits scarification of lignocellulosic biomass.

DISCUSSION

Based on the existing knowledge about the regulatory network of cellulase biosynthesis in *T. reesei*, great efforts have been made to reprogram cellulase transcription with the aim to enhance cellulase production by engineering endogenous



transcription factors. However, the regulatory mechanism of cellulase biosynthesis is still not fully clear, and the cross-regulation of transcription factors involved in cellulase biosynthesis is very complicated, which all limit the development of robust strains (Liu and Qu, 2019). Taking advantage of the diversity of zinc finger DBDs, AZFPs with the yeast Gal4_{AD} have been developed to increase cellulase production in *T. reesei* (Zhang et al., 2016). Yeast Gal4p has been identified as a transcription activator for regulation of genes involved in galactose catabolism, which contains an N-terminal DBD (1~147aa) and a C-terminal AD (768~881aa) (Hidalgo et al., 2001). The acidic part of the C-terminal activation region functions to stimulate transcription via the recruitment of SAGA (Spt-Ada-Gcn5-Acetyltransferase) *in vivo* (Larschan and Winston, 2001). The yeast Gcn5 orthologous protein encoding gene in *T. reesei* has also been identified, which plays a crucial role in regulation of cellulase gene expression (Xin et al., 2013). However, no further evidences showed that the exogenous Gal4_{AD} activates transcription by recruiting SAGA complex for the regulation of cellulase biosynthesis in *T. reesei* at present. Xyr1 (Xylanase regulator) is a Gal4-like binuclear Zn-cluster protein, which can activate the expression of cellulase and hemicellulase gene expression in *T. reesei*. Lack of Xyr1 resulted in not only the absence of lignocellulosic enzyme production, but also down-regulation of genes encoding MFS (Major facilitator superfamily) transporters and ABC (Adenosine triphosphate (ATP)-binding cassette) transporters in inducing medium (Dos Santos Castro et al., 2016). As shown in Figure 1A, the highly conserved domain of this protein contains the DBD (91~131aa) recognizing the nucleotide binding motif [GGC(T/A)₄] (Furukawa et al., 2009), as well as a middle homology region (MHR, 314~632aa) and a short acidic AD (767~940aa) within the distal portion of the C-terminus. The missing 140 C-terminal amino acids

of Xyr1 abolished cellulase production (Lichius et al., 2015). Recent studies have revealed the transcription factor Xyr1_{AD} could recruit SWI/SNF to remodel nucleosomes positioned in cellulase gene promoters for activating their transcription (Cao et al., 2019), suggesting the important role of this AD in regulation of cellulase gene expression. Therefore, we speculated that Xyr1_{AD} may function better than Gal4_{AD} to regulate cellulase gene expression in *T. reesei*. Moreover, it was reported that the mating type locus protein MAT1-2-1 could directly interact with the MHR and AD of Xyr1 to regulate expression of cellulase genes in response to light, which suggest that the MHR might be critical for enhancing transcription of target genes (Zheng et al., 2017). Herein, we used the endogenous Xyr1_{AD} including MHR instead of the original Gal4_{AD} to rebuild a new AZFP, and the results demonstrated that this optimization of AZFP not only improves cellulase production, but also balances cellulase system for efficient biomass conversion. In our recent work, it was found that the AZFP_{M2}-Gal4_{AD} could down-regulate the expression of a newly identified cellulase repressor Ctf1, resulting in relief of the repression of cellulase activator Vib-1 and Ace3 by Ctf1 for improvement of cellulase production (Meng et al., 2020), which was consistent with transcription analysis in Figure 3C (Fold change > 2). Here, the expression of *ctf1* was also significantly down-regulated by AZFP_{M2}-Gal4_{AD}, but not by AZFP_{M2}-Xyr1_{AD} (Supplementary Figure S2), which suggest that the regulatory mechanisms of these two AZFPs on cellulase biosynthesis are different due to the different effector domains. Taken together, our results proved the important roles of the effector domains in the AZFP regulating cellulase production in filamentous fungi. Using synthetic biology tools, other effector domains as well as synthetic effector domains can be created, and the numbers of effector domains can also be modulated in the AZFPs to improve cellulase production.

In order to compare the roles of the AZFP_{M2}-Gal4_{AD} and AZFP_{M2}-Xyr1_{AD} in cellulase biosynthesis, the *xyn3* gene locus was chosen for foreign DNA insertion, since the *xyn3* promoter was optimal for the expression of a specific gene and deletion of *xyn3* gene did not affect the cellulase activity (Rahman et al., 2009). The results showed that the activities of CMCase and pNPCase were improved significantly, which was consistent with transcription analysis in **Figure 3**. In the future work, various other integration sites can be evaluated to optimize the cellulase enzymatic complex. The cellulase produced by *T. reesei* QS2 displayed better performance in saccharification of lignocellulosic biomass comparing with that of *T. reesei* QS1. Besides the increased β -glucosidase activity in cellulase mixture of *T. reesei* QS2 in comparison to that of *T. reesei* QS1 (**Figure 2D**), another possible reason for enhanced hydrolysis efficiency is the enhancement of accessory protein components, such as Swo1, Cip1, Cip2, and Cel61A, the encoding genes of which were up-regulated in *T. reesei* QS2 (**Figure 3**). The protein Cip2 exhibits synergistic activity with the lytic polysaccharide monooxygenase (Cel61A) to break down the linkage present in the hemicellulose-lignin matrix (Duranová et al., 2009; Pierce et al., 2017). It will be important to explore regulation of accessory protein biosynthesis by the AZFP developed in this study, so that further synthetic biology design can be performed to increase hydrolysis efficiency of lignocellulosic biomass.

CONCLUSION

In this study, we designed a new artificial transcription factor AZFP_{M2}-Xyr1_{AD} in *T. reesei*, and found that AZFP_{M2}-Xyr1_{AD} could significantly improve the expression of major cellulase genes. Moreover, the cellulase produced by the *T. reesei* QS2 carrying AZFP_{M2}-Xyr1_{AD} was proven to be highly effective in the saccharification of the pretreated lignocellulosic biomass. As a result, we proved that the endogenous effector domain Xyr1_{AD} is more advantageous for construction of AZFP not only in improving cellulase production, but also in optimizing cellulase complex for biomass conversion.

REFERENCES

- Aro, N., Ilmén, M., Saloheimo, A., and Penttilä, M. (2003). ACEI of *Trichoderma reesei* is a repressor of cellulase and xylanase expression. *Appl. Environ. Microbiol.* 69, 56–65. doi: 10.1128/AEM.69.1.56-65.2003
- Aro, N., Saloheimo, A., Ilmen, M., and Penttilä, M. (2001). ACEII, a novel transcriptional activator involved in regulation of cellulase and xylanase genes of *Trichoderma reesei*. *J. Biol. Chem.* 276, 24309–24314. doi: 10.1074/jbc.M003624200
- Cao, Y., Zheng, F., Wang, L., Zhao, G., Chen, G., Zhang, W., et al. (2017). Rce1, a novel transcriptional repressor, regulates cellulase gene expression by antagonizing the transactivator Xyr1 in *Trichoderma reesei*. *Mol. Microbiol.* 105, 65–83. doi: 10.1111/mmi.13685
- Cao, Y., Zheng, F., Zhang, W., Meng, X., and Liu, W. (2019). *Trichoderma reesei* XYR1 recruits SWI/SNF to facilitate cellulase gene expression. *Mol. Microbiol.* 112, 1145–1162. doi: 10.1111/mmi.14352
- De Bhowmick, G., Sarmah, A. K., and Sen, R. (2018). Lignocellulosic biorefinery as a model for sustainable development of biofuels and value added products. *Bioresour. Technol.* 247, 1144–1154. doi: 10.1016/j.biortech.2017.09.163

DATA AVAILABILITY STATEMENT

All datasets generated for this study are included in the article/Supplementary Material.

AUTHOR CONTRIBUTIONS

X-QZ and Q-SM conceived the project and designed the experiments. Q-SM carried out experiments and measurements, and interpreted experimental data. WW, FZ, C-GL, X-QZ, and F-WB revised the manuscript. X-QZ supported the research funding. All authors read and approved the final manuscript.

FUNDING

This work was financially funded by the Natural Science Foundation of China (No. 21536006).

ACKNOWLEDGMENTS

We acknowledge the final support from the Open Funding Project of the State Key Laboratory of Bioreactor Engineering and the Fundamental Research Funds for the Central Universities (No. 222201714053) and State Key Laboratory of Microbial Technology Open Projects Fund (No. M2017-10). We are grateful to Dr. Jin-Soo Kim in ToolGen Inc., South Korea and Prof. Xu Fang in Shandong University for kindly providing the plasmids containing artificial zinc finger protein genes and *T. reesei* TU-6 strain, respectively.

SUPPLEMENTARY MATERIAL

The Supplementary Material for this article can be found online at: <https://www.frontiersin.org/articles/10.3389/fbioe.2020.00675/full#supplementary-material>

- Derntl, C., Gudynaite-Savitch, L., Calixte, S., White, T., Mach, R. L., and Mach-Aigner, A. R. (2013). Mutation of the Xylanase regulator 1 causes a glucose blind hydrolase expressing phenotype in industrially used *Trichoderma strains*. *Biotechnol. Biofuels.* 6:62. doi: 10.1186/1754-6834-6-62
- Derntl, C., Kiesenhofer, D. P., Mach, R. L., and Mach-Aigner, A. R. (2015). Novel strategies for genomic manipulation of *Trichoderma reesei* with the purpose of strain engineering. *Appl. Environ. Microbiol.* 81, 6314–6323. doi: 10.1128/AEM.01545-15
- Dos Santos Castro, L., de Paula, R. G., Antonieto, A. C., Persinoti, G. F., and Silva-Rocha, R. (2016). Understanding the role of the master regulator XYR1 in *Trichoderma reesei* by global transcriptional analysis. *Front. Microbiol.* 7:175. doi: 10.3389/fmicb.2016.00175
- Druzhinina, I. S., and Kubicek, C. P. (2017). Genetic engineering of *T. reesei* cellulases and their production. *Microb. Biotechnol.* 10, 1485–1499. doi: 10.1111/1751-7915.12726
- Duranová, M., Hirsch, J., Kolenová, K., and Biely, P. (2009). Fungal glucuronoyl esterases and substrate uronic acid recognition. *Biosci. Biotechnol. Biochem.* 73, 2483–2487. doi: 10.1271/bbb.90486

- Furukawa, T., Shida, Y., Kitagami, N., Mori, K., Kato, M., Kobayashi, T., et al. (2009). Identification of specific binding sites for XYR1, a transcriptional activator of cellulolytic and xylanolytic genes in *Trichoderma reesei*. *Fungal Genet. Biol.* 46, 564–574. doi: 10.1016/j.fgb.2009.04.001
- Gao, L., Li, Z., Xia, C., Qu, Y., Liu, M., Yang, P., et al. (2017). Combining manipulation of transcription factors and overexpression of the target genes to enhance lignocellulolytic enzyme production in *Penicillium oxalicum*. *Biotechnol. Biofuels* 10:100. doi: 10.1186/s13068-017-0783-3
- Gruber, F., Visser, J., Kubicek, C. P., and de Graaff, L. H. (1990). The development of a heterologous transformation system for the cellulolytic fungus *Trichoderma reesei* based on a pyrG-negative mutant strain. *Curr. Genet.* 18, 71–76. doi: 10.1007/bf00321118
- Hidalgo, P., Ansari, A. Z., Schmidt, P., Hare, B., Simkovich, N., Farrell, S., et al. (2001). Recruitment of the transcriptional machinery through GAL11P: structure and interactions of the GAL4 dimerization domain. *Genes Dev.* 15, 1007–1020. doi: 10.1101/gad.873901
- Klein-Marcuschamer, D., Oleskiewicz-Popiel, P., Simmons, B. A., and Blanch, H. W. (2012). The challenge of enzyme cost in the production of lignocellulosic biofuels. *Biotechnol. Bioeng.* 109, 1083–1087. doi: 10.1002/bit.24370
- Larschan, E., and Winston, F. (2001). The *S. cerevisiae* SAGA complex functions in vivo as a coactivator for transcriptional activation by Gal4. *Genes Dev.* 15, 1946–1956. doi: 10.1101/gad.911501
- Lichius, A., Bidard, F., Buchholz, F., Le Crom, S., Martin, J., Schackwitz, W., et al. (2015). Genome sequencing of the *Trichoderma reesei* QM9136 mutant identifies a truncation of the transcriptional regulator XYR1 as the cause for its cellulase-negative phenotype. *BMC Genomics* 16:326. doi: 10.1186/s12864-015-1526-0
- Liu, G., Qin, Y., Li, Z., and Qu, Y. (2013). Development of highly efficient, low-cost lignocellulolytic enzyme systems in the post-genomic era. *Biotechnol. Adv.* 31, 962–975. doi: 10.1016/j.biotechadv.2013.03.001
- Liu, G., and Qu, Y. (2019). Engineering of filamentous fungi for efficient conversion of lignocellulose: tools, recent advances and prospects. *Biotechnol. Adv.* 37, 519–529. doi: 10.1016/j.biotechadv.2018.12.004
- Liu, K., Dong, Y., Wang, F., Jiang, B., Wang, M., and Fang, X. (2016). Regulation of cellulase expression, sporulation, and morphogenesis by velvet family proteins in *Trichoderma reesei*. *Appl. Microbiol. Biotechnol.* 100, 769–779. doi: 10.1007/s00253-015-7059-2
- Livak, K. J., and Schmittgen, T. D. (2001). Analysis of relative gene expression data using real-time quantitative PCR and the 2^{(-Delta Delta C(T))} method. *Methods* 25, 402–408. doi: 10.1006/meth.2001.1262
- Lv, X., Zheng, F., Li, C., Zhang, W., Chen, G., and Liu, W. (2015). Characterization of a copper responsive promoter and its mediated overexpression of the xylanase regulator 1 results in an induction-independent production of cellulases in *Trichoderma reesei*. *Biotechnol. Biofuels* 8:67. doi: 10.1186/s13068-015-0249-4
- Ma, C., Wei, X., Sun, C., Zhang, F., Xu, J., Zhao, X., et al. (2015). Improvement of acetic acid tolerance of *Saccharomyces cerevisiae* using a zinc-finger-based artificial transcription factor and identification of novel genes involved in acetic acid tolerance. *Appl. Microbiol. Biotechnol.* 99, 2441–2449. doi: 10.1007/s00253-014-6343-x
- Meng, Q. S., Liu, C. G., Zhao, X. Q., and Bai, F. W. (2018). Engineering *Trichoderma reesei* Rut-C30 with the overexpression of egl1 at the ace1 locus to relieve repression on cellulase production and to adjust the ratio of cellulolytic enzymes for more efficient hydrolysis of lignocellulosic biomass. *J. Biotechnol.* 285, 56–63. doi: 10.1016/j.jbiotec.2018.09.001
- Meng, Q. S., Zhang, F., Liu, C. G., Zhao, X. Q., and Bai, F. W. (2020). Identification of a novel repressor encoded by the putative gene ctf1 for cellulase biosynthesis in *Trichoderma reesei* through artificial zinc finger engineering. *Biotechnol. Bioeng.* 117, 1747–1760. doi: 10.1002/bit.27321
- Park, K. S., Lee, D. K., Lee, H., Lee, Y., Jang, Y. S., Kim, Y. H., et al. (2003). Phenotypic alteration of eukaryotic cells using randomized libraries of artificial transcription factors. *Nat. Biotechnol.* 21, 1208–1214. doi: 10.1038/nbt868
- Pierce, B. C., Agger, J. W., Wichmann, J., and Meyer, A. S. (2017). Oxidative cleavage and hydrolytic boosting of cellulose in soybean spent flakes by *Trichoderma reesei* Cel61A lytic polysaccharide monoxygenase. *Enzyme Microb. Technol.* 98, 58–66. doi: 10.1016/j.enzymictec.2016.12.007
- Rahman, Z., Shida, Y., Furukawa, T., Suzuki, Y., Okada, H., Ogasawara, W., et al. (2009). Application of *Trichoderma reesei* cellulase and xylanase promoters through homologous recombination for enhanced production of extracellular β -glucosidase I. *Biosci. Biotechnol. Biochem.* 73, 1083–1089. doi: 10.1271/bbb.80852
- Rassinger, A., Gacek-Matthews, A., Strauss, J., Mach, R. L., and Mach-Aigner, A. R. (2018). Truncation of the transcriptional repressor protein Cre1 in *Trichoderma reesei* Rut-C30 turns it into an activator. *Fungal Biol. Biotechnol.* 5:15. doi: 10.2286/s40694-018-0059-0
- Steiger, M. G., Mach, R. L., and Mach-Aigner, A. R. (2010). An accurate normalization strategy for RT-qPCR in *Hypocrea jecorina* (*Trichoderma reesei*). *J. Biotechnol.* 145, 30–37. doi: 10.1016/j.jbiotec.2009.10.012
- Stricker, A. R., Grosstessner-Hain, K., Würleitner, E., and Mach, R. L. (2006). Xyr1 (xylanase regulator 1) regulates both the hydrolytic enzyme system and D-xylose metabolism in *Hypocrea jecorina*. *Eukaryot. Cell* 5, 2128–2137. doi: 10.1128/EC.00211-06
- Wang, F., Zhang, R., Han, L., Guo, W., Du, Z., Niu, K., et al. (2019). Use of fusion transcription factors to reprogram cellulase transcription and enable efficient cellulase production in *Trichoderma reesei*. *Biotechnol. Biofuels* 12:244. doi: 10.1186/s13068-019-1589-2
- Wang, H., Li, Z., Jia, R., Hou, Y., Yin, J., Bain, X., et al. (2016). RecET direct cloning and Red α recombineering of biosynthetic gene clusters, large operons or single genes for heterologous expression. *Nat. Protoc.* 11, 1175–1190. doi: 10.1038/nprot.2016.054
- Wood, T. M., and Bhat, K. M. (1988). Methods for measuring cellulase activities. *Methods Enzymol.* 160, 87–112. doi: 10.1016/0076-6879(88)60109-1
- Xin, Q., Gong, Y., Lv, X., Chen, G., and Liu, W. (2013). *Trichoderma reesei* histone acetyltransferase Gcn5 regulates fungal growth, condensation, and cellulase gene expression. *Curr. Microbiol.* 67, 580–589. doi: 10.1007/s00284-013-0396-4
- Zhang, F., Bai, F., and Zhao, X. (2016). Enhanced cellulase production from *Trichoderma reesei* Rut-C30 by engineering with an artificial zinc finger protein library. *Biotechnol. J.* 11, 1282–1290. doi: 10.1002/biot.201600227
- Zhang, F., Zhao, X., and Bai, F. (2018). Improvement of cellulase production in *Trichoderma reesei* Rut-C30 by overexpression of a novel regulatory gene Trvib-1. *Bioresour. Technol.* 247, 676–683. doi: 10.1016/j.biortech.2017.09.126
- Zhang, J., Zhang, G., Wang, W., and Wei, D. (2018). Enhanced cellulase production in *Trichoderma reesei* RUT-C30 via constitution of minimal transcriptional activators. *Microb. Cell Fact* 17:75. doi: 10.1186/s12934-018-0926-7
- Zhang, X., Li, Y., Zhao, X., and Bai, F. (2017). Constitutive cellulase production from glucose using the recombinant *Trichoderma reesei* strain overexpressing an artificial transcription activator. *Bioresour. Technol.* 223, 317–322. doi: 10.1016/j.biortech.2016.10.083
- Zheng, F., Cao, Y., Wang, L., Lv, X., Meng, X., Zhang, W., et al. (2017). The mating type locus protein MAT1-2-1 of *Trichoderma reesei* interacts with Xyr1 and regulates cellulase gene expression in response to light. *Sci. Rep.* 7:17346. doi: 10.1038/s41598-017-17439-2

Conflict of Interest: The authors declare that the research was conducted in the absence of any commercial or financial relationships that could be construed as a potential conflict of interest.

Copyright © 2020 Meng, Zhang, Wang, Liu, Zhao and Bai. This is an open-access article distributed under the terms of the Creative Commons Attribution License (CC BY). The use, distribution or reproduction in other forums is permitted, provided the original author(s) and the copyright owner(s) are credited and that the original publication in this journal is cited, in accordance with accepted academic practice. No use, distribution or reproduction is permitted which does not comply with these terms.



Acidic Versus Alkaline Bacterial Degradation of Lignin Through Engineered Strain *E. coli* BL21(Lacc): Exploring the Differences in Chemical Structure, Morphology, and Degradation Products

OPEN ACCESS

Edited by:

Shihui Yang,
Hubei University, China

Reviewed by:

Jinguan Hu,
University of Calgary, Canada
Fubao Sun,
Jiangnan University, China

*Correspondence:

Jianzhong Sun
jzsun1002@hotmail.com
Daochen Zhu
dczhucn@hotmail.com

† These authors have contributed
equally to this work

Specialty section:

This article was submitted to
Synthetic Biology,
a section of the journal
Frontiers in Bioengineering and
Biotechnology

Received: 16 January 2020

Accepted: 29 May 2020

Published: 30 June 2020

Citation:

Murillo Morales G, Ali SS, Si H,
Zhang W, Zhang R, Hosseini K, Sun J
and Zhu D (2020) Acidic Versus
Alkaline Bacterial Degradation
of Lignin Through Engineered Strain
E. coli BL21(Lacc): Exploring
the Differences in Chemical Structure,
Morphology, and Degradation
Products.
Front. Bioeng. Biotechnol. 8:671.
doi: 10.3389/fbioe.2020.00671

Gabriel Murillo Morales^{1†}, Sameh S. Ali^{1,3†}, Haibing Si¹, Weimin Zhang²,
Rongxian Zhang⁴, Keyvan Hosseini⁵, Jianzhong Sun^{1*} and Daochen Zhu^{1,2*}

¹ Biofuels Institute, School of Environmental Science and Safety Engineering, Jiangsu University, Zhenjiang, China, ² State Key Laboratory of Applied Microbiology Southern China, Guangdong Provincial Key Laboratory of Microbial Culture Collection and Application, Guangdong Open Laboratory of Applied Microbiology, Guangdong Institute of Microbiology, Guangdong Academy of Sciences, Guangzhou, China, ³ Botany Department, Faculty of Science, Tanta University, Tanta, Egypt, ⁴ School of Chemistry and Chemical Engineering, Jiangsu University, Zhenjiang, China, ⁵ School of Public Affairs, University of Science and Technology of China, Hefei, China

There is increasing interest in research on lignin biodegradation compounds as potential building blocks in applications related to renewable products. More attention is necessary to evaluate the effects of the initial pH conditions during the bacterial degradation of lignin. In this study we performed experiments on lignin biodegradation under acidic and mild alkaline conditions. For acidic biodegradation, lignin was chemically pretreated with hydrogen peroxide. Alkaline biodegradation was achieved by developing the bacterial growth on Luria and Bertani medium with alkali lignin as the sole carbon source. The mutant strain *Escherichia coli* BL21(Lacc) was used to carry out lignin biodegradation over 10 days of incubation. Results demonstrated that under acidic conditions there was a predominance of aliphatic compounds of the C₃–C₄ type. Alkaline biodegradation was produced in the context of oxidative stress, with a greater abundance of aryl compounds. The final pH values of acidic and alkaline biodegradation of lignin were 2.53 and 7.90, respectively. The results of the gas chromatography mass spectrometry analysis detected compounds such as crotonic acid, lactic acid and 3-hydroxybutanoic acid for acidic conditions, with potential applications for adhesives and polymer precursors. Under alkaline conditions, detected compounds included 2-phenylethanol and dehydroabietic acid, with potential applications for perfumery and anti tumor/anti-inflammatory medications. Size-exclusion chromatography analysis showed that the weight-average molecular weight of the alkaline biodegraded lignin increased by 6.75-fold compared to the acidic method, resulting in a repolymerization of its molecular structure. Lignin repolymerization coincided with an increase in the relative abundance of dehydroabietic acid and isovanillyl alcohol, from 2.70 and 3.96% on day

zero to 13.43 and 10.26% on 10th day. The results of the Fourier-transformed Infrared spectroscopy detected the presence of C = O bond and OH functional group associated with carboxylic acids in the acidic method. In the alkaline method there was a greater preponderance of signals related to skeletal aromatic structures, the amine functional group and the C – O – bond. Lignin biodegradation products from *E. coli* BL21(Lacc), under different initial pH conditions, demonstrated a promising potential to enlarge the spectrum of renewable products for biorefinery activities.

Keywords: lignin, *E. coli* BL21(Lacc), biodegradation compounds, acid/alkaline incubation, depolymerization/repolymerization

INTRODUCTION

Due to its abundance and complex polymeric structure, lignin represents a potential biomass resource for use in biorefinery activities (Saito et al., 2013). However, because of its intrinsic recalcitrance to depolymerization, its economical exploitation is still not feasible. Lignin's primary use is as energy source to produce heat and electricity for the paper and pulp industries (Chen and Wan, 2017; Van den Bosch et al., 2018). The microbiological partial degradation of lignin could represent a promising potential alternative to achieve a feasible production of renewable chemicals (Kosa and Ragauskas, 2013; Kohlstedt et al., 2018). Among the key advantages in the use of bacterial inoculation as approach to partial lignin biodegradation are its easy growth on a liquid medium, easy separation from the culture medium (facilitating recovery of the supernatants for analysis), and a flexible range of incubation temperatures. The whole cell bacterial degradation of lignin represents an opportunity to explore its potential as a source for renewable compounds. Taking advantage of the complex polymeric structure of lignin, could potentially produce a series of compounds of high interest for industries such as biofuels, bioplastics, food additives, pharmaceuticals, and others (Cline and Smith, 2017; Vinardell and Mitjans, 2017).

Laccase is among the most well-known ligninolytic enzymes under study. It is present in higher plants, fungi, and bacteria. Lignin partial biodegradation is achieved through redox reactions, via the oxidation of phenolic and non-phenolic structures and through the cleavage of some of the main lignin inter unit linkages such as β -O-4, β -O-5, β - β , etc. (Chatterjee and Saito, 2015), reducing molecular oxygen to water as a by-product. Researchers have demonstrated laccase's capacity to modify some functional groups of the lignin polymeric structure (Gianfreda et al., 1999; Hallac and Ragauskas, 2014; Constant et al., 2016; Zhu et al., 2018; Perez et al., 2019). Studies on lignin degradation through

bacterial laccase have especially focused their attention on the use of mediators, co-substrates, and optimal reaction temperature (Bourbonnais and Paice, 1990; Bourbonnais et al., 1997; Christopher et al., 2014). Additional studies have demonstrated that many microorganisms can display a series of specialized enzymes based on the availability of specific substrates (Kim et al., 2019). Nevertheless, to the best of our knowledge, studies assessing the partial degradation of lignin by microorganisms (in our particular case bacteria) under different pH conditions still remains obscure. Most studies on lignin biodegradation have paid little attention to the characterization of lignin degradation compounds and lignin chemical structure in the context of the pH incubation conditions.

Publications reporting on different lignin degradation compounds using whole-cell bacterial laccase strains under different pH conditions were recently reviewed. A study of lignin biodegradation using the bacterial strain *Comamonas* sp. B-9, isolated from eroded bamboo slips, performed the experiments on lignin mineral salt medium (KL-MSM) at an initial pH of 7.0, at 30°C, for 7 days. Some of the lignin degradation compounds found were isopropanol, 3-methyl-2-butanol and phenethyl alcohol (Chen et al., 2012). Another study on black liquor from rayon grade pulp paper industry reported its discoloring and detoxification with a potential bacterial consortium composed of *Serratia marcescens*, *Citrobacter* sp., and *Klebsiella pneumoniae*. The experimental conditions involved placing a solution of 10% (v/v) black liquor with 1% carbon and 0.5% nitrogen source in 100 mL volume in flasks of 250 mL for 8 days. After the first 24 h, the initial pH started to drop from 8.0 to approximately 6.5. From there the pH progressively rose to approximately 7.5 on day 8. Some of the lignin degradation compounds detected by gas chromatography/mass spectrometry (GC/MS) were carbamic acid, 1,2-benzenedicarboxylic acid and erythronitric acid (Chandra et al., 2011).

A study of directed biodegradation of Kraft lignin, without cosubstrates nor chemical pretreatment, was carried out with the bacterial strain *Cupriavidus basilensis* B-8. The incubation was tested along 7 days at 30°C, but the pH was not reported. The study focused on the measurement and characterization of the production of polyhydroxyalkanoates (PHA's), omitting the characterization of other lignin degradation compounds. The total concentration of PHA's was 319.4 mg L⁻¹, with (S)-3-hydroxy-butanoic acid, 3-hydroxy-butanoic acid, and

Abbreviations: ABTS, 2,2'-azino-bis(3-ethylbenzothiazoline-6-sulfonic acid); BSTFA-TMCS, N,O-Bis(trimethylsilyl)trifluoro-acetamide with trimethyl-chlorosilane; FTIR, Fourier-transformed infrared spectroscopy; GC-MS, gas chromatography-mass spectrometry; SEC, size exclusion chromatography; HPLC, high-performance liquid chromatography; IPTG, isopropyl β -D-thiogalactopyranoside; LB medium, Luria and Bertani broth or also known as Lysogeny broth; mM, milli molarity; M_n, number average molecular weight; M_w, weight average molecular weight; NaPSS, sodium polystyrene sulfonate; OD, optical density; OH, hydroxyl; PDI, polydispersity index; pH, hydronium potential; SEM, scanning electron microscopy; TGA, thermogravimetric analysis; UV, ultraviolet radiation.

3-hydroxybutyric acid in different percentages (Shi et al., 2017). Further studies reviewed reported the identification of value-added compounds from lignin biodegradation by bacteria (Duan et al., 2016; Suman et al., 2016; Zhu et al., 2017; Sapapporn et al., 2018; Shinoda et al., 2019; Yang et al., 2019). A thorough review of literature on lignin biodegradation identified the lack of research providing a systematic comparison of the lignin degradation in both sides of the pH spectrum using the same bacterial strain. Conducting such a study is necessary to advance research on lignin biodegradation by examining the resulting degradation compounds and the changes to lignin morphology, chemical structure, and molar mass accordingly.

To contribute to this gap in the research, our research group employed a recombinant strain of *Escherichia coli* BL21, produced through an intracellular harboring of a laccase gene from the bacterial strain of *Bacillus ligniniphilus* L1, which was previously isolated from the sediments of the South China Sea (Zhu et al., 2014; Zhu et al., 2017). Preliminary results suggest that this mutant bacterial strain has potential to aid in the development of innovative strategies for lignin bacterial degradation. Based on this demonstrated potential, one scientific question must be answered: How do lignin chemical structure, morphology, and molar mass, and lignin degradation compounds produced from the partial degradation activity of the mutant strain *E. coli* BL21(Lacc) differ under acidic and mild alkaline conditions? To answer this question, two different samples of lignin were used: (1) alkali lignin without any chemical pretreatment and (2) alkali lignin which underwent a chemical pretreatment. The initial pH conditions of the samples trigger to drive the pH values of the bacterial growth media to suitable conditions along the incubation. The samples were analyzed for characterization including optical density (OD₂₈₀), measurements of pH, morphology using scanning electron microscopy (SEM), changes in molar mass using size-exclusion chromatography (SEC), presence and identification of lignin degradation compounds using GC/MS and differences in the main functional groups using Fourier-transformed infrared spectroscopy (FTIR). Our results revealed remarkable differences in the lignin morphology, the chemical structure of some functional groups and the generation of biodegradation compounds. We performed experiments without the inoculation of the mutant strain *E. coli* BL21(Lacc) as controls. The results are described and discussed below.

MATERIALS AND METHODS

Materials

Reactants including alkali lignin (CAS number 8068-05-1), 2,2'-azino-bis(3-ethylbenzothiazoline-6-sulfonic acid) (ABTS), isopropyl β-D-thiogalactopyranoside (IPTG), kanamycin sulfate, 1,4-dioxane, pyridine, N,O-Bis(trimethylsilyl) trifluoro-acetamide with trimethylchlorosilane (BSTFA-TMCS), were purchased from Sigma-Aldrich, in St. Louis, MO, United States. Nitrogen gas (N₂) was purchased from

Shanghai Chemical Industry Park Pu River specialty gases Co., Ltd. The rest of the chemicals described to prepare the different bacterial culture media were purchased from Sinopharm Chemical Reagent Co., Ltd. All the reactants were of analytical grade and used without further purification. The mutant strain *E. coli* BL21(Lacc) with a harbored laccase gene was recombined at the Biofuels Institute of Jiangsu University.

Pretreatment of Lignin With Hydrogen Peroxide

A 500 mL solution of de-ionized water with alkali lignin at a concentration of 10 g L⁻¹ was prepared. The pH of the black liquor was set at 3.0 ± 0.1 by adding HCl to the aqueous solution. Hydrogen peroxide (30% v/v) at a concentration of 141.12 mM was added to the black liquor. A reactor (Weihai Zhengwei Machinery Equipment Co., Ltd., ZKCF-2L 1, China) submitted the substrates to anoxic conditions with dinitrogen gas at a temperature of 140 ± 5.0°C for 20 min at a pressure of approximately 400 kPa. The black liquor was dried in hot air at a temperature (Jintan Medical Equipment Factory, DHG-9245A, China) between 60–80°C for 4 days. The chemically pretreated lignin was used for bacterial degradation under low pH conditions. For the mild alkaline method, lignin was used after overnight vacuum drying at 60°C in a heat drier (YiHeng Scientific Instrument Co., Ltd., BPZ-6033, China) to remove moisture.

Preparation of Lignin Culture Medium for Acid and Mild Alkaline Degradation

The initial growth of the mutant strain *E. coli* BL21(Lacc) took place on LB medium for approximately 18–24 h. One milliliter of kanamycin sulfate solution (0.01 g mL⁻¹) was added before the inoculation and 100 μL of IPTG solution (0.1 mM) after 12 h of inoculation. For the alkaline biodegradation method, ABTS mediator was added to the LB medium before sterilization. After 24 h of incubation, 10 g L⁻¹ of alkali lignin (the lignin medium under alkaline conditions) were added.

For the acid method, the bacterial cells were precipitated from the LB culture medium via centrifugation at 10,000 rpm for 20 min. The pellets were transferred to the lignin medium under sterile conditions. The medium MM63 (used as lignin medium for acidic conditions) was prepared according to a method previously reported (Zhu et al., 2017). The medium MM63 consisted of 100 mM KH₂PO₄, 75 mM KOH, 15 mM (NH₄)₂SO₄, 1 mM MgSO₄ and 3.9 μM FeSO₄. Before sterilization, 1 g of lignin was added into 100 mL MM63 medium, along with 1 mM of ABTS as mediator. After sterilization (Sanyo, MLS-3750, Japan), 2.5 g of glucose dissolved in 20 mL of deionized water were added into the culture medium and filtered by 0.2 μm pore size filter for organic solutions. Next, H₂O₂ was added with a concentration of 0.50 mM and 1 mL of kanamycin sulfate solution (0.01 g mL⁻¹). For the mild alkaline method, lignin was used as a single carbon source without the addition of co-substrates. Before

inoculations, the initial pH for LB and MM63 media were set at 7.0 ± 0.10 .

After incubation, the bacterial cells were precipitated in a centrifuge (Beckman Advanti J-1, United States) at 12,000 rpm for 20 min. Afterward the supernatants were boiled in a heater at 130°C for 20 min. After cooling down the bacterial cells were precipitated again in the conditions described above. The supernatant was recovered, put into a refrigerator at -20°C for 24 h and submitted to freeze drying (Christ Beta 1–8 LD plus, Germany) for 7 days and kept at cool temperature conditions before analysis. For the preparation of samples for GC/MS analysis, the supernatants were not freeze-dried.

Optical Density Measures

Aliquots of 0.5 mL were centrifuged at 12,000 rpm for 5 min (Eppendorf, 5804R, Germany), boiled at 100°C for 20 min to inactivate and precipitate the bacterial cells and centrifuged again at the same rotational speed and time conditions. Before optical density readings, the samples were diluted in water at a factor of 1/1,000. The wavelength for optical density measures was set at 280 nm (OD_{280}) (Beckman DU 800 spectrophotometers, Beckman Coulter, Inc., United States). Deionized water was set as control. Readings were made in triplicate obtaining standard deviations smaller than or equal to 0.016.

pH Measures

The initial and final pH readings of the lignin media, and the initial and final pH of the chemically pretreated lignin solution with H_2O_2 were conducted with a pH meter (INESA, PHS-25, China) with a precision of 0.01. Intermediate readings were made with litmus paper. For litmus paper readings, a pH band of ± 0.50 was added throughout the readings.

Scanning Electron Microscopy

Dried samples were mounted on small adhesive tapes, coated with a gold–palladium alloy, and examined with SEM using 1 μm as reference scale (SEM, JSM-7800F, Japan).

Gas Chromatography Mass Spectrometry

The general procedures were prepared according to the method described by Zhu et al. (2017), with some modifications. For samples with bacterial activity at low pH, the pH was adjusted to 2.0 using 5 M of an aqueous solution of HCl. For the samples with bacterial activity above pH 7.0, there was no pH adjustment, to avoid inducing chemical modifications in the original compounds derived from the bacterial activity in the lignin medium and their controls. The samples were thoroughly mixed in twice their initial volume (15 mL) of ethyl acetate. The extraction mixture was collected and adjusted to approximately 1 mL via rotary evaporation at 37°C at vacuum, removing any presence of water with anhydrous Na_2SO_4 . The samples were stored in small glass bottles. Afterward, the samples were evaporated under a stream of dinitrogen gas. The silylation reaction was developed by adding 100 μL of 1,4-dioxane and

10 μL pyridine, followed by the addition of 50 μL of (BSTFA-TMCS). The organic solution was frequently shaken in a water bath at 80°C for 45 min. Before the final preparation of the samples for GC/MS analysis, the solutions were filtered using filter for organic solutions of 0.22 μm pore size and transferred to clean bottles for sampling with a syringe of 1 mL volume. A volume of 1 μL of silylated mixture was injected into the GC-MS equipment (Agilent Technologies, United States). The analytical column connected to the system was a PE-5MS capillary column (20 m \times 0.18 mm internal diameter, 0.18 mm film thickness). Helium was used as a carrier gas with a flow rate of 1 mL min^{-1} . The column temperature program was 50°C (5 min); $50\text{--}280^{\circ}\text{C}$ ($10^{\circ}\text{C min}^{-1}$, holding time of 6 min). The transfer line and the ion source temperatures were maintained at 200 and 250°C . A solvent delay of 3.0 min was selected. In the full-scan mode, electron ionization mass spectra in the range of 30–550 (m/z) were recorded at an electron energy of 70 eV.

Size-Exclusion Chromatography

Molar mass analysis was performed in a Shimadzu Series HPLC system (Shimadzu, Japan), equipped with a column oven unit CTO-20AC, a liquid chromatograph unit LC-20AD, a UV/VIS detector SPD-20A and a degassing unit DGU-20A. A column TSKgel GMPWxl, (Tosoh Corporation) was used for the analysis, based on methacrylate copolymer, with a length of 30 cm and a diameter of 7.80 mm, with an average copolymer particle size of 13 μm . The detection system was operated at a 280 nm wavelength, 50°C temperature and an 0.50 mL min^{-1} eluent flow rate. The sample volume was 200 μL . The retention time was adjusted according to the results obtained by the universal calibration procedure. The software used for the determination of the molar mass was provided by Shimadzu LabSolutions GPC.

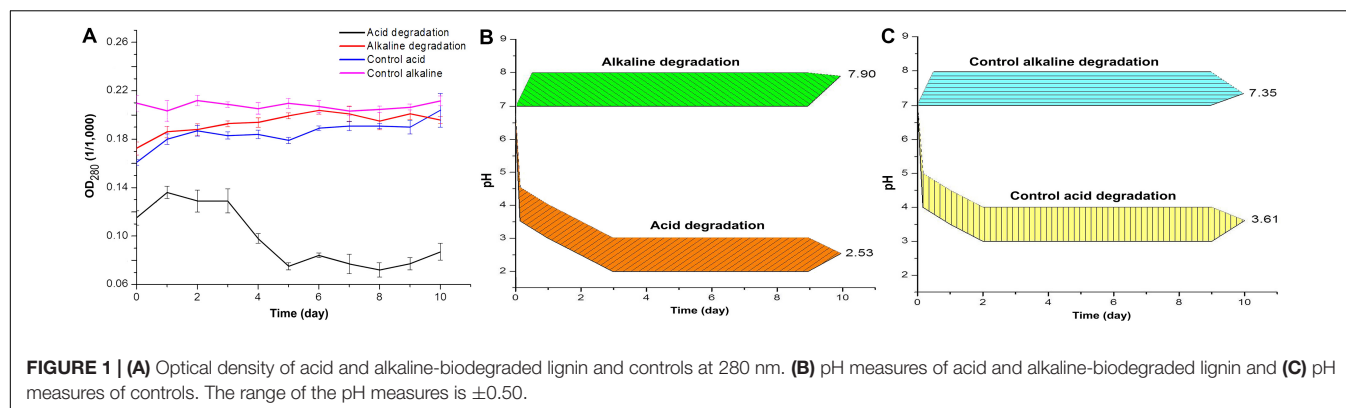
The universal calibration was made using five different types of NaPSS standards with different molecular weights – 1,690, 16,000, 33,400, 88,700, and 234,800 g mol^{-1} . The results were plotted with a logarithmic function of the molecular weight versus retention time. The solution used as eluent was NaNO_3 at a concentration of 0.1 M at $\text{pH } 7.0 \pm 0.1$. The concentration of the dissolved samples, as well as the standards, was 3 mg mL^{-1} with a minimum liquid volume of 5 mL per sample. Before the analysis, the samples were filtered in a 0.22 μm filter for organic solutions. The calculations for the different types of molecular weights (Mw, Mn) were based on the method previously reported (Andrianova et al., 2018).

Fourier-Transformed Infrared Spectroscopy

A Nicolet Nexus 470 spectrometer FT-IR with IR spectra between 400 and $4,000 \text{ cm}^{-1}$ performed measures at room temperature, applying 10 scans in transmission mode, using KBr pellets of 0.1 mm thickness. The weight of the samples were of approximately 1 mg.

Statistical Analysis

A statistical correlation between optical density and pH values was evaluated. The analysis was made with IBM SPSS Statistics



Software version 22. The correlations were considered significant at the 0.05 level.

RESULTS

Acidic and Alkaline Lignin Degradation With *E. coli* BL21(Lacc)

The results of optical density and pH measures suggest a modification of lignin chemical structure throughout the incubation time. **Figure 1A** shows the optical density at the wavelength of 280 nm (OD_{280}), which is related to the presence of phenolic groups in lignin (Sharma et al., 2019). For the acidic biodegradation sample, after day 3 the values of OD_{280} dropped, in an interval of 2 days, by 41.8%. In the case of the alkaline biodegraded sample, there was a steady increase in the optical density from day zero to day 6, for a total increase of 18.4%. The results suggest that the main changes on lignin chemical structure occurred after day 5 for the sample under acid biodegradation and after day 6 for the alkaline sample. The optical density values for the control of acidic biodegradation of lignin (hereafter acidic control) were relatively stable, experiencing two increments in the intervals between the days 5 and 6, and days 9 and 10, in 5.29 and 6.86%, respectively. In the control for alkaline biodegradation of lignin (hereafter alkaline control), the variation in the optical density was practically negligible. For the acid control, the initial variations in the optical density, particularly from day zero to day 1, were primarily due to dissolution of lignin in the growth medium. The controls showed no significant changes in optical density.

Figure 1B shows the changes in pH for acidic and alkaline biodegradation of lignin while **Figure 1C** shows the changes in pH for the controls of acidic and alkaline biodegradation (hereafter acidic and alkaline controls). Represented in **Figure 1B**, there is a very fast drop in pH in the first hours of reaction for the acidic lignin biodegradation. This might be caused by a chemical equilibrium in the pH between the lignin medium and the chemically pretreated lignin with hydrogen peroxide. From the days zero to 3, a less intense drop in pH occurred. This may be related to the initial bacterial growth and glucose depletion on the lignin medium. After day 3, the values of pH values remained relatively stable. The final pH value for

the acidic biodegradation sample was 2.53. In previous literature, few fungal or bacterial strains containing laccase have shown a good capacity for degrading lignin or lignin model compounds under very low pH (Gianfreda et al., 1999; Margot et al., 2013). Our results, however, demonstrated the utility of bacterial laccase for modifying the chemically pretreated lignin under very low pH, comparable with the optimal pH for ABTS activity in the oxidation of lignin model compounds (pH 3.0) (Bourbonnais et al., 1997; Margot et al., 2013).

Figure 1B also shows a single pH band between 7.0 and 8.0 during the 10 days of reaction, suggesting that the ionic equilibrium is more limited in the alkaline range for this particular bacterial strain under the performed experimental conditions. The final pH value was 7.90. This result demonstrates the capacity of the mutant strain *E. coli* BL21(Lacc) to tolerate alkaline conditions to some extent. Our findings of lignin biodegradation in mild alkaline medium are comparable to other reports of lignin degradation and lignin model compounds using bacterial and fungal laccase in the alkaline side of the pH spectrum (Xu, 1997; Ruijsenaars and Hartmans, 2004). **Figure 1C** shows the pH values for the acidic and alkaline controls. Both results showed similar patterns to those of the pH values of the main samples in **Figure 1B**. The acidic control also used chemically pretreated lignin and H_2O_2 as co-substrate, maintaining a very similar equilibrium in pH values during the first hours of reaction in the lignin medium compared to the of acidic biodegradation sample of lignin along the 10 days of agitation. The final pH value for acidic control was 3.61, 1.08 higher than the value measured for the acidic biodegraded sample, reflecting a difference in the concentration of hydronium ions [H_3O^+], favorable to the acidic biodegraded sample, of 2.7 mM. The pH values of the alkaline control fluctuated from 7.00 at the beginning of the reaction to 7.35 on day 10. As the pH of alkali lignin in aqueous solution at a concentration of 10 g L^{-1} is higher than 8.0, it is reasonable to assume that the pH could reach an equilibrium value in the first hours of reaction even higher than 7.50, progressively decreasing during the reaction time. A similar reaction is expected in the alkaline biodegraded lignin sample. In conclusion, optical density and pH measurements showed differences between the biodegradation samples and their controls, suggesting a bacterial degradation of lignin during the

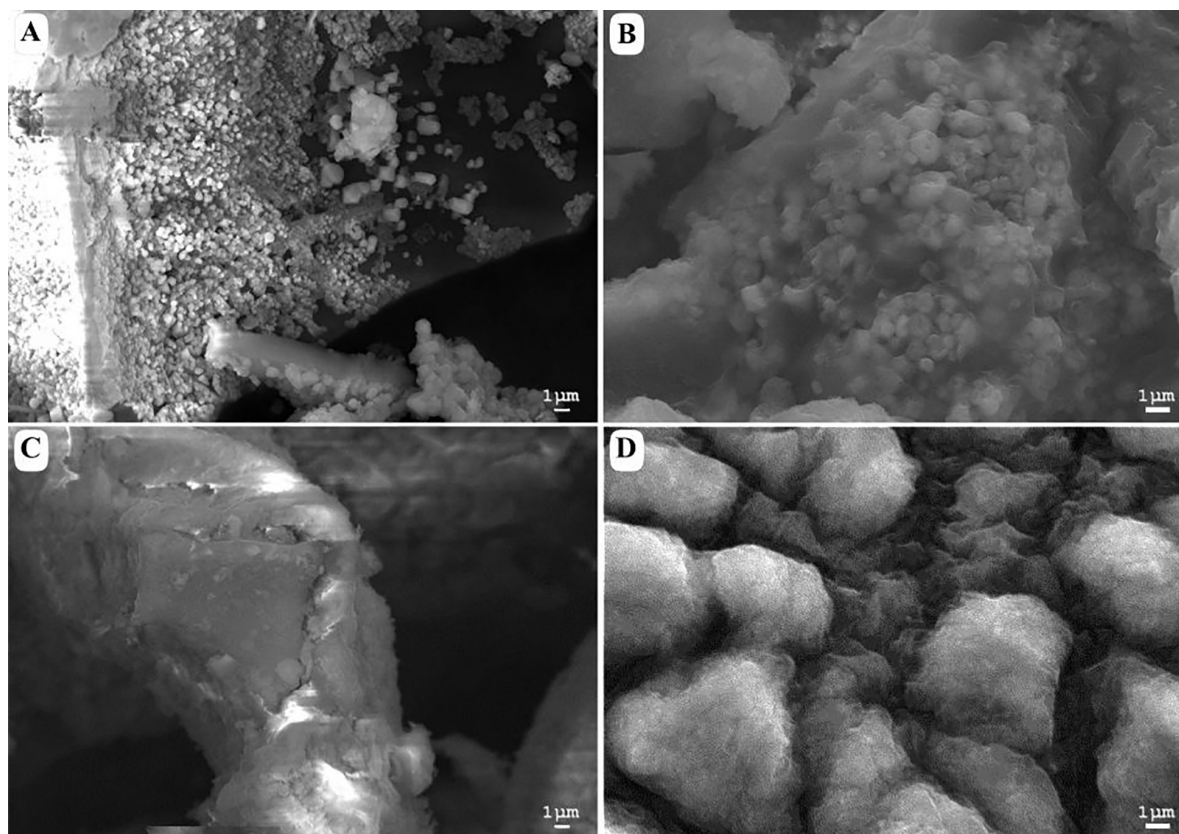


FIGURE 2 | Scanning electron microscopy images of (A) acid-biodegraded lignin, (B) alkaline-biodegraded lignin, (C) control of acid biodegradation, and (D) control of alkaline biodegradation. Scale of reference of 1 μm .

10 days of reaction. This conclusion is further confirmed in the analysis below.

Morphological Description

Figure 2 shows a morphological comparison using SEM between the samples of acidic and alkaline biodegradation of lignin and their controls, with a scale of reference of 1 μm . **Figure 2A** shows an acidic biodegradation sample of lignin with blocks in the background coated with a series of crystalline structures of minimum sizes of approximately 1 μm . **Figure 2B** shows a sample of alkaline biodegradation of lignin with blocks covered by non-crystalline moieties. The average size of the lignin moieties is also of approximately 1 μm . **Figure 2C** shows a sample of acidic control. Though the acidic control also used chemically pretreated lignin with H_2O_2 , the scanned image demonstrates the existence of well-defined lignin particles approximately 10 μm in size, without significant damage, and surrounded by foamy-like moieties. In the case of the alkaline control, an absence of clean lignin blocks appears in the background. The lignin moieties have an average size of approximately 5 μm . We conclude that the different pH conditions after lignin modification directly affected the final morphology of the samples. The differences are more notorious for the samples subjected to bacterial activity. Nevertheless, in the case of the alkaline control, there are

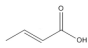
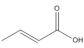
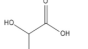
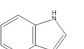
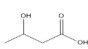
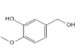
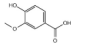

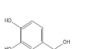
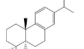
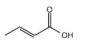
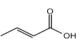
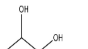
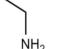
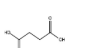
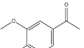
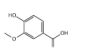
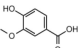
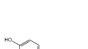
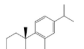
important modifications on its morphology. In comparison with a typical SEM image of untreated alkali lignin, the acidic control sample suffered less morphological modifications (see **Supplementary Figure S1**).

Identification of Lignin Biodegradation Compounds

Gas chromatography/mass spectrometry analysis gave valuable insights to elucidate if there are differences in lignin degradation compounds under bacterial activity at different pH conditions. A summary of five targeted peaks for each method and their controls, indicating their relative abundance and potential applications, is shown in **Table 1**. The results of the GC/MS spectral analysis for acidic, alkaline lignin biodegradation, and their controls are shown in **Figure 3**. The full list of all the compounds – excluding the functional group related to the thioacetolysis reaction – is shown in **Supplementary Table S1**. It is important to mention that most of the lignin degradation compounds were derived from vanillin, which was identified in a previous GC/MS analysis of alkali lignin – without any chemical pretreatment or bio treatment –, and with a relative abundance of approximately 32% (unpublished).

In **Table 1** it is the abundant presence of aliphatic compounds with the general structure $\text{C}_3\text{--C}_4$ namely carboxylic acids in

TABLE 1 | Summary of main degradation compounds from lignin degradation by *E. coli* BL21(Lacc) and controls.

Acid biodegradation of lignin					Alkaline biodegradation of lignin				
Retention time	Name of compound	Relative abundance (%)	Potential applications	Image of compound	Retention time	Name of compound	Relative abundance	Potential applications	Image of compound
7.73	Crotonic acid	5.22	Precursor for paints and adhesives		13.38	2-phenylethanol	3.75	Ingredient in flavors and fragrances	
10.53	DL-lactic acid	11.28	Polymer precursor, descaler, anti bacterial agent		16.38	1H-Indole	32.00	Bacterial signal	
12.33	3-hydroxy butanoic acid	3.32	Copolyester		18.80	Isovanillyl alcohol	10.26	Ingredient in flavors	
20.23	Vanillic acid	4.83	Flavoring agent		23.10	Hexadecanoic acid	4.33	Substrate for biofuels	
20.82	Protocatechuic acid	9.67	Antioxidant/anti inflammatory		26.17	Dehydroabietic acid	13.43	Anti microbial, anti tumor, anti inflammatory	
Control acid biodegradation of lignin					Control alkaline biodegradation of lignin				
7.73	Crotonic acid	6.31	Precursor for paints and adhesives		7.73	Crotonic acid	5.46	Precursor for paints and adhesives	
10.55	Propylene glycol	16.48	Thermoplastics, anti freeze, cosmetics		8.09	Ethanamine	5.91	Co-substrate in medical applications	
14.68	Succinic acid	7.10	Metabolic intermediate, platform for polymers		18.60	Apocynin	8.53	Anti inflammatory agent	
20.23	Vanillic acid	4.34	Flavoring agent		20.23	Vanillic acid	6.11	Flavoring agent	
20.82	Protocatechuic acid	7.88	Antioxidant/anti inflammatory		26.17	Dehydroabietic acid	4.47	Anti microbial, anti tumor, anti inflammatory	

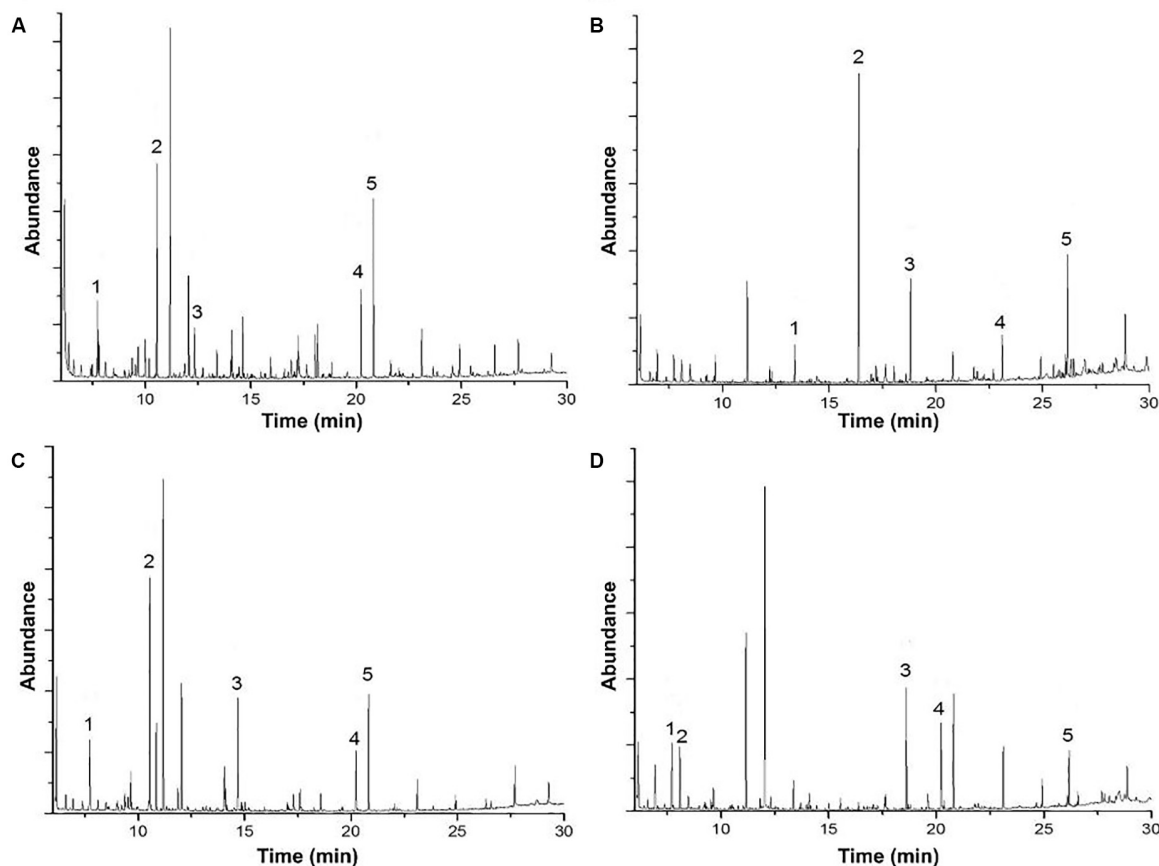


FIGURE 3 | Gas chromatography-mass spectrometry analysis of (A) acid biodegradation of lignin, (B) alkaline biodegradation of lignin, (C) control for acid biodegradation, and (D) control for alkaline biodegradation.

the acidic biodegradation sample, such as crotonic acid (#1), lactic acid (#2), and 3-hydroxybutanoic acid (#3), with relative abundances of 5.22, 11.28, and 3.32%, respectively. The short-chain carboxylic acids have potential applications as substrates for polymers and chemical precursors for paints, adhesives and other compounds (Doi et al., 1988; Rajan et al., 2014; Yang et al., 2018; Hack et al., 2019). Furthermore, two compounds with aromatic structures were also identified: vanillic acid (#4) and protocatechuic acid (#5), with relative abundances of 4.82 and 9.67%. These compounds are associated with the bacterial metabolism of vanillin. Vanillic acid was detected at the retention time of 20.228 min (see **Figures 3A,C**). Recently, researchers have reported on the use of vanillic acid as building block for copolymers (Gioia et al., 2018). Protocatechuic acid is well-known for its antioxidant capacity (Xi et al., 2016), and thus has potential for use in medicine/pharmaceutics.

The five targeted peaks of the alkaline biodegradation sample are 2-phenylethanol (#1), 1H-indole (#2), isovanillyl alcohol (#3), hexadecanoic acid (#4), and dehydroabietic acid (#5). The relative abundances represented 6.36, 16.48, 7.10, 4.34, and 7.88%, respectively. Compared with the lignin's acidic biodegradation sample, it is notable that in the acidic control the compounds in common also have similar relative abundances. For crotonic acid and vanillic acid, this suggests a limited metabolism of those compounds by the mutant bacterial

which is produced from some bacterial strains to regulate the transition from the exponential to the stationary phase. It is also related to a stress response and promotes resistance to a range of antibiotics and toxins through physical export and oxidative-stress protective mechanisms (Lee et al., 2010). Isovanillyl alcohol is an isovanilloid associated with vanillin, which is used as an ingredient in the food industry. Hexadecanoic acid is the only carboxylic acid on the list. It is used as a substrate for biofuels synthesis (Janßen and Steinbüchel, 2014). Dehydroabietic acid is found in resins or extracts of conifers and has being the subject of research for its anti-microbial, anti-tumor and anti-inflammatory properties (González, 2015; Vahermo et al., 2016).

The acidic and alkaline controls showed some similarities and differences compared to the samples under the bacterial activity of *E. coli* BL21(Lacc). The five compounds identified in **Table 1** for the acidic control were crotonic acid (#1), propylene glycol (#2), succinic acid (#3), vanillic acid (#4), and protocatechuic acid (#5). The relative abundances represented 6.36, 16.48, 7.10, 4.34, and 7.88%, respectively. Compared with the lignin's acidic biodegradation sample, it is notable that in the acidic control the compounds in common also have similar relative abundances. For crotonic acid and vanillic acid, this suggests a limited metabolism of those compounds by the mutant bacterial

strain. The differences of the lignin degradation compounds between the acidic biodegradation sample and its control are also evident. Some of the most remarkable differences rely on the presence of propylene glycol and succinic acid. On the other hand, the compounds in the acidic biodegradation sample are present in higher amounts, making up between 2.0 and 3.0%. The compounds found only in the acidic biodegradation sample include lactic acid, almost in the same retention time than propylene glycol (10.536 versus 10.55 min), glycerol (14.101 min), and adipic acid (17.235 min), among others (see Supporting Material 2). These results reflect an intense metabolic activity in the chemically modified lignin, which resulted in the degradation of the initially abundant aromatic compounds, suggesting that the addition of glucose as co-substrate, in synergy with the mutant bacterial strain could propitiate a more complex biological effects on lignin.

The alkaline control also exhibited some similarities and differences with the compounds found in the sample of alkaline biodegradation sample. For the alkaline control, are worth mentioning crotonic acid (#1), ethanamine (#2), apocynin (#3), vanillic acid (#4), and dehydroabietic acid (#5). Their relative abundances represented 5.46, 5.91, 8.53, 6.11, and 4.47%. From this list two compounds were also present in the acidic control: crotonic acid and vanillic acid. The differences between the products of the alkaline biodegradation sample were also notable. In the alkaline biodegradation sample, there was a preponderance of three compounds: 1H-indole, isovanillyl alcohol, and dehydroabietic acid. Dehydroabietic acid was also present in the alkaline control, but in the case of the alkaline biodegradation sample, the relative abundance was almost threefold higher. As expected, 1H-indole was not identified in the alkaline control sample, confirming the absence of bacterial activity. 1H-indole is produced as a bio signal for oxidative stress in the bacterial growth medium. Besides the high concentration of 1H-indole, the simultaneous absence of apocynin in the sample under biodegradation confirms the environment of oxidative the bacterial mutant strain was under during lignin oxidation in mild alkaline conditions (Stefanska and Pawliczak, 2008).

Contrasting with the large amount of lignin degradation compounds in the acidic biodegradation sample, the GC/MS analysis detected lower amounts of lignin degradation compounds in the alkaline biodegradation sample (see **Figures 3A,B**). In **Table 1**, the differences in their chemical structure are notable. The five targeted peaks of the alkaline biodegradation sample comprised 63.77% of the total detection by GC/MS, nearly double the amount measured in the acid biodegradation sample (32.81%). Most of the relative abundances in the alkaline method came from compounds containing at least one aromatic structure. Some of them originated from lignin degradation by *E. coli* BL 21(Lacc), and one was produced as a bio signal (1H-indole). A carboxylic acid molecule is present at the retention time of 23.107 min (hexadecanoic acid), which was also detected in the acidic method, in both cases a small amount. The presence of this compound in all the samples and their controls (see **Supplementary Table S1**) requires further study.

Due to their high relative abundances, particular attention was paid to 1H-indole and dehydroabietic acid. Samples were

analyzed using GC/MS on the days 0, 3, 7, and 10 to track the evolution of their relative abundances (see **Supplementary Table S2**). After several hours of the addition of lignin on day zero, the relative abundance of 1H-indole reached 19.71%. It is likely that 1H-indole was already produced before the addition of lignin due to the previous addition of tryptone for the preparation of the LB medium for the initial bacterial growth. On day 7, its abundance peaked at 56.52%, and then decreased to 32.00% on day 10. The initial pH conditions of the alkaline lignin medium could trigger high production of 1H-indole from resistant cells as an assistance to sensitive cells for their survival in the initial incubation conditions. The relative abundance of dehydroabietic acid on day zero was 2.70%, progressively increasing its value during the incubation time, reaching its maximum value of 13.44% on day 10. Interestingly, in the case of isovanillyl alcohol, there was also an increase in its relative abundance, starting with 3.96% on day 0, reaching a maximum value of 12.10% on day 7, and ending on day 10 with 10.26%. All of these compounds have a similar response in their relative abundances throughout the bacterial activity.

In conclusion, most of the lignin degradation compounds produced by the bacterial mutant strain activity of *E. coli* BL21(Lacc) could be conditioned by the evolution of the pH values during lignin biodegradation. The main trend was the production of carboxylic acids at low pH values, and a series of diverse aryl compounds in the alkaline side with an increase for some in their relative abundance under oxidative stress conditions after 7 days of reaction.

Statistical Analysis

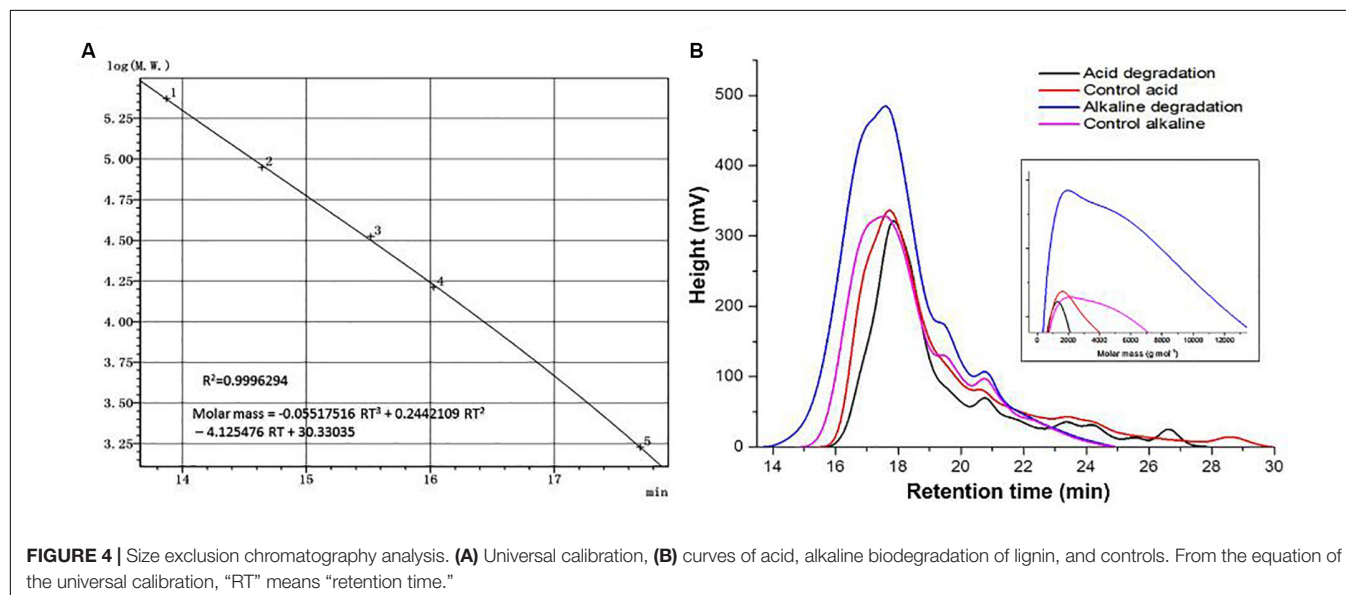
The Shapiro–Wilk test was initially performed to verify whether the optical density and pH values fit a normal probability distribution. The probability values (*p*-values) obtained from the Shapiro–Wilk test in the case of alkaline biodegradation of lignin experiment were greater than 0.05, which implied that the results were normally distributed. The correlation between the optical density and the PH values obtained throughout 11 observations for the experiment for alkaline biodegradation was equal to 0.829, indicating a high significant positive correlation (see **Table 2**).

The *p*-values obtained from Shapiro–Wilk test for the acidic biodegradation sample of lignin were smaller than 0.05, which indicated that the results did not follow a normal distribution. Thus, we performed the non-parametric Spearman correlation coefficient test for the 11 observations. The test revealed a high significant positive correlation of 0.726 (see **Table 2**). In the case of the acidic control sample, our results did not follow the normal distribution. Thus, we performed the non-parametric Spearman correlation coefficient test. The test revealed a high significant negative correlation of 0.852. For the results obtained from the of alkaline control sample, there was no significant correlation. The results of this analysis are shown in **Table 2**.

We conclude that for acidic and mild alkaline degradation of lignin using the mutant strain *E. coli* BL21(Lacc) there was a highly significant positive correlation between the values of OD₂₈₀ and pH throughout the 10 days of reaction.

TABLE 2 | Statistical correlation between optical density and pH for acid and alkaline biodegradation of lignin and controls.

Sample	Statistical correlation	Correlation test	Significance level
Acid biodegradation of lignin	0.726	Parametric Pearson	0.01
Control acid	-0.852	Parametric Pearson	0.01
Alkaline biodegradation of lignin	0.829	Non-parametric Spearman	0.01
Control alkaline	-0.227	Parametric Pearson	No significance



Molar Mass Analysis

Molar mass represents an important parameter which reflects quantitative changes on a quantitative basis. The universal calibration curve in **Figure 4A** shows a very high value in the coefficient of determination, allowing to use its equation for the estimations of M_n and M_w . **Figure 4B** shows the spectral curves for the samples of acidic and alkaline biodegradation of lignin and their controls, indicating the retention time in the abscissa of the main chart. The augmented chart of the curves of molar mass shows the equivalent values of the molar mass in the abscissa, in g mol^{-1} (from 0 to 13,000 g mol^{-1}). The main chart notes that the curves of the molar mass of acidic biodegradation of lignin and its control have broader late eluting portions (Chatterjee and Saito, 2015), evidence of ionic adsorptions between the lower molar mass fractions of lignin and the GPC column particles. In contrast, the of alkaline biodegradation samples of lignin and the alkaline control showed more compact configurations. For the alkaline biodegradation sample, its peak was found in a region of higher molar mass. A similar result was found for the curve of the molar mass of the alkaline control, but more moderate.

Table 3 shows the values of the number-average (M_n) and weight-average (M_w) molar mass of the lignin samples. The sample submitted to alkaline biodegradation underwent a 6.75-fold and 3.45-fold increase in its M_w and M_n values compared to the biodegraded sample in acidic conditions (32,325 and 7,095 g mol^{-1} for alkaline biodegradation of lignin

versus 11,254 and 2,054 g mol^{-1} for acidic biodegradation of lignin), and for alkaline biodegradation, the polydispersity index (PDI) was 4.55, a 1.96-fold increase compared to the PDI value of 2.32 for the acidic biodegradation of lignin (Chatterjee and Saito, 2015). It can be inferred that a repolymerization occurred on the molecular structure of the sample of alkaline biodegradation after the incubation time. This might be caused due to the degradation of the lightest molar mass lignin fractions in combination by complex chemical interactions during the bacterial activity of *E. coli* BL21(Lacc), viz., changes in polarity of lignin blocks, rearrangement of non-covalent bonds, etc. Our findings on the increase of lignin’s molar mass are in agreement with previously reported studies (Nugroho Prasetyo et al., 2010; Moya et al., 2011).

The acidic control showed slight differences compared to its corresponding biodegraded sample, reaching higher values on its M_n , and M_w values by 25 and 33%, respectively. The PDI value of the acidic biodegraded sample was higher than its control by 5.9%. Interestingly, in the case of the alkaline control there was an increase in the values of M_n , and M_w compared to the acidic control. The alkaline control experienced increments in the M_n , and M_w values by 59 and 87%, respectively. From these results we conclude that a depolymerization occurred in the acidic biodegradation sample of lignin where ring-opening reactions could occur, generating a series of short-chain aliphatic compounds with many carboxylic

acids among them. On the other hand, the alkaline conditions could trigger changes in the concentration of the main lignin monomers, which could be attributed to the interactions between reactive functional groups of lignin. This would lead to the rearrangement and reconfiguration of lignin's overall chemical structure after 10 days of shaking, producing a stronger repolymerization on the lignin degraded sample and a moderate repolymerization on its control.

In order to elucidate lignin repolymerization during the alkaline incubation, we also measured the molar mass on days 1 and 5. **Table 4** shows the results. From days 1–5, there was a twofold increase approximately in the values of M_n and M_w relative to the first day. From days 5 to 10, the increase ratio became larger, in the order by almost fourfold relative to day 5. The PDI values also changed over time, increasing from 2.78 on day 1, to 3.50 on day 5, and to 4.56 on day 10. These results suggest that the alkaline biodegradation of lignin could exert an important influence over the changes in the molar mass of lignin, particularly after the fifth day. Our results suggest that the changes in the molar mass of alkaline biodegradation of lignin could be a consequence of major changes in the lignin's polymeric structure. The changes in the relative abundance of some compounds reinforces this possibility. The increase of the relative abundance of dehydroabietic acid (molecular weight = 300.4 g mol⁻¹) on days 0, 3, 7, and 10, determined by GC/MS analysis, provides a clear example. The abundance of this metabolite was 2.7, 5.23, 13.14, and 13.44%, respectively (see **Supplementary Table S2**). A similar phenomenon was observed with isovanillyl alcohol.

Structural Characterization

The FTIR analysis method provided insights for a qualitative evaluation of the chemical structure of alkaline and acidic biodegraded lignins and their controls. The analysis confirmed the presence of guaiacyl (G) and syringyl (S) lignins (Gall et al., 2014). Some differences in the presence of functional groups among the lignin preparations were found and the results are shown in **Figure 5**. **Figure 5A** displays the overall FTIR spectra, **Figure 5B** shows more details from the wave numbers 450 to 1,300 cm⁻¹, while **Figure 5C** shows from 1,300 to 1,800 cm⁻¹ and **Figure 5D** shows from 2,250 to 3,700 cm⁻¹, respectively.

In **Figure 5B**, at the wave number of 1,228 cm⁻¹, there is a band displayed for the alkaline biodegradation sample and its control, which depicts the stretching of the C – O – C bond, providing important evidence of the stronger presence of aryl ether linkages, viz., β – O – 4' bond (Yang et al., 2007). In-plane deformations of C – H bonds in G type lignins (in aromatic structures and aliphatic moieties) are evidenced at wave numbers 1,147 and 883 cm⁻¹, while the band at 995 cm⁻¹ belongs to the deformations out of plane in the – CH = CH – group (Faix, 1991; Sun et al., 2003). The band at 1,080 cm⁻¹ is only present in the alkaline samples, corresponding to the stretching of the C – O bond, and reaffirming the previously described at the peak at 1,228 cm⁻¹ (Sun et al., 2003). The peak at 620 cm⁻¹ possibly describes the presence of a S – O bond, becoming particularly accentuated in the cases of acidic biodegradation of lignin and its control (Nugroho Prasetyo et al., 2010).

The band identified at the wave number 1,716 in **Figure 5C** is related to the C = O stretch for carboxylic acids. This result fits with the band assigned to the O–H bond for the acidic degradation sample and its control (El Mansouri and Salvadó, 2007; Faix, 1991). The alkaline samples showed a signal at the wave number of 1,633 cm⁻¹, assigned to the stretching of the C = C bonds of benzene rings in the IR spectra (Yang et al., 2007). Although is not confirmed, we surmise this could be associated with the repolymerization in alkaline conditions of the lignin biodegraded sample and its control. In contrast, at 1,602 cm⁻¹, all the samples displayed aromatic skeletal vibrations in the C – O bonds. This could be related to ether bonds, where the alkaline samples and the acidic control showed higher intensities, evidence of the preservation of ether linkages among aromatic structures (Faix, 1991; Sun et al., 2003; Gillgren et al., 2017). At 1,513 cm⁻¹ all the samples had a peak, corresponding to aromatic skeletal vibrations, G > S (Faix, 1991; Gordobil et al., 2016; Yu et al., 2019). The C–H stretch identified at 1,446; 1,423 and 1,404 cm⁻¹ are related to the C–H bonds in **Figure 5D** at the wave numbers 2,958, 2,875, and 2,852 cm⁻¹, respectively (Wade, 2013).

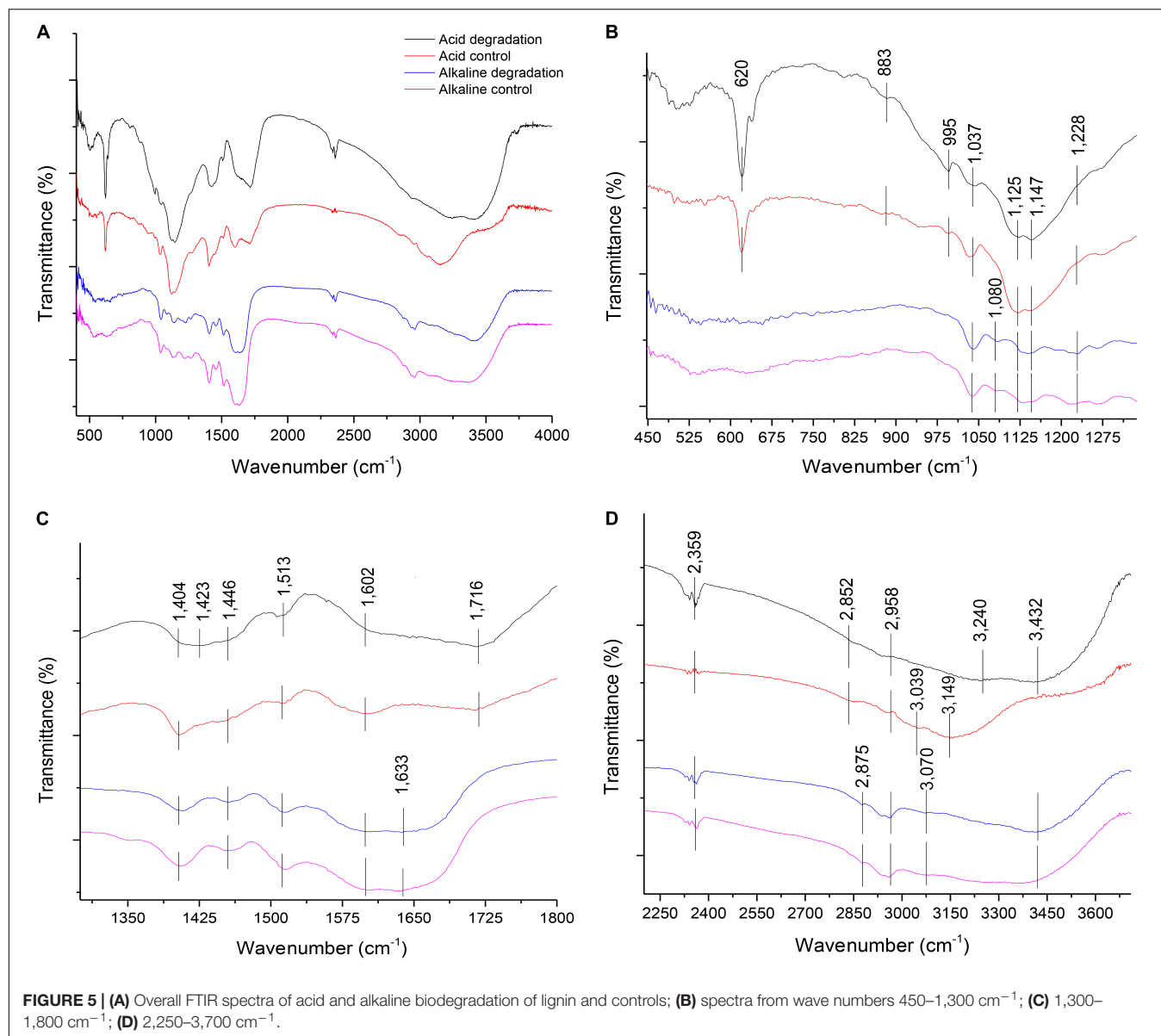
As reported in **Figure 5D**, all the lignin samples showed a broad response in the absorption band related to the O–H bond for aromatic structures at 3,432 cm⁻¹ (Cheng et al., 2016), with the exception of the acidic control, which was identified at 3,500 cm⁻¹. The acidic biodegradation sample and its control showed a second absorption band between the wave numbers 3,240 and 3,149 cm⁻¹. This band is assigned to the stretching of the O–H bond of carboxylic acids. For the biodegradation of lignin under low pH conditions, based on GC/MS data, the relative abundance of the carboxylic acids had an important share in the total detection of all the compounds, confirming the assignment of the wave number to this chemical bond (Yang et al., 2007). The alkaline samples of lignin displayed a signal at 3,070 cm⁻¹, which can be attributed to the N–H bond (Wade, 2013). We speculate that the band at 3,039 cm⁻¹, particularly strong in the sample of the acid control, could belong to a stronger presence of the stretching of the hybridized sp² C–H bond (Wade, 2013). The signals at the wave numbers 2,958, 2,875 and 2,852 cm⁻¹ are related to the asymmetric vibrations

TABLE 3 | Molar mass characterization of lignin samples.

Sample	M_w	M_n	PDI
Alkaline biodegradation of lignin	32,325	7,095	4.55
Acid biodegradation of lignin	4,782	2,054	2.32
Control acid	5,996	2,741	2.19
Control alkaline	11,254	4,362	2.58

TABLE 4 | Change in molar mass for alkaline biodegradation of lignin.

Day	M_n	M_w	PDI
1	2,083	5,798	2.78
5	2,767	9,671	3.50
10	7,095	32,325	4.56



and stretching of sp^3 hybridization of C–H bonds, particularly – CH_3 and – CH_2 – groups, associated to aliphatic and aromatic structures (El Mansouri and Salvadó, 2007; Wade, 2013; Yang et al., 2007; Reyes-Rivera and Terrazas, 2017). The band at $2,359\text{ cm}^{-1}$ was assigned to the presence of the nitrile functional group (– $\text{C}\equiv\text{N}$), which was confirmed in the results of GC/MS analysis (see **Supplementary Table S1**; Wade, 2013).

DISCUSSION

In this study, alkali lignin was submitted to partial biodegradation by the bacterial mutant strain *E. coli* BL21(Lacc) under acidic and mild alkaline conditions for 10 days. The final outcomes from those treatments were remarkably different in terms of optical density response,

pH evolution, morphology, detection of lignin degradation compounds, presence of functional groups, and changes in the molar mass.

The signals detected by the optical density measures at 280 nm, which indicates the presence of aromatic structures in lignin, showed a decay of 41.80% for the acidic lignin biodegradation sample and a peak of 18.40% in the alkaline lignin biodegradation sample. This is evidence that the lignin samples experienced two different chemical structure modification processes. These results indirectly reflected the phenomena of partial depolymerization for the acidic biodegradation and the repolymerization for the alkaline biodegradation of lignin. The existence of two possible modification mechanisms altering the chemical structure of lignin are strongly suggested by the chemical structures present for each case in the lignin biodegradation compounds identified by the GC/MS analysis.

In spite of the two different responses in the optical density, in both cases the statistical analysis showed a significant correlation between the OD₂₈₀ and the pH. Furthermore, based on the SEM images, referenced at the scale of 1 μm , the differences in the morphology of the lignin samples were notable. For the acidic biodegradation sample, the lignin blocks were coated on their surfaces by crystalline particles of sizes smaller than 1 μm . The specific lignin degradation compounds associated with that formation merit further studies.

Based on the results of GC/MS analysis, for acidic biodegradation of lignin, a plethora of compounds with aliphatic chemical structures were found, possibly as a result of intense aromatic ring-opening reactions. The majority of these compounds are alkyl compounds of the type C₃–C₄, associated to guaiacyl lignin degradation. This was confirmed by the identification of protocatechuic acid as one of the lignin metabolites (Xu et al., 2019). These compounds have potential applications as renewable substrates for food flavorings, biofuels and adhesives, and copolymers for bioplastics, among others. In contrast, most of the lignin degradation compounds identified in the alkaline biodegradation sample showed a tendency to preserve their aromatic structures. Some of these lignin degradation compounds have potential applications as food flavorings and as medical treatments for inflammations, and tumors.

The high concentration of 1H-indole provided clear evidence that the mild alkaline conditions for lignin biodegradation as a single carbon source represented a stressful environment for the activity of the mutant strain *E. coli* BL21(Lacc). In connection with this, a phenomenon of increase in the relative abundance of dehydroabietic acid and isovanillyl alcohol was notorious, which ceased until the production of 1H-indole peaked at the seventh day, suggesting the beginning of the stationary phase in the alkaline lignin incubation.

In the case of acidic biodegradation of lignin, reactions similar to aldol condensation may have occurred. For the alkaline biodegradation of lignin, presumably different condensation reactions were more predominant, especially those dependent on relative higher pH conditions which could activate phenyl groups. It is likely that phenyl intermediates have produced coupling reactions in a small extent of degradation of the aromatic structures, thus, triggering a repolymerization of the lignin backbone, which increased its Mw value 6.75-fold in relation to the acidic biodegraded sample (Sapapporn et al., 2018). In contrast, for the acidic lignin biodegradation, a repolymerization of the lignin backbone was not indicated, which may have been caused by the methylation of phenolic hydroxyl groups in the aromatic structures of lignin (Kim et al., 2017). Regarding the lignin degradation compounds in the in the acidic and alkaline control samples after 10 days shaking, the generation of those compounds may have been caused by the auto oxidation of reactive monomers, likely related to low molar mass fractions in lignin and mediated by ABTS. For lignin biodegradation

by whole bacterial cells, further studies are necessary to shed light on the synergistic reactions between laccase and putative secondary enzymes involved in lignin biodegradation (Li et al., 2014). In the case of the control samples, a better understanding of the mechanisms driving the auto oxidation reactions of the main lignin monomers is required, with vanillin as the main source of the biodegradation/auto oxidation-derived compounds.

Concerning the chemical structure of lignin, the results of FTIR analysis suggest a preponderance of G and S lignins in the samples, which is typical from softwood (Gall et al., 2014). FTIR results did not confirm the existence of H lignin. The chemical pretreatment of lignin in the acidic biodegradation method produced important modifications. The presence of the C = O bond and the OH functional group, predominantly associated with numerous carboxylic acid molecules were notable. The chemically pretreated alkali lignin with hydrogen peroxide at low pH values demonstrated its solubility in the liquid phase, without the precipitation of heavy molar mass fractions. This could be explained by the accentuation of the peak at 620 cm⁻¹, which presumably was caused by a S–O bond (Nugroho Prasetyo et al., 2010). The strong peak at this wave number could indicate the lack of interference from hydrogen bonds and other non-covalent bonds at very low pH values, demonstrating that this linkage was not affected by the bacterial activity of the mutant strain *E. coli* BL21(Lacc). The alkaline biodegraded sample showed the presence of the N–H bond (from amine functional groups), confirming the character of the alkalinity of the lignin medium. The FTIR results also displayed further evidence of the existence of the C–O–C bond in the alkaline samples, a key constituent of aryl-ether linkages, viz., β -O–4 bonds. This reinforced the idea that in this case the cleavage of such bonds occurred in a lesser extent (Helmich et al., 2016). Furthermore, for

TABLE 5 | Summary of a general comparison between acid versus alkaline biodegradation of lignin by *E. coli* BL21(Lacc).

	Acid biodegradation	Alkaline biodegradation
Changes in OD ₂₈₀	Drop in OD ₂₈₀ values by 41.8% after 2 days	OD ₂₈₀ values rose 18.4% after 6 days
Chemical pretreatment	140°C, N ₂ , 400 kPa, 141.12 mM H ₂ O ₂	No chemical pretreatment
Initial/final pH values	7.0/2.53	7.0/7.90
Lignin biodegradation compounds	Crotonic acid, DL-lactic acid, 3-hydroxybutanoic acid	2-Phenylethanol, isovanillyl alcohol, dehydroabietic acid
M _w /M _n	4,782/2,054	32,325/7,095
Final PDI	2.32	4.55
Main chemical structure	OH and C = O for carboxylic acids C = O stretch in GS lignins, –C≡N bond Strong signal of S–O bond	OH for alcohols, C = C stretching for aromatic structures, –C≡N bond N–H bonds Stronger signals of C–O–C bonds

the alkaline samples, the wave numbers related to aromatic skeletons/structures were more abundant, suggesting that the preponderant degradation mechanisms were not closely related to ring-opening reactions, as was the case for the acidic biodegradation sample. **Table 5** summarizes the most important differences between acidic and alkaline biodegradation of lignin previously discussed.

CONCLUSION

Partial biodegradation of industrial lignins by microorganisms with ligninolytic enzymes has demonstrated strong potential for producing compounds of interest for industries seeking alternative routes for the production of chemicals. In today's context, the synthesis of many goods still requires the use of non-renewable and toxic substrates, making the supply of more renewable compounds an urgent task. Alkali lignin is one of the industrial lignins that is produced in large amounts and can offer many opportunities due to its low valorization. The ligninolytic action of enzymes, such as bacterial laccase mediated in our case by ABTS, can further oxidize lignin monomers from low molar mass fractions, leading to the generation of many degradation compounds.

Our research strategy consisted of exploring the possibilities of the mutant bacterial strain *E. coli* BL21(Lacc) to partially degrade alkali lignin at acidic and mild alkaline conditions. In the low pH range of the spectrum, the mutant strain demonstrated its capacity to oxidize lignin monomers toward an abundant number of short-chain alkyl moieties with potential applications in the food, bio plastics, and adhesives sectors, among others. On the alkaline side of the spectrum, the metabolic activity of the bacterial mutant strain and increase in the relative abundance of compounds namely isovanillyl alcohol and dehydroabietic acid in the context of oxidative stress. Potential applications of these compounds are in the food and pharmacological industries. The possible reaction mechanism was the activation of phenyl radicals in aromatic structures, followed by substitution and repolymerization reactions, which increased its overall molar mass. This upgraded property in the alkaline biodegradation sample could render the building blocks for potential renewable substitutes in the biomaterials area.

By understanding the main reaction mechanisms involved in lignin biodegradation at different values on the pH spectrum, and by applying the appropriate chemical and biological pretreatment strategies, it is possible to unlock its potential, providing broader alternatives for renewable and bio-derived goods. Future work should tackle these issues.

REFERENCES

- Andrianova, A. A., Yeudakimenka, N. A., Lilak, S. L., Kozliak, E. I., Ugrinov, A., Sibi, M. P., et al. (2018). Size exclusion chromatography of lignin: the mechanistic aspects and elimination of undesired secondary interactions. *J. Chromatogr. A* 1534, 101–110. doi: 10.1016/j.chroma.2017.12.051

DATA AVAILABILITY STATEMENT

The original contributions presented in the study are included in the article/**Supplementary Material**, further inquiries can be directed to the corresponding author/s.

AUTHOR CONTRIBUTIONS

GM conception and execution of the experiments, interpretation of the results and, writing and preparation of the manuscript and **Supplementary Material**. SA assistance in preliminary tests, edition of the figures and, revision and correction of the manuscript. JS and DZ funding of the research work, supervision of the experiments and, revision and corrections of the manuscript. HS assistance in the preparation of the experiments of OD, GC-MS, and SEC analyses. WZ provision of the bacterial mutant strain *E. coli* BL21(Lacc). RZ assistance in the GC-MS tests arrangements and data analysis. KH preparation of statistical analysis. All authors read and approved the final manuscript.

FUNDING

This work was supported by the National Key R&D Program of China (Grant No. 2018YFE0107100); the National Natural Science Foundation of China (Grant No. 31772529); A Project Funded by the Priority Academic Program Development of Jiangsu Higher Education Institutions, and the Chinese Scholarship Council, under the number 2016GXYS4.

ACKNOWLEDGMENTS

We thank Mr. Ricardo Wu from the department of Food Science for providing technical assistance with the GC-MS and FTIR analysis. We thank Mrs. Laura C. Seithers from the College of Education and Human Development, University of Minnesota, United States for English language editing of this manuscript. We also thank Ms. Ting ting Lu from the Biofuels Institute of Jiangsu University for her contributions in the first trial tests of this study.

SUPPLEMENTARY MATERIAL

The Supplementary Material for this article can be found online at: <https://www.frontiersin.org/articles/10.3389/fbioe.2020.00671/full#supplementary-material>

- Bourbonnais, R., and Paice, M. G. (1990). Oxidation of non-phenolic substrates: an expanded role for laccase in lignin biodegradation. *FEBS Lett.* 267, 99–102. doi: 10.1016/0014-5793(90)80298-w
- Bourbonnais, R., Paice, M. G., Freiermuth, B., Bodie, E., and Borneman, S. (1997). Reactivities of various mediators and laccases with kraft pulp and lignin model compounds. *Appl. Environ. Microbiol.* 63, 4627–4632. doi: 10.1128/aem.63.12.4627-4632.1997

- Chandra, R., Abhishek, A., and Sankhwar, M. (2011). Bacterial decolorization and detoxification of black liquor from rayon grade pulp manufacturing paper industry and detection of their metabolic products. *Bioresour. Technol.* 102, 6429–6436. doi: 10.1016/j.biortech.2011.03.048
- Chatterjee, S., and Saito, T. (2015). Lignin-derived advanced carbon materials. *ChemSusChem* 8, 3941–3958. doi: 10.1002/cssc.201500692
- Chen, Y. H., Chai, L. Y., Zhu, Y. H., Yang, Z. H., Zheng, Y., and Zhang, H. (2012). Biodegradation of kraft lignin by a bacterial strain *Comamonas* sp. B-9 isolated from eroded bamboo slips. *J. Appl. Microbiol.* 112, 900–906. doi: 10.1111/j.1365-2672.2012.05275.x
- Chen, Z., and Wan, C. (2017). Biological valorization strategies for converting lignin into fuels and chemicals. *Ren. Sustain. Energy Rev.* 73, 610–621. doi: 10.1016/j.rser.2017.01.166
- Cheng, Y., Zhou, Z., Mehmet, A., Sun, D., Zhang, W., and Jiang, J. (2016). Direct liquefaction of alkali lignin in methanol and water mixture for the production of oligomeric phenols and aromatic Ethers. *J. Biobased Mater. Bioener.* 10, 76–80. doi: 10.1166/jbmb.2016.1572
- Christopher, L. P., Yao, B., and Ji, Y. (2014). Lignin biodegradation with laccase-mediator systems. *Front. Energy Res.* 2:12. doi: 10.3389/fenrg.2014.00012
- Cline, S. P., and Smith, P. M. (2017). Opportunities for lignin valorization: an exploratory process. *Energy Sustain. Soc.* 7:26.
- Constant, S., Wienk, H. L. J., Frissen, A. E., Peinder, P. D., Boelens, R., van Es, D. S., et al. (2016). New insights into the structure and composition of technical lignins: a comparative characterisation study. *Green Chem.* 18, 2651–2665. doi: 10.1039/c5gc03043a
- Doi, Y., Kunioka, M., Nakamura, Y., and Soga, K. (1988). Nuclear magnetic resonance studies on unusual bacterial copolyesters of 3-hydroxybutyrate and 4-hydroxybutyrate. *Macromolecules* 21, 2722–2727. doi: 10.1021/ma00187a012
- Duan, J., Huo, X., Du, W. J., Liang, J. D., Wang, D. Q., and Yang, S. C. (2016). Biodegradation of kraft lignin by a newly isolated anaerobic bacterial strain, *Acetanaerobium* sp. WJDL-Y2. *Lett. Appl. Microbiol.* 62, 55–62. doi: 10.1111/lam.12508
- El Mansouri, N.-E., and Salvadó, J. (2007). Analytical methods for determining functional groups in various technical lignins. *Ind. Crops Prod.* 26, 116–124. doi: 10.1016/j.indcrop.2007.02.006
- Faix, O. (1991). Classification of Lignins from Different Botanical Origins by FT-IR Spectroscopy. *Holzforschung Int. J. Biol. Chem. Phys. Technol. Wood* 45:21. doi: 10.1515/hfsg.1991.45.s1.21
- Gall, D. L., Ralph, J., Donohue, T. J., and Noguera, D. R. (2014). A group of sequence-related sphingomonad enzymes catalyzes cleavage of β -Aryl Ether linkages in lignin β -Guaiaacyl and β -Syringyl ether dimers. *Environ. Sci. Technol.* 48, 12454–12463. doi: 10.1021/es503886d
- Gianfreda, L., Xu, F., and Bollag, J.-M. (1999). Laccases: a useful group of oxidoreductive enzymes. *Bioremed. J.* 3, 1–26. doi: 10.1080/10889869991219163
- Gillgren, T., Hedenström, M., and Jönsson, L. J. (2017). Comparison of laccase-catalyzed cross-linking of organosolv lignin and lignosulfonates. *Int. J. Biol. Macromol.* 105, 438–446. doi: 10.1016/j.ijbiomac.2017.07.061
- Gioia, C., Banella, M. B., Totaro, G., Vannini, M., Marchese, P., Colonna, M., et al. (2018). Biobased vanillic acid and ricinoleic acid: building blocks for fully renewable copolyesters. *J. Ren. Mater.* 6, 126–135. doi: 10.7569/jrm.2017.634191
- González, M. A. (2015). Aromatic abietane diterpenoids: their biological activity and synthesis. *Nat. Prod. Rep.* 32, 684–704. doi: 10.1039/c4np00110a
- Gordobil, O., Moriana, R., Zhang, L., Labidi, J., and Sevastyanova, O. (2016). Assessment of technical lignins for uses in biofuels and biomaterials: structure-related properties, proximate analysis and chemical modification. *Ind. Crops Prod.* 83, 155–165. doi: 10.1016/j.indcrop.2015.12.048
- Hack, E., Hümmer, D., and Franzreb, M. (2019). Concentration of crotonic acid using capacitive deionization technology. *Separat. Purificat. Technol.* 209, 658–665. doi: 10.1016/j.seppur.2018.08.049
- Hallac, B. B., and Ragauskas, A. J. (2014). “CHAPTER 4 lignin modification to reduce the recalcitrance of biomass processing,” in *Biological Conversion of Biomass for Fuels and Chemicals: Explorations From Natural Utilization Systems*, (Cambridge, UK: Royal Society of Chemistry), 37–52. doi: 10.1039/9781849734738-00037
- Helmich, K. E., Pereira, J. H., Gall, D. L., Heins, R. A., McAndrew, R. P., Bingman, C., et al. (2016). Structural basis of stereospecificity in the bacterial enzymatic cleavage of β -Aryl ether bonds in lignin. *J. Biol. Chem.* 291, 5234–5246. doi: 10.1074/jbc.m115.694307
- Janßen, H. J., and Steinbüchel, A. (2014). Fatty acid synthesis in *Escherichia coli* and its applications towards the production of fatty acid based biofuels. *Biotechnol. Biofuels* 7:7. doi: 10.1186/1754-6834-7-7
- Kim, J., Kim, J., Um, Y., and Kim, K. H. (2019). Intracellular metabolite profiling and the evaluation of metabolite extraction solvents for *Clostridium carboxidivorans* fermenting carbon monoxide. *Proc. Biochem.* 89, 20–28. doi: 10.1016/j.procbio.2019.10.012
- Kim, K. H., Dutta, T., Walter, E. D., Isern, N. G., Cort, J. R., Simmons, B. A., et al. (2017). Chemoselective methylation of phenolic Hydroxyl group prevents quinone methide formation and repolymerization during lignin depolymerization. *ACS Sustain. Chem. Eng.* 5, 3913–3919. doi: 10.1021/acssuschemeng.6b03102
- Kohlstedt, M., Starck, S., Barton, N., Stolzenberger, J., Selzer, M., Mehlmann, K., et al. (2018). From lignin to nylon: cascaded chemical and biochemical conversion using metabolically engineered *Pseudomonas putida*. *Metab. Eng.* 47, 279–293. doi: 10.1016/j.ymben.2018.03.003
- Kosa, M., and Ragauskas, A. J. (2013). Lignin to lipid bioconversion by oleaginous rhodococci. *Green Chem.* 15, 2070–2074.
- Lee, H. H., Molla, M. N., Cantor, C. R., and Collins, J. J. (2010). Bacterial charity work leads to population-wide resistance. *Nature* 467, 82–85. doi: 10.1038/nature09354
- Li, Z., Nimtz, M., and Rinas, U. (2014). The metabolic potential of *Escherichia coli* BL21 in defined and rich medium. *Microb. Cell Fact.* 13, 45. doi: 10.1186/1475-2859-13-45
- Margot, J., Bennati-Granier, C., Maillard, J., Blázquez, P., Barry, D. A., and Holliger, C. (2013). Bacterial versus fungal laccase: potential for micropollutant degradation. *AMB Express* 3:63.
- Moya, R., Saastamoinen, P., Hernández, M., Suurnäkki, A., Arias, E., and Mattinen, M.-L. (2011). Reactivity of bacterial and fungal laccases with lignin under alkaline conditions. *Bioresour. Technol.* 102, 10006–10012.
- Nugroho Prasetyo, E., Kudanga, T., Østergaard, L., Rencoret, J., Gutiérrez, A., del Río, J. C., et al. (2010). Polymerization of lignosulfonates by the laccase-HBT (1-hydroxybenzotriazole) system improves dispersibility. *Bioresour. Technol.* 101, 5054–5062.
- Perez, J. M., Kontur, W. S., Alherech, M., Coplien, J., Karlen, S. D., Stahl, S. S., et al. (2019). Funneling aromatic products of chemically depolymerized lignin into 2-pyrone-4-6-dicarboxylic acid with *Novosphingobium aromaticivorans*. *Green Chem.* 21, 1340–1350.
- Rajan, R., Skrifvars, M., and Järvelä, P. (2014). “Lactic Acid Polymers: Synthesis, Properties, and Applications,” in *Handbook of Green Materials*, eds K. Oksman, P. P. Mathew, A. Bismarck, O. Rojas, and M. Sainpp (Singapore: World Scientific), 49–65.
- Reyes-Rivera, J., and Terrazas, T. (2017). Lignin Analysis by HPLC and FTIR. *Methods Mol. Biol.* 1544, 193–211.
- Ruijsenaars, H. J., and Hartmans, S. (2004). A cloned *Bacillus halodurans* multicopper oxidase exhibiting alkaline laccase activity. *Appl. Microbiol. Biotechnol.* 65, 177–182.
- Saito, T., Perkins, J. H., Jackson, D. C., Trammel, N. E., Hunt, M. A., and Naskar, A. K. (2013). Development of lignin-based polyurethane thermoplastics. *RSC Adv.* 3, 21832–21840.
- Sapaporn, N., Chaijamrus, S., Chatdumrong, W., and Tochampa, W. (2018). Degradation and polymerization of black liquor lignin using *Bacillus* sp. isolated from a pulp mill. *Bioresources* 14, 1049–1076.
- Sendovski, M., Nir, N., and Fishman, A. (2010). Bioproduction of 2-phenylethanol in a biphasic ionic liquid aqueous system. *J. Agric. Food Chem.* 58, 2260–2265.
- Sharma, R. K., Mukhopadhyay, D., and Gupta, P. (2019). Microbial fuel cell-mediated lignin depolymerization: a sustainable approach. *J. Chem. Technol. Biotechnol.* 94, 927–932.
- Shi, Y., Yan, X., Li, Q., Wang, X., Liu, M., Xie, S., et al. (2017). Directed bioconversion of Kraft lignin to polyhydroxyalkanoate by *Cupriavidus basilensis* B-8 without any pretreatment. *Process Biochem.* 52, 238–242.
- Shinoda, E., Takahashi, K., Abe, N., Kamimura, N., Sonoki, T., and Masai, E. (2019). Isolation of a novel platform bacterium for lignin valorization and its application in glucose-free cis,cis-muconate production. *J. Ind. Microbiol. Biotechnol.* 46, 1071–1080.

- Stefanska, J., and Pawliczak, R. (2008). Apocynin: molecular aptitudes. *Mediators Inflamm.* 2008, 106507–106507.
- Suman, S. K., Dhawaria, M., Tripathi, D., Raturi, V., Adhikari, D. K., and Kanaujia, P. K. (2016). Investigation of lignin biodegradation by *Trabulsiella* sp. isolated from termite gut. *Int. Biodeteriorat. Biodegradat.* 112, 12–17.
- Sun, J.-X., Sun, X.-F., Sun, R.-C., Fowler, P., and Baird, M. S. (2003). Inhomogeneities in the chemical structure of sugarcane bagasse lignin. *J. Agric. Food Chem.* 51, 6719–6725.
- Vahermo, M., Krogerus, S., Nasereddin, A., Kaiser, M., Brun, R., Jaffe, C. L., et al. (2016). Antiprotozoal activity of dehydroabietic acid derivatives against *Leishmania donovani* and *Trypanosoma cruzi*. *MedChemComm* 7, 457–463.
- Van den Bosch, S., Koelewijn, S. F., Renders, T., Van den Bossche, G., Vangeel, T., Schutyser, W., et al. (2018). Catalytic strategies towards lignin-derived chemicals. *Top. in Curr. Chem.* 376:36.
- Vinardell, M. P., and Mitjans, M. (2017). Lignins and their derivatives with beneficial effects on human health. *Int. J. Mol. Sci.* 18:1219.
- Wade, L. G. J. (2013). *Organic Chemistry*, 8th Edn. London: Pearson.
- Xi, X., Hu, S., Zhou, Z., Liu, X., Tang, J., and Shen, Y. (2016). Dendrimers with the protocatechuic acid building block for anticancer drug delivery. *J. Mater. Chem. B* 4, 5236–5245.
- Xu, F. (1997). Effects of redox potential and hydroxide inhibition on the pH activity profile of fungal laccases. *J. Biol. Chem.* 272, 924–928.
- Xu, Z., Lei, P., Zhai, R., Wen, Z., and Jin, M. (2019). Recent advances in lignin valorization with bacterial cultures: microorganisms, metabolic pathways, and bio-products. *Biotechnol. Biofuels* 12, 32–32.
- Yang, H., Yan, R., Chen, H., Lee, D. H., and Zheng, C. (2007). Characteristics of hemicellulose, cellulose and lignin pyrolysis. *Fuel* 86, 1781–1788.
- Yang, S., Yu, H., You, Y., Li, X., and Jiang, J. (2018). Effective lactic acid production from waste paper using *Streptococcus thermophilus* at low enzyme loading assisted by Gleditsia saponin. *Carbohydrate Polym.* 200, 122–127.
- Yang, Y., Song, W.-Y., Hur, H.-G., Kim, T.-Y., and Ghatge, S. (2019). Thermoalkaliphilic laccase treatment for enhanced production of high-value benzaldehyde chemicals from lignin. *Int. J. Biol. Macromol.* 124, 200–208.
- Yu, H., Hou, J., Yu, S., Liu, S., Li, L., Wu, Q., et al. (2019). Comprehensive understanding of the non-productive adsorption of cellulolytic enzymes onto lignins isolated from furfural residues. *Cellulose* 26, 3111–3125.
- Zhu, D., Si, H., Zhang, P., Geng, A., Zhang, W., Yang, B., et al. (2018). Genomics and biochemistry investigation on the metabolic pathway of milled wood and alkali lignin-derived aromatic metabolites of *Comamonas serinivorans* SP-35. *Biotechnol. Biofuels* 11:338.
- Zhu, D., Tanabe, S.-H., Xie, C., Honda, D., Sun, J., and Ai, L. (2014). *Bacillus ligniniphilus* sp. nov., an alkaliphilic and halotolerant bacterium isolated from sediments of the South China Sea. *Int. J. Syst. Evol. Microbiol.* 64, 1712–1717.
- Zhu, D., Zhang, P., Xie, C., Zhang, W., Sun, J., Qian, W.-J., et al. (2017). Biodegradation of alkaline lignin by *Bacillus ligniniphilus* L1. *Biotechnol. Biofuels* 10:4.

Conflict of Interest: The authors declare that the research was conducted in the absence of any commercial or financial relationships that could be construed as a potential conflict of interest.

Copyright © 2020 Murillo Morales, Ali, Si, Zhang, Zhang, Hosseini, Sun and Zhu. This is an open-access article distributed under the terms of the Creative Commons Attribution License (CC BY). The use, distribution or reproduction in other forums is permitted, provided the original author(s) and the copyright owner(s) are credited and that the original publication in this journal is cited, in accordance with accepted academic practice. No use, distribution or reproduction is permitted which does not comply with these terms.



Global Reprogramming of Gene Transcription in *Trichoderma reesei* by Overexpressing an Artificial Transcription Factor for Improved Cellulase Production and Identification of Ypr1 as an Associated Regulator

Fei Zhang¹, Jia-Xiang Li¹, Verawat Champreda², Chen-Guang Liu¹, Feng-Wu Bai¹ and Xin-Qing Zhao^{1*}

OPEN ACCESS

Edited by:

Min Jiang,
Nanjing Tech University, China

Reviewed by:

Fengxue Xin,
Nanjing Tech University, China
Jiazhang Lian,
Zhejiang University, China

*Correspondence:

Xin-Qing Zhao
xqzhao@sjtu.edu.cn

Specialty section:

This article was submitted to
Synthetic Biology,
a section of the journal
Frontiers in Bioengineering and
Biotechnology

Received: 20 March 2020

Accepted: 27 May 2020

Published: 03 July 2020

Citation:

Zhang F, Li J-X, Champreda V, Liu C-G, Bai F-W and Zhao X-Q (2020) Global Reprogramming of Gene Transcription in *Trichoderma reesei* by Overexpressing an Artificial Transcription Factor for Improved Cellulase Production and Identification of Ypr1 as an Associated Regulator. *Front. Bioeng. Biotechnol.* 8:649. doi: 10.3389/fbioe.2020.00649

¹ State Key Laboratory of Microbial Metabolism, Joint International Research Laboratory of Metabolic & Developmental Sciences, School of Life Sciences and Biotechnology, Shanghai Jiao Tong University, Shanghai, China, ² Biorefinery and Bioproduct Research Group, Enzyme Technology Laboratory, National Center for Genetic Engineering and Biotechnology, Pathum Thani, Thailand

Synthetic biology studies on filamentous fungi are providing unprecedented opportunities for optimizing this important category of microbial cell factory. Artificial transcription factor can be designed and used to offer novel modes of regulation on gene transcription network. *Trichoderma reesei* is commonly used for cellulase production. In our previous studies, a plasmid library harboring genes encoding artificial zinc finger proteins (AZFPs) was constructed for engineering *T. reesei*, and the mutant strains with improved cellulase production were selected. However, the underlying mechanism by which AZFP function remain unclear. In this study, a *T. reesei* Rut-C30 mutant strain *T. reesei* U5 bearing an AZFP named as AZFP-U5 was focused, which secretes high level protein and shows significantly improved cellulase and xylanase production comparing with its parental strain. In addition, enhanced sugar release was achieved from lignocellulosic biomass using the crude cellulase from *T. reesei* U5. Comparative transcriptome analysis was further performed, which showed reprogramming of global gene transcription and elevated transcription of genes encoding glycoside hydrolases by overexpressing AZFP-U5. Furthermore, 15 candidate regulatory genes which showed remarkable higher transcription levels by AZFP-U5 insertion were overexpressed in *T. reesei* Rut-C30 to examine their effects on cellulase biosynthesis. Among these genes, *TrC30_93861* (*ypr1*) and *TrC30_74374* showed stimulating effects on filter paper activity (FPase), but deletion of these two genes did not affect cellulase activity. In addition, increased yellow pigment production in *T. reesei* Rut-C30 by overexpression of gene *ypr1* was observed, and changes of cellulase gene transcription were revealed in the *ypr1* deletion mutant, suggesting possible interaction between pigment production and cellulase

gene transcription. The results in this study revealed novel aspects in regulation of cellulase gene expression by the artificial regulators. In addition, the candidate genes and processes identified in the transcriptome data can be further explored for synthetic biology design and metabolic engineering of *T. reesei* to enhance cellulase production.

Keywords: *Trichoderma reesei*, cellulase production, artificial zinc finger protein, comparative transcriptome analysis, transcription factor, lignocellulosic biomass

INTRODUCTION

Cellulase is widely used in detergents, textiles, pulp processing, food, and feed industries (Sharma et al., 2016). The application of cellulase in lignocellulosic biorefinery for producing renewable biofuels and biochemicals has particularly received widespread interest owing to the gradual depletion of fossil fuels and environmental concerns (Tiwari et al., 2018). Efficient production of cellulases is essential for reducing the bioconversion cost of lignocellulosic biomass. *Trichoderma reesei* (an anamorph of *Hypocrea jecorina*) and its derivative strains have been widely used for cellulase production (Bischof et al., 2016). However, so far high cellulase production cost is still a bottleneck for practical applications.

The *T. reesei* genome commonly contains over 220 putative genes encoding candidate carbohydrate-active enzymes (CAZymes), which include cellulases such as cellobiohydrolases (CBH), endoglucanases (EG), and β -glucosidases (BGL), as well as hemicellulases. In addition, auxiliary proteins that hydrolyze lignocellulose synergistically are also important for biodegradation of cellulosic feedstocks (Hakkinen et al., 2012). Cellulase biosynthesis by *T. reesei* is induced by various inducers such as cellulose, sophorose, lactose, and cellobiose, but is repressed by glucose. Besides these carbon sources, cellulase production is also responsive to a variety of environmental and physiological factors, such as Ca^{2+} , light, pH, and physiological state of the mitochondria (Abrahamo Neto et al., 1995; He et al., 2014; Chen et al., 2016; Schmoll, 2018). On the other hand, transcription factors also play important roles in cellulase production. So far, several key regulatory factors were well-characterized. Transcription factor Xyr1 is the major positive regulator governing a complex regulatory network for expression of (hemi-) cellulase genes, and recently, the function of Ace3 is characterized for cellulase production, and its cross talk with Xyr1 and Crt1 was revealed (Zhang et al., 2019). Furthermore, other regulators, such as Ace2, BglR, and Vib1 have also been identified to regulate cellulase production (Aro et al., 2001; Nitta et al., 2012; Zhang et al., 2018a). Recently, our group identified a novel repressor Ctf1 for cellulase biosynthesis in *T. reesei* Rut-C30 (Meng et al., 2020). In addition, transcription factor Cre1 mediates carbon catabolite repression (CCR) to suppress cellulase expression (Nakari-Setälä et al., 2009). However, the detailed regulatory mechanisms of cellulase production from *T. reesei* are known to be complicated and are still not fully clear.

Synthetic biology studies of *T. reesei* are still in its early stage, but have opened new opportunities for metabolic engineering of this important species (Druzhinina and Kubicek, 2017; Liu and Qu, 2019). Artificial transcription factors (ATFs) could perturb

and remodel the innate regulatory network, leading to new phenotypes (Yang et al., 2019). Several chimeric transcription factors were reported to have positive effects on cellulase production for *T. reesei*, which usually comprised DNA binding domains from characterized regulators with different effector domains, such as minimal transcriptional activators comprising DBDace2(cre1)-linker-VP16AD, regulators DBDxyl1-EDypr1, and Xyr1-DBDcre1 (Zhang et al., 2017, 2018b; Derntl et al., 2019). Also, some novel fused regulators containing DBDcre1 and activation domains of Ace3, Clr2, Ace2, or Xyr1 were found to regulate the cellulase production profile in *T. reesei*, especially for CBH1 (Wang et al., 2019).

In our previous studies, the artificial zinc finger protein (AZFP) AZFP-U3 containing Cyc2-His2 type DNA binding domain significantly enhanced cellulase production in *T. reesei* Rut-C30 (Zhang et al., 2016). In our recent report, AZFP-M2 also led to improved cellulase activity in *T. reesei* Rut-C30 (Meng et al., 2020), but these two AZFPs showed different stimulating patterns on cellulase compositions. It will be of great interest to test more AZFPs for their regulatory functions, and reveal how the ATFs regulate cellulase production in *T. reesei*.

In this study, an additional AZFP which we named AZFP-U5 was identified to have a positive effect on cellulase production in *T. reesei* Rut-C30, whose feature on the regulatory network was further analyzed by comparative transcriptome analysis. Meanwhile, candidate regulatory genes related to cellulase production were further explored. The results in this study would provide novel insights in synthetic biology design and metabolic engineering of *T. reesei* for cellulase production.

MATERIALS AND METHODS

Strains and Culture Media

T. reesei Rut-C30 was obtained from ARS Culture Collection (NRRL, Peoria, IL). Conidial suspensions were prepared by cultivating the strain on malt extract agar (MEA) medium (20 g/L Malt extract, 20 g/L Agar) at 28°C for 7 days. After harvesting, the conidia were suspended in 20% glycerol, which were then gauze-filtered, and stored at -80°C before use. Mandels-Andreotti (MA) medium (Mandels and Andreotti, 1978) containing 2% (m/v) microcrystalline cellulose (Merck, Germany) and 2% (m/v) wheat bran was used as a cellulase production medium. To induce cellulase production in the presence of soluble carbon sources, the carbon source in MA medium was replaced with 2% (m/v) glucose or 2% (m/v) lactose.

For cellulase production, the conidia of *Trichoderma* strains were collected from MEA medium, and cultured in 50 ml MA

medium in a 250 mL Erlenmeyer flask supplemented with 0.1% (w/v) peptone and 2% (w/v) glucose to induce spore germination. After pre-cultivation at 28°C and 150 rpm in a rotary shaker for 24 h, 5 mL mycelia were taken from the germination medium and were added into 45 mL cellulase production medium in a 250 mL flask (10% inoculation size).

Escherichia coli DH5 α was used for plasmid propagation and DNA manipulation. *Agrobacterium tumefaciens* AGL-1 was used for the *A. tumefaciens*-mediated genetic transformation (ATMT) of *T. reesei*. Transformation of *A. tumefaciens* AGL-1 with the pCB303-ZFP library and screening of *T. reesei* mutants were performed using the methods described previously (Zhang et al., 2016). The *T. reesei* U5 mutant strain selected from the mutants was preserved in China General Microbiological Culture Collection Center (CGMCC) with the accession number of CGMCC 10649.

Determination of Cellulase Activity, Protein Concentration, and Sporulation Assay

The *T. reesei* cultured sample (1 mL) was collected each day and centrifuged at 10,000 rpm for 5 min, from which the supernatant was used for cellulase activity measurement and protein concentration assay. Filter paper activity (FPase activity), endoglucanase (CMCase) activity, and β -glucosidase activity were measured according to the standard IUPAC procedures. The FPase activity is expressed as filter paper units, one unit of filter paper enzymatic activity is defined as the amount of enzyme that releases 1 μ mol of glucose per minute from 50 mg filter paper stripe. The total xylanase activity was assayed with 1% beechwood xylan (Sigma-Aldrich, USA) as the substrate according to the standard protocol (Bailey et al., 1992). Concentration of extracellular protein was measured by the Bio-Rad Protein Assay Kit (Bio-Rad, USA) following the manufacturer's instructions.

For sporulation assay, an aliquot of 10 μ L (10^8 /L) spores of the *T. reesei* strains were cultivated on MEA plates at 28°C for 7 days to obtain mature conidia, which were collected and counted using a hemocytometer.

Construction of *T. reesei* Mutants Overexpressing and Deleting Various Putative Regulatory Genes

All primers used for strain construction and confirmation were listed in Table S1. In order to study the effect of AZFP-U5 on cellulase synthesis in *T. reesei*, its nucleic acid sequence was amplified by PCR with the primers pCB303-U5-F and pCB303-U5-R, and the PCR product was ligated into the expression vector pCB303, then transformed into *T. reesei* Rut-C30 using the ATMT method. After confirmation of the correct transformants, the cellulase activities of at least three randomly selected transformants were determined.

For construction of the *T. reesei* mutants overexpressing endogenous putative regulators, the PCR products of 15 corresponding putative regulatory genes amplified from genomic cDNA were fused, respectively, into the pCZF3 vector (Zhang et al., 2018a) digested by *Nco* I and *Xba* I using Seamless Cloning Master Mix (Sangon Biotech, China). Each

ligated product was then transformed into *T. reesei* Rut-C30 using the ATMT method, putative regulatory genes were overexpressed individually, driven by the pyruvate decarboxylase (*pdh*) promoter.

Regarding the construction of *TrC30_93861* (*ypr1*) or *TrC30_74374* knockout strains, the 2,000-bp upstream and downstream region of the corresponding genes were amplified from *T. reesei* Rut-C30 genome as the homologous arms individually. The hygromycin B resistance gene *hph* was employed as the selected marker, and the expression cassette was amplified from the pCZF3 vector using primers hphCAS-F and hphCAS-R. Then, the *hph* expression cassette together with the 2,000-bp flanking arms were cloned into plasmid pZF-MCS at *Hind* III and *Eco* R I sites using ClonExpressTM II One Step Cloning Kit (Vazyme, China), resulting in the plasmid pZF-93861D and pZF-74374D. The plasmids pZF-93861D and pZF-74374D were then introduced into *T. reesei* Rut-C30 $\Delta ku70$ by the ATMT method. The correct deletion mutants were verified using four pairs of specific deletion primers, and the design scheme for strain constructions and verifications are provided in Figure S3.

Determination of the Copy Number and Integrated Site of AZFP-U5

To determine the copy number of the AZFP encoding gene *AZFP-U5* in the *T. reesei* U5, genomic DNA of *T. reesei* U5 was isolated and used as the template for quantitative PCR (qPCR) with the primers AZFPU5-F and AZFPU5-R. The qPCR method is the same as that described by Solomon et al. (2008), in which *tefla* (translation elongation factor 1- α) was used as a control for a single copy. Correspondingly, the integrated site of the *AZFP-U5* was determined by the thermal asymmetric interlaced PCR (TAIL-PCR) according to the procedure described elsewhere (Liu and Chen, 2007). Additionally, the copy number of *hph* expression cassette in respective regulator deletion mutants was verified by qPCR with the primers hphqPCR-F and hphqPCR-R. The primers used for qPCR and TAIL-PCR are listed in Table S2.

Comparative Transcriptome Analysis

T. reesei U5 and Rut-C30 were grown in the MA medium with cellulose as the carbon source, then, the total RNAs from the mycelia were isolated at 24 and 48 h using the RNA extraction kit (Sangon Biotech, China). RNA sequencing (RNA-Seq) was performed at the BGI Company (Shenzhen, China) using the Illumina HiSeq2000 system. Gene expression levels were calculated using the fragments per kilobase of exon model per million reads (FPKM) method (Mortazavi et al., 2008). Threshold values of $|\log_2$ FC (fold change of U5 to Rut-C30)| ≥ 1 and FDR (False Discovery Rate) < 0.001 were used to judge the significance. Genes were annotated according to the *T. reesei* Rut-C30 genome annotation, and proteins involved in CAZymes, transcription factors, transporters, secondary metabolism clusters, protein processing, and secretion were referred to genome database of Joint Genome Institute (https://mycocosm.jgi.doe.gov/pages/search-for-genes.jsf?organism=TrireRUTC30_1) (Grigoriev et al., 2014).

To elucidate the effects of *ypr1* in pigment production, *T. reesei* $\Delta ypr1$ and its parent strain *T. reesei* Rut-C30 $\Delta ku70$ were cultured in the MA medium with 2% glucose as a carbon source, then the mycelia of these two strains at 24 h were collected for total RNA extraction. The process of transcriptome analysis for *T. reesei* $\Delta ypr1$ and Rut-C30 $\Delta ku70$ is the same as described above for *T. reesei* U5 and Rut-C30. The mRNA profile for specific genes was also analyzed for verification of RNA-seq results with corresponding primers (Table S1). The NCBI accession numbers for transcriptome data of *T. reesei* U5 and Rut-C30, *T. reesei* $\Delta ypr1$ and Rut-C30 $\Delta ku70$ are PRJNA612708 and PRJNA613769, respectively.

Enzymatic Hydrolysis of the Pretreated Biomass

Biomass hydrolysis efficiency of cellulase produced by *T. reesei* was measured using alkaline pretreated corn stover (APCS). Corn stover was pretreated by 2% (w/v) sodium hydroxide and 2% (w/v) hydrogen peroxide, washed to reach neutral pH, and lignocellulose components and hydrolysis were measured according to the method described previously (Zhang et al., 2016). Hydrolysis experiment was carried out at 5% total solids loading with APCS as the substrate, and the cellulase loading was 30 mg per gram of dry biomass. The hydrolysis conditions are incubation at 50°C, pH 4.8, shaking at 150 rpm for 48 h, and samples were collected at an interval of 12 h. The sugar ingredients and concentrations released in the hydrolysate were analyzed by HPLC. The experiments were performed in triplicate, and the results are represented as the average values \pm standard deviation (SD).

RESULTS

Cellulase Properties of *T. reesei* Rut-C30 and U5

The mutant strain *T. reesei* U5 with improved cellulase production was selected from the *T. reesei* Rut-C30 transformants transformed by the AZFP library (Zhang et al., 2016). The AZFP sequence from the transformant *T. reesei* U5 was named as AZFP-U5, and the corresponding gene *AZFP-U5* was found to integrate into the genome as a single copy. The single integration site was identified to be located at the scaffold 33: 124903–124921 of *T. reesei* Rut-C30 chromosome, which is the intergenic region between terminators of two genes of *TrC30_91501* and *TrC30_91570*, indicating that *AZFP-U5* functions without disrupting other functional genes.

With cellulose as the carbon source in the MA medium, the FPase activity of *T. reesei* U5 was 2.1-folds of that from *T. reesei* Rut-C30, reaching 3.31 U/mL on the 7th day, while the FPase activity in the parental strain was 1.56 U/mL (Figure 1A). In addition to increasing the total FPase activity, U5 cellulase also exhibited superior profile for various cellulase components. As shown in Figure S1, the endoglucanase activity of *T. reesei* U5 reached 17.23 U/mL, increased by 1.88 times to that from Rut-C30. The activity of β -glucosidase secreted by U5 strain was 2.76 U/mL, much higher than that from *T. reesei* Rut-C30

(1.09 U/mL). The extracellular xylanase activities of *T. reesei* U5 and Rut-C30 were 596 and 388 U/mL, respectively. Meanwhile, the extracellular proteins of those two strains were significantly different, the amount of protein secretion from *T. reesei* U5 was increased by 86% relative to that from Rut-C30. The extracellular protein concentration from *T. reesei* U5 reached 2.62 mg/mL, while it was about 1.41 mg/mL for Rut-C30 (Figure 1B). When the re-constructed *AZFP-U5* plasmid was transformed into *T. reesei* Rut-C30, the enhanced cellulase production phenotypes were observed in all three randomly selected mutants.

In addition to cellulose, lactose also has an inducing effect on cellulase production. The FPase activities between cellulase U5 and Rut-C30 were found to be significantly different in the fermentation medium containing 2% glucose or lactose as carbon sources, as shown in Figure 1C. On the 6th day of fermentation in glucose medium, the FPase activity from U5 cellulase reached 0.28 U/mL, much higher than that in *T. reesei* Rut-C30 (0.12 U/mL). The FPase activities of cellulase U5 and Rut-C30 in the lactose medium were 0.83 and 0.20 U/mL, respectively, and over 4 times improvement was observed in cellulase U5 compared to that from Rut-C30, which demonstrates that *T. reesei* U5 partially abolished the CCR effect in the presence of glucose and lactose.

The hydrolytic ability for pretreated lignocellulose was further evaluated. In the course of hydrolysis on alkali pretreated corn stover by crude cellulase from *T. reesei* Rut-C30 and U5, the released glucose reached 35.22 g/L (corresponding to \sim 95% cellulose conversion) by the crude cellulase from *T. reesei* U5, which increased by 33.9% compared to that from Rut-C30 (26.30 g/L) at 48 h. Meanwhile, 31% higher xylose yields were also observed by the cellulase produced by *T. reesei* U5. At 48 h, slightly lower residual cellobiose was observed using the cellulase U5 (1.65 vs. 2.03 g/L from the parental strain) (Figure 2).

Transcriptional Changes of Major Cellulases and Transcription Factors

As shown in Figure 3, transcription levels of the five major cellulase components in *T. reesei* U5, including the major cellulase genes *cbh1/2*, *eg1/2*, and *bgl1*, increased significantly (2–16-fold) compared with that of *T. reesei* Rut-C30. In the U5 strain, the transcript of *bgl1* gene increased over 1-fold, and transcription of the endoglucanase genes *eg1* and *eg2* increased by 3-fold at 24 h compared to that in *T. reesei* Rut-C30. At 48 h, the transcription levels of main cellulase genes in *T. reesei* U5 increased by 4–16 times compared to that from Rut-C30, and the transcription levels of the two major xylanase genes *xyn1* and *xyn2* improved 32 and 128 times, respectively. Meanwhile, transcription of the major transcription factor *xyl1* gene also increased, of which the transcript in *T. reesei* U5 was 5-fold to that in Rut-C30 at 48 h. The transcription levels of other regulators for cellulase regulation were also remarkably increased, which include *ace1*, *ace2*, and *bglr*.

The artificial regulator *AZFP-U5* (Table S3) is composed of C₂H₂ type zinc finger and Gal4 effector domain. The zinc finger sequence of *AZFP-U5* is VSSR-RDER-ISNR-QNTQ, and the potential binding site is GYDGHGGAHATA (where Y represents C/T, D represents G/A/T, and H represents C/T/A)

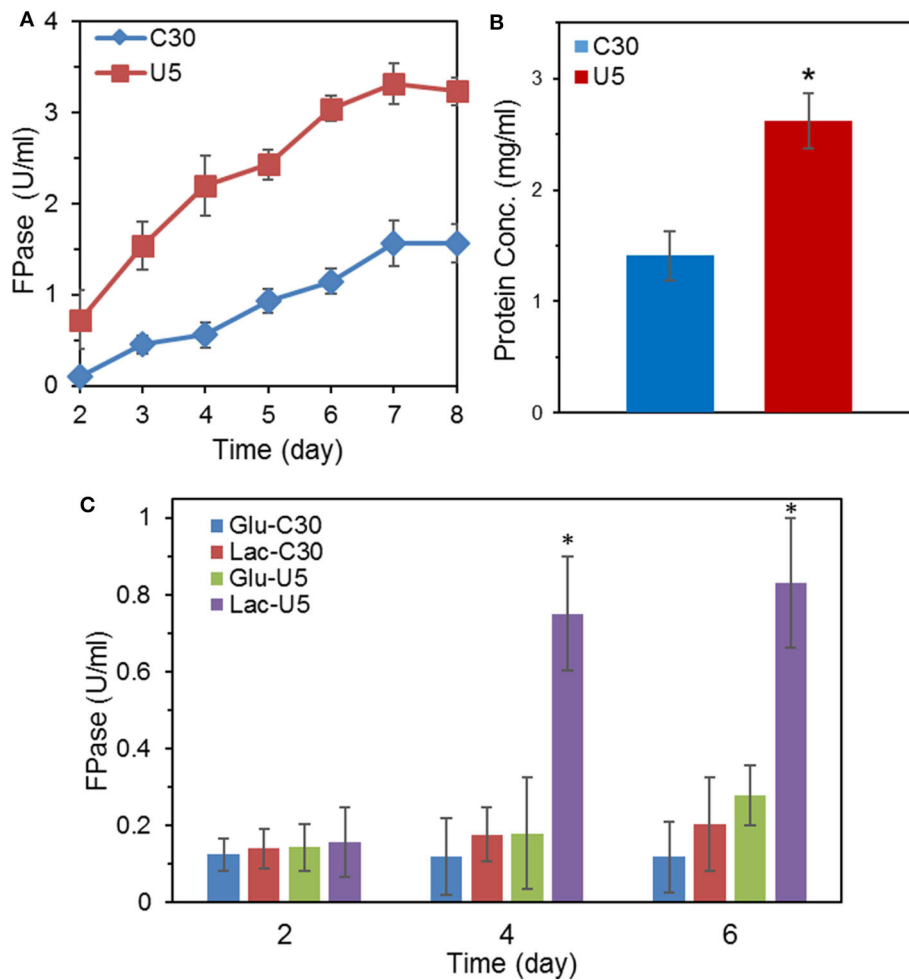


FIGURE 1 | Comparison of FPase activities and secreted protein concentration between the mutant *T. reesei* U5 and the parental strain Rut-C30. **(A)** FPase activities of *T. reesei* U5 and Rut-C30 in MA medium with 2% cellulose and 2% wheat bran as carbon source. **(B)** Extracellular protein concentration of *T. reesei* U5 and Rut-C30 at 7th day's fermentation. **(C)** FPase activities of *T. reesei* U5 and Rut-C30 in MA medium with 2% glucose or lactose as a carbon source. Asterisks indicate significant differences from reference strains (* $p < 0.05$, Student's *t*-test).

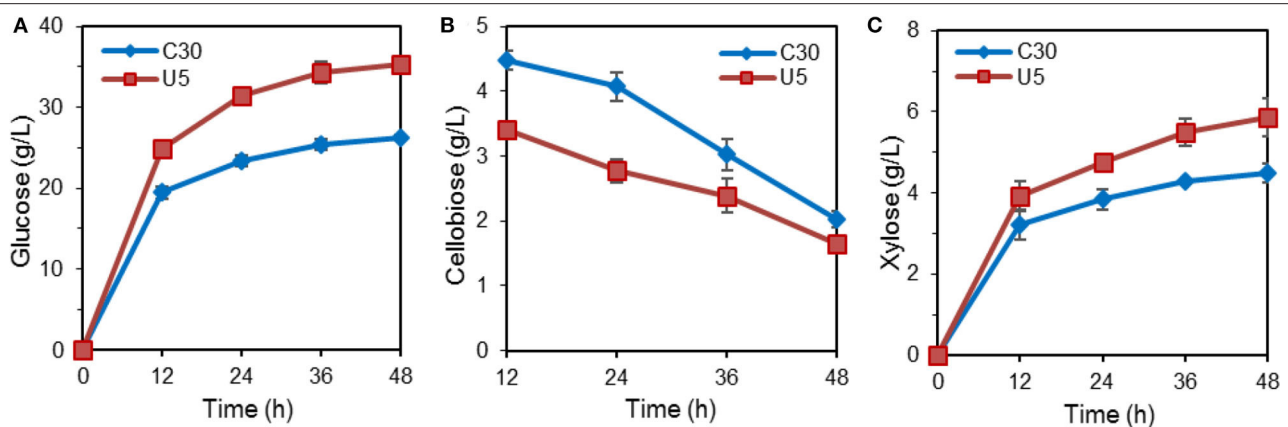
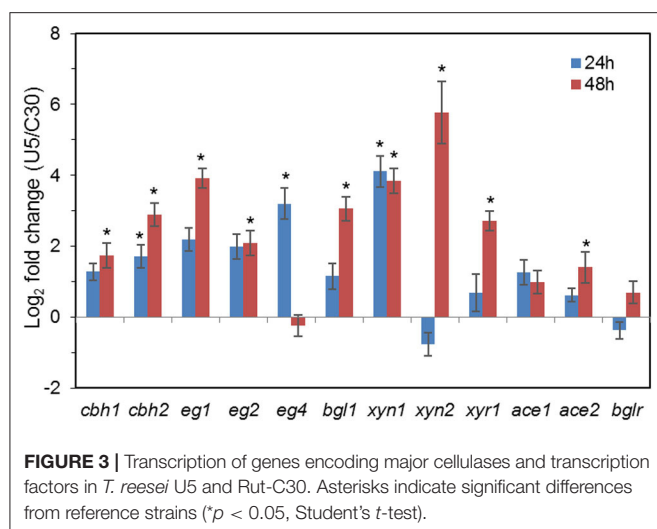


FIGURE 2 | Hydrolysis of pretreated corn stalk by cellulase produced by *T. reesei* U5 and Rut-C30. **(A)** Glucose releasing concentration. **(B)** Cellobiose releasing concentration. **(C)** Xylose releasing concentration.



(Park et al., 2003). After querying the corresponding binding sites in the Rut-C30 genome, 47 from 106 potential binding sites were identified to be located within 1,500 bp upstream of the coding region of specific genes. These 47 genes might be direct targets of the artificial regulator AZFP-U5, of which the profiles of transcripts and potential functions were provided in **Additional file 1**. These genes are related to carbohydrate and nucleic acid metabolism, transcriptional regulatory signaling pathways (transcription factors, protein kinases), protein folding and secretion, putative extracellular proteins, 13 of these 47 potential genes are classified as proteins with unknown functions. Since the transcription of major cellulase and hemicellulase genes in *T. reesei* U5 has increased significantly, it is speculated that proteins related to signal transduction and transcription regulation play a key role for AZFP-U5's regulatory effects. The putative sugar transporter gene (*TrC30_85306*), putative histidine kinase (*TrC30_129764*), and putative protein kinase (*TrC30_93459*) may participate in the cellulase induction and gene expression. The effect of *TrC30_129764* on cellulase production was further tested together with the other regulators, which were described in the section Exploration of New Regulators for *T. reesei* Cellulase Production.

Comparative Transcriptome Analysis of *T. reesei* U5 and Rut-C30

The total transcriptome reads of *T. reesei* U5 and C30 at 24 h were 48,803,620 and 49,017,490, respectively. At 48 h, the reads were 48,988,334 and 48,998,278, respectively, which have met the coverage assessment for the randomness and sequencing saturation assessment. Differentially expressed genes (DEGs) showed that there were 2,203 up-regulated genes and 786 down-regulated genes at 24 h, and 1,500 up-regulated genes and 383 down-regulated genes were observed at 48 h.

In addition to the five glycoside hydrolase genes, five down-regulated genes were randomly selected for RT-qPCR to verify the reliability of the transcriptome data (**Figure S2**). Similar trends of difference were observed by the RT-qPCR analysis

and the transcriptome analysis. Therefore, the transcriptome data of *T. reesei* U5 and C30 can be considered reliable for further analysis.

Gene Ontology (GO) and Functional Category of DEGs

In the course of transcriptome analysis, some functional DEGs exceed 40% of the total corresponding functionally classified genes in several GO terms at 24 h, including biological regulation, cell process regulation, stress response, antioxidant activity, transport activity, and transcriptional regulation (**Figure 4A**). At 48 h, the functional DEGs accounting for over 15% of the overall functional classification genes are located in the following categories, localization function, stress response, membrane fraction, transport activity, and transcription factors (**Figure 4B**). GO analysis at two time points indicated that the transcriptional changes of functional DEGs, such as stress response, transporter and transcription factor proteins, were relatively significant.

Besides the GO analysis, functional category of DEGs between *T. reesei* U5 and Rut-C30 was performed to evaluate statistically significant enrichment of gene functions (**Figure 5**). A number of DEGs were associated with metabolic functions, which account for 20.84 and 18.95% of total DEGs at 24 and 48 h, respectively. More importantly, the functional groups of DEGs included in protein fate (protein translation, folding, modification, sorting, and secretion), RNA processing (synthesis, modification, surveillance, and degradation), and transcription and signal transduction, take up 12.41%, 6.09%, and 10.17% of the total DEGs at 24 h, and 7.66%, 4.11%, and 7.90% at 48 h, respectively (**Table S4**, **Additional file 2**). The functional classification of DEGs demonstrates that RNA and protein processing kept active in *T. reesei* U5, especially at 24 h, which were analyzed in detail below.

Analysis of Genes Encoding Transcription Factors, GHs and Major Transporters

Regulators that potentially play crucial roles in the induction and production of cellulase in *T. reesei* were analyzed. Totally 420 genes in the *T. reesei* genome were predicted to encode transcriptional regulators, from which the transcripts of 223 genes (195 up-regulated; 38 down-regulated) and 91 genes (68 up-regulated; 23 down-regulated) changed significantly at 24 and 48 h, respectively (**Additional file 3**). Although the transcription levels of main cellulases improved remarkably in *T. reesei* U5 during the course of analysis, the known major transcription factor genes, such as *xyr1*, *ace2*, *ace3*, and *vib1*, have not changed consistently at 24 h, whose corresponding transcripts increased to a certain extent at 48 h in *T. reesei* U5 (**Figure 6A**). At 48 h, the transcription of *xyr1* gene in *T. reesei* U5 improved more than 2-folds compared to that in Rut-C30. Meanwhile, the transcript level of the positive regulatory gene *vib1* in *T. reesei* U5 reached 4-fold compared to that in Rut-C30 at 48 h. The Clr-2 homologous protein is the important glycoside hydrolase positive regulator in *Penicillium oxalicum* and *Neurospora crassa* (Coradetti et al., 2012; Li et al., 2015), whose transcript levels in *T. reesei* U5 were 3 and 2-folds to that of Rut-C30 at 24 and 48 h, respectively. Protein functions

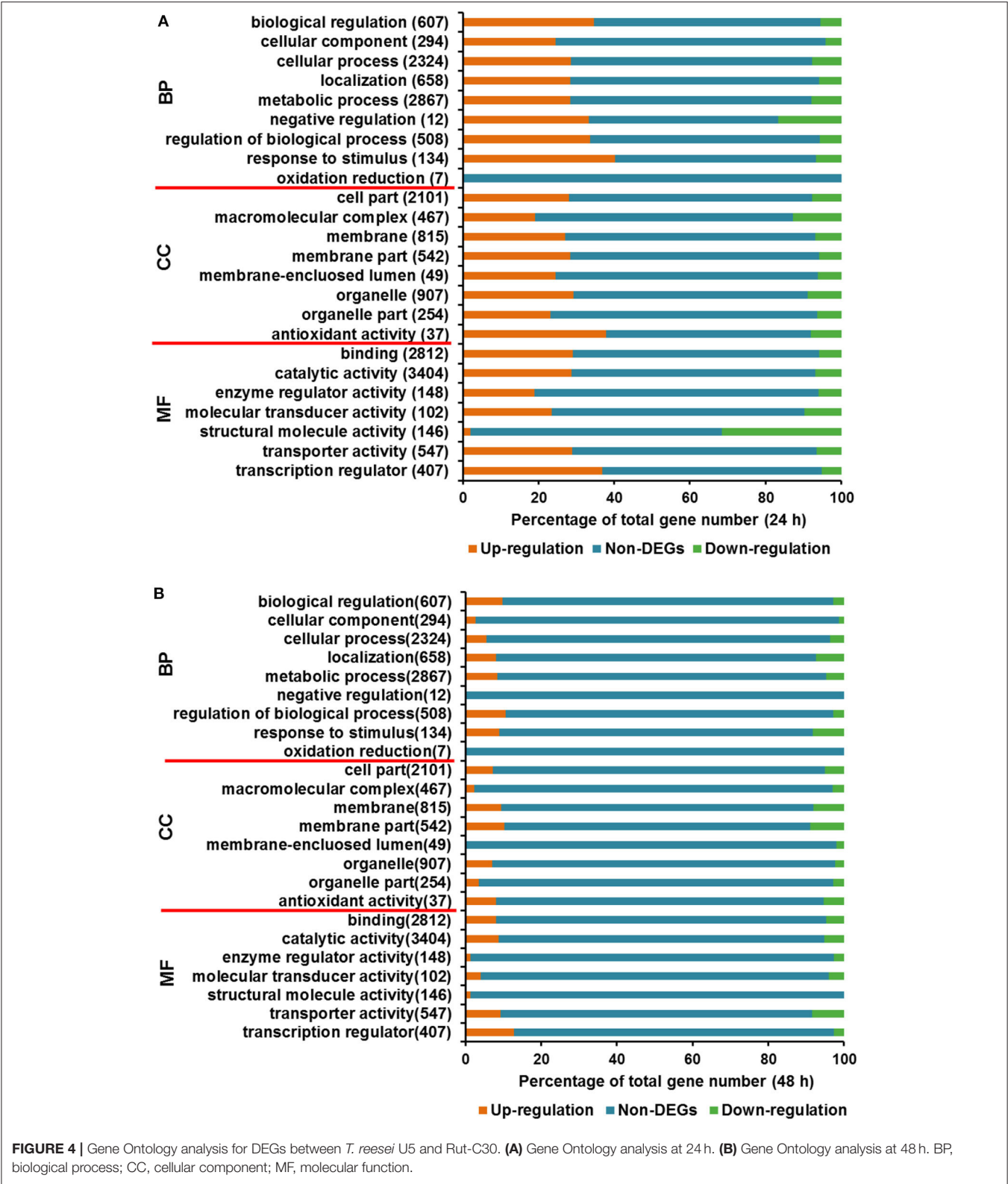
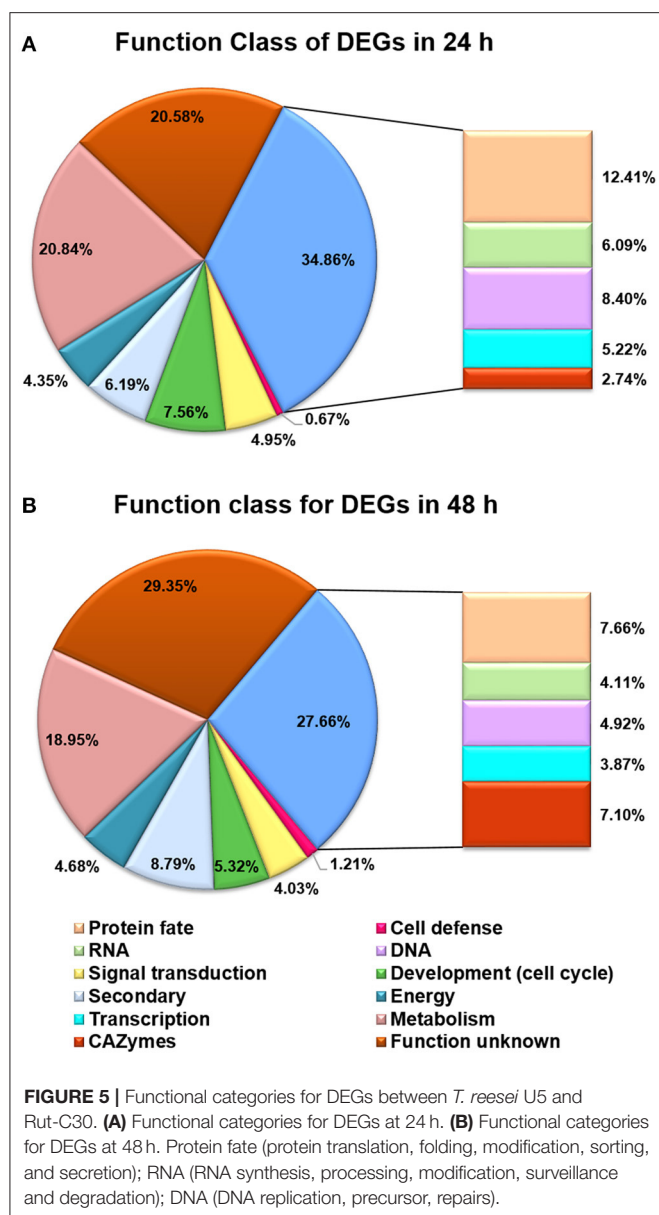


FIGURE 4 | Gene Ontology analysis for DEGs between *T. reesei* U5 and Rut-C30. **(A)** Gene Ontology analysis at 24 h. **(B)** Gene Ontology analysis at 48 h. BP, biological process; CC, cellular component; MF, molecular function.

of several differentially expressed transcription factors have been identified, among which overexpression of the gene *TrC30_81999* has a positive regulatory effect on cellulase production of *T. reesei* (Kubicek, 2013), and the gene *TrC30_101064* encoding the transcription factor Xpp1, has a feedback inhibitory effect on xylanase induction under high-concentration xylose induction



conditions (Derntl et al., 2015). The transcripts of *TrC30_74374* and *TrC30_96554* related to light-mediated regulation in *T. reesei* U5 were up-regulated 16-fold and down-regulated 8-fold at 24 h (Tisch and Schmoll, 2013). The results above provide a basis for further exploring novel regulators for cellulase synthesis and regulation. Interestingly, the transcripts of repressor genes for cellulase production, *ctf1* (*TrC30_10530*) (Meng et al., 2020) and *rce1* (*TrC30_6520*) (Cao et al., 2017), always improved about 1-2-fold in *T. reesei* U5 in the time course compared to that in Rut-C30. The velvet family proteins Ve1 and Ve2 possess positive effect on cellulase, however, the transcript levels of *ve1* (*TrC30_98965*), *ve2* (*TrC30_102739*) in *T. reesei* U5 were similar as that in Rut-C30. Genes *gcn5* (*TrC30_82854*) and *lae1* (*TrC30_9778*) encoding histone acetyltransferase and methyltransferase, respectively, whose functions were verified to

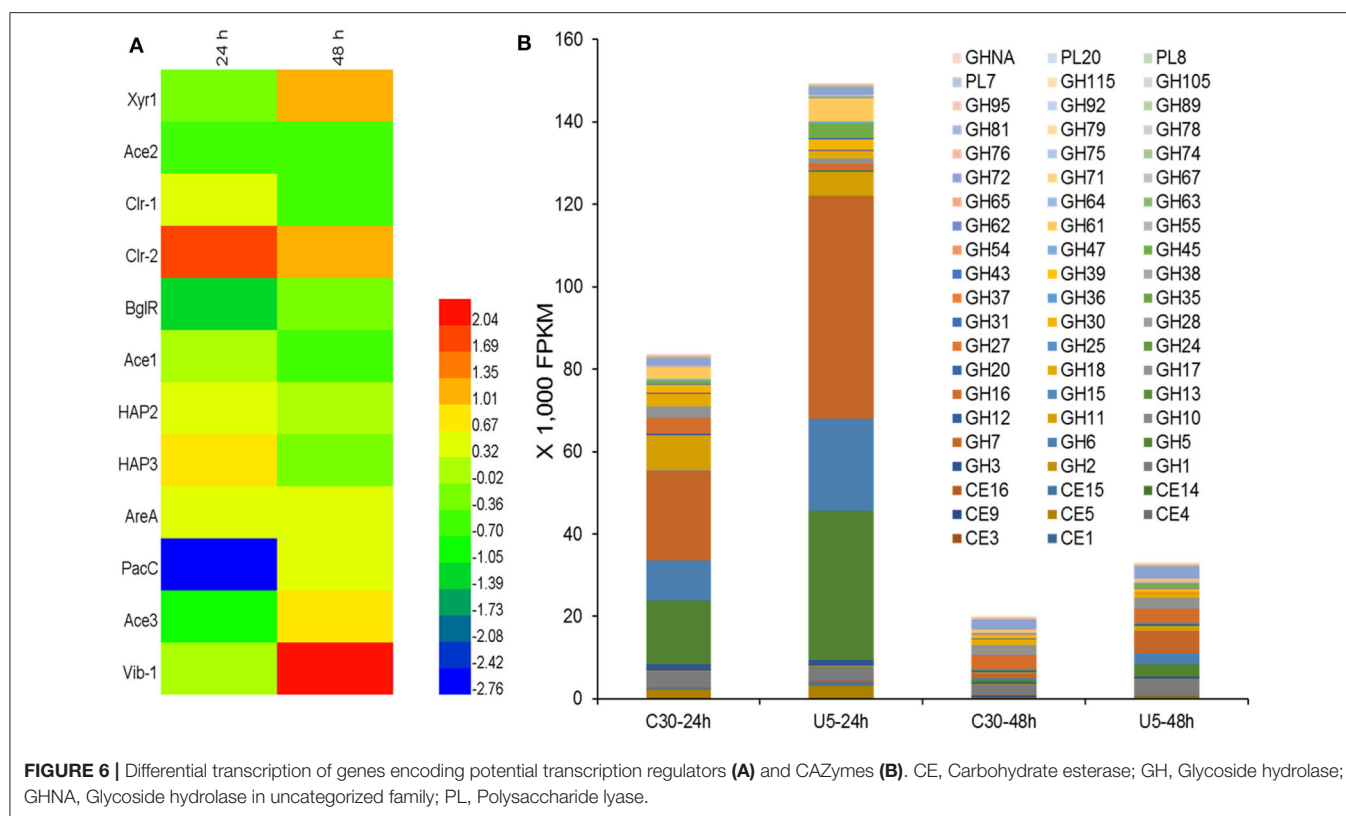
be relevant to cellulase regulation (Seiboth et al., 2012; Xin et al., 2013; Liu et al., 2016), also showed no significant changes.

The main transcription factors Xyr1 and Cre1 proteins could affect transporter family proteins in *T. reesei*, especially major facilitator superfamily (MFS) (dos Santos Castro et al., 2014, 2016), of which several sugar transporters transmit extracellular carbon-induced signals or transport oligosaccharide inducer into cell, such as the sugar transporters Cdt1 and Cdt2 in *N. crassa* (Znameroski et al., 2013), CltB in *Aspergillus nidulans* (dos Reis et al., 2016), and Crt1 (Zhang et al., 2013) in *T. reesei*. About 448 genes in the *T. reesei* genome are predicted to have transporter function (Chaudhary et al., 2016), among which 51 transporter genes changed significantly ($|\text{Log}_2\text{FC}| > 1$, $p < 0.05$). However, the transcription of *crt1* (*TrC30_109243*) kept the same level between *T. reesei* U5 and *T. reesei* Rut-C30. Besides ATP-binding cassette transporter superfamily genes, the transcripts of several predicted sugar transporters also showed the remarkable changes, in which the transcriptional levels of *TrC30_7623*, *TrC30_95062*, *TrC30_97401*, and *TrC30_12083* gene were up-regulated at least 2-fold, whereas transcripts of *TrC30_38765*, *TrC30_136619*, *TrC30_124396*, and *TrC30_133544* decreased at least 1-fold in comparison to that of Rut-C30. The sugar transporters above may play crucial roles on inducer transportation or transmission of carbon signals in *T. reesei* U5, which may re-modulate the profile of cellulase induction and production.

Transcription Analysis of Extracellular Protein Processing

As shown in Figure 6B, the transcript quantities of the major cellulases belonging to GH5, GH6, and GH7 families accounted for 56.2% of the total transcription of glycoside hydrolases (82,000 FPKM) in cellulase Rut-C30 at 24 h. However, the corresponding ratio is up to 75.5% for cellulase U5, whose total transcripts is 148,000 FPKM. The total transcripts of extracellular glycoside hydrolases, especially, major induced cellulases genes, such as genes *cbh1*, *cbh2*, *eg1*, and *eg2*, decreased significantly at 48 h compared to that at 24 h in two *Trichoderma* strains, probably due to repression under secretion stress (RESS) (Pakula et al., 2003). At 48 h, the transcription of extracellular major glycoside hydrolase genes in the two strains decreased significantly compared to that at 24 h, and the total FPKM values of extracellular protein U5 and Rut-C30 at 48 h decreased to 22–25% of that at 24 h, meanwhile, the transcripts of genes encoding the major cellulases from GH5, GH6, and GH7 families occupied 11.2% of the total cellulase transcripts in cellulase Rut-C30, 33.6% in cellulase U5 (Additional file 4). Furthermore, the transcripts of three major proteases genes (*TrC30_111063*, *TrC30_122545*, and *TrC30_26076*) in *T. reesei* U5 kept the same level to that of Rut-C30, which may exert negative effect on the stability of extracellular glycoside hydrolases (Qian et al., 2019).

Genes related to protein processing, folding, transporting, and secretion exhibited significant changes in *T. reesei* U5 compared to that of Rut-C30. At 24 h, the transcription levels of 14 aminoacyl-tRNA synthetase genes in *T. reesei* U5 were significantly higher than that in Rut-C30, whose transcript levels increased by 2 to 5.6 times. The transcriptional levels of genes encoding endoplasmic reticulum-related proteins



responsible for protein processing and folding were also changed in *T. reesei* U5, over 40% endoplasmic reticulum protein, transporting and sorting proteins were significantly up-regulated in *T. reesei* U5, which may be beneficial to protein secretion (Additional file 5). The transcription levels of genes related to N-glycosylation modification in the endoplasmic reticulum were significantly increased (Ruddock and Molinari, 2006). In addition, the transcription levels of genes such as mannosyl oligosaccharide glucosidase (*ERManI* homolog), α -1, 3 glucanase (*GlcII* homolog), and protein oligosaccharyltransferase (*UGGT* homolog) increased by 2–3.5 times, which all are the key glycosylation enzymes and hydrolases in the endoplasmic reticulum for protein processing. Furthermore, the *EDEM* homolog gene encoding the marker protein of the endoplasmic reticulum associated degradation pathway, was significantly up-regulated (8-fold) compared to that in Rut-C30 (Wang and Hebert, 2003). The transcription of the eukaryotic translation initiation factor 2 α kinase (*PERK* homolog) gene was improved 1.3-fold, which is a characteristic enzyme for endoplasmic reticulum stress response (Harding et al., 1999). Results above indicate the enhanced effect of endoplasmic reticulum-associated degradation (ERAD) on protein processing for glycoside hydrolases in *T. reesei* U5 at 24h. However, at 24h, the transcription levels of the genes encoding disulphide isomerase Pdi and ER-resident transmembrane kinase Ire1 proteins were not up-regulated, the transcript levels of *hac1* gene encoding regulator for UPR, and *bip1* gene encoding the luminal binding protein, an ER-localized member of the HSP70 family, also

kept in similar level between *T. reesei* U5 and Rut-C30 at 24h, which suggests that the unfolded protein response (UPR) was not changed in *T. reesei* U5. The positive function of genes above for protein processing in endoplasmic reticulum in *T. reesei* have been confirmed before (Saloheimo et al., 2003; Gao et al., 2018).

The ERAD and misfolding protein degradation pathway are always coupled. At 24h, transcription quantity of the ubiquitination-proteasome system-related genes in *T. reesei* U5 was significantly up-regulated, which is important to reduce the pressure on the endoplasmic reticulum owing to the accumulation of post-translated glycoside hydrolases. The transcription of genes encoding Derlin and Ubx family proteins involved in the ERAD pathway was increased in *T. reesei* U5, facilitating the entry of misfolding protein into the proteasome. In the course of protein ubiquitination, genes coding the ubiquitin-activating enzyme E1 family, the ubiquitin-binding enzyme E2 family, and the ubiquitin ligase E3 family in *T. reesei* U5 were all increased to various degrees, among which genes encoding ubiquitin-activating enzyme UBE1, UBLE1A, UBLE1B, and UBE1C were up-regulated by over 3-fold, and the ubiquitin-binding enzyme UBE2Q gene was up-regulated by 6-fold. Correspondingly, transcription levels of the proteasome subunit genes in *T. reesei* U5 also improved to various degrees, at least twice as high as that in Rut-C30 at both time points. Transcripts of genes in the ERAD pathway, as well as ubiquitination and proteasome-related genes increased remarkably, indicating that the protein processing of *T. reesei* U5 has begun speedily at 24h, which resulted in a large increase in extracellular

cellulase protein secretion in *T. reesei* U5 compared to that in *T. reesei* Rut-C30.

In addition, there are several significantly different transcriptional levels in metabolic pathways or cellular physiological activities between *T. reesei* U5 and Rut-C30 at 24 h, and the transcript level of genes in the following groups always improved remarkably in *T. reesei* U5: RNA polymerase II subunit and its basic transcriptional regulatory factors, mRNA regulatory pathways, RNA degradation, peroxisomes, CoA synthesis pathways, N-glycoside synthesis pathways, ammonia Acyl-tRNA synthesis pathway, nicotinamide metabolism pathway, fatty acid metabolism pathway, endoplasmic reticulum membrane protein processing, and proteasome complex (Additional file 2).

Exploration of New Regulators for *T. reesei* Cellulase Production

In the transcriptome data analysis of *T. reesei* U5, putative regulatory genes changing significantly at both 24 and 48 h are likely to be targets for activating the transcription of cellulase genes. Therefore, 15 genes possessing predicted regulatory function were selected as targets for further analysis. The predicted protein-encoding genes screened are shown in Table 1, which mainly include the fungal Zn₂Cys₆ type binuclear cluster transcription factor, histone kinase, LysR family regulatory proteins, helix-transition-helix regulatory proteins, and NmrA family regulatory proteins.

Recombinant strains with overexpression of the 15 putative regulators were obtained. With the exception of *T. reesei* Tr93861 strain overexpressing gene *TrC30_93861*, whose spore-forming ability was reduced significantly and mycelium growth was impaired, the other strains did not have significant changes in growth and mycelial morphology compared to *T. reesei* Rut-C30. Notably, the TrC30_93861 protein homolog in the wild-type strain *T. reesei* QM6a has been identified as the transcription factor Ypr1 (Derntl et al., 2016), so *TrC30_93861* gene is

named as *ypr1* in the following text. Through the fermentation performance of the transformants overexpressing 15 putative regulatory genes, it can be deduced that these regulators, when individually overexpressed, did not exert any positive regulation on cellulase production, and even the overall enzyme activities from some certain transformants showed a decreased level compared to Rut-C30, as shown in Figure 7. Gene *TrC30_129764* is the potential target gene regulated by AZFP-U5 directly, whose transcript also improved significantly in the *T. reesei* U5. However, *TrC30_129764* overexpressed strain showed similar cellulase activity profile with that in Rut-C30, which suggest that *TrC30_129764* is not a crucial factor for cellulase regulation. Furthermore, the transcript level of gene *TrC30_38522* encoding a putative transcriptional regulator in *T. reesei* U5 improved by over 50 and 2-fold at 24 and 48 h compared to that in Rut-C30, whose expressional level also elevated several folds when *T. reesei* Rut-C30 was cultured into the sugarcane bagasse medium (Borin et al., 2018). However, no difference was observed for cellulase production when *TrC30_38522* was overexpressed in *T. reesei* Rut-C30. Among the transformants, the strains overexpressing genes *ypr1* and *TrC30_74374* showed 38.8% and 42.7% higher FPase activities than that of Rut-C30, respectively. Meanwhile, the corresponding extracellular protein secretion increased by 29.44% and 36.54%, respectively.

Possible Crosslink Between Cellulase Production and Pigment Secretion

In order to further study the functions of *ypr1* or *TrC30_74374* in *T. reesei* Rut-C30, *ypr1*, and *TrC30_74374* gene knockout strains $\Delta ypr1$ and $\Delta 74374$ were constructed and verified individually with the correct integration as a single copy (Figure S4). Unexpectedly, no change in cellulase activities were observed in strains $\Delta ypr1$ and $\Delta 74374$ as to that in the control strain *T. reesei* Rut-C30 (Figure S5), suggesting that these two regulators are

TABLE 1 | Predicting differentially expressed genes with regulatory functions by overexpression of AZFP-U5.

Model ID	Prot ID	Log ₂ FC (24 h)	Log ₂ FC (48 h)	Annotation
estExt_Genemark1.C_1_t10198	23164	1.80	0.66	Fungal Zn(2)-Cys(6) binuclear regulator
estExt_Genemark1.C_1_t20246	23425	2.20	0.59	Fungal Zn(2)-Cys(6) binuclear regulator
estExt_fgenesh1_pg.C_110229	141745	0.68	1.72	Fungal Zn(2)-Cys(6) binuclear regulator
estExt_Genewise1Plus.C_17_t20040	102019	2.50	0.62	Fungal specific transcription factor
fgenesh1_pm.8_#_7	129764	2.14	0.82	Signal transduction histidine kinase
fgenesh1_pg.24_#_1	38417	0.75	6.17	LysR family regulatory protein
estExt_fgenesh2_kg.C_250078	124902	8.92	0.62	Helix-turn-helix containing protein
e_gw1.12.485.1	81999	6.73	0.73	Fungal Zn(2)-Cys(6) binuclear regulator
fgenesh1_pg.24_#_106	38522	5.72	1.49	Fungal specific transcription factor
estExt_Genewise1Plus.C_10_t10436	99728	3.22	1.93	Fungal specific transcription factor
e_gw1.47.20.1	93160	11.76	2.52	Fungal Zn(2)-Cys(6) binuclear regulator
estExt_Genemark1.C_270039	26551	5.37	1.96	NmrA-like family regulator
e_gw1.3.267.1	72675	4.98	1.36	Fungal Zn(2)-Cys(6) binuclear regulator
estExt_Genewise1Plus.C_1_t10373	93861	4.45	1.05	Fungal Zn(2)-Cys(6) binuclear regulator
e_gw1.4.341.1	74374	3.96	1.32	Fungal Zn(2)-Cys(6) binuclear regulator

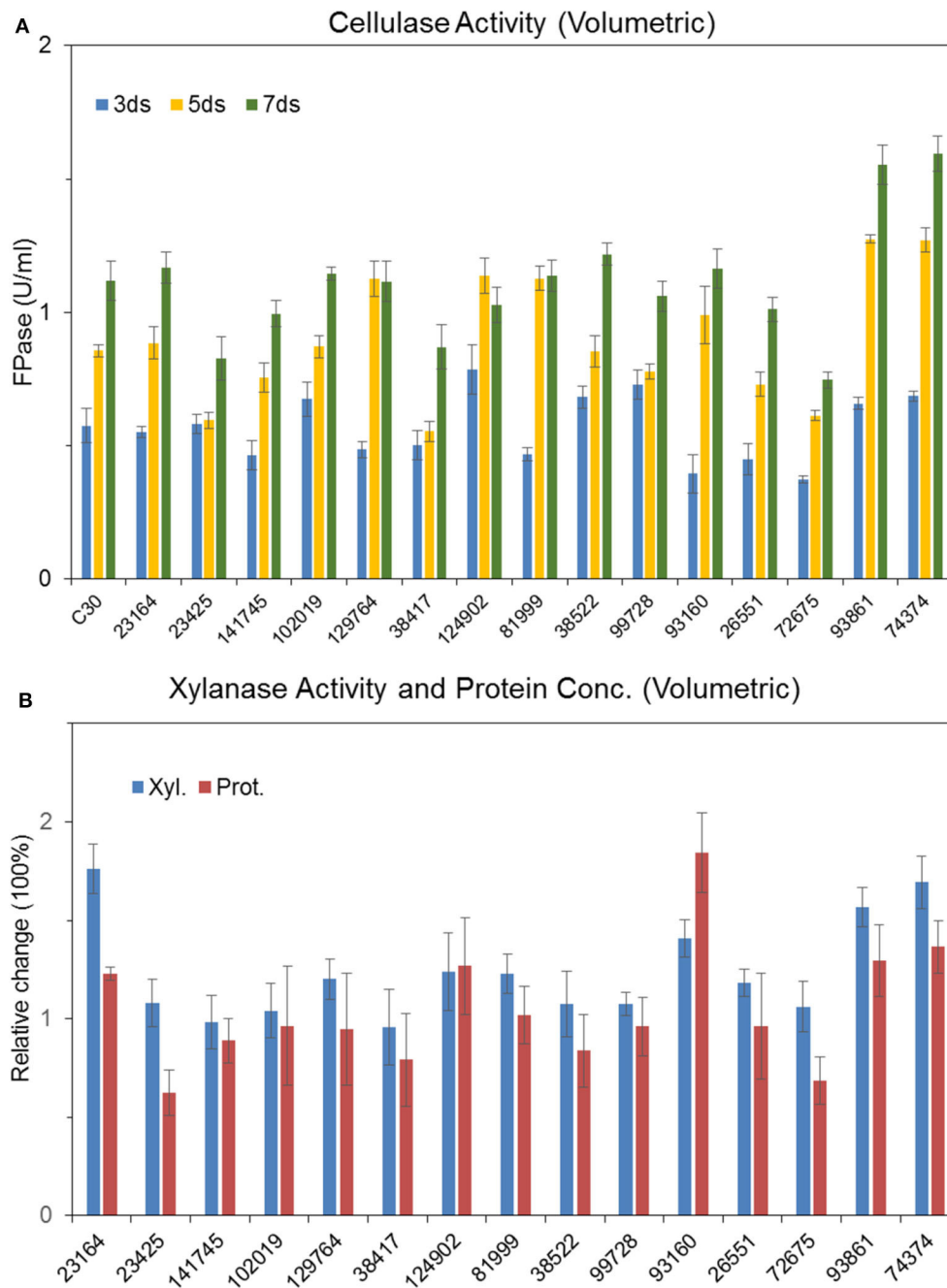


FIGURE 7 | Effects of overexpression of 15 transcription factors on cellulase production Cellulase (A), xylanase and protein productions (B) by *T. reesei* Rut-C30 recombinant strains overexpressing the 15 candidate transcription factors.

not essential for regulation of cellulase biosynthesis under the conditions used in this work.

In terms of cell morphology, the phenotype of *T. reesei* $\Delta 74374$ had no obvious change compared with the parental strain, and the fermentation broth was pale yellow under the condition of cellulose medium. *T. reesei* $\Delta ypr1$ recovered the similar level of spore-forming ability to the parental strain,

so did the growth biomass and mycelial morphology. During the cellulase fermentation process, the $\Delta ypr1$ strain no longer secreted yellow pigment, and the fermentation broth became white in contrast to Rut-C30. However, the yellow pigment production in the *ypr1* overexpression strain Tr93861 enhanced significantly. Meanwhile, conidiation of Tr93861 strain decreased remarkably (Figure 8). Hypersecretion of the yellow pigment

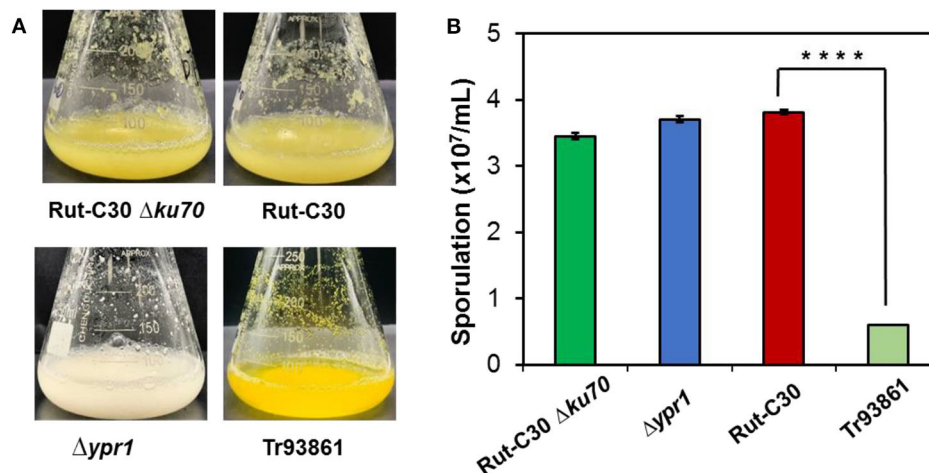


FIGURE 8 | Effects of *ypr1* on pigment production and sporulation. *T. reesei* Tr93861 is the mutant strain overexpressing *ypr1* in *T. reesei* Rut-C30, whereas strain $\Delta ypr1$ was obtained by deleting *ypr1* in *T. reesei* $\Delta ku70$. The mutant strains and their respective parental strains were cultured on cellulase production medium for 5 days, and pigment production was shown (A). The sporulation assay of the *T. reesei* strains was implemented when cultured on MEA for 7 days (B). Asterisks indicate significant differences from reference strains (**** $p < 0.001$, Student's *t*-test).

may be the direct cause of significant reduction in vegetative growth owing to the metabolic burden or the growth limiting effect of yellow pigment (Derntl et al., 2017a). The Ypr1 homolog in Rut-C30 (663 aa) have four regions of amino acid residues (insertions and deletions) in the C-terminal part of middle homology region (MHR) and regulatory region compared that of Ypr1 in QM6a (gene ID: 102499, 686 aa), which maybe resulted in the different regulatory profile for cellulase production and pigment secretion between Rut-C30 and QM6a (Figure S6).

To further analyze the effect of *ypr1* knockout on the secretion of *T. reesei* cellulase, comparative transcriptome analysis was performed for the knockout mutant *T. reesei* $\Delta ypr1$ and the parental strain Rut-C30 $\Delta ku70$ in MA medium with glucose as carbon source. Unexpectedly, we found that the transcription of the glycoside hydrolase genes in *T. reesei* $\Delta ypr1$ mutant were significantly changed compared to the parental strain *T. reesei* Rut-C30 $\Delta ku70$. Table 2 lists transcription changes in several major glycoside hydrolases and transcriptional regulator genes. The transcriptional quantity of major cellulases has been improved remarkably in *T. reesei* $\Delta ypr1$, the minimum change fold is 1-fold increased (*cbh1* gene), and the maximum transcript level change happened to the *egl* gene which increased by 3.8 times. The transcriptional levels for most hemicellulase genes are improved by at least 1.35-fold. Meanwhile, the transcriptions of *cel61a*, *cip1* genes encoding the auxiliary proteins, and *axe1* gene (encoding acetylxyylan esterase) have increased by 0.8, 1.6 and 2.4-fold, respectively, whose positions are located in close proximity to the gene *ypr1* locus (scaffold_1:507183-509547), which means that the deletion of Ypr1 protein facilitates the transcription of the surrounding glycoside hydrolase genes. Meanwhile, the transcripts of genes encoding the major cellulase regulatory factors, such as the genes of Xyr1 and Ace3, have increased significantly, except for Vib1.

TABLE 2 | Changes of major glycoside hydrolases and transcription factors in *T. reesei* $\Delta ypr1$ comparing with that of the control strain.

GeneID	Protein	Log ₂ FC*
125125	CBH1	0.99
122470	CBG2	1.78
5304	EG1	2.27
72489	EG2	1.69
124438	EG3	1.71
25940	EG5	1.06
136547	BGL1	1.52
38418	XYN1	1.89
124931	XYN2	0.31
23616	XYN3	1.38
90847	XYN4	1.23
134945	XYN5	1.31
140746	BXL1	1.10
139633	CEL61a	0.87
122518	CEL61b	0.42
104220	SWO1	1.42
121449	CIP1	1.40
125575	CIP2	0.68
98455	ACE3	1.18
98788	XYR1	1.58
31634	YPR2	-7.55
125610	Vib1	0.41

*FC, Fold change of the transcription of genes in *T. reesei* $\Delta ypr1$ over that in *T. reesei* Rut-C30 $\Delta ku70$.

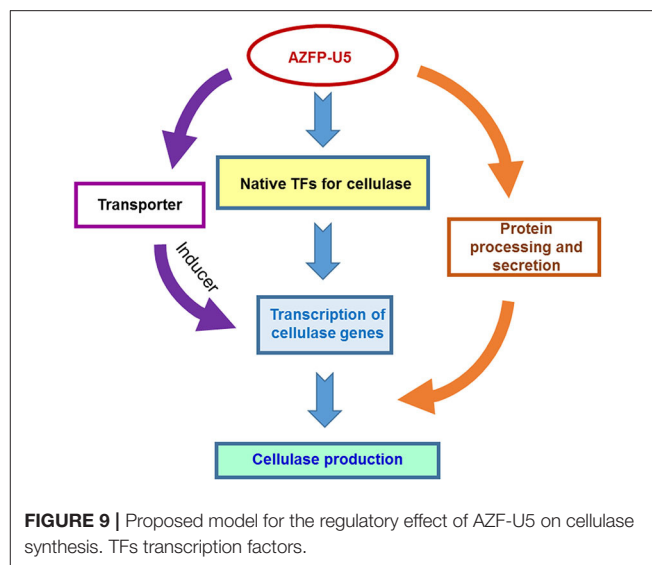
DISCUSSION

In our previous work, *T. reesei* strains overexpressing AZFP-U3 (Zhang et al., 2016) and AZFP-M2 (Meng et al., 2020) showed

enhanced cellulase production. Comparing with these two AZFP genes, AZFP-U5 has different sequence and also showed different regulatory patterns on cellulase biosynthesis. The strain overexpressing AZFP-U5 showed the best phenotypes among the three AZFP strains, with higher protein secretion level and higher activities of various cellulases and xylanases. Therefore, it is of great interest to further explore the mechanisms by which this AZFP functions.

In the previous studies, transcriptome analysis was performed using *T. reesei* grown in different carbon source (glucose, lactose, sophorose, or cellulose) and lignocellulose substrates, and data analysis has been focused on the functions of known major regulators, such as Xyr1 and Cre1 (dos Santos Castro et al., 2014, 2016; Hakkinen et al., 2014). Nevertheless, detailed analysis of global transcription as well as metabolic pathways for cellulase production in *T. reesei* is still lacking. In this work, we present extensive and comprehensive analysis of global transcription network reprogramming by the artificial regulator AZFP-U5, and assume that multiple pathways may be involved in cellulase biosynthesis by the function of AZFP-U5. For example, AZFP-U5 activates the transcription of glycoside hydrolase genes in the mRNA regulatory pathway, and also leads to changes of a series of metabolic processes, including mRNA synthesis, processing, and degradation, which may then lead to an increase in protein translation, processing, and secretion. Meanwhile, activation of the protein degradation pathway may be achieved by accumulation of unfolded proteins. The improvement of tRNA synthetase genes in the aminoacyl-tRNA synthesis pathway further indicated that the protein synthesis in *T. reesei* U5 were more active compared to that in *T. reesei* Rut-C30. In the reprogramming of global gene transcription, *T. reesei* U5 strain may be supplied with more energy, reducing power, and protein synthesis precursors by the activated intercellular metabolic pathways, which was also reflected from the comparative transcriptome results. After investigating dynamic changes of global transcription, we found different transcription profiles at 24 and 48 h. At 48 h, genes encoding marker proteins in the endoplasmic reticulum still have an up-regulation in *T. reesei* U5, indicating that AZFP-U5 may also have stimulating effects on protein processing, trafficking, and secretion pathway.

In addition to changes in the key metabolic processes, variation of transcription in several sugar transporters were discovered. AZFP-U5 may activate transcription of major transporter genes, which could transport potential carbon source inducers or transmit the carbon signal for induction, followed by transcriptional activation of the glycoside hydrolase genes regulated by AZFP-U5, directly, or indirectly. Meanwhile, the AZFP-U5 activates the stress response pathway and the transcription of the peroxisome protein genes, indicating that this artificial regulator has a potential positive effect on the release of reactive oxygen and external environmental stress response in protein and peptide synthesis. The possible mechanism by which AZFP-U5 works on cellulase production is shown in **Figure 9**. Further studies are needed to explore the directly regulated genes by AZFP-U5 as well as key genes on regulation of glycoside hydrolase genes.



During the transcriptome analysis, many putative regulator genes showed enhanced transcription by AZFP-U5 overexpression, of which 15 were selected for further investigation. However, the results did not show significant increase in cellulase production by overexpressing these regulators. It may be possible that individual expression of these regulators may not be sufficient to enhance cellulase biosynthesis, and the advantage of AZFP-U5 is that it simultaneously regulates multiple gene transcription by binding with various target genes, and induce changes in related signal transduction and metabolic pathways. It will be interesting to test the combinatory effects of the regulators for regulating cellulase production in the future work.

In this study, we found that Ypr1 in *T. reesei* Rut-C30 not only regulates the formation of secondary metabolites, but also participates in the transcriptional regulation of glycoside hydrolase genes when glucose was used as a carbon source. From transcriptome analysis, deletion of Ypr1 significantly increased the transcription of extracellular glycoside hydrolases and major transcription factor genes. We speculate that the secondary metabolites have a coupling effect with the cellulase production. This crosslink is also reflected in the transcription factor Xpp1 in *T. reesei*, the presence of Xpp1 can inhibit the synthesis of hemicellulase genes and inhibit the production of secondary metabolites in the cell, which acts as a switch function between the primary and secondary metabolism (Derntl et al., 2017b). Moreover, *T. reesei* ZC121 with up-regulated Ypr1 could overproduce the yellow pigment, but almost produce no extracellular cellulase (Li et al., 2018).

Ypr2 is a transcription factor that affects the production of yellow pigment, which has an inhibition effect on Ypr1 expression (Derntl et al., 2016). Deletion of Ypr1 also severely affected the transcription of Ypr2 (almost no ypr2 transcript in *T. reesei* $\Delta ypr1$ strain). Moreover, under dark conditions, Ypr2 (gene ID: 102497 in *T. reesei* QM6a, 664 aa) can affect the transcription of genes regulated by Cre1 in *T. reesei* QM6a,

and Ypr2 also could regulate Ypr1 (Hitzenhammer et al., 2019). However, the Ypr2 protein in *T. reesei* Rut-C30 (gene ID: *TrC30_31634*, 511 aa) contains a zinc finger-free DNA binding domain in *T. reesei* Rut-C30 (the first 175 amino acid residues missed), which will cause severe impact on DNA binding and regulatory function. Therefore, the specific role and function of Ypr2 lacking the binding domain in metabolism and pigment secretion requires further analysis (Figure S7).

The results in this study showed possible cross talk between cellulase production and pigment secretion in *T. reesei* regulated by the major regulator Ypr1 protein. Meanwhile, deletion of Ypr1 significantly increase the transcription of major glycoside hydrolase and transcription factor genes. Actually, CAZyme genes in *T. reesei* are non-randomly distributed within the genome, about (41%) CAZyme genes are found in 25 discrete regions containing specific regulators or secondary metabolites clusters (Martinez et al., 2008; Hakkinen et al., 2014). Ypr1 not only locates into nearly adjacent region of glycoside hydrolases, but also possess the co-regulated effect for *TrC30_69551* and some glycoside hydrolase genes, including *axe1*, *cip1*, and *cel61a*. However, there is no significant change in $\Delta ypr1$ for extracellular cellulase secretion compared to that from parental strain when cellulose or glucose is used as the substrate. In *T. reesei* $\Delta ypr1$, the transcript level of *ypr2* nearly disappeared ($\text{Log}_2\text{FC} = -7.5$), which may intensify CCR effect on cellulase translation and secretion. Another reason may be the existence of complex post-transcriptional or post-translational mechanisms for cellulase proteins, which need to be revealed in further studies.

CONCLUSION

T. reesei mutant U5 bearing an AZFP (AZFP-U5) was focused, which secretes more proteins and showed significantly higher cellulase and xylanase production than its parental strain *T. reesei* Rut-C30. Comparative transcriptome analysis showed enhanced transcription and post-translational modifications of glycoside

hydrolases by overexpression of AZFP-U5. Furthermore, deletion of *ypr1* and *TrC30_74374* did not affect cellulase production. Deletion of *ypr1* affected cellulase gene transcription, suggesting possible crosslink between pigment production and cellulase gene expression by the AZFP-U5-associated regulator Ypr1.

DATA AVAILABILITY STATEMENT

The raw data supporting the conclusions of this article will be made available by the authors, without undue reservation, to any qualified researcher.

AUTHOR CONTRIBUTIONS

FZ and X-QZ designed the experiments. FZ and J-XL performed the experiments as well as data analysis, and also prepared the draft of the manuscript. VC, C-GL, and F-WB participated in revision of the manuscript. X-QZ supervised the experiments and critically revise the manuscript. All authors contributed to the article and approved the submitted version.

ACKNOWLEDGMENTS

This work was financially funded by Natural Science Foundation of China with a grant reference number of 21536006, and the Open Funding Project of the State Key Laboratory of Bioreactor Engineering and the Fundamental Research Funds for the Central Universities (No. 222201714053). The authors acknowledge ToolGen Inc., South Korea for providing the plasmid containing artificial zinc finger protein genes.

SUPPLEMENTARY MATERIAL

The Supplementary Material for this article can be found online at: <https://www.frontiersin.org/articles/10.3389/fbioe.2020.00649/full#supplementary-material>

REFERENCES

- Abrahao Neto, J., Rossini, C., El-Gogary, S., Henrique-Silva, F., Crivellaro, O., and El-Dorry, H. (1995). Mitochondrial functions mediate cellulase gene expression in *Trichoderma reesei*. *Biochemistry* 34, 10456–10462. doi: 10.1021/bi00033a018
- Aro, N., Saloheimo, A., Ilmen, M., and Penttilä, M. (2001). ACEII, a novel transcriptional activator involved in regulation of cellulase and xylanase genes of *Trichoderma reesei*. *J. Biol. Chem.* 276, 24309–24314. doi: 10.1074/jbc.M003624200
- Bailey, M. J., Biely, P., and Poutanen, K. (1992). Interlaboratory testing of methods for assay of xylanase activity. *J. Biotechnol.* 23, 257–270. doi: 10.1016/0168-1656(92)90074-J
- Bischof, R. H., Ramoni, J., and Seiboth, B. (2016). Cellulases and beyond: the first 70 years of the enzyme producer *Trichoderma reesei*. *Microb. Cell Fact.* 15:106. doi: 10.1186/s12934-016-0507-6
- Borin, G. P., Carazzolle, M. F., dos Santos, R. A. C., Riaño-Pachón, D. M., and Oliveira, J. V. (2018). Gene co-expression network reveals potential new genes related to sugarcane bagasse degradation in *Trichoderma reesei* RUT-30. *Front. Bioeng. Biotechnol.* 6:151. doi: 10.3389/fbioe.2018.00151
- Cao, Y. L., Zheng, F. L., Wang, L., Zhao, G. L., Chen, G. J., Zhang, W. X., et al. (2017). Rce1, a novel transcriptional repressor, regulates cellulase gene expression by antagonizing the transactivator Xyr1 in *Trichoderma reesei*. *Mol. Microbiol.* 105, 65–83. doi: 10.1111/mmi.13685
- Chaudhary, N., Kumari, I., Sandhu, P., Ahmed, M., and Akhter, Y. (2016). Proteome scale census of major facilitator superfamily transporters in *Trichoderma reesei* using protein sequence and structure based classification enhanced ranking. *Gene* 585, 166–176. doi: 10.1016/j.gene.2016.03.043
- Chen, L., Zou, G., Wang, J. Z., Wang, J., Liu, R., Jiang, Y., et al. (2016). Characterization of the Ca^{2+} -responsive signaling pathway in regulating the expression and secretion of cellulases in *Trichoderma reesei* Rut-C30. *Mol. Microbiol.* 100, 560–575. doi: 10.1111/mmi.13334
- Coradetti, S. T., Craig, J. P., Xiong, Y., Shock, T., Tian, C., and Glass, N. L. (2012). Conserved and essential transcription factors for cellulase gene expression in ascomycete fungi. *Proc. Natl. Acad. Sci. U.S.A.* 109, 7397–7402. doi: 10.1073/pnas.1200785109
- Derntl, C., Guzmán-Chávez, F., Mello-de-Sousa, T. M., Busse, H.-J., Driessen, A. J., Mach, R. L., et al. (2017a). *In vivo* study of the sorbicillinoid gene cluster in *Trichoderma reesei*. *Front. Microbiol.* 8:2037. doi: 10.3389/fmicb.2017.02037
- Derntl, C., Kluger, B., Bueschl, C., Schuhmacher, R., Mach, R. L., and Mach-Aigner, A. R. (2017b). Transcription factor Xpp1 is a switch between primary and secondary fungal metabolism. *Proc. Natl. Acad. Sci. U.S.A.* 114, E560–E569. doi: 10.1073/pnas.1609348114

- Derntl, C., Mach, R. L., and Mach-Aigner, A. R. (2019). Fusion transcription factors for strong, constitutive expression of cellulases and xylanases in *Trichoderma reesei*. *Biotechnol. Biofuels* 12:231. doi: 10.1186/s13068-019-1575-8
- Derntl, C., Rassinger, A., Srebotnik, E., Mach, R. L., and Mach-Aigner, A. R. (2015). Xpp1 regulates the expression of xylanases, but not of cellulases in *Trichoderma reesei*. *Biotechnol. Biofuels* 8:112. doi: 10.1186/s13068-015-0298-8
- Derntl, C., Rassinger, A., Srebotnik, E., Mach, R. L., and Mach-Aigner, A. R. (2016). Identification of the main regulator responsible for synthesis of the typical yellow pigment produced by *Trichoderma reesei*. *Appl. Environ. Microbiol.* 82, 6247–6257. doi: 10.1128/AEM.01408-16
- dos Reis, T. F., de Lima, P. B., Parachin, N. S., Mingossi, F. B., de Castro Oliveira, J. V., Ries, L. N., et al. (2016). Identification and characterization of putative xylose and cellobiose transporters in *Aspergillus nidulans*. *Biotechnol. Biofuels* 9:204. doi: 10.1186/s13068-016-0611-1
- dos Santos Castro, L., de Paula, R. G., Antoniêto, A. C., Persinoti, G. F., Silva-Rocha, R., and Silva, R. N. (2016). Understanding the role of the master regulator XYR1 in *Trichoderma reesei* by global transcriptional analysis. *Front. Microbiol.* 7:175. doi: 10.3389/fmicb.2016.00175
- dos Santos Castro, L., Pedersoli, W. R., Antoniêto, A. C., Steindorff, A. S., Silva-Rocha, R., Martinez-Rossi, N. M., et al. (2014). Comparative metabolism of cellulose, sophorose and glucose in *Trichoderma reesei* using high-throughput genomic and proteomic analyses. *Biotechnol. Biofuels* 7:41. doi: 10.1186/1754-6834-7-41
- Druzhinina, I. S., and Kubicek, C. P. (2017). Genetic engineering of *Trichoderma reesei* cellulases and their production. *Microb. Biotechnol.* 10, 1485–1499. doi: 10.1111/1751-7915.12726
- Gao, F., Hao, Z. Z., Sun, X. H., Qin, L., Zhao, T., Liu, W. Q., et al. (2018). A versatile system for fast screening and isolation of *Trichoderma reesei* cellulase hyperproducers based on DsRed and fluorescence-assisted cell sorting. *Biotechnol. Biofuels* 11:261. doi: 10.1186/s13068-018-1264-z
- Grigoriev, I. V., Nikitin, R., Haridas, S., Kuo, A., Ohm, R., Otilar, R., et al. (2014). MycoCosm portal: gearing up for 1000 fungal genomes. *Nucleic Acids Res.* 42, D699–704. doi: 10.1093/nar/gkt1183
- Hakkinen, M., Arvas, M., Oja, M., Aro, N., Penttilä, M., Saloheimo, M., et al. (2012). Re-annotation of the CAZy genes of *Trichoderma reesei* and transcription in the presence of lignocellulosic substrates. *Microb. Cell Fact.* 11:134. doi: 10.1186/1475-2859-11-134
- Hakkinen, M., Valkonen, M. J., Westerholm-Parvinen, A., Aro, N., Arvas, M., Vitikainen, M., et al. (2014). Screening of candidate regulators for cellulase and hemicellulase production in *Trichoderma reesei* and identification of a factor essential for cellulase production. *Biotechnol. Biofuels* 7:14. doi: 10.1186/1754-6834-7-14
- Harding, H. P., Zhang, Y., and Ron, D. (1999). Protein translation and folding are coupled by an endoplasmic-reticulum-resident kinase. *Nature* 397:271. doi: 10.1038/16729
- He, R. L., Ma, L. J., Li, C., Jia, W. D., Li, D. M., Zhang, D. Y., et al. (2014). TrpA1, a pH response transcription regulator, is involved in cellulase gene expression in *Trichoderma reesei*. *Enzyme Microb. Technol.* 67, 17–26. doi: 10.1016/j.enzmictec.2014.08.013
- Hitzenhamer, E., Büschl, C., Sulyok, M., Schuhmacher, R., Kluger, B., Wischnitzki, E., et al. (2019). YPR2 is a regulator of light modulated carbon and secondary metabolism in *Trichoderma reesei*. *BMC Genomics* 20:211. doi: 10.1186/s12864-019-5574-8
- Kubicek, C. P. (2013). Systems biological approaches towards understanding cellulase production by *Trichoderma reesei*. *J. Biotechnol.* 163, 133–142. doi: 10.1016/j.jbiotec.2012.05.020
- Li, C. C., Lin, F. M., Sun, W., Yuan, S. X., Zhou, Z. H., Wu, F. G., et al. (2018). Constitutive hyperproduction of sorbicillinoids in *Trichoderma reesei* ZC121. *Biotechnol. Biofuels* 11:291. doi: 10.1186/s13068-018-1296-4
- Li, Z., Yao, G., Wu, R., Gao, L., Kan, Q., Liu, M., et al. (2015). Synergistic and dose-controlled regulation of cellulase gene expression in *Penicillium oxalicum*. *PLoS Genet.* 11:e1005509. doi: 10.1371/journal.pgen.1005509
- Liu, G. D., and Qu, Y. B. (2019). Engineering of filamentous fungi for efficient conversion of lignocellulose: Tools, recent advances and prospects. *Biotechnol. Adv.* 37, 519–529. doi: 10.1016/j.biotechadv.2018.12.004
- Liu, K., Dong, Y., Wang, F., Jiang, B., Wang, M., and Fang, X. (2016). Regulation of cellulase expression, sporulation, and morphogenesis by velvet family proteins in *Trichoderma reesei*. *Appl. Microbiol. Biotechnol.* 100, 769–779. doi: 10.1007/s00253-015-7059-2
- Liu, Y. G., and Chen, Y. L. (2007). High-efficiency thermal asymmetric interlaced PCR for amplification of unknown flanking sequences. *Biotechniques* 43, 649–656. doi: 10.2144/000112601
- Mandels, M., and Andreotti, R. (1978). Problems and challenges in the cellulose to cellulase fermentation. *Proc Biochem.* 13, 6–13.
- Martinez, D., Berka, R. M., Henrissat, B., Saloheimo, M., Arvas, M., Baker, S. E., et al. (2008). Genome sequencing and analysis of the biomass-degrading fungus *Trichoderma reesei* (syn. *Hypocrea jecorina*). *Nat. Biotechnol.* 26, 553–560. doi: 10.1038/nbt1403
- Meng, Q. S., Zhang, F., Liu, C. G., Zhao, X. Q., and Bai, F. W. (2020). Identification of a novel repressor encoded by the putative gene ctf1 for cellulase biosynthesis in *Trichoderma reesei* through artificial zinc finger engineering. *Biotechnol. Bioeng.* 117, 1747–1760. doi: 10.1002/bit.27321
- Mortazavi, A., Williams, B. A., McCue, K., Schaeffer, L., and Wold, B. (2008). Mapping and quantifying mammalian transcriptomes by RNA-Seq. *Nat. Methods* 5:621. doi: 10.1038/nmeth.1226
- Nakari-Setälä, T., Paloheimo, M., Kallio, J., Vehmaanpera, J., Penttilä, M., and Saloheimo, M. (2009). Genetic modification of carbon catabolite repression in *Trichoderma reesei* for improved protein production. *Appl. Environ. Microbiol.* 75, 4853–4860. doi: 10.1128/AEM.00282-09
- Nitta, M., Furukawa, T., Shida, Y., Mori, K., Kuhara, S., Morikawa, Y., et al. (2012). A new Zn(II)(2)Cys(6)-type transcription factor BglR regulates beta-glucosidase expression in *Trichoderma reesei*. *Fungal Genet. Biol.* 49, 388–397. doi: 10.1016/j.fgb.2012.02.009
- Pakula, T. M., Laxell, M., Huuskonen, A., Uusitalo, J., Saloheimo, M., and Penttilä, M. (2003). The effects of drugs inhibiting protein secretion in the filamentous fungus *Trichoderma reesei*. *J. Biol. Chem.* 278, 45011–45020. doi: 10.1074/jbc.M302372200
- Park, K. S., Lee, D. K., Lee, H., Lee, Y., Jang, Y. S., Kim, Y. H., et al. (2003). Phenotypic alteration of eukaryotic cells using randomized libraries of artificial transcription factors. *Nat. Biotechnol.* 21, 1208–1214. doi: 10.1038/nbt868
- Qian, Y. C., Zhong, L. X., Sun, Y., Sun, N. N., Zhang, L., Liu, W. F., et al. (2019). Enhancement of cellulase production in *Trichoderma reesei* via disruption of multiple protease genes identified by comparative secretomics. *Front. Microbiol.* 10:2784. doi: 10.3389/fmicb.2019.02784
- Ruddock, L. W., and Molinari, M. (2006). N-glycan processing in ER quality control. *J. Cell Sci.* 119, 4373–4380. doi: 10.1242/jcs.03225
- Saloheimo, M., Valkonen, M., and Penttilä, M. (2003). Activation mechanisms of the HAC1-mediated unfolded protein response in filamentous fungi. *Mol. Microbiol.* 47, 1149–1161. doi: 10.1046/j.1365-2958.2003.03363.x
- Schmoll, M. (2018). Regulation of plant cell wall degradation by light in *Trichoderma*. *Fungal Biol. Biotechnol.* 5:10. doi: 10.1186/s40694-018-0052-7
- Seiboth, B., Karimi, R. A., Phatale, P. A., Linke, R., Hartl, L., Sauer, D. G., et al. (2012). The putative protein methyltransferase LAE1 controls cellulase gene expression in *Trichoderma reesei*. *Mol. Microbiol.* 84, 1150–1164. doi: 10.1111/j.1365-2958.2012.08083.x
- Sharma, A., Tewari, R., Rana, S. S., Soni, R., and Soni, S. K. (2016). Cellulases: classification, methods of determination and industrial applications. *Appl. Biochem. Biotechnol.* 179, 1346–1380. doi: 10.1007/s12010-016-2070-3
- Solomon, P. S., Ipcho, S. V., Hane, J. K., Tan, K.-C., and Oliver, R. P. (2008). A quantitative PCR approach to determine gene copy number. *Fung. Gene. Rep.* 55:5–8. doi: 10.4148/1941-4765.1082
- Tisch, D., and Schmoll, M. (2013). Targets of light signalling in *Trichoderma reesei*. *BMC Genomics* 14:657. doi: 10.1186/1471-2164-14-657
- Tiwari, R., Nain, L., Labrou, N. E., and Shukla, P. (2018). Bioprospecting of functional cellulases from metagenome for second generation biofuel production: a review. *Crit. Rev. Microbiol.* 44, 244–257. doi: 10.1080/1040841X.2017.1337713
- Wang, F. Z., Zhang, R. Q., Han, L. J., Guo, W., Du, Z. Q., Niu, K. L., et al. (2019). Use of fusion transcription factors to reprogram cellulase transcription and enable efficient cellulase production in *Trichoderma reesei*. *Biotechnol. Biofuels* 12, 1–12. doi: 10.1186/s13068-019-1589-2
- Wang, T., and Hebert, D. N. (2003). EDEM an ER quality control receptor. *Nat. Struct. Mol. Biol.* 10:319. doi: 10.1038/nsb0503-319
- Xin, Q., Gong, Y. J., Lv, X. X., Chen, G. J., and Liu, W. F. (2013). *Trichoderma reesei* histone acetyltransferase Gcn5 regulates fungal growth,

- conidiation, and cellulase gene expression. *Curr. Microbiol.* 67, 580–589. doi: 10.1007/s00284-013-0396-4
- Yang, J., Kim, B., Kim, G. Y., Jung, G. Y., and Seo, S. W. (2019). Synthetic biology for evolutionary engineering: from perturbation of genotype to acquisition of desired phenotype. *Biotechnol. Biofuels* 12:113. doi: 10.1186/s13068-019-1460-5
- Zhang, F., Bai, F. W., and Zhao, X. Q. (2016). Enhanced cellulase production from *Trichoderma reesei* Rut-C30 by engineering with an artificial zinc finger protein library. *Biotechnol. J.* 11, 1282–1290. doi: 10.1002/biot.201600227
- Zhang, F., Zhao, X. Q., and Bai, F. W. (2018a). Improvement of cellulase production in *Trichoderma reesei* Rut-C30 by overexpression of a novel regulatory gene Trvib-1. *Bioresour. Technol.* 247, 676–683. doi: 10.1016/j.biortech.2017.09.126
- Zhang, J. J., Chen, Y. M., Wu, C., Liu, P., Wang, W., and Wei, D. Z. (2019). The transcription factor ACE3 controls cellulase activities and lactose metabolism via two additional regulators in the fungus *Trichoderma reesei*. *J. Biol. Chem.* 294, 18435–18450. doi: 10.1074/jbc.RA119.008497
- Zhang, J. J., Zhang, G. X., Wang, W., and Wei, D. Z. (2018b). Enhanced cellulase production in *Trichoderma reesei* RUT C30 via constitution of minimal transcriptional activators. *Microb. Cell Fact.* 17:75. doi: 10.1186/s12934-018-0926-7
- Zhang, W. X., Kou, Y. B., Xu, J. T., Cao, Y. L., Zhao, G. L., Shao, J., et al. (2013). Two major facilitator superfamily sugar transporters from *Trichoderma reesei* and their roles in induction of cellulase biosynthesis. *J. Biol. Chem.* 288, 32861–32872. doi: 10.1074/jbc.M113.505826
- Zhang, X. Y., Li, Y. H., Zhao, X. Q., and Bai, F. W. (2017). Constitutive cellulase production from glucose using the recombinant *Trichoderma reesei* strain overexpressing an artificial transcription activator. *Bioresour. Technol.* 223, 317–322. doi: 10.1016/j.biortech.2016.10.083
- Znameroski, E. A., Li, X., Tsai, J. C., Galazka, J. M., Glass, N. L., and Cate, J. H. (2013). Evidence for transceptor function of cellobiose transporters in *Neurospora crassa*. *J. Biol. Chem.* 289, 2610–2619. doi: 10.1074/jbc.M113.533273

Conflict of Interest: The authors declare that the research was conducted in the absence of any commercial or financial relationships that could be construed as a potential conflict of interest.

Copyright © 2020 Zhang, Li, Champreda, Liu, Bai and Zhao. This is an open-access article distributed under the terms of the Creative Commons Attribution License (CC BY). The use, distribution or reproduction in other forums is permitted, provided the original author(s) and the copyright owner(s) are credited and that the original publication in this journal is cited, in accordance with accepted academic practice. No use, distribution or reproduction is permitted which does not comply with these terms.



The Magnesium Concentration in Yeast Extracts Is a Major Determinant Affecting Ethanol Fermentation Performance of *Zymomonas mobilis*

Runxia Li¹, Mingjie Jin², Jun Du³, Mian Li⁴, Shouwen Chen¹ and Shihui Yang^{1*}

¹ State Key Laboratory of Biocatalysis and Enzyme Engineering, Environmental Microbial Technology Center of Hubei Province, School of Life Sciences, Hubei University, Wuhan, China, ² School of Environmental and Biological Engineering, Nanjing University of Science and Technology, Nanjing, China, ³ China Biotech Fermentation Industry Association, Beijing, China, ⁴ Zhejiang Huakang Pharmaceutical Co., Ltd., Quzhou, China

OPEN ACCESS

Edited by:

Maizirwan Mel,
International Islamic University
Malaysia, Malaysia

Reviewed by:

Pornthap Thanonkeo,
Khon Kaen University, Thailand
Bing-Zhi Li,
Tianjin University, China
Qiuqiang Gao,
Columbia University, United States

*Correspondence:

Shihui Yang
Shihui.Yang@hubu.edu.cn;
shhyoung@hotmail.com

Specialty section:

This article was submitted to
Bioprocess Engineering,
a section of the journal
Frontiers in Bioengineering and
Biotechnology

Received: 10 May 2020

Accepted: 23 July 2020

Published: 31 August 2020

Citation:

Li R, Jin M, Du J, Li M, Chen S
and Yang S (2020) The Magnesium
Concentration in Yeast Extracts Is
a Major Determinant Affecting Ethanol
Fermentation Performance
of *Zymomonas mobilis*.
Front. Bioeng. Biotechnol. 8:957.
doi: 10.3389/fbioe.2020.00957

Zymomonas mobilis is a model ethanologenic bacterium for diverse biochemical production. Rich medium (RM) is a complex medium that is routinely used to cultivate *Z. mobilis*, which contains carbon sources such as glucose, nitrogen sources such as yeast extract (YE), and KH_2PO_4 . Glucose consumption and cell growth of *Z. mobilis* is usually coupled during ethanol fermentation. However, sometimes glucose was not consumed during the exponential growth phase, and it took extended time for cells to consume glucose and produce ethanol, which eventually reduced the ethanol productivity. In this study, the effects of different nitrogen sources, as well as the supplementation of an additional nitrogen source into RM and minimal medium (MM), on cell growth and glucose consumption of *Z. mobilis* were investigated to understand the uncoupled cell growth and glucose consumption. Our results indicated that nitrogen sources such as YE from different companies affected cell growth, glucose utilization, and ethanol production. We also quantified the concentrations of major ion elements in different nitrogen sources using the quantitative analytic approach of Inductively Coupled Plasma Optical Emission Spectroscopy (ICP-OES), and demonstrated that magnesium ion in the media affected cell growth, glucose consumption, and ethanol production. The effect of magnesium on gene expression was further investigated using RNA-Seq transcriptomics. Our results indicated that the lack of Mg^{2+} triggered stress responses, and the expression of genes involved in energy metabolism was reduced. Our work thus demonstrated that Mg^{2+} concentration in nitrogen sources is essential for vigorous cell growth and ethanol fermentation, and the difference of Mg^{2+} concentration in different YE is one of the major factors affecting the coupled cell growth, glucose consumption and ethanol fermentation in *Z. mobilis*. We also revealed that genes responsive for Mg^{2+} deficiency in the medium were majorly related to stress

responses and energy conservation. The importance of magnesium on cell growth and ethanol fermentation suggests that metal ions should become one of the parameters for monitoring the quality of commercial nitrogen sources and optimizing microbial culture medium.

Keywords: *Zymomonas mobilis*, ethanol fermentation, nitrogen sources, yeast extract, magnesium, RNA-Seq, stress responses

INTRODUCTION

The Gram-negative bacterium *Zymomonas mobilis* is a natural ethanologen with many desirable industrial biocatalyst characteristics, which include high glucose consumption rate, high specific ethanol productivity, high ethanol tolerance, a broad pH range for production (pH 3.5–7.5), and its status being generally regarded as safe (GRAS) (Rogers et al., 1984, 2007; Panesar et al., 2006; He et al., 2014; Yang et al., 2016a; Wang et al., 2018). *Z. mobilis* utilizes glucose for ethanol production faster than *Saccharomyces cerevisiae* because of its high cell surface area which leads to higher ethanol productivity (Conway, 1992; Lawford and Rousseau, 1997; Rogers et al., 2007; He et al., 2014; Yang et al., 2016a; Wang et al., 2018).

Additionally, Compared with *S. cerevisiae*, the preferred biocatalyst using the Embden-Meyerhof-Parnas (EMP) pathway for industrial ethanol production with mature infrastructures, *Z. mobilis* has improved ethanol yield by using the Entner-Doudoroff (ED) pathway with 50% less ATP produced relative to the EMP pathway (Conway, 1992; Kingston et al., 1996; Dien et al., 2003). Recently, Jacobson et al. (2019) established a network-level approach that integrates quantitative metabolomics with ^2H and ^{13}C metabolic flux analysis to investigate the *in vivo* thermodynamics of the ED pathway and central carbon metabolism in *Z. mobilis*. Their result is consistent with previous *in silico* prediction (Flamholz et al., 2013) and demonstrated that ED pathway is twice as thermodynamically favorable as the EMP pathway in *E. coli* or *S. cerevisiae* (Jacobson et al., 2019).

Nitrogen sources in the medium are reported to affect the growth of *Z. mobilis*. For example, the morphology of *Z. mobilis* CP3 changes when cultured in a medium with a low nitrogen source (Ju et al., 1983). A medium commonly used to culture *Z. mobilis* is rich medium (RM). RM contains carbon sources such as glucose, nitrogen sources such as yeast extract (YE), and KH_2PO_4 that is often used as the phosphorus and potassium source and a buffering agent. Although nitrogen sources like peptone, corn steep liquid, and even N_2 can be used to sustain the cell growth of *Z. mobilis* (Ju et al., 1983; Lawford and Rousseau, 1997; Kremer et al., 2015), YE is the preferred nitrogen source because it can provide nitrogenous compounds, carbon, sulfur,

trace nutrients, vitamin B complex and other important growth factors for various microorganisms (Zarei et al., 2016).

Despite the fact that manufacturers produce different YE to have the same composition of total nitrogen content and free amino acid nitrogen, YE produced by different companies has different trace components such as growth factors and metal ions due to the differences in their production processes. This then affects the microbial cell growth because vitamins and metal ions (e.g., Mg^{2+} , Cu^{2+} , Zn^{2+} , and Fe^{2+}) are cofactors of enzymes involved in various metabolic activities. For example, Kosaka et al. (2020) investigated the effect of different metal ions on the thermotolerance of *Z. mobilis* TISTR548 and related mutants, and demonstrated that the addition of Mg^{2+} and K^+ reduced intracellular reactive oxygen species (ROS) accumulation at critical high temperature (CHT) with an increase of CHT by 1°C , which is probably due to the stabilization of both outer and inner membranes as well as the maintenance of homeostasis for cellular metabolism by the addition of Mg^{2+} and K^+ . In addition, the effect of supplementation of zinc on the ethanol fermentation performance of the self-flocculating yeast in the continuous ethanol fermentation was studied (Zhao et al., 2009; Xue et al., 2010; Ismail et al., 2014), and the roles of zinc and zinc containing proteins in yeast metabolism and cellular stress responses were summarized (Zhao and Bai, 2012).

With all nutrients needed for cell growth in the culture medium including a nitrogen source from YE, cell growth of *Z. mobilis* ZM4 is generally expected to be coupled with its glucose consumption and ethanol production. However, results and literature reports in a few studies from different research groups indicated that cell growth of *Z. mobilis* ZM4 and its glucose consumption were uncoupled, glucose was not completely consumed for ethanol production when cells reached stationary phase (Jones and Doelle, 1991; He et al., 2012; Yang et al., 2014a; Xia et al., 2018; Duan et al., 2019). This uncoupling phenomenon between growth and fermentation performance has also been reported in other microorganisms, including yeast, resulting in a prolonged fermentation time and decreased ethanol productivity (Cot et al., 2007; Pagliardini et al., 2013). For example, ethanol production of yeast cells was reported to be related to the length of the uncoupling phase during the batch fermentation process (Pagliardini et al., 2013).

A previous study in *E. coli* demonstrated that the inadequate amount of magnesium in the rich medium of buffered tryptone broth supplemented with glucose (TB7-glucose) is the major determinant leading to the uncoupled cell growth and glucose consumption (Christensen et al., 2017). They further demonstrated that the supplementation of sufficient magnesium can increase cell growth yield in other peptide-based media when

Abbreviations: CSL, corn steep liquid; ED, Entner-Doudoroff; EMP, Embden-Meyerhof-Parnas; GRAS, generally regarded as safe status; MM, minimum medium; ICP-OES, Inductively Coupled Plasma Optical Emission Spectroscopy; P, peptone; RM, rich medium; RM^{BD} , yeast extract in rich medium was from company Becton Dickinson (BD); RM^{OXOID} , yeast extract in rich medium was from company OXOID; RPKM, reads mapping to the genome per kilobase of transcript per million reads sequenced; T, tryptone; TRY, titer, rate, and yield; YE, yeast extract.

carbon is in excess. In addition, their study also showed that magnesium can increase cell growth of multiple *E. coli* strains and other bacterial species such as *Bacillus subtilis* and *Vibrio fischeri* (Christensen et al., 2017). Recently, Lozano Terol et al. (2019) studied protein overexpression for *E. coli* BL21 and five derived mutants in M9 minimal medium and TB7 complex medium, and discovered a similar phenomenon that carbon source of glucose or glycerol was not consumed during the exponential growth phase in TB7 complex medium but not M9.

The uncoupling of growth and fermentation in the late growth phase could be beneficial for ethanol fermentation since carbon source will be channeled into ethanol production instead of biomass buildup especially for yeast ethanol production. However, the uncoupling of growth and glucose consumption at early growth phase is unfavorable since there will be no sufficient cell biomass for efficient sugar fermentation to ethanol, which is mostly due to stressful physical and chemical growth conditions, such as extreme temperature, extreme pH, and toxic compounds in the medium. Limited nutrient sources of carbon, nitrogen and metal ions used for fermentation were also reported to affect cell growth and fermentation performance (Jones and Doelle, 1991; Cot et al., 2007; Pagliardini et al., 2013; Yang Y. et al., 2018). Although the effect of diverse nitrogen sources on cell growth and fermentation performance has been reported in various microorganisms, such as the ethanologenic yeast *S. cerevisiae* and lactate-producer *Sporolactobacillus inulinus* (Martinez-Moreno et al., 2012; Kemsawasd et al., 2015; Klotz et al., 2017), metal ions within nitrogen sources and their impact on cell growth and fermentation have not been investigated extensively.

To understand the uncoupling phenomenon of cell growth and glucose consumption for both efficient carbon utilization and maximum ethanol productivity, we investigated the effects of different nitrogen sources on cell growth, glucose consumption and ethanol production of *Z. mobilis* in this study to help achieve the goal of optimal titer, rate, and yield for economic bioethanol production using *Z. mobilis*. Our results demonstrated that glucose consumption and ethanol production can be coupled with cell growth by changing the nitrogen sources in the rich medium, and the concentration of metal ions such as Mg^{2+} in the nitrogen source is a major factor affecting cell growth and ethanol production.

RESULTS AND DISCUSSION

Effect of Supplementation of Nitrogen Sources Into RM

To understand the uncoupling of cell growth, glucose consumption and ethanol production in *Z. mobilis*, we evaluated factors in the medium affecting cell growth. The recipe of RM for *Z. mobilis* is relatively simple with carbon sources such as glucose, phosphate sources of KH_2PO_4 , and YE as the source of nitrogen, minerals, and vitamins. Thus, 10 mM NH_4Cl was added into RM using YE from the company OXOID (RM^{OXOID}) to increase inorganic nitrogen content. However, extra NH_4Cl supplemented into RM^{OXOID} did not reduce the time for glucose utilization and ethanol production of ZM4 (data not shown).

The effect of supplementing different organic nitrogen sources such as peptone and tryptone were then tested. Our results showed that the supplementation of peptone did not reduce the time of glucose utilization. It still took more than 24 h for cells to consume all glucose in the media with 20 g/L peptone supplemented into RM^{OXOID}. The final biomass in terms of OD₆₀₀ value did increase slightly in correspondence to the increase of peptone added (Figure 1).

Subsequently, different concentrations of tryptone were added in RM^{OXOID} in a separate experiment. The results showed that the addition of extra tryptone could significantly increase both cell biomass and glucose consumption of ZM4 (Figure 2). The addition of more than 5 g/L tryptone in RM^{OXOID} not only enhanced both cell growth and glucose utilization of ZM4, but also coupled the growth and ethanol fermentation of ZM4. The final highest OD₆₀₀ value of ZM4 in RM^{OXOID} with 5 g/L tryptone increased from 1.8 to 4.7, and all glucose was completely consumed within 12 h. *Z. mobilis* in medium without tryptone only utilized half the glucose at the same time point of 12-h post-inoculation (Figure 2).

The positive effect of adding tryptone into RM^{OXOID} was further evaluated by comparing cell growth along with glucose utilization and ethanol production of ZM4 in both RM^{OXOID} and RM^{OXOID} + 5T at different temperatures of 30, 36, and 40°C. The results demonstrated that the supplementation of tryptone increased the growth and fermentation performance of ZM4 at each of these different temperatures, including the specific growth rate (μ), ethanol yield ($Y_{p/s}$), and productivity (Q_p) (Table 1).

It also increased cell growth, glucose consumption rate, and ethanol productivity of ZM4 at higher temperatures of 36 and 40°C than those at the normal temperature of 30°C in RM^{OXOID} supplemented with 5 g/L tryptone, although ethanol yields were similar among these conditions (Table 1 and Figure 3). Compared with a normal temperature of 30°C, the time that ZM4 utilized all glucose at 36 and 40°C in RM^{OXOID} with extra tryptone was reduced by about 3 h, but 1 day was not sufficient for ZM4 to completely consume glucose at any of the aforementioned temperatures in RM^{OXOID} (Figure 3). ZM4 took less time to completely utilize glucose with maximum ethanol production achieved in RM^{OXOID} + 5T at 36 and 40°C (9 h) than at 30°C (12 h) with a corresponding higher growth rate and ethanol productivity, which was increased from 1.75 ± 0.01 at 30°C to 2.19 ± 0.22 and 2.23 ± 0.11 at 36 and 40°C, respectively (Table 1 and Figure 3).

Effect of Exchanging YE From OXOID With Different Brand Ones in RM

As briefly mentioned above, YE distributed by different companies are produced with different processes which may lead to different amounts of total nitrogen and trace elements such as growth factors and metal ions. Besides adding extra nitrogen sources into the RM^{OXOID} as discussed above (Figures 1–3), we also tested the effect of YE from different companies, including those from Becton Dickinson (YE^{BD}) and Sangon Biotech Co., Ltd. (YE^{SG}, Shanghai, China). In addition, another industrial

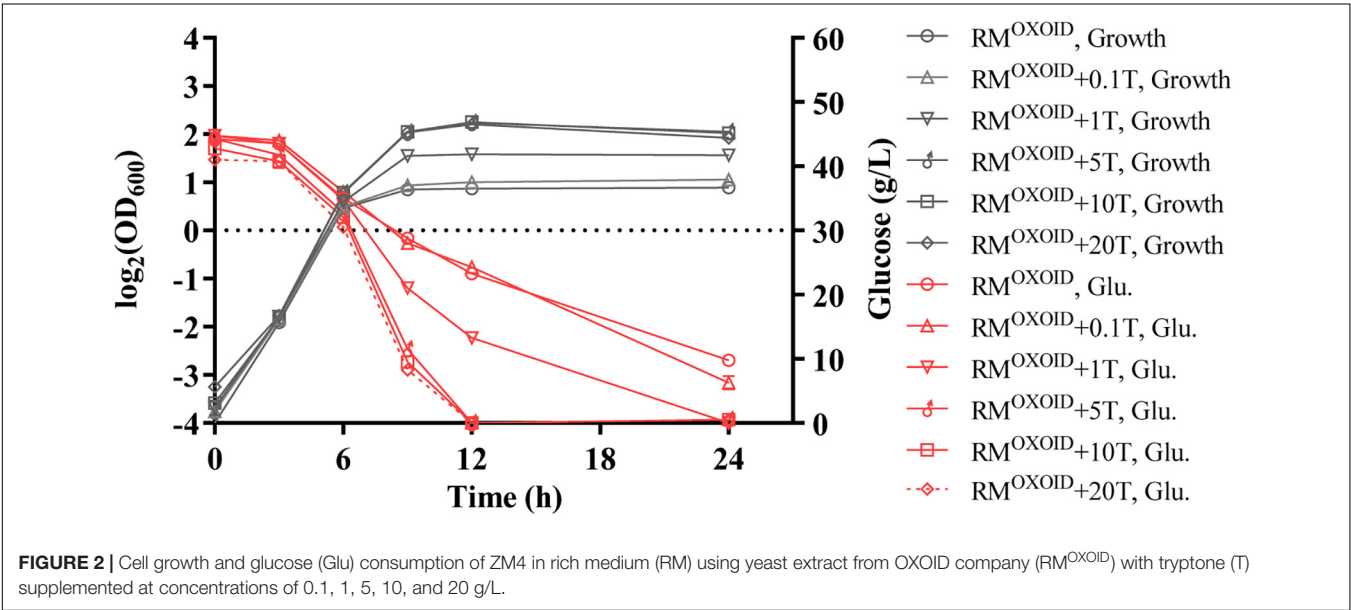
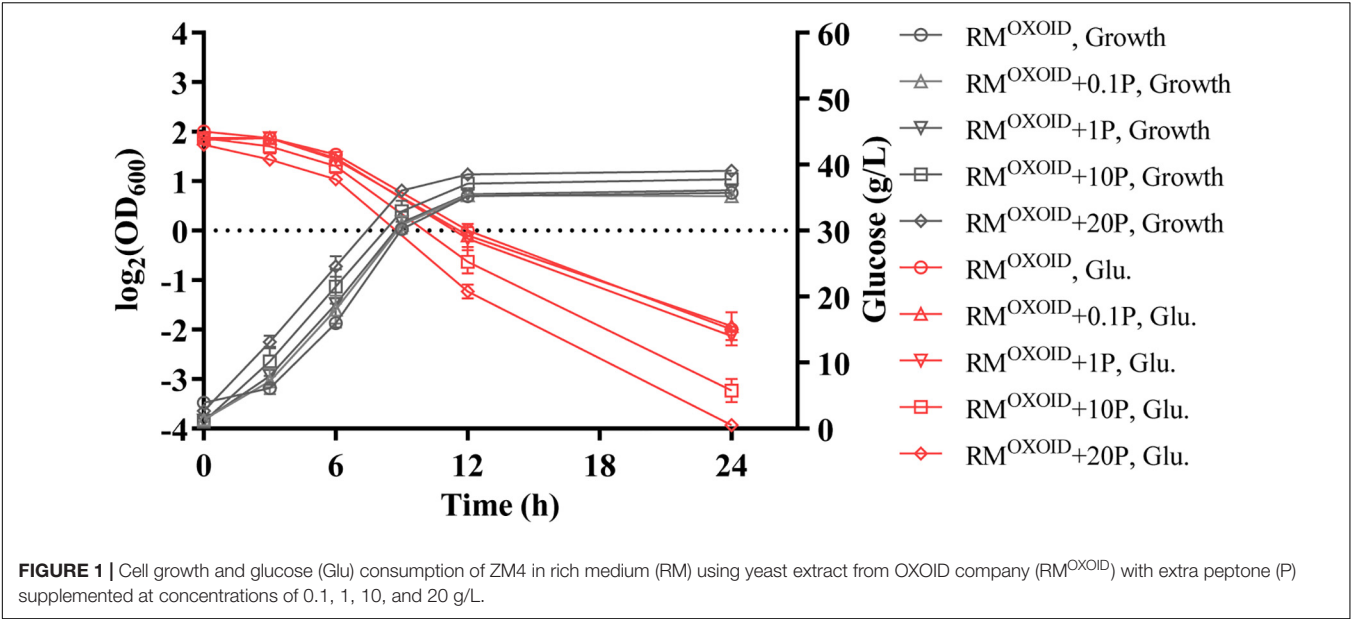
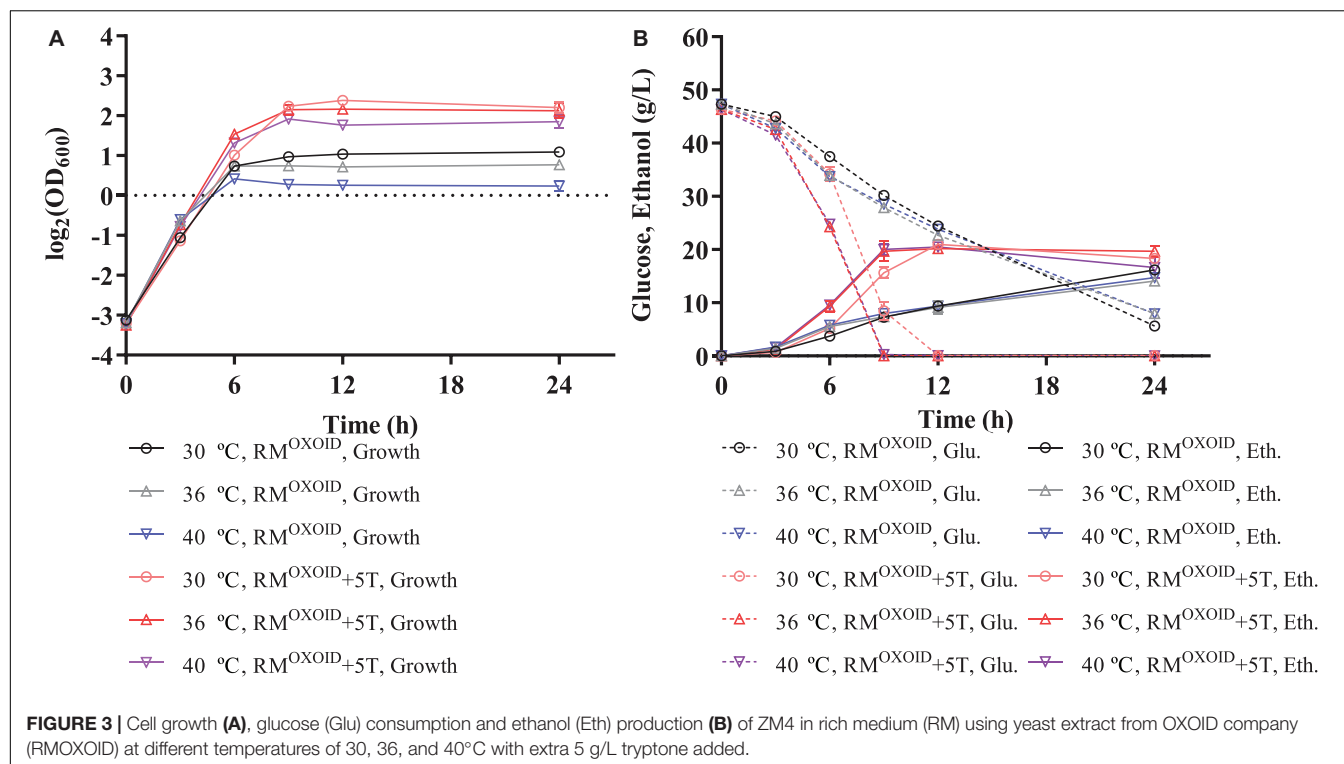


TABLE 1 | Glucose consumption (Y_s), ethanol yield ($Y_{p/s}$), theoretical ethanol yield ($\%Y_{p/s}$), ethanol productivity (Q_p), and specific growth rate (μ) of ZM4 in RM^{OXOID} and RM^{OXOID} supplemented with 5 g/L tryptone at different temperatures within 24 h.

Conditions	Y_s (g/L)	$Y_{p/s}$ (g/g)	$\%Y_{p/s}$ (g/g*100)	Q_p (g/L/h)	μ (h ⁻¹)
30°C, RM^{OXOID}	41.69 ± 0.27	0.39 ± 0.02	76 ± 4	0.67 ± 0.03	0.45 ± 0.01
36°C, RM^{OXOID}	39.36 ± 0.25**	0.36 ± 0.02	70 ± 4	0.59 ± 0.04	0.45 ± 0.01
40°C, RM^{OXOID}	39.40 ± 0.26**	0.37 ± 0.02	73 ± 4	0.61 ± 0.03	0.42 ± 0.00*
30°C, RM^{OXOID} + 5T	46.28 ± 0.04**	0.45 ± 0.00*	89 ± 1	1.75 ± 0.01**	0.49 ± 0.01*
36°C, RM^{OXOID} + 5T	46.29 ± 0.00**	0.43 ± 0.04	83 ± 8	2.19 ± 0.22*	0.55 ± 0.01**
40°C, RM^{OXOID} + 5T	46.08 ± 0.36**	0.44 ± 0.02	85 ± 4	2.23 ± 0.11**	0.53 ± 0.01*

Multiple comparisons were conducted using the values when cells were grown in RM^{OXOID} at 30°C as the control, *represents a significant difference (0.01 < P < 0.05), **represents a very significant difference (P < 0.01).



nitrogen source of corn steep liquid (CSL) from Macklin was evaluated at the same time as the two yeast-based nitrogen sources discussed above. All media used in this research are listed in Tables 5, 6.

YE^{OXOID} in RM^{OXOID} was replaced with different nitrogen sources including peptone (P), tryptone (T), CSL, YE^{BD}, and YE^{SG}. Cell growth, glucose utilization, and ethanol production of ZM4 cultured in these media were then examined. Our results showed ZM4 performed differently in these media (Figure 4). The biomass of ZM4 in RM(T) was about two times higher than that in RM^{OXOID}, while the biomass of ZM4 in RM(P) was the lowest (Figure 4B). Tryptone appeared to be better than YE^{OXOID} and peptone for cell growth, which was consistent with the aforementioned experiments of supplementation of nitrogen source into RM^{OXOID} (Figures 1, 2).

Except for the fact that the specific growth rates of ZM4 in RM with 1% of peptone or CSL as the sole nitrogen source were lower, which can be seen from the slopes of the lines in the exponential phase, the specific growth rates of ZM4 in other RM were almost the same (Figure 4A). Compared with YE^{OXOID} as the sole nitrogen source, YE^{BD}, YE^{SG}, and 5% CSL all increased the final biomass of ZM4 (Figure 4B), reduced the time of glucose consumption (Figure 4C), and coupled cell growth and ethanol production. The biomass of ZM4 in RM^{BD} was more than two times of that in RM^{OXOID} and the time for glucose consumption in RM^{BD} was about two-thirds shorter than that in RM^{OXOID} (Figures 4B,C). YE^{SG}, though cheaper than YE^{BD}, was almost just as good. In the future, YE^{SG} could be used in large-scale fermentation for ethanol production, and the appropriate

nitrogen source can be chosen as needed based on the results above (Figures 1–4).

Effect of Exchanging (NH₄)₂SO₄ in MM With Different Organic Nitrogen Sources

Although the RM recipe is relatively simple containing only three ingredients as discussed above, the composition of organic nitrogen sources such as YE is still complicated containing nitrogen, vitamins, metal ions, etc. Because the only nitrogen source in minimal medium (MM) is the inorganic nitrogen source (NH₄)₂SO₄, it was selected to further examine the effect of different organic nitrogen sources on ZM4. The representative organic nitrogen sources used to replace (NH₄)₂SO₄ in MM included YE^{BD}, YE^{OXOID}, and 5% CSL.

Our results demonstrated that the replacement of inorganic nitrogen source (NH₄)₂SO₄ with organic nitrogen source enhanced cell growth, glucose utilization, and ethanol productivity (Figure 5). Interestingly, ZM4 had similar growth and glucose consumption rates in two MM media with either YE^{BD} or YE^{OXOID} as the sole nitrogen source (Figure 5). These results differed from those when YE^{BD} or YE^{OXOID} was used as the sole nitrogen source in RM where ZM4 grew better in RM with YE^{BD} than in RM with YE^{OXOID} as the nitrogen source (Figure 4). Therefore, some ingredients must exist in MM which RM lacks when YE^{OXOID} is used as the nitrogen source. This difference is contingent on compositions of NaCl, Na₂MoO₄, and MgSO₄ which differ in the ingredients of the two media (Tables 5, 6).

Since magnesium ion is a cofactor of diverse enzymes involved in various metabolic activities, we investigated the effect of

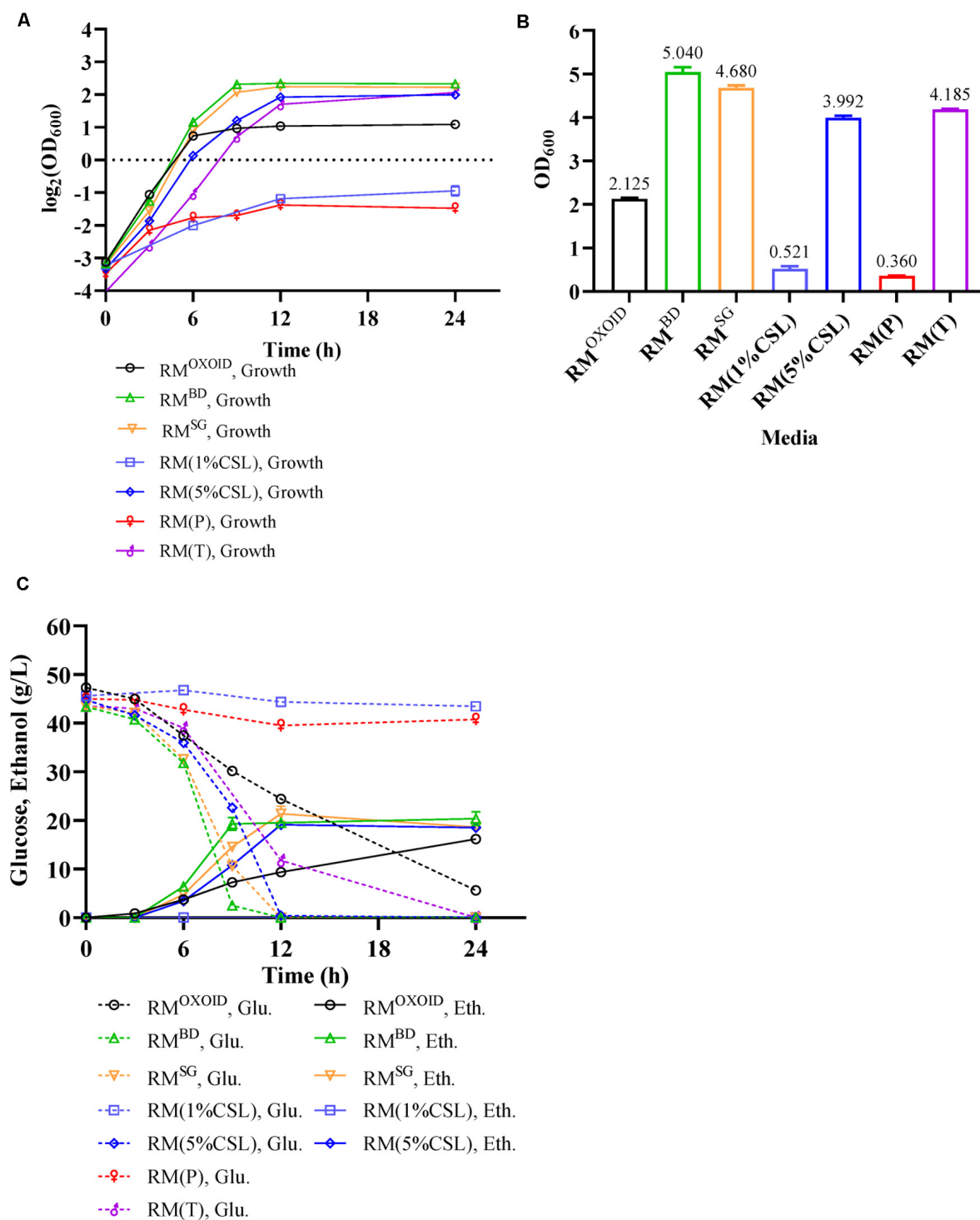


FIGURE 4 | Cell growth **(A)**, final OD_{600} value **(B)**, as well as glucose (Glu) consumption and ethanol (Eth) production **(C)** of ZM4 in RM with different nitrogen sources.

removing the magnesium ion from both MM^{BD} and MM^{OXOID} to test the growth and fermentation performance of ZM4. The lack of Mg^{2+} in MM^{BD} had no effect on the growth of ZM4, but

the biomass decreased in MM^{OXOID} lacking Mg^{2+} (**Figure 6**). This result indicates that the concentration of Mg^{2+} in YE^{OXOID} is different from that in YE^{BD}, and Mg^{2+} plays important roles in

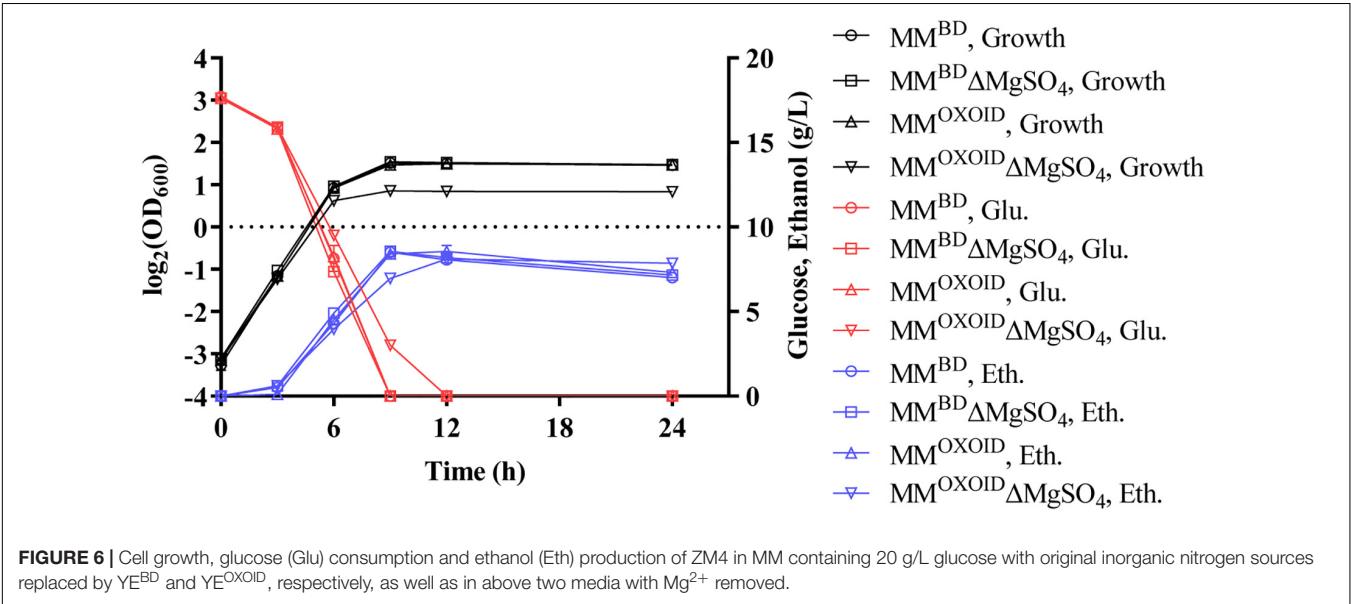
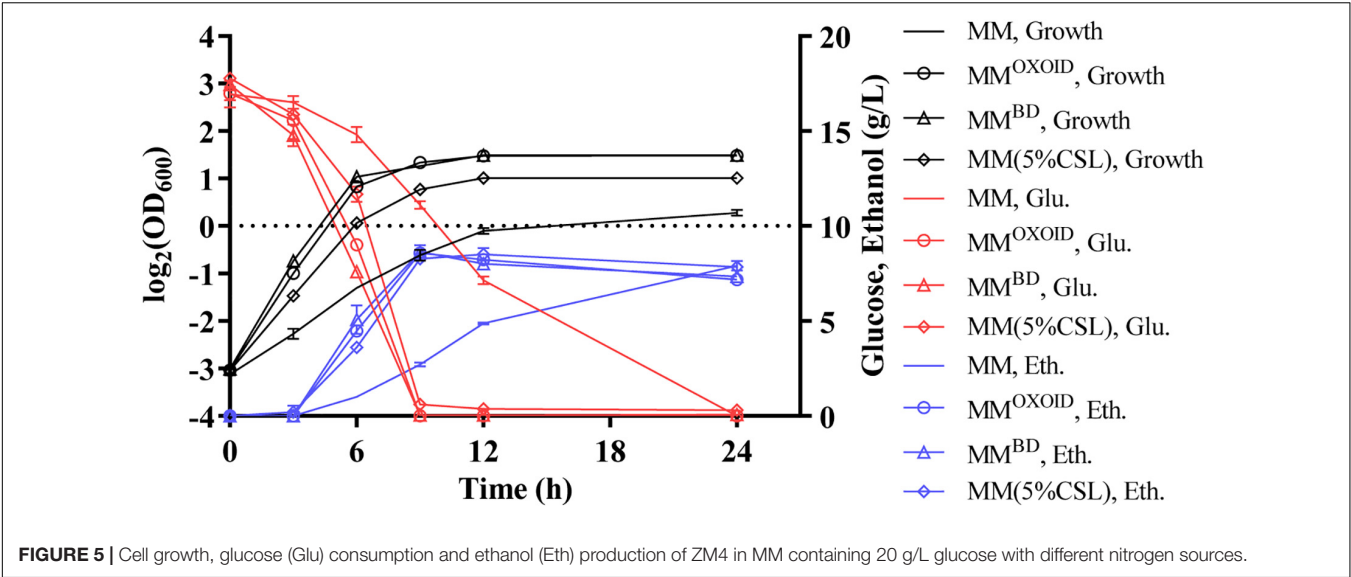


TABLE 2 | Concentrations of different ion elements in different nitrogen sources measured by ICP-OES.

Nitrogen sources	Fe (mg/L)	K (mg/L)	Mg (mg/L)	Na (mg/L)	P (mg/L)	S (mg/L)
1% YE ^{OXID}	0.51	492.74	2.32 ± 0.72	19.16	159.72	58.69
1% YE ^{BD}	0.42	456.13	10.62 ± 0.64**	48.83	129.1	85.92
1% YE ^{SG}	0.28	311.83	14.49 ± 5.60	131.3	278.3	65.59
1% Peptone	0.13	5.52	0.11 ± 0.07	27.8	2.67	5.21
1% Tryptone	0.13	1.07	6.87 ± 5.87	49.56	16.65	17.04
1% CSL	0.48	280.71	13.13 ± 4.82	20.61	198.13	56.88

Magnesium ion was tested twice while other ions were tested only once. Multiple comparisons of magnesium concentrations in different nitrogen sources were conducted with 1% YE^{OXID} as a control, **represents a significant difference ($P < 0.01$).

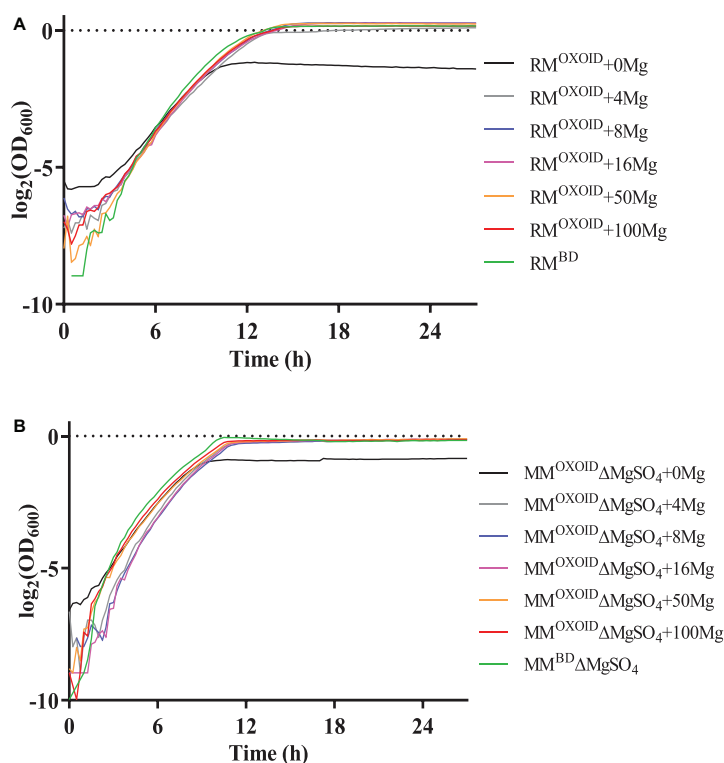


FIGURE 7 | Cell growth of ZM4 in RM^{OXOID} (A) or MM^{OXOID} without MgSO_4 ($\text{MM}^{\text{OXOID}} \Delta\text{MgSO}_4$) (B) with Mg^{2+} supplemented at different concentrations of 0, 4, 8, 16, 50, and 100 mg/L. RM^{BD} and $\text{MM}^{\text{BD}} \Delta\text{MgSO}_4$ were included as controls.

cell growth of *Z. mobilis*, and Mg^{2+} was likely one of the factors affecting the coupling of cell growth, glucose consumption and ethanol production.

Determination of Concentrations of Ions in Different Nitrogen Sources and the Impact of the Mg^{2+} on Fermentation Performance

In order to verify this hypothesis, the concentrations of several major ion elements in different organic nitrogen sources were then measured by ICP-OES. The result showed that the concentrations of these ion elements (Fe, K, Mg, P, S) were different among different nitrogen sources with peptone and tryptone containing fewer of these ions (Table 2). This may be one reason why cell growth and fermentation performance of *Z. mobilis* in media using tryptone and peptone as the sole nitrogen source was not as efficient as in other media using YE (Figure 4).

At the same concentration of nitrogen sources, the Mg^{2+} in the YE from OXOID was 8.3 mg/L less than that from Becton Dickinson. Mg^{2+} is the component with the major difference between these two nitrogen sources of YE from OXOID and BD companies, and therefore could be the reason that cell growth and ethanol fermentation of *Z. mobilis* in RM^{OXOID} was not as efficient as in RM^{BD} (Table 2). Since 0.5 g/L $\text{MgSO}_4 \cdot 7\text{H}_2\text{O}$ containing 49 mg/L Mg^{2+} was provided in MM

which was sufficient for cell growth (Tables 2, 4), the growth difference of *Z. mobilis* in MM^{OXOID} and MM^{BD} was therefore not as obvious as that in RM^{OXOID} and RM^{BD} (Figures 4, 5). The concentration of Mg^{2+} in peptone was the lowest, which could also be one reason that ZM4 grew poorly in $\text{RM}(\text{P})$ compared to other nitrogen sources (Figure 4). These results further confirm the importance of sufficient Mg^{2+} concentration in media for optimal cell growth, glucose consumption and ethanol fermentation. The result that the concentration of Mg^{2+} in tryptone was higher than that in YE^{OXOID} was consistent with the results of the nitrogen source supplement experiment (Kosaka et al., 2020), and provided a conjecture that perhaps the concentration of magnesium ion in nitrogen sources plays an important role in promoting temperature tolerance and cell growth (Figures 2, 3).

To verify the impact of Mg^{2+} on cell growth, different concentrations of Mg^{2+} were then added into the RM^{OXOID} and MM^{OXOID} without MgSO_4 ($\text{MM}^{\text{OXOID}} \Delta\text{MgSO}_4$), and the growth of ZM4 in these media was measured by the Bioscreen C (Figure 7). Our results indicated that in both RM^{OXOID} and $\text{MM}^{\text{OXOID}} \Delta\text{MgSO}_4$, even a small amount of Mg^{2+} at 4 mg/L could boost cell growth significantly.

Cell growth, glucose utilization, and ethanol production were further investigated using the shake flask experiment with OD_{600} values, glucose and ethanol concentrations measured (Figure 8). Consistent with the result of Bioscreen C (Figure 7), the supplementation of at least 8 mg/L of Mg^{2+} in RM^{OXOID} or

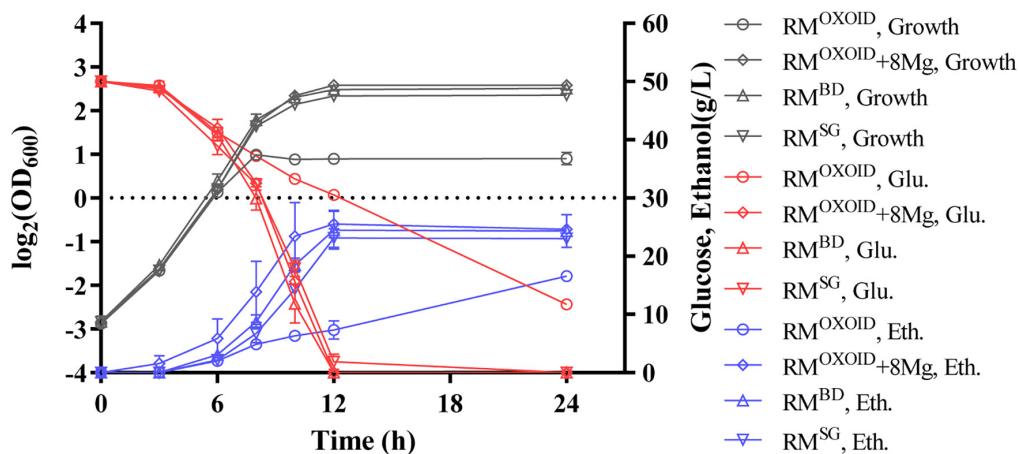


FIGURE 8 | Cell growth, glucose (Glu) consumption, and ethanol (Eth) production of ZM4 in RM^{OXOID} , $RM^{OXOID} + 8Mg$, RM^{BD} , and RM^{SG} . At least two independent experiments were carried out with similar results. Values are the mean of one representative experiment with two or more technical replicates. Error bars represent standard deviations.

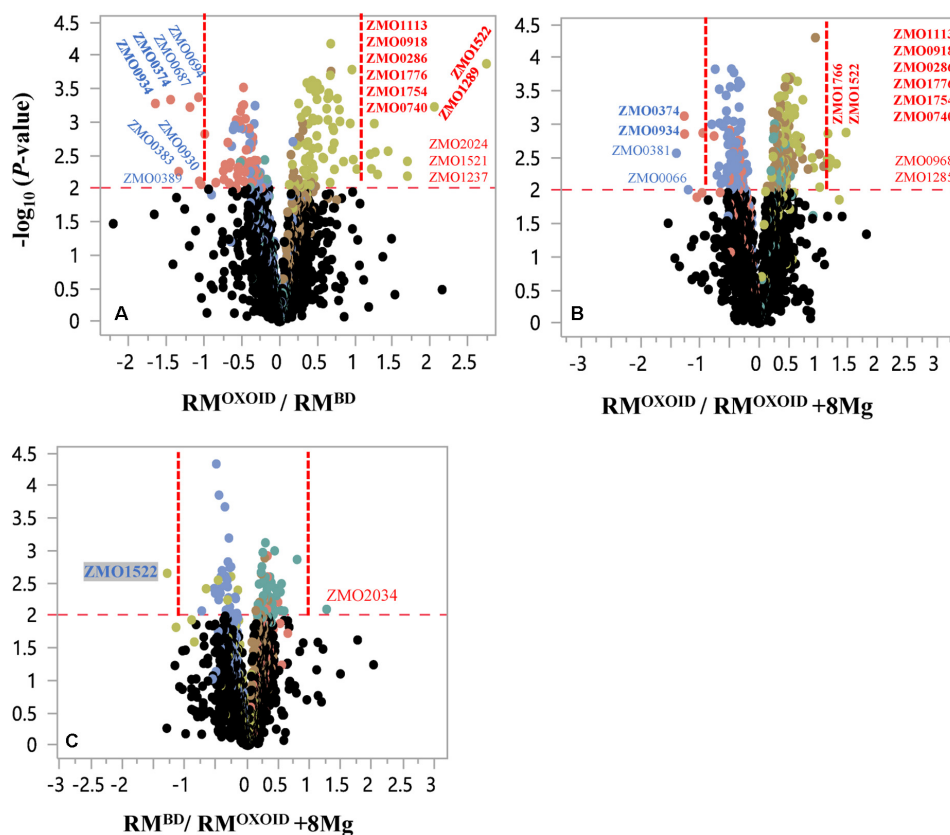


FIGURE 9 | Volcano plots of significantly differentially expressed genes of *Z. mobilis* cultured in RM^{OXOID} and RM^{BD} (RM^{OXOID}/RM^{BD} , (A), RM^{OXOID} and $RM^{OXOID} + 8Mg$ ($RM^{OXOID}/RM^{OXOID} + 8Mg$, (B), as well as RM^{BD} and $RM^{OXOID} + 8Mg$ ($RM^{BD}/RM^{OXOID} + 8Mg$, (C). X-axis is the \log_2 -based ratios between two conditions examined, and Y-axis is the $-\log_{10}(P\text{-value})$ of the difference. The dots above the horizontal red dash line indicate genes significantly differentially expressed, and the vertical red dash line indicate genes significantly differentially expressed with ratio greater than 2 (\log_2 -based ratio greater than 1). Gene name with red and blue color font indicates up-regulated and down-regulated ones, respectively. Gene names with bold font indicate common ones between different comparisons of RM^{OXOID}/RM^{BD} , $RM^{OXOID}/RM^{OXOID} + 8Mg$, and $RM^{BD}/RM^{OXOID} + 8Mg$.

MM^{OXID} Δ MgSO₄ allowed ZM4 to grow as well as in RM^{BD} or MM^{BD} Δ MgSO₄. At the same time, cell growth, glucose consumption, and ethanol production of ZM4 in RM^{OXID} with 8 mg/L Mg²⁺ added (RM^{OXID} + 8Mg) were coupled as in RM^{BD} (Figure 8). This suggests that Mg²⁺ is crucial for cell

growth, glucose consumption and fermentation performance of *Z. mobilis*, and a minimum concentration of at least 8 mg/L is needed for optimal cell growth and ethanol fermentation.

Effects of Mg²⁺ on Gene Expression of *Z. mobilis*

After confirmation of the impact of Mg²⁺ on cell growth and ethanol fermentation of *Z. mobilis* (Figure 8), next-generation sequencing (NGS)-based RNA-Seq transcriptomics was further applied to identify genes responsive for the uncoupling of cell growth, glucose consumption and ethanol fermentation due to the difference of Mg²⁺ concentration in the medium.

Despite that cell growth, glucose consumption and ethanol production exhibited apparent differences (Figure 8), RNA-Seq results showed that only a few genes were differentially expressed. There were seven and four genes down-regulated when *Z. mobilis* was cultured in RM^{OXID} and RM^{BD} (RM^{OXID}/RM^{BD}, Figure 9A and Table 3) as well as cultured in RM^{OXID} and RM^{OXID} + 8Mg (RM^{OXID}/RM^{OXID} + 8Mg, Figure 9B and Table 4), respectively. Although genes up-regulated in RM^{OXID} were more than those down-regulated (Figure 9 and Tables 3, 4), there were only 11 and 10 up-regulated genes identified when *Z. mobilis* was cultured in RM^{OXID} and RM^{BD} (RM^{OXID}/RM^{BD}, Figure 9A and Table 3) as well as cultured in

TABLE 3 | List of significantly differentially expressed genes between ZM4 cultured in RM^{BD} and RM^{OXID}.

Name	Product	Ratio	−log ₁₀ (P-value)
Up-regulated gene in ZM4 cultured in RM^{OXID} compared with RM^{BD}			
ZMO1113	NADH dehydrogenase	1.03	2.29
ZMO0918	Catalase	1.21	2.52
ZMO0286	DUF541 domain-containing protein	1.22	2.30
ZMO1776	Aminopeptidase N	1.26	2.98
ZMO1754	Succinate-semialdehyde dehydrogenase SSADH	1.27	2.55
ZMO2024	Hypothetical protein	1.30	2.21
ZMO0740	General stress protein CsbD	1.44	2.56
ZMO1521	Hypothetical protein	1.70	2.41
ZMO1237	Lactate dehydrogenase	1.70	2.19
ZMO1289	Putative transglycosylase-associated protein	2.06	3.23
ZMO1522	TonB-dependent receptor	2.75	3.88
Down-regulated gene in ZM4 cultured in RM^{OXID} compared with RM^{BD}			
ZMO0934	Secretion-related protein	−1.65	3.28
ZMO0374	Levansucrase	−1.45	3.34
ZMO0383	Hypothetical protein	−1.34	2.26
ZMO0687	Acetolactate synthase large subunit	−1.19	3.23
ZMO0694	Hypothetical protein	−1.08	3.38
ZMO0930	Hypothetical protein	−1.06	2.11
ZMO0389	Constituent protein	−1.04	2.07

Ratio is the log₂-based expression difference between ZM4 cultured in RM^{OXID} and RM^{BD} (RM^{OXID}/RM^{BD}).

TABLE 4 | List of significantly differentially expressed genes between ZM4 cultured in RM^{OXID} and RM^{OXID} + 8Mg.

Name	Product	Ratio	−log ₁₀ (P-value)
Up-regulated gene in ZM4 cultured in RM^{OXID} compared with RM+8Mg			
ZMO1522	TonB-dependent receptor	1.47	2.88
ZMO0286	DUF541 domain-containing protein	1.31	2.40
ZMO1754	Succinate-semialdehyde dehydrogenase SSADH	1.21	2.47
ZMO0918	Catalase	1.18	2.49
ZMO1289	Putative transglycosylase-associated protein	1.17	2.35
ZMO1776	Aminopeptidase N	1.17	2.86
ZMO1113	NADH dehydrogenase	1.15	2.47
ZMO0968	Hypothetical protein	1.09	2.37
ZMO0740	General stress protein CsbD	1.03	2.05
ZMO1285	Sorbitol dehydrogenase large subunit	1.02	2.55
Down-regulated gene in ZM4 cultured in RM^{OXID} compared with RM+8Mg			
ZMO0066	Hypothetical protein	−1.20	2.02
ZMO0934	Secretion-related protein	−1.26	2.85
ZMO0374	Levansucrase	−1.26	3.12
ZMO0381	Hypothetical protein	−1.40	2.56

Ratio is the log₂-based expression difference between ZM4 cultured in RM^{OXID} and RM^{OXID} + 8Mg (RM^{OXID}/RM^{OXID} + 8Mg).

TABLE 5 | Recipes of different rich medium (RM) with different nitrogen sources used in this work.

Media	Nitrogen sources
RM(P)	Peptone (10 g/L)
RM(T)	Tryptone (10 g/L)
RM(1%CSL)	CSL (10 g/L)
RM(5%CSL)	CSL (50 g/L)
RM ^{BD}	YE ^{BD} (10 g/L)
RM ^{SG}	YE ^{SG} (10 g/L)
RM ^{OXID}	YE ^{OXID} (10 g/L)
RM + P	YE ^{OXID} (10 g/L) + peptone
RM + T	YE ^{OXID} (10 g/L) + tryptone

All media contained ingredients of glucose (50 g/L), KH₂PO₄ (2 g/L), and nitrogen sources. YE, Yeast extract; CSL, corn steep liquid. The media supplemented with CSL were filter-sterilized, others were autoclaved (108°C, 30 min).

TABLE 6 | Recipes of different minimal medium (MM) with different nitrogen sources and metal ions of Mg²⁺ and MoO₄^{2−} used in this work.

Media	Nitrogen sources	MgSO ₄ ·7H ₂ O (0.5 g/L)
MM	(NH ₄) ₂ SO ₄ (1 g/L)	+
MM(5%CSL)	CSL (50 g/L)	+
MM ^{OXID}	YE ^{OXID} (10 g/L)	+
MM ^{BD}	YE ^{BD} (10 g/L)	+
MM ^{OXID} Δ MgSO ₄	YE ^{OXID} (10 g/L)	−
MM ^{BD} Δ MgSO ₄	YE ^{BD} (10 g/L)	−

YE, Yeast extract; CSL, corn steep liquid. All media contained ingredients of glucose (20 g/L), K₂HPO₄ (1 g/L), KHP₂O₄ (1 g/L), NaCl (0.5 g/L), and nitrogen sources. The media supplemented with CSL were filter-sterilized, others were autoclaved (108°C, 30 min). After the autoclavation, the filter-sterilized Na₂MoO₄·2H₂O (0.025 g/L) was then added into the media, and the filter-sterilized MgSO₄·7H₂O (0.5 g/L) was also added into the media as needed +: with the component in the medium; −: without the component in the medium.

RM^{OXOID} and RM^{OXOID} + 8Mg (RM^{OXOID}/RM^{OXOID} + 8Mg, **Figure 9B** and **Table 4**), respectively. Two and eight of these down-regulated and up-regulated ones are common between these two comparisons (**Figure 9** and **Tables 3, 4**).

Genes related to stress responses were up-regulated while genes related to protein secretion were down-regulated in RM^{OXOID} medium compared with in RM^{OXOID} + 8Mg or RM^{BD} medium (**Figure 9** and **Tables 3, 4**). For example, genes encoding catalase (*ZMO0918*), general stress protein CsbD (*ZMO0740*), NADH dehydrogenase (*ZMO1113*), and succinate-semialdehyde dehydrogenase SSADH (*ZMO1754*) were up-regulated when RM^{OXOID} was used compared with those in RM^{OXOID} + 8Mg or RM^{BD} (**Figure 9** and **Tables 3, 4**). These results indicate that Mg²⁺, a key element of cofactor, is essential for vigorous cell growth, and the lack of Mg²⁺ will trigger energy-consuming stress responses while slowing down energy-consuming metabolism with genes encoding levansucrase (*ZMO0374*) and secretion-related protein (*ZMO0934*) being down-regulated (**Figure 9** and **Tables 3, 4**).

Considering that the supplementation of 8 mg/L Mg²⁺ into RM^{OXOID} (RM^{OXOID} + 8Mg) could restore the coupling of cell growth, glucose consumption and ethanol fermentation of *Z. mobilis* (**Figure 8**) and that there was only one gene up-regulated (*ZMO2034*) and one down-regulated (*ZMO1522*) when *Z. mobilis* grew in RM^{BD} compared with RM^{OXOID} + 8Mg (**Figure 9C**), the transcriptomics study further confirmed our hypothesis that the difference of Mg²⁺ concentrations in different nitrogen sources is one of the determinants affecting the coupling of cell growth, glucose consumption and ethanol fermentation in *Z. mobilis*.

CONCLUSION

The effects of nitrogen sources on cell growth, glucose consumption, and ethanol fermentation performance of *Z. mobilis* ZM4 were investigated to understand the uncoupling of cell growth, glucose consumption and ethanol fermentation of ZM4 in this study. Through the supplementation and replacement of inorganic or organic nitrogen sources in both RM and MM, we found that YE^{BD}, YE^{SG}, or 5% CSL were better than YE^{OXOID}. We also quantified the ion elements in different nitrogen sources using ICP-OES, and demonstrated that the difference of magnesium ion in YE is one of the major factors affecting cell growth and ethanol fermentation. We further verified the impact of Mg²⁺ on cell growth of ZM4 by supplementing various concentrations of Mg²⁺ into the medium, and used the RNA-Seq transcriptomics approach to identify genes responsive for the uncoupling of cell growth, glucose consumption and ethanol fermentation when the medium lacked Mg²⁺. These findings can be used as a reference for the selection and/or modification of nitrogen sources using *Z. mobilis* ZM4. The concentrations of ion elements in nitrogen sources affecting cell growth and fermentation performance can also be used as a parameter for optimizing and monitoring the components of nitrogen sources for efficient cell growth and fermentation using other microorganisms.

MATERIALS AND METHODS

Bacterial Strain, Media, and Growth Conditions

Zymomonas mobilis ZM4 (ATCC 31821) was revived from frozen glycerol stocks in 10 mL RM^{OXOID} (50 g/L glucose, 10 g/L YE, 2 g/L KH₂PO₄) at 30°C for about 6–8 h prior to inoculating overnight seed cultures at 30°C at 100 rpm in RM^{OXOID} using shake flasks with a sealing gas permeable membrane sealed filled to 80% capacity. Glucose, KH₂PO₄, K₂HPO₄, NaCl, MgSO₄·7H₂O, Na₂MoO₄·2H₂O, and NH₄Cl were purchased from Sinopharm Chemical Reagent Co., Ltd. (Shanghai, China). YE was purchased from OXOID, Becton Dickinson, and Sangon Biotech (Shanghai) Co., Ltd. (Shanghai, China). Tryptone was purchased from OXOID. Peptone was purchased from Becton Dickinson. Corn steep liquid (CSL) was purchased from Shanghai Macklin Biochemical Co., Ltd. (Shanghai, China).

The recipes of different rich medium (RM) and minimal medium (MM) with different nitrogen sources used in this work were listed in **Tables 5, 6**, respectively.

Growth Test by Bioscreen C

The Bioscreen C automatic growth curve analyzer has the functions of culturing cells and measuring cell turbidity. It is similar to the plate reader, but can continuously measure the turbidity of cells, while maintaining a constant temperature and rotation speed to maintain normal cell growth.

The seed culture of *Z. mobilis* was centrifuged to remove RM^{OXOID}. Cells were resuspended with test medium. Bioscreen C assays were carried out as described previously (Frandsen et al., 2009; Yang et al., 2010, 2014a,b, 2016b; Yang S. et al., 2018) except that cells were inoculated into Bioscreen C wells containing a total volume of 200 µL test medium at an initial OD₆₀₀ value of 0.05 and incubated without shaking at 30°C. Triplicate were used for each condition, and turbidity measurements (OD₆₀₀) were taken every 15 min till cells grew into stationary phase. At least two independent experiments were carried out with similar results. Values are the mean of one representative experiment with two or more technical replicates. Error bars represent standard deviations.

Flask Fermentation and Analytical Analysis

The seed culture of *Z. mobilis* was used to inoculate the shake flask containing 80% of test medium with a sealing gas permeable membrane sealed at an initial OD₆₀₀ of 0.1, and cultured at 30°C, 100 rpm. At least two replicates were used for each condition.

The OD₆₀₀ values of the bacterial culture was measured by UV-visible spectrophotometer UV-1800 (AoYi Instrument Co., Ltd., Shanghai, China) every 3 h. At the same time, 1-mL culture was centrifuged at 12,000 rpm for 1 min to obtain the supernatant for measuring the glucose and ethanol concentrations in the culture. Biosensor analyzer M-100 (Sieman Technology Co., Ltd., Shenzhen, China) was used for quick assessment of the

concentrations of glucose and ethanol. The supernatant was also filtered through a 0.45 μm filter before applying on a Shimadzu LC-2030 high pressure liquid chromatography (HPLC) with refractive index detector (RID). Bio-Rad Aminex HPX-87H (300 \times 7.8 mm) column was used to separate the fermentation products, and 0.005 M H_2SO_4 was used as the mobile phase at a flow rate of 0.5 mL/min. Temperatures of detector and column were 40 and 60°C, respectively. The measurement of glucose and ethanol by HPLC and Biosensor analyzer M-100 was compared, and the results showed that the measurement data of the two instruments on the same sample were close (data not shown). At least two independent experiments were carried out with similar results. Values are the mean of one representative experiment with two or more technical replicates. Error bars represent standard deviations.

One percent (w/v) of different organic nitrogen sources were prepared in ddH₂O and then filter-sterilized. The concentrations of different ions in these samples were then measured by Inductively Coupled Plasma Optical Emission Spectroscopy (ICP-OES, Wuhan SouSepad Testing Technology Co., Ltd., Wuhan, China).

Ethanol Production Calculations

Cell growth was monitored by optical density spectrophotometrically at 600 nm. The time points when cells reached stationary phase and when glucose was completely consumed with the maximum ethanol produced were recorded. The concentrations of glucose and ethanol determined by HPLC or Biosensor analyzer M-100 were then used for the calculation of the ethanol yield ($Y_{p/s}$), theoretical ethanol yield ($\%Y_{p/s}$), ethanol productivity (Q_p), and specific growth rate (μ) using the formula below:

$Y_{p/s}$ = maximum ethanol (g)/consumed glucose (g);

$\%Y_{p/s}$ = (ethanol(g)/(consumed sugar(g)*0.511))*100;

Q_p = maximum ethanol titer (g/L)/time to reach the maximum ethanol.

μ = $\ln((\text{OD}_{600} \text{ at } t_2)/(\text{OD}_{600} \text{ at } t_1))/(t_2 - t_1)$, t_1 and t_2 are the time points in the log phase.

Transcriptomic Analysis

The transcriptomics study followed previous work (Frandsen et al., 2009; Zhao et al., 2009; Martinez-Moreno et al., 2012; Kemsawasd et al., 2015; Klotz et al., 2017; Yang S. et al., 2018; Lozano Terol et al., 2019). Briefly, cell culture samples were collected during the exponential phase with the OD₆₀₀ values around 0.6–0.8. RNA-Seq was performed using paired-end sequencing technology according to standard Illumina protocols (Genewiz Inc., Suzhou, China). The quality of RNA-Seq fastq data was evaluated using FastQC software (Babraham Bioinformatics, United States). Data passing the quality control were imported

into CLC Genomics Workbench (Ver. 11.0) for RNA-Seq analysis to get the RPKM value (reads mapping to the genome per kilobase of transcript per million reads sequenced) of each gene with the reference genome. Genome sequence of *Z. mobilis* was used as the reference for RPKM calculation (Yang et al., 2010; Martinez-Moreno et al., 2012). The RPKM value of each gene was then imported into JMP Genomics (Ver. 9.0); data normalization and statistical analysis were conducted to identify differentially expressed genes when three different media were used. Duplicate samples were used for each condition. RNA-Seq raw data were deposited at Sequence Read Archive (SRA) database with the Bioproject accession number of PRJNA601020.

DATA AVAILABILITY STATEMENT

The RNA-Seq raw data was deposited at Sequence Read Archive (SRA) database with the BioProject accession number PRJNA601020.

AUTHOR CONTRIBUTIONS

SY conceived and designed the experiments with inputs from RL, MJ, SC, ML, and JD. RL performed the experiments. RL and SY wrote the manuscript. MJ, ML, SC, and JD conducted the extensive manuscript review. All authors contributed to the article and approved the submitted version.

FUNDING

This work was supported by the National Key Research and Development Program of China (2018YFA0900300), the National Science Foundation of China (21978071 and U1932141), the Technical Innovation Special Fund of Hubei Province (2019AHB055 and 2018ACA149), and the Leading Innovative and Entrepreneur Team Introduction Program of Zhejiang Province (2018R01014). We also acknowledge the support from State Key Laboratory of Biocatalysis and Enzyme Engineering.

ACKNOWLEDGMENTS

This manuscript has been released as a pre-print at Research Square: RL, MJ, JD, SC, SY, Underlying Mechanism of Uncoupled Cell Growth and Ethanol Fermentation of *Zymomonas mobilis* using Different Nitrogen Sources, doi: 10.21203/rs.2.21812/v1. We appreciate the reviewers for their valuable advice.

REFERENCES

- Christensen, D. G., Orr, J. S., Rao, C. V., and Wolfe, A. J. (2017). Increasing growth yield and decreasing acetylation in *Escherichia coli* by optimizing the carbon-to-magnesium ratio in peptide-based media. *Appl. Environ. Microbiol.* 83:AEM.03034-16. doi: 10.1128/AEM.03034-16
- Conway, T. (1992). The entner-doudoroff pathway. history, physiology and molecular biology. *FEMS Microbiol. Rev.* 9, 1–27.
- Cot, M., Loret, M. O., Francois, J., and Benbadis, L. (2007). Physiological behaviour of *Saccharomyces cerevisiae* in aerated fed-batch fermentation for high level production of bioethanol. *FEMS Yeast Res.* 7, 22–32. doi: 10.1111/j.1567-1364.2006.00152.x

- Dien, B. S., Cotta, M. A., and Jeffries, T. W. (2003). *Bacteria* engineered for fuel ethanol production. current status. *Appl. Microbiol. Biotechnol.* 63, 258–266. doi: 10.1007/s00253-003-1444-y
- Duan, G., Wu, B., Qin, H., Wang, W., Tan, Q., Dai, Y., et al. (2019). Replacing water and nutrients for ethanol production by ARTP derived biogas slurry tolerant *Zymomonas mobilis* strain. *Biotechnol. Biofuels* 12:124.
- Flamholz, A., Noor, E., Bar-Even, A., Liebermeister, W., and Milo, R. (2013). Glycolytic strategy as a tradeoff between energy yield and protein cost. *Proc. Natl. Acad. Sci. U.S.A.* 110, 10039–10044. doi: 10.1073/pnas.1215283110
- Frandsen, M. A., Pienkos, P. T., and Zhang, M. (2009). Development of a high-throughput method to evaluate the impact of inhibitory compounds from lignocellulosic hydrolysates on the growth of *Zymomonas mobilis*. *J. Biotechnol.* 144, 259–267. doi: 10.1016/j.jbiotec.2009.08.006
- He, M. X., Wu, B., Qin, H., Ruan, Z. Y., Tan, F. R., Wang, J. L., et al. (2014). *Zymomonas mobilis*, a novel platform for future biorefineries. *Biotechnol. Biofuels* 7:101. doi: 10.1186/1754-6834-7-101
- He, M. X., Wu, B., Shui, Z. X., Hu, Q. C., Wang, W. G., Tan, F. R., et al. (2012). Transcriptome profiling of *Zymomonas mobilis* under ethanol stress. *Biotechnol. Biofuels* 5:75. doi: 10.1186/1754-6834-5-75
- Ismail, K. S., Sakamoto, T., Hasunuma, T., Zhao, X. Q., and Kondo, A. (2014). Zinc, magnesium, and calcium ion supplementation confers tolerance to acetic acid stress in industrial *Saccharomyces cerevisiae* utilizing xylose. *Biotechnol. J.* 9, 1519–1525. doi: 10.1002/biot.201300553
- Jacobson, T. B., Adamczyk, P. A., Stevenson, D. M., Regner, M., Ralph, J., Reed, J. L., et al. (2019). 2H and 13C metabolic flux analysis elucidates in vivo thermodynamics of the ED pathway in *Zymomonas mobilis*. *Metab. Eng.* 54, 301–316. doi: 10.1016/j.ymben.2019.05.006
- Jones, C. W., and Doelle, H. W. (1991). Kinetic control of ethanol production by *Zymomonas mobilis*. *Appl. Microbiol. Biotechnol.* 35, 4–9.
- Ju, N. H., Damiano, D., Shin, C. S., Kim, N. K., and Wang, S. S. (1983). Continuous ethanol fermentation of *Zymomonas mobilis* using soy flour as a protective agent. *Biotechnol. Lett.* 5, 837–842. doi: 10.1007/bf01386658
- Kemsawasd, V., Viana, T., Ardo, Y., and Arneborg, N. (2015). Influence of nitrogen sources on growth and fermentation performance of different wine yeast species during alcoholic fermentation. *Appl. Microbiol. Biotechnol.* 99, 10191–10207. doi: 10.1007/s00253-015-6835-3
- Kingston, R. L., Scopes, R. K., and Baker, E. N. (1996). The structure of glucose-fructose oxidoreductase from *Zymomonas mobilis*, an osmoprotective periplasmic enzyme containing non-dissociable NADP. *Structure* 4, 1413–1428. doi: 10.1016/s0969-2126(96)00149-9
- Klotz, S., Kuenz, A., and Prüße, U. (2017). Nutritional requirements and the impact of yeast extract on the d-lactic acid production by *Sporolactobacillus inulinus*. *Green Chem.* 19, 4633–4641. doi: 10.1039/c7gc01796k
- Kosaka, T., Nishioka, A., Sakurada, T., Miura, K., Anggarini, S., and Yamada, M. (2020). Enhancement of thermal resistance by metal ions in thermotolerant *Zymomonas mobilis* TISTR 548. *Front. Microbiol.* 11:502. doi: 10.3389/fmicb.2020.00502
- Kremer, T. A., LaSarre, B., Posto, A. L., and McKinlay, J. B. (2015). N₂ gas is an effective fertilizer for bioethanol production by *Zymomonas mobilis*. *Proc. Natl. Acad. Sci. U.S.A.* 112, 2222–2226. doi: 10.1073/pnas.1420663112
- Lawford, H. G., and Rousseau, J. D. (1997). Corn steep liquor as a cost-effective nutrition adjunct in high-performance *Zymomonas* ethanol fermentations. *Appl. Biochem. Biotechnol.* 6, 287–304. doi: 10.1007/978-1-4612-2312-2_25
- Lozano Terol, G., Gallego-Jara, J., Sola Martínez, R. A., Cánovas Díaz, M., and de Diego Puente, T. (2019). Engineering protein production by rationally choosing a carbon and nitrogen source using *E. coli* BL21 acetate metabolism knockout strains. *Microbial. Cell Factories* 18:151.
- Martinez-Moreno, R., Morales, P., Gonzalez, R., Mas, A., and Beltran, G. (2012). Biomass production and alcoholic fermentation performance of *Saccharomyces cerevisiae* as a function of nitrogen source. *FEMS Yeast Res.* 12, 477–485. doi: 10.1111/j.1567-1364.2012.00802.x
- Pagliardini, J., Hubmann, G., Alfenore, S., Nevoigt, E., Bideaux, C., and Guillouet, S. E. (2013). The metabolic costs of improving ethanol yield by reducing glycerol formation capacity under anaerobic conditions in *Saccharomyces cerevisiae*. *Microb. Cell Fact.* 12:29. doi: 10.1186/1475-2859-12-29
- Panesar, P. S., Marwaha, S. S., and Kennedy, J. F. (2006). *Zymomonas mobilis*, an alternative ethanol producer. *J. Chem. Technol. Biotechnol.* 81, 623–635. doi: 10.1002/jctb.1448
- Rogers, P. L., Goodman, A. E., and Heyes, R. H. (1984). *Zymomonas* ethanol fermentations. *Microbiol. Sci.* 1, 133–136.
- Rogers, P. L., Jeon, Y. J., Lee, K. J., and Lawford, H. G. (2007). *Zymomonas mobilis* for fuel ethanol and higher value products. *Adv. Biochem. Eng. Biotechnol.* 108, 263–288. doi: 10.1007/10_2007_060
- Wang, X., He, Q., Yang, Y., Wang, J., Haning, K., Hu, Y., et al. (2018). Advances and prospects in metabolic engineering of *Zymomonas mobilis*. *Metab. Eng.* 50, 57–73. doi: 10.1016/j.ymben.2018.04.001
- Xia, J., Liu, C. G., Zhao, X. Q., Xiao, Y., Xia, X. X., and Bai, F. W. (2018). Contribution of cellulose synthesis, formation of fibrils and their entanglement to the self-flocculation of *Zymomonas mobilis*. *Biotechnol. Bioeng.* 115, 2714–2725. doi: 10.1002/bit.26806
- Xue, C., Zhao, X. Q., and Bai, F. W. (2010). Effect of the size of yeast flocs and zinc supplementation on continuous ethanol fermentation performance and metabolic flux distribution under very high concentration conditions. *Biotechnol. Bioeng.* 105, 935–944.
- Yang, S., Fei, Q., Zhang, Y., Contreras, L. M., Utturkar, S. M., Brown, S. D., et al. (2016a). *Zymomonas mobilis* as a model system for production of biofuels and biochemicals. *Microb. Biotechnol.* 9, 699–717. doi: 10.1111/1751-7915.12408
- Yang, S., Mohagheghi, A., Frandsen, M. A., Chou, Y. C., Chen, X., Dowe, N., et al. (2016b). Metabolic engineering of *Zymomonas mobilis* for 2,3-butanediol production from lignocellulosic biomass sugars. *Biotechnol. Biofuels* 9:189.
- Yang, S., Frandsen, M. A., Brown, S. D., Chou, Y. C., Pienkos, P. T., and Zhang, M. (2014a). Insights into acetate toxicity in *Zymomonas mobilis* 8b using different substrates. *Biotechnol. Biofuels* 7:140.
- Yang, S., Pan, C., Hurst, G. B., Dice, L., Davison, B. H., and Brown, S. D. (2014b). Elucidation of *Zymomonas mobilis* physiology and stress responses by quantitative proteomics and transcriptomics. *Front. Microbiol.* 5:246. doi: 10.3389/fmicb.2014.00246
- Yang, S., Frandsen, M. A., Yang, Q., Chou, Y. C., Zhang, M., and Pienkos, P. T. (2018). Identification of inhibitors in lignocellulosic slurries and determination of their effect on hydrocarbon-producing microorganisms. *Front. Bioeng. Biotechnol.* 6:23. doi: 10.3389/fbioe.2018.00023
- Yang, S., Land, M. L., Klingeman, D. M., Pelletier, D. A., Lu, T. Y., Martin, S. L., et al. (2010). Paradigm for industrial strain improvement identifies sodium acetate tolerance loci in *Zymomonas mobilis* and *Saccharomyces cerevisiae*. *Proc. Natl. Acad. Sci. U.S.A.* 107, 10395–10400. doi: 10.1073/pnas.0914506107
- Yang, Y., Hu, M., Tang, Y., Geng, B., Qiu, M., He, Q., et al. (2018). Progress and perspective on lignocellulosic hydrolysate inhibitor tolerance improvement in *Zymomonas mobilis*. *Bioresour. Bioprocess.* 5:6.
- Zarei, O., Dastmalchi, S., and Hamzeh-Mivehroud, M. (2016). A simple and rapid protocol for producing yeast extract from *Saccharomyces cerevisiae* suitable for preparing bacterial culture media. *Iran J. Pharm. Res.* 15, 907–913.
- Zhao, X. Q., and Bai, F. W. (2012). Zinc and yeast stress tolerance. micronutrient plays a big role. *J. Biotechnol.* 158, 176–183. doi: 10.1016/j.jbiotec.2011.06.038
- Zhao, X. Q., Xue, C., Ge, X. M., Yuan, W. J., Wang, J. Y., and Bai, F. W. (2009). Impact of zinc supplementation on the improvement of ethanol tolerance and yield of self-flocculating yeast in continuous ethanol fermentation. *J. Biotechnol.* 139, 55–60. doi: 10.1016/j.jbiotec.2008.08.013

Conflict of Interest: JD was employed by China Biotech Fermentation Industry Association. ML was employed by Zhejiang Huakang Pharmaceutical Co., Ltd.

The remaining authors declare that the research was conducted in the absence of any commercial or financial relationships that could be construed as a potential conflict of interest.

The reviewer QG declared a past co-authorship with one of the authors SY to the handling editor.

Copyright © 2020 Li, Jin, Du, Li, Chen and Yang. This is an open-access article distributed under the terms of the Creative Commons Attribution License (CC BY). The use, distribution or reproduction in other forums is permitted, provided the original author(s) and the copyright owner(s) are credited and that the original publication in this journal is cited, in accordance with accepted academic practice. No use, distribution or reproduction is permitted which does not comply with these terms.



A Novel Butanol Tolerance-Promoting Function of the Transcription Factor Rob in *Escherichia coli*

Zhiquan Wang^{1,2†}, Tingli Xue^{1,2†}, Dongsheng Hu^{1,2} and Yuanyuan Ma^{1,3,4,5*}

¹ Biomass Conversion Laboratory, R&D Center for Petrochemical Technology, Tianjin University, Tianjin, China, ² Department of Biochemical Engineering, School of Chemical Engineering and Technology, Tianjin University, Tianjin, China, ³ Collaborative Innovation Centre of Chemical Science and Engineering, and Key Laboratory for Green Chemical Technology, Tianjin University, Tianjin, China, ⁴ State Key Laboratory of Biobased Material and Green Papermaking, Qilu University of Technology, Shandong Academy of Sciences, Jinan, China, ⁵ Frontier Technology Institute, Tianjin University, Tianjin, China

OPEN ACCESS

Edited by:

Min Jiang,
Nanjing Tech University, China

Reviewed by:

Fu-Li Li,
Qingdao Institute of Bioenergy
and Bioprocess Technology (CAS),
China
Jingyu Chen,
China Agricultural University, China

*Correspondence:

Yuanyuan Ma
myy@tju.edu.cn

[†] These authors have contributed
equally to this work

Specialty section:

This article was submitted to
Synthetic Biology,
a section of the journal
Frontiers in Bioengineering and
Biotechnology

Received: 03 January 2020

Accepted: 24 August 2020

Published: 22 September 2020

Citation:

Wang Z, Xue T, Hu D and Ma Y
(2020) A Novel Butanol
Tolerance-Promoting Function of the
Transcription Factor Rob
in *Escherichia coli*.
Front. Bioeng. Biotechnol. 8:524198.
doi: 10.3389/fbioe.2020.524198

Producing high concentrations of biobutanol is challenging, primarily because of the toxicity of butanol toward cells. In our previous study, several butanol tolerance-promoting genes were identified from butanol-tolerant *Escherichia coli* mutants and inactivation of the transcriptional regulator factor Rob was shown to improve butanol tolerance. Here, the butanol tolerance characteristics and mechanism regulated by inactivated Rob are investigated. Comparative transcriptome analysis of strain DTrob, with a truncated *rob* in the genome, and the control BW25113 revealed 285 differentially expressed genes (DEGs) to be associated with butanol tolerance and categorized as having transport, localization, and oxidoreductase activities. Expression of 25 DEGs representing different functional categories was analyzed by quantitative reverse transcription PCR (qRT-PCR) to assess the reliability of the RNA-Seq data, and 92% of the genes showed the same expression trend. Based on functional complementation experiments of key DEGs, deletions of *glgS* and *yibT* increased the butanol tolerance of *E. coli*, whereas overexpression of *fadB* resulted in increased cell density and a slight increase in butanol tolerance. A metabolic network analysis of these DEGs revealed that six genes (*fadA*, *fadB*, *fadD*, *fadL*, *poxB*, and *acs*) associated with acetyl-CoA production were significantly upregulated in DTrob, suggesting that Rob inactivation might enhance butanol tolerance by increasing acetyl-CoA. Interestingly, DTrob produced more acetate in response to butanol stress than the wild-type strain, resulting in the upregulation expression of some genes involved in acetate metabolism. Altogether, the results of this study reveal the mechanism underlying increased butanol tolerance in *E. coli* regulated by Rob inactivation.

Keywords: butanol, tolerance, *rob*, RNA-Seq, function investigation, acetate

INTRODUCTION

Butanol has received increased attention as a high-energy-density fuel and bulk chemical feedstock (Gu et al., 2011). Only biobutanol can be used in the pharmaceutical and cosmetics industries, and biomass-based butanol production can reduce environmental pollution compared to petrochemical-based production (Jiang et al., 2015b). Traditional biobutanol is produced by *Clostridium* species and can reach a titer of approximately 20 g/L (Qureshi and Blaschek, 2000). The butanol titers produced by engineered *Escherichia coli* strains can also reach approximately 20 g/L in batch fermentation without any antibiotics or inducers and up to 30 g/L with the continuous removal of butanol (Shen et al., 2011; Jang and Lee, 2015; Dong et al., 2017), indicating that *E. coli* is a potential butanol-producing bacterium. However, the current production of butanol is limited to approximately 20 g/L due to the toxicity of butanol toward bacteria; indeed, this toxicity is a bottleneck in butanol production (Qureshi and Blaschek, 2000). Therefore, it is important to improve the butanol tolerance of chassis strains and to explore tolerance-associated mechanisms to promote the highly efficient production of butanol.

Due to its hydrophobicity, butanol binds to lipid chains of the bacterial cytoplasmic membrane, which results in toxicity to the cells (Jones and Woods, 1986; Nielsen and Prather, 2009). The mechanism of this toxicity involves increased membrane fluidity and permeability in the presence of butanol, causing leakage of protons and ATP and interference with the correct folding of proteins, which leads to cell damage or even death (Sikkema et al., 1995; Isken and de Bont, 1998). Bacteria alter their physiological and biochemical characteristics to respond to butanol stress in the following ways: (1) membrane composition changes, including increasing efflux capacity of toxins, preventing leakage of intracellular components, and protecting cells from damage due to the solvent (Reyes et al., 2011; Bui et al., 2015; Royce et al., 2015; Sandoval and Papoutsakis, 2016); (2) physiological responses similar to those involved in responses to osmotic, oxidizing, respiratory, and heat shock stresses (e.g., altered osmotic pressure) (Purvis et al., 2005; Chin et al., 2017), reactive oxygen species (ROS) accumulation (Kaczmarzyk et al., 2014) and enhanced metabolic transport and molecular chaperone levels (Peralta-Yahya et al., 2012); and (3) up- or downregulation of expression of regulatory genes, such as those encoding sensor proteins, transcription factors (TFs), and those involved in regulating expression of small RNAs (Peralta-Yahya et al., 2012), to modulate gene expression profiles to protect against butanol stress (Reyes et al., 2011, 2012).

Escherichia coli expresses 304 TFs (Perez-Rueda et al., 2015), though only a few have been reported to regulate butanol tolerance-related genes (Reyes et al., 2012; Horinouchi et al., 2018). Furthermore, the corresponding genes regulated by these TFs and the associated regulatory mechanism have not yet been clarified (Aquino et al., 2017), limiting the improvement of butanol-tolerant chassis strains using a rational-design engineering strategy. In our previous study, a mutant strain (BW1847) able to tolerate 2% (v/v) butanol was obtained, and among the genes mutated or deleted, *rob* (GenBank No.

RS22900), *acrB* (GenBank No. RS02385), and *tqsA* (GenBank No. RS08380) have been identified as having a function in enhancing butanol tolerance (He et al., 2019). The DTrob strain, with an AT_{686–7} base deletion within *rob* in the genome, and the *rob*-deletion mutant Δrob produced much higher cell densities than did the wild-type strain under 0.75% butanol stress (He et al., 2019), indicating that partial and full inactivation of Rob both result in improved butanol tolerance. The *rob* gene encodes a right oriC-binding transcriptional activator (Nakajima et al., 1995) that interacts with a superoxide response regulon transcriptional activator (SoxS) and a multiple antibiotic resistance transcriptional regulator (MarA) and can activate genes involved in antibiotic, oxygen pressure and organic solvent resistance (Nakajima et al., 1995). The *rob*-deleted strain exhibited decreased tolerance to antibiotics, oxygen stress, cyclohexane and n-pentane (Nakajima et al., 1995; White et al., 1997; Bennik et al., 2000). However, inactivation of Rob yielded increased butanol tolerance in our previous study. These contrasting results are due to the extensive, intricate and multiple regulatory mechanisms of Rob, and the corresponding butanol-tolerant mechanism regulated by Rob is unknown. Strain DTrob with truncated Rob exhibited a butanol tolerance characteristic and can be used to investigate the interaction mechanism between Rob and its target genes. DTrob is thus an ideal candidate for studying the butanol tolerance mechanism caused by Rob inactivation.

Therefore, in this study, butanol stress response genes regulated by the Rob-inactivated mutant were evaluated by RNA-Seq. In addition, key genes involved in butanol tolerance were functionally identified, and a potential tolerance mechanism was determined to demonstrate the novel roles of Rob in response to butanol stress.

MATERIALS AND METHODS

Growth Assays and Extracellular n-Butanol Measurements

The site-specific mutant DTrob (AT_{686–7} deletion in the *rob* gene) was constructed in a previous study (He et al., 2019). The DTrob strain and BW25113 (Supplementary Table S1) were precultured in lysogeny broth (LB) until the late exponential phase, after which the cultures were concentrated to an OD₆₀₀ of 20. The concentrated cells were then used to inoculate 50 mL of LB medium containing 0, 0.75, 1, and 1.25% (v/v) butanol at an initial OD₆₀₀ of 0.1–0.15 to evaluate cell growth. A total of 0.7 mL of culture was taken to measure the OD₆₀₀ with a Cary 50 Conc spectrophotometer (Varian, Palo Alto, CA, United States); 1 mL of culture was collected at the appropriate time to measure butanol and acetate concentrations in the medium. The collected samples were centrifuged, and the supernatants were used to measure butanol and acetate contents by high-performance liquid chromatography (HPLC). HPLC was performed using an organic acid analytical column (Aminex HPX-87H Ion Exclusion Column, 300 mm × 7.8 mm) at 45°C; sulfuric acid (4 mM) was used as the mobile phase at 0.8 mL/min. The butanol and acetate concentrations in each sample were calculated by comparisons

with the peak area of the standard. The per unit intracellular butanol concentration (PIC) was calculated according to previous reports (He et al., 2019), with a slight modification, as shown by the following equation:

$$\text{PIC} = \frac{C_{\text{initial}} - C_{\text{final}}}{N}$$

where “PIC” indicates “per unit intracellular butanol concentration” ($\mu\text{g/L}$) and “ C_{initial} ” and “ C_{final} ” indicate “initial extracellular butanol concentration” and “final extracellular butanol concentration”, respectively; “N” indicates the number of cells; and 1 OD cells at 600 nm corresponds to 8.3×10^8 cells mL^{-1} . $N = \text{OD}_{600} \times 8.3 \times 10^8 \text{ mL}^{-1}$. The values of the mean and standard deviation are plotted using the bar and error bar.

Overexpression strains (**Supplementary Table S1**) were precultured in LB until the late exponential phase, and the cultures were concentrated to an OD_{600} of 20. The concentrated cells were then used to inoculate LB medium containing 0.2% (w/v) L-arabinose, 100 $\mu\text{g/mL}$ ampicillin, and a gradient concentration of butanol at an initial $\text{OD}_{600} = 0.2$. A total of 1 mL of culture was collected at a suitable time point for cell concentration measurements.

RNA-Seq and Data Processing

The strains BW25113 and DTrob were cultured in 50 mL of LB containing 0.75% (v/v) butanol until the OD_{600} reached 0.6–1.1; 3-mL aliquots were harvested, and the cells were washed with ice-cold PBS (phosphate buffer saline) buffer. Total RNA was extracted with TRIzol reagent (Invitrogen, Carlsbad, CA, United States) according to the manufacturer’s instructions. The quality of the total RNA extracted was assessed spectrophotometrically at 230, 260, and 280 nm. The RNA sample with an $\text{OD}_{260}/\text{OD}_{230}$ ratio higher than 1.8 and an $\text{OD}_{260}/\text{OD}_{280}$ ratio between 1.8 and 2.1 was considered as pure and used to cDNA library construction. cDNA library preparation and sequencing were conducted by the Allwegene Technology Company in Beijing, China. Individual libraries were sequenced using the Illumina HiSeq 4000 platform (Illumina, Inc., San Diego, CA, United States). The original fluorescent images were converted into raw sequence reads by CASAVA software. The raw reads were then processed to remove reads with adapters, reads containing poly-N ($N > 1\%$) and low-quality reads (more than 50% bases with Q-score ≤ 20), yielding clean reads (Gao et al., 2018; Wang et al., 2018). The clean data were deposited in Gene Expression Omnibus (GEO) at NCBI (Accession Number GSE120032) and mapped to the genome of the reference strain BW25113 (LOCUS NZ_CP009273) using Bowtie2 (Kim et al., 2018). Gene expression levels were analyzed using fragments per kilobase of exon model per million mapped reads (FPKM). Differentially expressed genes (DEGs) between the two samples were identified using the DESeq package (v1.24.0), and $|\log_2(\text{FoldChange})| > 1$ and $q\text{-value} < 0.005$ were used as the threshold to identify significant differences in gene expression. Analysis of Gene Ontology (GO), which assigns genes into functional categories, was performed using the GOSec (v1.22) and top GO (v2.22) R packages.

Quantitative Reverse Transcription PCR Analysis

The expression levels of eighteen DEGs representing different functional categories were assessed by real-time quantitative reverse transcription PCR (qRT-PCR) to validate the reliability of the RNA-Seq data. Total RNA from DTrob and BW25113 cells was extracted as described above, and RQ1 RNase-Free DNase (Promega, Madison, WI, United States) was added to the RNA to remove genomic DNA. PCR reaction was performed using the total RNA as template in order to check for genomic DNA contamination. No product was observed, demonstrating that the sample had no genomic DNA contaminants and was suitable for qRT-PCR assay. Subsequently, reverse transcription was performed using iScript cDNA Synthesis Kit (Bio-Rad) with 2 μg of total RNA following the manufacturer’s instructions. qRT-PCR experiments were performed using CFX96 Real-Time System (Bio-Rad). Each reaction contained 2 μL of diluted (1/10) cDNA, Taq SYBR Green qPCR Premix (Yugong Biolabs Inc., Jiangsu, China) and the corresponding primer pairs (**Supplementary Table S2**). The 16S rRNA gene was used as a reference to normalize the qRT-PCR data. The expression level of each gene was calculated according to the following formula: expression level = $2^{-\Delta\Delta C_t}$ (Livak and Schmittgen, 2001). The relative mRNA level is presented as the percent (%) ratio of the gene expression level in DTrob to that in BW25113.

Construction of Knockout Strains

Strains deleted for the *glgS* and *yibT* genes were constructed using the CRISPR-Cas9 system (Ran et al., 2013; Jiang et al., 2015a; **Supplementary Figure S1**). Inverse PCR was performed using pTargetF plasmid as a template to introduce the target sequence of N20 (20-bp complementary region) upstream of the single-guide RNA (sgRNA) in the pTargetF plasmid. The N20 sequence was introduced into the primers shown in **Supplementary Table S3**. The inverse PCR products were digested with the methylation-sensitive restriction enzyme DMT (TransGen Biotech, Shanghai, China) to remove methylated plasmid templates, after which the DNA was transformed into DH5 α competent cells (Biomed, Beijing, China). Positive clones were identified by PCR with the appropriate geneN20F/pTargetF-IR primer pairs (**Supplementary Table S3**), and the resulting plasmid was correspondingly named pTargetF-geneN20. DNA fragments containing left and right homologous arms located upstream and downstream of the target gene were amplified with the primer pairs geneDLF/geneDLR and geneDRF/geneDRR (**Supplementary Table S3**), respectively. The two fragments were then fused together by overlap PCR with the appropriate geneDLF/geneDRR primer pairs (**Supplementary Table S3**), and the resulting fused PCR fragment was used as donor DNA to delete the target gene by homologous recombination. Approximately 500 ng of donor DNA and the corresponding pTargetF-geneN20 plasmid were co-transformed into BW25113 (pCas) competent cells. Positive clones were screened on LB plates containing 100 mg/L kanamycin and spectinomycin and subsequently identified by PCR using the appropriate geneDLF/geneDRR primer pairs (**Supplementary Table S3**).

The deletion was confirmed by sequencing, and the positive clones were cultured in LB medium supplemented with 50 mg/L kanamycin and 0.5 mM IPTG to eliminate the pTargetF-geneN20 plasmid. The temperature-sensitive plasmid pCas was then removed by growing the culture overnight at 37°C.

Overexpression Analysis of Several Upregulated Genes

Thirteen upregulated genes (Supplementary Table S5) were chosen for overexpression analysis. Plasmids harboring the target genes were constructed on the basis of pBAD30 (Guzman et al., 1995). PCR amplification of the target genes from the genomic DNA of BW25113 was performed using the primer pairs shown in Supplementary Table S4. The plasmid pBAD30 was digested with the restriction endonucleases *SacI* and *HindIII*, and the aforementioned PCR products were cloned into the *SacI/HindIII* sites of pBAD30 using GenBuilder Cloning Kit (GenScript, Nanjing, China). The mixture was transformed into competent DH5 α cells and screened on LB agar plates containing 100 μ g/mL ampicillin. Single clones were identified by PCR using the primers pBADIup/pBADIdown (Supplementary Table S4). Plasmids were extracted using TIANprep Mini Plasmid Kit (TIANGEN, Beijing, China) and verified by sequencing (Sangon Biotech, Shanghai, China). The overexpression plasmids were transformed into BW25113 by electroporation, and the positive transformants were correspondingly named BW25113 (gene) (Supplementary Table S1).

RESULTS

Enhanced Butanol Tolerance by the Truncated Rob in DTrob

The DTrob strain has an AT_{686–7} base deletion of *rob* in the genome, which leads to an early termination of translation of *rob* mRNA, and the resulting truncated protein only has 229 amino acids (He et al., 2019). Strain DTrob showed a similar growth trend to control BW25113 in absence of butanol (Figure 1A), and the maximum cell density of the DTrob exhibit 94, 49, and 18% higher than that of BW25113 under 0.75, 1, and 1.25% (v/v) butanol stress, respectively, indicating that the DTrob strain was able to tolerate 1–1.25% and that the improvement in relative growth decreased with increasing butanol concentrations. The PIC of the DTrob strain was 76, 56, and 78% of that of the control BW25113 under 0.75, 1, and 1.25% (v/v) butanol stress at 4 h (logarithmic phase), respectively (Figures 1B–D), which shows that inactivation of Rob can result in an enhanced ability to efflux butanol out of the cell to improve the tolerance, and the highest efflux capacity was shown in the presence of 1% butanol. The PIC value of DTrob was 32–60% of that of BW25113 in 0.75–1% (v/v) butanol at 12 h, demonstrating a higher efflux capacity than at 4 h. Nevertheless, interestingly, the PICs of both BW25113 and DTrob in a higher concentration of butanol (1.25%) were decreased at 12 h compared to 4 h, and the two strains had similar intracellular butanol concentration. It is due to that the strains grown in 1.25% butanol have entered the decline phase

at 12 h (Figure 1D), and the cell death causes more butanol to be released into the medium, thus resulting in a decreased sharply butanol content in these cells and lower PIC value than at 4 h. Therefore, the alleviated toxicity by butanol efflux in log stage is one reason for the improved butanol tolerance of DTrob.

Transcriptomic Differences Between the DTrob and Control Strains Under Butanol Stress

RNA-Seq of the wild-type BW25113 and DTrob strains was performed to assess differences in gene expression between them. Genes with a “q-value < 0.005” and “|log₂(FoldChange)| > 1” were defined as DEGs. A total of 285 (6.2% of genes) DEGs were identified in DTrob compared with the control. In the late logarithmic phase, 184 and 101 genes were upregulated and downregulated in DTrob compared with BW25113, respectively (Supplementary Figure S2A). The 285 DEGs were then subjected to GO enrichment analysis and grouped into three primary categories: biological process, molecular function and cellular component. GO annotations were found for 202 of these genes. The significantly enriched GO terms and number of DEGs with GO annotations were as follows: “localization” (32.7%, 66/202), “transport” (31.7%, 64/202), “establishment of localization” (31.7%, 64/202), “oxidoreductase activity” (17.82%, 36/202), and “transporter activity” (20.30%, 41/202) (Supplementary Figure S2B). In addition, the 285 DEGs were examined by Kyoto Encyclopedia of Genes and Genomes (KEGG) pathway analysis using KOBAS (v2.0), revealing 68 pathways, 53 of which were different from the KEGG pathways in previous reports (Reyes et al., 2012; Si et al., 2016; Guo et al., 2019). The significant KEGG terms are primarily associated with the biosynthesis of antibiotics, biosynthesis of secondary metabolites and fatty acid degradation (Supplementary Figure S3).

Hundreds of potential genes involved in the n-butanol tolerance response have been identified by DNA microarrays and comparative genome hybridization microarrays (array-CGH); nevertheless, only approximately 20 candidate genes were identified as being associated with butanol tolerance through overexpression or knockout experiments (Supplementary Table S6; Rutherford et al., 2010; Reyes et al., 2011; Si et al., 2016). Among the 285 DEGs identified by RNA-Seq in the present study, *ompF*, *acrB*, *glcF*, *ybjC*, *yibT* and *cpxP* have been reported to be associated with butanol tolerance (Rutherford et al., 2010; Reyes et al., 2011; Si et al., 2016); however, most of the DEGs have not yet been reported to be involved in butanol tolerance. Therefore, the results of this study reveal potential functional genes related to the development of butanol-tolerant strains for further exploration of butanol tolerance mechanisms.

Validation of RNA-Seq Data Using Real-Time qRT-PCR

Twenty five genes representing different GO functional categories and different expression levels were classified based

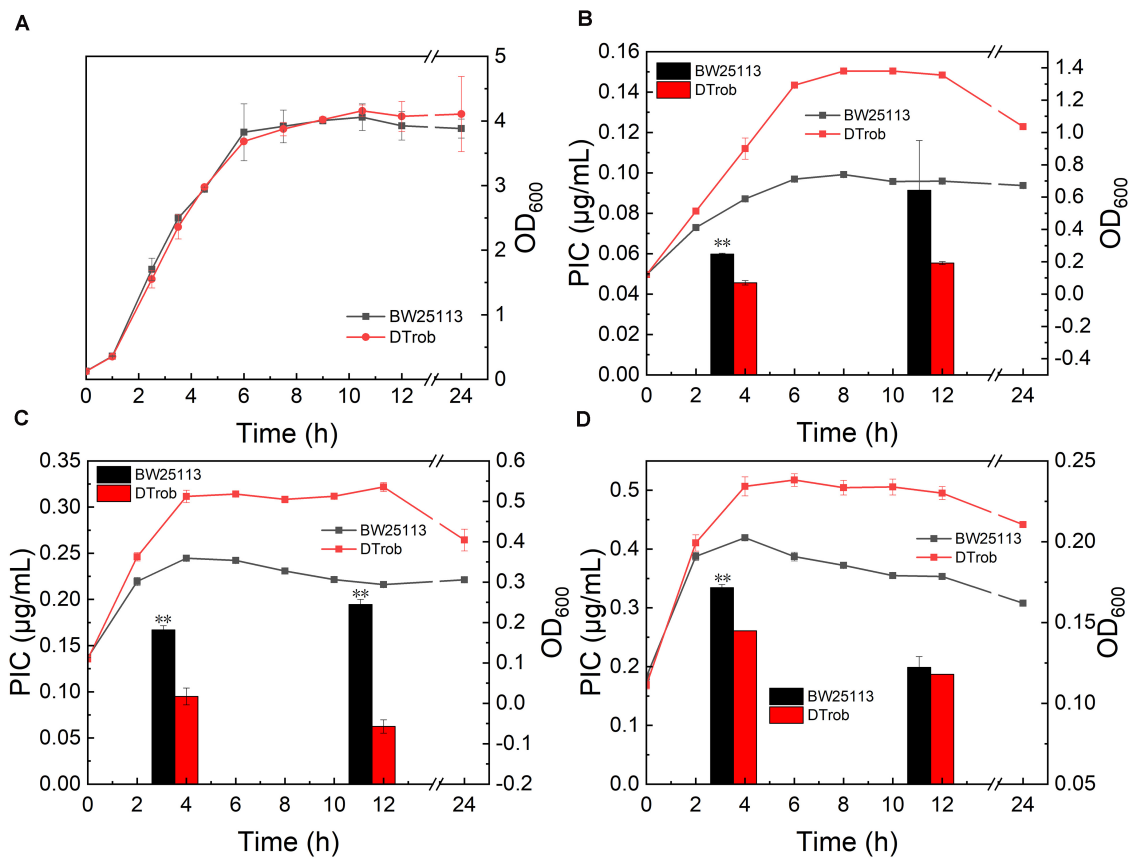


FIGURE 1 | Growth assays for the DTrob strain in the presence of butanol. **(A)** Without butanol; **(B)** with 0.75% (v/v) butanol; **(C)** with 1% butanol; and **(D)** with 1.25% butanol. The line graph shows the growth curve, and the bar graph shows the unit intracellular butanol concentration. Error bars represent one standard deviation. Statistical significance of the differences between DTrob and BW25113 was analyzed by a one-way analysis of variance (ANOVA). * $P < 0.05$ was considered statistically significant and ** $p < 0.01$ was considered extremely significant. Growth assays were performed in triplicate in screw-cap flasks.

on annotations in the NCBI database (Table 1) and primarily classified into four groups: regulatory factors (ChaC, GadE, GlgS, and YiaG), transport and membrane proteins (ActP, ElaB, PspG, FadL, MdtD, OmpW, Slp, YacH, YibT, YdcL, and YjcH), stress response proteins (HdeB, InaA, and YhbO), and enzymes (Acs, AstC, NarG, FadA, FadB, FadD, and PoxB). The expression levels of 25 DEGs between the DTrob and BW25113 strains under butanol stress were analyzed by qRT-PCR to confirm the reliability of the RNA-Seq data obtained. The log₂-fold change values of the 25 DEGs were also examined to compare the consistency of the RNA-Seq and qRT-PCR data, and a strong correlation ($R = 0.8318$) was observed between the RNA-Seq and qRT-PCR data (Supplementary Figure S4). Based on the qRT-PCR results, the expression trends of 23 of these candidate genes were consistent with the RNA-Seq data. Among these 23 genes, *acs*, *actP*, *astC*, *elaB*, *fadA*, *fadB*, *fadD*, *fadL*, *yiaG*, *yhbO*, and *yjcH* were obviously upregulated (263–11503%) (Table 1) and *gadE*, *hdeB*, and *slp* slightly upregulated (153–194%) in the DTrob strain compared to the control strain, whereas *chaC*, *glgS*, *inaA*, *narG*, *mdtD*, *yibT*, *ycdL*, and *yacH* were notably downregulated (65–99%) (Table 1). Therefore, 92% of the candidate genes exhibited consistent qRT-PCR

and RNA-Seq results, indicating that the RNA-Seq data were of good quality.

Functional Analysis of Significant Differentially Expressed Genes

Based on GO enrichment and the gene expression levels of the DEGs, fifteen representative DEGs in each cluster were selected (Supplementary Table S5) for investigation of their function in promoting butanol tolerance by growth evaluation under butanol stress. To determine their direct impacts on the butanol tolerance phenotype, the selected upregulated and downregulated genes were overexpressed and deleted, respectively. Deletion mutants of *glgS* and *yibT* were obtained using the CRISPR-Cas9 system and named $\Delta glgS$ and $\Delta yibT$, respectively. The growth evaluation results showed that the maximum cell density of the $\Delta glgS$ (pBAD30) and $\Delta yibT$ (pBAD30) strains was increased by 7.7–23.6% compared to that of BW25113 in the presence of 1–1.25% (v/v) n-butanol, indicating that the absence of Rob or downregulated expression improved butanol tolerance (Figure 2). The complementation strains $\Delta glgS$ (pBAD-*glgS*) and $\Delta yibT$ (pBAD-*yibT*) of the two genes displayed a lower cell

TABLE 1 | Functional categories and qRT-PCR results of 25 DEGs associated with butanol tolerance.

Functional group and gene	Description	Fold change ^a	Relative expression by qRT-PCR ^b (%)	True or false ^c
Regulator				
<i>gadE</i>	Transcriptional regulator GadE	2.68	153	True
<i>chaC</i>	Cation transport regulator	−2.65	30	True
<i>glgS</i>	Glycogen synthase surface composition regulator/motility and biofilm regulator	−5.83	1	True
<i>yiaG</i>	Transcriptional regulator	2.03	4095	True
Stress related				
<i>hdeB</i>	Acid stress chaperone HdeB	3.23	181	True
<i>inaA</i>	Acid-inducible Kdo/WaaP family putative kinase	−3.06	8	True
<i>yhbO</i>	Stress-resistance protein	2.38	263	True
Metabolism				
<i>narG</i>	Respiratory nitrate reductase 1 alpha chain	−3.55	27	True
<i>acs</i>	Acetyl-coenzyme A synthetase	3.33	3000	True
<i>astC</i>	Succinylornithine aminotransferase	3.98	3928	True
<i>fadA</i>	Acetyl-CoA C-acyltransferase FadA	3.63	2508	True
<i>fadB</i>	Fatty acid oxidation complex subunit alpha FadB	3.27	4580	True
<i>fadD</i>	Acyl-CoA synthetase	2.14	1068	True
<i>poxB</i>	Pyruvate dehydrogenase	1.36	5686	True
Membrane and transport related				
<i>pspG</i>	Envelope stress response protein PspG	−2.7	124	False
<i>elaB</i>	DUF883 family protein, putative membrane-anchored ribosome-binding protein	2.19	11503	True
<i>fadL</i>	Long-chain fatty acid transporter	2.81	7286	True
<i>actP</i>	Cation acetate symporter	3.11	797	True
<i>mdtD</i>	MFS (major facilitator superfamily) transporter	−3.06	23	True
<i>yibT</i>	Uncharacterized protein Hypothetical protein	−5.76	2	True
<i>yjcH</i>	DUF485 family inner membrane protein	3.01	736	True
<i>slp</i>	Outer membrane protein slp	2.80	194	True
<i>ydcl</i>	Lipoprotein	−2.36	13	True
<i>ompW</i>	Outer membrane protein W	3.03	64	False
<i>yach</i>	DUF3300 domain-containing protein	−4.06	35	True

^aFold change indicates the log₂ ratios between the corresponding transcript levels of the DTrob and BW25113 strains in the RNA-Seq data; a log₂ fold change of “+” indicates that the gene is upregulated in the DTrob strain relative to the BW25113 strain, and a “−” indicates that a gene is downregulated. ^bThe percentage ratio of the expression levels of the target gene in the DTrob strain compared to that observed in the BW25113 strain. ^c“True” and “False” indicate that the real-time qRT-PCR verification result is consistent and inconsistent with the RNA-Seq data, respectively.

density than their deletion strains $\Delta glgS$ and $\Delta yibT$, indicating that their overexpression can lead to a decrease in butanol tolerance (**Figures 2C,D**). Overexpression of these two genes in the wild-type strain also reduced butanol tolerance compared to the control strain BW25113 (pBAD30) (**Figure 2D**). These results indicate that a reduced level of *glgS* and *yibT* expression is beneficial for enhancing butanol tolerance.

Thirteen upregulated genes verified by qRT-PCR were selected for investigating their function in promoting butanol tolerance, and engineered strains were cultured in the presence or absence of butanol. The maximum cell density of BW25113 (pBAD-*fadB*) was increased by 25.5, 12.7, and 5.1% under 0, 0.5, and 0.75% (v/v) butanol stress, respectively, compared with that of the control strain BW25113 (pBAD30) (**Figure 3**).

These results indicate that *fadB* overexpression can promote cell growth and that the cell density of *E. coli* under butanol stress can also be increased to some extent. The maximum cell density of the *slp*-, *acs*-, and *fadL*-overexpressing strains was decreased by 31.9, 8.3, and 27.7%, respectively, compared with the control strain in the absence of butanol (**Figure 3A**, with a significant decrease under butanol stress (**Figures 3B,C**). These results indicate that overexpression of these three genes inhibits the growth of the cells, resulting in a decreased cell density under butanol stress.

Unlike *fadB*, *slp*, *acs*, and *fadL*, overexpression of the other nine upregulated genes did not cause an increase or decrease in cell growth under butanol stress (data not shown), indicating that overexpression of these nine genes does not

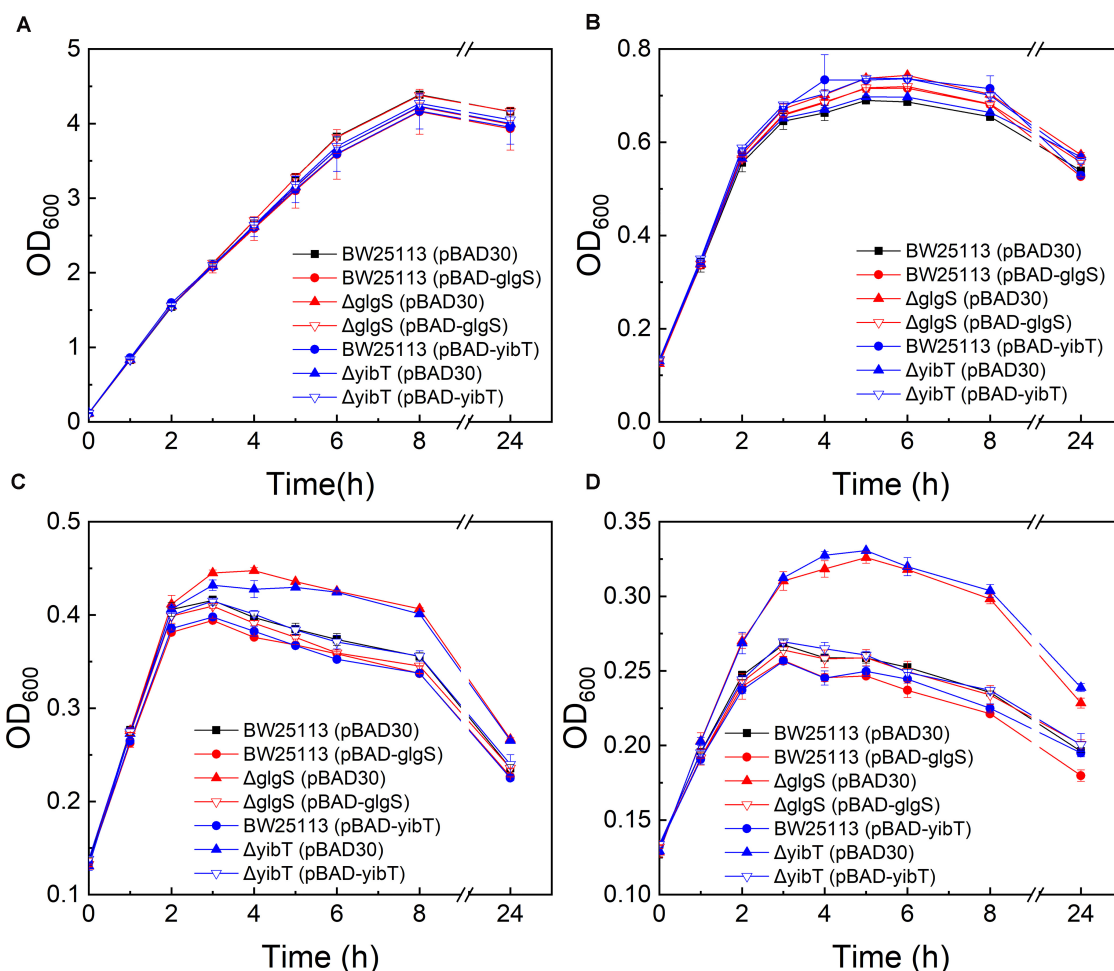


FIGURE 2 | Butanol tolerance evaluation of the *glgS* or *yibT* deletion and complement strains. All strains were cultured in LB medium containing 0% (A), 0.75% (B), 1% (C), and 1.25% (v/v) (D) butanol.

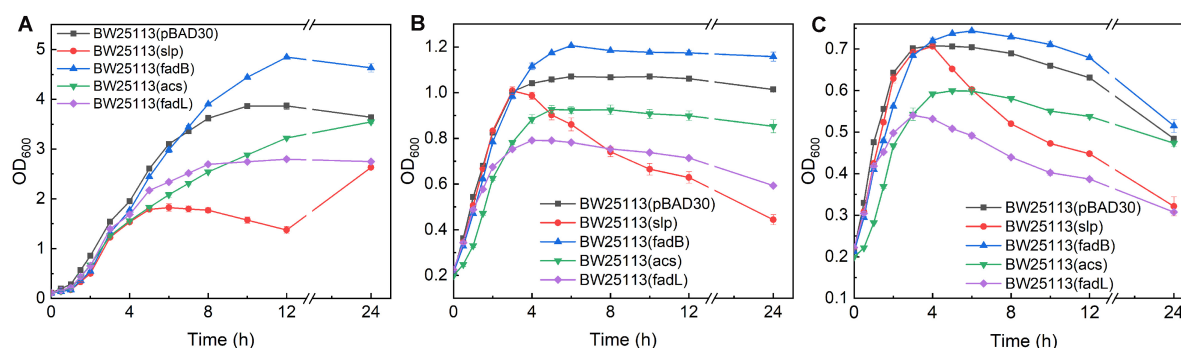


FIGURE 3 | Growth evaluation of overexpression strains. (A–C) Growth curves of *acs*-, *fadB*-, *fadL*-, and *slp*-overexpressing strains exposed to 0, 0.5, and 0.75% (v/v) butanol. BW25113 (pBAD30) was used as a control.

alter butanol tolerance. It is possible that most responsive genes do not exhibit a significant butanol tolerance function; it also may be that simultaneous changes in the expression of multiple DEGs cause synergistic physiological and biochemical

responses to resist butanol stress. Therefore, the function and classification of the DEGs is not well illustrated merely by functional complementation via knockout or overexpression of a certain gene. Correspondingly, the metabolic network of these

DEGs was also analyzed, and the following interesting response mechanism was observed.

DTrob Responds to Butanol Stress by Altering Acetyl-CoA and Acetate Production

The expression levels of *poxB*, encoding pyruvate dehydrogenase (PoxB), and *acs*, encoding acetyl-CoA synthetase (Acs), were upregulated in the DTrob strain, as shown by the RNA-Seq and qRT-PCR data (Figure 5). PoxB and Acs convert pyruvate to acetyl-CoA in a two-step enzymatic reaction (Figure 4A). Four genes (*fadA*, *fadB*, *fadD*, and *fadL*) involved in fatty acid β -oxidation were also significantly upregulated in the DTrob strain, and the final product of fatty acid β -oxidation is acetyl-CoA (Figure 4A). An enhanced acetyl-CoA pool has been demonstrated to be achieved through modification of a fatty acid β -oxidation pathway (Zhang et al., 2019), and acetyl-CoA is a key molecule in microbial central carbon metabolism and involved in a variety of cellular processes (Krivoruchko et al., 2015). Thus, upregulation of the six genes (Figure 5 and Table 1) caused by inactivation of Rob might result in increased acetyl-CoA levels, which would provide more raw material and energy for a number of physiological processes and cell growth. Nonetheless, the acetyl-CoA content of BW25113 and DTrob was not significantly different under 0.75% butanol stress (data not shown). It is possible that the increased acetyl-CoA in DTrob is quickly transferred to other metabolic pathways, such as the TCA cycle to provide energy for cell growth, or provides acetyl groups for acetylation of histones to promote cell growth and proliferation (Cai et al., 2011). Accordingly, no obvious accumulation of acetyl-CoA was observed in DTrob, although which showed a higher cell density than BW25113 under butanol stress.

In addition, expression of ten genes (*Slp*, *hdeA*, *hdeB*, *hdeD*, *gadA*, *gadB*, *gadC*, *gadE*, *yiaG*, and *yccJ*) upregulated in the DTrob strain has been reported to be increased when cells are subjected to acid stress (Ma et al., 2003; Tucker et al., 2003; Hommais et al., 2004). Indeed, upregulation of PoxB, which converts pyruvate to acetate (Dittrich et al., 2005), would lead to an increase in acetate levels, and the extracellular acetate concentration in the DTrob culture was higher than that of the BW25113 strain in the log phase (Figure 4B). These results indicate that upregulated expression of some genes in the DTrob strain might promote the production of acetyl-CoA and result in acetate accumulation, in turn inducing expression of genes involved in the response to acid stress.

DISCUSSION

Mutation of the transcription regulator *rob* in *E. coli* altered the expression levels of 285 genes in response to butanol stress. Deletion of the genes *glgS* and *yibT*, encoding a transcriptional regulator and a membrane-associated protein, respectively, directly increased butanol tolerance. In addition, overexpression of the *fadB* gene, encoding a fatty acid oxidation-related enzyme, promoted the growth of *E. coli* and slightly enhanced butanol tolerance. Deletion of *glgS* has been reported to improve the production of both flagella and type 1 fimbriae, resulting in enhanced swarming motility of bacterial cells. Such enhanced motility protects cells from toxicity by allowing them to escape from toxic environments, such as those containing n-butanol (Rahimpour et al., 2013; Kim et al., 2016). However, the Δ *glgS* strain showed an increased capacity to initiate biofilm formation (Rahimpour et al., 2013), and biofilms provide good protection for cells as a permeability barrier and also enhance the ability of bacteria to adapt to adverse environments, including butanol

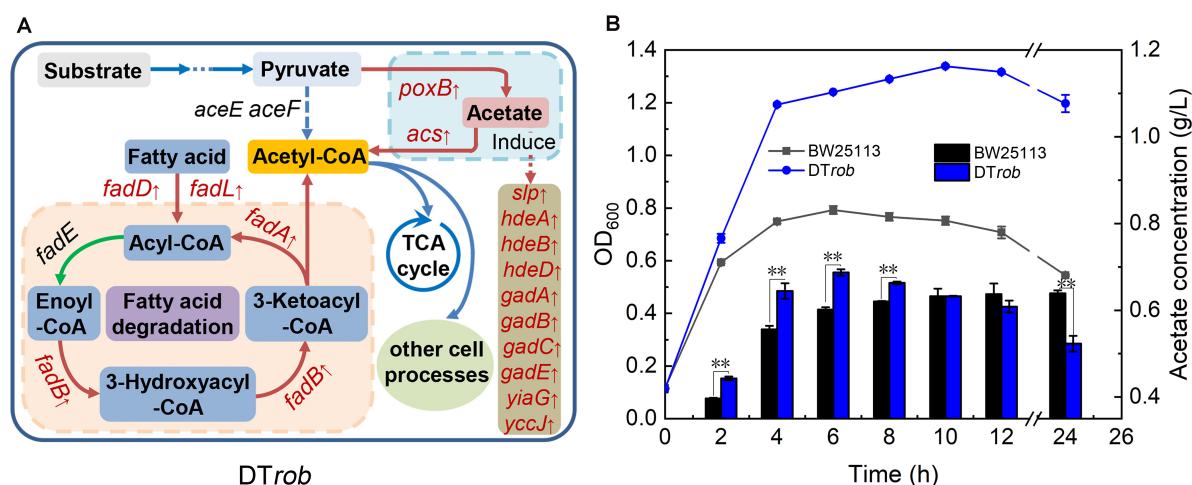
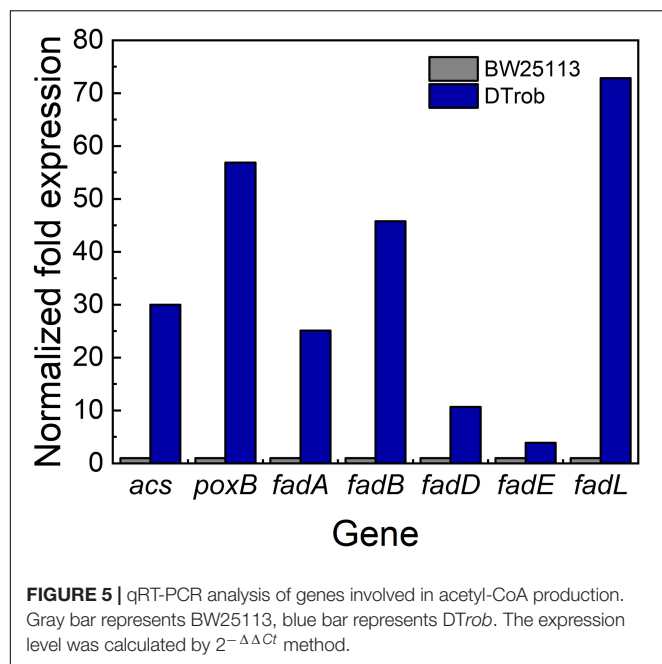


FIGURE 4 | Mechanism of butanol tolerance regulated by Rob via an increase in acetyl-CoA. **(A)** The fatty acid oxidation and acetate metabolism pathways regulated by Rob. Genes marked in red font were upregulated in DTrob. **(B)** Acetate levels in the BW25113 and DTrob strains under 0.75% (v/v) butanol stress. The line graph shows the growth curve, and the bar graph shows the extracellular acetate concentration. Error bars represent one standard deviation. Statistical significance of the differences between DTrob and BW25113 was analyzed by a one-way ANOVA. **P* < 0.05 was considered statistically significant and ***p* < 0.01 was considered extremely significant. Growth assays were carried out in triplicate in screw-cap flasks.



stress (Li et al., 2016). It has been reported that deletion of *yibT* can increase the proportion of unsaturated fatty acids in the membrane, resulting in lower membrane fluidity and higher membrane rigidity and integrity, protecting cells from organic solvent stress (Si et al., 2016). Therefore, *yibT* deletion can improve the butanol tolerance of *E. coli*.

The gene *fadB* encodes the α -subunit of a multienzyme complex that is involved in fatty acid β -oxidation (Fujita et al., 2007) and responsible for the hydration of enoyl-CoA and oxidation of 3-hydroxyacyl-CoA (Figure 4A). Overexpression of *fadB* may accelerate the two-step enzymatic reaction and the conversion of fatty acids to acetyl-CoA. Additional acetyl-CoA entering the tricarboxylic acid cycle would provide more energy for cell growth, resulting in an increase in cell density. This growth improvement may also result in a higher cell density under butanol stress.

Interestingly, overexpression of *acs*, *slp*, and *fadL* did not increase the butanol tolerance of *E. coli* and even led to inhibition of cell growth. The *acs*, *slp*, and *fadL* genes encode the Acs (Brown et al., 1977), outer membrane protein Slp (Alexander and St John, 1994) and fatty acid transporter FadL (van den Berg et al., 2004), respectively, and the results of previous studies also showed that overexpression of these three genes inhibits cell growth (Black et al., 1985; Alexander and St John, 1994; Zhang et al., 2019). However, individually overexpressing these three genes does not improve butanol tolerance, as they function in synergy with other genes in the same GO functional category to resist butanol stress. Moreover, Acs and PoxB may function together to promote the production of acetyl-CoA; FadL may act in conjunction with proteins encoded by *fadA*, *fadB*, and *fadD* to promote fatty acid degradation, and Slp may act in conjunction with some proteins to promote acid tolerance in response to acetate stress (Figure 4A). Therefore,

the proteins encoded by these genes synergistically respond to butanol stress.

Among the 15 DEGs identified by functional complementation experiments, only *fadB*, *glgS*, and *yibT* were identified to be involved in significant butanol tolerance in this study. Correspondingly, among thirteen DEGs investigated, only five contribute to the increased butanol tolerance of the mutant B8 (Si et al., 2016). These results demonstrate that changes in the expression of a few genes may be valuable for functional improvements in butanol tolerance. Furthermore, the enhanced tolerance regulated by a TF may result from the combined actions of simultaneous changes in the expression levels of multiple genes. In addition, metabolic network and GO analyses of DEGs are necessary to identify potential mechanisms regulated by TFs, which would provide a basis for further elucidating the elaborate molecular interplay between a TF and its interacting proteins or responsive genes.

CONCLUSION

In summary, the *rob* gene-mutant strain DTrob was shown to exhibit higher butanol tolerance than BW25113, and 285 DEGs between the two strains were identified. Deletion of *glgS* and *yibT* and overexpression of *fadB* improved the butanol tolerance of *E. coli*. Furthermore, this is the first study to report that *glgS* can impact butanol tolerance directly. Analysis of the metabolic network of DEGs revealed that inactivation of Rob upregulated some genes that may be involved in the synergistic increase in acetyl-CoA production to promote cell growth under butanol stress. Thus, the results of this study provide a deeper understanding of the regulatory mechanism of Rob in the resistance of *E. coli* to butanol stress.

DATA AVAILABILITY STATEMENT

The datasets generated for this study can be found in the Gene Expression Omnibus (GEO) of NCBI, GSE120032, <https://www.ncbi.nlm.nih.gov/geo/query/acc.cgi?acc=GSE120032>.

AUTHOR CONTRIBUTIONS

YM conceived of the project, analyzed the data, and wrote the manuscript. YM, TX, and ZW designed the experiments and drafted the manuscript. TX, ZW, and DH performed the experiments. All authors analyzed the data, prepared the manuscript, and approved the final version.

FUNDING

This work was supported by the National Natural Science Foundation of China (NSFC-30900033), the Tianjin Science and Technology Council (18JCYBJC24200), and the Foundation

(No. KF201815) of State Key Laboratory of Biobased Material and Green Papermaking, Qilu University of Technology, Shandong Academy of Sciences.

ACKNOWLEDGMENTS

We gratefully appreciate Dr. Yang Sheng (Chinese Acad Sci, Shanghai Inst Biol Sci, Inst Plant Physiol and Ecol, Key Lab

Synthet Biol, Shanghai, China) for providing us with the plasmids and strains related to the CRISPR-Cas9 system.

SUPPLEMENTARY MATERIAL

The Supplementary Material for this article can be found online at: <https://www.frontiersin.org/articles/10.3389/fbioe.2020.524198/full#supplementary-material>

REFERENCES

- Alexander, D. M., and St John, A. C. (1994). Characterization of the carbon starvation-inducible and stationary phase-inducible gene *slp* encoding an outer membrane lipoprotein in *Escherichia coli*. *Mol. Microbiol.* 11, 1059–1071. doi: 10.1111/j.1365-2958.1994.tb00383.x
- Aquino, P., Honda, B., Jaini, S., Lyubetskaya, A., Hosur, K., Chiu, J. G., et al. (2017). Coordinated regulation of acid resistance in *Escherichia coli*. *BMC Syst. Biol.* 11:1. doi: 10.1186/s12918-016-0376-y
- Bennik, M. H. J., Pomposiello, P. J., Thorne, D. F., and Demple, B. (2000). Defining a *rob* regulon in *Escherichia coli* by using transposon mutagenesis. *J. Bacteriol.* 182, 3794–3801. doi: 10.1128/jb.182.13.3794-3801.2000
- Black, P. N., Kianian, S. F., DiRusso, C. C., and Nunn, W. D. (1985). Long-chain fatty acid transport in *Escherichia coli*. *Cloning Mapp. Exp. fadL Gene* 260, 1780–1789.
- Brown, T. D. K., Jones-mortimer, M. C., and Kornberg, H. L. (1977). The enzymic interconversion of acetate and acetyl-coenzyme a in *Escherichia coli*. *J. Gen. Microbiol.* 102, 327–336. doi: 10.1099/00221287-102-2-327
- Bui, L. M., Lee, J. Y., Gerdali, A., Rahman, Z., Lee, J. H., and Kim, S. C. (2015). Improved n-butanol tolerance in *Escherichia coli* by controlling membrane related functions. *J. Biotechnol.* 204, 33–44. doi: 10.1016/j.jbiotec.2015.03.025
- Cai, L., Sutter, B. M., Li, B., and Tu, B. P. (2011). Acetyl-CoA induces cell growth and proliferation by promoting the acetylation of histones at growth genes. *Mol. Cell* 42, 426–437. doi: 10.1016/j.molcel.2011.05.004
- Chin, W. C., Lin, K. H., Liu, C. C., Tsuge, K., and Huang, C. C. (2017). Improved n-butanol production via co-expression of membrane-targeted tilapia metallothionein and the clostridial metabolic pathway in *Escherichia coli*. *BMC Biotechnol.* 17:36. doi: 10.1186/s12896-017-0356-3
- Dittrich, C. R., Bennett, G. N., and San, K.-Y. (2005). Characterization of the acetate-producing pathways in *Escherichia coli*. *Biotechnol. Prog.* 21, 1062–1067. doi: 10.1021/bp050073s
- Dong, H. J., Zhao, C. H., Zhang, T. R., Zhu, H. W., Lin, Z., Tao, W. W., et al. (2017). A systematically chromosomally engineered *Escherichia coli* efficiently produces butanol. *Metab. Eng.* 44, 284–292. doi: 10.1016/j.ymben.2017.10.014
- Fujita, Y., Matsuoka, H., and Hirooka, K. (2007). Regulation of fatty acid metabolism in bacteria. *Mol. Microbiol.* 66, 829–839. doi: 10.1111/j.1365-2958.2007.05947.x
- Gao, C., Zhai, J., Dang, S., and Zheng, S. (2018). Analysis of alternative splicing in chicken embryo fibroblasts in response to reticuloendotheliosis virus infection. *Avian Pathol.* 47, 585–594. doi: 10.1080/03079457.2018.1511047
- Gu, Y., Jiang, Y., Wu, H., Liu, X., Li, Z., Li, J., et al. (2011). Economical challenges to microbial producers of butanol: feedstock, butanol ratio and titer. *Biotechnol. J.* 6, 1348–1357. doi: 10.1002/biot.201100046
- Guo, Y., Lu, B., Tang, H., Bi, D., Zhang, Z., Lin, L., et al. (2019). Tolerance against butanol stress by disrupting succinylglutamate desuccinylase in *Escherichia coli*. *RSC Adv.* 9, 11683–11695. doi: 10.1039/c8ra09711a
- Guzman, L. M., Belin, D., Carson, M. J., and Beckwith, J. (1995). Tight regulation, modulation, and high-level expression by vectors containing the arabinose PBAD promoter. *J. Bacteriol.* 177:4121. doi: 10.1128/jb.177.14.4121-4130.1995
- He, X., Xue, T., Ma, Y., Zhang, J., Wang, Z., Hong, J., et al. (2019). Identification of functional butanol-tolerant genes from *Escherichia coli* mutants derived from error-prone PCR-based whole-genome shuffling. *Biotechnol. Biofuels* 12:73. doi: 10.1186/s13068-019-1405-z
- Hommais, F., Krin, E., Coppee, J. Y., Lacroix, C., Yeramian, E., Danchin, A., et al. (2004). GadE (YhiE): a novel activator involved in the response to acid environment in *Escherichia coli*. *Microbiology* 150(Pt 1), 61–72. doi: 10.1099/mic.0.26659-0
- Horinouchi, T., Maeda, T., and Furusawa, C. (2018). Understanding and engineering alcohol-tolerant bacteria using OMICS technology. *World J. Microbiol. Biotechnol.* 34:157. doi: 10.1007/s11274-018-2542-4
- Isken, S., and de Bont, J. A. M. (1998). Bacteria tolerant to organic solvents. *Extremophiles* 2, 229–238. doi: 10.1007/s007920050065
- Jang, Y.-S., and Lee, S. Y. (2015). Recent advances in biobutanol production. *Ind. Biotechnol.* 11, 316–321. doi: 10.1089/ind.2015.0023
- Jiang, Y., Chen, B., Duan, C. L., Sun, B. B., Yang, J. J., and Yang, S. (2015a). Multigene editing in the *Escherichia coli* genome via the CRISPR-Cas9 system. *Appl. Environ. Microbiol.* 81, 2506–2514. doi: 10.1128/aem.04023-14
- Jiang, Y., Liu, J. L., Jiang, W. H., Yang, Y. L., and Yang, S. (2015b). Current status and prospects of industrial bio-production of n-butanol in China. *Biotechnol. Adv.* 33, 1493–1501. doi: 10.1016/j.biotechadv.2014.10.007
- Jones, D. T., and Woods, D. R. (1986). Acetone-butanol fermentation revisited. *Microbiol. Rev.* 50, 484–524. doi: 10.1128/mmbr.50.4.484-524.1986
- Kaczmarzyk, D., Anfelt, J., Sarnegrim, A., and Hudson, E. P. (2014). Overexpression of sigma factor SigB improves temperature and butanol tolerance of *Synechocystis* sp PCC6803. *J. Biotechnol.* 182, 54–60. doi: 10.1016/j.jbiotec.2014.04.017
- Kim, M., Hatt, J. K., Weigand, M. R., Krishnan, R., Pavlostathis, S. G., and Konstantinidis, K. T. (2018). Genomic and transcriptomic insights into how bacteria withstand high concentrations of benzalkonium chloride biocides. *Appl. Environ. Microbiol.* 84:e00197-18.
- Kim, Y. J., Im, S. Y., Lee, J. O., and Kim, O. B. (2016). Potential Swimming Motility Variation by AcrR in *Escherichia coli*. *J. Microbiol. Biotechnol.* 26, 1824–1828. doi: 10.4014/jmb.1607.07058
- Krivoruchko, A., Zhang, Y., Siewers, V., Chen, Y., and Nielsen, J. (2015). Microbial acetyl-CoA metabolism and metabolic engineering. *Metab. Eng.* 28, 28–42. doi: 10.1016/j.ymben.2014.11.009
- Li, H. G., Ma, X. X., Zhang, Q. H., Luo, W., Wu, Y. Q., and Li, X. H. (2016). Enhanced butanol production by solvent tolerance *Clostridium acetobutylicum* SE25 from cassava flour in a fibrous bed bioreactor. *Bioresour. Technol.* 221, 412–418. doi: 10.1016/j.biortech.2016.08.120
- Livak, K. J., and Schmittgen, T. D. (2001). Analysis of relative gene expression data using real-time quantitative PCR and the 2^{(-Delta Delta C(T))} Method. *Methods* 25, 402–408. doi: 10.1006/meth.2001.1262
- Ma, Z., Gong, S., Richard, H., Tucker, D. L., Conway, T., and Foster, J. W. (2003). GadE (YhiE) activates glutamate decarboxylase-dependent acid resistance in *Escherichia coli* K-12. *Mol. Microbiol.* 49, 1309–1320. doi: 10.1046/j.1365-2958.2003.03633.x
- Nakajima, H., Kobayashi, K., Kobayashi, M., Asako, H., and Aono, R. (1995). Overexpression of the *robA* gene increases organic solvent tolerance and multiple antibiotic and heavy metal ion resistance in *Escherichia coli*. *Appl. Environ. Microbiol.* 61:2302. doi: 10.1128/aem.61.6.2302-2307.1995
- Nielsen, D. R., and Prather, K. J. (2009). In situ product recovery of n-butanol using polymeric resins. *Biotechnol. Bioeng.* 102, 811–821. doi: 10.1002/bit.22109
- Peralta-Yahya, P. P., Zhang, F. Z., del Cardayre, S. B., and Keasling, J. D. (2012). Microbial engineering for the production of advanced biofuels. *Nature* 488, 320–328.
- Perez-Rueda, E., Tenorio-Salgado, S., Huerta-Saquero, A., Balderas-Martinez, Y. I., and Moreno-Hagelsieb, G. (2015). The functional landscape bound to the transcription factors of *Escherichia coli* K-12. *Comput. Biol. Chem.* 58, 93–103. doi: 10.1016/j.compbiolchem.2015.06.002

- Purvis, J. E., Yomano, L. P., and Ingram, L. O. (2005). Enhanced trehalose production improves growth of *Escherichia coli* under osmotic stress. *Appl. Environ. Microbiol.* 71, 3761–3769. doi: 10.1128/aem.71.7.3761-3769.2005
- Qureshi, N., and Blaschek, H. P. (2000). Butanol production using *Clostridium beijerinckii* BA101 hyper-butanol producing mutant strain and recovery by pervaporation. *Appl. Biochem. Biotechnol.* 84–6, 225–235. doi: 10.1385/abab:84-86:1-9:225
- Rahimpour, M., Montero, M., Almagro, G., Viale, A. M., Sevilla, A., Canovas, M., et al. (2013). GlgS, described previously as a glycogen synthesis control protein, negatively regulates motility and biofilm formation in *Escherichia coli*. *Biochem. J.* 452, 559–573. doi: 10.1042/bj20130154
- Ran, F. A., Hsu, P. D., Wright, J., Agarwala, V., Scott, D. A., and Zhang, F. (2013). Genome engineering using the CRISPR-Cas9 system. *Nat. Protoc.* 8, 2281–2308.
- Reyes, L. H., Almario, M. P., and Kao, K. C. (2011). Genomic library screens for genes involved in n-butanol tolerance in *Escherichia coli*. *PLoS One* 6:e17678. doi: 10.1371/journal.pone.0017678
- Reyes, L. H., Almario, M. P., Winkler, J., Orozco, M. M., and Kao, K. C. (2012). Visualizing evolution in real time to determine the molecular mechanisms of n-butanol tolerance in *Escherichia coli*. *Metab. Eng.* 14, 579–590. doi: 10.1016/j.ymben.2012.05.002
- Royce, L. A., Yoon, J. M., Chen, Y. X., Rickenbach, E., Shanks, J. V., and Jarboe, L. R. (2015). Evolution for exogenous octanoic acid tolerance improves carboxylic acid production and membrane integrity. *Metab. Eng.* 29, 180–188. doi: 10.1016/j.ymben.2015.03.014
- Rutherford, B. J., Dahl, R. H., Price, R. E., Szmidt, H. L., Benke, P. I., Mukhopadhyay, A., et al. (2010). Functional genomic study of exogenous n-butanol stress in *Escherichia coli*. *Appl. Environ. Microbiol.* 76, 1935–1945. doi: 10.1128/AEM.02323-09
- Sandoval, N. R., and Papoutsakis, E. T. (2016). Engineering membrane and cell-wall programs for tolerance to toxic chemicals: beyond solo genes. *Curr. Opin. Microbiol.* 33, 56–66. doi: 10.1016/j.mib.2016.06.005
- Shen, C. R., Lan, E. I., Dekishima, Y., Baez, A., Cho, K. M., and Liao, J. C. (2011). Driving forces enable high-titer anaerobic 1-butanol synthesis in *Escherichia coli*. *Appl. Environ. Microbiol.* 77, 2905–2915. doi: 10.1128/aem.03034-10
- Si, H. M., Zhang, F., Wu, A. N., Han, R. Z., Xu, G. C., and Ni, Y. (2016). DNA microarray of global transcription factor mutant reveals membrane-related proteins involved in n-butanol tolerance in *Escherichia coli*. *Biotechnol. Biofuels* 9:114.
- Sikkema, J., de Bont, J. A., and Poolman, B. (1995). Mechanisms of membrane toxicity of hydrocarbons. *Microbiol. Rev.* 59:201. doi: 10.1128/mmbr.59.2.201-222.1995
- Tucker, D. L., Tucker, N., Ma, Z., Foster, J. W., Miranda, R. L., Cohen, P. S., et al. (2003). Genes of the GadX-GadW regulon in *Escherichia coli*. *J. Bacteriol.* 185, 3190–3201. doi: 10.1128/jb.185.10.3190-3201.2003
- van den Berg, B., Black, P. N., Clemons, W. M., and Rapoport, T. A. (2004). Crystal structure of the long-chain fatty acid transporter FadL. *Science* 304:1506. doi: 10.1126/science.1097524
- Wang, X. J., Zhang, X., Yang, J. T., and Wang, Z. X. (2018). Effect on transcriptome and metabolome of stacked transgenic maize containing insecticidal cry and glyphosate tolerance epsps genes. *Plant J.* 93, 1007–1016. doi: 10.1111/tpj.13825
- White, D. G., Goldman, J. D., Demple, B., and Levy, S. B. (1997). Role of the acrAB locus in organic solvent tolerance mediated by expression of marA, soxS, or robA in *Escherichia coli*. *J. Bacteriol.* 179:6122. doi: 10.1128/jb.179.19.6122-6126.1997
- Zhang, S., Yang, W., Chen, H., Liu, B., Lin, B., and Tao, Y. (2019). Metabolic engineering for efficient supply of acetyl-CoA from different carbon sources in *Escherichia coli*. *Microb. Cell Fact.* 18:130. doi: 10.1186/s12934-019-1177-y

Conflict of Interest: The authors declare that the research was conducted in the absence of any commercial or financial relationships that could be construed as a potential conflict of interest.

Copyright © 2020 Wang, Xue, Hu and Ma. This is an open-access article distributed under the terms of the Creative Commons Attribution License (CC BY). The use, distribution or reproduction in other forums is permitted, provided the original author(s) and the copyright owner(s) are credited and that the original publication in this journal is cited, in accordance with accepted academic practice. No use, distribution or reproduction is permitted which does not comply with these terms.

Frontiers in Bioengineering and Biotechnology

Accelerates the development of therapies,
devices, and technologies to improve our lives

A multidisciplinary journal that accelerates the
development of biological therapies, devices,
processes and technologies to improve our lives
by bridging the gap between discoveries and their
application.

Discover the latest Research Topics

See more →

Frontiers

Avenue du Tribunal-Fédéral 34
1005 Lausanne, Switzerland
frontiersin.org

Contact us

+41 (0)21 510 17 00
frontiersin.org/about/contact



Frontiers in
Bioengineering
and Biotechnology

